frontiers | Research Topics

Fertilization and early embryogenesis: from research to clinical practice

Edited by
Martin Anger, Katerina Komrskova, Jason Knott, Ahmed Balboula and Paolo Rinaudo

Published in
Frontiers in Cell and Developmental Biology

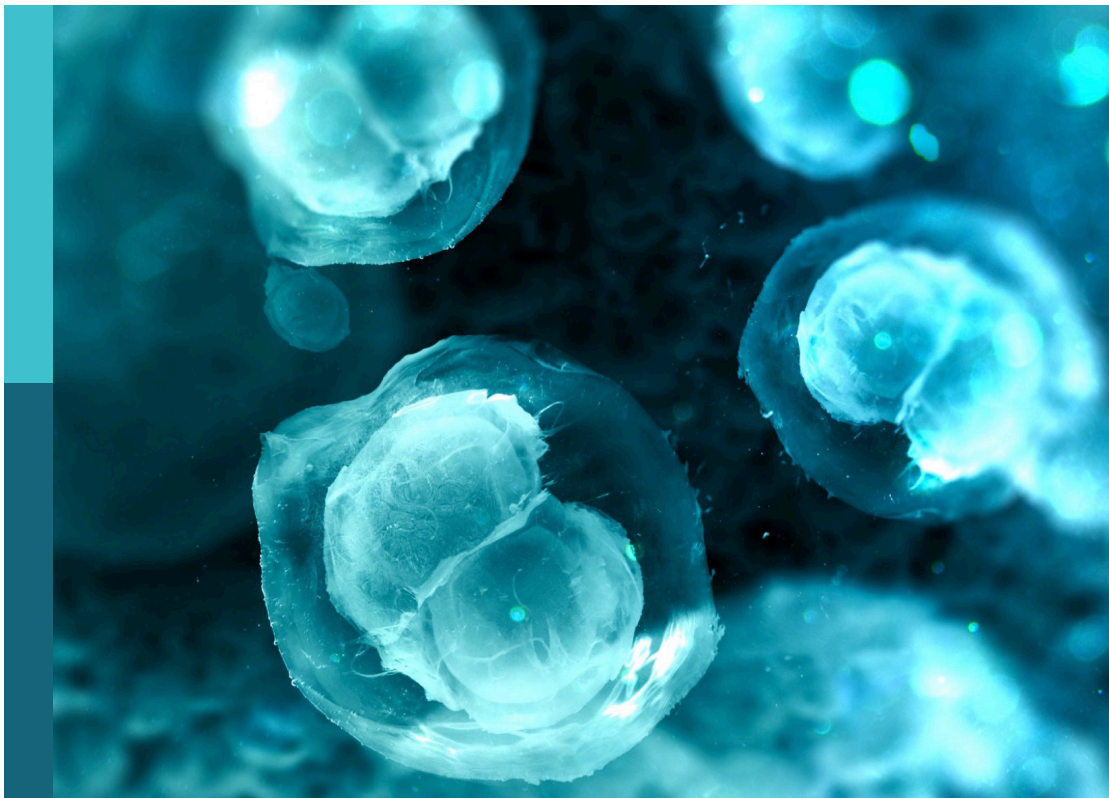

FRONTIERS EBOOK COPYRIGHT STATEMENT

The copyright in the text of individual articles in this ebook is the property of their respective authors or their respective institutions or funders. The copyright in graphics and images within each article may be subject to copyright of other parties. In both cases this is subject to a license granted to Frontiers.

The compilation of articles constituting this ebook is the property of Frontiers.

Each article within this ebook, and the ebook itself, are published under the most recent version of the Creative Commons CC-BY licence. The version current at the date of publication of this ebook is CC-BY 4.0. If the CC-BY licence is updated, the licence granted by Frontiers is automatically updated to the new version.

When exercising any right under the CC-BY licence, Frontiers must be attributed as the original publisher of the article or ebook, as applicable.

Authors have the responsibility of ensuring that any graphics or other materials which are the property of others may be included in the CC-BY licence, but this should be checked before relying on the CC-BY licence to reproduce those materials. Any copyright notices relating to those materials must be complied with.

Copyright and source acknowledgement notices may not be removed and must be displayed in any copy, derivative work or partial copy which includes the elements in question.

All copyright, and all rights therein, are protected by national and international copyright laws. The above represents a summary only. For further information please read Frontiers' Conditions for Website Use and Copyright Statement, and the applicable CC-BY licence.

ISSN 1664-8714
ISBN 978-2-8325-5925-3
DOI 10.3389/978-2-8325-5925-3

About Frontiers

Frontiers is more than just an open access publisher of scholarly articles: it is a pioneering approach to the world of academia, radically improving the way scholarly research is managed. The grand vision of Frontiers is a world where all people have an equal opportunity to seek, share and generate knowledge. Frontiers provides immediate and permanent online open access to all its publications, but this alone is not enough to realize our grand goals.

Frontiers journal series

The Frontiers journal series is a multi-tier and interdisciplinary set of open-access, online journals, promising a paradigm shift from the current review, selection and dissemination processes in academic publishing. All Frontiers journals are driven by researchers for researchers; therefore, they constitute a service to the scholarly community. At the same time, the *Frontiers journal series* operates on a revolutionary invention, the tiered publishing system, initially addressing specific communities of scholars, and gradually climbing up to broader public understanding, thus serving the interests of the lay society, too.

Dedication to quality

Each Frontiers article is a landmark of the highest quality, thanks to genuinely collaborative interactions between authors and review editors, who include some of the world's best academicians. Research must be certified by peers before entering a stream of knowledge that may eventually reach the public - and shape society; therefore, Frontiers only applies the most rigorous and unbiased reviews. Frontiers revolutionizes research publishing by freely delivering the most outstanding research, evaluated with no bias from both the academic and social point of view. By applying the most advanced information technologies, Frontiers is catapulting scholarly publishing into a new generation.

What are Frontiers Research Topics?

Frontiers Research Topics are very popular trademarks of the *Frontiers journals series*: they are collections of at least ten articles, all centered on a particular subject. With their unique mix of varied contributions from Original Research to Review Articles, Frontiers Research Topics unify the most influential researchers, the latest key findings and historical advances in a hot research area.

Find out more on how to host your own Frontiers Research Topic or contribute to one as an author by contacting the Frontiers editorial office: frontiersin.org/about/contact

Fertilization and early embryogenesis: from research to clinical practice

Topic editors

Martin Anger — Institute of Animal Physiology and Genetics, Academy of Sciences of the Czech Republic (ASCR), Czechia

Katerina Komrskova — Institute of Biotechnology (ASCR), Czechia

Jason Knott — Michigan State University, United States

Ahmed Balboula — University of Missouri, United States

Paolo Rinaudo — University of California, San Francisco, United States

Citation

Anger, M., Komrskova, K., Knott, J., Balboula, A., Rinaudo, P., eds. (2025). *Fertilization and early embryogenesis: from research to clinical practice*. Lausanne: Frontiers Media SA. doi: 10.3389/978-2-8325-5925-3

Table of contents

frontiers | Frontiers in Cell and Developmental Biology

TYPE Editorial
PUBLISHED 09 January 2025
DOI 10.3389/fcell.2024.1547205

Check for updates

OPEN ACCESS

EDITED AND REVIEWED BY
Natraj Krishnan,
Mississippi State University, United States

*CORRESPONDENCE
Martin Anger,
martin.anger@vri.cz
Jason G. Knott,
knottj@msu.edu

RECEIVED 17 December 2024
ACCEPTED 26 December 2024
PUBLISHED 09 January 2025

CITATION
Anger M, Komrskova K, Balboula AZ, Rinaudo P and Knott JG (2025) Editorial: Fertilization and early embryogenesis: from research to clinical practice.
Front. Cell Dev. Biol. 12:1547205.
doi: 10.3389/fcell.2024.1547205

COPYRIGHT
© 2025 Anger, Komrskova, Balboula, Rinaudo and Knott. This is an open-access article distributed under the terms of the Creative Commons Attribution License (CC BY). The use, distribution or reproduction in other forums is permitted, provided the original author(s) and the copyright owner(s) are credited and that the original publication in this journal is cited, in accordance with accepted academic practice. No use, distribution or reproduction is permitted which does not comply with these terms.

Editorial: Fertilization and early embryogenesis: from research to clinical practice

Martin Anger[1,2]*, Katerina Komrskova[3,4], Ahmed Z. Balboula[5], Paolo Rinaudo[6] and Jason G. Knott[7]*

[1]Department of Genetics and Reproductive Biotechnologies, Veterinary Research Institute, Brno, Czechia, [2]Institute of Animal Physiology and Genetics, Czech Academy of Sciences, Libechov, Czechia, [3]Laboratory of Reproductive Biology, Institute of Biotechnology, Czech Academy of Sciences, BIOCEV, Vestec, Czechia, [4]Department of Zoology, Faculty of Science, Charles University, Prague, Czechia, [5]Division of Animal Sciences, University of Missouri, Columbia, MO, United States, [6]Department of Obstetrics Gynecology and Reproductive Sciences, University of California, San Francisco, San Francisco, CA, United States, [7]Developmental Epigenetics Laboratory, Department of Animal Science, Reproductive and Developmental Sciences Program, Michigan State University, East Lansing, MI, United States

KEYWORDS

oocyte, sperm, preimplantation embryo, aneuploidy, human assisted reproduction, epigenetic regulation, placentation, maternal immune response

Editorial on the Research Topic
Fertilization and early embryogenesis: from research to clinical practice

The fusion of an egg and a sperm triggers a complex plethora of events that will ultimately lead to the formation of a new individual. Embryonic development requires the precise orchestration of a formidable number of events. Although our knowledge of the underlying mechanisms involved has significantly increased over the last 2 decades, new discoveries continue to surprise us, further underlining the complexity and diversity of ontogenesis in different species. The intricacy of events that occur during early development, with the rapid changes in cellular morphology and behavior, may serve as an explanation for the frequent failure of mammalian embryos. This Research Topic, "Fertilization and early embryogenesis: from Research to clinical practice," is comprised of thirteen publications that cover the complexity of germ cell, embryonic, and fetal development in a diverse number of species, including mice, cattle, pigs, humans, *Xenopus*, and axolotls. The Research Topic of these papers range from basic research on animal germ cells and embryos to clinical studies on human IVF embryos to placentation and postimplantation events.

Five studies focused on chromosomal and epigenetic aspects of early development. These include retrospective and clinical studies in humans. In Sanovec et al., the authors identified a potential new link between chromatin defects and disturbed mobility in sperm. The interaction between the DNA packaging protein protamine 2, nuclear envelope component lamin B2/3, and the cytoskeletal protein septin 12, provide a mechanistical link between abnormal sperm chromatin condensation and altered motility in a mouse model. The authors further provided evidence that a similar connection exists in human sperm. For instance, the altered expression and localization of homologue proteins is associated with low sperm motility known as asthenozoospermia.

Embryonic development is known to be prone to errors during chromosome segregation. In the study by Horakova et al., the authors showed that the spindle assembly checkpoint (SAC), a surveillance mechanism that ensures accurate chromosome attachment to spindle microtubules prior to cell division, is not utilized by early mouse embryos. Instead, the blastomeres of 2-cell embryos activate a complex known as the anaphase promoting complex (APC/C) immediately after nuclear envelope breakdown (NEBD). Therefore, the absence of SAC may partially explain the higher frequency of aneuploidy in embryos.

In the study by Ma et al., the authors recruited two female patients from a family characterized by recurrent early embryo failure after IVF or ICSI. Using whole-exome sequencing on zygotes, the authors identified a mutation in a gene that encodes for regulator of G protein signaling 12 (RGS12). Phenotypic analysis of oocytes and zygotes from these patients revealed defects in calcium signaling, prolonged CSF arrest, and the inability to activate APC/C sufficiently, resulting in arrest after the 1-cell stage. The authors postulate that the RGS12 gene mutation plays a causal role in recurrent early embryo failure.

Human IVF embryos can exhibit unusual patterns of cell division after IVF or ICSI such as fast cell (FC) division to the 3-cell stage via two consecutive divisions or instant direct cleavage (IDC) into 3 blastomeres. The utilization rate of embryos that exert these types of cleavage is not known. In a retrospective study by Nemerovsky et al., the authors show that although FC dividing embryos exhibited reduced development into blastocysts, the pregnancy rate was similar to controls. Most IDC embryos arrested on day 3, and those that developed into blastocysts did not produce a pregnancy. Since blastomeres resulting from fast division might be aneuploid, this illustrates that developing human embryos exhibit a surprising degree of plasticity and redundancy.

The review by Montgomery et al. provides an exquisite overview of the developmental dynamics of DNA methylation and the role of ten-eleven translocation (TET) enzymes in demethylation in oocytes, preimplantation embryos, primordial germ cells, and adults. These enzymes are not only essential for epigenetic reprogramming during normal development, but their malfunction is associated with various types of cancer and developmental disorders. The authors further discuss the implications of TET enzymes in human ART.

Two studies focused on the microscopic assessment of oocytes and preimplantation embryos and the impact of oil-covered culture media on the efficacy of small molecule inhibitors. Oocyte and embryo quality is paramount for their utilization in ART. However, it is not always possible to assess oocytes and early embryos without compromising the developmental potential. Thanks to the recent progress in live imaging and micromanipulation, the biomechanical properties of oocytes and embryos can be assessed using noninvasive techniques. Fluks et al. provide a comprehensive review on the biomechanical properties of oocytes and preimplantation embryos and discuss various techniques that are used to evaluate these properties.

In the laboratory it is a common practice to use small molecule inhibitors to block the activity of key cell-cycle regulators and signaling proteins in oocytes and preimplantation embryos. In Rémillard-Labrosse et al., the authors demonstrated that several different inhibitors lose activity in standard oil-covered culture media, likely by partitioning into the oil. The authors conclude that researchers should be extremely cautious when using oil to culture oocytes and embryos in the presence of small molecule inhibitors and recommend using oil-free culture systems.

Three studies focused on embryonic development and tetraploid complementation. In Šimková et al., the authors assessed spatiotemporal changes in expression of various transcripts during early development in axolotl. Since the localization of specific transcripts is essential for the development of the body plan, the comparison was aimed at identifying similarities and differences between axolotls and *Xenopus*. The authors reported surprising differences between both species. One notable difference was the development of primordial germ cells, indicating that even fundamental processes might not be conserved between closely related species.

In Kang et al., the authors focused on the effect of growth differentiation factor 8 (GDF-8) on the *in vitro* development of bovine oocytes and embryos. The authors demonstrated that the supplementation of culture media with GDF-8 improved embryo quality by increasing the total number of cells in blastocysts and enhancing the expression of multiple transcripts, including mRNAs that encode for tight junction proteins important for blastocyst cavitation. The authors further show that cryopreserved GDF-8 treated blastocysts recovered and re-expanded better than untreated embryos.

Tetraploid complementation is highly efficient method for testing the developmental potential of pluripotent cells. Lee et al. compared various methods for producing tetraploid embryos in pigs and discovered that tetraploids produced by the electrofusion of 2-cell blastomeres in parthenogenetic embryos, exhibited the greatest developmental potential with significantly lower rates of apoptosis compared to the other methods tested.

Lastly, three papers focused on the role of the maternal immune system during pregnancy, the importance of *in vitro* models for placental research, and research on fetal steroidogenesis. It is well known that the functional modifications of the maternal immune system are essential for successful embryonic and fetal development. However, we still do not fully understand how immune tolerance of the sperm and embryo is established in the reproductive tract while the immune system is still able to react to most pathogens. Recent literature on this subject is elegantly reviewed by Visnyaiová et al. The authors provide an extensive overview on the diverse population of immune cells that occupy the uterine tube. They discuss the possibility of immune privilege as a mechanism to tolerate sperm and embryos in the uterine tube. The authors conclude that more studies concerning the specificity of the maternal immune system and its interaction with the developing embryo and fetus are needed.

A prerequisite for a successful pregnancy is the establishment of a healthy placenta, a transient organ that supports the growth and health of the fetus. Alterations in placentation or placental function can have a profound impact on embryonic and fetal development and the health of the offspring. In Liu et al., the authors provide an expansive review on the biology of the human placenta and the available *in vitro* models used for studying human placentation and placental function. Examples of these models include placental-derived trophoblastic stem cell (TSC) models, primary trophoblast cells, and organoid models. The advantages and limitations of each model are discussed.

In adults, it is well established that testosterone is produced by Leydig cells in part through the actions of the enzyme 17β-hydroxysteroid dehydrogenase (HSD17B3). However, the cell-specific expression and localization of HSD17B3 during human fetal development is not as clear. In Planinic et al., the authors used a unique cohort of human fetal testes samples to follow the expression and localization of HSD17B3. They traced its origin to the Sertoli cells during the second trimester, which is similar to the Sertoli cell-specific expression observed in rodents. The authors postulate that perturbations in the transition of steroidogenesis from Sertoli cells to Leydig cells could be a potential source of problems in the development of the testes and future sperm production.

Author contributions

MA: Writing–original draft, Writing–review and editing. KK: Writing–original draft, Writing–review and editing. AB: Writing–original draft, Writing–review and editing. PR: Writing–original draft, Writing–review and editing. JK: Writing–original draft, Writing–review and editing.

Funding

The author(s) declare that financial support was received for the research, authorship, and/or publication of this article. JK was supported by a grant from the National Institutes of Child Health and Development (NICHD) (R01HD095371) and Michigan State University AgBioResearch. PR was supported by a grant from the NICHD (R01HD108166). AB was supported by two grants from the NIH (R35 GM142537 and R01HD113358), and the National Institute of Food and Agriculture, grant number 2022-67015-36301. MA was supported by Czech Science Foundation Project 20-25850S and by institutional support projects MZE-RO0518 to Veterinary Research Institute and RVO 67985904 to Institute of Animal Physiology and Genetics. KK was supported by Science Foundation Projects GC20-20217J and GA23-06591S; institutional support by Institute of Biotechnology of the Czech Academy of Sciences RVO 86652036 and COST Action CA20119 (ANDRONET) supported by European Cooperation in Science and Technology (www.cost.eu).

Conflict of interest

The authors declare that the work was conducted in the absence of any commercial or financial relationships that could be construed as a potential conflict of interest.

Generative AI statement

The author(s) declare that no Generative AI was used in the creation of this manuscript.

Publisher's note

All claims expressed in this article are solely those of the authors and do not necessarily represent those of their affiliated organizations, or those of the publisher, the editors and the reviewers. Any product that may be evaluated in this article, or claim that may be made by its manufacturer, is not guaranteed or endorsed by the publisher.

frontiers | Frontiers in Cell and Developmental Biology

TYPE Original Research
PUBLISHED 19 October 2023
DOI 10.3389/fcell.2023.1260795

Check for updates

OPEN ACCESS

EDITED BY
Jason Knott,
Michigan State University, United States

REVIEWED BY
Prayag Murawala,
Mount Desert Island Biological Laboratory, United States
Stephan Q. Schneider,
Academia Sinica, Taiwan
Francisco Pelegri,
University of Wisconsin-Madison, United States

*CORRESPONDENCE
Radek Šindelka,
sindelka@ibt.cas.cz

†These authors have contributed equally to this work

RECEIVED 18 July 2023
ACCEPTED 26 September 2023
PUBLISHED 19 October 2023

CITATION
Šimková K, Naraine R, Vintr J, Soukup V and Šindelka R (2023), RNA localization during early development of the axolotl. *Front. Cell Dev. Biol.* 11:1260795. doi: 10.3389/fcell.2023.1260795

COPYRIGHT
© 2023 Šimková, Naraine, Vintr, Soukup and Šindelka. This is an open-access article distributed under the terms of the Creative Commons Attribution License (CC BY). The use, distribution or reproduction in other forums is permitted, provided the original author(s) and the copyright owner(s) are credited and that the original publication in this journal is cited, in accordance with accepted academic practice. No use, distribution or reproduction is permitted which does not comply with these terms.

RNA localization during early development of the axolotl

Kateřina Šimková[1†], Ravindra Naraine[1†], Jan Vintr[2], Vladimír Soukup[2] and Radek Šindelka[1*]

[1]Laboratory of Gene Expression, Institute of Biotechnology of the Czech Academy of Sciences, Vestec, Czechia, [2]Department of Zoology, Faculty of Science, Charles University, Prague, Czechia

The asymmetric localization of biomolecules is critical for body plan development. One of the most popular model organisms for early embryogenesis studies is *Xenopus laevis* but there is a lack of information in other animal species. Here, we compared the early development of two amphibian species—the frog *X. laevis* and the axolotl *Ambystoma mexicanum*. This study aimed to identify asymmetrically localized RNAs along the animal-vegetal axis during the early development of *A. mexicanum*. For that purpose, we performed spatial transcriptome-wide analysis at low resolution, which revealed dynamic changes along the animal-vegetal axis classified into the following categories: profile alteration, *de novo* synthesis and degradation. Surprisingly, our results showed that many of the vegetally localized genes, which are important for germ cell development, are degraded during early development. Furthermore, we assessed the motif presence in UTRs of degraded mRNAs and revealed the enrichment of several motifs in RNAs of germ cell markers. Our results suggest novel reorganization of the transcriptome during embryogenesis of *A. mexicanum* to converge to the similar developmental pattern as the *X. laevis*.

KEYWORDS

RNA localization, early development, *Ambystoma mexicanum*, animal-vegetal axis, TOMO-seq

Introduction

Asymmetric distribution of biomolecules and asymmetric cell division is a crucial mechanism during stem cell division and the development of body tissues and internal organs. Moreover, it plays a critical role in the early development of many animal species. Maternal determinants such as proteins and RNAs (coding and non-coding), are asymmetrically distributed within the oocyte and early embryos. Thus, cell division often results in two unequal daughter cells with distinct fates. This phenomenon has been observed mainly in fish—*Danio rerio* (Howley and Ho, 2000)—and anuran amphibians—*Xenopus laevis* (Forristall et al., 1995; Kloc and Etkin, 1995; Sindelka et al., 2018; 2010) or *Rana pipiens* (Nath et al., 2005)—but interestingly there is no evidence of determinants localization in early mammalian embryos (Vinot et al., 2005). Likewise, our knowledge on the early development of other non-mammalian vertebrates, such as urodeles amphibians is still limited. In one of these urodeles, the Mexican axolotl (*Ambystoma mexicanum*), the maternal asymmetrical localization of several genes during the early development has been described (Vaur et al., 2003; Bachvarova et al., 2004). However, the whole transcriptome analysis, which could have the potential to reveal the similarities and differences between embryos of two close amphibian orders, is still missing. Therefore, we performed the comparison of RNA localization during the early development of the frog *X. laevis* (order *Anura*) and the axolotl *A. mexicanum* (order *Urodela*).

The anuran amphibian, like *X. laevis*, lays a copious number of large sized eggs (~1.3 mm) which show a clear delineation of two hemispheres. The animal hemisphere is typically dark due to pigment granules and contains the germinal vesicle, while the vegetal hemisphere is light and full of yolk proteins and contains important organelles such as the endoplasmic reticulum, Golgi apparatus and mitochondria (Dumont, 1972). Eggs of urodele amphibians, like *A. mexicanum,* are typically larger (~2 mm) and also show a clear animal and vegetal hemisphere (Schreckenberg and Jacobson, 1975; Bordzilovskaya and Dettlaff, 1979). In amphibians, the hemispheric distinction occurs during oogenesis, and simultaneously asymmetric distribution of maternal RNAs and proteins is established. The gradient formation of maternal molecules is the first step in the establishment of the animal-vegetal (A-V) axis, which is important for the development of the germ layers. In *X. laevis,* the blastomere fate mapping shows that the animal part of the embryo contributes to the ectoderm formation, the vegetal part into endoderm structures and the equatorial segment into mesodermal structures (Moody, 1987a; Moody, 1987b). To study Urodeles gastrulation, cell lineage tracing was performed in *A. mexicanum* (Lundmark, 1986), but comparatively thorough blastomere fate mapping of early embryos has never been done. On the other hand, the fate mapping in related urodele *Pleurodeles waltl* shows a similar blastomeres contribution to the formation of body structures as in *X. laevis* (Delarue et al., 1997). However, it is still unknown to what extent the gross similarities in blastomere fate-mapping reflect similarities in the distribution of molecular components along the A-V axis.

In our laboratory, we focus on the identification of asymmetrically distributed biomolecules in oocytes and early embryos of many animal species. Recently, we identified about 15000 maternal transcripts asymmetrically localized along the animal-vegetal axis in *X. laevis* oocytes (Sindelka et al., 2018). These mRNAs were classified into four localization profile groups: extremely animal, animal, vegetal and extremely vegetal. We identified most of the mRNAs in the animal hemisphere—94%. The extremely animal group contains 2.8% mRNAs, which are important mainly in transcription and translation regulation. While animal localization is probably formed through diffusion, the localization in extremely animal sections seems to be caused by the yet undiscovered active transport mechanism. In the vegetal and extremely vegetal sections, we identified 1.3% and 0.2% of the total mRNAs respectively.

Previous studies have shown the presence of three distinct pathways for vegetal RNA localization. The first one is called the early pathway (also known as METRO) and is used mainly for the localization of germ plasm determinants such as *nanos1* (Forristall et al., 1995; Kloc and Etkin, 1995; Zhou and King, 1996), *dazl* (Houston et al., 1998) and *ddx25* (MacArthur et al., 2000). During early oogenesis, mRNAs diffuse from the nucleus to be entrapped by the mitochondrial cloud (in fish, called Balbiani body). Later the whole structure is transported towards the vegetal pole to be anchored in the narrow region of the oocyte vegetal cortex (Forristall et al., 1995; Chang et al., 2004). The localization through the late pathway takes place at later stages of oogenesis. This pathway includes mainly mRNAs essential for the germ layer development, such as *gdf1* (also called *Vg1*) (Melton, 1987; Forristall et al., 1995; Kloc and Etkin, 1995; Deshler et al., 1997) and *vegt* (Lustig et al., 1996; Stennard et al., 1996; Zhang and King, 1996). The late pathway components are localized to the vegetal region by a microtubule-dependent mechanism and then anchored in the wide region of the vegetal cortex. In addition, the existence of mRNAs sharing some characteristics of both major pathways led to the categorization of the new intermediate pathway. Examples of such mRNAs include *dnd1* (Horvay et al., 2006), *grip2* (Claußen et al., 2011) and *plin2* (Chan et al., 1999).

In anuran amphibians and teleost fish, the primordial germ cells (PGCs) are produced from germ plasm determinants that migrated to the vegetal hemisphere during oogenesis. (Mahowald and Hennen, 1971; Whitington and Dixon, 1975; Heasman et al., 1984; Knaut et al., 2000). This mechanism of PGCs formation, known as preformation, involves germ plasm repression of transcription of somatic genes in the primordial germ cells (PGCs) leading to germ line segregation (Venkatarama et al., 2010). Another mechanism of PGCs determination, epigenesis (also called induction), is found in *M. musculus*, and involves the production of PGCs through the induction of pluripotent cells of early gastrula by extracellular signals in a germ plasm-independent manner (Tam and Zhou, 1996). Germ plasm has never been observed in urodele oocytes or eggs and therefore it is believed that the germ line of these amphibians is also most probably determined by epigenesis (Johnson et al., 2001).

In teleost fish, such as *D. rerio*, the maternal determinant gradients along the animal-vegetal axis are established during oogenesis similarly to amphibians. Surprisingly, these gradients are disrupted shortly after fertilization in the RNA translocation phenomenon, which is indispensable for germline and germ layer development. This is observed for the vegetally localized germ plasm components (*dnd1, nanos1* and *ddx4*) which migrate to the animal pole after fertilization (Howley and Ho, 2000; Weidinger et al., 2003; Theusch et al., 2006). The post-fertilization translocation is connected with the cytoplasm segregation from the vitelloplasm resulting in the creation of a blastodisc, that will give rise to the embryo (reviewed in Fuentes et al., 2018). The process is accompanied with slow and fast cytoplasmic flow. While the actin-dependent slow cytoplasmic flow translocates vegetally localized *dazl* towards the animal pole, fast cytoplasmic flow transports dorsal determinants (*grip2a* and *wnt8a*) along microtubules to the dorsal side of the embryo (Lu et al., 2011; Tran et al., 2012; Ge et al., 2014; Welch and Pelegri, 2015). During cell division, the cells at the base of blastodisc containing germ plasm markers adopt a germ cell lineage fate (Hashimoto et al., 2004; Kosaka et al., 2007).

When the animal-vegetal axis is established the determination of the left-right and dorsal-ventral axis can start. The first step in the establishment of the dorsal-ventral axis occurs in *X. laevis* shortly after fertilization. The sperm penetrates to the future ventral side and this event leads to the process known as cortical rotation. The cytoplasmic movement and cytoskeleton reorganization give rise to a grey crescent, which is the base for the origin of the Niewkoop center and the gastrulation induction center—The Spemann organizer (Vincent et al., 1986; Vincent et al., 1987). The Spemann organizer is formed through the crosstalk of two signaling pathways (Agius et al., 2000; Nishita et al., 2000). For the activation of the Wnt pathway, it is necessary to stabilize β-catenin on the dorsal side of the embryo. The stabilizing factors are originally present in the vegetal hemisphere but are transported to the dorsal side after the cortical rotation. Here, stabilizing factors can act on β-catenin leading to the expression of zygotic genes (*siamois, twin*) (Brannon et al., 1997; Laurent et al., 1997). The second signaling pathway occurs shortly after fertilization. It is

known that some vegetally localized mRNAs (*vegt*) are translated after fertilization and proteins diffuse to the equatorial region of the egg. These proteins regulate the gene expression of *transforming growth factor-beta* (TGFβ) family members (Kofron et al., 1999) The cooperation of β-catenin-activated genes and TGFβ family genes direct the formation of Spemann organizer and initiate gastrulation (Agius et al., 2000; Nishita et al., 2000).

While the role of asymmetric RNA distribution in the animal-vegetal axis establishment has been confirmed, the induction of dorsal-ventral and left-right axes appears to be independent on RNA localization in *X. laevis*. In (Levin et al.,2002) revealed the asymmetric distribution of mRNA H+-V-ATPase using *in situ* hybridization and he outlined a possible role in left-right axis induction, but this hypothesis has been disproven a few years later. The single blastomere transcriptome analysis of 8-cell stage *Xenopus tropicalis* embryos also revealed the absence of any RNA pattern along the dorsal-ventral and left-right axis (De Domenico et al., 2015). Moreover, in our laboratory, we analyzed the expression of genes that have been previously connected with the dorsal-ventral pattern (for example *dvl2, dvl3, gsk3b, ctnnb1* and *wnt11*) and confirmed the non-existence of RNA asymmetry (Flachsova et al., 2013). These results indicate the involvement of other biomolecules, such as proteins, in the establishment of these axes in anurans.

Previously, we compared localization profiles of matured eggs along the animal-vegetal axis among various model organisms (*X. laevis, D. rerio, A. mexicanum* and *Acipenser ruthenus*) and revealed the relatively low conservation in RNA localization (Naraine et al., 2022). Here, we continue using urodele *A. mexicanum* to study the spatiotemporal changes during early development in comparison to anuran amphibians. We identified asymmetrically localized RNAs along the animal-vegetal axis and revealed that many identified RNAs show dynamic pattern changes in stages before the onset of mid-blastula transition (MBT), the event of embryonic genome activation. The detected changes were classified into two groups. The first group contains genes that are transcribed *de novo* before MBT, showing the gradual activation of the embryonic genome. In the second group, there are genes whose transcripts are partially degraded after fertilization. Surprisingly many degraded genes are germ plasm markers suggesting preformation as a conserved mechanism for vertebrates as mentioned in (Škugor et al., 2016). Many of *de novo* or degraded transcripts shows altering profiles during development. In addition, we found motifs conserved in PGC transcripts of *A. mexicanum* and suggested its possible role in the early development of urodeles.

Methods

Ethics approval

All experimental procedures involving model organism *A. mexicanum* were carried out in accordance with the Czech Law 246/1992 on animal welfare. *A. mexicanum* animals were from the colony of the Department of Zoology, Faculty of Science, Charles University, Prague, Czech Republic, and all protocols were approved by the Faculty of Sciences of Charles University.

Embryos collection

A. mexicanum male and female adults were kept together in an aquarium and after natural stimulation, the females laid eggs. Samples were prepared in two independent experiments and using two different females and males. The gel envelope was first removed from the eggs using tweezers. Eggs were then collected and incubated in sterile 1× Steinberg's solution containing Pen-Strep (Sigma). Embryos at the 1-, 4-, 64- and 1K-cell stages were embedded in Tissue-Tek O.C.T. Compound (Sakura) with the animal pole oriented at the top. All samples were then stored in the freezer at −80°C.

Sample preparation

Samples were subsequently incubated in the cryostat chamber (Leica CM 1950, USA) at −24°C for 10 min and then cut into 30 µm slices along the animal-vegetal axis as shown in Figure 1A. The slices were pooled and equally distributed into 5 tubes. The tube labelling corresponded to embryo orientation: A—extremely animal segment, B—animal, C—central, D—vegetal, E—extremely vegetal.

RNA isolation and reverse transcription

The samples were homogenized in 300 µl of TRIReagent® (Sigma-Aldrich, USA) and total RNA was extracted according to the manufacturer's protocol. LiCl precipitation was performed to remove inhibitors present in the yolky vegetal hemisphere. The concentration of RNA was measured using NanoDrop-2000 (ThermoFisher, USA) and sample quality was assessed using 5200 Fragment Analyzer (Agilent, USA).

The cDNA was prepared using 30 ng of total RNA and RNase-free distilled water (ThermoFisher, USA) in a volume of 5.5 µl and a reaction mixture was added containing 0.5 µl of dNTPs (10 µM each, ThermoFisher, USA), 0.5 µl of oligo-dT and random hexamer (1:1 mixture, 50 µM each, ThermoFisher, USA), and 0.5 µl of RNA-spike (TATAA biocentre, Sweden). The mixture was incubated for 5 min at 65°C and 10 min at 4°C. During the second step, the second mixture was added containing 2 µl of 5xRT Buffer (ThermoFisher, USA), 0.5 µl of RnaseOUT (ThermoFisher, USA) and 0.5 µl of Maxima H Minus Reverse Transcriptase (ThermoFisher, USA). The reaction proceeded as follows—10 min at 25°C, 30 min at 50°C, 5 min at 85°C and cooling to 4°C. The cDNA was diluted to 100 µl using Tris-EDTA buffer solution (Sigma-Aldrich, USA) and stored at −20°C.

Primer design and qPCR

qPCR was performed to detect the localization of known genes (list of used primers is attached in Supplementary Table S1). PCR primers were designed using Primer3 (Untergasser et al., 2012). The expected length of qPCR products was 80–120 bp and the annealing temperature was 60°C. Geneious prime (version 2021.2) was used to increase the specificity of designed primers and to avoid targeting RNA isoforms.

qPCR reaction mix with a total volume of 7 µl contained 2 µl of cDNA, 0.29 µl of forward and reverse primers mix (1:1, 10 µM each),

3.5 µl of 2x TATAA SYBR® GrandMaster® Mix (TATAA Biocenter, Sweden) and 1.21 µl of RNase-free distilled water (ThermoFisher, USA). qPCR was performed using CFX384 Real-Time System (Bio-Rad, USA) as follows: the initial denaturation for 3 min at 95°C, 45 cycles of denaturation for 15 s at 95°C, annealing at 60°C for 20 s and extension at 72°C for 20 s. qPCR melting curves were analyzed to test the reaction specificity. qPCR data were analyzed using workflow published in Sindelka et al., 2008.

Library preparation

We used 100 ng of a total RNA for library preparation. Ribosomal RNA depletion was performed using Ribocop rRNA Depletion Kit V1.3 (Lexogen, Austria). Libraries were prepared using NEBNext® Ultra™ II Directional RNA Library Prep Kit for Illumina® (New England Biolabs, USA). The number of PCR cycles was set at 12 cycles according to the initial RNA concentration. Library concentration was measured with a Qubit 4 Fluorometer (ThermoFisher, USA) and quality was assessed using a 5200 Fragment Analyzer (Agilent, USA). The pooled libraries were sequenced using Illumina NextSeq 500, high-output 150 bp run.

Molecular cloning

The cDNA of *grip2, dnd1, rbpms2* and AMEXTC_0340000004005 was PCR amplified using primers (Supplementary Table S2) designed for a full length cDNA. PCR reaction mix contained 5x Phusion green HF buffer (ThermoFisher, USA), 10 µM $MgCl_2$ (ThermoFisher, USA), 10 µM $dNTP_3$ (ThermoFisher, USA), Phusion Hot Start II DNA Polymerase (ThermoFisher, USA), UltraPure dH_2O (Invitrogen, USA) and forward and reverse primers. PCR program run as follows: initial denaturation at 98°C for 30 s, 39 cycles of denaturation for 10 s, annealing at 55°C for 30 s and extension at 72°C for 2 min.

The plasmid pBluescript II KS+ and amplified cDNA were digested using *XhoI* and *NotI* (New England Biolabs, USA). 5′-ends of DNA were dephosphorylated using CIP (calf intestinal alkaline phosphatase, New England Biolabs, USA) and then DNA insert was inserted into vector DNA in a ligation reaction. Ligation mix contained T4 DNA Ligase Buffer (New England Biolabs, USA), vector DNA, insert DNA, RNase-free distilled water (ThermoFisher) and T4 DNA ligase (New England Biolabs, USA). The mix was incubated overnight at 16°C. Then, the reaction was stopped at 65°C for 10 min.

NEB 5-alpha competent *E. coli* was used for a transformation (High efficiency, # C2987I, New England Biolabs, USA) according to the manufacturer's protocol: High Efficiency Transformation Protocol (C2987H/C2987I). After that, the individual clones were sequenced to screen for the presence of the expected sequences. Correct plasmids were purified using Plasmid Midi Kit (Qiagen, Germany).

Probes preparation and whole mount *in situ* hybridization

Plasmids were linearized in the restriction digest reaction. The mix contained 7 µg of plasmid DNA, NEB restriction enzyme (New England Biolabs, USA) and 10x NEB buffer 3.1 (New England Biolabs, USA). Mix was incubated overnight in a 37°C water bath. Linear DNA was cleaned up using QIAquick PCR Purification Kit (Qiagen, Germany). During the transcription reaction, we mixed 2 µg of linear template, 4 µl of 5x transcription buffer (Agilent, USA), 2 µl DIG RNA labelling mix (Roche, Switzerland), 2 µl of the T7 polymerase (Agilent, USA) and water in total volume of 20 µl. The mixture was incubated in a 37°C water bath for 3 h. Then, the mix was cleaned using LiCl. Finally, the RNA probe quality was tested using formaldehyde gel.

In situ hybridization was performed on whole mounts as described previously (Soukup et al., 2021) with slight modifications. Briefly, rehydrated *A. mexicanum* albino (d/d) embryos were digested in 60 µg/ml Proteinase K in PBS, fixed in 4% formaldehyde + 0.2% glutaraldehyde for 30–120 min, transferred into hybridization solution (50% formamide, 1x Denhardt's, 1 mg/ml yeast RNA, 0.1% Tween-20, 10% dextran sulfate, 1x salt solution containing 0.2 M NaCl, 8.9 mM Tris-HCl, 1.1 mM Tris base, 5 mM $NaH_2PO_4.H_2O$, 5 mM Na_2HPO_4 and 5 mM EDTA), and incubated overnight in hybridization solution containing RNA probe (1:1,000–1:100). Next day, the specimens were washed several times in post-hybridization solution (50% formamide, 4 × SSC, 0.5% Tween-20) and transferred via MABT buffer (100 mM maleic acid, 150 mM NaCl, 0.1% Tween-20) into blocking solution (2% blocking reagent, 20% sheep serum, in MABT buffer). Following blocking, the specimens were incubated overnight in the blocking solution containing alkaline phosphatase-conjugated antibody against DIG (Roche, 1:3,000) at 4°C. The specimens were washed several times in the MABT buffer. Following the overnight MABT wash, the samples were transferred into NTMT buffer (0.1 M Tris, 0.1 M NaCl, 0.05 M $MgCl_2$, 0.1% Tween-20) and incubated in BM Purple substrate (Roche) at 4°C until desired signal developed.

RNA-seq data processing and analysis

RNA-seq reads were processed as previously described in Naraine et al. (2022). Adaptor sequences and low quality reads were removed using TrimmomaticPE (v. 0.36) (Bolger et al., 2014) using the parameters, "HEADCROP:12 ILLUMINACLIP:~/TruSeq-PE3.fa:2:30:10 LEADING:3 TRAILING:3 SLIDINGWINDOW:4:15 MINLEN:36." Mitochondrial RNA reads (GenBank id: AY659991.1) and any remaining rRNA reads were removed using SortMeRNA (v. 2.1b) (Kopylova et al., 2012). The reads were then pseudo-aligned to the *A. mexicanum* transcriptome AmexT_v34 (Nowoshilow and Tanaka, 2020) using kallisto (v. 0.43.1) (Bray et al., 2016). The data were deposited in the National Center for Biotechnology Information's Gene Expression Omnibus (GEO: GSE240796).

Raw counts were initially filtered to keep transcripts with counts greater than 30 in at least one sample. DESeq2 (v. 1.32.0) (Love et al., 2014) was used to normalize the counts using the median-of-ratios method followed by differential expression analysis to determine differential localization of transcripts along the animal-vegetal sections in the 1-cell, 4-cell, 64-cell, 1K-cell stages; changes in the sectional profile across all stages; and changes in the total transcript across the stages. The

median-of-ratios normalization method was used to focus primarily on the extremely localized transcripts.

The following DESeq2 design models were used:

1) Alteration between the sections at the same stage:
   a) design: ~replicate + position; reduced design: ~replicate
2) Alteration in the profiles across the different stages:
   a) Transcripts with altered profiles: design: ~Stage + position + Stage:position; reduced: ~Stage + position
   b) Transcripts with altered magnitudes: design: ~Stage + position; reduced: ~Stage
3) Alteration of the total transcript count between the different stages:
   a) design: ~Stage; reduced: ~1; uses the sum of the normalized counts for each sample as input counts

The Principal Component Analysis (PCA) of the top 500 variable transcripts was assessed for the presence of any outlier samples. Differentially localized transcripts (DLTs) were defined as those with an adjusted *p*-value (padj) value less than 0.01 and also a total transcript count greater than 20 within at least one stage. Human gene symbols were assigned based on the previous ortholog analysis from Naraine et al., 2022, whereby *A. mexicanum* gene symbols were either matched against all known *Homo sapiens* gene symbols or derived from the similarity between its protein sequences as compared against the *H. sapiens* proteome using the reciprocal best alignment heuristic tool Proteinortho (v. 6.0.9) (Lechner et al., 2011).

The spatial expression profiles of the DLTs were then characterized into five discrete categories (extreme animal, animal, central, vegetal, extreme vegetal) based on the parameters previously described in Naraine et al., 2022. The central category represents a new category of localized maternal transcripts that was observed primarily in the eggs of *A. mexicanum* and *A. ruthenus* (Naraine et al., 2022). The other four profile parameters remained unchanged from the previous publication describing sub-location in *X.* laevis (Sindelka et al., 2018). DLTs that did not fit into these defined parameters were labelled as unclassified. Profile changes in the DLTs across the whole stages and within the stages were assessed using the degPatterns function from DEGreport (v. 1.28.0) package (Pantano et al., 2023). Profiles where the DLTs showed a fold change of 3x or 2x difference between either the stages or the sections respectively were selected. The validity of the profiles was verified using optCluster (v. 1.3.0) with the "Diana" clustering algorithm (Sekula et al., 2017).

Gene ontology terms associated with the genes were obtained using online software g:Profiler (access date: 14/02/23) using the default parameters of the annotated human reference, multiple testing correction using g:SCS threshold with a cutoff of 0.05 (Raudvere et al., 2019). Gene ontology terms clustering and removal of redundant terms were done using Revigo (access date: 14/02/23) with the default parameters of the whole UniProt reference database and SimRel semantic similarity measurement (Supek et al., 2011).

Motif analysis

We analyzed the presence of motifs unique within the UTRs of *A. mexicanum* PGC markers that might be responsible for its degradation. This was done by comparing their 3′ and 5′UTRs against shuffled versions of their sequences or the UTRs from *X. laevis* PGC genes. We also analyzed for enrichment of motifs within the vegetal and animal transcripts using the previously observed vegetal and animal motifs that were detected in *A. mexicanum* oocytes (previously published by Naraine et al., 2022). Analyzing the 3′UTR sequences, we also checked for *de novo* motifs that might be enriched selectively within the degraded transcripts versus the *de novo* transcripts and also between the animal and vegetal groups.

Motifs were detected using the STREME software (v. 5.5.2) (Bailey, 2021) under the following conditions: *p*-value < 0.05 and motif width = 6 to 25. The motif enrichment in primary sequences compared with control sequences was assessed using AME (e-value ≤ 0.05) (v. 5.5.2) (McLeay and Bailey, 2010). FIMO software (*p*-value ≤ 0.0001) (v. 5.5.2) (Grant et al., 2011) was used to scan the identified motifs against primary and control sequences. Using FIMO we obtained information about motif position within the sequences, and it was used to assemble a map of the motif distribution.

The enrichment of the previously observed vegetal and animal motifs from the paper (Naraine et al., 2022) was analysed against the UTRs of the animal and vegetal transcripts observed during embryogenesis. Significantly enriched motifs were deemed as those that gave an AME e-value ≤ 0.05 and a 3x fold enrichment in the vegetal UTRs versus the animal UTRs. In the case of the occurrence of the same or very similar motifs, we selected the motif with the lowest e-value.

Using only the PGC dataset, we continued with the analysis of putative regulatory elements in the UTRs that might explain its temporal degradation. To identify known protein binding sites and RNA binding proteins (RBPs) within the 3′UTR, we used Scan For Motif (access date: 16/03/23) with the datasets from TransTerm (E-value <= 0.175 per thousand bases) and RBPDB (E-value <= 0.001) and selected results with E-value thresholds < 0.001 (Biswas and Brown, 2014). The motifs recognized by these RBPs were compared against the list of *de novo* motifs detected by STREME using the comparison tool Tomtom (v. 5.5.2) (Gupta et al., 2007). The position probability matrices for the motif of these RBPs were downloaded from several online databases: CIS-BP-RNA (v. 0.6) (Ray et al., 2013), RBPDB (v. 1.3.1) (Cook et al., 2011) and oRNAment (access date: 12/06/23) (Benoit Bouvrette et al., 2020). Within 3′ and 5′UTR, the BEAM software (v. 1.6.1.) (Pietrosanto et al., 2018) was used to find RNA secondary structures using a *p*-value threshold cutoff of 0.01. The BEAGLE software (access date: 23/05/23) (Mattei et al., 2015) was then used to identify a conserved secondary structure either shared across all the *A. mexicanum* PGCs or unique to *A. mexicanum* relative to the PGCs in *X. laevis*, using a *p*-value threshold cutoff of 0.01. BRIO (*p*-value < 0.05) (Guarracino et al., 2021) was used to identify known sequences and structure RNA-binding motifs that are recognized by RBPs in the UTRs of *H. sapiens* and *M. musculus* from PAR-CLIP, eCLIP and HITS experiments. The AURA database (v. 2.7) was then used to screen the identified RBPs for their selective preference to either the 3′ or 5′ UTR regions (Dassi et al., 2014). For the discovery of putative binding sites for miRNA within the 3′UTR of the PGC markers, miRDB (v. 6.0) (Chen and Wang, 2020) was used with the human dataset as a reference.

Results

Asymmetric distribution of maternal RNA in early embryos

To describe RNA localization during early embryogenesis of *A. mexicanum*, we collected the stage of a fertilized egg (1-cell stage), 4-, 64- and 1K-cell (early blastula), which are expected to be pre-embryonic genome activation (MBT).

Embryos were sectioned along the animal-vegetal axis using the TOMO-seq method (Figure 1A). The results were first analyzed using PCA of the 500 most variable transcripts (Figure 1B). PC1 showed high variability during early development, mainly between the 1-cell stage and late embryos. PC2 revealed the clear distinction among individual sections in all stages. The variability in the sections decreased as the embryos progressed towards the later stages, indicating a disruption or reduction in the original asymmetrical gradients. Additionally the largest sectional differences were observed between the D and E sections, while minimal between the A and B sections.

The average number of coding genes identified at each stage was 28909 (using threshold >30 transcript counts in any sample). The complete dataset containing genes with asymmetrical distribution are listed in Supplementary Table S3. More than 2,200 DLTs (padj < 0.01, using threshold >20 transcripts in at least one stage) with sectional changes per stage were identified in embryos at 4, 64 and 1K-cell stages and twice as many were identified at the 1-cell stage (4,076 DLTs). The diagram in Figure 1C shows the overlap of the shared DLTs across the stages with 1,216 shared in all analyzed stages. Most of the DLTs were classified into one of the five localization categories: extremely animal, animal, central, vegetal and extremely vegetal (Fig. 1Da). In extremely animal and animal categories, we identified 284–675 DLTs in each stage (Fig. 1Db). Majority of DLTs are localized in vegetal or extremely vegetal sections at the 1-cell stage—1,114 and 1,083. The number of extreme vegetal DLTs dramatically decreased during development and only 240 were found at the 1K-cell stage.

We performed RT-qPCR validation of a few members within the extremely vegetal and animal transcript categories. In the extremely vegetal category, we confirmed the localization profile of *grip2* and *dnd1* (Supplementary Figure S1A), and in the animal category, we confirmed the localization of *ankhd1* and *akt2* (Supplementary Figure S1B).

Sectional profile alteration during the early development

In total 4,850 DLTs were observed to change their sectional profile or its sectional amplitude across the analyzed stages. 781 of these DLTs had a ≥2x fold change between a given section and showed two profile alteration processes—alteration of vegetal profiles and alteration of animal profiles (Supplementary Table S4).

Vegetal alteration

The vegetal alteration was observed for 673 DLTs and several groups depicting different types of alterations were described (Figure 2). A pronounced vegetal profile was created either at the 1K cell stage (22 DLTs, Figure 2A) or from the 4-cell stage (77 DLTs, Figure 2B). Next group showed the vegetal profile already established at the 1-cell stage (405 DLTs), while a uniformed/reduced distribution during the other developmental stages (Figure 2C). In the last group, the vegetal profile is also present at the 1-cell stage (Figure 2D). However, in contrast to the slow progression towards the uniform distribution, it was already established at the 4-cell stage (169 DLTs).

Due to the low number of genes in the mentioned groups or the limited number of annotated genes, the GO enrichment analysis was performed only on the third group (Vegetal at the 1 cell/Gradual decrease in late stages; Supplementary Table S5). Enriched GO terms were associated with biological processes affiliated with localization and protein folding, and molecular function in oxidoreductase activity and protein binding.

Animal alteration

The animal profile alteration comprised of 108 DLTs which can be classified into three groups (Figure 3). In the first group, the transcript uniform distribution persisted until the stage of 64-cell, after which at 1K-cell the animal profile was more visible (29 DLTs, Figure 3A). DLTs in the second group were uniformly distributed only at the 1-cell stage and later formed animal gradients (74 DLTs, Figure 3B). The third group showed clear animal profile at the 1-cell (5 DLTs, Figure 3C), but its animal distribution was disrupted leading to homogenous distribution in the later stages.

GO enrichment was performed only on the second group (Homogenous/slightly animal at the 1-cell stage, animal in late stages) as it contained sufficient numbers of genes. The genes in this group may play a role as the cellular components of the centrosome, cytoplasm, and cytoskeleton. No molecular function or biological process connected with the transcripts in this group was observed.

Transcript count alteration during the early development

Alteration in transcript count caused by synthesis or degradation was detected for 6,811 DLTs (padj <0.01, >20 transcripts in at least one stage). Out of these, we observed 960 DLTs with at least 3-fold change across individual stages (Supplementary Table S6). Two main groups were created reflecting *de novo* synthesis and degradation.

Transcripts degradation detected using the TOMO-seq approach was validated by RT-qPCR for 2 DLTs—*plin2* and *velo1* (Supplementary Figure S1C). *De novo* synthesis of *mok* and *nynrin-like* was also validated by RT-qPCR (Supplementary Figure S1D).

De novo transcription in early embryogenesis

De novo transcription of 519 DLTs was detected in the analyzed time points (Figure 4). 250 DLTs showed transcript increase right after fertilization at the 4-cell stage (Figure 4A). Out of these DLTs, 19 established vegetal profiles during development (e.g., *dusp1*) and 14 created animal profiles after the 1-cell stage (e.g., *prmt1*) (Supplementary Table S7).

The second wave of *de novo* transcription was observed at the 64-cell stage (193 DLTs, Figure 4B). Only 3 DLTs set up a vegetal profile at the 1K cell stage and 1 DLT created an animal profile at the 1K cell stage (not annotated transcripts).

The third *de novo* transcription was detected at the 1K-cell stage with 76 DLTs being synthesized at this time point. 6 DLTs showed

10.3389/fcell.2023.1260795

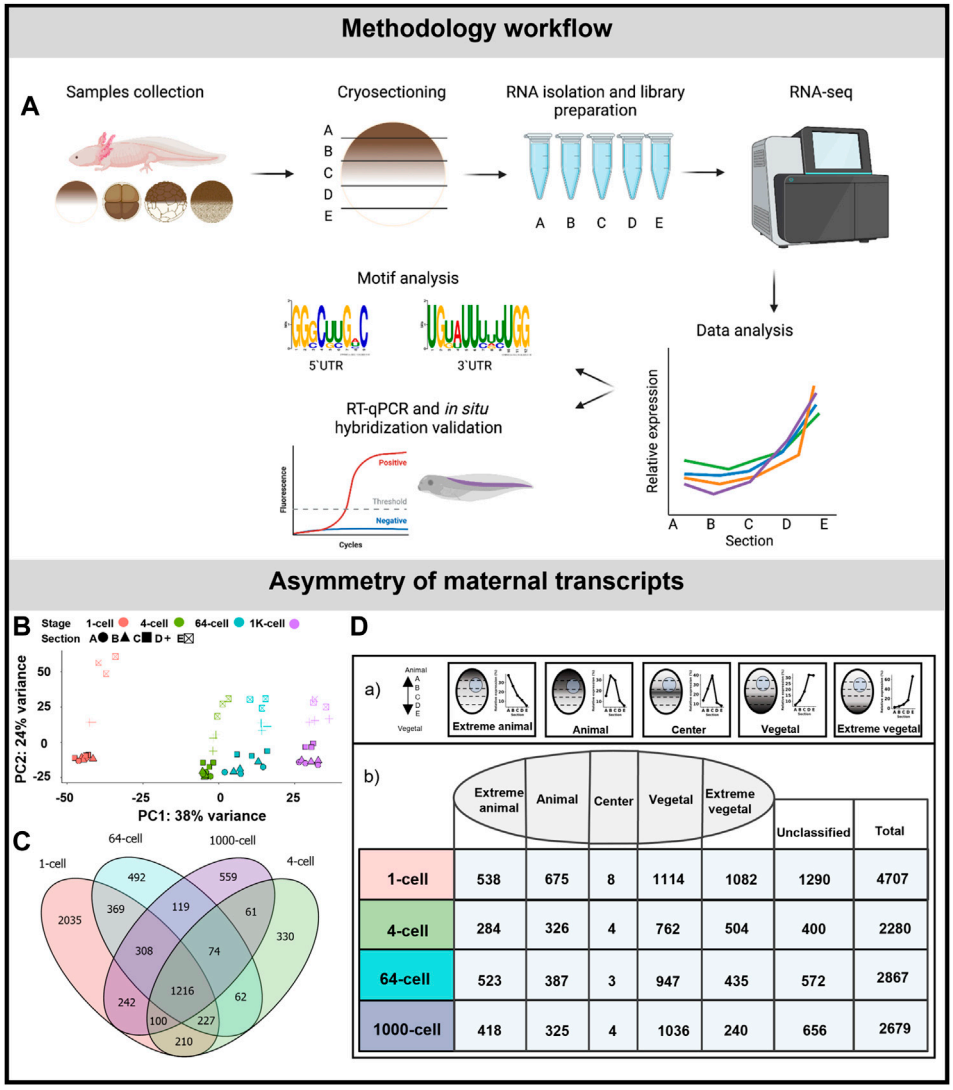

	Extreme animal	Animal	Center	Vegetal	Extreme vegetal	Unclassified	Total
1-cell	538	675	8	1114	1082	1290	4707
4-cell	284	326	4	762	504	400	2280
64-cell	523	387	3	947	435	572	2867
1000-cell	418	325	4	1036	240	656	2679

FIGURE 1
Asymmetric localization of maternal transcript in *A. mexicanum* early embryos. **(A)** Schematic representation of the workflow. **(B)** PCA of 500 most variable transcripts show high variability among developmental stages and embryo sections. **(C)** The diagram of shared DLTs among developmental stages. **(D)** Number of DLTs in each localization category. DLTs in the unclassified category represent those that did not fit into any of the five defined profiles.

preferential enrichment to the animal section (e.g., *rpl12*) and only 1 DLT was synthesized in the vegetal hemisphere at the 1K-cell stage (not annotated transcript).

Gene ontology terms associated with transcripts synthesized at the 4-cell stage proposed their role mainly in biological processes such as cell regulation and biosynthesis. Although it was not possible to perform gene ontology analysis on the remaining subgroups due to missing gene annotations, several interesting genes were revealed. For example, we identified several DLTs linked with ribosomal proteins at the 64-cell stage.

Transcript degradation during early embryogenesis

A 3-fold decrease in 441 DLTs was observed between the 1-cell and 4-cell stages (Figure 5A). Out of these, 2 DLTs initially localized in the animal hemisphere but later lost their localization pattern due to degradation after the 1-cell stage (not annotated transcripts). 28 DLTs (e.g., *sys1*) were vegetal only at the 1-cell stage and their profile became uniform at the 4-cell stage. 33 DLTs (e.g., *sh3bp4*) were gradually degraded after the 1-cell stage and kept a slight vegetal profile even at later stages (Supplementary Table S7). In contrast, no significant degradation cluster was detected at the 64 or 1K-cell stages.

Gene ontology analysis supported the role of degraded DLTs in many biological processes, such as cell regulation, localization and development (Figure 5B). Moreover, the GO enrichment analysis suggests a molecular function of DLTs in the binding of specific molecules, such as proteins or RNAs (Supplementary Table S5).

Degradation of PGC markers during *A. mexicanum* development

A separate subgroup included genes that are known as the PGC markers. In this group, we observed the degradation of

10.3389/fcell.2023.1260795

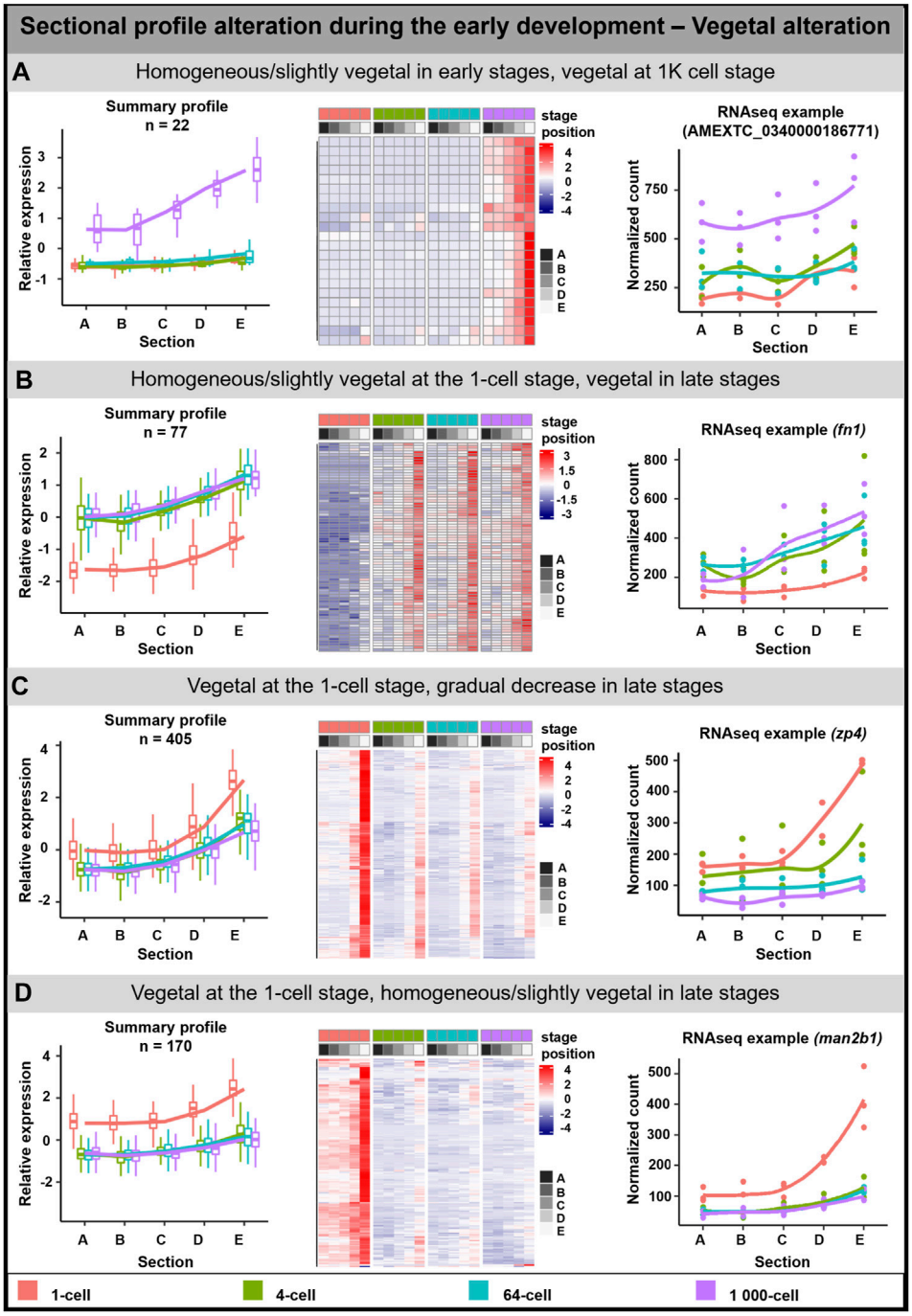

FIGURE 2
Vegetal sectional profile alteration. During the early development of *A. mexicanum,* 4 groups of vegetal DLTs altering profiles were observable. **(A)** Homogenous or slightly vegetal localization from the 1-cell stage until the 64-cell stage and vegetal localization at the 1K-cell stage. **(B)** Homogenous or slightly vegetal localization at the 1-cell stage and vegetal localization from the 4-cell stage and later. **(C)** Vegetal localization at the 1-cell stage and from the 4-cell stage until the 1K-cell stage the gradual decrease of transcript amount. **(D)** Vegetal localization at the 1-cell stage and from the 4-cell stage the localization is homogenous or slightly vegetal. Line plots represent the averaged z-score expression for the genes with shared localization profiles. Heatmap shows the z-score of the averaged relative expression across the replicates. DLTs represent genes that had a padj < 0.01 and greater than 20 transcripts per stage. DLTs were further filtered to show those that were 2x greater in either amplitude or relative to another section across the stages. 3 biological replicates were used. Embryos sections: A - extremely animal, B - animal, C - central, D - vegetal, E - extremely vegetal.

DLTs affecting profile pattern—from extremely vegetal to slightly vegetal or homogeneous distribution (Figure 5C). The transcript level of all PGC transcripts—*dnd1, rbmps2-1, rbpms2-2, grip2-1, grip2-2, nanos1, velo1-1* and *velo1-2*—significantly decreased after the 1-cell stage (Figure 5C; Supplementary Figure S2A). Even if some transcripts did not

10.3389/fcell.2023.1260795

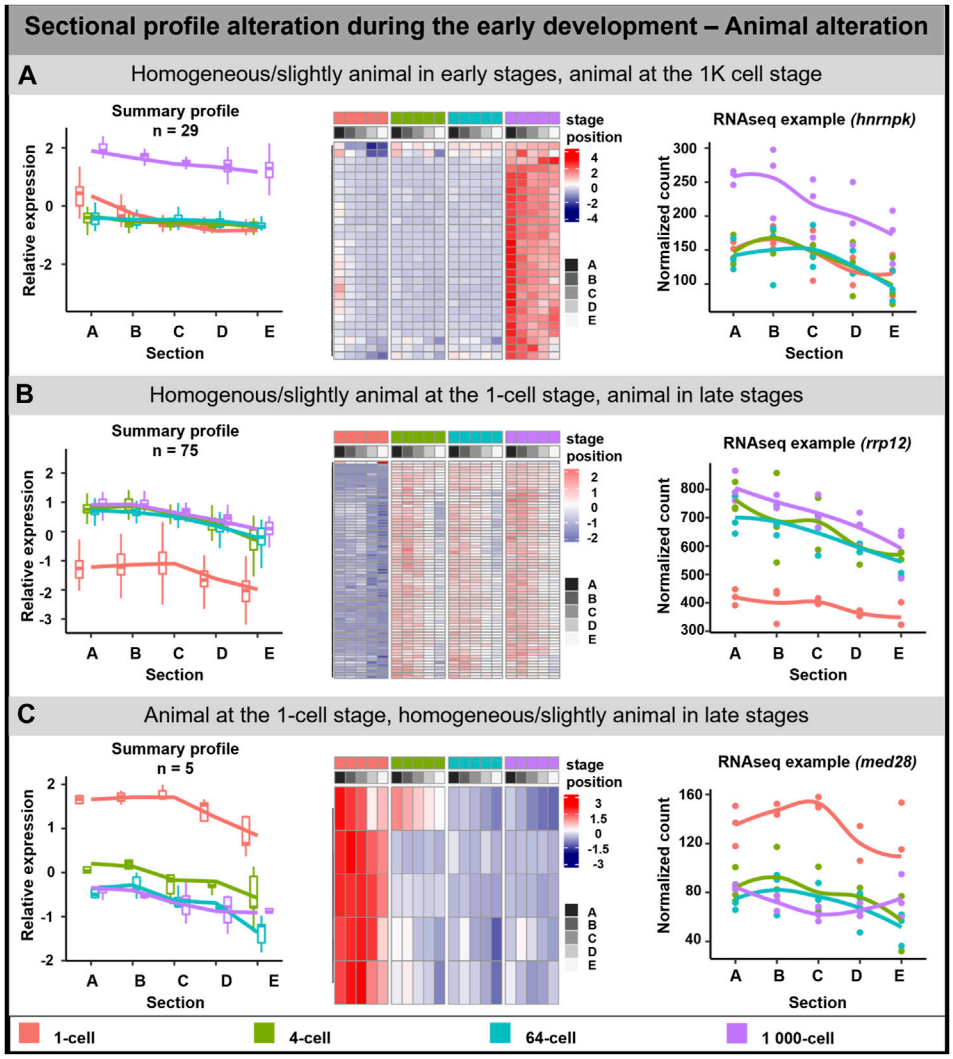

FIGURE 3
Animal sectional profile alteration. During the early development of *A. mexicanum,* 3 groups of animal DLTs altering profiles were observable. **(A)** Homogeneous or slightly animal from 1-cell until the 64-cell stage and the creation of animal profile at the 1K-cell stage. **(B)** Homogeneous or slightly animal at the 1-cell stage and animal at the 4-cell stage and later. **(C)** Animal localization at the 1-cell stage and homogenous or slightly animal localization from 4-cell until the 1K-cell stage. Line plots represent the averaged z-score expression for the genes with shared localization profiles. Heatmap shows the z-score of the averaged relative expression across the replicates. DLTs represent genes that had a padj < 0.01 and greater than 20 transcripts per stage. DLTs were further filtered to show those that were 2x greater in either amplitude or relative to another section across the stages. 3 biological replicates were used. Embryos sections: A – extremely animal, B – animal, C – central, D – vegetal, E – extremely vegetal.

meet the criteria to be included in the total transcript alteration (3-fold change) or sectional profile alteration (2-fold change), the profile change was pronounced enough to suggest that vegetal degradation is occurring. To identify whether degraded transcripts are present in PGC in later development, we selected 3 genes from this group showing vegetal degradation (*rbmps2-1*, *grip2-1*, *dnd1*) and 1 gene (AMEXTC_0340000004005) with the opposite trend—zero count at the 1-cell stage and *de novo* transcription mainly in the vegetal hemisphere from the 4-cell stage—for *in situ* hybridization. All transcripts were detected in the embryo at around stage 33 in the presumptive germ line (Figure 5C) and surprisingly also in the heart and pronephros (Supplementary Figure S2B).

Motif enrichment in primordial germ cell markers

For a deeper understanding of the PGC markers degradation process, we performed motif analysis searching for any conserved regulatory sequence within the 3′ and 5’ UTR sequences. Using data from previous publication (Naraine et al., 2022) and Xenbase.org we obtained UTRs of 5 transcripts in each organism (Listed in Supplementary Figure S2A). There were no statistically significant motifs enriched within the PGCs RNAs of the *A. mexicanum* versus those from the *X. laevis*. However, this is most likely due to the low number of genes used for the analysis (~5 genes). Due to this limitation, FIMO was instead used to assess whether the detected motifs were found exclusively or in a high

10.3389/fcell.2023.1260795

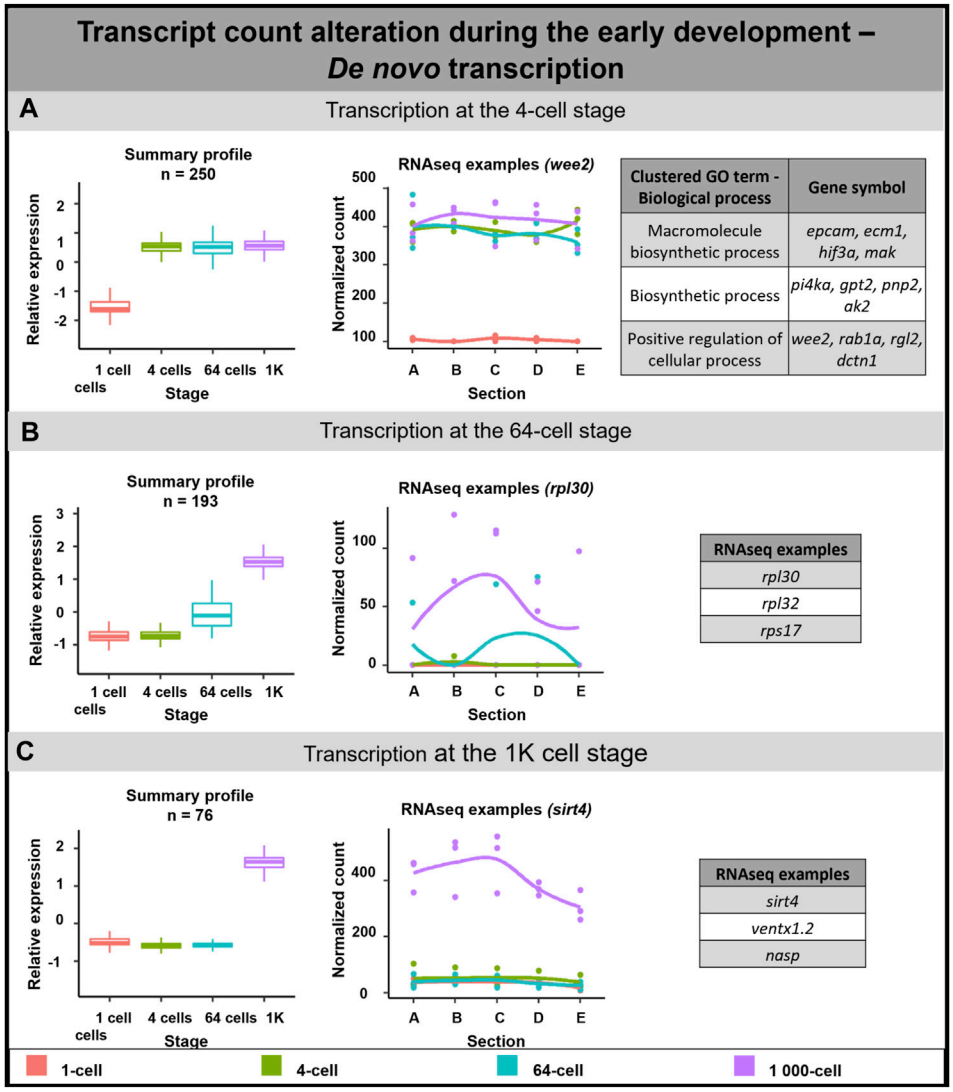

FIGURE 4
De novo transcription during early embryogenesis of *A. mexicanum*. **(A)** *De novo* transcription at the 4-cell stage and biological role of DLTs proposed using gene ontology analysis. **(B)** *De novo* transcription at the 64-cell stage and RNA-seq gene examples. **(C)** *De novo* transcription at the 1K-cell and RNA-seq gene examples. Box plots in the first column represent the averaged z-score expression for the averaged total transcript across the stage replicates. Line plots in the second column represent the normalized counts for each replicate for a specific gene across the stages. DLTs represent genes that had a padj < 0.01 and greater than 20 transcripts per stage. DLTs were further filtered to show those that were 3x greater in either amplitude or relative to another section across the stages. 3 biological replicates were used. Embryos sections: A - extremely animal, B - animal, C - central, D - vegetal, E - extremely vegetal.

proportion within the UTRs of the *A. mexicanum* PGCs versus the other models.

The *de novo* motif analysis within the 3′UTR of PGC marker genes revealed 7 motifs enriched in the *A. mexicanum* compared with either the *X. laevis* marker genes or the shuffled sequences (Figure 6A). Most of the motifs were uridine rich. 5 of the identified motifs were present exclusively in *A. mexicanum* but not in *X. laevis*. Then, the motif presence was also estimated in the other model organisms—*M. musculus, H. sapiens, D. melanogaster, A. ruthenus* and *D. rerio*—and only 1 motif (Motif 6) was exclusive to *A. mexicanum*. We observed no significant enrichment of these 7 motifs when comparing the *de novo* transcripts against the degraded ones, or the vegetal sectional changes against the animal sectional changes.

In total, we identified 10 motifs conserved within the 5′UTR of PGC markers in *A. mexicanum* and none of them were present in *X. laevis* or the shuffled sequences (Figure 6B). Most of the motifs were enriched with either cytosine or guanosine. Two motifs (Motif 1 and 6)—had CAC core. All the motifs were scanned against PGC sequences of the 4 model organisms and 4 motifs were unique exclusively to *A. mexicanum*. We observed no significant enrichment of these 10 motifs when comparing the *de novo* transcripts against the degraded ones, or the vegetal sectional changes against the animal sectional changes.

10.3389/fcell.2023.1260795

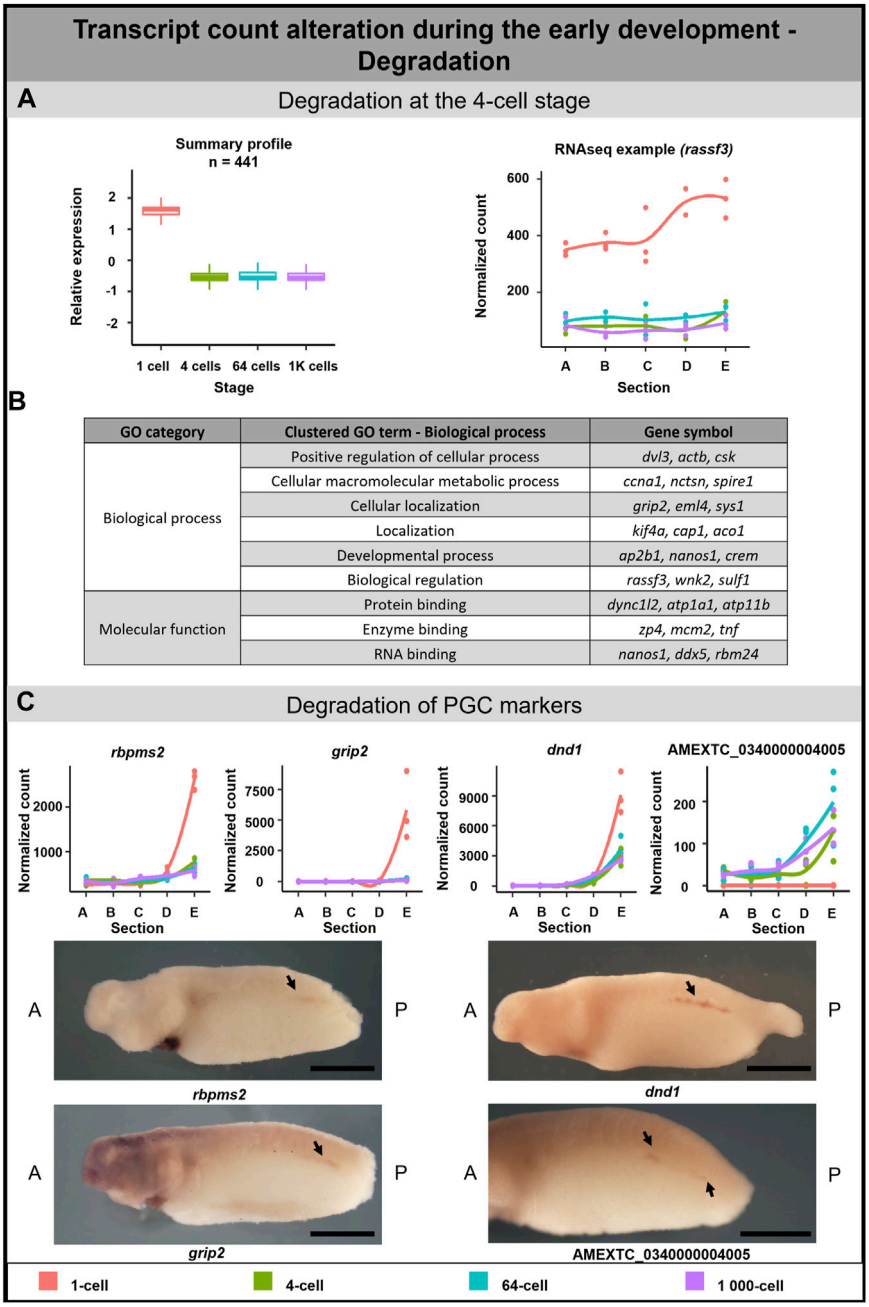

GO category	Clustered GO term - Biological process	Gene symbol
Biological process	Positive regulation of cellular process	*dvl3, actb, csk*
	Cellular macromolecular metabolic process	*ccna1, nctsn, spire1*
	Cellular localization	*grip2, eml4, sys1*
	Localization	*kif4a, cap1, aco1*
	Developmental process	*ap2b1, nanos1, crem*
	Biological regulation	*rassf3, wnk2, sulf1*
Molecular function	Protein binding	*dync1l2, atp1a1, atp11b*
	Enzyme binding	*zp4, mcm2, tnf*
	RNA binding	*nanos1, ddx5, rbm24*

FIGURE 5
Transcription degradation during early embryogenesis of *A. mexicanum*. **(A)** The massive degradation was observed only after the 1-cell stage. Box plot in the first column represents the averaged z-score expression for the averaged total transcript across the stage replicates. Line plot in the second column represents the normalized counts for each replicate for a specific gene across the stages. DLTs represent genes that had a padj < 0.01 and greater than 20 transcripts per stage. DLTs were further filtered to show those that were 3x greater in either amplitude or relative to another section across the stages. 3 biological replicates were used. **(B)** Gene ontology analysis of degraded DLTs. **(C)** Degradation of PGC markers. Line plots show the localization profile and total amount of selected PGC markers change during the development. Whole-mount *in situ* hybridization shows the gene expression of 3 known PGC markers and 1 unknown gene within presumptive germ cells (arrow). Detection of PGC in *A. mexicanum* embryos at around stage 33 using *in situ* hybridization. Lateral view, with A-Anterior, B-Posterior. Scale bar = 2 mm.

We used the Scan for motif software to identify putative RBP sites within the 3′UTR of PGC markers. The analysis revealed several RBPs which can affect RNA stability, degradation and translation, such as PUM2, KHSRP and ZFP36. However, all the RBPs affecting RNA stability were also detected in *X. laevis* PGC markers (Complete list of RBPs in Supplementary Table S8). To compare *de novo* motifs with motifs recognized by known RBPs we used the Tomtom tool, which helped us to identify 2 motifs which resembled previously discovered motifs. Motif 5 was similar to RBFOX1 (UGCAUG) binding sites and motif 6 was similar to PUM2 (UGUA) and ZFP36 (UUAUUUAWK) (Figure 6A).

10.3389/fcell.2023.1260795

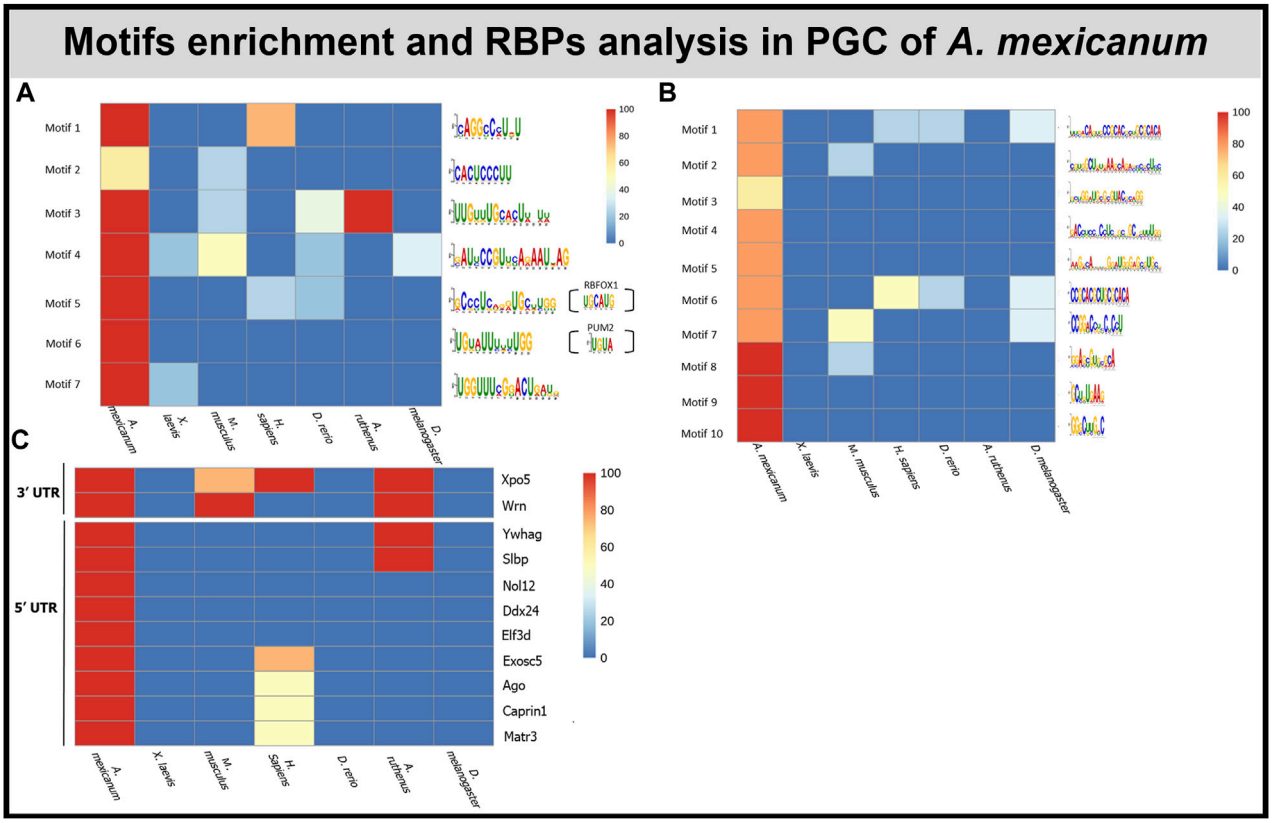

FIGURE 6
Motif and RBP enrichment in PGC. **(A)** *De novo* motif analysis within 3′UTR of *A. mexicanum*. Enriched motifs were also scanned in other model organisms. Sequences of motifs 5 and 6 probably can be bound by 2 known RBPS—PUM2 and RBFOX1. **(B)** *De novo* motifs analysis within 5′UTR of *A. mexicanum*. Enriched motifs were also scanned in other model organisms. **(C)** Identification of RBP binding motifs using BRIO within 3′ and 5′ UTR of *A.mexicanum*. The RBP presence was also assessed in other model organisms.

BRIO software was used to search for known primary sequences and secondary structures associated with RBP binding motifs within the 3′ and 5′ UTRs of *A. mexicanum* PGC markers. We identified 5 (3′UTR) and 17 (5′UTR) RBPs binding motifs unique to *A. mexicanum* compared with *X. laevis* (Supplementary Table S9). Using the available resources, we selected 2 (3′UTR) and 9 (5′UTR) proteins potentially playing a role in transcript degradation (Figure 6C). BEAM was used to find structural motifs present in the RNA secondary structure, but no motif was shared in all 5 *A. mexicanum* PGC markers within 3′ or 5′UTR.

As it is known, miRNA can induce mRNA degradation or translational repression (reviewed in O'Brien et al., 2018). Therefore, we searched for miRNAs that may target the *A. mexicanum* PGC transcripts using the online miRNA database miRDB. We discovered 41 miRNAs present only in *A. mexicanum,* but none of them was shared in all PGC genes. Similarly, 50 miRNAs were specific only for *X. laevis* but were not shared in all its PGC genes (Supplementary Table S10).

Conservation of vegetal and animal motifs

Analysis was carried out to determine if previously conserved animal and vegetal motifs detected in the oocyte of the *A. mexicanum* (Naraine et al., 2022) can also be seen preferentially enriched within the vegetal and animal transcripts during embryogenesis. Motifs were scanned using FIMO against the following datasets of developing *A. mexicanum* embryos: animal, vegetal, sectional profile altering, stage altering *de novo* and degraded DLTs.

Within the 3′ and 5′ UTR of transcripts from the *A. mexicanum* embryos, we observed the enrichment of the previously detected putative localization motifs that were found shared between both *A. mexicanum* and *X. laevis* oocytes and also those that were unique only for *A. mexicanum* oocytes (Supplementary Figure S3) (Naraine et al., 2022). The conserved motifs were detected only in the vegetally localized DLTs of *A. mexicanum* embryos and were mostly enriched with CAC or guanine-rich sequences.

The map of identified *de novo* motifs, miRNAs, RBPs and motifs from previous publication (Naraine et al., 2022) was assembled for selected PGC markers (Supplementary Figure S4).

Discussion

Localization of transcripts established in the mature egg during oogenesis has a crucial role in asymmetric cell division during embryo development. Previously we identified thousands of DLTs in the maturating oocytes of *X. laevis* and *A. ruthenus*

(Iegorova et al., 2022) and mature eggs of *X. laevis, A. mexicanum, A. ruthenus* and *D. rerio* (Naraine et al., 2022). The comparison of the evolutionary conservation of localized transcripts revealed many differences among analyzed species such as a low correlation in vegetal localization and dynamic changes in transcript levels. Based on these results we proposed that the development of different vertebrate species can be regulated in many ways.

To assess this, we performed a spatiotemporal analysis of transcript localization in early embryos of the urodele amphibian *A. mexicanum* and compared our results with available data from the anuran *X. laevis*. The transcriptome analysis in four developmental stages of *A. mexicanum* revealed very dynamic changes in RNA profiles and uncovered three divergent alterations—sectional profile alteration, *de novo* transcription and degradation. Early embryonic development is dependent on maternal RNA and protein storages in the absence of transcription, after which during MBT the transcription from the embryonic genome is initiated. In *X. laevis*, the MBT occurs after the 12th cycle of cell division, but in *A. mexicanum,* it can be either after the 9th cycle (Lefresne et al., 1998) or the 12th cycle of cell division (Jiang et al., 2017). Despite the first theories that transcription does not occur before MBT, later it has been shown in many species (e.g., *X. laevis* (Yang et al., 2002; Skirkanich et al., 2011), *M. musculus* (Bouniol et al., 1995; Aoki et al., 1997; Abe et al., 2018)) that a small number of genes can be transcribed even shortly after fertilization. In *A. mexicanum*, we identified more than 1.7% of maternal transcripts transcribed during the period from the fertilized egg until the early blastula (1K-cell) stage. Our findings support Jiang et al., 2017 and determine the onset of MBT after the 12th cycle of cell division. According to the GO analysis, *de novo* transcripts synthesized during this period have a structural and functional role in nascent cells. For example, *pi4ka* encodes kinase contributing to cell membrane synthesis (Wong and Cantley, 1994) and *epcam* is one of the main cell-to-cell adhesion molecules (Litvinov et al., 1994). Moreover, we identified *de novo* synthesis of *wee2*, whose zygotic expression was previously described in *X. laevis*. Leise and Mueller, 2002 proposed the possible mitosis-inhibiting role of Wee2 kinase in specific embryo tissues lacking proliferating cells.

The clearance of maternal transcripts before embryonic genome activation is required to regulate early embryo development and prepare the embryo for MBT. In *X. laevis*, deadenylation and transcript degradation can be mediated via RBPs recognizing specific RNA elements—deadenylation elements (Paillard et al., 1998) and AU-rich elements (Voeltz and Steitz, 1998)—or through zygotic miRNA (Lund et al., 2009; Koebernick et al., 2010). In *A. mexicanum,* we revealed the degradation of more than 1.5% of maternal transcripts. Previously, the degradation of several mRNAs (*wnt1, wnt5a, wnt5b*) during *A. mexicanum* early development was noticed (Caulet et al., 2010), but we are the first to describe the degradation in transcriptome-wide view in this model. Degraded maternal transcripts are enriched for GO terms related to cell cycle regulation, localization and the developmental process. For example, we have detected degradation of *actb,* which can be caused by actin disassembly at the cleaving egg (Field et al., 2019), and *ccna1*, which regulates cell cycle control (G1/S and G2/M). Degradation of the *ccna1* may be due to cyclin A1 redundancy given that the G1 phase is absent in the axolotl (Lefresne et al., 1998). Previously, Hamatani et al., 2004 described massive degradation of transcripts involved in the cell cycle also in *M. musculus* early embryos.

The PGC markers were previously identified to be localized to the vegetal pole in the eggs of *X. laevis* and *A. mexicanum* (Naraine et al., 2022), and have been corroborated by our research. While in *X. laevis*, the vegetal localization is established through the mitochondrial cloud (Kloc and Etkin, 1995), in *A. mexicanum*, this structure is probably absent and the mechanisms of mRNA localization remain unknown (Ikenishi and Nieuwkoop, 1978; Johnson et al., 2001). The interesting view on germ cell development in urodele was proposed by Škugor et al., 2016. In *A. mexicanum*, they described the functional loss of protein encoded by *velo1* which probably played an ancestral role in germ plasm assembly and proposed its role in germline formation in the ancestors of vertebrates. Therefore, they concluded that preformation is an ancestral mechanism and the inductive germ line determination occurred in vertebrates lacking germ plasm (e.g., urodeles, primates, rodents) due to convergent evolution. Our results may support this hypothesis because we detected the partial degradation of several PGC markers shortly after fertilization. Johnson et al. (2001) described the first appearance of *dazl,* another PGC marker, at stage 40 as well as the first formation of primordial germ cells. Therefore, to confirm, that the expression of PGC markers again starts after gastrulation (Johnson et al., 2001), we decided to detect 3 PGC markers (*grip2, dnd1* and *rbpms2*) and 1 vegetally localized unknown transcript using *in situ* hybridization. While *grip2* and *dnd1* were previously detected in PGCs (Tarbashevich et al., 2007; Koebernick et al., 2010), *rbpms2* was detected only in oocytes and developing heart in *X.laevis* (Gerber et al., 1999; Zearfoss et al., 2004). Indeed, all of them was localized in the region of *A. mexicanum* presumptive germ cells at the stage 35 (Figure 5C), which is 5 stages earlier than reported by Johnson et al. (2001).

To take a deeper look into the processes of partial degradation of PGC markers, we analyzed their UTRs for a motif enrichment that may cause the degradation. We identified 1 motif (Motif 6, Figure 6A) within 3′UTR, which is exclusive for *A. mexicanum* PGC. It is interesting that the motif possibly binds PUM2 and ZFP36, which are RBPs involved in mRNA repression (Lai et al., 1999; Lai et al., 2003; Van Etten et al., 2012). Therefore, we concluded that this motif may potentially plays an important role in the partial degradation of the PGC marker RNAs after fertilization. Moreover, we identified 4 motifs exclusive in the 5′UTR of *A. mexicanum* PGCs mRNAs, but the role of these motifs is not known. Also, we identified several RBPs, potentially playing a role in degradation, which recognize binding sited within 3′UTR of PGCs mRNAs, but for these RBPs, the role in embryonic developmental degradation has not yet been described.

To find motifs specific for degradation or *de novo* synthesis, we searched motif enrichment within 3′ and 5′UTRs of maternal transcript in the degradation/*de novo* group, but no significant enrichment was observed. Moreover, we searched within animal or vegetal groups, to find enriched motifs for localization, but we did not find any significant enrichment. However, previously detected motifs enriched within the UTRs of vegetal and animally transcripts in the egg of the *A. mexicanum* (Naraine et al., 2022), revealed 5 motifs enriched within the 3′ and 5′UTRs of *A. mexicanum* embryos. These motifs are enriched with CAC core, a known localization motif, as well as some with guanine or cytosine-rich sequences, which may be potentially new localization elements.

The final mechanism on how the transcript can be regulated during early development is through profile alteration. We have determined sectional profile alteration in both vegetal and animal

hemispheres. The formation or disruption of the vegetal profile was detected in a total of 2.3% DLTs. Out of these, 9% DLTs disrupt their vegetal profile due to transcript degradation and 3.4% DLTs create the profile due to *de novo* synthesis. The remaining 87.6% of transcripts show less than 3x fold change count across stages. Therefore, the sectional profile alteration for these remaining transcripts can be caused by either lower levels of degradation/*de novo* synthesis or active relocalization. GO term analysis performed on a subgroup containing transcripts whose vegetal localization gradually changed into uniform/slightly vegetal distribution, revealed their functions mainly in localization and protein folding. In *X. laevis*, for instance, Grip2 protein is indispensable for proper PGC migration (Kirilenko et al., 2008) and *kif4*, encoding microtubule motor protein, is essential for somatic cell division and its maternal paralog for meiotic division (Samwer et al., 2013; Ems-McClung et al., 2019). GO terms associated with transcripts whose vegetal profile rapidly changed into uniform/slightly vegetal distribution after the 1-cell stage, revealed their connection mainly with cellular components. As an example, *man2b1* (Malm and Nilssen, 2008) and *fuca1* (Willems et al., 1999) encode lysosomal enzymes and Sys1 protein is involved in protein trafficking (Behnia et al., 2004).

The alteration in animal profile was detected in almost 0.4% of DLTs. Of the total number of DLTs altering the animal profile, 78.7% of DLTs show less than 3x fold count change across individual stages. The animal alteration caused by transcript degradation was detected only in 1.9% DLTs, while *de novo* transcription was revealed in 19.4% DLTs. Transcripts forming animal profiles after the 1-cell stage are enriched for GO terms related to structural and functional components of the cell. Examples include *nek9*, encoding serine/threonine kinase, which plays an important role in mitotic spindle formation (Rapley et al., 2008) and Rrp12 protein important for ribosome assembly (Oeffinger et al., 2004).

Overall, our findings describing the regulation of maternal transcripts in early *A. mexicanum* embryos showed that after fertilization, maternal transcripts undergo multiple dynamic changes. These include alteration in localization or abundance and suggest that even related amphibians, such as *A. mexicanum* and *X. laevis*, can regulate their early development differently. The most prominent difference is probably the partial degradation of PGC markers, which indicates relevance for the differential development of germ cell establishment in the two amphibian orders. Our results support the necessity of cross-species comparison for a better understanding of aspects of the regulation of embryonic development.

Data availability statement

The datasets presented in this study can be found in online repositories. The names of the repository/repositories and accession number(s) can be found below: NCBI GEO under GSE240796.

Ethics statement

The animal studies were approved by the Faculty of Sciences of the Charles University. The studies were conducted in accordance with the local legislation and institutional requirements. Written informed consent was obtained from the owners for the participation of their animals in this study.

Author contributions

KŠ: Conceptualization, Formal Analysis, Investigation, Methodology, Validation, Visualization, Writing–original draft, Writing–review and editing, Data curation. RN: Conceptualization, Data curation, Formal Analysis, Investigation, Methodology, Visualization, Writing–review and editing. JV: Methodology, Validation, Visualization, Writing–review and editing. VS: Writing–review and editing, Methodology, Resources, Validation, Visualization. RŠ: Conceptualization, Funding acquisition, Investigation, Project administration, Resources, Supervision, Writing–review and editing.

Funding

The author(s) declare financial support was received for the research, authorship, and/or publication of this article. This work was supported by 86652036 from RVO; the Czech Science Foundation (Grant Number. 20-23836S); the Ministry of Education, Youth and Sports of the Czech Republic project CENAKVA (LM2023038).

Acknowledgments

We thank the GeneCore facility in BIOCEV for assistance during library preparation and Dr. Pavel Abaffy for help during data analysis. Image for the methodology workflow was created with BioRender.com.

Conflict of interest

The authors declare that the research was conducted in the absence of any commercial or financial relationships that could be construed as a potential conflict of interest.

Publisher's note

All claims expressed in this article are solely those of the authors and do not necessarily represent those of their affiliated organizations, or those of the publisher, the editors and the reviewers. Any product that may be evaluated in this article, or claim that may be made by its manufacturer, is not guaranteed or endorsed by the publisher.

Supplementary material

The Supplementary Material for this article can be found online at: https://www.frontiersin.org/articles/10.3389/fcell.2023.1260795/full#supplementary-material

References

Abe, K., Funaya, S., Tsukioka, D., Kawamura, M., Suzuki, Y., Suzuki, M., et al. (2018). Minor zygotic gene activation is essential for mouse preimplantation development. *PNAS* 115, E6780–E6788. doi:10.1073/pnas.1804309115

Agius, E., Oelgeschlager, M., Wessely, O., Kemp, C., and De Robertis, E. M. (2000). Endodermal Nodal-related signals and mesoderm induction in Xenopus. *Development* 127, 1173–1183. doi:10.1242/dev.127.6.1173

Aoki, F., Worrad, D. M., and Schultz, R. M. (1997). Regulation of transcriptional activity during the first and second cell cycles in the preimplantation mouse embryo. *Dev. Biol.* 181, 296–307. doi:10.1006/dbio.1996.8466

Bachvarova, R. F., Masi, T., Drum, M., Parker, N., Mason, K., Patient, R., et al. (2004). Gene expression in the axolotl germ line: axdazl, axvh, axoct-4, and axkit. *Dev. Dyn.* 231, 871–880. doi:10.1002/dvdy.20195

Bailey, T. L. (2021). STREME: accurate and versatile sequence motif discovery. *Bioinformatics* 37, 2834–2840. doi:10.1093/bioinformatics/btab203

Behnia, R., Panic, B., Whyte, J. R. C., and Munro, S. (2004). Targeting of the arf-like GTPase Arl3p to the Golgi requires N-terminal acetylation and the membrane protein Sys1p. *Nat. Cell Biol.* 6, 405–413. doi:10.1038/ncb1120

Benoit Bouvrette, L. P., Bovaird, S., Blanchette, M., and Lécuyer, E. (2020). oRNAment: a database of putative RNA binding protein target sites in the transcriptomes of model species. *Nucleic Acids Res.* 48, D166-D173–D173. doi:10.1093/nar/gkz986

Biswas, A., and Brown, C. M. (2014). Scan for motifs: a webserver for the analysis of post-transcriptional regulatory elements in the 3′ untranslated regions (3′ UTRs) of mRNAs. *BMC Bioinforma.* 15, 174. doi:10.1186/1471-2105-15-174

Bolger, A. M., Lohse, M., and Usadel, B. (2014). Trimmomatic: a flexible trimmer for Illumina sequence data. *Bioinformatics* 30, 2114–2120. doi:10.1093/bioinformatics/btu170

Bordzilovskaya, N. P., and Dettlaff, T. A. (1979). Table of stages of the normal development of axolotl embryos. 1-6. *Axolotl Newsl.* 7, 2–22.

Bouniol, C., Nguyen, E., and Debey, P. (1995). Endogenous transcription occurs at the 1-cell stage in the mouse embryo. *Exp. Cell Res.* 218, 57–62. doi:10.1006/excr.1995.1130

Brannon, M., Gomperts, M., Sumoy, L., Moon, R. T., and Kimelman, D. (1997). A beta-catenin/XTcf-3 complex binds to the siamois promoter to regulate dorsal axis specification in Xenopus. *Genes Dev.* 11, 2359–2370. doi:10.1101/gad.11.18.2359

Bray, N. L., Pimentel, H., Melsted, P., and Pachter, L. (2016). Near-optimal probabilistic RNA-seq quantification. *Nat. Biotechnol.* 34, 525–527. doi:10.1038/nbt.3519

Caulet, S., Pelczar, H., and Andéol, Y. (2010). Multiple sequences and factors are involved in stability/degradation of Awnt-1, Awnt-5A and Awnt-5B mRNAs during axolotl development. *Development growth and differentiation* 52 (2) 209–222. doi:10.1111/j.1440-169X.2009.01156.x

Chan, A. P., Kloc, M., and Etkin, L. D. (1999). Fatvg encodes a new localized RNA that uses a 25-nucleotide element (FVLE1) to localize to the vegetal cortex of Xenopus oocytes. *Development* 126, 4943–4953. doi:10.1242/dev.126.22.4943

Chang, P., Torres, J., Lewis, R. A., Mowry, K. L., Houliston, E., and King, M. L. (2004). Localization of RNAs to the mitochondrial cloud in Xenopus oocytes through entrapment and association with endoplasmic reticulum. *Mol. Biol. Cell.* 15, 4669–4681. doi:10.1091/mbc.e04-03-0265

Chen, Y., and Wang, X. (2020). miRDB: an online database for prediction of functional microRNA targets. *Nucleic Acids Res.* 48, D127-D131–D131. doi:10.1093/nar/gkz757

Claußen, M., Tarbashevich, K., and Pieler, T. (2011). Functional dissection of the RNA signal sequence responsible for vegetal localization of XGrip2.1 mRNA in Xenopus oocytes. *RNA Biol.* 8, 873–882. doi:10.4161/rna.8.5.16028

Cook, K. B., Kazan, H., Zuberi, K., Morris, Q., and Hughes, T. R. (2011). RBPDB: a database of RNA-binding specificities. *Nucleic Acids Res.* 39, D301–D308. doi:10.1093/nar/gkq1069

Dassi, E., Re, A., Leo, S., Tebaldi, T., Pasini, L., Peroni, D., et al. (2014). AURA 2: empowering discovery of post-transcriptional networks. *Transl. (Austin)* 2, e27738. doi:10.4161/trla.27738

De Domenico, E., Owens, N. D. L., Grant, I. M., Gomes-Faria, R., and Gilchrist, M. J. (2015). Molecular asymmetry in the 8-cell stage Xenopus tropicalis embryo described by single blastomere transcript sequencing. *Dev. Biol.* 408, 252–268. doi:10.1016/j.ydbio.2015.06.010

Delarue, M., Sáez, F. J., Johnson, K. E., and Boucaut, J. C. (1997). Fates of the blastomeres of the 32-cell stage *Pleurodeles waltl* embryo. *Dev. Dyn.* 210, 236–248. doi:10.1002/(SICI)1097-0177(199711)210:3<236::AID-AJA5>3.0.CO;2-H

Deshler, J. O., Highett, M. I., and Schnapp, B. J. (1997). Localization of Xenopus Vg1 mRNA by vera protein and the endoplasmic reticulum. *Science* 276, 1128–1131. doi:10.1126/science.276.5315.1128

Dumont, J. (1972). Oogenesis in *Xenopus laevis* (Daudin). I. Stages of oocyte development in laboratory maintained animals. *J. Morphol.* 136, 153–179. doi:10.1002/jmor.1051360203

Ems-McClung, S. C., Emch, M., Zhang, S., Mahnoor, S., Weaver, L. N., and Walczak, C. E. (2019). RanGTP induces an effector gradient of XCTK2 and importin α/β for spindle microtubule cross-linking. *J. Cell Biol.* 219, e201906045. doi:10.1083/jcb.201906045

Field, C. M., Pelletier, J. F., and Mitchison, T. J. (2019). Disassembly of actin and keratin networks by aurora B kinase at the midplane of cleaving *Xenopus laevis* eggs. *Curr. Biol.* 29, 1999–2008. doi:10.1016/j.cub.2019.05.016

Flachsova, M., Sindelka, R., and Kubista, M. (2013). Single blastomere expression profiling of *Xenopus laevis* embryos of 8 to 32-cells reveals developmental asymmetry. *Sci. Rep.* 3, 2278. doi:10.1038/srep02278

Forristall, C., Pondel, M., Chen, L., and King, M. L. (1995). Patterns of localization and cytoskeletal association of two vegetally localized RNAs, Vg1 and Xcat-2. *Dev* 121, 201–208. doi:10.1242/dev.121.1.201

Fuentes, R., Mullins, M. C., and Fernández, J. (2018). Formation and dynamics of cytoplasmic domains and their genetic regulation during the zebrafish oocyte-to-embryo transition. *Mech. Dev.* 154, 259–269. doi:10.1016/j.mod.2018.08.001

Ge, X., Grotjahn, D., Welch, E., Lyman-Gingerich, J., Holguin, C., Dimitrova, E., et al. (2014). Hecate/Grip2a acts to reorganize the cytoskeleton in the symmetry-breaking event of embryonic Axis induction. *PLOS Genet.* 10, e1004422. doi:10.1371/journal.pgen.1004422

Gerber, W. V., Yatskievych, T. A., Antin, P. B., Correia, K. M., Conlon, R. A., and Krieg, P. A. (1999). The RNA-binding protein gene, hermes, is expressed at high levels in the developing heart. *Mech. Dev.* 80, 77–86. doi:10.1016/s0925-4773(98)00195-6

Grant, C. E., Bailey, T. L., and Noble, W. S. (2011). FIMO: scanning for occurrences of a given motif. *Bioinformatics* 27, 1017–1018. doi:10.1093/bioinformatics/btr064

Guarracino, A., Pepe, G., Ballesio, F., Adinolfi, M., Pietrosanto, M., Sangiovanni, E., et al. (2021). BRIO: a web server for RNA sequence and structure motif scan. *Nucleic Acids Res.* 49, W67–W71. doi:10.1093/nar/gkab400

Gupta, S., Stamatoyannopoulos, J. A., Bailey, T. L., and Noble, W. S. (2007). Quantifying similarity between motifs. *Genome Biol.* 8, R24. doi:10.1186/gb-2007-8-2-r24

Hamatani, T., Carter, M. G., Sharov, A. A., and Ko, M. S. H. (2004). Dynamics of global gene expression changes during mouse preimplantation development. *Dev. Cell* 6, 117–131. doi:10.1016/s1534-5807(03)00373-3

Hashimoto, Y., Maegawa, S., Nagai, T., Yamaha, E., Suzuki, H., Yasuda, K., et al. (2004). Localized maternal factors are required for zebrafish germ cell formation. *Dev. Biol.* 268, 152–161. doi:10.1016/j.ydbio.2003.12.013

Heasman, J., Quarmby, J., and Wylie, C. C. (1984). The mitochondrial cloud of Xenopus oocytes: the source of germinal granule material. *Dev. Biol.* 105, 458–469. doi:10.1016/0012-1606(84)90303-8

Horvay, K., Claußen, M., Katzer, M., Landgrebe, J., and Pieler, T. (2006). Xenopus Dead end mRNA is a localized maternal determinant that serves a conserved function in germ cell development. *Dev. Biol.* 291, 1–11. doi:10.1016/j.ydbio.2005.06.013

Houston, D. W., Zhang, J., Maines, J. Z., Wasserman, S. A., and King, M. L. (1998). A Xenopus DAZ-like gene encodes an RNA component of germ plasm and is a functional homologue of Drosophila boule. *Development* 125, 171–180. doi:10.1242/dev.125.2.171

Howley, C., and Ho, R. K. (2000). mRNA localization patterns in zebrafish oocytes. *Mech. Dev.* 92, 305–309. doi:10.1016/s0925-4773(00)00247-1

Iegorova, V., Naraine, R., Psenicka, M., Zelazowska, M., and Sindelka, R. (2022). Comparison of RNA localization during oogenesis within *Acipenser ruthenus* and *Xenopus laevis*. *Front. Cell. Dev. Biol.* 10, 982732. doi:10.3389/fcell.2022.982732

Ikenishi, K., and Nieuwkoop, P. D. (1978). Location and ultrastructure of primordial germ cells (PGCs) in *Ambystoma mexicanum*. *Dev. Growth Differ.* 20, 1–9. doi:10.1111/j.1440-169X.1978.00001.x

Jiang, P., Nelson, J. D., Leng, N., Collins, M., Swanson, S., Dewey, C. N., et al. (2017). Analysis of embryonic development in the unsequenced axolotl: waves of transcriptomic upheaval and stability. *Dev. Biol. Xenopus Genomes* 426, 143–154. doi:10.1016/j.ydbio.2016.05.024

Johnson, A. D., Bachvarova, R. F., Drum, M., and Masi, T. (2001). Expression of axolotl DAZL RNA, a marker of germ plasm: widespread maternal RNA and onset of expression in germ cells approaching the gonad. *Dev. Biol.* 234, 402–415. doi:10.1006/dbio.2001.0264

Kirilenko, P., Weierud, F. K., Zorn, A. M., and Woodland, H. R. (2008). The efficiency of Xenopus primordial germ cell migration depends on the germplasm mRNA encoding the PDZ domain protein Grip2. *Differentiation* 76, 392–403. doi:10.1111/j.1432-0436.2007.00229.x

Kloc, M., and Etkin, L. D. (1995). Two distinct pathways for the localization of RNAs at the vegetal cortex in Xenopus oocytes. *Development* 121, 287–297. doi:10.1242/dev.121.2.287

Knaut, H., Pelegri, F., Bohmann, K., Schwarz, H., and Nüsslein-Volhard, C. (2000). Zebrafish vasa RNA but not its protein is a component of the germ plasm and segregates

asymmetrically before germline specification. *J. Cell Biol.* 149, 875–888. doi:10.1083/jcb.149.4.875

Koebernick, K., Loeber, J., Arthur, P. K., Tarbashevich, K., and Pieler, T. (2010). Elr-type proteins protect Xenopus Dead end mRNA from miR-18-mediated clearance in the soma. *PNAS* 107, 16148–16153. doi:10.1073/pnas.1004401107

Kofron, M., Demel, T., Xanthos, J., Lohr, J., Sun, B., Sive, H., et al. (1999). Mesoderm induction in Xenopus is a zygotic event regulated by maternal VegT via TGFbeta growth factors. *Development* 126, 5759–5770. doi:10.1242/dev.126.24.5759

Kopylova, E., Noé, L., and Touzet, H. (2012). SortMeRNA: fast and accurate filtering of ribosomal RNAs in metatranscriptomic data. *Bioinformatics* 28, 3211–3217. doi:10.1093/bioinformatics/bts611

Kosaka, K., Kawakami, K., Sakamoto, H., and Inoue, K. (2007). Spatiotemporal localization of germ plasm RNAs during zebrafish oogenesis. *Mech. Dev.* 124, 279–289. doi:10.1016/j.mod.2007.01.003

Lai, W. S., Carballo, E., Strum, J. R., Kennington, E. A., Phillips, R. S., and Blackshear, P. J. (1999). Evidence that tristetraprolin binds to AU-rich elements and promotes the deadenylation and destabilization of tumor necrosis factor alpha mRNA. *Mol. Cell Biol.* 19, 4311–4323. doi:10.1128/mcb.19.6.4311

Lai, W. S., Kennington, E. A., and Blackshear, P. J. (2003). Tristetraprolin and its family members can promote the cell-free deadenylation of AU-rich element-containing mRNAs by poly(A) ribonuclease. *Mol. Cell Biol.* 23, 3798–3812. doi:10.1128/mcb.23.11.3798-3812.2003

Laurent, M. N., Blitz, I. L., Hashimoto, C., Rothbächer, U., and Cho, K. W. (1997). The Xenopus homeobox gene twin mediates Wnt induction of goosecoid in establishment of Spemann's organizer. *Development* 124, 4905–4916. doi:10.1242/dev.124.23.4905

Lechner, M., Findeiss, S., Steiner, L., Marz, M., Stadler, P. F., and Prohaska, S. J. (2011). Proteinortho: detection of (co-)orthologs in large-scale analysis. *BMC Bioinforma.* 12, 124. doi:10.1186/1471-2105-12-124

Lefresne, J., Andéol, Y., and Signoret, J. (1998). Evidence for introduction of a variable G1 phase at the midblastula transition during early development in axolotl. *Dev. Growth Differ.* 40, 497–508. doi:10.1046/j.1440-169x.1998.t01-3-00004.x

Leise, W. F., and Mueller, P. R. (2002). Multiple Cdk1 inhibitory kinases regulate the cell cycle during development. *Dev. Biol.* 249, 156–173. doi:10.1006/dbio.2002.0743

Levin, M., Thorlin, T., Robinson, K. R., Nogi, T., and Mercola, M. (2002). Asymmetries in H+/K+-ATPase and cell membrane potentials comprise a very early step in left-right patterning. *Development* 111 (1) 77–89. doi:10.1016/S0092-8674(02)00939-X

Litvinov, S. V., Velders, M. P., Bakker, H. A., Fleuren, G. J., and Warnar, S. O. (1994). Ep-CAM: a human epithelial antigen is a homophilic cell-cell adhesion molecule. *J. Cell Biol.* 125, 437–446. doi:10.1083/jcb.125.2.437

Love, M. I., Huber, W., and Anders, S. (2014). Moderated estimation of fold change and dispersion for RNA-seq data with DESeq2. *Genome Biol.* 15, 550. doi:10.1186/s13059-014-0550-8

Lu, F.-I., Thisse, C., and Thisse, B. (2011). Identification and mechanism of regulation of the zebrafish dorsal determinant. *Proc. Natl. Acad. Sci.* 108, 15876–15880. doi:10.1073/pnas.1106801108

Lund, E., Liu, M., Hartley, R. S., Sheets, M. D., and Dahlberg, J. E. (2009). Deadenylation of maternal mRNAs mediated by miR-427 in *Xenopus laevis* embryos. *RNA* 15, 2351–2363. doi:10.1261/rna.1882009

Lundmark, C. (1986). Role of bilateral zones of ingressing superficial cells during gastrulation of *Ambystoma mexicanum*. *Development* 97, 47–62. doi:10.1242/dev.97.1.47

Lustig, K. D., Kroll, K. L., Sun, E. E., and Kirschner, M. W. (1996). Expression cloning of a Xenopus T-related gene (Xombi) involved in mesodermal patterning and blastopore lip formation. *Development* 122, 4001–4012. doi:10.1242/dev.122.12.4001

McLeay, R. C., and Bailey, T. L. (2010). Motif enrichment analysis: a unified framework and an evaluation on ChIP data. *BMC Bioinforma.* 11, 165. doi:10.1186/1471-2105-11-165

MacArthur, H., Houston, D. W., Bubunenko, M., Mosquera, L., and King, M. L. (2000). DEADSouth is a germ plasm specific DEAD-box RNA helicase in Xenopus related to eIF4A. *Mech. Dev.* 95, 291–295. doi:10.1016/s0925-4773(00)00357-9

Mahowald, A. P., and Hennen, S. (1971). Ultrastructure of the "germ plasm" in eggs and embryos of *Rana pipiens*. *Dev. Biol.* 24, 37–53. doi:10.1016/0012-1606(71)90045-5

Malm, D., and Nilssen, Ø. (2008). Alpha-mannosidosis. *Orphanet J. Rare Dis.* 3, 21. doi:10.1186/1750-1172-3-21

Mattei, E., Pietrosanto, M., Ferrè, F., and Helmer-Citterich, M. (2015). Web-beagle: a web server for the alignment of RNA secondary structures. *Nucleic Acids Res.* 43, W493–W497. doi:10.1093/nar/gkv489

Melton, D. A. (1987). Translocation of a localized maternal mRNA to the vegetal pole of Xenopus oocytes. *Nature* 328, 80–82. doi:10.1038/328080a0

Moody, S. A. (1987a). Fates of the blastomeres of the 16-cell stage Xenopus embryo. *Dev. Biol.* 119, 560–578. doi:10.1016/0012-1606(87)90059-5

Moody, S. A. (1987b). Fates of the blastomeres of the 32-cell-stage Xenopus embryo. *Dev. Biol.* 122, 300–319. doi:10.1016/0012-1606(87)90296-x

Naraine, R., Iegorova, V., Abaffy, P., Franek, R., Soukup, V., Psenicka, M., et al. (2022). Evolutionary conservation of maternal RNA localization in fishes and amphibians revealed by TOMO-Seq. *Dev. Biol.* 489, 146–160. doi:10.1016/j.ydbio.2022.06.013

Nath, K., Boorech, J. L., Beckham, Y. M., Burns, M. M., and Elinson, R. P. (2005). Status of RNAs, localized in *Xenopus laevis* oocytes, in the frogs *Rana pipiens* and Eleutherodactylus coqui. *J. Exp. Zool.* 304B, 28–39. doi:10.1002/jez.b.21020

Nishita, M., Hashimoto, M. K., Ogata, S., Laurent, M. N., Ueno, N., Shibuya, H., et al. (2000). Interaction between Wnt and TGF-beta signalling pathways during formation of Spemann's organizer. *Nature* 403, 781–785. doi:10.1038/35001602

Nowoshilow, S., and Tanaka, E. M. (2020). Introducing www.axolotl-omics.org – an integrated -omics data portal for the axolotl research community. *Exp. Cell Res* 394 (1) 112143. doi:10.1016/j.yexcr.2020.112143

O'Brien, J., Hayder, H., Zayed, Y., and Peng, C. (2018). Overview of MicroRNA biogenesis, mechanisms of actions, and circulation. *Front. Endocrinol.* 9, 402. doi:10.3389/fendo.2018.00402

Oeffinger, M., Dlakić, M., and Tollervey, D. (2004). A pre-ribosome-associated HEAT-repeat protein is required for export of both ribosomal subunits. *Genes Dev.* 18, 196–209. doi:10.1101/gad.285604

Paillard, L., Omilli, F., Legagneux, V., Bassez, T., Maniey, D., and Osborne, H. B. (1998). EDEN and EDEN-BP, a cis element and an associated factor that mediate sequence-specific mRNA deadenylation in Xenopus embryos. *EMBO J.* 17, 278–287. doi:10.1093/emboj/17.1.278

Pantano, L., Hutchinson, J., Barrera, V., Piper, M., Khetani, R., Daily, K., et al. (2023). *DEGreport: Report of DEG analysis*. Available at: http://lpantano.github.io/DEGreport/.

Pietrosanto, M., Adinolfi, M., Casula, R., Ausiello, G., Ferrè, F., and Helmer-Citterich, M. (2018). BEAM web server: a tool for structural RNA motif discovery. *Bioinformatics* 34, 1058–1060. doi:10.1093/bioinformatics/btx704

Rapley, J., Nicolàs, M., Groen, A., Regué, L., Bertran, M. T., Caelles, C., et al. (2008). The NIMA-family kinase Nek6 phosphorylates the kinesin Eg5 at a novel site necessary for mitotic spindle formation. *J. Cell Sci.* 121, 3912–3921. doi:10.1242/jcs.035360

Raudvere, U., Kolberg, L., Kuzmin, I., Arak, T., Adler, P., Peterson, H., et al. (2019). g:Profiler: a web server for functional enrichment analysis and conversions of gene lists (2019 update). *Nucleic Acids Res.* 47, W191-W198–W198. doi:10.1093/nar/gkz369

Ray, D., Kazan, H., Cook, K. B., Weirauch, M. T., Najafabadi, H. S., Li, X., et al. (2013). A compendium of RNA-binding motifs for decoding gene regulation. *Nature* 499, 172–177. doi:10.1038/nature12311

Samwer, M., Dehne, H.-J., Spira, F., Kollmar, M., Gerlich, D. W., Urlaub, H., et al. (2013). The nuclear F-actin interactome of Xenopus oocytes reveals an actin-bundling kinesin that is essential for meiotic cytokinesis. *EMBO J.* 32, 1886–1902. doi:10.1038/emboj.2013.108

Schreckenberg, G. M., and Jacobson, A. G. (1975). Normal stages of development of the axolotl. *Ambystoma mexicanum*. *Dev. Biol.* 42, 391–400. doi:10.1016/0012-1606(75)90343-7

Sekula, M., Datta, S., and Datta, S. (2017). optCluster: an R Package for determining the optimal clustering algorithm. *Bioinformation* 13, 101–103. doi:10.6026/97320630013101

Sindelka, R., Abaffy, P., Qu, Y., Tomankova, S., Sidova, M., Naraine, R., et al. (2018). Asymmetric distribution of biomolecules of maternal origin in the *Xenopus laevis* egg and their impact on the developmental plan. *Sci. Rep.* 8, 8315. doi:10.1038/s41598-018-26592-1

Sindelka, R., Jonák, J., Hands, R., Bustin, S. A., and Kubista, M. (2008). Intracellular expression profiles measured by real-time PCR tomography in the *Xenopus laevis* oocyte. *Nucleic Acids Res.* 36, 387–392. doi:10.1093/nar/gkm1024

Sindelka, R., Sidova, M., Svec, D., and Kubista, M. (2010). Spatial expression profiles in the *Xenopus laevis* oocytes measured with qPCR tomography. *Methods, Xenopus Oocytes as Exp. Syst.* 51, 87–91. doi:10.1016/j.ymeth.2009.12.011

Skirkanich, J., Luxardi, G., Yang, J., Kodjabachian, L., and Klein, P. S. (2011). An essential role for transcription before the MBT in *Xenopus laevis*. *Dev. Biol.* 357, 478–491. doi:10.1016/j.ydbio.2011.06.010

Škugor, A., Tveiten, H., Johnsen, H., and Andersen, Ø. (2016). Multiplicity of Buc copies in Atlantic salmon contrasts with loss of the germ cell determinant in primates, rodents and axolotl. *BMC Evol. Biol.* 16, 232. doi:10.1186/s12862-016-0809-7

Soukup, V., Tazaki, A., Yamazaki, Y., Pospisilova, A., Epperlein, H.-H., Tanaka, E. M., et al. (2021). Oral and palatal dentition of axolotl arises from a common tooth-competent zone along the ecto-endodermal boundary. *Front. Cell. Dev. Biol.* 8, 622308. doi:10.3389/fcell.2020.622308

Stennard, F., Carnac, G., and Gurdon, J. B. (1996). The Xenopus T-box gene, Antipodean, encodes a vegetally localised maternal mRNA and can trigger mesoderm formation. *Development* 122, 4179–4188. doi:10.1242/dev.122.12.4179

Supek, F., Bošnjak, M., Škunca, N., and Šmuc, T. (2011). REVIGO summarizes and visualizes long lists of gene ontology terms. *PLOS ONE* 6, e21800. doi:10.1371/journal.pone.0021800

Tam, P. P., and Zhou, S. X. (1996). The allocation of epiblast cells to ectodermal and germ-line lineages is influenced by the position of the cells in the gastrulating mouse embryo. *Dev. Biol.* 178, 124–132. doi:10.1006/dbio.1996.0203

Tarbashevich, K., Koebernick, K., and Pieler, T. (2007). XGRIP2.1 is encoded by a vegetally localizing, maternal mRNA and functions in germ cell development and anteroposterior PGC positioning in *Xenopus laevis*. *Dev. Biol.* 311, 554–565. doi:10.1016/j.ydbio.2007.09.012

Theusch, E. V., Brown, K. J., and Pelegri, F. (2006). Separate pathways of RNA recruitment lead to the compartmentalization of the zebrafish germ plasm. *Dev. Biol.* 292, 129–141. doi:10.1016/j.ydbio.2005.12.045

Tran, L. D., Hino, H., Quach, H., Lim, S., Shindo, A., Mimori-Kiyosue, Y., et al. (2012). Dynamic microtubules at the vegetal cortex predict the embryonic axis in zebrafish. *Development* 139, 3644–3652. doi:10.1242/dev.082362

Untergasser, A., Cutcutache, I., Koressaar, T., Ye, J., Faircloth, B. C., Remm, M., et al. (2012). Primer3--new capabilities and interfaces. *Nucleic Acids Res.* 40, e115. doi:10.1093/nar/gks596

Van Etten, J., Schagat, T. L., Hrit, J., Weidmann, C. A., Brumbaugh, J., Coon, J. J., et al. (2012). Human Pumilio proteins recruit multiple deadenylases to efficiently repress messenger RNAs. *J. Biol. Chem.* 287, 36370–36383. doi:10.1074/jbc.M112.373522

Vaur, S., Montreau, N., Dautry, F., and Andeol, Y. (2003). Differential post-transcriptional regulations of wnt mRNAs upon axolotl meiotic maturation. *Int. J. Dev. Biol.* 46, 731–739.

Venkatarama, T., Lai, F., Luo, X., Zhou, Y., Newman, K., and King, M. L. (2010). Repression of zygotic gene expression in the Xenopus germline. *Development* 137, 651–660. doi:10.1242/dev.038554

Vincent, J.-P., Oster, G. F., and Gerhart, J. C. (1986). Kinematics of gray crescent formation in Xenopus eggs: the displacement of subcortical cytoplasm relative to the egg surface. *Dev. Biol.* 113, 484–500. doi:10.1016/0012-1606(86)90184-3

Vincent, J.-P., Scharf, S. R., and Gerhart, J. C. (1987). Subcortical rotation in Xenopus eggs: A preliminary study of its mechanochemical basis. *Cell Motil.* 8, 143–154. doi:10.1002/cm.970080206

Vinot, S., Le, T., Ohno, S., Pawson, T., Maro, B., and Louvet-Vallée, S. (2005). Asymmetric distribution of PAR proteins in the mouse embryo begins at the 8-cell stage during compaction. *Dev. Biol.* 282, 307–319. doi:10.1016/j.ydbio.2005.03.001

Voeltz, G. K., and Steitz, J. A. (1998). AUUUA sequences direct mRNA deadenylation uncoupled from decay during Xenopus early development. *Mol. Cell. Biol.* 18, 7537–7545. doi:10.1128/mcb.18.12.7537

Weidinger, G., Stebler, J., Slanchev, K., Dumstrei, K., Wise, C., Lovell-Badge, R., et al. (2003). dead end, a novel vertebrate germ plasm component, is required for zebrafish primordial germ cell migration and survival. *Curr. Biol.* 13, 1429–1434. doi:10.1016/s0960-9822(03)00537-2

Welch, E., and Pelegri, F. (2015). Cortical depth and differential transport of vegetally localized dorsal and germ line determinants in the zebrafish embryo. *BioArchitecture* 5, 13–26. doi:10.1080/19490992.2015.1080891

Whitington, P. M. D., and Dixon, K. E. (1975). Quantitative studies of germ plasm and germ cells during early embryogenesis of *Xenopus laevis*. *Development* 33, 57–74. doi:10.1242/dev.33.1.57

Willems, P. J., Seo, H.-C., Coucke, P., Tonlorenzi, R., and O'Brien, J. S. (1999). Spectrum of mutations in fucosidosis. *Eur. J. Hum. Genet.* 7, 60–67. doi:10.1038/sj.ejhg.5200272

Wong, K., and Cantley, L. C. (1994). Cloning and characterization of a human phosphatidylinositol 4-kinase. *J. Biol. Chem.* 269, 28878–28884. doi:10.1016/s0021-9258(19)61989-7

Yang, J., Tan, C., Darken, R. S., Wilson, P. A., and Klein, P. S. (2002). Beta-catenin/Tcf-regulated transcription prior to the midblastula transition. *Development* 129, 5743–5752. doi:10.1242/dev.00150

Zearfoss, N. R., Chan, A. P., Wu, C. F., Kloc, M., and Etkin, L. D. (2004). Hermes is a localized factor regulating cleavage of vegetal blastomeres in *Xenopus laevis*. *Dev. Biol.* 267, 60–71. doi:10.1016/j.ydbio.2003.10.032

Zhang, J., and King, M. L. (1996). Xenopus VegT RNA is localized to the vegetal cortex during oogenesis and encodes a novel T-box transcription factor involved in mesodermal patterning. *Development* 122, 4119–4129. doi:10.1242/dev.122.12.4119

Zhou, Y., and King, M. L. (1996). Localization of Xcat-2 RNA, a putative germ plasm component, to the mitochondrial cloud in Xenopus stage I oocytes. *Development* 122, 2947–2953. doi:10.1242/dev.122.9.2947

frontiers | Frontiers in Cell and Developmental Biology

TYPE Review
PUBLISHED 14 November 2023
DOI 10.3389/fcell.2023.1279227

Check for updates

OPEN ACCESS

EDITED BY
Jason Knott,
Michigan State University, United States

REVIEWED BY
Xuan Shao,
Chinese Academy of Sciences (CAS), China
Zhaowei Tu,
Third Affiliated Hospital of Guangzhou Medical University, China
Soumen Paul,
University of Kansas Medical Center, United States

*CORRESPONDENCE
Qinghua Li,
liqinghua_0729@163.com
Weiwei Yang,
yangww@wfmc.edu.cn

†These authors share first authorship

RECEIVED 17 August 2023
ACCEPTED 30 October 2023
PUBLISHED 14 November 2023

CITATION
Liu X, Wang G, Huang H, Lv X, Si Y, Bai L, Wang G, Li Q and Yang W (2023), Exploring maternal-fetal interface with in vitro placental and trophoblastic models. *Front. Cell Dev. Biol.* 11:1279227. doi: 10.3389/fcell.2023.1279227

COPYRIGHT
© 2023 Liu, Wang, Huang, Lv, Si, Bai, Wang, Li and Yang. This is an open-access article distributed under the terms of the Creative Commons Attribution License (CC BY). The use, distribution or reproduction in other forums is permitted, provided the original author(s) and the copyright owner(s) are credited and that the original publication in this journal is cited, in accordance with accepted academic practice. No use, distribution or reproduction is permitted which does not comply with these terms.

Exploring maternal-fetal interface with in vitro placental and trophoblastic models

Xinlu Liu[1†], Gang Wang[2†], Haiqin Huang[1], Xin Lv[1], Yanru Si[1], Lixia Bai[1], Guohui Wang[1], Qinghua Li[3*] and Weiwei Yang[1*]

[1]School of Biosciences and Biotechnology, Weifang Medical University, Weifang, Shandong, China , [2]Department of Emergency, Affiliated Hospital of Weifang Medical University, Weifang, Shandong, China, [3]School of Public Health, Weifang Medical University, Weifang, Shandong, China

The placenta, being a temporary organ, plays a crucial role in facilitating the exchange of nutrients and gases between the mother and the fetus during pregnancy. Any abnormalities in the development of this vital organ not only lead to various pregnancy-related disorders that can result in fetal injury or death, but also have long-term effects on maternal health. *In vitro* models have been employed to study the physiological features and molecular regulatory mechanisms of placental development, aiming to gain a detailed understanding of the pathogenesis of pregnancy-related diseases. Among these models, trophoblast stem cell culture and organoids show great promise. In this review, we provide a comprehensive overview of the current mature trophoblast stem cell models and emerging organoid models, while also discussing other models in a systematic manner. We believe that this knowledge will be valuable in guiding further exploration of the complex maternal-fetal interface.

KEYWORDS

placenta, trophoblast cells, trophoblast stem cells, organoids, *in vitro* models

1 Introduction

The placenta is an extra-embryonic organ that plays a crucial role in supporting and facilitating fetal development within the uterus. It serves as a vital conduit for oxygen, nutrients, and waste removal (Maltepe and Fisher, 2015). Impaired placental function can have profound implications on both maternal and fetal health, potentially leading to serious pregnancy complications (Silasi et al., 2010; Zhou et al., 2013; Mele et al., 2014; Liu et al., 2022). However, our current understanding of the human placenta remains limited due to the absence of functional experimental models. This constraint has impeded research efforts aimed at elucidating the etiology of placental disorders and developing effective therapeutic interventions. Therefore, establishing *in vitro* models can enhance our comprehension of intricate placental diseases while also enabling novel therapeutic strategies.

2 Human placenta

2.1 Macroscopic structure of the placenta

The placenta, which originates from both the embryonic and maternal endometrium, plays a crucial role in facilitating material exchange between the fetus and the mother

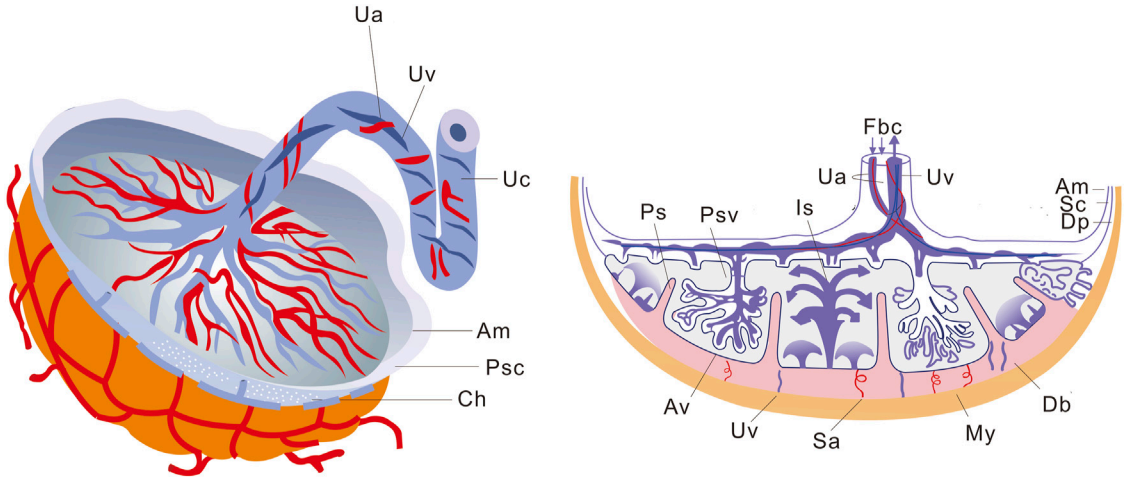

FIGURE 1
Schematic representation of placental structure. The macroscopic structure of the placenta is shown on the left, and the sagittal section of the placenta is shown on the right. *Ua*, Umbilical artery; *Uv*, Umbilical vein; *Uc*, Umbilical cord; *Am*, Amnion; *Psc*, Placental stem cells; *Ch*, Chorion; *Fbc*, Fetal blood circulation; *Is*, Intervillous space; *Ps*, Placental septum; *Psv*, Primary stem villus; *Sc*, Smooth chorion; *Dp*, Decidua parietalis; *Db*, Decidua basalis; *My*, Myometrium; *Sa*, Spiral arteries; *Av*, Anchoring villus.

(Covarrubias et al., 2023). It is disc-shaped and remains embedded in the inner wall of the uterus until delivery, when it is expelled due to myometrial contractions (Leiser and Kaufmann, 1994; Wheeler and Oyen, 2021). Figure 1 illustrates that the placental thickness is greater at its center and thinner at its margin. The smooth side facing inward is called the chorionic plate, to which the umbilical cord attaches, connecting each villus. On the rough basal plate, there are dendritic villus, which constitute a major component of the placenta. These finger-like blood vessels allow for maternal blood flow through the intervillous space, enabling material exchange across their intricate network, from mother to fetus, while waste products are excreted.

2.2 Major components of the placenta

The placenta is a complex organ consisting of three main components: the amnion, chorion, and decidua basalis (Huppertz, 2008). The amniotic membrane serves as both the innermost layer of the placenta and umbilical cord, as well as the fetal part of the placenta. It has a smooth texture without any vascular or lymphatic structures and exhibits a certain level of elasticity (Chuva de Sousa Lopes et al., 2022). Initially, the amniotic membrane was attached to the edge of the embryonic disc. As it expanded within the amniotic cavity, it surrounded the ventral surface of the embryo's body stalk, resulting in the formation of the primitive umbilical cord (Huppertz, 2008).

The decidua basalis, although a small portion of the term placenta, plays a crucial role in immune regulation as it is an integral component of maternal tissue (Zhang and Wei, 2021; Jin et al., 2023). The decidua basalis surface is coated with a layer of trophoblast cells originating from the fixed chorionic villus. This bottom metaphase, along with the trophoblast cells, constitutes the base of the chorionic interstices, known as the decidua plate. From this plate, several decidua intervals extend towards the chorionic membrane, dividing the maternal side of the placenta into approximately 20 visible maternal lobes.

The chorion, which is the main component of the fetus, is covered by the chorionic membrane. This membrane directly contacts the endometrium and other accessory structures. Within the intervillous space, there are villus filled with maternal blood and basal decidua-embedded villus (Huppertz, 2008). The development of these villus enhances the contact between the chorion and uterine decidua, allowing for material exchange between the embryo and mother (O'Brien and Wang, 2023).

The villus in contact with the decidua basalis are well developed due to the abundance of nutrients and are referred to as phyllodes chorion. The ends of the villus that are suspended in the intervillous space, filled with maternal blood, are known as free villus, while those growing into the decidua basalis are called fixed villus. The fetal lobe is partially separated into maternal lobes, with each maternal lobe containing several fetal lobes. Each fetal lobe has its own spiral artery for blood supply (Gruenwald, 1977).

The uterine spiral artery passes through the decidual plate and enters the maternal lobe. Material exchange between the mother and the fetus occurs at the villus of the fetal lobule (Pijnenborg et al., 2006). This indicates that fetal blood exchanges with maternal blood in the intervillous space through the umbilical artery until it reaches the capillary network in the villus. It is important to note that fetal blood and maternal blood do not communicate directly (Cindrova-Davies and Sferruzzi-Perri, 2022). In a well-structured placenta, maternal nutrients enter the fetal blood through six layers of tissue. These layers include the endothelial cell layer of the maternal microvascular wall, the connective tissue layer, the epithelial layer of the endometrium, the germinal layer of the fetal chorionic membrane, the connective tissue layer of the fetal villus core, and the endothelial cell layer of the fetal microvascular wall.

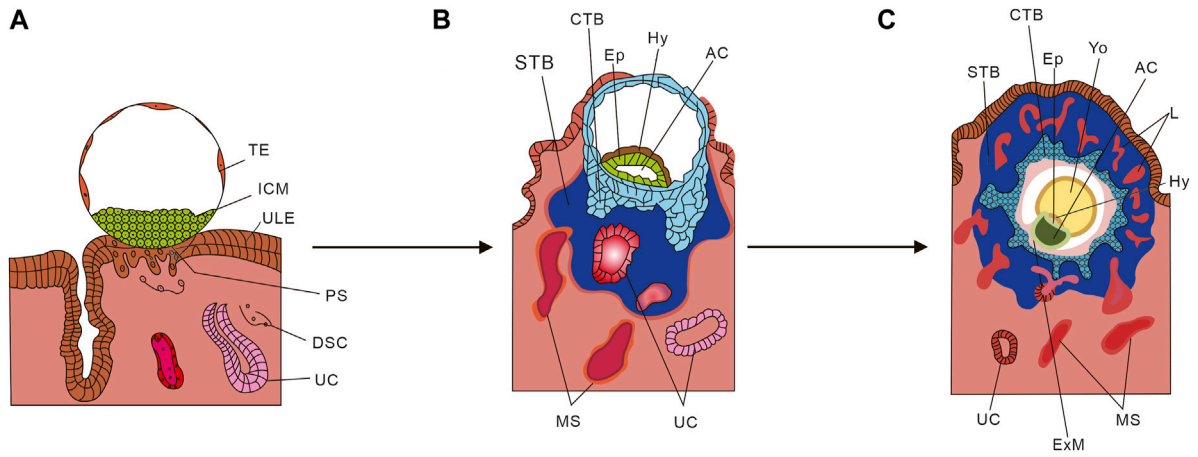

FIGURE 2
Schematic diagram of placental development. **(A)** Human blastocyst implanting into the pregnant uterus. **(B)** Development of the first placental structures and the embryonic disc. **(C)** Formation of primary villus and yolk sac. *TE*, Trophectoderm; *ICM*, Inner cell mass; *ULE*, Uterine luminal epithelium; *PS*, Primitive syncytium; *DSC*, Decidual stromal cell; *UC*, Uterine capillary; *Hy*, Hypoblast Ep; *STB*, Syncytiotrophoblasts; *CTB*, Cytotrophoblast; *MS*, Maternal blood sinusoid; *Yo*, Yolk sac; *L*, Lacunae system; *AC*, Amniotic cavity; *ExM*, Extraembryonic mesoderm. (From Cindrova-Davies T, Sferruzzi-Perri AN. Human placental development and function. Semin Cell Dev Biol. 2022 Nov; 131:66-77. doi: 10.1016/j.semcdb.2022.03.039. Epub 2022 Apr 4. And make some changes).

2.3 Development of the human placenta

The development of the human placenta involves a collaborative interaction between the trophoblast layer of the placenta and the maternal endometrium. Trophectoderm (TE) is the initial cell type that gives rise to all trophoblast cells and it starts developing 4–5 days after fertilization. Once the TE separates from the inner cell mass (ICM), the ICM proceeds to form an embryo. As depicted in Figure 2A, the first stage of placental development involves the implantation of a human blastocyst into the uterus of the pregnant individual. This process typically begins around 6–7 days after fertilization, during which the wall of the blastocyst differentiates into the placenta upon implantation. Figure 2B depicts the initial development of the primary structures of the placenta. Once the embryo attaches to the uterus, the trophoblast cells infiltrate the endometrium (Bentin-Ley et al., 2000; Illsley et al., 2020) and undergo primary syncytiotrophoblast (STB) formation (Shao et al., 2021). During this stage, the inner cell mass (ICM) transforms into a bilaminar epithelial structure comprising of the epiblast (Ep) and hypoblast (Hy; also known as primitive endoderm). Subsequently, a significant number of STB infiltrate between the endometrial cells, leading to the transformation of the endometrium into a specialized tissue known as decidua (Ruiz-Magaña et al., 2022). Trophoblast cells that do not come into contact with the intima do not undergo the primary integration process and become cytotrophoblast (CTB) (Shao et al., 2022). The period between 7 and 8 days after fertilization is referred to as the prelacunar period of placental development. On the 8th day after fertilization, vacuole-like structures start to appear in the hypertrophic STB at the implantation site. These vacuoles gradually enlarge and merge with each other, forming a complete lacunar space, indicating the transition of placental development into the lacunar period (Enders, 1995).

From day 8 to day 13 after fertilization, the cytotrophoblast (CTB) in the blastocyst undergoes proliferation and gradually merges with the syncytiotrophoblast (STB), resulting in its thickening and eventual envelopment of the entire blastocyst with lacunae. During this process, the CTB proliferates in layers to form trophoblast columns, while the STB penetrates the maternal uterine capillary (UC), giving rise to discontinuous maternal blood sinus (MS). As depicted in Figure 2C, around day 14 after fertilization, the CTB completely infiltrates the STB and forms the cytotrophoblast sheath, which signifies the onset of the villous stage of placental development. In this period, lamellar or columnar STB extend branches composed of CTB, known as primary villous stems, which branch out to form a dendritic complete villous structure. At this point, the aforementioned cavity structure is officially referred to as the intervillous space (Cindrova-Davies and Sferruzzi-Perri, 2022).

The cytotrophoblast sheath initiates a process of deep invasion and migration when it comes into contact with the maternal decidua (Gude et al., 2004). At this stage, the CTB separates from the villous structure and transforms into extravillous trophoblast (EVT). The EVT that penetrate the deep layer of endometrium are referred to as interstitial EVT (iEVT), while the remaining portion of EVT cells is known as endovascular EVT (enEVT) (Brkić et al., 2018). During early placental development, enEVT infiltrates into the spiral arteries of the endometrium and gradually remodels by interacting with endothelial cells (Sato, 2020). The invasion of placental trophoblast cells into the endometrial matrix and subsequent reconstruction of uterine spiral arteries are crucial physiological processes for maintaining a successful pregnancy. They also play a pivotal role in establishing utero open blood circulation (Albrecht and Pepe, 2020).

During pregnancy, the CTB undergoes continuous development, leading to the formation of a fully developed STB. The STB envelops the surface of placental formation and establishes

a selectively permeable barrier between the maternal and fetal compartments. Additionally, it serves as a crucial structural link connecting these compartments.

The placenta has two main functions in establishing and maintaining an optimal growth environment for the embryo. Firstly, it facilitates the circulation and exchange of materials between the mother's uterus and the fetus. This involves the transfer of substances between the fetal blood vessels and the maternal blood through the semi-permeable barrier created by the villus. Secondly, trophoblast cells invade and remodel the uterine blood vessels, further enhancing this complex process (Staff et al., 2022). The placenta also plays a role in maintaining the growth environment by ensuring the fetal growth microenvironment and promoting maternal-fetal immune tolerance. This is achieved through the maintenance of decidualization of the endometrium and the control of uterine contractile response by progesterone (Amini et al., 2019). The placental chorion has an immunomodulatory effect, which includes inhibiting excessive inflammation after blastocyst implantation, regulating uterine natural killer cells (Xie et al., 2022), and promoting the proliferation of regulatory T cells (Paolino et al., 2021).

The placenta plays a crucial role in pregnancy by synthesizing various hormones, enzymes, and cytokines. It produces hormones similar to those produced by the pituitary and ovary to support pregnancy. During early pregnancy, the placenta secretes human chorionic gonadotropin (hCG), which is similar to luteinizing hormone (LH) and helps maintain the development of the ovary's corpus luteum. It also promotes the secretion of estrogen and progesterone by the corpus luteum. Additionally, the placenta secretes human placental prolactin (hPL), a hormone that stimulates the growth of both the placenta and fetus, as well as the development of the maternal mammary gland. The placenta, through the secretion of hCG, hPL, progesterone, and alpha-fetoprotein synthesized by the fetal liver, inhibits the maternal immune response, allowing normal fetal development in the uterus without triggering an immune reaction. Furthermore, the placenta possesses various properties such as anti-inflammatory, antibacterial, and anti-scar activities. These properties, combined with the common practice of discarding the placenta after childbirth, have facilitated its use in cell therapy research, regenerative medicine, and *in vitro* organ-tissue related studies. Overall, the placenta is a dynamic and multifaceted organ that supports the development and survival of the embryo and fetus.

The placenta is capable of synthesizing various hormones, enzymes, and cytokines. It secretes hormones similar to those produced by the pituitary and ovary to support pregnancy. Additionally, it produces short-range hormones similar to peptides from the hypothalamus. During early pregnancy, the placenta secretes hCG (Stenman et al., 2006; Barrera et al., 2008), which is similar to luteinizing hormone (LH) and helps maintain the development of the ovary's corpus luteum. It also promotes the secretion of estrogen and progesterone by the corpus luteum. Another hormone secreted by the placenta is hPL, which promotes the growth of the placenta, fetus, and maternal mammary gland (Walker et al., 1991). The placenta also secretes progesterone (Kolatorova et al., 2022) and alpha-fetoprotein (Melamed et al., 2023), synthesized by the fetal liver, which inhibit the maternal immune response, allowing normal development of the fetus in the uterus without causing rejection. Furthermore, the placenta is a dynamic and multifaceted organ that supports the development and survival of the embryo and fetus (Tan et al., 2023). It possesses anti-inflammatory properties (Aggarwal et al., 2019), as well as antibacterial and anti-scar activity. These characteristics, combined with the common practice of discarding the placenta after childbirth, have facilitated its use in cell therapy research, regenerative medicine, and *in vitro* organ-tissue related studies.

3 Cell models

Trophoblast cells, which are epithelial cells in the placenta, play a crucial role in fetal growth and development throughout pregnancy. Abnormal trophoblast differentiation has been linked to complications such as miscarriage (Wang et al., 2021), preeclampsia (Huppertz, 2018), and fetal growth restriction. To understand placental disorders better, it is essential to have a comprehensive understanding of trophoblast structure and function during pregnancy. However, studying trophoblast cells has been challenging due to the lack of reproducible and widely used model systems. This has hindered significant advancements in this field. Fortunately, there has been recent progress in our ability to model this critical cell type at the maternal-fetal interface.

3.1 Placental derived TSCs models

Trophoblastic stem cells (TSCs) are derived from the trophectoderm, which corresponds to embryonic pluripotent stem cells (ESCs) derived from the inner cell mass of blastocysts. These TSCs have the ability to differentiate into various placental trophoblast cells during subsequent development, making them an invaluable *in vitro* model for studying the molecular mechanisms of placental development. Previous studies have successfully cultured mouse TSCs, providing a powerful *in vitro* platform for investigating the molecular mechanisms and functions of mouse embryonic development (Kidder, 2020; Ohinata et al., 2022; Seong et al., 2022). TSCs were first isolated and cultured from mouse extraembryonic ectoderm (ExE) (Tanaka et al., 1998). When mouse ExE cells were cultured in the presence of fibroblast growth factor 4 (FGF4) (Roberts and Fisher, 2011), highly proliferative epithelial colonies expressing Errb, Cdx2, Fgfr2, and Eomes were generated. The establishment of a mouse TSCs model has enabled researchers to comprehend the key gene network (Oct4, Ets2, Fgf4, Elf5) that maintains mouse TSCs in an undifferentiated state or identify key regulators involved in trophoblast cell differentiation (Tfap2c, Eomes, Cdx2, Gata3) (Kuijk et al., 2008; Rossant, 2008; Chen et al., 2021). It is crucial to establish a reliable model of human trophoblast cells in order to compare differences in early developmental embryos from human embryos using the same conditions.

In 2018, Okae et al. (2018) made a significant advancement in trophoblast cell research by successfully isolating TSCs from blastocysts and early pregnancy villus. These cells can be cultured for a long time for purification or cryopreserved for future use. The

researchers achieved this by activating the Wnt signaling pathway (Sonderegger et al., 2010) and inhibiting Rho-associated protein (ROCK), histone deacetylase, and TGF-β. The TSCs also expressed trophoblastic markers such as TEAD4, GATA3, TP63 and ELF5 (Kuijk et al., 2008; Rossant, 2008; Chen et al., 2021). Additionally, they demonstrated the ability to differentiate into hCG^+ STB (Horii et al., 2019) and HLA-G^+ EVT (Xu et al., 2020).

The recent study by Vento-Tormo et al. (2018) utilized single-cell RNA sequencing to examine the cellular heterogeneity in early pregnancy and term placentas. Consequently, there are variations between TSCs models derived from early pregnancy and those derived from term placentas. Wang et al. (2022) established an effective method for obtaining TSCs from term placenta. Their research revealed that the induction efficiency of CTB is influenced by the functional antagonism between the placental transcription factor GCM1 and the stemness regulator ΔNp63α. This antagonism reduces the transcriptional activity of GCM1, while GCM1 inhibits ΔNp63α oligomerization and autoregulation. GCM1 serves as a major transcriptional regulator for trophoblast cell differentiation, promoting fusion, invasion, and hormone secretion of trophoblast cells. It is crucial for the differentiation of STB and EVT (Liang et al., 2010; Cheong et al., 2015; Jeyarajah et al., 2022). ΔNp63α, an isoform of the p63 transcription factor, exhibits high expression in CTBS (Lee et al., 2007; Li et al., 2013). By inducing ΔNp63α activity, inhibiting GCM1 expression through EGF/CASVY, and further disrupting GCM1 expression through hypoxia, the researchers successfully transformed CTB cells from term placenta into TSCs. This breakthrough provides a new avenue for investigating pregnancy diseases and trophoblast cell differentiation.

Significant progress has been made in TSCs research, and it is now possible to obtain equivalent cell lines from human blastocysts for studying the development and function of human trophoblast cells. However, there are still some challenges that need to be addressed. Firstly, ethical and legal issues, as well as potential diseases associated with the use of these cells, may limit their applicability, similar to primary cells obtained from these tissue sources. Secondly, although the characteristics of these cells, such as ITGA6 expression (Wu et al., 2022), suggest their origin from cytotrophoblast blasts, their exact location in the placenta remains unknown. Therefore, further studies are required to establish a comprehensive and systematic model.

3.2 ESCs and pluripotent stem cells (PSCs) derived TSCs models

ESCs are totipotent cells derived from early mammalian embryos that can proliferate indefinitely *in vitro* and remain undifferentiated (Evans and Kaufman, 1981). Extensive research has been conducted on ECSs derived from mice, which have significantly contributed to our understanding of various molecular mechanisms (Baribault and Kemler, 1989; Sato and Nakano, 2001; Lau et al., 2022). Additionally, non-human primate ES cell lines have been utilized as accurate *in vitro* models for studying the differentiation of human tissues (Lester et al., 2004; Kishimoto et al., 2021). However, due to ethical and practical reasons, human relevant models have not been extensively explored. In 1998, Thomson et al. (1998) reported the development of pluripotent cell lines derived from human blastocysts. These cell lines exhibited normal karyotypes and expressed high levels of telomerase activity, as well as cell surface markers characteristic of primate ESCs. Although the characterization of other early cell lineages was not performed, these cells retained their developmental potential even after 4–5 months of *in vitro* proliferation. They were capable of forming trophoblasts and derivatives of all three embryonic germ layers, including the intestinal epithelium (endoderm), cartilage, bone, smooth muscle, and striated muscle (mesoderm), as well as neuroepithelium, embryonic ganglia, and stratified squamous epithelium (ectoderm). These cell lines hold immense promise in the fields of human developmental biology, drug discovery, and transplantation medicine (Gearhart, 1998). However, they also give rise to scientific hopes and pose legal issues (Marshall, 1998).

Then Ezashi et al. (2012) utilized human embryonic stem cells (hESC) as a model to investigate trophoblast differentiation. They exposed both hESCs and iPSCs to the growth factor BMP4 (Xu et al., 2002; Koel et al., 2017) in order to generate trophoblast lineage cells. This model system allowed them to explore the initial events that determine the specification of trophoblasts and their subsequent transformation into more specialized lineages, as well as the role of oxygen in this differentiation process. Additionally, they extensively described the significant role of BMP4 in differentiating ESCs and PSC into trophoblast lineages (Ezashi et al., 2005; Das et al., 2007; Karvas et al., 2018). The original hESC model, which employed only BMP4 without FGF2, has been widely used to study trophoblast development. However, there have been some concerns suggesting that this differentiation primarily leads to mesoderm rather than trophoblast. In 2013, R. Michael Roberts and his team demonstrated that hesCs grown in mouse embryonic fibroblast medium containing BMP4 but no FGF2 rapidly transformed into epithelial cells expressing more trophoblastic markers and fewer mesodermal markers. In response to doubts regarding whether the BMP4/hESC *in vitro* model primarily differentiates into mesoderm rather than trophoblast (Bernardo et al., 2011), they indicated that it can indeed be utilized to study the emergence and differentiation of trophoblast cells. This study revealed that optimal trophoblast differentiation can be achieved by maximizing BMP4 signaling while minimizing MEK/ERK signaling (Amita et al., 2013). Subsequently, in 2015, they reported a new study on BMP4, which demonstrated that transient exposure to BMP4 for 24–36 h increased the potency of PSCs. When combined with ACTIVIN signaling inhibitors A83-01 and FGF2, this led to the acquisition of unique stem cell phenotypes from hESCs and iPSCs (Yang et al., 2015; Roberts et al., 2018). It has been demonstrated that BMP4 can induce human hPSCs to a self-renewing alternative state that allows trophoblast development, with implications for the regulation of lineage determination in early embryos.

In 2016, Horii et al. (2016) proposed a reproducible two-step protocol to differentiate into hPSCs dual-energy TSCs, followed by redifferentiation into fully functional trophoblast cells. The protocol involved inducing hPSCs to differentiate into CDX2+/p63+CTB stem cells using a specific medium containing BMP4. These CTB stem cells demonstrated self-renewal capacity and the potential to differentiate into STB and EVT cells, as confirmed by marker expression, hormone secretion, and invasive capacity. To evaluate

TABLE 1 Representive Trophoblastic Models in recent years.

The author	Date	Source	Differentiation direction	Main methods, etc.
Gaël Castel et al.	2020	Somatic cell and pluripotent stem cell	Blastocysts and first trimester CTB	Reprogramming or cell fate conversion
Jessica K Cinkornpumin et al.	2020	Naive hESCs	HTSCs derived from human placenta or blastocys	Transdifferentiation
Chen Dong et al.	2020	Naïve hPSCs	Extravillous and STB	Differentiation
Yanxing Wei et al.	2021	Primed PSCs	TSCs	Chromatin accessibility dynamics and histone modifications
Zhuosi Li et al.	2019	hTSCs	STB and EVT	Micromesh culture technique
Adam Mischler et al.	2021	hPSCs	Two distinct stem cell types of the trophectoderm	Derivative of differentiation
Gaël Castel et al.	2022	hPSCs	CTB, EVT	Reprogram somatic cells
Jia Ping Tan	2022	Fibroblasts	hTSCs	Reprogramming
Dong C et al.	2022	Human Naïve PSCs	hTSCs	Derivation of cells

the applicability of hPSCs-derived CTBs, the researchers successfully replicated the delayed CTB maturation and impaired STB differentiation observed in trisomy 21 syndrome (T21) (Gerbaud et al., 2019) hPSCs. Overall, their study emphasizes that hPSCs provide a reliable model for studying human trophoblast development and accurately replicating trophoblast cell differentiation defects. In 2022, the researchers used a new protocol to generate functional TSCs from primed hPSCs. They followed the previously established two-step protocol to differentiate induced hPSCs into functional trophoblasts and then switched to the newly developed TSCs medium to generate authentic TSC (Soncin et al., 2022). Through sequencing and transcriptome analysis, they found that these cells resembled placenta and naive hPSC-derived TSCs, and exhibited similar differentiation potential both *in vitro* and *in vivo*. The new scheme offers a simpler approach that can be applied to a wide range of existing hPSCs, including induced PSCs derived from patients with known birth outcomes.

Mammalian embryonic development initiates with the formation of the inner cell mass and trophectoderm, although the exact mechanism remains unclear. In a study conducted by Kobayashi et al. (2022) in 2022, it was discovered that naive human embryonic stem cells (hESCs) have the ability to transdifferentiate into TSCs, whereas priming hESCs cannot. This discrepancy was attributed to the highly active primate-specific miRNA cluster (C19MC) located on chromosome 19 of naive hESCs, which triggers post-HES silencing. Further investigation revealed that C19MC is crucial for maintaining hTSC cells, and the activation of hESCs cells can generate hTSCs cells. These findings demonstrate that the activation of C19MC equips hESCs cells with the potential to differentiate into trophoblast cell lineages, thereby providing a significant molecular mechanism for the development of TSCs models.

Table 1 presents trophoblast cell models developed in recent years, summarizing their sources and direction of differentiation, along with the main methods used for their construction. Simulating real-time pathophysiological changes *in vivo* remains a challenge for cell models, despite the attention garnered by TSCs models obtained from different sources and using different methods (Li et al., 2019; Castel et al., 2020; Cinkornpumin et al., 2020; Dong et al., 2020; Mischler et al., 2021; Wei et al., 2021; Castel and David, 2022; Dong and Theunissen, 2022; Tan et al., 2022). While traditional 2D cell culture has been convenient and widely adopted for many years, it lacks the ability to closely mimic *in vivo* conditions. In contrast, 3D tissue culture offers a physiologically relevant environment that more closely resembles *in vivo* conditions. As a result, researchers have started exploring 3D environments to observe physiological and pathological changes in cells and organs.

3.3 Primary trophoblasts

Primary cells are obtained from living tissues through isolation methods and are not immortalized like cell lines. They retain their original genetic characteristics and closely resemble the growth status of cells *in vivo*. This makes them ideal for experimental research, including drug testing, cell differentiation, and transformation (Anvarian et al., 2019).

In recent decades, studies on primary trophoblast cells have been conducted using placental tissue from various stages of pregnancy. The most easily accessible samples are obtained after normal full-term pregnancies and late-gestation deliveries. However, it is difficult to determine whether placental pathology is a cause or a consequence of EVT function, which plays a crucial role in the development of pregnancy disorders such as preeclampsia during early placental formation. The invasiveness and motility of EVT are significantly reduced at term. Quenby et al. (2004) investigated the impact of heparin and aspirin on EVT; however, their study did not establish any correlation between this effect and markers such as PP13 (Piskun et al., 2022), PIGF (Author Anyonoums, 2019; Wang et al., 2020), PAPP-A (Conover and Oxvig, 2023), or any other known predictive markers for preeclampsia (Townsend et al., 2019). Therefore, researchers are still searching for new molecules that can serve as markers for EVT. Consequently, the *in vitro* formation of STB during different developmental processes of trophoblast cells can effectively be studied using human full-term placenta.

The isolation of chorionic trophoblast cells has been conducted in multiple laboratories, followed by freezing and storage for various programs (Sagrillo-Fagundes et al., 2016). In the 1980s, a traditional tryptic digestive procedure was established and has been utilized since then. Kliman et al. (1986) later introduced the Percoll gradient procedure, which significantly enhanced the purity of chorionic trophoblast cells. Additionally, the use of magnetic beads allowed for further purification of these cells (Douglas and King, 1989). It was not until 2002 that Guilbert et al. (2002) (Huppertz et al., 1999) and Tannetta et al. developed methods to isolate CTB from mononuclear ensemble fragments.

However, Tannetta et al. (2008) demonstrated that isolated primary trophoblast cells no longer proliferate in culture. They tested the effects of antioxidants vitamin C and vitamin E on cultured primary trophoblast cells and found that after 96 h of culture, the cells underwent apoptosis, as evidenced by the loss of pase9 and Caspase3. Additionally, there was an increased shedding of CTB cell debris accompanied by apoptosis. Vitamins C and E were able to prevent apoptosis and shedding of CTB fragments, but they also resulted in decreased fusion of isolated trophoblast cells. Therefore, further studies on effective *in vitro* model systems are still pending.

3.4 Human placental passage cell lines

Human trophoblast cell lines BeWo, JEG-3, and JAR have been extensively utilized in studying the functions of trophoblast cells when human samples are not available. BeWo is an endocrine cell line derived from malignant gestational choriocarcinoma tissue (Pattillo and Gey, 1968). JEG-3 is one of the six different cell lines derived from choriocarcinoma clones, established serially (Kohler and Bridson, 1971). JAR, on the other hand, was established from placental trophoblast cell tumors. These cell lines exhibit similar foreign body metabolism enzymes to human placenta, such as CYP1A1 and CYP19 (Wójtowicz et al., 2011), making them suitable for investigating placental hormone secretion, uptake, efflux, and metabolism of exogenous foreign substances by placental cells.

JEG-3 and BeWo cell lines are commonly used as trophoblast cell models in early pregnancy. Champoothiri et al. (Nampoothiri et al., 2007) studied the protein profile of the BeWo cell line induced by forskolin. Additionally, the JEG-3 cytotrophoblast cell line can serve as a model for studying the function of isoforms of ADAMTS (a disintegrin and metalloproteinase with thrombospondin repeats) in epithelial cell proliferation (Beristain et al., 2011). The BeWo b30 cell line is commonly used to investigate placental barrier function at the cellular level. It forms tightly polarized monolayer cells on Transwell culture plates, although it has been associated with P-gp (Mark and Waddell, 2006). Furthermore, JEG-3 and BeWo b24 cell lines have the potential to develop monolayer polarized tight junctions, making them promising models for *in vitro* studies on placental drug transport after optimizing the appropriate conditions (Ikeda et al., 2011; Crowe and Keelan, 2012).

The BeWo cell line is widely used as a model for choriotrophoblast cells. It shares many characteristics with choriotrophoblast cells, such as the ability to fuse and integrate. However, due to the complex origin of BeWo cells, it is unclear which stage of pregnancy they represent. Additionally, BeWo cells can cause different changes in cell lines and varying fusion rates. Therefore, it is important to compare BeWo cells with primary trophoblast cells at different stages of pregnancy. Comparisons between BeWo and JEG-3 cells showed that they had the same DNA profile and similar secretory activity. However, BeWo cells were found to be highly sensitive to forskolin-induced syncytial formation (Vargas et al., 2009; Schneider et al., 2011), while JAR cells retained many of the morphological and endocrine features observed in human trophoblasts. Furthermore, the expression of certain proteins in the immortalized cell lines did not align with that of primary cells. For example, the expression of P-gp in BeWo, JAR, and JEG-3 cell lines was lower compared to primary trophoblasts isolated from term placentas (Evseenko et al., 2006). The expression of BCRP in BeWo and JAR cells was similar to that in human placenta, except for JEG-3. BeWo and JAR cells exhibited higher levels of ABCC2 and lower levels of ABCC1 compared to primary trophoblasts (Wolfe, 2006).

Although the cell line has the advantage of being repetitive and stable, the method of changing telomerase and viral transformation also leads to alterations in gene expression (Shiverick et al., 2001), thereby necessitating further improvement in the cell line model. However, these cell models still have certain limitations, such as their inability to simulate real-time pathophysiological changes *in vivo*. While traditional 2D cell culture has been widely adopted for many years due to its convenience, 3D tissue culture offers a more physiologically relevant environment that closely mimics *in vivo* conditions. As a result, researchers have started exploring 3D models to observe physiological and pathological changes in cells and organs.

4 Trophoblast organoid models

4.1 Introduction to organoids

In recent years, organoids have become indispensable tools for studying disease mechanisms (Corrò et al., 2020). They utilize various types of stem cells, including ESCs, induced pluripotent stem cells (iPSCs), and adult stem cells (ASCs), to self-organize in a 3D culture environment through cell sorting and space restriction (Hagen and Hinds, 2019). Organoids are small, simulated organs that closely resemble real organs in structure and function, although they do not possess full functionality. They exhibit remarkable self-renewal and self-organization capabilities and can replicate the organ-specific functions of the tissues they originate from (Hagen and Hinds, 2019).

The concept of 3D organoid culture dates back to the early 20th century, with Wilson et al. first demonstrating the self-organization and regeneration ability of isolated sponge cells to become complete organisms in 1907 (Wilson, 1907). However, in 2009, Hans Clevers and his team pioneered the intestinal organoid culture system, marking the beginning of a “new era” of organoid technology (Barker et al., 2009). Since then, organoids have revolutionized various fields, including basic research, medicine, and regenerative medicine. Their ability to faithfully reproduce complex 3D structures, different cell types, and specific organ functions makes them valuable models for studying organ

development and disease. As a result, they hold great potential for a wide range of biological and medical applications (Rossi et al., 2018; Hofbauer et al., 2021).

4.2 Trophoblastic organoids (CTB-ORGs) models

In 2018, the groundbreaking research conducted by Turco et al. (2018) led to the establishment of CTB-ORGs. This model provides a powerful tool for studying the complex interactions between maternal and fetal cells during human placenta formation. The objective of this study is to effectively replicate the dual differentiation pathways of early placental trophoblast cells, specifically migration and infiltration. By doing so, it establishes a platform for observing and understanding the interaction between early placental development and trophoblast cells.

First, the researchers studied the Wnt and MAPK signaling pathways during the 6–8 weeks of gestation. They identified the basal medium components, including epidermal growth factor (EGF) (Cheng et al., 2022) and fibroblast growth factor 2 (FGF-2) (Martinez-Fierro et al., 2022), and enzymatically digested the placenta during early pregnancy. EpCAM-labeled trophoblast cells, which are a specific subtype of trophoblast cells, were obtained. These labeled trophoblast cells were then seeded in Matrigel drops rich in medium to support the stable growth of trophoblast cells (Zhao et al., 2022). In this study, proliferating EpCAM$^+$ CTB were successfully isolated from first-trimester villus. Subsequently, human first-trimester trophoblast organoids were generated by activating the Wnt signaling pathway and inhibiting the TGF-β signaling pathway (Ye et al., 2022). Transcriptome microarray analysis revealed that the organoids exhibited similar transcriptome and methylation profiles to primiparous placentas. Mass spectrometry showed that the hormones and proteins secreted by the villus in the organoids were similar to those secreted by the placenta. The origin of the cells was confirmed by HLA typing, while their identity was verified according to specific criteria for four trophoblast cell types (Lee et al., 2016).

Turco et al. (2018) successfully generated human trophoblast organoids using villous trophoblast cells (VCT) and syncytial trophoblast cells (SCT). These organoids closely resemble the *in vivo* villous placenta in terms of anatomy and function, presenting complex 3D structures. Additionally, HLA-G positive EVT, which exhibited strong invasion ability in a 3D environment, was also identified during the experiment. The *in vitro* organoid model offers a significant advantage as it can replicate the complex placental structure and produce both STB and EVT. This model facilitates the study of mother-to-child transmission of xenobiotics, drugs, pathogens, proteins, and hormones from STB. Consequently, these trophoblastic organoids hold great promise in understanding maternal-fetal interactions post-implantation and exploring maternal physiological changes in metabolism and hormonal regulation during pregnancy.

However, the study of placental development has been stagnant due to the lack of models that can autonomously renew and differentiate, such as STB and EVT. One of the challenges is accurately reproducing the human trophoblast model of early placental development (Ma et al., 2023). In 2018, Haider et al. (2016) developed an organoid model with autonomous differentiation and renewal ability using purified CTB cells from early pregnancy. This model provides a valuable foundation for understanding the initial development mechanism of trophoblast cells, as well as cell proliferation and differentiation. Haider et al. (2016) cultured purified VCT extracted from early primiparous pregnancy placental tissue in Matrigel, supplemented with various growth factors and signal transduction inhibitors like A83-01 and GSK-3α/β. Within a few days of culture with these factors, small cell clusters rapidly formed and developed into 16 different organoid cultures with 100% derivation efficiency in 2–3 weeks. These organoids could be stably passaged for 5 months. CTB-ORGs, which are the organoids, express markers of trophoblast stemness and proliferation like ELF5 (Lee and Ormandy, 2012), CDX2 (Nishioka et al., 2009), TEAD4 (Saha et al., 2020; Stamatiadis et al., 2022), GATA3 (Chiu and Chen, 2016), and AP-2a (Orso et al., 2007). They have been identified and gene sequenced, confirming their long-term expansion ability and similarity to primary CTBs in terms of gene expression.

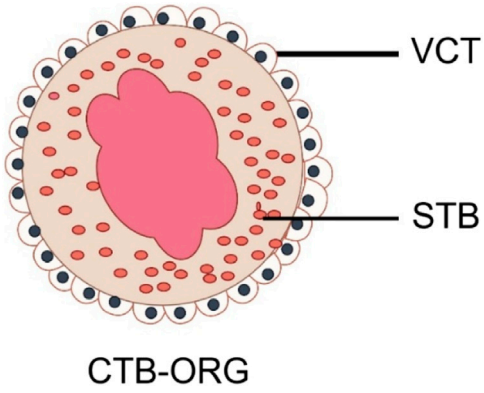

FIGURE 3
Schematic diagram of trophoblast organoid. *VCT*, Cytotrophoblast; *STB*, Syncytiotrophoblast (By Figdraw).

The presence of EGF (Cheng et al., 2022) and A83-01 was found to be essential for the long-term expansion of CTB-ORGs. On the other hand, the absence of Wnt inducers (R-pondin and CHIR99021) promoted the growth and differentiation of trophoblast cells. This suggests that WNT signaling plays a crucial role in organoid formation by controlling self-renewal, lineage delineation, and differentiation. Exogenous stimulation of Wnt signaling can maintain the growth of CTB-ORGs. Additionally, it was observed that the withdrawal of R-spondin and CHIR99021 led to a transient increase in cyclin A expression, promoting the growth of trophoblast cells and the development of proliferative NOTCH1$^+$ progenitor cells. These findings provide a valuable molecular mechanism for future research.

Due to the limited lifetime of TSCs *in vivo*, the self-renewal capacity of most sorted organ tissues will diminish over time. However, the study by Haider et al. discovered self-renewing vCTB precursors within CTB-ORGs through molecular analysis. These cells rely on Wnt signaling and have the ability to fuse and generate Notch1-positive EVT precursors after Wnt stimulation is lost, making them bipotent CTB stem cells. The model successfully

replicates the development of trophoblast progenitors and different subtypes, including STB and EVT, in a 3D environment. Its ability to grow and differentiate under precise culture conditions makes it a valuable tool for modeling placental diseases and studying trophoblast development and function. Figure 3 briefly depicts a model diagram of their constructed trophoblast organoids.

Both trophoblast cells and decidual tissues play crucial roles in maternal and fetal immune responses. While various models and organoids derived from uterine glands have been utilized to simulate different physiological processes, there remains a dearth of innate infection models. To investigate their specific contributions to virus resistance, Yang et al. (2022) developed trophoblast cells and decidual tissue organoids to mimic the HCMV virus model. The reactivity of these two types of organs to HCMV infection was assessed, along with their observed differences. Furthermore, a co-culture technique was employed to examine the interaction between trophoblast cells and decidual epithelial cells. This model offers a straightforward and accessible approach to explore the interconnected responses among distinct pregnancy tissues.

At present, a study conducted by Karvas et al. (2022) in 2022 introduced a new model that combines stem cells and organoids, specifically TSCs derived from immature hPSCs that spontaneously form trophoblast organoids (SC-TOs) with villus structures similar to primary trophoblast organoids. The study utilized single-cell transcriptome analysis to identify distinct clusters of CTB, STB, and EVT, which are closely associated with trophoblast identity in the postimplantation embryo. Additionally, the study revealed that these organoid cultures exhibited the clonal X chromosome inactivation pattern observed in human placenta (Andoh-Noda et al., 2017) and showed selective susceptibility to emerging pathogens such as SARS-CoV-2 and Zika virus, which correlated with the expression levels of their respective entry factors. The SC-TOs provide an accessible 3D model system for studying the developing placenta and its susceptibility to emerging pathogens, offering comparable tissue architecture, placental hormone secretion, and long-term self-renewal capacity to previous trophoblast organoids. This study not only demonstrated the trophoblast identity and differentiation capacity of multiple cells in organoids but also characterized the X chromosome inactivation dynamics during the process from naive hiPSCs to organoid establishment. Furthermore, this model was utilized to explore placental development and susceptibility to different pathogens.

In the same year, Qin Jianhua's team utilized biology and engineering technologies to establish a 3D model of hiPSCs-derived trophoblasts *in vitro*. This model was created using cell and organ chip technology, allowing for the simulation of developmental characteristics of early human placenta and the effects of hydrodynamic factors on placental tissue differentiation and secretion function (Cui et al., 2022). The researchers perfused hiPSCs in a fluid device, resulting in the formation of trophoblastic tissue in a biomimetic microenvironment. The device incorporated the extracellular matrix (ECM) and facilitated the generation of 3D clusters with major cell types of the human placenta, including trophoblast progenitors, STBs, and EVTs, through long-term 3D culture. RNA-seq analysis confirmed that the resulting CTB-ORGs exhibited phenotypic features highly similar to human first-trimester placental tissue. Further studies demonstrated that the organoids responded to stimulation by TNF-α and VEGF receptor inhibitors, effectively mimicking the physiological and pathological characteristics of placental tissue *in vivo*.

The advantage of their model is that, under dynamic culture conditions, the formed tissues exhibit enhanced expression of CTB, STB, and EVT-related markers at the gene and protein levels. RNA-seq analysis showed higher expression of trophoblast-specific genes in 3D tissues, indicating the important role of fluid flow in promoting trophoblast differentiation of hiPSCs. The established 3D placenta model combines bioengineering strategies with developmental principles and provides a comprehensive platform for studying placental biology in the biomimetic microenvironment of health and disease. It includes various trophoblast cell subtypes, vascular-like structures, and key functional characteristics of tissues, offering new insights into the study of human early placental development, preeclampsia, and pathogen infection.

4.3 Culture system of trophoblast organoids

In 2020, Sheridan et al. (2020) conducted a study on the limitations of current *in vitro* models of trophoblast cells and gained new insights into the cultivation of placental organoids. Moreover, the use of animal models poses inherent limitations in studying human placental development and function due to species variations. Consequently, creating precise *in vitro* models that accurately represent the distinct characteristics of the human placenta has been a significant hurdle.

The culture system used by Sheridan et al. (year) to extract organoids from early human placental specimens was based on existing organoid systems. In this method, cells isolated from tissues are encapsulated in Matrigel droplets supplemented with specific media (Sato et al., 2009). Through repeated refinement and validation, they established an optimized basic formulation for the growth of trophoblast cell organoids. The formulation includes EGF, hepatocyte growth factor (HGF), FGF-2 as a MAPK activator (Hempstock et al., 2004; Paiva et al., 2011; Kunath et al., 2014), CHIR99021 and R-Spinin-1 as Wnt pathway activators (Sonderegger et al., 2007), Y-27632 as a ROCK inhibitor (Shiokawa et al., 2002), PGE-2 as a cAMP/Akt pathway activator (Meadows et al., 2004), and A83-01 as a TGF-β inhibitor (Wu et al., 2017). Additionally, a simple enzymatic treatment with Accutase during culture significantly increased the expansion and proliferation of trophoblast cells (Lai et al., 2022).

CTB-ORGs are trophoblast cells isolated from first-trimester placentas and cultured in a 3D system to promote their long-term expansion as trophoblastic organoplasm. These organ tissues can be established within 2–3 weeks, passaged every 7–10 days, and maintained over a year. Under these optimized conditions, the organ tissue exhibits a villous structure composed of STB and CTB that have the ability to continuously proliferate. The structural arrangement of these human trophoblast organ tissues closely resembles that observed in villous placentas, with a layer of proliferating CTBs and the potential to differentiate into overlapping STB (Sheridan et al., 2020). Efficient generation of EVT was achieved by removing all growth factors and Wnt activators, inhibiting TGF-β, and introducing NRG1 (Maenhoudt et al., 2020). These EVT cells demonstrated rapid migration and invasion when placed in Matrigel droplets.

TABLE 2 Emerging Trophoblastic Organoid Models.

Author	Date	Source	Direction of differentiation	Advantage	Trophoblastic specific criteria
Margherita Y. Turco et al.	2018	VCT	EVT	To study human placental development and to study the interaction between the local and systemic maternal environment of the trophoblast	Yes
Sandra Haider et al.	2018	CTB	STB and HLA-G-EVT	To summarize the formation of trophoblast progenitor cells and differentiated subtypes in the 3D direction	Yes
Jian-Hua Qin et al.	2022	hiPSC	Trophoblast progenitor cells, STB and EVT	3D placental models combine bioengineering strategies with developmental principles	Yes
Rowan M Karvas et al.	2022	Naïve hPSCs	CTB, STB and EVT	An accessible 3D model system of the developing placenta and its susceptibility to emerging pathogens is provided	Yes

This organoid culture system offers a unique experimental model for studying the development, function, and interaction between trophoblast cells and the local and systemic maternal environment of the human placenta. It effectively addresses the limitations of previous models and allows for the exploration of various aspects of placental biology and pathology in a more physiological context.

4.4 Advantages and limitations of trophoblast organoids

This study provides a convenient and efficient system for studying various aspects of the placenta, including trophoblast differentiation pathways and interactions with other cell types. Additionally, 3D organoid models offer significant advantages over 2D cell culture as they allow for the modeling of specific cell-cell interactions and mechanical cues that arise from the structural complexity during early placental formation. Moreover, the creation of CTB-ORGs opens up opportunities for clinical *in vitro* drug studies. In the future, investigating trophoblast cell-like organoid cultures under pathological pregnancy conditions, such as preeclampsia, could help us understand potential mechanisms associated with related diseases and advance our knowledge of these disorders. Table 2 presents a summary of the trophoblast organoid models discussed earlier, indicating their sources and differentiation directions. Additionally, it provides a brief overview of the advantages associated with each model. This allows researchers to choose different experimental models based on their specific experimental requirements.

However, it is important to acknowledge the limitations and shortcomings of CTB-ORGs. One notable challenge is the misplacement of CTB and STB in organoids compared to placental villus. CTB spontaneously fuse in the center of organoids to form ENDOU, GCM1, and hCG^{+} STB, while there is a gradual decrease in cell proliferation from the outer edges of the organoids to the center. Overcoming this problem would open up more possibilities for studying the initiation of syncretization of trophoblast cells and uncovering the physiological functions of the placenta. Additionally, it should be noted that current trophoblast cell-like organoid tissues are exclusively derived from primordial placental tissue, which raises ethical and legal concerns and limits their applicability in potential diseases. Therefore, in order to broaden the scope and relevance of trophoblast cell organoid research, further investigations on the utilization of whole placental tissue to create similar organoids are necessary, although this will undoubtedly pose a difficult challenge.

5 Placenta explants

Explant from the human placenta is commonly utilized for studying cell proliferation and differentiation (Orendi et al., 2011), as well as placental transporters and metabolic enzyme studies (Lee et al., 2013). These explants are typically categorized into two groups. Explants from normal pregnancies are employed to investigate the impact of external factors on tissue function, as well as to compare normal pregnancy tissues of the same gestational age with explants from placentas affected by known pathologies (e.g., preeclampsia and intrauterine growth restriction) (Miller et al., 2005; Mehendale et al., 2007). While both early and late placentas can be used to study functions related to chorionic trophoblast cells, the early placenta cultures are specifically used to investigate chorionic EVT differentiation and invasion as they better maintain complete functionality. Additionally, unlike primary cells, the placental tissue used for culturing the explant cannot undergo freezing or thawing.

Depending on the purpose of the study, chorionic explants are cultured under different conditions. For instance, during early gestation, chorionic explants are typically cultured at the bottom of a well or embedded in an insert with a polycarbonate film underneath. On the other hand, during late gestation, chorionic explants are cultured at the bottom of a well, free-suspended, and then free-floating chorionic villus can be suspended in culture on styrene blocks or through a mesh support (Sooranna et al., 1999; Simán et al., 2001; Matalon et al., 2005; Toro et al., 2014).

In vitro culture of placental villus explants is commonly performed under static conditions. However, it is important to note that static placental villus explant culture differs significantly from the *in vivo* situation. *In vivo*, trophoblast cells invade the spiral arteries, leading to vascular end dilation. Additionally, free-floating placental villus adapt to fluid shear stresses caused by placental perfusion of maternal plasma and blood. Therefore, it is necessary to establish functional and indigenous chorionic villus explants. In a study by Kupper et al. (2021), a milder and simpler flow culture method for placental villus explants was established as an alternative

to the commonly used static method. The study simulated the perfusion of the interchorionic space using an *in vitro* flow system, mimicking the intrauterine environment. The explant was positioned in a chamber to avoid direct exposure to the flow of medium and only passed through the top. The flow rate of the chorionic explant was set at 1 mL/min (Burton et al., 2009; Wang and Zhao, 2010). By analyzing the effect of the blood flow system on the activity and structural integrity of placental tissues using unbiased morphological and biochemical parameters, the study demonstrated the benefits of culturing tissues under flow conditions. The data showed a higher tendency of tissue disintegration in static cultured tissue compared to flow cultured tissue.

In both early and late pregnancy tissues, the STB undergoes progressive degeneration, believed to be driven by apoptosis (Palmer et al., 1997; Sooranna et al., 1999; Simán et al., 2001). However, Kupper et al. (2021) discovered that apoptosis increased in static cultured tissues after 48 h, but this degradation appeared to decrease or at least remain at the same level after flow culture. There are two advantages to flow-cultured explants: first, the placental vascular endothelial cells within the explants remain intact, and second, there are fewer vesicular structures on the chorionic surface of explants cultured under flow conditions. The use of placental explants cultured under flow conditions enables the analysis of the fetal-maternal interface, aiding in the understanding of various pregnancy pathologies such as preeclampsia. Additionally, it can be utilized for early pregnancy placental tissue culture and to simulate different pregnancy conditions by altering the experimental conditions.

6 Isolated placental perfusion models

Many studies involving the placenta cannot be directly conducted in humans due to ethical issues. Although animal experiments provide some reference significance, it is challenging to fully extrapolate their results to humans. To address this problem, the isolated placenta perfusion model was proposed. This model, initially suggested by Panigel et al. (1967), involves connecting the umbilical vein and umbilical artery supplying the same placental leaflet through a perfusion tube to establish fetal collateral circulation. Additionally, the perfusion tube is inserted into the stump of the spiral artery to establish maternal collateral circulation. This model has been further improved by Schneider et al. (1972) and Miller et al. (1985), eventually evolving into the mature isolated placenta perfusion model.

To preserve the intact placenta, we collected it for lavage. We ligated the umbilical vein that supplies the same placental leaflet to the branch of the umbilical artery. Then, we inserted tubes through puncture to establish fetal circulation in that placental leaflet. We ensured that the amount of perfusion at the end of the umbilical artery was equal to the amount of outflow at the end of the umbilical vein, indicating no leakage of the placental leaflet. Next, we removed the excess placental tissue and inserted two perfusion tubes 2–3 mm into the chorionic gap on the maternal side of the placenta to establish maternal circulation. Once the isolated placental perfusion model was established, we oxygenated the maternal-side perfusate with a mixture of 95% O_2 and 5% CO_2. Additionally, we inflated the fetus with a mixture of 95% N_2 and 5% CO_2 to simulate the *in vivo* state of maternal blood and fetal umbilical artery blood. Typically, the loss of fetal collateral perfusate does not exceed 2–4 mL/min, indicating the successful establishment of the cycle (Mathiesen et al., 2010).

In vitro placental perfusion models have been developed in various laboratories to facilitate research on the human placenta. These models have been used to study placental transport of nutrients and exogenous substances (Lee et al., 2018; Warth et al., 2019; Kurosawa et al., 2020), immune factors (Jain et al., 2014), trophoblast responses to infectious agents (Desforges et al., 2018), toxic substances (Bongaerts et al., 2021), and endogenous substances (Eshkoli et al., 2013). However, there are limitations to these models. The complexity of the perfusion system makes it difficult to establish and standardize, limiting widespread use. Additionally, although the isolated placenta is tested under near-physiological conditions, there are some differences compared to *in vivo* conditions, such as enzyme activity, number of transporters, and damage caused by ischemia and hypoxia during the preparation process. Despite these shortcomings, *ex vivo* placental perfusion remains a popular choice among researchers as the classical method to study placental function. Future studies should aim to gain a deeper understanding of the factors affecting *ex vivo* placental perfusion in order to develop a model that closely resembles the *in vivo* environment.

7 Comparison between trophoblast cell models and organoid models

CTB-ORGs and TSCs are valuable tools for gaining further insight into human placental development. Human trophoblast stem cells are obtained from the by-products of the blastocyst or early gestational placenta and can be cultured for extended periods or induced to differentiate into stem cell transplants or EVT. Additionally, trophoblast cell-like organs are derived from the placenta during early pregnancy and form chorionic structures comprised of proliferative VCTs that naturally transform into multinucleated STB. Under specific culture conditions, these organs readily promote differentiation into EVT. Both trophoblast-like organs and trophoblast stem cells originate from the chorionic cell trophoblast and differentiate into EVT or STB.

Both models have been reported to meet the following criteria for characterizing the trophoblast in early pregnancy *in vivo*: 1) expression of typical trophoblast markers; 2) unique features of human leukocyte antigen (HLA) class I molecules; 3) expression of microRNAs (miRNAs) from chromosome 19 cluster (C19MC); and 4) methylation of the ELF5 promoter. However, there are also notable differences between the two models, as reported by Megan A. Sheridan et al. TSCs resemble cells at the bottom of the cell column of EVT origin and do not readily undergo STB differentiation. On the other hand, organoids exhibit similarities to VCT and undergo spontaneous STB differentiation. A key characteristic of human trophoblast cells is that VCT and STB are human leukocyte antigen HLA null, while EVT expresses HLA-C, HLA-G, and HLA-E molecules. Trophoblast-like organoids retain these HLA expressions *in vivo*. Trophoblast stem cells, however, express only classical HLA-A and HLA-B molecules and maintain their expression even after EVT differentiation, while also upregulating HLA-G. Furthermore, the HLA expression of trophoblast stem cells in the 3D environment

differs from that in the 2D environment. Therefore, trophoblast stem cells are more suitable for studies in the 2D environment, whereas trophoblast cell-like organoids are better suited for the 3D environment (Sheridan et al., 2021).

8 Conclusion and prospects

The human placenta is commonly used for *in vitro* studies due to its easy availability post-delivery. Various *in vitro* methods and experimental models have been established to investigate placental function. The trophoblast cell model and the trophoblast organoid model serve as effective *in vitro* models for studying the trophoblast and placenta from 2D and 3D perspectives, respectively. The acquisition of trophoblast stem cells not only provides a source for studying physiological changes in placental cells during pregnancy but also plays a crucial role in constructing cell and organoid models. Additionally, the establishment of placental trophoblast cellular organoids offers a reliable platform to explore maternal-fetal interactions during pregnancy and visualize physiological and pathological changes in 3D. Furthermore, the placenta explant and placenta isolated perfusion models serve as valuable *in vitro* models for studying the trophoblast and placenta from both 2D and 3D perspectives. These models, which closely mimic physiological conditions, have also significantly contributed to the study of various diseases' physiological models.

Although many of them are organoid and stem cell models derived from trophoblast cells and chorionic villus explants, the advancement of technology will lead to a better understanding of the placenta as a transient organ. As a result, placental organoids and *in vitro* models of the placenta will become increasingly common and play a significant role in addressing various illnesses and challenges encountered during pregnancy.

Author contributions

XL: Writing–original draft, Writing–review and editing. HH: Writing–review and editing. YS: Writing–review and editing. LB: Writing–review and editing. GW: Writing–review and editing. QL: Writing–review and editing. WY: Writing–original draft, Writing–review and editing.

Funding

The author(s) declare financial support was received for the research, authorship, and/or publication of this article. This project was funded by Natural Science Foundation of Shandong (ZR2022MH195 ZR2023MH211, and X2023116), and the Graduate Student Research Grant from Weifang Medical University.

Conflict of interest

The authors declare that the research was conducted in the absence of any commercial or financial relationships that could be construed as a potential conflict of interest.

Publisher's note

All claims expressed in this article are solely those of the authors and do not necessarily represent those of their affiliated organizations, or those of the publisher, the editors and the reviewers. Any product that may be evaluated in this article, or claim that may be made by its manufacturer, is not guaranteed or endorsed by the publisher.

References

Aggarwal, R., Jain, A. K., Mittal, P., Kohli, M., Jawanjal, P., and Rath, G. (2019). Association of pro- and anti-inflammatory cytokines in preeclampsia. *J. Clin. Lab. Anal.* 33 (4), e22834. doi:10.1002/jcla.22834

Albrecht, E. D., and Pepe, G. J. (2020). Regulation of uterine spiral artery remodeling: a review. *Reprod. Sci.* 27 (10), 1932–1942. doi:10.1007/s43032-020-00212-8

Amini, P., Wilson, R., Wang, J., Tan, H., Yi, L., Koeblitz, W. K., et al. (2019). Progesterone and cAMP synergize to inhibit responsiveness of myometrial cells to pro-inflammatory/pro-labor stimuli. *Mol. Cell Endocrinol.* 479, 1–11. doi:10.1016/j.mce.2018.08.005

Amita, M., Adachi, K., Alexenko, A. P., Sinha, S., Schust, D. J., Schulz, L. C., et al. (2013). Complete and unidirectional conversion of human embryonic stem cells to trophoblast by BMP4. *Proc. Natl. Acad. Sci. U. S. A.* 110 (13), E1212–E1221. doi:10.1073/pnas.1303094110

Andoh-Noda, T., Akamatsu, W., Miyake, K., Kobayashi, T., Ohyama, M., Kurosawa, H., et al. (2017). Differential X chromosome inactivation patterns during the propagation of human induced pluripotent stem cells. *Keio J. Med.* 66 (1), 1–8. doi:10.2302/kjm.2016-0015-OA

Anvarian, Z., Mykytyn, K., Mukhopadhyay, S., Pedersen, L. B., and Christensen, S. T. (2019). Cellular signalling by primary cilia in development, organ function and disease. *Nat. Rev. Nephrol.* 15 (4), 199–219. doi:10.1038/s41581-019-0116-9

Author Anyonoums (2019). Measuring PIGF speeds up pre-eclampsia diagnosis. *Drug Ther. Bull.* 57 (9), 132. doi:10.1136/dtb.2019.000053

Baribault, H., and Kemler, R. (1989). Embryonic stem cell culture and gene targeting in transgenic mice. *Mol. Biol. Med.* 6 (6), 481–492.

Barker, N., Ridgway, R. A., van Es, J. H., van de Wetering, M., Begthel, H., van den Born, M., et al. (2009). Crypt stem cells as the cells-of-origin of intestinal cancer. *Nature* 457 (7229), 608–611. doi:10.1038/nature07602

Barrera, D., Chirinos, M., and García-Becerra, R. (2008). Mecanismos de regulación de la síntesis y secreción de la gonadotropina coriónica humana (hCG) durante el embarazo [Mechanism of regulation of synthesis and secretion of human chorionic gonadotropin (hCG) during pregnancy]. *Rev. Invest. Clin.* 60 (2), 124–132.

Bentin-Ley, U., Horn, T., Sjögren, A., Sorensen, S., Falck Larsen, J., and Hamberger, L. (2000). Ultrastructure of human blastocyst-endometrial interactions *in vitro*. *J. Reprod. Fertil.* 120 (2), 337–350. doi:10.1530/jrf.0.1200337

Beristain, A. G., Zhu, H., and Leung, P. C. (2011). Regulated expression of ADAMTS-12 in human trophoblastic cells: a role for ADAMTS-12 in epithelial cell invasion? *PLoS One* 6 (4), e18473. doi:10.1371/journal.pone.0018473

Bernardo, A. S., Faial, T., Gardner, L., Niakan, K. K., Ortmann, D., Senner, C. E., et al. (2011). BRACHYURY and CDX2 mediate BMP-induced differentiation of human and mouse pluripotent stem cells into embryonic and extraembryonic lineages. *Cell Stem Cell* 9 (2), 144–155. doi:10.1016/j.stem.2011.06.015

Bongaerts, E., Aengenheister, L., Dugershaw, B. B., Manser, P., Roeffaers, M. B. J., Ameloot, M., et al. (2021). Label-free detection of uptake, accumulation, and translocation of diesel exhaust particles in *ex vivo* perfused human placenta. *J. Nanobiotechnology* 19 (1), 144. doi:10.1186/s12951-021-00886-5

Brkić, J., Dunk, C., O'Brien, J., Fu, G., Nadeem, L., Wang, Y. L., et al. (2018). MicroRNA-218-5p promotes endovascular trophoblast differentiation and spiral artery remodeling. *Mol. Ther.* 26 (9), 2189–2205. doi:10.1016/j.ymthe.2018.07.009

Burton, G. J., Woods, A. W., Jauniaux, E., and Kingdom, J. C. (2009). Rheological and physiological consequences of conversion of the maternal spiral arteries for uteroplacental blood flow during human pregnancy. *Placenta* 30 (6), 473–482. doi:10.1016/j.placenta.2009.02.009

Castel, G., and David, L. (2022). Induction of human trophoblast stem cells. *Nat. Protoc.* 17 (12), 2760–2783. doi:10.1038/s41596-022-00744-0

Castel, G., Meistermann, D., Bretin, B., Firmin, J., Blin, J., Loubersac, S., et al. (2020). Induction of human trophoblast stem cells from somatic cells and pluripotent stem cells. *Cell Rep.* 33 (8), 108419. doi:10.1016/j.celrep.2020.108419

Chen, L., Sun, F., Li, M., Qian, J., Du, M., Li, D., et al. (2021). Decreased level of Eomes+dCD8+ T cells with altered function might be associated with miscarriage. *Reproduction* 162 (2), 107–115. doi:10.1530/REP-20-0639

Cheng, J. C., Gao, Y., Chen, J., Meng, Q., and Fang, L. (2022). EGF promotes human trophoblast cell invasion by downregulating CTGF expression via PI3K/AKT signaling. *Reproduction* 165 (1), 113–122. doi:10.1530/REP-22-0247

Cheong, M. L., Wang, L. J., Chuang, P. Y., Chang, C. W., Lee, Y. S., Lo, H. F., et al. (2015). A positive feedback loop between glial cells missing 1 and human chorionic gonadotropin (hCG) regulates placental hCGβ expression and cell differentiation. *Mol. Cell Biol.* 36 (1), 197–209. doi:10.1128/MCB.00655-15

Chiu, Y. H., and Chen, H. (2016). GATA3 inhibits GCM1 activity and trophoblast cell invasion. *Sci. Rep.* 6, 21630. doi:10.1038/srep21630

Chuva de Sousa Lopes, S. M., Roelen, B. A. J., Lawson, K. A., and Zwijsen, A. (2022). The development of the amnion in mice and other amniotes. *Philos. Trans. R. Soc. Lond B Biol. Sci.* 377 (1865), 20210258. doi:10.1098/rstb.2021.0258

Cindrova-Davies, T., and Sferruzzi-Perri, A. N. (2022). Human placental development and function. *Semin. Cell Dev. Biol.* 131, 66–77. doi:10.1016/j.semcdb.2022.03.039

Cinkornpumin, J. K., Kwon, S. Y., Guo, Y., Hossain, I., Sirois, J., Russett, C. S., et al. (2020). Naive human embryonic stem cells can give rise to cells with a trophoblast-like transcriptome and methylome. *Stem Cell Rep.* 15 (1), 198–213. doi:10.1016/j.stemcr.2020.06.003

Conover, C. A., and Oxvig, C. (2023). The pregnancy-associated plasma protein-A (PAPP-A) story. *Endocr. Rev.*, bnad017. doi:10.1210/endrev/bnad017

Corrò, C., Novellasdemunt, L., and Li, V. S. W. (2020). A brief history of organoids. *Am. J. Physiol. Cell Physiol.* 319 (1), C151–C165. doi:10.1152/ajpcell.00120.2020

Covarrubias, A., Aguilera-Olguín, M., Carrasco-Wong, I., Pardo, F., Díaz-Astudillo, P., and Martín, S. S. (2023). Feto-placental unit: from development to function. *Adv. Exp. Med. Biol.* 1428, 1–29. Erratum in: Adv Exp Med Biol. 2023;1428:C1. PMID: 37466767. doi:10.1007/978-3-031-32554-0_1

Crowe, A., and Keelan, J. A. (2012). Development of a model for functional studies of ABCG2 (breast cancer resistance protein) efflux employing a standard BeWo clone (B24). *Assay. Drug Dev. Technol.* 10 (5), 476–484. doi:10.1089/adt.2011.441

Cui, K., Chen, T., Zhu, Y., Shi, Y., Guo, Y., and Qin, J. (2022). Engineering placenta-like organoids containing endogenous vascular cells from human-induced pluripotent stem cells. *Bioeng. Transl. Med.* 8 (1), e10390. doi:10.1002/btm2.10390

Das, P., Ezashi, T., Schulz, L. C., Westfall, S. D., Livingston, K. A., and Roberts, R. M. (2007). Effects of fgf2 and oxygen in the bmp4-driven differentiation of trophoblast from human embryonic stem cells. *Stem Cell Res.* 1 (1), 61–74. doi:10.1016/j.scr.2007.09.004

Desforges, M., Rogue, A., Pearson, N., Rossi, C., Olearo, E., Forster, R., et al. (2018). Vitro human placental studies to support adenovirus-mediated VEGF-dδnδc maternal gene therapy for the treatment of severe early-onset fetal growth restriction. *Hum. Gene Ther. Clin. Dev.* 29 (1), 10–23. doi:10.1089/humc.2017.090

Dong, C., Beltcheva, M., Gontarz, P., Zhang, B., Popli, P., Fischer, L. A., et al. (2020). Derivation of trophoblast stem cells from naïve human pluripotent stem cells. *Elife* 9, e52504. doi:10.7554/eLife.52504

Dong, C., and Theunissen, T. W. (2022). Generating trophoblast stem cells from human naïve pluripotent stem cells. *Methods Mol. Biol.* 2416, 91–104. doi:10.1007/978-1-0716-1908-7_7

Douglas, G. C., and King, B. F. (1989). Isolation of pure villous cytotrophoblast from term human placenta using immunomagnetic microspheres. *J. Immunol. Methods* 119 (2), 259–268. doi:10.1016/0022-1759(89)90405-5

Enders, A. C. (1995). Transition from lacunar to villous stage of implantation in the macaque, including establishment of the trophoblastic shell. *Acta Anat. (Basel)* 152 (3), 151–169. doi:10.1159/000147694

Eshkoli, T., Holcberg, G., Bronfenmacher, B., Amash, A., Huleihel, M., and Erez, O. (2013). Perfusion with magnesium sulfate increases sFlt-1 secretion only in the fetal side of placenta of women with preeclampsia. *J. Matern. Fetal Neonatal Med.* 26 (2), 116–122. doi:10.3109/14767058.2012.722725

Evans, M. J., and Kaufman, M. H. (1981). Establishment in culture of pluripotential cells from mouse embryos. *Nature* 292 (5819), 154–156. doi:10.1038/292154a0

Evseenko, D. A., Paxton, J. W., and Keelan, J. A. (2006). ABC drug transporter expression and functional activity in trophoblast-like cell lines and differentiating primary trophoblast. *Am. J. Physiol. Regul. Integr. Comp. Physiol.* 290 (5), R1357–R1365. doi:10.1152/ajpregu.00630.2005

Ezashi, T., Das, P., and Roberts, R. M. (2005). Low O2 tensions and the prevention of differentiation of hES cells. *Proc. Natl. Acad. Sci. U. S. A.* 102 (13), 4783–4788. doi:10.1073/pnas.0501283102

Ezashi, T., Telugu, B. P., and Roberts, R. M. (2012). Model systems for studying trophoblast differentiation from human pluripotent stem cells. *Cell Tissue Res.* 349 (3), 809–824. doi:10.1007/s00441-012-1371-2

Gearhart, J. (1998). New potential for human embryonic stem cells. *Science* 282 (5391), 1061–1062. doi:10.1126/science.282.5391.1061

Gerbaud, P., Murthi, P., Guibourdenche, J., Guimiot, F., Sarazin, B., Evain-Brion, D., et al. (2019). Study of human T21 placenta suggests a potential role of mesenchymal spondin-2 in placental vascular development. *Endocrinology* 160 (3), 684–698. doi:10.1210/en.2018-00826

Gruenwald, P. (1977). The development of the placental lobular pattern in the human. Review and reinterpretation of the material. *Obstet. Gynecol.* 49 (6), 728–732.

Gude, N. M., Roberts, C. T., Kalionis, B., and King, R. G. (2004). Growth and function of the normal human placenta. *Thromb. Res.* 114 (5-6), 397–407. doi:10.1016/j.thromres.2004.06.038

Guilbert, L. J., Winkler-Lowen, B., Sherburne, R., Rote, N. S., Li, H., and Morrish, D. W. (2002). Preparation and functional characterization of villous cytotrophoblasts free of syncytial fragments. *Placenta* 23 (2-3), 175–183. doi:10.1053/plac.2001.0756

Hagen, M. W., and Hinds, M. T. (2019). Static spatial growth restriction micropatterning of endothelial colony forming cells influences their morphology and gene expression. *PLoS One* 14 (6), e0218197. doi:10.1371/journal.pone.0218197

Haider, S., Meinhardt, G., Saleh, L., Fiala, C., Pollheimer, J., and Knöfler, M. (2016). Notch1 controls development of the extravillous trophoblast lineage in the human placenta. *Proc. Natl. Acad. Sci. U. S. A.* 113 (48), E7710–E7719. doi:10.1073/pnas.1612335113

Hempstock, J., Cindrova-Davies, T., Jauniaux, E., and Burton, G. J. (2004). Endometrial glands as a source of nutrients, growth factors and cytokines during the first trimester of human pregnancy: a morphological and immunohistochemical study. *Reprod. Biol. Endocrinol.* 2, 58. doi:10.1186/1477-7827-2-58

Hofbauer, P., Jahnel, S. M., Papai, N., Giesshammer, M., Deyett, A., Schmidt, C., et al. (2021). Cardioids reveal self-organizing principles of human cardiogenesis. *Cell* 184 (12), 3299–3317.e22. doi:10.1016/j.cell.2021.04.034

Horii, M., Bui, T., Touma, O., Cho, H. Y., and Parast, M. M. (2019). An improved two-step protocol for trophoblast differentiation of human pluripotent stem cells. *Curr. Protoc. Stem Cell Biol.* 50 (1), e96. doi:10.1002/cpsc.96

Horii, M., Li, Y., Wakeland, A. K., Pizzo, D. P., Nelson, K. K., Sabatini, K., et al. (2016). Human pluripotent stem cells as a model of trophoblast differentiation in both normal development and disease. *Proc. Natl. Acad. Sci. U. S. A.* 113 (27), E3882–E3891. doi:10.1073/pnas.1604747113

Huppertz, B. (2008). The anatomy of the normal placenta. *J. Clin. Pathol.* 61 (12), 1296–1302. doi:10.1136/jcp.2008.055277

Huppertz, B. (2018). The critical role of abnormal trophoblast development in the etiology of preeclampsia. *Curr. Pharm. Biotechnol.* 19 (10), 771–780. doi:10.2174/1389201019666180427110547

Huppertz, B., Frank, H. G., Reister, F., Kingdom, J., Korr, H., and Kaufmann, P. (1999). Apoptosis cascade progresses during turnover of human trophoblast: analysis of villous cytotrophoblast and syncytial fragments *in vitro*. *Lab. Invest.* 79 (12), 1687–1702.

Ikeda, K., Utoguchi, N., Tsutsui, H., Yamaue, S., Homemoto, M., Nakao, E., et al. (2011). *In vitro* approaches to evaluate placental drug transport by using differentiating JEG-3 human choriocarcinoma cells. *Basic Clin. Pharmacol. Toxicol.* 108 (2), 138–145. doi:10.1111/j.1742-7843.2010.00634.x

Illsley, N. P., DaSilva-Arnold, S. C., Zamudio, S., Alvarez, M., and Al-Khan, A. (2020). Trophoblast invasion: lessons from abnormally invasive placenta (placenta accreta). *Placenta* 102, 61–66. doi:10.1016/j.placenta.2020.01.004

Jain, A., Ezashi, T., Roberts, R. M., and Tuteja, G. (2017). Deciphering transcriptional regulation in human embryonic stem cells specified towards a trophoblast fate. *Sci. Rep.* 7 (1), 17257. doi:10.1038/s41598-017-17614-5

Jain, A., Schneider, H., Aliyev, E., Soydemir, F., Baumann, M., Surbek, D., et al. (2014). Hypoxic treatment of human dual placental perfusion induces a preeclampsia-like inflammatory response. *Lab. Invest.* 94 (8), 873–880. doi:10.1038/labinvest.2014.76

Jeyarajah, M. J., Jaju Bhattad, G., Kelly, R. D., Baines, K. J., Jaremek, A., Yang, F. P., et al. (2022). The multifaceted role of GCM1 during trophoblast differentiation in the human placenta. *Proc. Natl. Acad. Sci. U. S. A.* 119 (49), e2203071119. Epub 2022 Nov 28. Erratum in: Proc Natl Acad Sci U S A. 2023 Feb 7;120(6):e2300603120. doi:10.1073/pnas.2203071119

Jin, F., Liu, W., Cheng, G., Cai, S., Yin, T., and Diao, L. (2023). The function of decidua natural killer cells in physiology and pathology of pregnancy. *Am. J. Reprod. Immunol.* 90 (3), e13755. doi:10.1111/aji.13755

Karvas, R. M., Khan, S. A., Verma, S., Yin, Y., Kulkarni, D., Dong, C., et al. (2022). Stem-cell-derived trophoblast organoids model human placental development and susceptibility to emerging pathogens. *Cell Stem Cell* 29 (5), 810–825.e8. doi:10.1016/j.stem.2022.04.004

Karvas, R. M., Yang, Y., Ezashi, T., Schust, D. J., Roberts, R. M., and Schulz, L. C. (2018). ITGA1 is upregulated in response to oxygen over time in a BMP4 model of trophoblast. *Mol. Reprod. Dev.* 85 (8-9), 738–739. doi:10.1002/mrd.23047

Kidder, B. L. (2020). Simultaneous derivation of embryonic and trophoblast stem cells from mouse blastocysts. *Methods Mol. Biol.* 2117, 235–241. doi:10.1007/978-1-0716-0301-7_14

Kishimoto, K., Shimada, A., Shinohara, H., Takahashi, T., Yamada, Y., Higuchi, Y., et al. (2021). Establishment of novel common marmoset embryonic stem cell lines under various conditions. *Stem Cell Res.* 53, 102252. doi:10.1016/j.scr.2021.102252

Kliman, H. J., Nestler, J. E., Sermasi, E., Sanger, J. M., and Strauss, J. F., 3rd (1986). Purification, characterization, and *in vitro* differentiation of cytotrophoblasts from human term placentae. *Endocrinology* 118 (4), 1567–1582. doi:10.1210/endo-118-4-1567

Kobayashi, N., Okae, H., Hiura, H., Kubota, N., Kobayashi, E. H., Shibata, S., et al. (2022). The microRNA cluster C19MC confers differentiation potential into trophoblast lineages upon human pluripotent stem cells. *Nat. Commun.* 13 (1), 3071. doi:10.1038/s41467-022-30775-w

Koel, M., Võsa, U., Krjutškov, K., Einarsdottir, E., Kere, J., Tapanainen, J., et al. (2017). Optimizing bone morphogenic protein 4-mediated human embryonic stem cell differentiation into trophoblast-like cells using fibroblast growth factor 2 and transforming growth factor-β/activin/nodal signalling inhibition. *Reprod. Biomed. Online* 35 (3), 253–263. doi:10.1016/j.rbmo.2017.06.003

Kohler, P. O., and Bridson, W. E. (1971). Isolation of hormone-producing clonal lines of human choriocarcinoma. *J. Clin. Endocrinol. Metab.* 32 (5), 683–687. doi:10.1210/jcem-32-5-683

Kolatorova, L., Vitku, J., Suchopar, J., Hill, M., and Parizek, A. (2022). Progesterone: a steroid with wide range of effects in physiology as well as human medicine. *Int. J. Mol. Sci.* 23 (14), 7989. doi:10.3390/ijms23147989

Kuijk, E. W., Du Puy, L., Van Tol, H. T., Oei, C. H., Haagsman, H. P., Colenbrander, B., et al. (2008). Differences in early lineage segregation between mammals. *Dev. Dyn.* 237 (4), 918–927. doi:10.1002/dvdy.21480

Kunath, T., Yamanaka, Y., Detmar, J., MacPhee, D., Caniggia, I., Rossant, J., et al. (2014). Developmental differences in the expression of FGF receptors between human and mouse embryos. *Placenta* 35 (12), 1079–1088. doi:10.1016/j.placenta.2014.09.008

Kupper, N., Pritz, E., Siwetz, M., Guettler, J., and Huppertz, B. (2021). Placental villous explant culture 2.0: flow culture allows studies closer to the *in vivo* situation. *Int. J. Mol. Sci.* 22 (14), 7464. doi:10.3390/ijms22147464

Kurosawa, K., Chiba, K., Noguchi, S., Nishimura, T., and Tomi, M. (2020). Development of a pharmacokinetic model of transplacental transfer of metformin to predict *in vivo* fetal exposure. *Drug Metab. Dispos.* 48 (12), 1293–1302. doi:10.1124/dmd.120.000127

Lai, T. Y., Cao, J., Ou-Yang, P., Tsai, C. Y., Lin, C. W., Chen, C. C., et al. (2022). Different methods of detaching adherent cells and their effects on the cell surface expression of Fas receptor and Fas ligand. *Sci. Rep.* 12 (1), 5713. doi:10.1038/s41598-022-09605-y

Lau, K. Y. C., Rubinstein, H., Gantner, C. W., Hadas, R., Amadei, G., Stelzer, Y., et al. (2022). Mouse embryo model derived exclusively from embryonic stem cells undergoes neurulation and heart development. *Cell Stem Cell* 29 (10), 1445–1458.e8. doi:10.1016/j.stem.2022.08.013

Lee, C. Q., Gardner, L., Turco, M., Zhao, N., Murray, M. J., Coleman, N., et al. (2016). What is trophoblast? A combination of criteria define human first-trimester trophoblast. *Stem Cell Rep.* 6 (2), 257–272. doi:10.1016/j.stemcr.2016.01.006

Lee, H. J., and Ormandy, C. J. (2012). Elf5, hormones and cell fate. *Trends Endocrinol. Metab.* 23 (6), 292–298. doi:10.1016/j.tem.2012.02.006

Lee, N., Hebert, M. F., Wagner, D. J., Easterling, T. R., Liang, C. J., Rice, K., et al. (2018). Organic cation transporter 3 facilitates fetal exposure to metformin during pregnancy. *Mol. Pharmacol.* 94 (4), 1125–1131. doi:10.1124/mol.118.112482

Lee, Y., Jung, J., Cho, K. J., Lee, S. K., Park, J. W., Oh, I. H., et al. (2013). Increased SCF/c-kit by hypoxia promotes autophagy of human placental chorionic plate-derived mesenchymal stem cells via regulating the phosphorylation of mTOR. *J. Cell Biochem.* 114 (1), 79–88. doi:10.1002/jcb.24303

Lee, Y., Kim, K. R., McKeon, F., Yang, A., Boyd, T. K., Crum, C. P., et al. (2007). A unifying concept of trophoblastic differentiation and malignancy defined by biomarker expression. *Hum. Pathol.* 38 (7), 1003–1013. doi:10.1016/j.humpath.2006.12.012

Leiser, R., and Kaufmann, P. (1994). Placental structure: in a comparative aspect. *Exp. Clin. Endocrinol.* 102 (3), 122–134. doi:10.1055/s-0029-1211275

Lester, L. B., Kuo, H. C., Andrews, L., Nauert, B., and Wolf, D. P. (2004). Directed differentiation of rhesus monkey ES cells into pancreatic cell phenotypes. *Reprod. Biol. Endocrinol.* 2, 42. doi:10.1186/1477-7827-2-42

Li, Y., Moretto-Zita, M., Soncin, F., Wakeland, A., Wolfe, L., Leon-Garcia, S., et al. (2013). BMP4-directed trophoblast differentiation of human embryonic stem cells is mediated through a ΔNp63+ cytotrophoblast stem cell state. *Development* 140 (19), 3965–3976. doi:10.1242/dev.092155

Li, Z., Kurosawa, O., and Iwata, H. (2019). Establishment of human trophoblast stem cells from human induced pluripotent stem cell-derived cystic cells under micromesh culture. *Stem Cell Res. Ther.* 10 (1), 245. doi:10.1186/s13287-019-1339-1

Liang, C. Y., Wang, L. J., Chen, C. P., Chen, L. F., Chen, Y. H., and Chen, H. (2010). GCM1 regulation of the expression of syncytin 2 and its cognate receptor MFSD2A in human placenta. *Biol. Reprod.* 83 (3), 387–395. doi:10.1095/biolreprod.110.083915

Liu, D., Gao, Q., Wang, Y., and Xiong, T. (2022). Placental dysfunction: the core mechanism for poor neurodevelopmental outcomes in the offspring of preeclampsia pregnancies. *Placenta* 126, 224–232. doi:10.1016/j.placenta.2022.07.014

Ma, Y., Hu, Y., and Ma, J. (2023). Animal models of the placenta accreta spectrum: current status and further perspectives. *Front. Endocrinol. (Lausanne)* 14, 1118168. doi:10.3389/fendo.2023.1118168

Maenhoudt, N., Defraye, C., Boretto, M., Jan, Z., Heremans, R., Boeckx, B., et al. (2020). Developing organoids from ovarian cancer as experimental and preclinical models. *Stem Cell Rep.* 14 (4), 717–729. doi:10.1016/j.stemcr.2020.03.004

Maltepe, E., and Fisher, S. J. (2015). Placenta: the forgotten organ. *Annu. Rev. Cell Dev. Biol.* 31, 523–552. doi:10.1146/annurev-cellbio-100814-125620

Mark, P. J., and Waddell, B. J. (2006). P-glycoprotein restricts access of cortisol and dexamethasone to the glucocorticoid receptor in placental BeWo cells. *Endocrinology* 147 (11), 5147–5152. doi:10.1210/en.2006-0633

Marshall, E. (1998). A versatile cell line raises scientific hopes, legal questions. *Science* 282 (5391), 1014–1015. doi:10.1126/science.282.5391.1014

Martinez-Fierro, M. L., Garza-Veloz, I., Castañeda-Lopez, M. E., Wasike, D., Castruita-De la Rosa, C., Rodriguez-Sanchez, I. P., et al. (2022). Evaluation of the effect of the fibroblast growth factor type 2 (FGF-2) administration on placental gene expression in a murine model of preeclampsia induced by L-NAME. *Int. J. Mol. Sci.* 23 (17), 10129. doi:10.3390/ijms231710129

Matalon, S. T., Ornoy, A., Fishman, A., Drucker, L., and Lishner, M. (2005). The effect of 6-mercaptopurine on early human placental explants. *Hum. Reprod.* 20 (5), 1390–1397. doi:10.1093/humrep/deh721

Mathiesen, L., Mose, T., Mørck, T. J., Nielsen, J. K., Nielsen, L. K., Maroun, L. L., et al. (2010). Quality assessment of a placental perfusion protocol. *Reprod. Toxicol.* 30 (1), 138–146. doi:10.1016/j.reprotox.2010.01.006

Meadows, J. W., Pitzer, B., Brockman, D. E., and Myatt, L. (2004). Differential localization of prostaglandin E synthase isoforms in human placental cell types. *Placenta* 25 (4), 259–265. doi:10.1016/j.placenta.2003.09.004

Mehendale, R., Hibbard, J., Fazleabas, A., and Leach, R. (2007). Placental angiogenesis markers sFlt-1 and PlGF: response to cigarette smoke. *Am. J. Obstet. Gynecol.* 197 (4), 363.e1–5. doi:10.1016/j.ajog.2007.06.025

Melamed, N., Okun, N., Huang, T., Mei-Dan, E., Aviram, A., Allen, M., et al. (2023). Obesity and hypertension in pregnancy research network) and SOON (southern ontario obstetrical network) investigators. Maternal first-trimester alpha-fetoprotein and placenta-mediated pregnancy complications. *Hypertension*. doi:10.1161/HYPERTENSIONAHA.123.21568

Mele, J., Muralimanoharan, S., Maloyan, A., and Myatt, L. (2014). Impaired mitochondrial function in human placenta with increased maternal adiposity. *Am. J. Physiol. Endocrinol. Metab.* 307 (5), E419–E425. doi:10.1152/ajpendo.00025.2014

Miller, R. K., Genbacev, O., Turner, M. A., Aplin, J. D., Caniggia, I., and Huppertz, B. (2005). Human placental explants in culture: approaches and assessments. *Placenta* 26 (6), 439–448. doi:10.1016/j.placenta.2004.10.002

Miller, R. K., Wier, P. J., Maulik, D., and di Sant'Agnese, P. A. (1985). Human placenta *in vitro*: characterization during 12 h of dual perfusion. *Contrib. Gynecol. Obstet.* 13, 77–84.

Mischler, A., Karakis, V., Mahinthakumar, J., Carberry, C. K., San Miguel, A., Rager, J. E., et al. (2021). Two distinct trophectoderm lineage stem cells from human pluripotent stem cells. *J. Biol. Chem.* 296, 100386. doi:10.1016/j.jbc.2021.100386

Nampoothiri, L. P., Neelima, P. S., and Rao, A. J. (2007). Proteomic profiling of forskolin-induced differentiated BeWo cells: an *in-vitro* model of cytotrophoblast differentiation. *Reprod. Biomed. Online* 14 (4), 477–487. doi:10.1016/s1472-6483(10)60896-6

Nishioka, N., Inoue, K., Adachi, K., Kiyonari, H., Ota, M., Ralston, A., et al. (2009). The Hippo signaling pathway components Lats and Yap pattern Tead4 activity to distinguish mouse trophectoderm from inner cell mass. *Dev. Cell* 16 (3), 398–410. doi:10.1016/j.devcel.2009.02.003

O'Brien, K., and Wang, Y. (2023). The placenta: a maternofetal interface. *Annu. Rev. Nutr.* 43, 301–325. doi:10.1146/annurev-nutr-061121-085246

Ohinata, Y., Endo, T. A., Sugishita, H., Watanabe, T., Iizuka, Y., Kawamoto, Y., et al. (2022). Establishment of mouse stem cells that can recapitulate the developmental potential of primitive endoderm. *Science* 375 (6580), 574–578. doi:10.1126/science.aay3325

Okae, H., Toh, H., Sato, T., Hiura, H., Takahashi, S., Shirane, K., et al. (2018). Derivation of human trophoblast stem cells. *Cell Stem Cell* 22 (1), 50–63.e6. doi:10.1016/j.stem.2017.11.004

Orendi, K., Kivity, V., Sammar, M., Grimpel, Y., Gonen, R., Meiri, H., et al. (2011). Placental and trophoblastic *in vitro* models to study preventive and therapeutic agents for preeclampsia. *Placenta* 32 (Suppl. l), S49–S54. doi:10.1016/j.placenta.2010.11.023

Orso, F., Fassetta, M., Penna, E., Solero, A., De Filippo, K., Sismondi, P., et al. (2007). The AP-2alpha transcription factor regulates tumor cell migration and apoptosis. *Adv. Exp. Med. Biol.* 604, 87–95. doi:10.1007/978-0-387-69116-9_6

Paiva, P., Hannan, N. J., Hincks, C., Meehan, K. L., Pruysers, E., Dimitriadis, E., et al. (2011). Human chorionic gonadotrophin regulates FGF2 and other cytokines produced

by human endometrial epithelial cells, providing a mechanism for enhancing endometrial receptivity. *Hum. Reprod.* 26 (5), 1153–1162. doi:10.1093/humrep/der027

Palmer, M. E., Watson, A. L., and Burton, G. J. (1997). Morphological analysis of degeneration and regeneration of syncytiotrophoblast in first trimester placental villi during organ culture. *Hum. Reprod.* 12 (2), 379–382. doi:10.1093/humrep/12.2.379

Panigel, M., Pascaud, M., and Brun, J. L. (1967). Etude radioangiographique de la circulation dans les villosités et l'espace intervilleux du cotylédon placentaire humain isolé mantenu en survie paperfusion [Radioangiographic study of circulation in the villi and intervillous space of isolated human placental cotyledon kept viable by perfusion]. *J. Physiol. Paris.* 59 (1 Suppl. l), 277.

Paolino, M., Koglgruber, R., Cronin, S. J. F., Uribesalgo, I., Rauscher, E., Harreiter, J., et al. (2021). RANK links thymic regulatory T cells to fetal loss and gestational diabetes in pregnancy. *Nature* 589 (7842), 442–447. doi:10.1038/s41586-020-03071-0

Pattillo, R. A., and Gey, G. O. (1968). The establishment of a cell line of human hormone-synthesizing trophoblastic cells *in vitro*. *Cancer Res.* 28 (7), 1231–1236.

Pijnenborg, R., Vercruysse, L., and Hanssens, M. (2006). The uterine spiral arteries in human pregnancy: facts and controversies. *Placenta* 27 (9-10), 939–958. doi:10.1016/j.placenta.2005.12.006

Piskun, A., Dmytro, K., Honcharenko, O., Rud, V., and Klimas, L. (2022). PLACENTAL BIOMARKERS: PP13, VEGF IN DIAGNOSTICS OF EARLY AND LATE PREECLAMPSIA. *Wiad. Lek.* 75 (12), 3041–3045. doi:10.36740/WLek202212125

Quenby, S., Mountfield, S., Cartwright, J. E., Whitley, G. S., and Vince, G. (2004). Effects of low-molecular-weight and unfractionated heparin on trophoblast function. *Obstet. Gynecol.* 104 (2), 354–361. doi:10.1097/01.AOG.0000128902.84876.d4

Roberts, R. M., Ezashi, T., Sheridan, M. A., and Yang, Y. (2018). Specification of trophoblast from embryonic stem cells exposed to BMP4. *Biol. Reprod.* 99 (1), 212–224. doi:10.1093/biolre/ioy070

Roberts, R. M., Ezashi, T., Temple, J., Owen, J. R., Soncin, F., and Parast, M. M. (2022). The role of BMP4 signaling in trophoblast emergence from pluripotency. *Cell Mol. Life Sci.* 79 (8), 447. doi:10.1007/s00018-022-04478-w

Roberts, R. M., and Fisher, S. J. (2011). Trophoblast stem cells. *Biol. Reprod.* 84 (3), 412–421. doi:10.1095/biolreprod.110.088724

Roberts, R. M., Loh, K. M., Amita, M., Bernardo, A. S., Adachi, K., Alexenko, A. P., et al. (2014). Differentiation of trophoblast cells from human embryonic stem cells: to be or not to be? *Reproduction* 147 (5), D1–D12. doi:10.1530/REP-14-0080

Rossant, J. (2008). Stem cells and early lineage development. *Cell* 132 (4), 527–531. doi:10.1016/j.cell.2008.01.039

Rossi, G., Manfrin, A., and Lutolf, M. P. (2018). Progress and potential in organoid research. *Nat. Rev. Genet.* 19 (11), 671–687. doi:10.1038/s41576-018-0051-9

Ruiz-Magaña, M. J., Llorca, T., Martinez-Aguilar, R., Abadia-Molina, A. C., Ruiz-Ruiz, C., and Olivares, E. G. (2022). Stromal cells of the endometrium and decidua: in search of a name and an identity. *Biol. Reprod.* 107 (5), 1166–1176. doi:10.1093/biolre/ioac158

Sagrillo-Fagundes, L., Clabault, H., Laurent, L., Hudon-Thibeault, A. A., Salustiano, E. M., Fortier, M., et al. (2016). Human primary trophoblast cell culture model to study the protective effects of melatonin against hypoxia/reoxygenation-induced disruption. *J. Vis. Exp.* (113), 54228. doi:10.3791/54228

Saha, B., Ganguly, A., Home, P., Bhattacharya, B., Ray, S., Ghosh, A., et al. (2020). TEAD4 ensures postimplantation development by promoting trophoblast self-renewal: an implication in early human pregnancy loss. *Proc. Natl. Acad. Sci. U. S. A.* 117 (30), 17864–17875. doi:10.1073/pnas.2002449117

Sato, M., and Nakano, T. (2001). Embryonic stem cell. *Intern Med.* 40 (3), 195–200. doi:10.2169/internalmedicine.40.195

Sato, T., Vries, R. G., Snippert, H. J., van de Wetering, M., Barker, N., Stange, D. E., et al. (2009). Single Lgr5 stem cells build crypt-villus structures *in vitro* without a mesenchymal niche. *Nature* 459 (7244), 262–265. doi:10.1038/nature07935

Sato, Y. (2020). Endovascular trophoblast and spiral artery remodeling. *Mol. Cell Endocrinol.* 503, 110699. doi:10.1016/j.mce.2019.110699

Schneider, H., Panigel, M., and Dancis, J. (1972). Transfer across the perfused human placenta of antipyrine, sodium and leucine. *Am. J. Obstet. Gynecol.* 114 (6), 822–828. doi:10.1016/0002-9378(72)90909-x

Schneider, R., Borges, M., and Kadyrov, M. (2011). Forskolin-induced differentiation of BeWo cells stimulates increased tumor growth in the chorioallantoic membrane (CAM) of the Turkey (*Meleagris gallopavo*) egg. *Ann. Anat.* 193 (3), 220–223. doi:10.1016/j.aanat.2011.02.007

Seetharam, A. S., Vu, H. T. H., Choi, S., Khan, T., Sheridan, M. A., Ezashi, T., et al. (2022). The product of BMP-directed differentiation protocols for human primed pluripotent stem cells is placental trophoblast and not amnion. *Stem Cell Rep.* 17 (6), 1289–1302. doi:10.1016/j.stemcr.2022.04.014

Seong, J., Frias-Aldeguer, J., Holzmann, V., Kagawa, H., Sestini, G., Heidari Khoei, H., et al. (2022). Epiblast inducers capture mouse trophectoderm stem cells *in vitro* and pattern blastoids for implantation *in utero*. *Cell Stem Cell* 29 (7), 1102–1118.e8. doi:10.1016/j.stem.2022.06.002

Shao, X., Cao, G., Chen, D., Liu, J., Yu, B., Liu, M., et al. (2021). Placental trophoblast syncytialization potentiates macropinocytosis via mTOR signaling to adapt to reduced amino acid supply. *Proc. Natl. Acad. Sci. U. S. A.* 118 (3), e2017092118. doi:10.1073/pnas.2017092118

Shao, X., Yu, W., Yang, Y., Wang, F., Yu, X., Wu, H., et al. (2022). The mystery of the life tree: the placentas. *Biol. Reprod.* 107 (1), 301–316. doi:10.1093/biolre/ioac095

Sheridan, M. A., Fernando, R. C., Gardner, L., Hollinshead, M. S., Burton, G. J., Moffett, A., et al. (2020). Establishment and differentiation of long-term trophoblast organoid cultures from the human placenta. *Nat. Protoc.* 15 (10), 3441–3463. doi:10.1038/s41596-020-0381-x

Sheridan, M. A., Zhao, X., Fernando, R. C., Gardner, L., Perez-Garcia, V., Li, Q., et al. (2021). Characterization of primary models of human trophoblast. *Development* 148 (21), dev199749. doi:10.1242/dev.199749

Shiokawa, S., Iwashita, M., Akimoto, Y., Nagamatsu, S., Sakai, K., Hanashi, H., et al. (2002). Small guanosine triphospatase RhoA and Rho-associated kinase as regulators of trophoblast migration. *J. Clin. Endocrinol. Metab.* 87 (12), 5808–5816. doi:10.1210/jc.2002-020376

Shiverick, K. T., King, A., Frank, H., Whitley, G. S., Cartwright, J. E., and Schneider, H. (2001). Cell culture models of human trophoblast II: trophoblast cell lines--a workshop report. *Placenta* 22 (Suppl. A), S104–S106. doi:10.1053/plac.2001.0647

Silasi, M., Cohen, B., Karumanchi, S. A., and Rana, S. (2010). Abnormal placentation, angiogenic factors, and the pathogenesis of preeclampsia. *Obstet. Gynecol. Clin. North Am.* 37 (2), 239–253. doi:10.1016/j.ogc.2010.02.013

Simán, C. M., Sibley, C. P., Jones, C. J., Turner, M. A., and Greenwood, S. L. (2001). The functional regeneration of syncytiotrophoblast in cultured explants of term placenta. *Am. J. Physiol. Regul. Integr. Comp. Physiol.* 280 (4), R1116–R1122. doi:10.1152/ajpregu.2001.280.4.R1116

Soncin, F., Morey, R., Bui, T., Requena, D. F., Cheung, V. C., Kallol, S., et al. (2022). Derivation of functional trophoblast stem cells from primed human pluripotent stem cells. *Stem Cell Rep.* 17 (6), 1303–1317. doi:10.1016/j.stemcr.2022.04.013

Sonderegger, S., Husslein, H., Leisser, C., and Knöfler, M. (2007). Complex expression pattern of Wnt ligands and frizzled receptors in human placenta and its trophoblast subtypes. *Placenta.* 28,S97–S102. doi:10.1016/j.placenta.2006.11.003

Sonderegger, S., Pollheimer, J., and Knöfler, M. (2010). Wnt signalling in implantation, decidualisation and placental differentiation--review. *Placenta* 31 (10), 839–847. doi:10.1016/j.placenta.2010.07.011

Sooranna, S. R., Oteng-Ntim, E., Meah, R., Ryder, T. A., and Bajoria, R. (1999). Characterization of human placental explants: morphological, biochemical and physiological studies using first and third trimester placenta. *Hum. Reprod.* 14 (2), 536–541. doi:10.1093/humrep/14.2.536

Staff, A. C., Fjeldstad, H. E., Fosheim, I. K., Moe, K., Turowski, G., Johnsen, G. M., et al. (2022). Failure of physiological transformation and spiral artery atherosis: their roles in preeclampsia. *Am. J. Obstet. Gynecol.* 226 (2S), S895–S906. doi:10.1016/j.ajog.2020.09.026

Stamatiadis, P., Cosemans, G., Boel, A., Menten, B., De Sutter, P., Stoop, D., et al. (2022). TEAD4 regulates trophectoderm differentiation upstream of CDX2 in a GATA3-independent manner in the human preimplantation embryo. *Hum. Reprod.* 37 (8), 1760–1773. doi:10.1093/humrep/deac138

Stenman, U. H., Tiitinen, A., Alfthan, H., and Valmu, L. (2006). The classification, functions and clinical use of different isoforms of HCG. *Hum. Reprod. Update* 12 (6), 769–784. doi:10.1093/humupd/dml029

Tan, B., Zhou, C., Zang, X., Zhao, X., Xiao, L., Zeng, J., et al. (2023). Integrated analysis of DNA methylation and gene expression in porcine placental development. *Int. J. Mol. Sci.* 24 (6), 5169. doi:10.3390/ijms24065169

Tan, J. P., Liu, X., and Polo, J. M. (2022). Establishment of human induced trophoblast stem cells via reprogramming of fibroblasts. *Nat. Protoc.* 17 (12), 2739–2759. doi:10.1038/s41596-022-00742-2

Tanaka, S., Kunath, T., Hadjantonakis, A. K., Nagy, A., and Rossant, J. (1998). Promotion of trophoblast stem cell proliferation by FGF4. *Science* 282 (5396), 2072–2075. doi:10.1126/science.282.5396.2072

Tannetta, D. S., Sargent, I. L., Linton, E. A., and Redman, C. W. (2008). Vitamins C and E inhibit apoptosis of cultured human term placenta trophoblast. *Placenta* 29 (8), 680–690. doi:10.1016/j.placenta.2008.04.009

Thomson, J. A., Itskovitz-Eldor, J., Shapiro, S. S., Waknitz, M. A., Swiergiel, J. J., Marshall, V. S., et al. (1998). Embryonic stem cell lines derived from human blastocysts. *Science* 282 (5391), 1145–1147. Erratum in: Science 1998 Dec 4;282(5395):1827. doi:10.1126/science.282.5391.1145

Toro, A. R., Maymó, J. L., Ibarbalz, F. M., Pérez-Pérez, A., Maskin, B., Faletti, A. G., et al. (2014). Leptin is an anti-apoptotic effector in placental cells involving p53 downregulation. *PLoS One* 9 (6), e99187. Erratum in: PLoS One. 2014;9(9):e107632. doi:10.1371/journal.pone.0099187

Townsend, R., Khalil, A., Premakumar, Y., Allotey, J., Snell, K. I. E., Chan, C., et al. (2019). IPPIC Network. Prediction of pre-eclampsia: review of reviews. *Ultrasound Obstet. Gynecol.* 54 (1), 16–27. doi:10.1002/uog.20117

Turco, M. Y., Gardner, L., Kay, R. G., Hamilton, R. S., Prater, M., Hollinshead, M. S., et al. (2018). Trophoblast organoids as a model for maternal-fetal interactions during human placentation. *Nature* 564 (7735), 263–267. doi:10.1038/s41586-018-0753-3

Vargas, A., Moreau, J., Landry, S., LeBellego, F., Toufaily, C., Rassart, E., et al. (2009). Syncytin-2 plays an important role in the fusion of human trophoblast cells. *J. Mol. Biol.* 392 (2), 301–318. doi:10.1016/j.jmb.2009.07.025

Vento-Tormo, R., Efremova, M., Botting, R. A., Turco, M. Y., Vento-Tormo, M., and Meyer, K. B. (2018). Single-cell reconstruction of the early maternal-fetal interface in humans. *Nature* 563 (7731), 347–353. doi:10.1038/s41586-018-0698-6

Walker, W. H., Fitzpatrick, S. L., Barrera-Saldaña, H. A., Resendez-Perez, D., and Saunders, G. F. (1991). The human placental lactogen genes: structure, function, evolution and transcriptional regulation. *Endocr. Rev.* 12 (4), 316–328. doi:10.1210/edrv-12-4-316

Wang, F., Zhang, L., Zhang, F., Wang, J., Wang, Y., and Man, D. (2020). First trimester serum PIGF is associated with placenta accreta. *Placenta* 101, 39–44. doi:10.1016/j.placenta.2020.08.023

Wang, J., Ding, J., Zhang, S., Chen, X., Yan, S., Zhang, Y., et al. (2021). Decreased USP2a expression inhibits trophoblast invasion and associates with recurrent miscarriage. *Front. Immunol.* 12, 717370. doi:10.3389/fimmu.2021.717370

Wang, L. J., Chen, C. P., Lee, Y. S., Ng, P. S., Chang, G. D., Pao, Y. H., et al. (2022). Functional antagonism between ΔNp63α and GCM1 regulates human trophoblast stemness and differentiation. *Nat. Commun.* 13 (1), 1626. doi:10.1038/s41467-022-29312-6

Wang, Y., and Zhao, S. (2010). *Vascular biology of the placenta*. San Rafael (CA): Morgan & Claypool Life Sciences.

Warth, B., Preindl, K., Manser, P., Wick, P., Marko, D., and Buerki-Thurnherr, T. (2019). Transfer and metabolism of the xenoestrogen zearalenone in human perfused placenta. *Environ. Health Perspect.* 127 (10), 107004. doi:10.1289/EHP4860

Wei, Y., Wang, T., Ma, L., Zhang, Y., Zhao, Y., Lye, K., et al. (2021). Efficient derivation of human trophoblast stem cells from primed pluripotent stem cells. *Sci. Adv.* 7 (33), eabf4416. doi:10.1126/sciadv.abf4416

Wheeler, M. L., and Oyen, M. L. (2021). Bioengineering approaches for placental research. *Ann. Biomed. Eng.* 49 (8), 1805–1818. doi:10.1007/s10439-020-02714-7

Wilson, H. V. (1907). A NEW METHOD BY WHICH SPONGES MAY BE ARTIFICIALLY REARED. *Science* 25 (649), 912–915. doi:10.1126/science.25.649.912

Wójtowicz, A. K., Honkisz, E., Zięba-Przybylska, D., Milewicz, T., and Kajta, M. (2011). Effects of two isomers of DDT and their metabolite DDE on CYP1A1 and AhR function in human placental cells. *Pharmacol. Rep.* 63 (6), 1460–1468. doi:10.1016/s1734-1140(11)70710-1

Wolfe, M. W. (2006). Culture and transfection of human choriocarcinoma cells. *Methods Mol. Med.* 121, 229–239. doi:10.1385/1-59259-983-4:227

Wu, S., Liu, H., Zhou, M., Shang, Y., Luo, L., Chen, J., et al. (2022). The miR-410-5p/ITGA6 axis participates in the pathogenesis of recurrent abortion by regulating the biological function of trophoblast. *J. Reprod. Immunol.* 152, 103647. doi:10.1016/j.jri.2022.103647

Wu, Y., Tran, T., Dwabe, S., Sarkissyan, M., Kim, J., Nava, M., et al. (2017). A83-01 inhibits TGF-β-induced upregulation of Wnt3 and epithelial to mesenchymal transition in HER2-overexpressing breast cancer cells. *Breast Cancer Res. Treat.* 163 (3), 449–460. doi:10.1007/s10549-017-4211-y

Xie, M., Li, Y., Meng, Y. Z., Xu, P., Yang, Y. G., Dong, S., et al. (2022). Uterine natural killer cells: a rising star in human pregnancy regulation. *Front. Immunol.* 13, 918550. doi:10.3389/fimmu.2022.918550

Xu, R. H., Chen, X., Li, D. S., Li, R., Addicks, G. C., Glennon, C., et al. (2002). BMP4 initiates human embryonic stem cell differentiation to trophoblast. *Nat. Biotechnol.* 20 (12), 1261–1264. doi:10.1038/nbt761

Xu, X., Zhou, Y., and Wei, H. (2020). Roles of HLA-G in the maternal-fetal immune microenvironment. *Front. Immunol.* 11, 592010. doi:10.3389/fimmu.2020.592010

Yabe, S., Alexenko, A. P., Amita, M., Yang, Y., Schust, D. J., Sadovsky, Y., et al. (2016). Comparison of syncytiotrophoblast generated from human embryonic stem cells and from term placentas. *Proc. Natl. Acad. Sci. U. S. A.* 113 (19), E2598–E2607. doi:10.1073/pnas.1601630113

Yang, L., Semmes, E. C., Ovies, C., Megli, C., Permar, S., Gilner, J. B., et al. (2022). Innate immune signaling in trophoblast and decidua organoids defines differential antiviral defenses at the maternal-fetal interface. *Elife* 11, e79794. doi:10.7554/eLife.79794

Yang, Y., Adachi, K., Sheridan, M. A., Alexenko, A. P., Schust, D. J., Schulz, L. C., et al. (2015). Heightened potency of human pluripotent stem cell lines created by transient BMP4 exposure. *Proc. Natl. Acad. Sci. U. S. A.* 112 (18), E2337–E2346. doi:10.1073/pnas.1504778112

Ye, Z., Kilic, G., Dabelsteen, S., Marinova, I. N., Thøfner, J. F. B., Song, M., et al. (2022). Characterization of TGF-β signaling in a human organotypic skin model reveals that loss of TGF-βRII induces invasive tissue growth. *Sci. Signal* 15 (761), eabo2206. doi:10.1126/scisignal.abo2206

Zhang, X., and Wei, H. (2021). Role of decidual natural killer cells in human pregnancy and related pregnancy complications. *Front. Immunol.* 12, 728291. doi:10.3389/fimmu.2021.728291

Zhao, Z., Zhu, D., Liu, Y., Zhou, Q., Qiu, J., Xu, C., et al. (2022). Embryotoxic effects of tribromophenol on early post-implantation development of mouse embryos *in vitro*. *Environ. Sci. Pollut. Res. Int.* 29 (8), 12085–12099. doi:10.1007/s11356-021-16614-3

Zhou, Y., Gormley, M. J., Hunkapiller, N. M., Kapidzic, M., Stolyarov, Y., Feng, V., et al. (2013). Reversal of gene dysregulation in cultured cytotrophoblasts reveals possible causes of preeclampsia. *J. Clin. Invest.* 123 (7), 2862–2872. Epub 2013 Jun 24. Erratum in: J Clin Invest. 2013 Oct 1;123(10):4541. doi:10.1172/JCI66966

frontiers | Frontiers in Cell and Developmental Biology

TYPE Original Research
PUBLISHED 16 November 2023
DOI 10.3389/fcell.2023.1239448

Check for updates

OPEN ACCESS

EDITED BY
Ahmed Balboula,
University of Missouri, United States

REVIEWED BY
Inchul Choi,
Chungnam National University, Republic of Korea
Jiawei Sun,
Massachusetts General Hospital, Harvard Medical School, United States

*CORRESPONDENCE
Sang-Hwan Hyun,
shhyun@cbu.ac.kr

RECEIVED 13 June 2023
ACCEPTED 01 November 2023
PUBLISHED 16 November 2023

CITATION
Lee J, Cai L, Kim M, Choi H, Oh D, Jawad A, Lee E and Hyun S-H (2023), Tetraploid embryo aggregation produces high-quality blastocysts with an increased trophectoderm in pigs. *Front. Cell Dev. Biol.* 11:1239448. doi: 10.3389/fcell.2023.1239448

COPYRIGHT
© 2023 Lee, Cai, Kim, Choi, Oh, Jawad, Lee and Hyun. This is an open-access article distributed under the terms of the Creative Commons Attribution License (CC BY). The use, distribution or reproduction in other forums is permitted, provided the original author(s) and the copyright owner(s) are credited and that the original publication in this journal is cited, in accordance with accepted academic practice. No use, distribution or reproduction is permitted which does not comply with these terms.

Tetraploid embryo aggregation produces high-quality blastocysts with an increased trophectoderm in pigs

Joohyeong Lee[1], Lian Cai[2,3,4], Mirae Kim[2,3], Hyerin Choi[2,3], Dongjin Oh[2,3], Ali Jawad[2,3], Eunsong Lee[5] and Sang-Hwan Hyun[2,3,4]*

[1]Department of Companion Animal Industry, College of Healthcare and Biotechnology, Semyung University, Jecheon, Republic of Korea, [2]Laboratory of Veterinary Embryology and Biotechnology (VETEMBIO), Veterinary Medical Center and College of Veterinary Medicine, Chungbuk National University, Cheongju, Republic of Korea, [3]Institute of Stem Cell and Regenerative Medicine (ISCRM), Chungbuk National University, Cheongju, Republic of Korea, [4]Graduate School of Veterinary Biosecurity and Protection, Chungbuk National University, Cheongju, Republic of Korea, [5]College of Veterinary Medicine, Kangwon National University, Chuncheon, Republic of Korea

Tetraploid complementation is an ideal method for demonstrating the differentiation potential of pluripotent stem cells. In this study, we selected the most efficient tetraploid production method for porcine embryos and investigated whether tetraploid blastomere aggregation could enhance the quality of tetraploid embryos. Three methods were investigated to produce tetraploid embryos: First, tetraploid embryos were produced using electro-fusion of two-cell stage parthenogenetic blastomere (FUTP). Second, somatic cell was injected into the mature oocyte and fused to produce tetraploid embryos. Third, oocytes were matured with Cytochalasin B (CB) for the late 22 h of *in vitro* maturation to inhibit the first polar body (PB1). Following that, non-PB1 oocytes were treated with CB for 4 h after parthenogenetic activation. There was no significant difference in the blastocyst development rate and tetraploid production rate of the embryos produced through the three methods. However, FUTP-derived blastocysts had a significantly lower percentage of apoptotic cells compared to other methods. The developmental competence of embryos, expression of trophectoderm cell marker genes, and distribution of YAP1 protein were investigated in tetraploid embryos produced using the FUTP method. The FUTP method most effectively prevented apoptosis during porcine tetraploid embryo formation. Tetraploid aggregation-derived blastocysts have a high proportion of trophectoderm with increased expression of the CDX2 mRNA and high YAP1 intensity. High-quality blastocysts derived from a tetraploid

Abbreviations: AI/TI, Anaphase I/telophase I; CB, Cytochalasin B; CoCs, Cumulus oocyte complexes; ES, Embryonic stem cells; GV, Germinal vesicles; iPS, Induced pluripotent stem cells; IVC, *In vitro* culture medium; MI, Metaphase I; MII, Metaphase II; PA, parthenogenetic activation; PHA-L, Phytohemagglutinin-L; PZM-3, Porcine zygote medium; qRT-PCR, Quantitative real-time polymerase chain reaction; TE, Trophectoderm; TS, Tyrode's Solution.

embryo aggregation can serve as suitable source material for testing the differentiation potential of pluripotent stem cells for blastocyst complementation in pigs.

KEYWORDS

tetraploid, blastomere aggregation, trophectoderm, parthenogenetic activation, pig

1 Introduction

Blastocyst complementation refers to the injection of cells into a blastocoel. This technique allows the production of chimeric animals (Wu et al., 2016), which have the potential to be used as an unlimited source of organs (Oldani et al., 2017). Tetraploid complementation is a method that ideally proves the differentiation potential of pluripotent stem cells such as embryonic stem (ES) or induced pluripotent stem (iPS) cells. Pluripotent stem cells can differentiate into cells of all tissues except placental tissue. When pluripotent stem cells are combined with embryos capable of differentiating into placental tissue, they can be grown into whole animals. Tetraploid complementation allows pluripotent stem cells to be produced as a complete organism by supplementing embryos capable of forming placental tissue. Previous studies have shown that the mouse naïve pluripotent stem cells can pass the tetraploid complementation test (Zhou et al., 2015; Li et al., 2017). However, mammalian species other than rats and mice have not yet succeeded in producing offspring using the tetraploid complementation method, and pluripotency of the injected cells has not been demonstrated.

Animal models for human disease are essential in medical research. Pigs are more anatomically and physiologically similar to humans than small rodents such as mice; therefore, pigs are an attractive option for modeling human disease (Walters and Prather, 2013). Recent advances in genetic engineering have facilitated the rapid expansion of pig models for the study of human disease (Hou et al., 2022). However, the production of ES cells, representative pluripotent stem cells, has not been established in pigs (Brevini et al., 2010; Vassiliev et al., 2010; Hou et al., 2016). The published cell lines usually do not meet the stringent criteria for pluripotency and are frequently called "ES-like" cells. Besides studies on the production of pluripotent cell lines in pigs, extensive investigations are required to enhance the quality of blastocyst used for tetraploid complementation.

In general, embryos produced *in vitro* are inferior to *in vivo*-derived embryos (Holm et al., 2002; Stokes et al., 2005). Pig embryos used in assisted reproductive technology are mostly derived from *in vitro*-derived oocytes. The low-quality *in vitro*-derived embryos often leads to the low-quality donor blastocysts used for tetraploid complementation. In addition, the total number of cells in a tetraploid blastocyst is lower than that in a diploid blastocyst (Ishiguro et al., 2005; Kawaguchi et al., 2009; Park et al., 2011). Therefore, a method to overcome these disadvantages must be investigated to produce good-quality embryos.

Several researchers have studied various methods of tetraploid embryo production. The most commonly used method in mammalian species is the production of blastomere of a two-cell stage embryo by fusing (Curnow et al., 2000; Krivokharchenko et al., 2002; Atikuzzaman et al., 2011; Kong and Liu, 2019). A method for producing tetraploid embryos by inserting a somatic cell nucleus into an intact metaphase II (MII) oocyte followed by activation and Cytochalasin B (CB) treatment has been introduced (Fu et al., 2016). Another method for producing tetraploid embryos is to inhibit the extrusion of the first polar body (PB1) and second polar body (PB2) through CB treatment during maturation and after activation (Lin et al., 2019). It is necessary to determine which of these methods for producing tetraploid embryos in pigs is the most effective.

The embryo aggregation method is widely used in various mammals to improve production efficiency by compensating for developmental deficits of *in vitro*-derived embryos (Lee et al., 2022). This strategy consists of placing two or more zona pellucida (ZP)-free embryos in close proximity during *in vitro* culture so that the blastomeres self-organize to form one single blastocyst of improved quality (Savy et al., 2021). These improvements are due to "epigenetic compensation" between higher cell numbers, aggregate structures, or both early in development (Boiani et al., 2003; Eckardt and McLaughlin, 2004). The blastomere aggregation method can be an effective tool to improve low-quality tetraploid embryos. However, whether aggregated tetraploid porcine blastocysts have characteristics such as morphology, blastocyst cell composition, and expression of transcription factors remains unknown.

In this study, we selected the most efficient tetraploid production method for porcine embryos and investigated whether blastomere aggregation could improve the quality of tetraploid embryos. Our findings help gain insight into the evolution and regulation of pluripotency across mammalian species.

2 Materials and methods

2.1 Ethics statement and animal information

The animal experiments were reviewed, and the experimental protocol was approved by the Committee on Ethics of Animal Experiments of the Chungbuk National University (Permit Number: CBNUA-1733-22-01). The animals employed in this study were treated in compliance with the standard operating procedures set forth by the Institutional Animal Care and Use Committee. The specific anesthesia and analgesia protocols are delineated in the following subsections. The authors of this article further confirm that the experiments, statistical analyses, and information presented here adhere to the recommendations outlined in the guidelines of Animal Research: Reporting of *in vivo* Experiments.

2.2 Culture media

All chemicals were purchased from Sigma-Aldrich Corporation (St. Louis, MO, United States) unless otherwise stated. Oocytes were matured in Medium-199 (Invitrogen, Grand Island, NY,

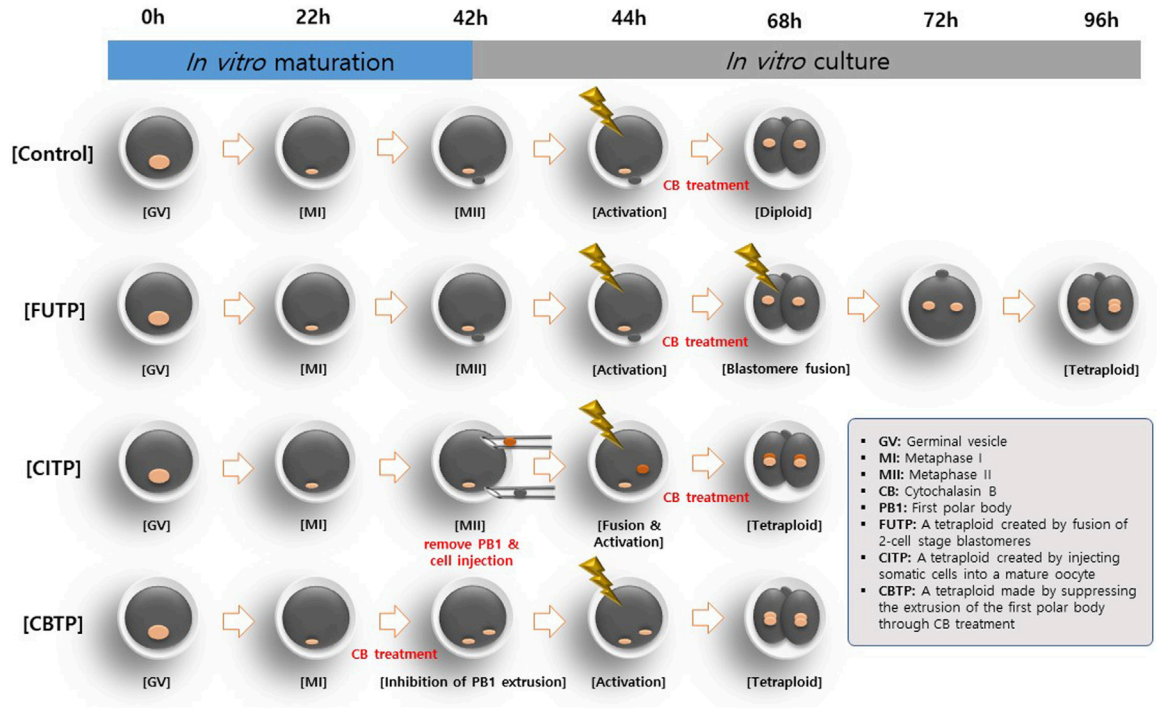

FIGURE 1
Different methods for generating tetraploid embryos in pigs. Tetraploid embryos were produced by electro-fusion of two-cell stage PA embryos (FUTP). The diploid somatic cell was injected into the mature oocyte and fused to produce tetraploid embryos (CITP). Oocytes were matured with CB for the late 22 h of *in vitro* maturation to inhibit the PB1. Thereafter, non-PB1 oocytes were treated with CB for 4 h after parthenogenetic activation (CBTP).

United States) supplemented with 0.91 mM pyruvate, 0.6 mM cysteine, 10 ng/mL epidermal growth factor, and 1 μg/mL insulin, and 10% (v/v) porcine follicular fluid was used as basal medium for *in vitro* maturation (IVM). Porcine zygote medium (PZM)-3 containing 0.3% (w/v) bovine serum albumin (BSA) was used as *in vitro* culture (IVC) medium. On day 4, we transferred embryos into PZM-3 droplets containing 10% fetal bovine serum (Thermo Fisher Scientific, Waltham, MA, United States).

2.3 Experimental design

In the first experiment, we evaluated the preimplantation developmental competence of embryos using three methods to produce tetraploid as shown in Figure 1: First, tetraploid embryos were produced using electro-fusion of the two-cell stage parthenogenetic activation (PA) blastomere (FUTP). Second, the diploid somatic cell (porcine ear fibroblasts) was injected into the mature oocyte and fused to produce tetraploid blastomere (CITP). Third, oocytes were matured with 5 μg/mL CB for the late 22 h of IVM to inhibit the PB1. Subsequently, non-PB1 oocytes were treated with CB for 4 h after PA (CBTP). In the second experiment, the proportion of blastocysts constructed as tetraploids were investigated by analyzing the nuclear ploidy of the blastocysts aggregated through the three tetraploid production methods. In the third experiment, the apoptotic cell rates of blastocysts were investigated according to the three methods of producing tetraploid embryos. In the fourth experiment, the diameter and surface area of blastocysts produced through embryo aggregation was calculated. In the fifth experiment, the developmental competence of embryos was investigated through the aggregation of tetraploid embryos produced by the FUTP method. In the sixth experiment, the expression of pluripotency and trophectoderm (TE) cell markers genes in aggregated embryo-derived blastocysts were investigated. In the seventh experiment, the distribution of YAP1 protein in aggregated embryo-derived blastocysts was investigated.

2.4 Oocyte collection and IVM

The IVM of oocytes was performed in the same manner as described by Lee et al. (Lee et al., 2021). The ovaries of prepubertal gilts obtained from a local abattoir were transported to the laboratory at 34°C–37°C. Cumulus oocyte complexes (COCs) were aspirated from follicles with diameters ranging from 3 to 8 mm. COCs with multiple layers of compacted cumulus cells were selected and washed three times in HEPES-buffered Tyrode's medium (TLH) containing 0.05% (w/v) polyvinyl alcohol (TLH-PVA). COCs were placed in each well of a four-well multi-dish (Nunc, Roskilde, Denmark). Each well contained 500 μL of IVM with 10 IU/mL equine chronic gonadotropin and 10 IU/mL human chorionic gonadotropin (Intervet, Boxmeer, Netherland). After 22 h, the COCs were transferred to a fresh IVM medium, without equine or human chorionic gonadotropin, and incubated for 22 h. IVM was performed at 39°C and 5% CO_2 in a humid incubator (Astec, Fukuoka, Japan). For the CBTP treatment

group, oocytes were cultured in an IVM medium supplemented with 5 μg/mL CB for the last 22 h of IVM. After IVM, COCs were denuded by gentle pipetting with 0.1% hyaluronidase.

2.5 Assessment of nuclear status of oocyte and chromosome ploidy of blastocyst

The nuclear status of oocytes was assessed in the same manner as described by Cai et al. (2022). The nuclear state of oocytes derived from the CBTP-treated group was examined. The denuded oocytes were washed thrice in TLH-PVA medium and stained with 5 μg/mL Hoechst 33,342 in TLH-PVA for 10 min. The stained oocytes were examined using an epifluorescence microscope (Nikon, Tokyo, Japan) with an ultraviolet (UV) filter (370 nm) and were classified according to the meiotic maturation stage as germinal vesicles (GV), or being in the metaphase I (MI), anaphase I/telophase I (AI/TI), or MII stage. The blastocysts derived from each treatment group were subjected to karyotyping to confirm the chromosome ploidy. Porcine blastocysts were treated with 0.4 μg/mL demecolcine for 6 h. Blastocysts were then added to a hypotonic solution (0.075 M KCl). Swollen blastocysts were fixed on a clean glass slide immersed in a fixative (acetic acid/methanol = 1:3 v/v). Chromosome spreads were stained with 10% (v/v) Giemsa before imaging.

2.6 Donor cell injection and fusion

Before the experiments, one male Jeju mini pig weighing 30–45 kg was provided *ad libitum* access to food and water and fasted for 12 h. For skin biopsies, 10 mg/kg ketamine hydrochloride (Yuhan, Seoul, Korea) was intramuscularly injected, followed by initial sedation, and respiratory anesthesia was maintained by using Isoflurane (Hana Pharm, Seoul, Korea). Skin ear tissue was recovered from three places using a 3-mm biopsy punch (Kai industries, Tokyo, Japan) and sterilized with 10% povidone iodine and 70% alcohol. Sufficient hemostasis and antibiotic ointment were applied post biopsy to prevent infection. For the CITP treatment group, porcine ear fibroblasts or cumulus cells were inserted into the MII oocyte. Porcine ear fibroblasts were cultured in Dulbecco's modified Eagle's medium F-12 (Invitrogen) supplemented with 10% (v/v) fetal bovine serum until a complete monolayer of cells was formed. A suspension of single cells was prepared by trypsinization using EDTA-trypsin and resuspending in TLH containing 0.4% (w/v) bovine serum albumin (TLH-BSA) before cell injection. IVM oocytes were incubated for 10 min in TLH-BSA medium, washed twice with fresh TLH-BSA medium, and then transferred to a droplet of TLH-BSA containing 5 μg/mL CB covered with mineral oil. The PB1 were enucleated aspiration using a 16-μm polar body biopsy pipette (sunlight Medical, FL, United States). A donor cell was inserted into the perivitelline space of an MII oocyte. The reconstituted single cell-oocyte couplets were simultaneously induced to fuse and activate through a single electrical stimulation. Fusion-activation was induced by applying an alternating current field of 2 V at 1 MHz for 2 s, followed by two pulses of 170 V/mm direct current for 30 μs using an Electro Cell Fusion Generator (LF101; NepaGene, Chiba, Japan) in a fusion-activation medium containing 280 mM mannitol, 0.05 mM $MgCl_2$, and 0.1 mM $CaCl_2$. After electrical stimulation, oocytes were transferred to TLH-BSA medium and fused oocyte was checked 30 min later. Fused oocytes were transferred to PZM-3 supplemented with 5 μg/mL CB for 4 h at 39°C temperature and in a humidified atmosphere of 5% CO_2, 5% O_2, and 90% N_2. Embryos were transferred to PZM-3 and cultured until the next step at 39°C temperature in a humidified atmosphere of 5% CO_2, 5% O_2, and 90% N_2.

2.7 PA and blastomere fusion

The PA of oocytes for FUTP and CBTP methods were performed as previously described by Lee et al. (Lee et al., 2021). Only oocytes from which the PB1 was released after IVM were selected for PA. They were placed between two wires in a 1-mm fusion chamber coated with a fusion-activation medium. Oocyte activation was stimulated with a direct current pulse of 120 V/mm for 60 μs using a Cell Fusion Generator. Electrically stimulated oocytes were transferred to PZM-3 with 5 μg/mL CB and cultured for 4 h at 39°C temperature and in a humidified atmosphere of 5% CO_2, 5% O_2, and 90% N_2. PA embryos were transferred to PZM-3 and cultured until the next step at 39 °C temperature in a humidified atmosphere of 5% CO_2, 5% O_2, and 90% N_2. To produce tetraploid embryos through the FUTP method, only embryos with evenly divided blastomeres were selected 24 h after *in vitro* culture. Two-cell stage embryos were transferred to an electro-fusion chamber coated with fusion-activation medium. The division plane of the embryo was placed horizontal to the electrode and then two pulses of 170 V/mm direct current for 30 μs were supplied using an electric cell fusion generator. After electrical stimulation, 2-cell stage embryos were transferred to PZM-3 and fusion of blastomeres was checked 30 min later.

2.8 ZP removal and blastomere aggregation

According to the experimental design, the two-cell stage PA embryos were collected 24 h after electrical activation. The collected embryos were incubated with acidic Tyrode′s Solution (TS) to remove the ZP, as previously described by Lee et al. (Lee et al., 2022). The collected embryos were incubated in 50% TS solution for 1 min, then in 100% TS solution for 30 s, and then sufficiently removed using a glass pipette. The ZP-free blastomeres were aggregated using phytohemagglutinin-L (PHA-L) (Lee et al., 2022). The blastomeres were aggregated by culturing for 20 min in an IVC medium with 15 μg/mL PHA-L. Aggregated blastomeres were transferred to PZM-3 and cultured for 144 h at 39°C in a humidified atmosphere of 5% CO_2, 5% O_2, and 90% N_2.

2.9 Evaluation of developmental competence of blastocyst and total cell count

Day 0 was regarded as the day on which PA was initiated. On day 1, cleavage formation was analyzed. Blastocyst formation was

assessed on day 7. To calculate the total cell number of blastocysts on day 7, the blastocysts were washed in TLH-PVA and fixed in 4% (v/v) paraformaldehyde in phosphate-buffered saline containing 0.05% PVA and stained for 10 min with 5 μg/mL of Hoechst-33342. Then, the blastocysts from each group were transferred to a drop of 100% glycerol on a glass slide and gently covered with a coverslip. The stained blastocysts were observed using a fluorescence microscope (Nikon, Tokyo, Japan) at ×200 magnification.

2.10 Terminal deoxynucleotidyl transferase dUTP nick-end labeling (TUNEL) assay

Analysis of apoptosis was performed as previously described by Lee et al. (Lee et al., 2022). To analyze apoptosis in blastocysts, they were fixed with 4% (v/v) paraformaldehyde for 1 h at room temperature, washed with Dulbecco's phosphate-buffered saline (DPBS) containing 0.05% PVA, and permeabilized with 0.1% (v/v) Triton X-100 in 0.1% (w/v) sodium citrate for 1 h at 20°C–25°C. After rinsing with DPBS containing 0.05% PVA, the embryos were stained with 45 μL of TUNEL-Label solution (Roche, Mannheim, Germany) supplemented with 5 μL TUNEL-Enzyme solution (Roche) for 1 h at 39°C in a dark, humidified atmosphere. Subsequently, the nuclei were stained with 5 μg/mL Hoechst-33342 for 10 min.

2.11 Diameter measurement and surface area conversion of blastocyst

Blastocysts in each group were recorded at ×2 magnification using a digital camera (DS-L3; Nikon) attached to an inverted microscope (TE-300; Nikon). The diameter of the blastocyst was measured using the ImageJ software, version 1.46 (National Institutes of Health, Bethesda, MD, United States). The surface area of the blastocyst was converted based on the diameter of the blastocyst described in Supplementary Figure S1.

2.12 Gene expression analysis via quantitative real-time polymerase chain reaction (qRT-PCR)

qRT-PCR was performed as previously described by Lee et al. (Lee et al., 2022). The relative expression of porcine pluripotency-related genes (*POU5F1*, *NANOG*, and *SOX2*) and TE markers (*CDX2*) in aggregated tetraploid blastocysts was investigated. The blastocysts were washed once in DPBS, centrifuged, and the supernatant was removed and stored at −80°C until analysis. Gene expression was analyzed using the CFX96 Touch Deep Well Real-Time PCR Detection System (BIO-RAD, Hercules, CA, United States). After mRNA extraction and cDNA synthesis, qRT-PCR was performed using 2 μL of cDNA template with 10 μL of 2X SYBR Premix Ex Taq (Takara Bio Inc., Shiga, Japan) containing primers specific to *CDX2, POU5F1, SOX2*, and *NANOG* (Supplementary Table S1). Reactions were performed for 40 cycles under the following conditions: denaturation at 95°C for 30 s, annealing at 57°C for 15 s, and extension at 72°C for 30 s. Gene expression was quantified relative to the reference gene *RN18S*. Relative quantification was based on a comparison of the threshold cycle (Ct) at a constant fluorescence intensity. Relative mRNA expression was calculated using the following equation: $R = 2^{-[\Delta Ct\ sample - \Delta Ct\ control]}$. Expression values were normalized to those of *RN18S*.

2.13 Immunofluorescence analysis

Immunofluorescence analysis was performed as previously described by Lee et al. [21]. For immunofluorescence analysis, blastocysts fixed with 4% paraformaldehyde were washed three times with phosphate-buffered saline (PBS) and permeabilized with 0.5% Triton X-100 for 30 min. Then, blastocysts were co-incubated with blocking solution (10% goat serum in PBS) and primary antibody overnight at 4°C. The primary antibodies used were anti-SOX2, anti-CDX2, and anti-YAP1, described in Supplementary Table S2. After washing three times with a washing medium (Tween 20, Triton X-100, and PBS), the blastocysts were incubated with the appropriate secondary antibodies. Secondary antibodies were applied, and the cells were incubated at 20°C–25°C for 1 h. Nuclei were stained with Hoechst-33342. The stained blastocysts were observed using a fluorescence microscope (Nikon, Tokyo, Japan) at ×200 magnification.

2.14 Statistical analysis

Statistical analysis was performed using Statistical Analysis System software (version 9.4; SAS Institute, Cary, NC, United States). In experiments 1 to 3, the standard diploid embryo generation method and three tetraploid generation methods were analyzed as independent variables. Proportions of oocytes reached MII, cleavage rate, blastocyst rate, nuclear states, and TUNEL-positive nuclei were analyzed as dependent variables. In experiments 4 to 7, the standard diploid embryo generation method, FUTP, and 3X FUTP methods were analyzed as independent variables. Proportions of cells in blastocyst, diameter of blastocyst, surface area of blastocyst, gene expression, and YAP1 intensity were analyzed as dependent variables. The data were subjected to analysis of variance (ANOVA) using a general linear model procedure. Post-hoc analyses to identify between-group differences were performed using the least significant difference test when treatments differed at a ($p < 0.05$). Percentage data were arcsine transformed prior to analysis to maintain homogeneity of variance. Results are expressed as mean ± standard error of the mean (SEM).

3 Results

3.1 Developmental competence of tetraploid embryos according to the methods of producing tetraploid

We investigated the *in vitro* developmental competence of embryos according to the tetraploid production method

TABLE 1 *In vitro* **developmental competence according to various methods for generating tetraploid embryos in pigs.**

Treatment	No. (%) of oocytes that reached MII	No. (%) of oocytes fused	No. (%) of cleaved oocytes	No. (%) of two-cell	No. (%) of blastomere fused	No. (%) of embryos developed to blastocyst/ two-cell
Control (Diploid)	910/1093 (83.5 ± 0.9)[a]	_	380/453 (75.3 ± 4.0)	283/453 (61.6 ± 4.0)[c]	_	96/122 (76.3 ± 4.7)[c]
FUTP		_			153/156 (98.1 ± 1.0)	100/153 (62.7 ± 4.5) [cd]
CITP		276/407 (68.0 ± 6.0)	190/262 (71.3 ± 2.6)	141/262 (55.9 ± 6.5) [cd]	_	84/141 (55.9 ± 6.5)[d]
CBTP	29/343 (9.2 ± 2.1)[b]	_	219/298 (72.3 ± 4.5)	157/298 (51.4 ± 3.5)[d]	_	109/157 (68.7 ± 5.4) [cd]

Ten replicates.
[a,b] Values in the same column with different superscript letters are significantly different ($p < 0.01$).
[c,d] Values in the same column with different superscript letters are significantly different ($p < 0.05$).

TABLE 2 Nuclear state of blastocysts according to various methods for generating tetraploid embryos in pigs.

Treatment	No. of blastocysts evaluated *	Nuclear states (%)			
		Haploid	Diploid	Polyploid	Tetraploid
Control (Diploid)	20	2 (10.4 ± 6.3)[a]	17 (84.6 ± 5.4)[a]	0 (0.0 ± 0.0)	1 (5.0 ± 5.0)[a]
FUTP	21	0 (0.0 ± 0.0)[b]	3 (14.0 ± 5.2)[b]	0 (0.0 ± 0.0)	18 (86.0 ± 5.2)[b]
CITP	20	0 (0.0 ± 0.0)[b]	3 (17.1 ± 7.5)[b]	1 (2.5 ± 2.5)	16 (80.4 ± 7.1)[b]
CBTP	21	0 (0.0 ± 0.0)[b]	4 (25.4 ± 8.6)[b]	0 (0.0 ± 0.0)	17 (74.6 ± 8.6)[b]

*Four replicates.
[a,b] Values in the same column with different superscript letters are significantly different ($p < 0.01$).

(Table 1). The average nuclear maturation rate of the oocytes used in control, FUTP, and CBPT was 83.5% ± 0.9%, and that of the CBTP group was 9.2% ± 2.1%. During the last 22 h of IVM, 96.7% ± 1.2% of CB-treated oocytes (CBTP) were arrested in the MI stage (Supplementary Table S3). In the CBTP group, there was no significant difference in the cleavage rate at 24 h after activation compared with that in the control group, but the ratio in the two-cell stage was significantly reduced (61.6% ± 4.0% vs. 51.4% ± 3.5%). The blastocyst development rate of the CITP group (55.9% ± 6.5%) was significantly ($p < 0.05$) lower than that of the control group (76.3% ± 4.7%), but there was no significant difference when compared to the FUTP and CBTP groups (62.7%–68.7%).

3.2 Chromosome ploidy of the blastocysts according to the methods of producing tetraploid

We analyzed the chromosome ploidy of blastocysts derived from the tetraploid production method (Table 2). The tetraploid production method groups showed a significantly ($p < 0.01$) lower diploid ratio (14.0%–25.4% vs. 84.6%) and a higher tetraploid ratio (74.6%–86.0% vs. 5.0%) than did the control group. Representative images of blastocysts and chromosome ploidy from each treatment group are shown in Figure 2.

3.3 Apoptotic cell rates of blastocysts according to the methods of producing tetraploid

Control and tetraploid blastocysts were examined for the percentage of apoptotic cells using the TUNEL assay. Representative images of blastocyst nuclei and TUNEL-positive cells from each treatment group are shown in Figure 3A. The FUTP (1.8%) group showed significantly ($p < 0.05$) lower apoptotic cell rates than did the CITP (5.3%) and CBTP (4.8%) groups, but there was no significant difference from the control group (2.6%) (Figure 3B).

3.4 Diameter and surface area of blastocysts produced through embryo aggregation

We investigated the effect of tetraploid embryo aggregation on the size of the blastocyst, and the number of cells was compared with the surface area of the blastocyst (Tables 3, 4). The 3X FUTP group showed a significantly ($p < 0.05$) larger blastocyst diameter than did the control and FUTP groups (294.4 ± 9.8 μm vs. 190.9 ± 10.3 μm vs. 199.0 ± 11.3 μm). In addition, the nucleus in the tetraploid blastocysts showed a significantly ($p < 0.05$) larger diameter than that in the control group (19.2–19.4 μm vs. 14.1 μm). The average surface area of blastocysts was converted from the diameter of blastocysts derived from each treatment group. When the surface area of the blastocyst per cell in the control group was normalized to "1", the FUTP and 3X FUTP groups were 1.43 and 1.34, respectively.

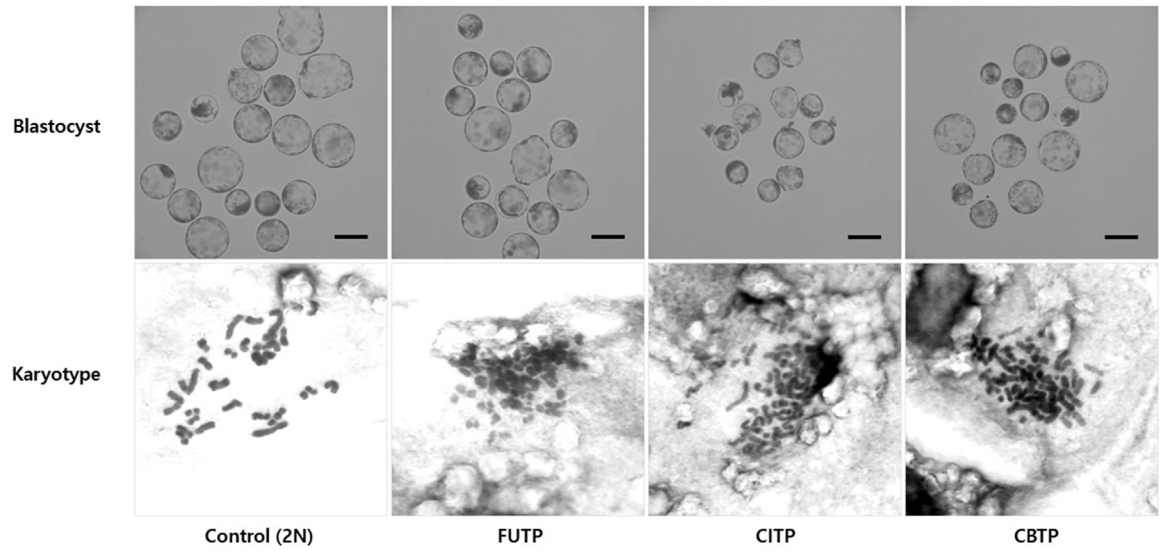

FIGURE 2
Morphology of blastocysts derived from various methods of producing tetraploid embryos. The chromosome ploidy of the blastocyst was observed at 400×, a blastocyst with about 38 chromosomes was recognized as a diploid, and a blastocyst with about 76 chromosomes as a tetraploid. Scale bar = 200 μm.

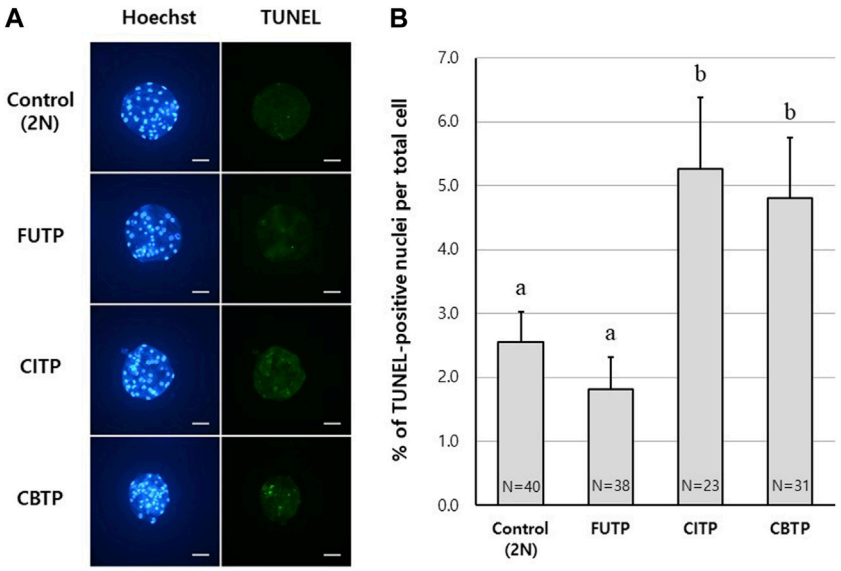

FIGURE 3
Apoptotic cell rates of blastocysts according to the methods of producing tetraploid. **(A)** Representative image of TUNEL assay according to tetraploid embryo-producing method. Scale bar = 50 μm. **(B)** Apoptotic cell index (%) according to the tetraploid embryo-producing method. N = the number of blastocysts analyzed. Data are the mean ± SEM. [a, b] Values in the same column with different superscript letters are significantly different ($p < 0.05$).

3.5 Developmental competence of aggregated tetraploid embryos

The morphological changes in the blastocyst formation process through tetraploid embryo formation and blastomere aggregation are shown in Figure 4. The FUTP-derived tetraploid-derived embryos were cultured singly (FUTP) or in aggregates of three embryos (3X FUTP). The blastocysts derived from each group were examined for the number of inner cell mass (ICM) using SOX2 immunostaining (Figure 5). The 3X FUTP group showed a significantly ($p < 0.05$) higher blastocyst development rate than did the FUTP group (77.2% ± 2.3% vs. 63.1% ± 2.9%). The 3X FUTP group showed a significantly ($p < 0.05$) higher total cell number in the blastocyst than did the control and FUTP groups (71.3% ± 3.9% vs. 39.2% ± 2.5% vs. 29.8% ± 2.1%, respectively).

TABLE 3 Effect of tetraploid blastomere aggregation on blastocyst rate, cell number, the proportion of ICM and TE cells in blastocysts.

Type of blastomere	No. (%) of embryos [aggregate] developed to blastocyst/two-cell	No. of blastocyst evaluated *	No. of total cells in blastocyst	No. of ICM in blastocyst	ICM ratio (%)	No. of TE cell in blastocyst	TE cell ratio (%)
Control (Diploid)	55/77 (71.2 ± 3.9) ^{ab}	30	39.2 ± 2.5^{a}	6.4 ± 1.0^{a}	14.7 ± 1.8^{a}	32.8 ± 1.9^{a}	85.3 ± 1.8^{a}
FUTP	43/68 (63.1 ± 2.9)^{a}	28	29.8 ± 2.1^{b}	3.1 ± 0.4^{b}	10.1 ± 1.6^{b}	26.8 ± 1.9^{a}	89.7 ± 1.6^{b}
3X FUTP	42/[57] (77.2 ± 2.3)^{b}	30	71.3 ± 3.9^{c}	5.7 ± 0.7 ^{ab}	8.2 ± 1.1^{b}	65.5 ± 3.7^{b}	92.5 ± 1.1^{b}

*Six replicates.
^{a,b,c} Values in the same column with different superscript letters are significantly different ($p < 0.05$).

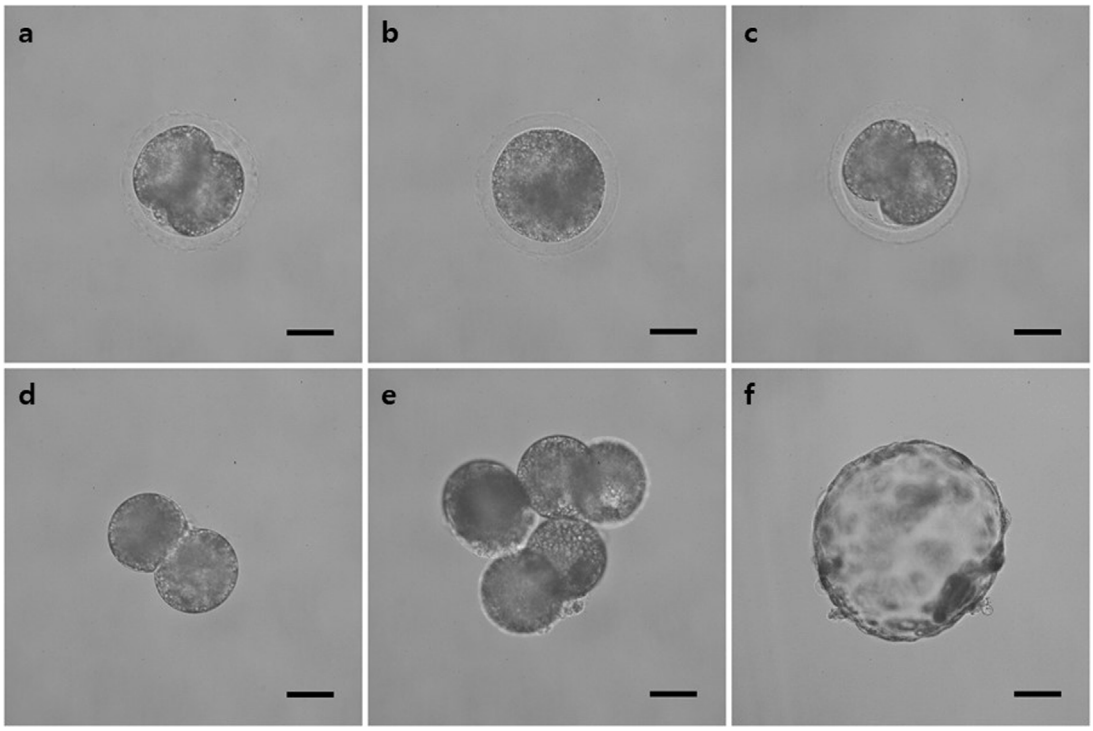

FIGURE 4
Representative image of the tetraploid blastocyst production process using the FUTP method. **(A)** Two-cell stage embryo 24 h after parthenogenetic activation; **(B)** embryo in which two blastomeres were fused through electrical stimulation; **(C)** re-cleaved embryos 24 h after fusion; **(D)** re-cleaved embryo with the zona pellucida removed; **(E)** Aggregated three re-cleaved embryos; **(F)** blastocysts of aggregated tetraploid embryos on day 7 after parthenogenetic activation.

The FUTP group showed a significantly ($p < 0.05$) lower total number of blastocyst cells than did the control group. The FUTP and 3X FUTP groups showed a significantly ($p < 0.05$) lower ICM ratio than did the control group (8.2%–10.1% vs. 14.7%) and a significantly higher TE cell ratio (89.7%–92.5% vs. 85.3%).

3.6 Expression of pluripotency and TE cell markers genes in aggregated embryo-derived blastocysts

Using RT-PCR, we investigated the relative gene expression of pluripotency markers *POU5F1*, *NANOG*, *SOX2*, and TE cell marker *CDX2* in blastocysts (Figure 6). Expression of the *CDX2* gene was significantly ($p < 0.05$) higher in the 3X FUTP group than in the control and FUTP groups. There was no significant difference in the relative expression of the pluripotency markers *POU5F1*, *NANOG*, and *SOX2* genes in all groups.

3.7 Distribution of YAP1 protein in aggregated embryo-derived blastocysts

The blastocysts derived from each treatment group were examined for YAP1 protein expression intensity in the whole blastocyst and nucleus through immunostaining (Figure 7A). The

TABLE 4 Effect of tetraploid blastomere aggregation on diameter and surface area of the blastocyst.

Type of blastomere	No. of blastocysts evaluated *	Dimeter of blastocyst (μm)	No. of blastocyst nucleus evaluated	Diameter of the blastocyst nucleus (μm)	Surface area of blastocyst ($μm^2$)	Surface area/ cell ($μm^2$)	Relative proportion[A]
Control (Diploid)	21	190.9 ± 10.3[a]	100	14.1 ± 0.3[a]	121,095 ± 13,406[a]	3,089	1
FUTP	21	199.0 ± 11.3[a]	100	19.2 ± 0.4[b]	132,356 ± 15,041[a]	4,442	1.43
3X FUTP	21	294.4 ± 9.8 [b]	100	19.4 ± 0.4[b]	278,183 ± 18,643[b]	3,902	1.34

*Five replicates.

[a,b] Values in the same column with different superscript letters are significantly different ($p < 0.05$).

[A] The relative ratio of blastocyst surface area per cell was calculated by normalizing the control to "1".

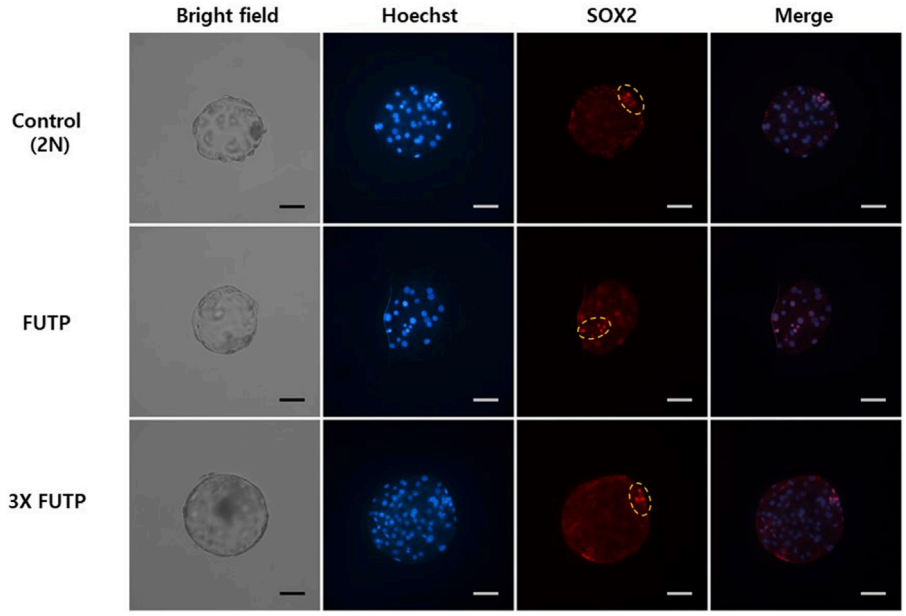

FIGURE 5
Representative images of fluorescent immunostaining. Nuclei (blue) and inner cell mass (red) of aggregated tetraploid blastocysts. The yellow dotted circle indicates the inner cell mass of the blastocyst.

3X FUTP group showed significantly ($p < 0.05$) higher YAP1 expression in the nucleus than did the control and FUTP groups. In the cytoplasm of the entire blastocyst, including the nucleus, the 3X FUTP group showed significantly ($p < 0.05$) higher YAP1 expression than did the FUTP group, but there was no significant difference in the control group (Figure 7B).

4 Discussion

Tetraploid complementation is a method that ideally proves the differentiation potential to differentiate into all tissue cells except for placental tissue. In other words, when pluripotent stem cells and placenta-forming cells are combined and implanted, an individual composed of 100% pluripotent stem cell-derived cells can be created. To make this practically possible, the TE that forms the placenta and pluripotent stem cells should be combined and implanted. To facilitate this through experimentation, a more stable supply of tetraploid blastocysts must be established. However, there is limited evidence to measure gene products in tetraploid mammalian cells (Eakin and Behringer, 2003).

In this study, PA embryos were used to produce tetraploid embryos. Although PA embryos cannot maintain normal pregnancy, it is a good material for observing developmental competence and characteristics in the preimplantation embryo stage. IVF embryos can be used for this study, but in the case of pigs, the fertility rate varies greatly depending on the quality of semen. Furthermore, a high polyspermy rate of porcine IVF embryos increases karyotypic abnormalities (McCauley et al., 2003; Nguyen et al., 2020), which can be an obstacle to analyzing the efficiency of tetraploid production. The tetraploid production technology established in this study can use pig embryos derived from IVF or somatic cell nuclear transfer in the future.

In the first experiment, there was no significant difference in cleavage rate in all treatment groups after 24 h of electrical stimulation for PA. However, blastocysts derived from the CITP group showed a significantly lower blastocyst development rate than did the blastocysts derived from the control group (diploid). In

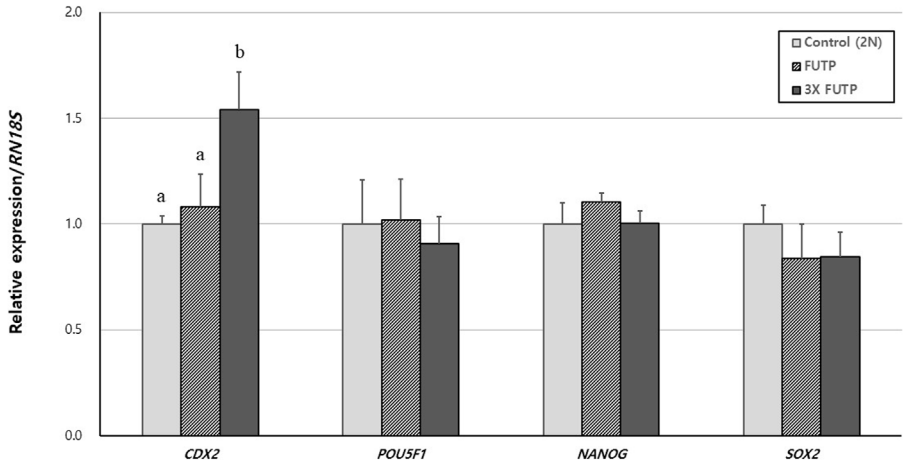

FIGURE 6
Relative expression of porcine pluripotency-related genes and trophectoderm markers in aggregated tetraploid blastocysts. The mRNA levels of the genes were analyzed using quantitative real-time polymerase chain reaction, with three replicates per sample. The expression of each gene was normalized against *RN18S* mRNA. Data are the mean ± SEM. [a, b] Values in the same column with different superscript letters are significantly different ($p < 0.05$).

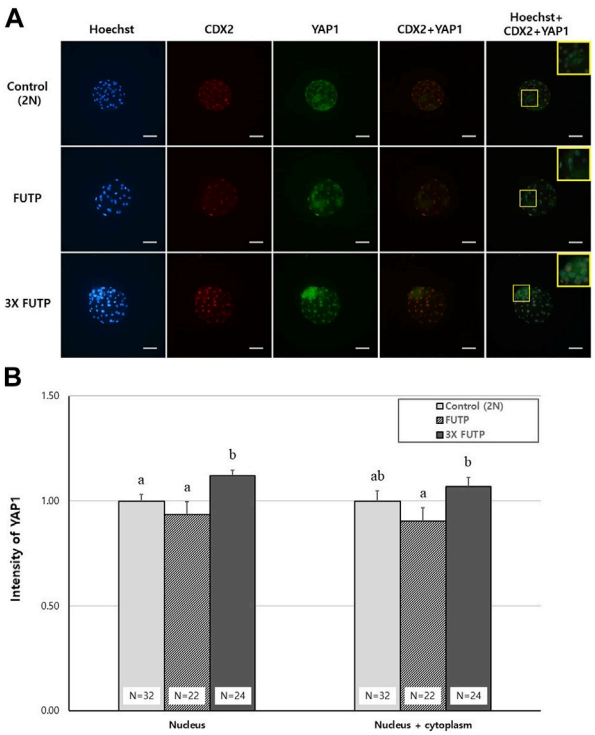

FIGURE 7
YAP1 protein expression intensity in the whole blastocyst and nucleus through immunostaining. **(A)** Representative images of blastocysts from each treatment group immunostained with Hoechst (blue), CDX2 (red), and YAP1 (green). The yellow box is a two-fold magnified image of the ICM region of the blastocyst. Scale bar = 50 μm. **(B)** The blastocysts from each treatment group were examined for YAP1 expression in the entire cytoplasm, including the nucleus or nucleus, through YAP1 immunostaining. N = the number of blastocysts analyzed. Data are the mean ± SEM. [a, b] Values in the same column with different superscript letters are significantly different ($p < 0.05$).

addition, the fact that the CITP group shows differences in fusion rate and blastocyst quality depending on the type of donor cells injected may be a disadvantage in the production of tetraploid embryos.

In the second experiment, we investigated the nuclear ploidy of blastocysts from each treatment group. In the control group, 84% of the blastocysts were diploid. The tetraploid ratio of blastocysts derived from FUTP, CITP, and CBTP was also investigated at 74.6%–86%, showing high tetraploid formation in all methods. Several previous studies have also shown that these methods have a high tetraploid formation rate (Sembon et al., 2011; Kong and Liu, 2019).

A study by Lin et al. reported that there was no significant difference in the frequency of apoptotic cells in tetraploid blastocysts produced through CBTP and FUTP methods (Lin et al., 2019). However, our results showed that blastocysts derived from the CITP-treated group and CBTP-treated group showed a significantly higher percentage of apoptotic cells than the FUTP-treated group and the control group. For the oocytes used in the other treatment groups except for the CBTP treatment group; only MII oocytes are selected for PA after IVM. Hence, oocytes that do not spontaneously mature to MII are filtered out. However, CBTP-derived oocytes in which extrusion of the PB1 is inhibited by CB treatment did not filter out oocytes that did not naturally mature. These oocytes may have been responsible for the high rate of apoptosis when they reach the blastocyst. The low developmental capacity of somatic cell nuclear transfer has been primarily attributed to incomplete reprogramming of the donor (Zhang et al., 2020; Glanzner et al., 2022). Donor cells injected for the production of CITP-derived tetraploid embryos also have processing similar to somatic cell nuclear transfer. Factors such as the synchrony of the cell cycle stages of the donor cells, various ages, and tissue origin may have caused low reprogramming and increased the rate of cell death. Based on the results of experiments 1, 2, and 3, we selected the FUTP method as the most suitable method for producing porcine tetraploid embryos.

The size of a tetraploid blastocyst remains approximately the same as that of a diploid blastocyst at the same stage (Edwards, 1958; Eakin and Behringer, 2003). In the results of the fourth experiment, the size of the tetraploid blastocyst remained almost the same as that of the diploid blastocyst at the same stage. However, it was confirmed that the average cell nucleus diameter of tetraploid-derived blastocysts was significantly larger than that of diploids. This result can be attributed to two reasons. The size of the nucleus gradually decreases during preimplantation development in mice (Tsichlaki and FitzHarris, 2016), which means that tetraploid blastocysts can have large nuclei because the cell cycle is slower than that of diploids. Another reason is that tetraploid blastocysts are similar in size to diploid blastocysts but contain fewer cells. This means that the cells of a tetraploid blastocyst constitute a larger area of blastocyst surface area per cell. Based on the morphological values of the blastocysts measured in this experiment, the relative area ratio of 1 cell constituting the blastocyst was calculated. As a result, it was determined that the cells of the tetraploid blastocyst cover areas 1.34 to 1.43 times more than the cells of the diploid blastocyst. Although no similar references can be found for pigs, it is evident from other literature that used mouse embryos, which reported that the size of the cell nucleus in the early preimplantation embryo is affected by the size of the cytoplasm (Tsichlaki and FitzHarris, 2016). Therefore, it can be assumed that the nucleus of a tetraploid with a relatively large cytoplasm is larger than that of a diploid blastocyst.

There have been reports in pigs that aggregation of diploid embryos improves blastocyst quality (Terashita et al., 2011; Buemo et al., 2016), but this has not been reported for cases of tetraploid embryos. In the fifth experiment, we demonstrated that the aggregation of porcine tetraploid embryos increases the rate of development into blastocysts and the number of cells in blastocysts. The tetraploid blastocyst showed a significantly higher TE cell ratio than did the diploid blastocyst (control), and the ratio of ICM and TE did not change depending on blastomere aggregation. As the embryo develops from a morula to a blastocyst, it divides into ICM and TE. In the sixth experiment, *CDX2* mRNA expression was significantly higher in the 3X FUTP group with the highest number of TE cells than in the other groups. This result demonstrates that there is a close relationship between high *CDX2* expression and the number of TE cells in aggregated tetraploid embryos, probably because most of the cells in the tetraploid blastocyst must consist of outer cells to construct a similar size to the diploid blastocyst, with a relatively small number of cells compared to the diploid. Cells inside the morula differentiate into ICM expressing *OCT4* (*POU5F1*) and *NANOG*, and cells outside the morula differentiate into trophoblast expressing CDX2. This mechanism originates from the inside-outside hypothesis of Tarkowski and Wróblewska (1967) (Tarkowski and Wróblewska, 1967).

We further investigated whether the high percentage of TE cells in aggregated tetraploid blastocysts was due to outer cell origin. During the development of the mammalian embryo, differentiation of the ICM and TE during the transition from morula to blastocyst is regulated by the Hippo signaling pathway (Pedersen et al., 1986; Karasek et al., 2020). However, the function of the Hippo signaling pathway in porcine embryogenesis remains relatively unexplored.

Hippo pathway is known to play important roles in the ICM/TE decision in murine (Nishioka et al., 2009; Hirate et al., 2013). The downstream effector YAP1 is the core component of the Hippo pathway. At the morula stage, the Hippo pathway is quiescent in the outer cells, and YAP1 is not phosphorylated by Lats1/2 kinases. Thus, YAP1 can localize to the nucleus and combine with Tead4 to induce the expression of TE-related genes such as *CDX2* (Yagi et al., 2007; Nishioka et al., 2008; Nishioka et al., 2009; Home et al., 2012; Rayon et al., 2014). In our seventh experiment, the expression of the YAP1 protein was more clearly observed in the nuclei of TE cells, and most SOX2-positive nuclei were YAP1-negative. This trend is consistent with the results of Emura et al. that in porcine blastocyst stage embryos, nuclear YAP1 signals were observed at least in TE cells (Emura et al., 2020). Aggregated tetraploid blastocysts with an increased proportion of TE cells can display higher efficiency in implantation and placenta formation after tetraploid complementation using pigs. However, this study has limitations in that the results were obtained using PA embryos that cannot develop into complete organisms. Another limitation is that the efficiency of embryos produced through condensed tetraploid blastocyst complementation was not verified *in vivo*. Therefore, further studies are needed to determine whether tetraploid aggregated blastocysts derived from *in vivo* embryos or IVF embryos can sustain intact pregnancies when used in tetraploid complementation.

This study demonstrated that the FUTP method was the most efficient method for producing tetraploid blastocysts in pigs with a low apoptosis rate. Tetraploid embryos had fewer cells in the blastocyst than did diploid embryos, but this disadvantage can be overcome through tetraploid embryo aggregation. In addition, the aggregated FUTP-treated group maintained a high ratio of TE based on the increased expression of the *CDX2* gene and high YAP1 intensity in the nucleus. The established method could improve the quality of donor blastocysts used in tetraploid complementation and provide insight into understanding the evolution and regulation of pluripotency across mammalian species.

Data availability statement

The original contributions presented in the study are included in the article/Supplementary Material, further inquiries can be directed to the corresponding authors.

Ethics statement

The animal studies were approved by the Committee on Ethics of Animal Experiments of the Chungbuk National University. The studies were conducted in accordance with the local legislation and institutional requirements. Written informed consent was obtained from the owners for the participation of their animals in this study.

Author contributions

JL was involved in the design of the study, executed experiments, and wrote and edited the manuscript. LC and

MK were involved in the execution and analysis of qRT-PCR and cell culture. HC and DO were involved in the TUNEL assay and embryo culture. AJ was involved in sample collection and cell maintenance. EL contributed to data interpretation and edited the manuscript. S-HH devised and supervised the study, contributed to data interpretation, and edited the manuscript. All authors contributed to the article and approved the submitted version.

Funding

This work was supported by the Basic Science Research Program through the National Research Foundation of Korea, funded by the Ministry of Education (NRF-2021R1C1C2013954).

Acknowledgments

The authors are very grateful to Eunjeong Kim for her support with several techniques, including ovary sampling.

Conflict of interest

The authors declare that the research was conducted in the absence of any commercial or financial relationships that could be construed as a potential conflict of interest.

Publisher's note

All claims expressed in this article are solely those of the authors and do not necessarily represent those of their affiliated organizations, or those of the publisher, the editors and the reviewers. Any product that may be evaluated in this article, or claim that may be made by its manufacturer, is not guaranteed or endorsed by the publisher.

Supplementary material

The Supplementary Material for this article can be found online at: https://www.frontiersin.org/articles/10.3389/fcell.2023.1239448/full#supplementary-material

References

Atikuzzaman, M., Koo, O. J., Kang, J. T., Kwon, D. K., Park, S. J., Kim, S. J., et al. (2011). The 9-cis retinoic acid signaling pathway and its regulation of prostaglandin-endoperoxide synthase 2 during *in vitro* maturation of pig cumulus cell-oocyte complexes and effects on parthenogenetic embryo production. *Biol. Reprod.* 84, 1272–1281. doi:10.1095/biolreprod.110.086595

Boiani, M., Eckardt, S., Leu, N. A., Schöler, H. R., and McLaughlin, K. J. (2003). Pluripotency deficit in clones overcome by clone-clone aggregation: epigenetic complementation? *EMBO J.* 22, 5304–5312. doi:10.1093/emboj/cdg507

Brevini, T. A., Pennarossa, G., Attanasio, L., Vanelli, A., Gasparrini, B., and Gandolfi, F. (2010). Culture conditions and signalling networks promoting the establishment of cell lines from parthenogenetic and biparental pig embryos. *Stem Cell. Rev. Rep.* 6, 484–495. doi:10.1007/s12015-010-9153-2

Buemo, C. P., Gambini, A., Moro, L. N., Hiriart, M. I., Fernández-Martín, R., Collas, P., et al. (2016). Embryo aggregation in pig improves cloning efficiency and embryo quality. *PLOS ONE* 11, e0146390. doi:10.1371/journal.pone.0146390

Cai, L., Yoon, J. D., Hwang, S. U., Lee, J., Kim, E., Kim, M., et al. (2022). Exploring the mechanism of trehalose: dual functions of PI3K/Akt and VPS34/mTOR pathways in porcine oocytes and cumulus cells. *Biol. Reprod.* 107, 432–445. doi:10.1093/biolre/ioac060

Curnow, E. C., Gunn, I. M., and Trounson, A. O. (2000). Electrofusion of two-cell bovine embryos for the production of tetraploid blastocysts *in vitro*. *Mol. Reprod. Dev.* 56, 372–377. doi:10.1002/1098-2795(200007)56:3<372::AID-MRD7>3.0.CO;2-W3.0.CO;2-W

Eakin, G. S., and Behringer, R. R. (2003). Tetraploid development in the mouse. *Dev. Dyn.* 228, 751–766. doi:10.1002/dvdy.10363

Eckardt, S., and McLaughlin, K. J. (2004). Interpretation of reprogramming to predict the success of somatic cell cloning. *Anim. Reprod. Sci. 82–* 83, 97–108. doi:10.1016/j.anireprosci.2004.04.017

Edwards, R. G. (1958). Colchicine-induced heteroploidy in the mouse. II. The induction of tetraploidy and other types of heteroploidy. *J. Exp. Zool.* 137, 349–362. doi:10.1002/jez.1401370207

Emura, N., Saito, Y., Miura, R., and Sawai, K. (2020). Effect of downregulating the hippo pathway members YAP1 and LATS2 transcripts on early development and gene expression involved in differentiation in porcine embryos. *Cell. Reprogr.* 22, 62–70. doi:10.1089/cell.2019.0082

Fu, B., Liu, D., Ma, H., Guo, Z. H., Wang, L., Li, Z. Q., et al. (2016). Development of porcine tetraploid somatic cell nuclear transfer embryos is influenced by oocyte nuclei. *Cell. Biol. Int.* 40, 214–222. doi:10.1002/cbin.10554

Glanzner, W. G., de Macedo, M. P., Gutierrez, K., and Bordignon, V. (2022). Enhancement of chromatin and epigenetic reprogramming in porcine SCNT embryos-progresses and perspectives. *Front. Cell. Dev. Biol.* 10, 940197. doi:10.3389/fcell.2022.940197

Hirate, Y., Hirahara, S., Inoue, K. I., Suzuki, A., Alarcon, V. B., Akimoto, K., et al. (2013). Polarity-dependent distribution of angiomotin localizes Hippo signaling in preimplantation embryos. *Curr. Biol.* 23, 1181–1194. doi:10.1016/j.cub.2013.05.014

Holm, P., Booth, P. J., and Callesen, H. (2002). Kinetics of early *in vitro* development of bovine *in vivo*- and *in vitro*-derived zygotes produced and/or cultured in chemically defined or serum-containing media. *Reproduction* 123, 553–565. doi:10.1530/rep.0.1230553

Home, P., Saha, B., Ray, S., Dutta, D., Gunewardena, S., Yoo, B., et al. (2012). Altered subcellular localization of transcription factor TEAD4 regulates first mammalian cell lineage commitment. *Proc. Natl. Acad. Sci. U. S. A.* 109, 7362–7367. doi:10.1073/pnas.1201595109

Hou, D. R., Jin, Y., Nie, X. W., Zhang, M. L., Ta, N., Zhao, L. H., et al. (2016). Derivation of porcine embryonic stem-like cells from *in vitro*-produced blastocyst-stage embryos. *Sci. Rep.* 6, 25838. doi:10.1038/srep25838

Hou, N., Du, X., and Wu, S. (2022). Advances in pig models of human diseases. *Anim. Model. Exp. Med.* 5, 141–152. doi:10.1002/ame2.12223

Ishiguro, N., Kano, K., Yamamoto, Y., and Taniguchi, K. (2005). Tetraploid cells of enhanced green fluorescent protein transgenic mice in tetraploid/diploid-chimeric embryos. *J. Reprod. Dev.* 51, 567–572. doi:10.1262/jrd.17004

Karasek, C., Ashry, M., Driscoll, C. S., and Knott, J. G. (2020). A tale of two cell-fates: role of the Hippo signaling pathway and transcription factors in early lineage formation in mouse preimplantation embryos. *Mol. Hum. Reprod.* 26, 653–664. doi:10.1093/molehr/gaaa052

Kawaguchi, J., Kano, K., and Naito, K. (2009). Expression profiling of tetraploid mouse embryos in the developmental stages using a cDNA microarray analysis. *J. Reprod. Dev.* 55, 670–675. doi:10.1262/jrd.09-127a

Kong, Q., and Liu, Z. (2019). Electrofusion of 2-cell embryos for porcine tetraploid embryo production. *Methods Mol. Biol.* 1874, 361–371. doi:10.1007/978-1-4939-8831-0_21

Krivokharchenko, A., Galat, V., Ganten, D., and Bader, M. (2002). *In vitro* formation of tetraploid rat blastocysts after fusion of two-cell embryos. *Mol. Reprod. Dev.* 61, 460–465. doi:10.1002/mrd.90001

Lee, J., Cai, L., Kim, M., Choi, H., Oh, D., Jawad, A., et al. (2022). Blastomere aggregation using phytohemagglutinin-L improves the establishment efficiency of porcine parthenogenesis-derived embryonic stem-like cell lines. *Front. Cell. Dev. Biol.* 10, 948778. doi:10.3389/fcell.2022.948778

Lee, J., Kim, E., Hwang, S. U., Cai, L., Kim, M., Choi, H., et al. (2021). Effect of D-glucuronic acid and N-acetyl-D-glucosamine treatment during *in vitro* maturation on embryonic development after parthenogenesis and somatic cell nuclear transfer in pigs. *Anim. (Basel)* 11, 1034. doi:10.3390/ani11041034

Li, T. D., Feng, G. H., Li, Y. F., Wang, M., Mao, J. J., Wang, J. Q., et al. (2017). Rat embryonic stem cells produce fertile offspring through tetraploid complementation. *Proc. Natl. Acad. Sci. U. S. A.* 114, 11974–11979. doi:10.1073/pnas.1708710114

Lin, T., Lee, J. E., Shin, H. Y., Lee, J. B., Kim, S. Y., and Jin, D. I. (2019). Production and development of porcine tetraploid parthenogenetic embryos. *J. Anim. Sci. Technol.* 61, 225–233. doi:10.5187/jast.2019.61.4.225

McCauley, T. C., Mazza, M. R., Didion, B. A., Mao, J., Wu, G., Coppola, G., et al. (2003). Chromosomal abnormalities in Day-6, *in vitro*-produced pig embryos. *Theriogenology* 60, 1569–1580. doi:10.1016/s0093-691x(03)00172-9

Nguyen, H. T., Dang-Nguyen, T. Q., Somfai, T., Men, N. T., Viet Linh, N., Xuan Nguyen, B., et al. (2020). Selection based on morphological features of porcine embryos produced by *in vitro* fertilization: timing of early cleavages and the effect of polyspermy. *Anim. Sci. J.* 91, e13401. doi:10.1111/asj.13401

Nishioka, N., Inoue, K. I., Adachi, K., Kiyonari, H., Ota, M., Ralston, A., et al. (2009). The Hippo signaling pathway components Lats and Yap pattern Tead4 activity to distinguish mouse trophectoderm from inner cell mass. *Dev. Cell.* 16, 398–410. doi:10.1016/j.devcel.2009.02.003

Nishioka, N., Yamamoto, S., Kiyonari, H., Sato, H., Sawada, A., Ota, M., et al. (2008). Tead4 is required for specification of trophectoderm in pre-implantation mouse embryos. *Mech. Dev.* 125, 270–283. doi:10.1016/j.mod.2007.11.002

Oldani, G., Peloso, A., Lacotte, S., Meier, R., and Toso, C. (2017). Xenogeneic chimera-generated by blastocyst complementation-As a potential unlimited source of recipient-tailored organs. *Xenotransplantation* 24. doi:10.1111/xen.12327

Park, M. R., Lee, A. R., Bui, H. T., Park, C., Park, K. K., Cho, S. G., et al. (2011). Chromosome remodeling and differentiation of tetraploid embryos during preimplantation development. *Dev. Dyn.* 240, 1660–1669. doi:10.1002/dvdy.22653

Pedersen, R. A., Wu, K., and BaŁakier, H. (1986). Origin of the inner cell mass in mouse embryos: cell lineage analysis by microinjection. *Dev. Biol.* 117, 581–595. doi:10.1016/0012-1606(86)90327-1

Rayon, T., Menchero, S., Nieto, A., Xenopoulos, P., Crespo, M., Cockburn, K., et al. (2014). Notch and hippo converge on Cdx2 to specify the trophectoderm lineage in the mouse blastocyst. *Dev. Cell.* 30, 410–422. doi:10.1016/j.devcel.2014.06.019

Savy, V., Alberio, V., Vans Landschoot, G., Moro, L. N., Olea, F. D., Rodríguez-Álvarez, L., et al. (2021). Effect of embryo aggregation on *in vitro* development of adipose-derived mesenchymal stem cell-derived bovine clones. *Cell. Reprogr.* 23, 277–289. doi:10.1089/cell.2021.0026

Sembon, S., Fuchimoto, D., Iwamoto, M., Suzuki, S., Yoshioka, K., and Onishi, A. (2011). A simple method for producing tetraploid porcine parthenogenetic embryos. *Theriogenology* 76, 598–606. doi:10.1016/j.theriogenology.2011.03.010

Stokes, P. J., Abeydeera, L. R., and Leese, H. J. (2005). Development of porcine embryos *in vivo* and *in vitro*; evidence for embryo 'cross talk' *in vitro*. *Dev. Biol.* 284, 62–71. doi:10.1016/j.ydbio.2005.05.001

Tarkowski, A. K., and Wróblewska, J. (1967). Development of blastomeres of mouse eggs isolated at the 4- and 8-cell stage. *J. Embryol. Exp. Morphol.* 18, 155–180. doi:10.1242/dev.18.1.155

Terashita, Y., Sugimura, S., Kudo, Y., Amano, R., Hiradate, Y., and Sato, E. (2011). Improving the quality of miniature pig somatic cell nuclear transfer blastocysts: aggregation of SCNT embryos at the four-cell stage. *Reprod. Domest. Anim.* 46, 189–196. doi:10.1111/j.1439-0531.2010.01614.x

Tsichlaki, E., and FitzHarris, G. (2016). Nucleus downscaling in mouse embryos is regulated by cooperative developmental and geometric programs. *Sci. Rep.* 6, 28040. doi:10.1038/srep28040

Vassiliev, I., Vassilieva, S., Beebe, L. F., Harrison, S. J., McIlfatrick, S. M., and Nottle, M. B. (2010). *In vitro* and *in vivo* characterization of putative porcine embryonic stem cells. *Cell. Reprogr.* 12, 223–230. doi:10.1089/cell.2009.0053

Walters, E. M., and Prather, R. S. (2013). Advancing swine models for human health and diseases. *Mo. Med.* 110, 212–215.

Wu, J., Greely, H. T., Jaenisch, R., Nakauchi, H., Rossant, J., and Belmonte, J. C. (2016). Stem cells and interspecies chimaeras. *Nature* 540, 51–59. doi:10.1038/nature20573

Yagi, R., Kohn, M. J., Karavanova, I., Kaneko, K. J., Vullhorst, D., DePamphilis, M. L., et al. (2007). Transcription factor TEAD4 specifies the trophectoderm lineage at the beginning of mammalian development. *Development* 134, 3827–3836. doi:10.1242/dev.010223

Zhang, J., Hao, L., Wei, Q., Zhang, S., Cheng, H., Zhai, Y., et al. (2020). TET3 overexpression facilitates DNA reprogramming and early development of bovine SCNT embryos. *Reproduction* 160, 379–391. doi:10.1530/REP-20-0021

Zhou, C., Cai, X., Fu, Y., Wei, X., Fu, N., Xie, J., et al. (2015). Tetraploid complementation proves pluripotency of induced pluripotent stem cells derived from adipose tissue. *Cell. Prolif.* 48, 39–46. doi:10.1111/cpr.12152

frontiers | Frontiers in Cell and Developmental Biology

TYPE Review
PUBLISHED 15 February 2024
DOI 10.3389/fcell.2024.1342905

Check for updates

OPEN ACCESS

EDITED BY
Ahmed Balboula,
University of Missouri, United States

REVIEWED BY
Zuzana Holubcová,
Masaryk University, Czechia
Ahmed Gad,
Colorado State University, United States

*CORRESPONDENCE
Monika Fluks,
m.fluks@uw.edu.pl,
mfluks@jcu.cz

RECEIVED 22 November 2023
ACCEPTED 01 February 2024
PUBLISHED 15 February 2024

CITATION
Fluks M, Collier R, Walewska A, Bruce AW and Ajduk A (2024), How great thou ART: biomechanical properties of oocytes and embryos as indicators of quality in assisted reproductive technologies.
Front. Cell Dev. Biol. 12:1342905.
doi: 10.3389/fcell.2024.1342905

COPYRIGHT
© 2024 Fluks, Collier, Walewska, Bruce and Ajduk. This is an open-access article distributed under the terms of the Creative Commons Attribution License (CC BY). The use, distribution or reproduction in other forums is permitted, provided the original author(s) and the copyright owner(s) are credited and that the original publication in this journal is cited, in accordance with accepted academic practice. No use, distribution or reproduction is permitted which does not comply with these terms.

How great thou ART: biomechanical properties of oocytes and embryos as indicators of quality in assisted reproductive technologies

Monika Fluks[1,2]*, Rebecca Collier[2], Agnieszka Walewska[1], Alexander W. Bruce[2] and Anna Ajduk[1]

[1]Department of Embryology, Institute of Developmental Biology and Biomedical Sciences, Faculty of Biology, University of Warsaw, Warsaw, Poland, [2]Department of Molecular Biology and Genetics, Faculty of Science, University of South Bohemia in České Budějovice, České Budějovice, Czechia

Assisted Reproductive Technologies (ART) have revolutionized infertility treatment and animal breeding, but their success largely depends on selecting high-quality oocytes for fertilization and embryos for transfer. During preimplantation development, embryos undergo complex morphogenetic processes, such as compaction and cavitation, driven by cellular forces dependent on cytoskeletal dynamics and cell-cell interactions. These processes are pivotal in dictating an embryo's capacity to implant and progress to full-term development. Hence, a comprehensive grasp of the biomechanical attributes characterizing healthy oocytes and embryos is essential for selecting those with higher developmental potential. Various noninvasive techniques have emerged as valuable tools for assessing biomechanical properties without disturbing the oocyte or embryo physiological state, including morphokinetics, analysis of cytoplasmic movement velocity, or quantification of cortical tension and elasticity using microaspiration. By shedding light on the cytoskeletal processes involved in chromosome segregation, cytokinesis, cellular trafficking, and cell adhesion, underlying oogenesis, and embryonic development, this review explores the significance of embryo biomechanics in ART and its potential implications for improving clinical IVF outcomes, offering valuable insights and research directions to enhance oocyte and embryo selection procedures.

KEYWORDS

oocyte, embryo, mouse, preimplantation development, biomechanics, cytoskeleton, quality assessment, assisted reproductive technologies

Abbreviations: ART, assisted reproductive technologies; CT, cortical tension; EPI, epiblast; HGM, harmonic generation microscopy, ICM, inner cell mass; IVF, *in vitro* fertilization; OCM, optical coherence microscopy; PE, primitive endoderm; PIV, particle image velocimetry; PLM, polarized light microscopy; QPI, quantitative phase imaging; ROS, reactive oxygen species; TE, trophectoderm.

1 Introduction

Infertility has been recognized by the World Health Organization (WHO) as a disease and a global public health issue since 2013, following 2 decades of research into its personal and social consequences suffered by those affected (Fidler, 1999; Daar and Merali, 2002; Inhorn et al., 2002; Macaluso et al., 2010; Lemoine and Ravitsky, 2013; Rouchou, 2013; Gimenes et al., 2014; Nik Hazlina et al., 2022). It is estimated that it affects around 10% of couples of reproductive age (Vander Borght and Wyns, 2018), and even 15% of all women (Sadecki et al., 2022).

Assisted Reproductive Technologies (ART), especially *in vitro* fertilization (IVF), have become one of the most important procedures for treating infertility. Although there have been great advancements in IVF procedures over the years, the live birth rate per ART cycle remains low, especially for patients in advanced maternal age. While women below 35 may be expecting, depending on the reporting institution, about 33%/40%/18% success rate, women over 40 face only about 29%/15%/9% chance to give birth (according to Human Fertilisation & Embryology Authority [HEFA], 2021; Society for Assisted Reproductive Technology [SART], 2022; European Society of Human Reproduction and Embryology [ESHRE], 2023, respectively). Consequently, many couples must undergo several IVF cycles to succeed. This brings additional health risks for women, resulting in their psychological and emotional distress (especially in societies where infertility and ART are stigmatized), and further limits ART accessibility due to economic barriers (Daar and Merali, 2002; Cui, 2010; Macaluso et al., 2010; Rouchou, 2013; Nik Hazlina et al., 2022).

Additionally, IVF is an important method in livestock breeding programs (Silber et al., 2013; Sirard, 2018), and the production of phenotypically valuable livestock (Hansen, 2014), which has been a steadily growing area of commerce (Blondin, 2017; Moore and Hasler, 2017; Sanches et al., 2019; Viana, 2019). IVF is also used as a means of overcoming the significant challenges of managing small, isolated populations in zoos (Herrick, 2019) and the preservation of endangered species (Saragusty et al., 2016; Hildebrandt et al., 2018; Kochan et al., 2019; Lanyon and Burgess, 2019).

IVF is increasingly often accompanied by other procedures, such as *in vitro* oocyte maturation and cryopreservation of gametes and embryos. Around 25% of female chemotherapy-treated patients, before the age of 30, develop acute ovarian failure or premature menopause (Letourneau et al., 2012) and the risk reaches 40% for women under 40 and more than 80% for women over 40 (Rosenberg and Partridge, 2013). A strategy to preserve fertility in certain groups of female cancer patients is the cryopreservation of ovarian follicles ahead of the oncological treatment and *in vitro* maturation of oocytes before fertilization after recovery. This approach may also be applied to women with polycystic ovary syndrome, a group of patients with a high risk of ovarian hyperstimulation syndrome (Walls et al., 2015). Both oocyte and sperm cryopreservation are a fertility conservation option for transgender individuals undergoing hormone replacement therapy and genital reconstructive surgery (De Roo et al., 2016) and serve as an efficient banking method of gametes and embryos for infertility patients (Di Santo et al., 2012; Liang and Motan, 2016) and donors (Lindheim and Klock, 2018; Mignini Renzini et al., 2021). *In vitro* maturation and cryopreservation are also widely used tools in assisted reproduction of domestic and endangered animals (Gandolfi and Brevini, 2010; Hildebrandt et al., 2018; Sjunnesson, 2020).

The efficiency of IVF can be raised by transferring multiple embryos in a single cycle, but it can result in multiple pregnancies and, as a consequence, in serious health complications for mothers and their offspring (Ombelet et al., 2005; Skora and Frankfurter, 2012). Many clinics have therefore introduced elective single embryo transfers (eSET), according to guidelines of good clinical practice. Consequently, scientists and the medical industry are urged to develop novel and reliable methods to select high-quality embryos for transfer. Thus, protocols for noninvasive assessment of embryo competence are a valuable addition to the IVF procedures. Furthermore, the evaluation of oocyte quality serves the purpose of selecting the most suitable oocytes for fertilization. This becomes especially vital when legal restrictions limit the number of eggs that can be fertilized (e.g., six in Poland, unless specific medical conditions or age criteria are met). Reliable evaluation processes allow embryologists to personalize IVF treatments for each patient, including considerations such as the logistics of oocyte cryobanking and helping to manage patient expectations. Equally significant, the outcome of oocyte evaluation can yield supplementary insights that prove valuable in assessing the quality of the resulting embryos.

Plenty of methods for oocyte and embryo selection have been previously proposed (Patrizio et al., 2007; Rienzi et al., 2011; Ajduk and Zernicka-Goetz, 2013; Anagnostopoulou et al., 2022), but their adaptation into a clinical setting has proved challenging, either due to conflicting results or time, personnel, and financial constraints (Ajduk and Zernicka-Goetz, 2013). Current methods used in clinics are primarily based on the assessment of oocyte or embryo morphology, often combined with time-lapse imaging providing extra information on cellular divisions and morphogenetic events occurring during embryo preimplantation development (so called morphokinetics). However, morphology assessment of oocytes is often more informative than predictive (Nikiforov et al., 2022), and in embryos—it allows for excluding low-quality specimens, but not necessarily for indicating those of the highest viability (Gardner and Balaban, 2016). Moreover, this approach is prone to intra- and interobserver bias (Paternot et al., 2009; Bormann et al., 2020). Recently, artificial intelligence algorithms have been explored as a means of enhancing these methods (Zaninovic and Rosenwaks, 2020). However, some scholars point out that this approach still requires proper standardization of methodology (Kragh and Karstoft, 2021). Another technique applied in the evaluation of embryos is preimplantation genetic testing (PGT; Madero et al., 2023). Preimplantation genetic testing for monogenic gene defects (PGT-M) is a well-established method for selecting embryos devoid of disease-related mutations. However, the efficiency and accuracy of preimplantation genetic testing for aneuploidy (PGT-A) and preimplantation genetic testing for structural rearrangements (PGT-SR) remains limited, due to embryonic mosaicism (Popovic et al., 2020; Giuliano et al., 2023). Moreover, all types of preimplantation genetic testing are highly invasive, requiring biopsy of embryonic cells (as a source of genetic material for analysis). Furthermore, PGT-A is controversial due to the lack of unambiguous evidence to support its use (Mastenbroek et al., 2021).

TABLE 1 Advantages and limitations of noninvasive techniques used in assessment of biomechanical properties of oocytes and embryos.

Technique	Type of information provided	Advantages	Disadvantages
Analysis of cavitation dynamics	- Timing and extent of blastocoel expansion	- Enables estimation of the biomechanical properties of the blastocyst	- Requires *in vitro* culture up to expanded blastocyst stage and periodic exposure to light (time-lapse imaging)
	- Parameters describing amplitude, frequency, and duration of expansion-contraction cycles of the blastocoel	- May utilize standard time-lapse recordings obtained for morphokinetic analysis	- Does not offer information about sub-cellular structures
		- Quantifiable data	
Analysis of cytoplasmic velocity	- Velocity and direction of the cytoplasmic movement	- Simple technique providing biomechanically relevant measurements	- Measurements are very easily disrupted by external movement of the analyzed cells
	- Fast cytoplasmic movements typical for freshly fertilized oocytes precisely mimic the pattern of sperm-induced Ca^{2+} oscillations	- Quantifiable data	- Until now has been applied only in experimental setting
Atomic force spectroscopy (AFS)	- Young's modulus, stiffness, and adhesion force	- Provides precise biomechanical measurements at the nanoscale	- Limited to studies of the *zona pellucida* (making it imprecise for oocyte/embryo properties assessment) or requiring *zona* removal (making it invasive)
		- Quantifiable data	- Expensive setup and maintenance costs
			- Until now has been applied only in experimental setting
Cortical tension (CT) measurements by microaspiration	- Measures the force required to aspirate a portion of the cell, providing information about its surface tension or viscoelastic properties	- Simple technique providing biomechanically relevant measurements	- Limited to studies of the *zona pellucida* (making it imprecise for oocyte/embryo properties assessment) or requiring *zona* removal (making it invasive)
		- Quantifiable data	- Until now has been applied only in experimental setting
Harmonic generation microscopy (HGM)	- Imaging of sub-cellular morphology, including metaphase spindles, based on nonlinear optical processes	- Provides 3D sub-cellular structural information	- If light of longer wavelength is used, low spatial resolution limits detailed analysis, for shorter wavelengths—potentially invasive
			- Obtained data is only indirectly related to cellular biomechanics
			- Requires an expensive setup and maintenance
			- Until now has been applied only in experimental setting
Optical coherence microscopy (OCM)	- 3D reconstructions of intracellular architecture, including metaphase spindles, based on intrinsic contrasting of back-scattered coherent light	- Offers 3D sub-cellular structural information	- Limited spatial resolution affecting detailed structural analysis
		- Quantifiable data	- Obtained data is only indirectly related to cellular biomechanics
			- Requires a fairly expensive setup
			- Until now has been applied only in experimental setting
Polarized light microscopy (PLM)	- Visualization of anisotropic cellular structures, such as metaphase spindles or zona pellucida, based on detection of changes in refractive indices and birefringence	- Used in ART on every-day basis	- Obtained data is only indirectly related to cellular biomechanics
		- Simple technique	
		- Quantifiable data	
Quantitative phase imaging (QPI)	- Captures phase shifts and refractive indices using off-axis illumination	- Offers 3D sub-cellular structural information	- Applicability limited to high refractive index structures within cells
	- Quantitative imaging of sub-cellular morphology	- Quantifiable data	- Obtained data is only indirectly related to cellular biomechanics
			- Until now has been applied only in experimental setting

As quality assessment protocols still require improvement, numerous novel methods of quality assessment have been proposed in recent years. One is the metabolic profiling of the embryos, which is achieved by the chemical analysis of spent culture media (Nagy et al., 2009; Zhao et al., 2013; Salmerón et al., 2021). Another technique, fluorescent lifetime imaging microscopy (FLIM) uses the differences in the exponential decay rate of the photon emission of autofluorescent coenzymes NAD(P)H and FAD^{2+} and allows for quantification of their concentration and thus energy metabolism of the embryo (Ma et al., 2019; Venturas et al., 2022; Venturas et al., 2023). This technique, however, uses UV light to excite autofluorescence, raising concerns about its invasiveness. Finally, it is also possible to analyze the chemical composition of oocytes and embryos using coherent anti-Stokes Raman scattering (CARS; Bogliolo et al., 2013; Davidson et al., 2013; Bradley et al., 2016; Jasensky et al., 2016; Ishigaki et al., 2017; Rusciano et al., 2017; Arena et al., 2021). CARS detects the vibrational spectra of biomolecules, depending on the mass of the atoms constituting the molecule and the strength of their respective bonds (Robert, 2009). Although not particularly efficient in identifying proteins, CARS provides a reliable quantitative analysis of lipids (Evans and Xie, 2008; Zumbusch et al., 2013).

Recently, the application of biomechanical quality assessment in ART has been a growing area of research as well. Biomechanical properties of oocytes and embryos reflect the functionality of key cellular components, including cytoskeleton and intracellular junctions. Therefore, examination of the oocyte/embryo biomechanics may provide novel insights into the quality of those intracellular structures, and, in consequence, improve oocyte/embryo evaluation protocols. Many invasive approaches to the analysis of the biomechanical properties of cells have been proposed. Structure of biomechanically relevant cellular components may be studied with fluorescent probes and confocal microscopy (Kölle et al., 2009). On the other hand, confocal microscopy, together with special nanomechanical chips, can be used to assess the intracellular pressure (Gómez-Martínez et al., 2013). The chip comprises of a mechanical sensor and an optical reference area created by two parallel reflecting membranes, separated by a vacuum gap. Waves can only pass through the reference area when they are in resonance with it. By analyzing the reflected light's intensity, the system can quantify the pressure-induced membrane deflection. Another interesting method is the implementation of magnetically responsive ferrofluid microdroplets that enable highly precise measurements of mechanical properties, such as viscosity in tissues and embryos (Campàs, 2016; Serwane et al., 2017). The viscosity of tissue affects the movement and deformation of the microdroplets under the influence of the magnetic field, allowing for precise quantitative measurements of mechanical properties. While these approaches have shown promise in research, their application in ART is limited due to concerns about their potential to disrupt natural developmental processes. Noninvasive techniques described in this review (Table 1) represent an alternative, yet promising, avenue for gaining deeper insights into the biomechanical aspects of oocytes and embryos during ART, offering valuable contributions to improving clinical outcomes and reproductive health.

2 Cytoskeletal functions, dynamics, and alternations in oocytes

The developmental capabilities of mammalian embryos are largely determined by the oocyte cargo (Stitzel and Seydoux, 2007; Li et al., 2010). Although fragmentation of DNA or other deterioration of sperm can diminish an embryo's potency, the oocyte contributes the vast majority of the cytoplasmic contents: cytoskeleton components essential for a multitude of inter- and intracellular processes, mitochondria providing energy to the embryo, lipid droplets supplying metabolic reserves, and maternal mRNA and proteins accumulated during oocyte growth, required as a guiding template before embryonic genome activation. Identifying features of a high-quality oocyte can therefore facilitate ART procedures.

Studies have shown that the biomechanical properties of mammalian oocytes reflect their developmental competence (Ebner et al., 2003; Liu et al., 2010). Whilst these properties stem partially from the *zona pellucida*'s mechanical characteristics, they predominantly depend on cellular biomechanics. The zona may harden as a result of cortical granule exocytosis at fertilization (the main element of the polyspermy block; Murayama et al., 2006; Shen et al., 2019), but also, as shown in the mouse, during premature cortical granule exocytosis in the *in vitro* matured and vitrified oocytes (Carroll et al., 1990; Ducibella et al., 1990). Premature zona hardening inhibits *in vitro* fertilization via gamete co-incubation, as sperm cannot penetrate the zona (Carroll et al., 1990). Conversely, cellular mechanics, *i.e.*, elastic (ability to resist deformation) and plastic (ability to undergo permanent deformation) behavior of cells, reflect their cytoskeletal functionality (Larson et al., 2010; Chaigne et al., 2013; Chaigne et al., 2015; Mackenzie et al., 2016). The cytoskeleton plays a key role in the segregation of chromosomes, cytokinesis, and cellular trafficking, each of which is important for cell cycle progression (Tang, 2012; D'Avino et al., 2015; Prosser and Pelletier, 2017). Microtubules build metaphase spindles, while actin and myosin are required for the spindle positioning and formation of the cytokinetic contraction ring (Schuh and Ellenberg, 2008). Disturbances in the function of these components can result in aneuploidy, which has detrimental effects on future embryonic development, especially when first appearing in meiosis (McCoy et al., 2023). A functioning actomyosin cytoskeleton is also invaluable during so-called cytoplasmic maturation, a process concurrent with the meiotic maturation of oocytes. Research conducted predominantly on mouse oocytes indicates that during cytoplasmic maturation relocation of organelles occurs. Mitochondria move from the perinuclear region towards the cell periphery (Dalton and Carroll, 2013), the Golgi apparatus fragments and shifts to the center of the gamete (Moreno et al., 2002), and the endoplasmic reticulum gathers in the cortical region (Mehlmann et al., 1995; FitzHarris et al., 2007). These changes in organelle distribution depend on intact actin filaments (Dalton and Carroll, 2013). Simultaneously, dynamic changes in the cytoskeleton itself occur. In mouse oocytes, metaphase I spindle migration is supported by an ARP2/3-dependent thickening of the cortical F-actin meshwork, nucleated by formin-2 (Leader et al., 2002; Dumont et al., 2007; Schuh and Ellenberg, 2008) and Spire 1/2 (Pfender et al., 2011). As the cortical F-actin thickens, myosin-II is excluded from the cortex, leading to its softening (Chaigne et al., 2013). These

events are regulated by phosphorylated (active) myosin-II regulatory light chain and phosphorylated ezrin-radixin-moesin complex and coordinated temporally by the MOS-MAPK pathway (Larson et al., 2010; Chaigne et al., 2013; Chaigne et al., 2015). Cortical tension (CT) resulting from the force generated by the actomyosin cytoskeleton must be strictly regulated to allow normal spindle migration and positioning: too low or too high CT both lead to spindle anomalies (Chaigne et al., 2013; Chaigne et al., 2015). As shown for human and mouse oocytes, actin filaments may also infiltrate the meiotic spindle and regulate the correct alignment and segregation of the chromosomes (Mogessie and Schuh, 2017).

Interestingly, Larson and others show that there are some discrepancies in cytoskeleton modifications during meiotic maturation between *in vivo*- and *in vitro*-matured mouse oocytes (Larson et al., 2010). This could be linked to lower developmental capabilities of *in vitro* matured human metaphase II oocytes (Jurema and Nogueira, 2006). The cellular cytoskeleton is often damaged during freezing and thawing procedures as well (Hosu et al., 2008; Hendriks et al., 2015). Various cytoskeletal elements can also be affected by postovulatory aging (*i.e.*, the extended period between ovulation and fertilization; reviewed in Miao et al., 2009; Takahashi et al., 2013); in particular, actin distribution and myosin functionality (McGinnis et al., 2015; Mackenzie et al., 2016). Some authors have even suggested that reduced myosin light chain kinase activity in aged mouse oocytes is linked to their susceptibility to parthenogenetic activation, potentially by dysregulation of membrane ion channels (McGinnis et al., 2015; Mackenzie et al., 2016).

Cytoskeletal damage can be caused by reactive oxygen species (ROS; Lord et al., 2013). In somatic cells, proteins damaged by oxidation, such as carbonylated or glycated proteins, accumulate with age and in several pathological states (Stadtman, 1992; Levine, 2002). These proteins are rendered inactive and tend to form large aggregates in the cytoplasm. Similarly, the mammalian germline accumulates these dysfunctional proteins (Hernebring et al., 2006; Haucke et al., 2014), but they are eliminated to some extent during embryo development (Hernebring et al., 2006). Oocytes may carry varying amounts of advanced glycation end (AGE) products and carbonylated or otherwise modified proteins, depending on maternal age and overall female health. Notably, actin is a common target for carbonylation (Aksenov et al., 2001; Soreghan et al., 2003). Mouse oocytes subjected to postovulatory aging or obtained from females of advanced reproductive age feature increased ROS concentrations (Szpila et al., 2019; Czajkowska and Ajduk, 2023). Similarly, vitrification is known to cause oxidative stress in murine, porcine, and human oocytes (reviewed in Tatone et al., 2010). Some studies report that increased ROS levels can be also observed during murine and bovine oocyte *in vitro* maturation (Morado et al., 2009; Xie et al., 2016). It is feasible that carbonylation/glycation of proteins occurs not only in oocytes obtained from old females but also in oocytes otherwise subjected to oxidative stress (Berlett and Stadtman, 1997), including postovulatory aging and vitrification. It can be speculated that these oocytes' cytoskeletal dysfunction could be, at least in part, caused by the oxidation of cytoskeletal proteins (Mihalas et al., 2018).

Cytoskeletal functionality is intricately linked to the successful progression of meiosis, making it a pivotal factor in oocyte and early embryo development. As a result, the assessment of cytoskeleton quality in these cells, reflected among others by their biomechanical properties, emerges as a valuable and predictive indicator, offering critical insights into the outcomes of IVF procedures, thus enhancing the understanding and potential success of ART.

3 Quality assessment of oocytes based on cytoskeletal and biomechanical properties

Some biomarkers indicative of the biomechanical properties, e.g., *zona pellucida* and metaphase spindle, can be observed using polarized light microscopy (PLM; Oldenbourg, 2013; Ajduk and Szkulmowski, 2019). Importantly, zona birefringence also indicates its ability to participate in the acrosome reaction and ability to undergo proper polyspermy block, whereas shape of the metaphase spindle can be associated with the ploidy and the maturation status of the oocyte (Caamaño et al., 2010; Montag et al., 2013; Omidi et al., 2017).

Alas, even PLM does not provide detailed information on inner cell architecture, nor does it have a high in-depth resolution. These limitations might be overcome by harmonic generation microscopy (HGM; Hsieh et al., 2008; Thayil et al., 2011), which obtains contrasts by the sample's ability to emit photons with half the wavelength of incident light. HGM has been shown to obtain 3D images of microtubules in the spindle (Yu et al., 2014; Sanchez et al., 2019) and myosin heavy-chain B (Mohler et al., 2003). However, HGM is beset by the choice between the imaging depth when using longer excitation wavelengths, which are less harmful to biomaterials, and high spatial resolution when using shorter but more invasive wavelengths (Aghigh et al., 2023). These limitations are shared by optical coherence microscopy (OCM), which can be used for metaphase spindle visualization (Karnowski et al., 2017). In addition, both methods typically require a complex and expensive setup, which might not be readily available in prospective fertility clinics. A simpler solution can perhaps be found in quantitative phase imaging (QPI) techniques, such as holographic microscopy or interferometric phase imaging, which can provide quantitative information about cell morphology based on 3D refractive index distribution (Nguyen et al., 2022). These methods can be used to study cytoskeletal organization and dynamics (Bon et al., 2014), however, to date QPI has mostly been employed to study membranous organelles such as mitochondria, which have a higher refractive index (Sandoz et al., 2019; Salucci et al., 2020).

Cellular mechanics depend on cytoskeletal function, thus probing oocytes or embryos for their biomechanical characteristics can provide insight into their developmental potential. One such method is the analysis of cytoplasmic velocity. Cytoplasmic velocity measurement combines time-lapse imaging with particle image velocimetry (PIV) analysis. PIV is an algorithm frequently used in fluid dynamics that follows the displacement of bright and dark pixel patterns in consecutive images to establish the velocity and direction of the fluid (cytoplasm) movement (Westerweel, 1997; Figure 1). Studies have demonstrated that cytoplasmic velocity monitored at the time of fertilization reflects the capacity of mouse zygotes to correctly complete preimplantation and full-term development

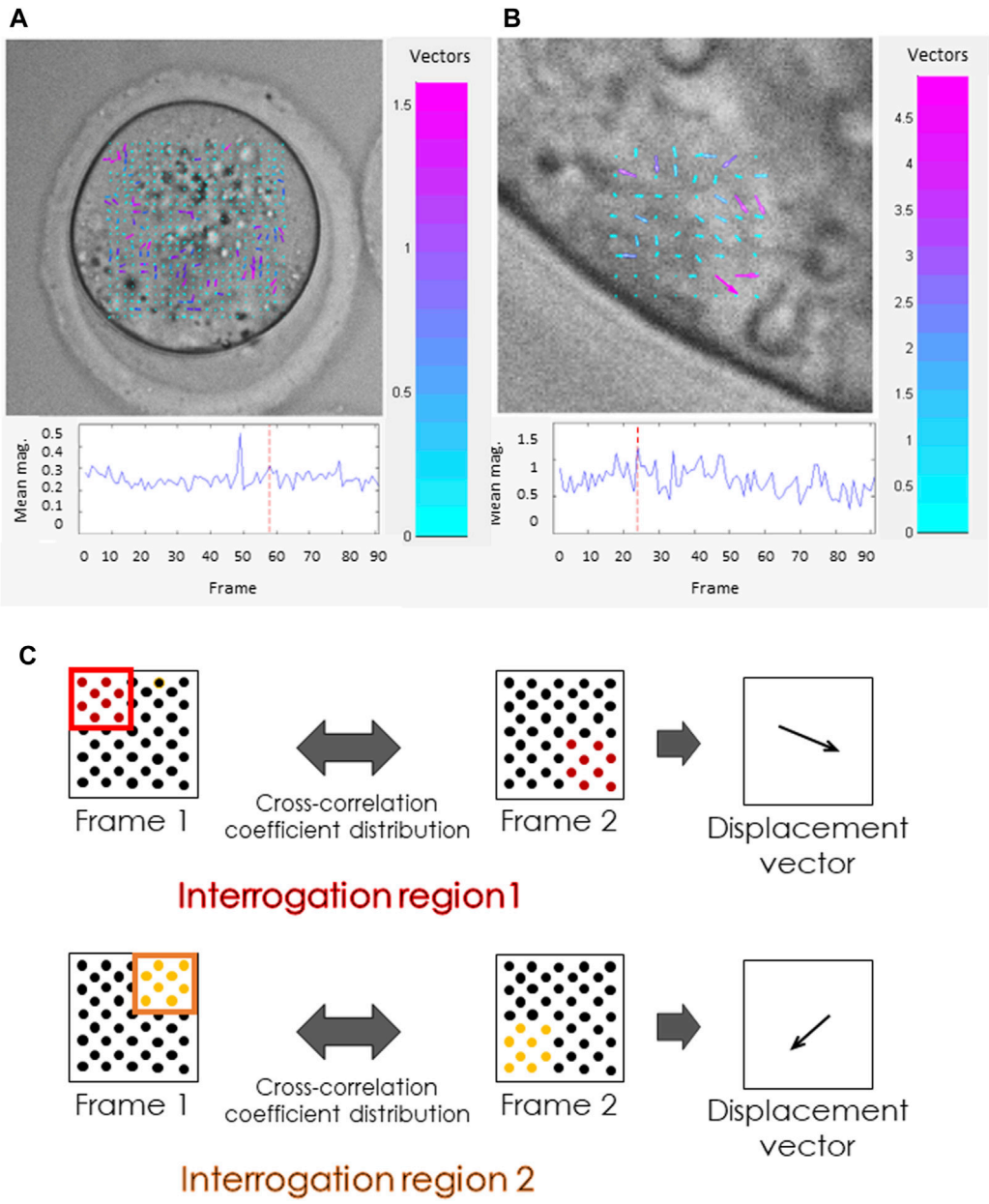

FIGURE 1
Cytoplasmic movement velocity (CMV) assessment by Particle Image Velocimetry (PIV). **(A, B)** Images from the PIV software used by some of the authors (Ajduk et al., 2011). PIV analysis was conducted for high-resolution time-lapse images of **(A)** mouse metaphase II oocyte, **(B)** polar trophectoderm cell in a mouse blastocyst. Both the length and the color of the vectors visible inside the cells reflect the cytoplasmic velocity. Cyan represents the slowest-moving vectors. Magenta represents the fastest-moving vectors. The graphs (below) show the mean cytoplasmic velocity in the analyzed region over time. The direction of the vectors indicates the direction of cytoplasm displacement between frames. **(C)** Schematic representation of the PIV algorithm. The algorithm divides the images into small interrogation windows, identifying the pattern of pixels in each window, and calculating the displacement of particles between frames. This information is used to generate a map of velocity vectors representing the cytoplasmic flow and to calculate mean cytoplasmic velocity.

(Ajduk et al., 2011). These movements can also be observed in human zygotes (Swann et al., 2012). Fast directional cytoplasmic movements (the so-called "speed-peaks") correspond to rhythmic actomyosin-mediated spasms, coincident with fertilization-induced Ca^{2+} oscillations (Ajduk et al., 2011). The mean basal speed represents the average velocity of cytoplasmic movement between speed-peaks, thereby providing information on the functionality of the zygote actomyosin cytoskeleton. For example, a relative decrease in mean basal speed is concurrent with both depolymerization and overstabilization of actin filaments and inhibition of myosin (Ajduk et al., 2011). Moreover, the mean basal speed in freshly fertilized mouse oocytes correlates with the length of the second embryonic cell cycle, the percentage of cells with fragmented nuclei, and the percentage of primitive endoderm cells in the blastocyst (Milewski et al., 2018). The basal velocity of cytoplasmic movement in unfertilized (metaphase II) oocytes is slower than in their

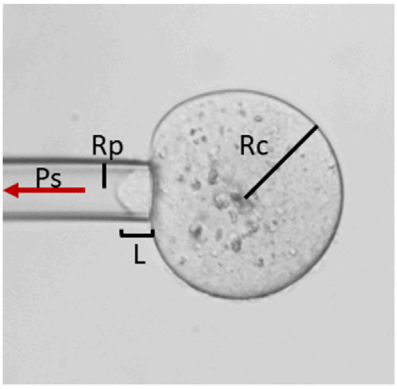

Rc – Cell curvature radius (μm)
Rp – Pipette radius (μm)
Ps– Aspiration pressure (nN/μm^2)
L – Deformation length (μm)

$$\gamma = \frac{Ps}{2}\left(\frac{1}{Rp} - \frac{1}{Rc}\right)$$

FIGURE 2
Cortical tension (CT, γ) analysis. CT analysis can be conducted by micropipette aspiration. Assessment of CT requires the measurement of cell curvature radius and aspiration pressure (Ps) when the deformation length (L) becomes equal to the micropipette radius (Rp) and utilizes the Young–Laplace equation.

fertilized counterparts (Ajduk et al., 2011). Both maternal and postovulatory types of aging are detrimental to the actomyosin cytoskeleton of mammalian, including human, metaphase II oocytes (Pickering et al., 1988; Sun et al., 2012; McGinnis et al., 2015; Mackenzie et al., 2016; Dunkley et al., 2022), which might influence the cytoplasmic dynamics, resulting in lower basal speed in aged oocytes.

Interestingly, the mean basal cytoplasmic speed is also indicative of immature oocyte (so-called GV oocyte) quality (Bui et al., 2017). There are two populations of GV oocytes, which are known to have distinct developmental capabilities: oocytes with surrounded nucleolus (or SN oocytes) that have already transcribed all necessary RNAs and are transcriptionally inactive, and oocytes with non-surrounded nucleolus (or NSN oocytes) that are still transcribing (reviewed in: Tan et al., 2009). These two types of GV oocytes differ in terms of the basal speed at various stages of *in vitro* maturation (Bui et al., 2017).

Assessment of oocyte quality based on the monitoring of actomyosin cytoskeleton-mediated cell mechanics can also utilize techniques such as micropipette aspiration (Mackenzie et al., 2016; Yanez et al., 2016) and indentation (Liu et al., 2012). Applying negative pressure through a micropipette or positive force through a microlever, results in the deformation of the cell allowing for the calculation of the cell's physical properties, such as CT or elasticity (Figure 2). CT reflects the biochemical and structural features of the oocyte cortex (Larson et al., 2010; Chaigne et al., 2013; Chaigne et al., 2015; Mackenzie et al., 2016) and *zona pellucida* (Khalilian et al., 2010; Shen et al., 2019). Studies on mouse oocytes devoid of *zona pellucida* have shown that CT decreases six-fold during maturation, then increases about 1.6-fold after fertilization (Larson et al., 2010). Also, mature mouse oocytes are polarized, with CT differing 2.5-fold between the stiff cortex over the meiotic spindle (the amicrovillar domain) and the softer, opposing cortex, where the sperm binds (microvillar domain; Larson et al., 2010). The purpose of this asymmetry is unclear. However, *in vitro* matured oocytes have reduced tension in the amicrovillar domain (Larson et al., 2010). Viscoelastic equilibrium in the cortex is essential to achieve asymmetric cytokinesis (Chaigne et al., 2013; Chaigne et al., 2015). This equilibrium is characteristic of a viable oocyte (Yanez et al., 2016). Too elastic or too plastic cortex results in anomalous spindle migration (Chaigne et al., 2013; Chaigne et al., 2015) and lowered developmental competence, likely due to less effective cortical granule release at fertilization, which could lead to polyspermy (Yanez et al., 2016). CT is also reduced in both maternally (Liu et al., 2012) and postovulatory-aged oocytes (Mackenzie et al., 2016). These differences in viscoelastic properties, hence cytoskeletal properties, offer a valuable tool for quality assessment. Methods for testing oocyte and embryo cytoskeletal properties by CT analysis, however, are relatively time-consuming and labor-intensive. Additionally, most protocols presented to date feature the removal of the zona, which may negatively affect overall embryo development (Fan et al., 2022).

Another method to measure surface forces is atomic force spectroscopy. Here, a sharp tip attached to a cantilever runs over the surface of the sample. The deflection of the cantilever across the sample surface is measured using a laser beam, which is reflected onto a photodetector (Figure 3). The amount of deflection is used to calculate the force exerted on the tip by the sample's surface (Viljoen et al., 2021). In its noninvasive form, in a similar manner to CT measurements, atomic force spectroscopy is limited to the studies of the *zona pellucida* (Boccaccio et al., 2012; Andolfi et al., 2016; Battistella et al., 2022).

4 Molecular basis of embryo biomechanics

The success of *in vitro* fertilization procedures is also contingent on sperm quality and conditions of embryo culture (Chapuis et al., 2017; Colaco and Sakkas, 2018; Consensus Group, 2020). Various molecular mechanisms reflected in changes in biomechanical properties are at play before the blastocyst, the last stage of mammalian preimplantation development, is formed. A blastocyst is built of an inner cell mass (ICM) and an outer trophectoderm (TE) epithelial layer. As the blastocyst expands, ICM cells differentiate into two lineages: the centrally located epiblast (EPI) and the primitive endoderm (PE), also called hypoblast, adjoined to the blastocyst cavity (blastocoel). The TE,

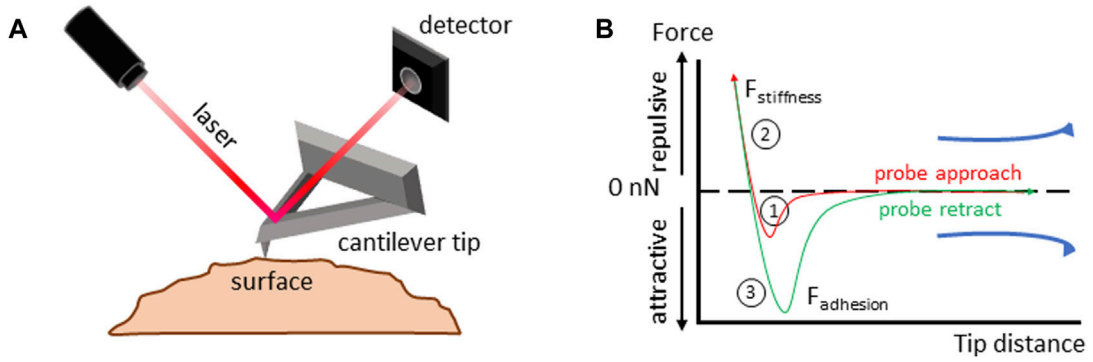

FIGURE 3
Atomic force spectroscopy. **(A)** Atomic force spectroscopy setup diagram. Details in the main text. **(B)** Force-distance curve analysis to measure the viscoelastic properties of a material. 1) The cantilever tip approaches the sample until it makes contact, and the force at the interaction between the tip and the sample is measured; 2) the tip is further compressed into the sample, deforming its surface, the forces acting on the tip during compression are recorded, allowing for calculation of the surface stiffness; 3) the tip is retracted from the sample surface. Forces acting on the tip as it moves away from the sample are measured allowing for calculation of surface adhesion.

on the other hand, differentiates into the polar TE surrounding the ICM and the mural TE surrounding the blastocyst cavity. The ICM that will give rise to the embryo proper (resulting from the EPI) as well as additional extraembryonic membranes (derived from the PE), and the TE will participate in embryo implantation in the uterus and form the future placenta.

Preimplantation development consists of multiple mitotic divisions, which are highly dependent on actin networks (Chaigne et al., 2016). Importantly, zygotic genome activation (ZGA) is connected with maternal protein degradation (Toralova et al., 2020), and considerable changes in cytoskeletal makeup. During embryonic development, the configuration of cells and cell lineages is shaped by the contractile nature of the actomyosin cortex (Murrell et al., 2015; Coravos et al., 2017; Özgüç and Maître, 2020). These cortical contractile forces are essential for the formation of the cleavage furrow during cytokinesis (Fujiwara and Pollard, 1976; Straight et al., 2003; Yamamoto et al., 2021), the movement of cells during migration and maintenance of appropriate cell positioning (Eddy et al., 2000; Tsai et al., 2019), and the withdrawal of cellular blebs (Charras et al., 2006; Taneja and Burnette, 2019). Moreover, changes in actomyosin contractility drive processes such as apical constriction (Martin et al., 2009; Solon et al., 2009) and the restructuring of cell-cell contacts (Bertet et al., 2004; Maître et al., 2012).

Significant biomechanical alterations occur particularly during the compaction of preimplantation embryos, a process that occurs at the 8-cell stage in mice, 16-cell stage in humans, and 32-cell stage in rabbits and cattle (Płusa and Piliszek, 2020). Compaction is accompanied by intra-cellular polarization of blastomeres along the apical-basal axis. In pre-compacted mouse embryos, actomyosin is uniformly distributed in the cellular cortex, whereas during compaction, it accumulates gradually in the apical, contact-free region, and becomes excluded from the cell-cell contact sites (Zhu et al., 2017). Moreover, as the mouse embryo undergoes compaction, the cell adhesion protein, epithelial cadherin (E-cadherin), translocates and becomes phosphorylated at the cell-cell contact sites (Winkel et al., 1990). Additionally, ezrin, a protein responsible for establishing and maintaining microvilli, undergoes phosphorylation and relocates to the contact-free regions of the membranes (Louvet et al., 1996).

Translocation of actomyosin occurring during compaction leads to the progressive increase of the CT on the contact-free interface of the blastomeres. At the same time, junctional E-cadherin keeps actomyosin contractility low at the cell-cell contacts (Maître et al., 2015). As a result, the inner and outer cells of a compacted embryo differ in contractility (Maître et al., 2016). These changes in cellular adhesion and CT are crucial not only for mouse embryo compaction but also for the internalization of the cells that will later form the inner cell mass (ICM; Samarage et al., 2015; Maître et al., 2016).

The biomechanical properties of preimplantation embryos are dynamically regulated by various molecular pathways. The initiation and maintenance of symmetry breaking in a compacting mouse embryo depend on the activity of PLC-PKC signaling (Zhu et al., 2017). On the other hand, formin regulates contractility in preimplantation morphogenesis (Özgüç et al., 2022). The actin nucleator ARP2/3 is critical for blastomere cytokinesis, and its inhibition leads to the failure of blastocyst formation. The RHO-associated coiled-coil-containing protein kinase (ROCK), associated with cell migration and adhesion, vesicular trafficking, and cytoskeletal dynamics, is involved in apicobasal cell polarity proteins maintenance (Marikawa and Alarcon, 2018), and the regulation of angiomotin (AMOT) localization (Mihajlović and Bruce, 2016). AMOT is a scaffolding protein involved in cell-cell junctions. As an activator of the Hippo pathway, it is crucial for the specification of TE and ICM cells in the mouse blastocysts (reviewed in: Mihajlović and Bruce, 2017). Interestingly, recently published data on mouse and human embryos indicate that there is a tight link between actomyosin contractility, lamin-A, a component of the nuclear lamina, and AMOT stability (Skory et al., 2023). Nuclear lamina is linked to the blastomere cortex via an F-actin network. As actomyosin contractility increases during embryo development, lamin-A levels rise as well. However, in cells that underwent internalization in compacted embryos and lost their apical, actomyosin-rich domain, lamin-A becomes downregulated. This leads to the relocalization of actin nucleators from the nucleus to the cytoplasm and an increase in cytoplasmic F-actin. In consequence,

AMOT is stabilized and YAP, a key transcription coregulator involved in cell lineage differentiation, undergoes phosphorylation (Hippo pathway activated). Active Hippo pathway directs inner cells towards the ICM fate. By contrast, in outer cells, lamin-A levels are upregulated. This destabilizes AMOT and prevents YAP phosphorylation (Hippo pathway inactive), promoting TE cell fate (Skory et al., 2023).

A critical and final event in preimplantation development is the formation of a blastocyst cavity, in which the radial symmetry of the embryo is broken. In mouse, the apicobasal polarity of outer TE permits the formation of an osmotic gradient that draws water from the external environment via the apical compartment of blastomeres (Eckert et al., 2004; Madan et al., 2007; Moriwaki et al., 2007) into the basal intercellular regions sealed by tight junctions (Zenker et al., 2018). Such fluid accumulation is driven by the secretion of cytoplasmic actin-coated vesicles into the intercellular space (Ryan et al., 2019). Hundreds of microlumens form throughout the mouse embryo between cell-cell contacts by hydraulic fracturing, directed by cadherin reorganization (Dumortier et al., 2019). Some microlumens also display enrichment of the apical marker, phosphorylated ezrin-radixin-moesin complex (Ryan et al., 2019). Microlumens show a swelling phase followed by a siphoning of all the fluid to a single cavity, guided by actomyosin contractions (Dumortier et al., 2019; Schliffka et al., 2023).

Existing data clearly indicate that TE functionality depends on the quality of its cytoskeleton and intracellular junctions that determine the epithelial character of this layer. Additionally, the expression and activity of proteins transporting ions, thus allowing for osmotic gradient formation and consequent cavitation (Bazer et al., 2009; Posfai et al., 2019), also play an important role in TE functioning. These factors are associated with the biomechanical properties of TE cells. It has been shown that inhibition of Na^+/K^+ pumps or claudins in tight junctions affects the CT of TE cells (Chan et al., 2019). Decreased TE cell tension also coincides with the disassembly of vinculin from tight junctions and disrupts tight junction seal integrity (Chan et al., 2019). Vinculin has been shown to regulate traction force transmission via myosin contractility-dependent adhesion (Dumbauld et al., 2013). Additionally, actin filament remodeling, required to form a sealed TE epithelium, is tension-sensitive (Zenker et al., 2018). Interestingly, it has been shown in mouse embryos that mechanical stretching, typical for TE cells during cavity expansion, facilitates *Cdx2* expression (Watanabe et al., 2017). *Cdx2* expression is a prerequisite for TE function (although not always for early stages of TE differentiation) in mice, humans, and domestic animals (reviewed in: Piliszek and Madeja, 2018; Posfai et al., 2019). Notably, keratins have been recently proven to be another regulator of TE fate in both mouse and human embryos: they enhance apical polarity and *Cdx2* expression in outer cells (Lim et al., 2020). Although keratin knockouts display trophoblast fragility, placental bleeding, and lethality after implantation (Baribault et al., 1993; Hesse et al., 2000; Tamai et al., 2000), depletion of keratins 8 and/or 18 (*i.e.*, variants that are the most abundant in preimplantation embryos; Lu et al., 2005) does not lead to severe phenotypes up to blastocyst stage, either in mice or in cattle (Goossens et al., 2010; Lim et al., 2020). Interestingly, in mouse embryos, keratin 8/18-knockdown cells display a reduced nuclear expression of YAP (required for *Cdx2* transcription) and CDX2 itself in TE cells.

Immediately prior to implantation, blastocysts hatch from the *zona pellucida*, exposing the TE, which attaches to the endometrial epithelium of the uterus. Blastocyst attachment initiates a complex cascade of events that lead to the implantation and development of a placenta. Importantly, implantation requires functional TE (Bazer et al., 2009; Aplin and Ruane, 2017; Posfai et al., 2019) and failure in implantation is the main source of reproduction loss in mammals, including humans and cattle (Aplin and Ruane, 2017; D'Occhio et al., 2020).

In summary, it is clear that the biomechanical properties of embryos are highly associated with their developmental potential. By gaining insights into how biomechanical factors influence the formation and quality of embryos, and their subsequent implantation, researchers can set forth noninvasive and robust methods of assessing such properties which could help ART practitioners make more informed decisions when selecting embryos for transfer.

5 Quality assessment based on embryo biomechanical properties

Time-lapse recordings used for classical morphogenetic analysis of preimplantation embryos, if only covering cavitation and blastocysts expansion events, may be applied for the assessment of the biomechanical properties of TE. Mouse blastocysts with inhibited actomyosin contractility, Na^+/K^+ pumps, or perturbed tight junctions displayed a slower expansion rate (Chan et al., 2019). Moreover, it has been shown in mouse embryos that experimentally reduced cavity size and hydraulic pressure inside the cavity are associated with the increased number of ICM cells and perturbed specification and spatial separation of ICM lineages (EPI and PE; Chan et al., 2019; Ryan et al., 2019). Analysis of the extent of blastocyst expansion has been shown to be a predictor of pregnancy success in human embryos (Du et al., 2016), and expansion kinetics have been related to a human embryo's ploidy: euploid embryos expanded faster than aneuploid embryos (Huang et al., 2019). The rate of blastocoel re-expansion in frozen-thawed embryos also has been associated with pregnancy likelihood in both humans and domestic animals (Leoni et al., 2008; Yin et al., 2016; Ebner et al., 2017; Lin et al., 2017; Zhao et al., 2019). Interestingly, the rate of human blastocyst re-expansion correlates with the number of TE cells (Iwasawa et al., 2019). This observation has also been confirmed in mouse embryos: smaller blastocyst size is associated with slower blastocoel expansion (Chan et al., 2019).

Blastocyst cavity volume tends to oscillate during the expansion period, undergoing contraction-expansion cycles (Figure 4). This feature seems to be an intrinsic property of the blastocysts in all animals examined, including humans (Niimura, 2003; Huang et al., 2016), and is associated with waves of mitotic divisions in TE and increasing TE cortical tension (Chan et al., 2019). However, the interpretation of these contraction-expansion cycles in terms of embryo quality is ambiguous. It has been reported that human blastocysts that transiently collapsed have less potential to give rise to pregnancy (Marcos et al., 2015; Gazzo et al., 2020; Sciorio et al., 2020) and are characterized by higher aneuploidy odds (Gazzo et al., 2020). Others have claimed that the occurrence of blastocyst collapse is not an independent predictor of reduced live birth rate (Bodri et al., 2016). It has been shown that mouse blastocysts exhibiting stronger contractions of the lumen are less likely to hatch (Shimoda

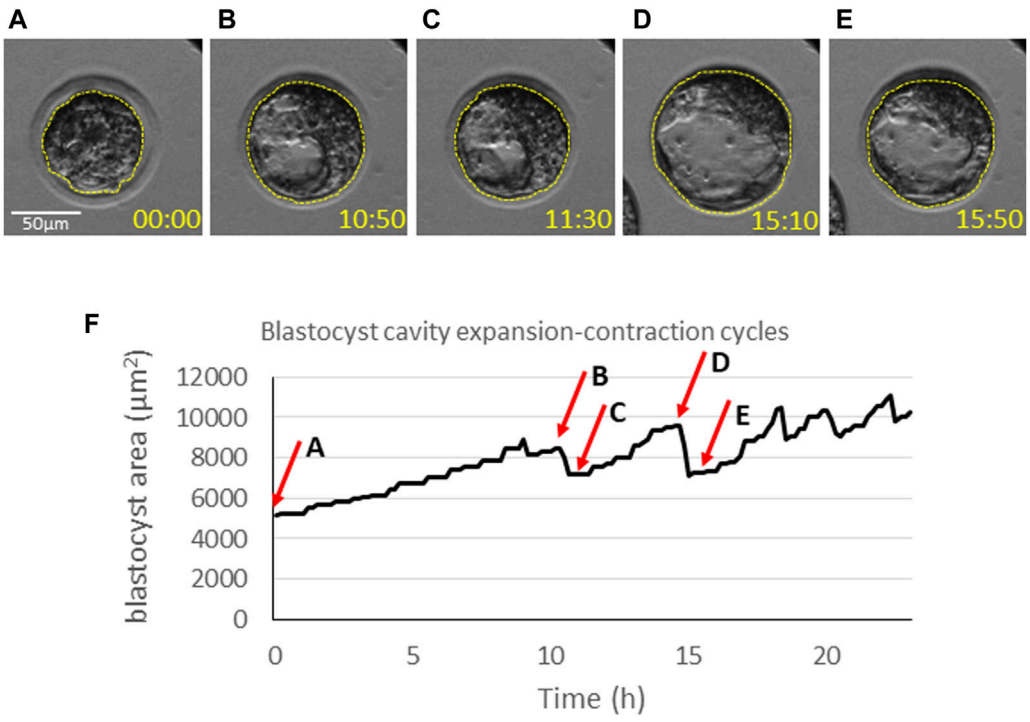

FIGURE 4
Dynamics of blastocyst cavitation. The equatorial area of blastocysts (dashed line) is measured at **(A)** the onset of cavitation, **(B)** the time-point of maximum expansion just before the first contraction, **(C)** the last phase of the first contraction, **(D)** the time-point of maximum expansion before the next contraction, **(E)** the last phase of the contraction. Time points (hh:mm) indicate the time of imaging and correspond to the graph below **(F)**. **(F)** A graph representing oscillations of the blastocyst size over time. The arrows indicate the time points corresponding to the measurements in **(A–E)**.

et al., 2016). Moreover, unusually frequent blastocoel contractions in mouse embryos can be caused by aberrant intracellular junctions in TE (Togashi et al., 2015). While the interpretation of contraction-expansion cycles in blastocysts remains inconclusive, monitoring cavitation dynamics might provide useful insights into the quality of blastocyst cytoskeleton as well as the functionality of intracellular junctions and proteins involved in filling blastocoel with fluid. Further research is essential to validate the efficacy of such an approach and its potential for application in ART.

PIV-based analysis of cytoplasmic movement in blastomeres is yet another method to provide insights into the biomechanical properties of embryos. Cytoplasmic motion reflects the reorganization of cytoskeletal elements that are key for the movement of signaling vesicles, and, as described above, for both compaction and cavitation (Coumailleau et al., 2009; Derivery et al., 2015; Zenker et al., 2017). The reorganization of the actinomyosin cytoskeleton can be observed with PIV analysis (Özgüç et al., 2022), and holds promise as a means to monitor and assess the dynamics of these crucial phases in preimplantation embryo development. Additionally, the analysis of cytoplasmic velocity with the PIV algorithm could be applied in TE cells (Figure 1), where it is associated with the functionality of keratin cytoskeleton, crucial for subsequent implantation: keratin-depleted TE cells have a more mobile (less "rigid") cytoplasm (Lim et al., 2020).

Keratin 8/18 depletion also increased the apical curvature of TE cells, which is indicative of lower apical tension (Lim et al., 2020). Therefore, microaspiration or indentation methods may help in detecting embryos with keratin defects. Interestingly, in mice, CT of TE cells is associated with the embryo size at least at the early blastocyst stage: smaller embryos (obtained by dissection of the whole embryo in halves or quarters) display higher CT (Chan et al., 2019). Therefore, measuring the CT of cells could provide information on the functionality of the cellular cytoskeleton, intracellular junctions, and ion pumps required for cavitation in TE cells (Chan et al., 2019; Lim et al., 2020).

6 Summary

This review offers a comprehensive overview of the molecular mechanisms that underlie the biomechanical properties of oocytes and embryos, along with the potential noninvasive techniques for assessing those properties. Our intent is to bridge the gap between scientific research and practical applications, providing a background for the suitability of the proposed techniques in the context of ART.

As highlighted here, cytoskeletal proteins play a pivotal role in determining the developmental potential of oocytes and embryos. Cytoskeleton, particularly its actomyosin component, governs key intracellular processes such as cell cycle progression or organelle trafficking, and intercellular processes such as compaction and cavitation. Elucidating biomechanical biomarkers characterizing a high-quality oocyte and properly developing preimplantation embryo with functional TE could provide a novel approach for evaluating quality beyond conventional morphological assessment. We draw attention to promising techniques, such as analysis of cytoplasmic movement or cavitation-related morphokinetic

parameters as well as cortical tension and elasticity measurements, which may offer novel insights into oocyte and embryo viability.

The integration of biomechanical assessments into ART could refine currently used procedures. Conventional methods of oocyte and embryo evaluation based solely on morphological criteria have limitations in predicting implantation and pregnancy rates accurately. Biomechanical assessment provides a more comprehensive understanding of oocyte and embryo quality, potentially enhancing the selection of oocytes and embryos with higher developmental potential. While some questions and ambiguities persist, and further research and validation are imperative to establish the reliability and effectiveness of these techniques in a clinical setting, ongoing research in cellular biomechanics holds great potential for enhancing the success rates of fertility treatments.

Author contributions

MF: Project administration, Writing–original draft, Writing–review and editing, Data curation. RC: Writing–review and editing. AW: Writing–review and editing, Data curation. AWB: Writing–review and editing. AA: Supervision, Writing–review and editing, Data curation.

Funding

The author(s) declare financial support was received for the research, authorship, and/or publication of this article. Funding from National Science Centre, Poland: MF was supported by Preludium grant (UMO-2020/37/N/NZ5/02733; awarded to MF) and Opus grant (UMO-2017/27/B/NZ5/00405; awarded to AA); AW was supported by Opus grant (UMO-2020/39/B/NZ5/02962; awarded to AA); AA was supported by both Opus grants. Funding from Czech Science Foundation: RC and AWB were supported by GACR Standard (21-03305S) grant awarded to AWB.

Acknowledgments

We would like to thank Ewa Kosyl for her help with preparing the figure on cavitation dynamics.

Conflict of interest

AA is a co-inventor in the patent "Methods for predicting mammalian embryo viability" (patent no. US 9 410 939 B2) on the application of cytoplasmic movement analysis in evaluation of embryo quality.

The remaining authors declare that the research was conducted in the absence of any commercial or financial relationships that could be construed as a potential conflict of interest.

Publisher's note

All claims expressed in this article are solely those of the authors and do not necessarily represent those of their affiliated organizations, or those of the publisher, the editors and the reviewers. Any product that may be evaluated in this article, or claim that may be made by its manufacturer, is not guaranteed or endorsed by the publisher.

References

Aghigh, A., Bancelin, S., Rivard, M., Pinsard, M., Ibrahim, H., and Légaré, F. (2023). Second harmonic generation microscopy: a powerful tool for bio-imaging. *Biophys. Rev.* 15, 43–70. doi:10.1007/S12551-022-01041-6

Ajduk, A., Ilozue, T., Windsor, S., Yu, Y., Seres, K. B., Bomphrey, R. J., et al. (2011). Rhythmic actomyosin-driven contractions induced by sperm entry predict mammalian embryo viability. *Nat. Commun.* 2, 417–7. doi:10.1038/ncomms1424

Ajduk, A., and Szkulmowski, M. (2019). Light microscopy of mammalian gametes and embryos: methods and applications. *Int. J. Dev. Biol.* 63, 235–244. doi:10.1387/ijdb.180300aa

Ajduk, A., and Zernicka-Goetz, M. (2013). Quality control of embryo development. *Mol. Asp. Med.* 34, 903–918. doi:10.1016/j.mam.2013.03.001

Aksenov, M. Y., Aksenova, M. V., Butterfield, D. A., Geddes, J. W., and Markesbery, W. R. (2001). Protein oxidation in the brain in Alzheimer's disease. *Neuroscience* 103, 373–383. doi:10.1016/S0306-4522(00)00580-7

Anagnostopoulou, C., Maldonado Rosas, I., Singh, N., Gugnani, N., Chockalingham, A., Singh, K., et al. (2022). Oocyte quality and embryo selection strategies: a review for the embryologists, by the embryologists. *Panminerva Med.* 64, 171–184. doi:10.23736/S0031-0808.22.04680-8

Andolfi, L., Masiero, E., Giolo, E., Martinelli, M., Luppi, S., Dal Zilio, S., et al. (2016). Investigating the mechanical properties of zona pellucida of whole human oocytes by atomic force spectroscopy. *Integr. Biol.* 8, 886–893. doi:10.1039/C6IB00044D

Aplin, J. D., and Ruane, P. T. (2017). Embryo-epithelium interactions during implantation at a glance. *J. Cell Sci.* 130, 15–22. doi:10.1242/jcs.175943

Arena, R., Bisogno, S., Gasior, Ł., Rudnicka, J., Bernhardt, L., Haaf, T., et al. (2021). Lipid droplets in mammalian eggs are utilized during embryonic diapause. *Proc. Natl. Acad. Sci. U.S.A.* 118, e2018362118. doi:10.1073/pnas.2018362118

Baribault, H., Price, J., Miyai, K., and Oshima, R. G. (1993). Mid-gestational lethality in mice lacking keratin 8. *Genes Dev.* 7, 1191–1202. doi:10.1101/gad.7.7a.1191

Battistella, A., Andolfi, L., Zanetti, M., Dal Zilio, S., Stebel, M., Ricci, G., et al. (2022). Atomic force spectroscopy-based essay to evaluate oocyte postovulatory aging. *Bioeng. Transl. Med.* 7, e10294. doi:10.1002/BTM2.10294

Bazer, F. W., Spencer, T. E., Johnson, G. A., Burghardt, R. C., and Wu, G. (2009). Comparative aspects of implantation. *Reproduction* 138, 195–209. doi:10.1530/REP-09-0158

Berlett, B. S., and Stadtman, E. R. (1997). Protein oxidation in aging, disease, and oxidative stress. *J. Biol. Chem.* 272, 20313–20316. doi:10.1074/jbc.272.33.20313

Bertet, C., Sulak, L., and Lecuit, T. (2004). Myosin-dependent junction remodelling controls planar cell intercalation and axis elongation. *Nature* 429, 667–671. doi:10.1038/nature02590

Blondin, P. (2017). Logistics of large scale commercial IVF embryo production. *Reprod. Fertil. Dev.* 29, 32–36. doi:10.1071/RD16317

Boccaccio, A., Frassanito, M. C., Lamberti, L., Brunelli, R., Maulucci, G., Monaci, M., et al. (2012). Nanoscale characterization of the biomechanical hardening of bovine zona pellucida. *J. R. Soc. Interface* 9, 2871–2882. doi:10.1098/RSIF.2012.0269

Bodri, D., Sugimoto, T., Yao Serna, J., Kawachiya, S., Kato, R., and Matsumoto, T. (2016). Blastocyst collapse is not an independent predictor of reduced live birth: a time-lapse study. *Fertil. Steril.* 105, 1476–1483. doi:10.1016/j.fertnstert.2016.02.014

Bogliolo, L., Murrone, O., Di Emidio, G., Piccinini, M., Ariu, F., Ledda, S., et al. (2013). Raman spectroscopy-based approach to detect aging-related oxidative damage in the mouse oocyte. *J. Assist. Reprod. Genet.* 30, 877–882. doi:10.1007/s10815-013-0046-6

Bon, P., Lécart, S., Fort, E., and Lévêque-Fort, S. (2014). Fast label-free cytoskeletal network imaging in living mammalian cells. *Biophys. J.* 106, 1588–1595. doi:10.1016/J.BPJ.2014.02.023

Bormann, C. L., Thirumalaraju, P., Kanakasabapathy, M. K., Kandula, H., Souter, I., Dimitriadis, I., et al. (2020). Consistency and objectivity of automated embryo assessments using deep neural networks. *Fertil. Steril.* 113, 781–787. doi:10.1016/j.fertnstert.2019.12.004

Bradley, J., Pope, I., Masia, F., Sanusi, R., Langbein, W., Swann, K., et al. (2016). Quantitative imaging of lipids in live mouse oocytes and early embryos using CARS microscopy. *Development* 143, 2238–2247. doi:10.1242/dev.129908

Bui, T. T. H., Belli, M., Fassina, L., Vigone, G., Merico, V., Garagna, S., et al. (2017). Cytoplasmic movement profiles of mouse surrounding nucleolus and not-surrounding nucleolus antral oocytes during meiotic resumption. *Mol. Reprod. Dev.* 84, 356–362. doi:10.1002/mrd.22788

Caamaño, J. N., Muñoz, M., Diez, C., and Gómez, E. (2010). Polarized light microscopy in mammalian oocytes. *Reprod. Domest. Anim.* 45, 49–56. doi:10.1111/j.1439-0531.2010.01621.x

Campàs, O. (2016). A toolbox to explore the mechanics of living embryonic tissues. *Semin. Cell Dev. Biol.* 55, 119–130. doi:10.1016/J.SEMCDB.2016.03.011

Carroll, J., Depypere, H., and Matthews, C. D. (1990). Freeze-thaw-induced changes of the zona pellucida explains decreased rates of fertilization in frozen-thawed mouse oocytes. *J. Reprod. Fertil.* 90, 547–553. doi:10.1530/jrf.0.0900547

Chaigne, A., Campillo, C., Gov, N. S., Voituriez, R., Azoury, J., Umaña-Diaz, C., et al. (2013). A soft cortex is essential for asymmetric spindle positioning in mouse oocytes. *Nat. Cell Biol.* 15, 958–966. doi:10.1038/ncb2799

Chaigne, A., Campillo, C., Gov, N. S., Voituriez, R., Sykes, C., Verlhac, M. H., et al. (2015). A narrow window of cortical tension guides asymmetric spindle positioning in the mouse oocyte. *Nat. Commun.* 6, 6027. doi:10.1038/ncomms7027

Chaigne, A., Campillo, C., Voituriez, R., Gov, N. S., Sykes, C., Verlhac, M. H., et al. (2016). F-actin mechanics control spindle centring in the mouse zygote. *Nat. Commun.* 7, 10253. doi:10.1038/ncomms10253

Chan, C. J., Costanzo, M., Ruiz-Herrero, T., Mönke, G., Petrie, R. J., Bergert, M., et al. (2019). Hydraulic control of mammalian embryo size and cell fate. *Nature* 571, 112–116. doi:10.1038/s41586-019-1309-x

Chapuis, A., Gala, A., Ferrières-Hoa, A., Mullet, T., Bringer-Deutsch, S., Vintejoux, E., et al. (2017). Sperm quality and paternal age: effect on blastocyst formation and pregnancy rates. *Basic Clin. Androl.* 27, 2. doi:10.1186/s12610-016-0045-4

Charras, G. T., Hu, C. K., Coughlin, M., and Mitchison, T. J. (2006). Reassembly of contractile actin cortex in cell blebs. *J. Cell Biol.* 175, 477–490. doi:10.1083/jcb.200602085

Colaco, S., and Sakkas, D. (2018). Paternal factors contributing to embryo quality. *J. Assist. Reprod. Genet.* 35, 1953–1968. doi:10.1007/s10815-018-1304-4

Consensus Group, C. (2020). 'There is only one thing that is truly important in an IVF laboratory: everything' Cairo Consensus Guidelines on IVF Culture Conditions. *Reprod. Biomed. Online* 40, 33–60. doi:10.1016/j.rbmo.2019.10.003

Coravos, J. S., Mason, F. M., and Martin, A. C. (2017). Actomyosin pulsing in tissue integrity maintenance during morphogenesis. *Trends Cell Biol.* 27, 276–283. doi:10.1016/j.tcb.2016.11.008

Coumailleau, F., Fürthauer, M., Knoblich, J. A., and González-Gaitán, M. (2009). Directional Delta and Notch trafficking in Sara endosomes during asymmetric cell division. *Nature* 458, 1051–1055. doi:10.1038/nature07854

Cui, W. (2010). Mother or nothing: the agony of infertility. *Bull. World Health Organ.* 88, 881–882. doi:10.2471/blt.10.011210

Czajkowska, K., and Ajduk, A. (2023). Mitochondrial activity and redox status in oocytes from old mice: the interplay between maternal and postovulatory aging. *Theriogenology* 204, 18–30. doi:10.1016/j.theriogenology.2023.03.022

Daar, A. S., and Merali, Z. (2002). "Infertility and social suffering: the case of ART in developing countries," in *"Medical, ethical and social aspects of assisted reproduction" held at WHO headquarters in Geneva, Switzerland 17–21 september 2001*. Editors E. Vayena, P. J. Rowe, and D. P. Griffin (Geneva: World Health Organization), 15–21.

Dalton, C. M., and Carroll, J. (2013). Biased inheritance of mitochondria during asymmetric cell division in the mouse oocyte. *J. Cell Sci.* 126, 2955–2964. doi:10.1242/jcs.128744

Davidson, B., Murray, A. A., Elfick, A., and Spears, N. (2013). Raman micro-spectroscopy can Be used to investigate the developmental stage of the mouse oocyte. *PLoS ONE* 8, e67972. doi:10.1371/journal.pone.0067972

D'Avino, P. P., Giansanti, M. G., and Petronczki, M. (2015). Cytokinesis in animal cells. *Cold Spring Harb. Perspect. Biol.* 7, a015834. doi:10.1101/cshperspect.a015834

Derivery, E., Seum, C., Daeden, A., Loubéry, S., Holtzer, L., Jülicher, F., et al. (2015). Polarized endosome dynamics by spindle asymmetry during asymmetric cell division. *Nature* 528, 280–285. doi:10.1038/nature16443

De Roo, C., Tilleman, K., Tsjoen, G., and De Sutter, P. (2016). Fertility options in transgender people. *Int. Rev. Psychiatry.* 28, 112–119. doi:10.3109/09540261.2015.1084275

Di Santo, M., Tarozzi, N., Nadalini, M., and Borini, A. (2012). Human sperm cryopreservation: update on techniques, effect on DNA integrity, and implications for ART. *Adv. Urol.* 2012, 854837. doi:10.1155/2012/854837

D'Occhio, M. J., Campanile, G., Zicarelli, L., Visintin, J. A., and Baruselli, P. S. (2020). Adhesion molecules in gamete transport, fertilization, early embryonic development, and implantation—role in establishing a pregnancy in cattle: a review. *Mol. Reprod. Dev.* 87, 206–222. doi:10.1002/mrd.23312

Du, Q. Y., Wang, E. Y., Huang, Y., Guo, X. Y., Xiong, Y. J., Yu, Y. P., et al. (2016). Blastocoele expansion degree predicts live birth after single blastocyst transfer for fresh and vitrified/warmed single blastocyst transfer cycles. *Fertil. Steril.* 105, 910–919. doi:10.1016/j.fertnstert.2015.12.014

Ducibella, T., Kurasawa, S., Rangarajan, S., Kopf, G. S., and Schultz, R. M. (1990). Precocious loss of cortical granules during mouse oocyte meiotic maturation and correlation with an egg-induced modification of the zona pellucida. *Dev. Biol.* 137, 46–55. doi:10.1016/0012-1606(90)90006-5

Dumbauld, D. W., Lee, T. T., Singh, A., Scrimgeour, J., Gersbach, C. A., Zamir, E. A., et al. (2013). How vinculin regulates force transmission. *Proc. Natl. Acad. Sci. U. S. A.* 110, 9788–9793. doi:10.1073/PNAS.1216209110

Dumont, J., Million, K., Sunderland, K., Rassinier, P., Lim, H., Leader, B., et al. (2007). Formin-2 is required for spindle migration and for the late steps of cytokinesis in mouse oocytes. *Dev. Biol.* 301, 254–265. doi:10.1016/j.ydbio.2006.08.044

Dumortier, J. G., Le Verge-Serandour, M., Tortorelli, A. F., Mielke, A., De Plater, L., Turlier, H., et al. (2019). Hydraulic fracturing and active coarsening position the lumen of the mouse blastocyst. *Sci. (80-.)* 365, 465–468. doi:10.1126/science.aaw7709

Dunkley, S., Scheffler, K., and Mogessie, B. (2022). Cytoskeletal form and function in mammalian oocytes and zygotes. *Curr. Opin. Cell Biol.* 75, 102073. doi:10.1016/J.CEB.2022.02.007

Ebner, T., Moser, M., Sommergruber, M., Puchner, M., Wiesinger, R., and Tews, G. (2003). Developmental competence of oocytes showing increased cytoplasmic viscosity. *Hum. Reprod.* 18, 1294–1298. doi:10.1093/humrep/deg232

Ebner, T., Oppelt, P., Radler, E., Allerstorfer, C., Habelsberger, A., Mayer, R. B., et al. (2017). Morphokinetics of vitrified and warmed blastocysts predicts implantation potential. *J. Assist. Reprod. Genet.* 34, 239–244. doi:10.1007/s10815-016-0855-5

Eckert, J. J., McCallum, A., Mears, A., Rumsby, M. G., Cameron, I. T., and Fleming, T. P. (2004). Specific PKC isoforms regulate blastocoel formation during mouse preimplantation development. *Dev. Biol.* 274, 384–401. doi:10.1016/J.YDBIO.2004.07.027

Eddy, R. J., Pierini, L. M., Matsumura, F., and Maxfield, F. R. (2000). Ca2+-dependent myosin II activation is required for uropod retraction during neutrophil migration. *J. Cell Sci.* 113, 1287–1298. doi:10.1242/jcs.113.7.1287

European Society of Human Reproduction and Embryology (ESHRE) (2023). ART in Europe, 2019: results generated from European registries by ESHRE. Available from: https://www.eshre.eu.

Evans, C. L., and Xie, X. S. (2008). Coherent anti-Stokes Raman scattering microscopy: chemical imaging for biology and medicine. *Annu. Rev. Anal. Chem.* 1, 883–909. doi:10.1146/annurev.anchem.1.031207.112754

Fan, W., Huang, T., Wu, T., Bai, H., Kawahara, M., and Takahashi, M. (2022). Zona pellucida removal by acid Tyrode's solution affects pre- and post-implantation development and gene expression in mouse embryos†. *Biol. Reprod.* 107, 1228–1241. doi:10.1093/biolre/ioac155

Fidler, A. T., and Bernstein, J. (1999). Infertility: from a personal to a public health problem. *Public Health Rep.* 14, 494–511. doi:10.1093/phr/114.6.494

FitzHarris, G., Marangos, P., and Carroll, J. (2007). Changes in endoplasmic reticulum structure during mouse oocyte maturation are controlled by the cytoskeleton and cytoplasmic dynein. *Dev. Biol.* 305, 133–144. doi:10.1016/j.ydbio.2007.02.006

Fujiwara, K., and Pollard, T. D. (1976). Fluorescent antibody localization of myosin in the cytoplasm, cleavage furrow, and mitotic spindle of human cells. *J. Cell Biol.* 71, 848–875. doi:10.1083/jcb.71.3.848

Gandolfi, F., and Brevini, T. A. L. (2010). RFD Award Lecture 2009. *in vitro* maturation of farm animal oocytes: a useful tool for investigating the mechanisms leading to full-term development. *Reprod. Fertil. Dev.* 22, 495–507. doi:10.1071/RD09151

Gardner, D. K., and Balaban, B. (2016). Assessment of human embryo development using morphological criteria in an era of time-lapse, algorithms and 'OMICS': is looking good still important? *Mol. Hum. Rep.* 22, 704–718. doi:10.1093/molehr/gaw057

Gazzo, E., Peña, F., Valdéz, F., Chung, A., Velit, M., Ascenzo, M., et al. (2020). Blastocyst contractions are strongly related with aneuploidy, lower implantation rates, and slow-cleaving embryos: a time lapse study. *J. Bras. Reprod. Assist.* 24, 77–81. doi:10.5935/1518-0557.20190053

Gimenes, F., Souza, R. P., Bento, J. C., Teixeira, J. J. V., Maria-Engler, S. S., Bonini, M. G., et al. (2014). Male infertility: a public health issue caused by sexually transmitted pathogens. *Nat. Rev. Urol.* 11, 672–687. doi:10.1038/nrurol.2014.285

Giuliano, R., Maione, A., Vallefuoco, A., Sorrentino, U., and Zuccarello, D. (2023). Preimplantation genetic testing for genetic diseases: limits and review of current literature. *Genes* 14, 2095. doi:10.3390/genes14112095

Gómez-Martínez, R., Hernández-Pinto, A. M., Duch, M., Vázquez, P., Zinoviev, K., De La Rosa, E. J., et al. (2013). Silicon chips detect intracellular pressure changes in living cells. *Nat. Nanotechnol.* 8, 517–521. doi:10.1038/nnano.2013.118

Goossens, K., Tesfaye, D., Rings, F., Schellander, K., Hölker, M., Van Poucke, M., et al. (2010). Suppression of keratin 18 gene expression in bovine blastocysts by RNA interference. *Reprod. Fertil. Dev.* 22, 395–404. doi:10.1071/RD09080

Hansen, P. J. (2014). Current and future assisted reproductive technologies for mammalian farm animals. *Adv. Exp. Med. Biol.* 752, 1–22. doi:10.1007/978-1-4614-8887-3_1

Haucke, E., Santos, A. N., Simm, A., Henning, C., Glomb, M. A., Gürke, J., et al. (2014). Accumulation of advanced glycation end products in the rabbit blastocyst under maternal diabetes. *Reproduction* 148, 169–178. doi:10.1530/REP-14-0149

Hendriks, W. K., Roelen, B. A. J., Colenbrander, B., and Stout, T. A. E. (2015). Cellular damage suffered by equine embryos after exposure to cryoprotectants or cryopreservation by slow-freezing or vitrification. *Equine Vet. J.* 47, 701–707. doi:10.1111/evj.12341

Hernebring, M., Brolén, G., Aguilaniu, H., Semb, H., and Nyström, T. (2006). Elimination of damaged proteins during differentiation of embryonic stem cells. *Proc. Natl. Acad. Sci. U. S. A.* 103, 7700–7705. doi:10.1073/pnas.0510944103

Herrick, J. R. (2019). Assisted reproductive technologies for endangered species conservation: developing sophisticated protocols with limited access to animals with unique reproductive mechanisms. *Biol. Reprod.* 100, 1158–1170. doi:10.1093/biolre/ioz025

Hesse, M., Franz, T., Tamai, Y., Taketo, M. M., and Magin, T. M. (2000). Targeted deletion of keratins 18 and 19 leads to trophoblast fragility and early embryonic lethality. *EMBO J.* 19, 5060–5070. doi:10.1093/emboj/19.19.5060

Hildebrandt, T. B., Hermes, R., Colleoni, S., Diecke, S., Holtze, S., Renfree, M. B., et al. (2018). Embryos and embryonic stem cells from the white rhinoceros. *Nat. Commun.* 9, 2589. doi:10.1038/s41467-018-04959-2

Hosu, B. G., Mullen, S. F., Critser, J. K., and Forgacs, G. (2008). Reversible disassembly of the actin cytoskeleton improves the survival rate and developmental competence of cryopreserved mouse oocytes. *PLoS One* 3, e2787, e2787. doi:10.1371/journal.pone.0002787

Hsieh, C.-S., Chen, S.-U., Lee, Y.-W., Yang, Y.-S., and Sun, C.-K. (2008). Higher harmonic generation microscopy of *in vitro* cultured mammal oocytes and embryos. *Opt. Express* 16, 11574–11588. doi:10.1364/oe.16.011574

Huang, T. T., Huang, D. H., Ahn, H. J., Arnett, C., and Huang, C. T. (2019). Early blastocyst expansion in euploid and aneuploid human embryos: evidence for a non-invasive and quantitative marker for embryo selection. *Reprod. Biomed. Online* 39, 27–39. doi:10.1016/j.rbmo.2019.01.010

Huang, T. T. F., Chinn, K., Kosasa, T., Ahn, H. J., and Kessel, B. (2016). Morphokinetics of human blastocyst expansion *in vitro*. *Reprod. Biomed. Online* 33, 659–667. doi:10.1016/j.rbmo.2016.08.020

Human Fertilisation and Embryology Authority (HEFA) (2021). HFEA Fertility treatment 2019: trends and figures. Available from: https://www.hfea.gov.uk.

Inhorn, M. C., van Balen, F., Sandelowski, M., de Lacey, S., Thompson, C. M., Greil, A. L., et al. (2002). *Infertility around the globe: new thinking on childlessness, gender, and reproductive technologies., infertility around the globe*. Berkeley: University of California Press. doi:10.1525/9780520927810

Ishigaki, M., Hashimoto, K., Sato, H., and Ozaki, Y. (2017). Non-destructive monitoring of mouse embryo development and its qualitative evaluation at the molecular level using Raman spectroscopy. *Sci. Rep.* 7, 43942. doi:10.1038/srep43942

Iwasawa, T., Takahashi, K., Goto, M., Anzai, M., Shirasawa, H., Sato, W., et al. (2019). Human frozen-thawed blastocyst morphokinetics observed using time-lapse cinematography reflects the number of trophectoderm cells. *PLoS One* 14, e0210992. doi:10.1371/journal.pone.0210992

Jasensky, J., Boughton, A. P., Khmaladze, A., Ding, J., Zhang, C., Swain, J. E., et al. (2016). Live-cell quantification and comparison of mammalian oocyte cytosolic lipid content between species, during development, and in relation to body composition using nonlinear vibrational microscopy. *Analyst* 141, 4694–4706. doi:10.1039/c6an00629a

Jurema, M. W., and Nogueira, D. (2006). *In vitro* maturation of human oocytes for assisted reproduction. *Fertil. Steril.* 86, 1277–1291. doi:10.1016/j.fertnstert.2006.02.126

Karnowski, K., Ajduk, A., Wieloch, B., Tamborski, S., Krawiec, K., Wojtkowski, M., et al. (2017). Optical coherence microscopy as a novel, non-invasive method for the 4D live imaging of early mammalian embryos. *Sci. Rep.* 7, 4165. doi:10.1038/s41598-017-04220-8

Khalilian, M., Navidbakhsh, M., Valojerdi, M. R., Chizari, M., and Yazdi, P. E. (2010). Estimating Young's modulus of zona pellucida by micropipette aspiration in combination with theoretical models of ovum. *J. R. Soc. Interface* 7, 687–694. doi:10.1098/rsif.2009.0380

Kochan, J., Niżański, W., Moreira, N., Cubas, Z. S., Nowak, A., Prochowska, S., et al. (2019). ARTs in wild felid conservation programmes in Poland and in the world. *J. Vet. Res.* 63, 457–464. doi:10.2478/jvetres-2019-0043

Kölle, S., Reese, S., and Kummer, W. (2009). New aspects of gamete transport, fertilization, and embryonic development in the oviduct gained by means of live cell imaging. *Theriogenology* 73, 786–795. doi:10.1016/j.theriogenology.2009.11.002

Kragh, M. F., and Karstoft, H. (2021). Embryo selection with artificial intelligence: how to evaluate and compare methods? *J. Assist. Reprod. Genet.* 38, 1675–1689. doi:10.1007/s10815-021-02254-6

Lanyon, J. M., and Burgess, E. A. (2019). "Reproductive science methods for wild, fully-marine mammals: current approaches and future applications," in *Advances in experimental medicine and Biology* (New York LLC: Springer), 363–411. doi:10.1007/978-3-030-23633-5_13

Larson, S. M., Lee, H. J., Hung, P. H., Matthews, L. M., Robinson, D. N., and Evans, J. P. (2010). Cortical mechanics and meiosis II completion in mammalian oocytes are mediated by myosin-II and Ezrin-Radixin-Moesin (ERM) proteins. *Mol. Biol. Cell* 21, 3182–3192. doi:10.1091/mbc.E10-01-0066

Leader, B., Lim, H., Carabatsos, M. J., Harrington, A., Ecsedy, J., Pellman, D., et al. (2002). Formin-2, polyploidy, hypofertility and positioning of the meiotic spindle in mouse oocytes. *Nat. Cell Biol.* 4, 921–928. doi:10.1038/ncb880

Lemoine, M. E., and Ravitsky, V. (2013). Toward a public health approach to infertility: the ethical dimensions of infertility prevention. *Public Health Ethics* 6, 287–301. doi:10.1093/phe/pht026

Leoni, G. G., Berlinguer, F., Succu, S., Bebbere, D., Mossa, F., Madeddu, M., et al. (2008). A new selection criterion to assess good quality ovine blastocysts after vitrification and to predict their transfer into recipients. *Mol. Reprod. Dev.* 75, 373–382. doi:10.1002/mrd.20754

Letourneau, J. M., Ebbel, E. E., Katz, P. P., Oktay, K. H., McCulloch, C. E., Ai, W. Z., et al. (2012). Acute ovarian failure underestimates age-specific reproductive impairment for young women undergoing chemotherapy for cancer. *Cancer* 118, 1933–1939. doi:10.1002/cncr.26403

Levine, R. L. (2002). Carbonyl modified proteins in cellular regulation, aging, and disease. *Free Radic. Biol. Med.* 32, 790–796. doi:10.1016/S0891-5849(02)00765-7

Li, L., Zheng, P., and Dean, J. (2010). Maternal control of early mouse development. *Development* 137, 859–870. doi:10.1242/dev.039487

Liang, T., and Motan, T. (2016). Mature oocyte cryopreservation for fertility preservation. *Adv. Exp. Med. Biol.* 951, 155–161. doi:10.1007/978-3-319-45457-3_13

Lim, H. Y. G., Alvarez, Y. D., Gasnier, M., Wang, Y., Tetlak, P., Bissiere, S., et al. (2020). Keratins are asymmetrically inherited fate determinants in the mammalian embryo. *Nature* 585, 404–409. doi:10.1038/s41586-020-2647-4

Lin, R., Feng, G., Shu, J., Zhang, B., Zhou, H., Gan, X., et al. (2017). Blastocoele re-expansion time in vitrified–warmed cycles is a strong predictor of clinical pregnancy outcome. *J. Obstet. Gynaecol. Res.* 43, 689–695. doi:10.1111/jog.13257

Lindheim, S. R., and Klock, S. C. (2018). Oocyte donation: lessons from the past, directions for the future. *Fertil. Steril.* 110, 979–980. doi:10.1016/j.fertnstert.2018.09.019

Liu, X., Fernandes, R., Jurisicova, A., Casper, R., Sun, Yu, Liu, X., et al. (2010). *In situ* mechanical characterization of mouse oocytes using a cell holding device. *Lab. Chip* 10, 2154–2161. doi:10.1039/C004706F

Liu, X., Shi, J., Zong, Z., Wan, K. T., and Sun, Y. (2012). Elastic and viscoelastic characterization of mouse oocytes using micropipette indentation. *Ann. Biomed. Eng.* 40, 2122–2130. doi:10.1007/s10439-012-0595-3

Lord, T., Aitken, J. R., John Aitken, R., and Aitken, J. R. (2013). Oxidative stress and ageing of the post-ovulatory oocyte. *Reproduction* 146, 217–227. doi:10.1530/rep-13-0111

Louvet, S., Aghion, J., Santa-Maria, A., Mangeat, P., and Maro, B. (1996). Ezrin becomes restricted to outer cells following asymmetrical division in the preimplantation mouse embryo. *Dev. Biol.* 177, 568–579. doi:10.1006/dbio.1996.0186

Lu, H., Hesse, M., Peters, B., and Magin, T. M. (2005). Type II keratins precede type I keratins during early embryonic development. *Eur. J. Cell Biol.* 84, 709–718. doi:10.1016/j.ejcb.2005.04.001

Ma, N., Mochel, N. R., Pham, P. D., Yoo, T. Y., Cho, K. W. Y., and Digman, M. A. (2019). Label-free assessment of pre-implantation embryo quality by the Fluorescence Lifetime Imaging Microscopy (FLIM)-phasor approach. *Sci. Rep.* 9, 13206. doi:10.1038/s41598-019-48107-2

Macaluso, M., Wright-Schnapp, T. J., Chandra, A., Johnson, R., Satterwhite, C. L., Pulver, A., et al. (2010). A public health focus on infertility prevention, detection, and management. *Fertil. Steril.* 93, 16.e1–10. doi:10.1016/j.fertnstert.2008.09.046

Mackenzie, A. C. L., Kyle, D. D., McGinnis, L. A., Lee, H. J., Aldana, N., Robinson, D. N., et al. (2016). Cortical mechanics and myosin-II abnormalities associated with post-ovulatory aging: implications for functional defects in aged eggs. *Mol. Hum. Reprod.* 22, 397–409. doi:10.1093/molehr/gaw019

Madan, P., Rose, K., and Watson, A. J. (2007). Na/K-ATPase beta1 subunit expression is required for blastocyst formation and normal assembly of trophectoderm tight junction-associated proteins. *J. Biol. Chem.* 282, 12127–12134. doi:10.1074/JBC.M700696200

Madero, J. I., Manotas, M. C., García-Acero, M., López Cáceres, A., and López Jaimes, C. (2023). Preimplantation genetic testing in assisted reproduction. *Minerva Obstet. Gynecol.* 75, 260–272. doi:10.23736/S2724-606X.21.04805-3

Maître, J. L., Berthoumieux, H., Krens, S. F. G., Salbreux, G., Jülicher, F., Paluch, E., et al. (2012). Adhesion functions in cell sorting by mechanically coupling the cortices of adhering cells. *Science* 338, 253–256. doi:10.1126/science.1225399

Maître, J. L., Niwayama, R., Turlier, H., Nedelec, F., and Hiiragi, T. (2015). Pulsatile cell-autonomous contractility drives compaction in the mouse embryo. *Nat. Cell Biol.* 17, 849–855. doi:10.1038/ncb3185

Maître, J. L., Turlier, H., Illukkumbura, R., Eismann, B., Niwayama, R., Nédélec, F., et al. (2016). Asymmetric division of contractile domains couples cell positioning and fate specification. *Nature* 536, 344–348. doi:10.1038/nature18958

Marcos, J., Pérez-Albalá, S., Mifsud, A., Molla, M., Landeras, J., and Meseguer, M. (2015). Collapse of blastocysts is strongly related to lower implantation success: a time-lapse study. *Hum. Reprod.* 30, 2501–2508. doi:10.1093/humrep/dev216

Marikawa, Y., and Alarcon, V. B. (2018). RHOA activity in expanding blastocysts is essential to regulate HIPPO-YAP signaling and to maintain the trophectoderm-specific gene expression program in a ROCK/actin filament-independent manner. *Mol. Hum. Reprod.* 25, 43–60. doi:10.1093/molehr/gay048

Martin, A. C., Kaschube, M., and Wieschaus, E. F. (2009). Pulsed contractions of an actin-myosin network drive apical constriction. *Nature* 457, 495–499. doi:10.1038/nature07522

Mastenbroek, S., de Wert, G., and Adashi, E. Y. (2021). The imperative of responsible innovation in reproductive medicine. *N. Engl. J. Med.* 385, 2096–2100. doi:10.1056/NEJMsb2101718

McCoy, R. C., Summers, M. C., McCollin, A., Ottolini, C. S., Ahuja, K., and Handyside, A. H. (2023). Meiotic and mitotic aneuploidies drive arrest of *in vitro* fertilized human preimplantation embryos. *Genome Med.* 15, 77. doi:10.1186/S13073-023-01231-1

McGinnis, L. A., Lee, H. J., Robinson, D. N., and Evans, J. P. (2015). MAPK3/1 (ERK1/2) and myosin light chain kinase in mammalian eggs affect myosin-II function and regulate the metaphase II state in a calcium- and zinc-dependent manner. *Biol. Reprod.* 92, 146. doi:10.1095/biolreprod.114.127027

Mehlmann, L. M., Terasaki, M., Jaffe, L. A., and Kline, D. (1995). Reorganization of the endoplasmic reticulum during meiotic maturation of the mouse oocyte. *Dev. Biol.* 170, 607–615. doi:10.1006/dbio.1995.1240

Miao, Y. L., Kikuchi, K., Sun, Q. Y., and Schatten, H. (2009). Oocyte aging: cellular and molecular changes, developmental potential and reversal possibility. *Hum. Reprod. Update.* 15, 573–585. doi:10.1093/humupd/dmp014

Mignini Renzini, M., Dal Canto, M., Guglielmo, M. C., Garcia, D., De Ponti, E., La Marca, A., et al. (2021). Sperm donation: an alternative to improve post-ICSI live birth rates in advanced maternal age patients. *Hum. Reprod.* 36, 2148–2156. doi:10.1093/humrep/deab148

Mihajlović, A. I., and Bruce, A. W. (2016). Rho-associated protein kinase regulates subcellular localisation of Angiomotin and Hippo-signalling during preimplantation mouse embryo development. *Reprod. Biomed. Online* 33, 381–390. doi:10.1016/j.rbmo.2016.06.028

Mihajlović, A. I., and Bruce, A. W. (2017). The first cell-fate decision of mouse preimplantation embryo development: integrating cell position and polarity. *Open Biol.* 7, 170210. doi:10.1098/rsob.170210

Mihalas, B. P., Bromfield, E. G., Sutherland, J. M., De Iuliis, G. N., McLaughlin, E. A., John Aitken, R., et al. (2018). Oxidative damage in naturally aged mouse oocytes is exacerbated by dysregulation of proteasomal activity. *J. Biol. Chem.* 293, 18944–18964. doi:10.1074/jbc.RA118.005751

Milewski, R., Szpila, M., and Ajduk, A. (2018). Dynamics of cytoplasm and cleavage divisions correlates with preimplantation embryo development. *Reproduction* 155, 1–14. doi:10.1530/REP-17-0230

Mogessie, B., and Schuh, M. (2017). Actin protects mammalian eggs against chromosome segregation errors. *Science* 357, 1647. doi:10.1126/science.aal1647

Mohler, W., Millard, A. C., and Campagnola, P. J. (2003). Second harmonic generation imaging of endogenous structural proteins. *Methods* 29, 97–109. doi:10.1016/S1046-2023(02)00292-X

Montag, M., Toth, B., and Strowitzki, T. (2013). New approaches to embryo selection. *Reprod. Biomed. Online* 27, 539–546. doi:10.1016/j.rbmo.2013.05.013

Moore, S. G., and Hasler, J. F. (2017). A 100-Year Review: reproductive technologies in dairy science. *J. Dairy Sci.* 100, 10314–10331. doi:10.3168/JDS.2017-13138

Morado, S. A., Cetica, P. D., Beconi, M. T., and Dalvit, G. C. (2009). Reactive oxygen species in bovine oocyte maturation *in vitro*. *Reprod. Fertil. Dev.* 21, 608–614. doi:10.1071/RD08198

Moreno, R. D., Schatten, G., and Ramalho-Santos, J. (2002). Golgi apparatus dynamics during mouse oocyte *in vitro* maturation: effect of the membrane trafficking inhibitor brefeldin A. *Biol. Reprod.* 66, 1259–1266. doi:10.1095/biolreprod66.5.1259

Moriwaki, K., Tsukita, S., and Furuse, M. (2007). Tight junctions containing claudin 4 and 6 are essential for blastocyst formation in preimplantation mouse embryos. *Dev. Biol.* 312, 509–522. doi:10.1016/J.YDBIO.2007.09.049

Murayama, Y., Mizuno, J., Kamakura, H., Fueta, Y., Nakamura, H., Akaishi, K., et al. (2006). Mouse zona pellucida dynamically changes its elasticity during oocyte maturation, fertilization, and early embryo development. *Hum. Cell* 19, 119–125. doi:10.1111/j.1749-0774.2006.00019.x

Murrell, M., Oakes, P. W., Lenz, M., and Gardel, M. L. (2015). Forcing cells into shape: the mechanics of actomyosin contractility. *Nat. Rev. Mol. Cell Biol.* 16, 486–498. doi:10.1038/nrm4012

Nagy, Z. P., Jones-Colon, S., Roos, P., Botros, L., Greco, E., Dasig, J., et al. (2009). Metabolomic assessment of oocyte viability. *Reprod. Biomed. Online* 18, 219–225. doi:10.1016/s1472-6483(10)60259-3

Nguyen, T. L., Pradeep, S., Judson-Torres, R. L., Reed, J., Teitell, M. A., and Zangle, T. A. (2022). Quantitative phase imaging: recent advances and expanding potential in biomedicine. *ACS Nano* 16, 11516–11544. doi:10.1021/ACSNANO.1C11507

Niimura, S. (2003). Time-lapse videomicrographic analyses of contractions in mouse blastocysts. *J. Reprod. Dev.* 49, 413–423. doi:10.1262/jrd.49.413

Nik Hazlina, N. H., Norhayati, M. N., Shaiful Bahari, I., and Nik Muhammad Arif, N. A. (2022). Worldwide prevalence, risk factors and psychological impact of infertility among women: a systematic review and meta-analysis. *BMJ Open* 12, e057132. doi:10.1136/bmjopen-2021-057132

Nikiforov, D., Grøndahl, M. L., Hreinsson, J., and Andersen, C. Y. (2022). Human oocyte morphology and outcomes of infertility treatment: a systematic review. *Reprod. Sci.* 29, 2768–2785. doi:10.1007/s43032-021-00723-y

Oldenbourg, R. (2013). Polarized light microscopy: principles and practice. *Cold Spring Harb. Protoc.* 2013, 078600. doi:10.1101/pdb.top078600

Ombelet, W., De Sutter, P., Van der Elst, J., and Martens, G. (2005). Multiple gestation and infertility treatment: registration, reflection and reaction - the Belgian project. *Hum. Reprod. Update* 11, 3–14. doi:10.1093/humupd/dmh048

Omidi, M., Faramarzi, A., Agharahimi, A., and Khalili, M. A. (2017). Noninvasive imaging systems for gametes and embryo selection in IVF programs: a review. *J. Microsc.* 267, 253–264. doi:10.1111/jmi.12573

Özgüç, Ö., de Plater, L., Kapoor, V., Tortorelli, A. F., Clark, A. G., and Maître, J. L. (2022). Cortical softening elicits zygotic contractility during mouse preimplantation development. *PLoS Biol.* 20, e3001593. doi:10.1371/journal.pbio.3001593

Özgüç, Ö., and Maître, J. L. (2020). Multiscale morphogenesis of the mouse blastocyst by actomyosin contractility. *Curr. Opin. Cell Biol.* 66, 123–129. doi:10.1016/j.ceb.2020.05.002

Paternot, G., Devroe, J., Debrock, S., D'Hooghe, T. M., and Spiessens, C. (2009). Intra- and inter-observer analysis in the morphological assessment of early-stage embryos. *Reprod. Biol. Endocrinol.* 7, 105. doi:10.1186/1477-7827-7-105

Patrizio, P., Fragouli, E., Bianchi, V., Borini, A., and Wells, D. (2007). Molecular methods for selection of the ideal oocyte. *Reprod. Biomed. Online* 15, 346–353. doi:10.1016/S1472-6483(10)60349-5

Pfender, S., Kuznetsov, V., Pleiser, S., Kerkhoff, E., and Schuh, M. (2011). Spire-type actin nucleators cooperate with formin-2 to drive asymmetric oocyte division. *Curr. Biol.* 21, 955–960. doi:10.1016/j.cub.2011.04.029

Pickering, S. J., Johnson, M. H., Braude, P. R., and Houliston, E. (1988). Cytoskeletal organization in fresh, aged and spontaneously activated human oocytes. *Hum. Reprod.* 3, 978–989. doi:10.1093/oxfordjournals.humrep.a136828

Piliszek, A., and Madeja, Z. E. (2018). "Pre-implantation development of domestic animals," in *Current topics in developmental Biology* (United States: Academic Press), 267–294. doi:10.1016/bs.ctdb.2017.11.005

Płusa, B., and Piliszek, A. (2020). Common principles of early mammalian embryo self-organisation. *Development* 147, 183079. doi:10.1242/DEV.183079

Popovic, M., Dhaenens, L., Boel, A., Menten, B., and Heindryckx, B. (2020). Chromosomal mosaicism in human blastocysts: the ultimate diagnostic dilemma. *Hum. Reprod. Update* 26, 313–334. doi:10.1093/humupd/dmz050

Posfai, E., Rovic, I., and Jurisicova, A. (2019). The mammalian embryo's first agenda: making trophectoderm. *Int. J. Dev. Biol.* 63, 157–170. doi:10.1387/ijdb.180404ep

Prosser, S. L., and Pelletier, L. (2017). Mitotic spindle assembly in animal cells: a fine balancing act. *Nat. Rev. Mol. Cell Biol.* 18, 187–201. doi:10.1038/nrm.2016.162

Rienzi, L., Vajta, G., and Ubaldi, F. (2011). Predictive value of oocyte morphology in human IVF: a systematic review of the literature. *Hum. Reprod. Update.* 17, 34–45. doi:10.1093/humupd/dmq029

Robert, B. (2009). Resonance Raman spectroscopy. *Photosynth. Res.* 101, 147–155. doi:10.1007/s11120-009-9440-4

Rosenberg, S. M., and Partridge, A. H. (2013). Premature menopause in young breast cancer: effects on quality of life and treatment interventions. *J. Thorac. Dis.* 5 Suppl 1, S55–S61. doi:10.3978/j.issn.2072-1439.2013.06.20

Rouchou, B. (2013). Consequences of infertility in developing countries. *Perspect. Public Health* 133, 174–179. doi:10.1177/1757913912472415

Rusciano, G., De Canditiis, C., Zito, G., Rubessa, M., Roca, M. S., Carotenuto, R., et al. (2017). Raman-microscopy investigation of vitrification-induced structural damages in mature bovine oocytes. *PLoS ONE* 12, e0177677. doi:10.1371/journal.pone.0177677

Ryan, A. Q., Chan, C. J., Graner, F., and Hiiragi, T. (2019). Lumen expansion facilitates epiblast-primitive endoderm fate specification during mouse blastocyst formation. *Dev. Cell* 51, 684–697. doi:10.1016/j.devcel.2019.10.011

Sadecki, E., Weaver, A., Zhao, Y., Stewart, E. A., and Ainsworth, A. J. (2022). Fertility trends and comparisons in a historical cohort of US women with primary infertility. *Reprod. Health* 19, 13. doi:10.1186/s12978-021-01313-6

Salmerón, A. M., Abreu, A. C., Vilches-Ferrón, M., and Fernández, I. (2021). Solution NMR in human embryo culture media as an option for assessment of embryo implantation potential. *NMR Biomed.* 34, e4536. doi:10.1002/nbm.4536

Salucci, S., Battistelli, M., Burattini, S., Sbrana, F., and Falcieri, E. (2020). Holotomographic microscopy: a new approach to detect apoptotic cell features. *Microsc. Res. Tech.* 83, 1464–1470. doi:10.1002/JEMT.23539

Samarage, C. R., White, M. D., Álvarez, Y. D., Fierro-González, J. C., Henon, Y., Jesudason, E. C., et al. (2015). Cortical tension allocates the first inner cells of the mammalian embryo. *Dev. Cell* 34, 435–447. doi:10.1016/j.devcel.2015.07.004

Sanches, B. V., Zangirolamo, A. F., and Seneda, M. M. (2019). Intensive use of IVF by large-scale dairy programs. *Anim. Reprod.* 16, 394–401. doi:10.21451/1984-3143-AR2019-0058

Sanchez, T., Venturas, M., Aghvami, S. A., Yang, X., Fraden, S., Sakkas, D., et al. (2019). Combined noninvasive metabolic and spindle imaging as potential tools for embryo and oocyte assessment. *Hum. Reprod.* 34, 2349–2361. doi:10.1093/humrep/dez210

Sandoz, P. A., Tremblay, C., Gisou van der Goot, F., and Frechin, M. (2019). Image-based analysis of living mammalian cells using label-free 3D refractive index maps reveals new organelle dynamics and dry mass flux. *PLoS Biol.* 17, e3000553. doi:10.1371/JOURNAL.PBIO.3000553

Saragusty, J., Diecke, S., Drukker, M., Durrant, B., Friedrich Ben-Nun, I., Galli, C., et al. (2016). Rewinding the process of mammalian extinction. *Zoo. Biol.* 35, 280–292. doi:10.1002/zoo.21284

Schliffka, M. F., Dumortier, J. G., Pelzer, D., Mukherjee, A., and Maître, J. L. (2023). *Inverse blebs operate as hydraulic pumps during mouse blastocyst formation*. bioRxiv, 2023.05.03.539105. doi:10.1101/2023.05.03.539105

Schuh, M., and Ellenberg, J. (2008). A new model for asymmetric spindle positioning in mouse oocytes. *Curr. Biol.* 18, 1986–1992. doi:10.1016/j.cub.2008.11.022

Sciorio, R., Thong, K. J., and Pickering, S. J. (2020). Spontaneous blastocyst collapse as an embryo marker of low pregnancy outcome: a time-lapse study. *J. Bras. Reprod. Assist.* 24, 34–40. doi:10.5935/1518-0557.20190044

Serwane, F., Mongera, A., Rowghanian, P., Kealhofer, D. A., Lucio, A. A., Hockenbery, Z. M., et al. (2017). *In vivo* quantification of spatially varying mechanical properties in developing tissues. *Nat. Methods* 14, 181–186. doi:10.1038/nmeth.4101

Shen, T., Benet, E., Sridhar, S. L., Abadie, J., Piat, E., and Vernerey, F. J. (2019). Separating the contributions of zona pellucida and cytoplasm in the viscoelastic response of human oocytes. *Acta Biomater.* 85, 253–262. doi:10.1016/j.actbio.2018.12.034

Shimoda, Y., Kumagai, J., Anzai, M., Kabashima, K., Togashi, K., Miura, Y., et al. (2016). Time-lapse monitoring reveals that vitrification increases the frequency of contraction during the pre-hatching stage in mouse embryos. *J. Reprod. Dev.* 62, 187–193. doi:10.1262/JRD.2015-150

Silber, S. J., Barbey, N., Lenahan, K., and Silber, D. Z. (2013). Applying clinically proven human techniques for contraception and fertility to endangered species and zoo animals: a review. *J. Zoo. Wildl. Med.* 44, 111–S122. doi:10.1638/1042-7260-44.4S.S111

Sirard, M. A. (2018). 40 years of bovine IVF in the new genomic selection context. *Reproduction* 156, R1. doi:10.1530/REP-18-0008

Sjunnesson, Y. (2020). *In vitro* fertilisation in domestic mammals—a brief overview. *J. Med. Sci.* 125, 68–76. doi:10.1080/03009734.2019.1697911

Skora, D., and Frankfurter, D. (2012). Adverse perinatal events associated with ART. *Semin. Reprod. Med.* 30, 84–91. doi:10.1055/s-0032-1307416

Skory, R. M., Moverley, A. A., Ardestani, G., Alvarez, Y., Domingo-Muelas, A., Pomp, O., et al. (2023). The nuclear lamina couples mechanical forces to cell fate in the preimplantation embryo via actin organization. *Nat. Commun.* 14, 3101–3114. doi:10.1038/s41467-023-38770-5

Society for Assisted Reproductive Technology (SART) (2022). Final national summary report for 2020. Available from: https://sartcorsonline.com.

Solon, J., Kaya-Çopur, A., Colombelli, J., and Brunner, D. (2009). Pulsed forces timed by a ratchet-like mechanism drive directed tissue movement during dorsal closure. *Cell* 137, 1331–1342. doi:10.1016/j.cell.2009.03.050

Soreghan, B. A., Yang, F., Thomas, S. N., Hsu, J., and Yang, A. J. (2003). High-throughput proteomic-based identification of oxidatively induced protein carbonylation in mouse brain. *Pharm. Res.* 20, 1713–1720. doi:10.1023/B:PHAM.0000003366.25263.78

Stadtman, E. R. (1992). Protein oxidation and aging. *Science* 257, 1220–1224. doi:10.1126/science.1355616

Stitzel, M. L., and Seydoux, G. (2007). Regulation of the oocyte-to-zygote transition. *Science* 316, 407–408. doi:10.1126/science.1138236

Straight, A. F., Cheung, A., Limouze, J., Chen, I., Westwood, N. J., Sellers, J. R., et al. (2003). Dissecting temporal and spatial control of cytokinesis with a myosin II inhibitor. *Science* 299, 1743–1747. doi:10.1126/science.1081412

Sun, S. C., Gao, W. W., Xu, Y. N., Jin, Y. X., Wang, Q. L., Yin, X. J., et al. (2012). Degradation of actin nucleators affects cortical polarity of aged mouse oocytes. *Fertil. Steril.* 97, 984–990. doi:10.1016/j.fertnstert.2012.01.101

Swann, K., Windsor, S., Campbell, K., Elgmati, K., Nomikos, M., Zernicka-Goetz, M., et al. (2012). Phospholipase C-ζ-induced Ca 2+ oscillations cause coincident cytoplasmic movements in human oocytes that failed to fertilize after intracytoplasmic sperm injection. *Fertil. Steril.* 97, 742–747. doi:10.1016/j.fertnstert.2011.12.013

Szpila, M., Walewska, A., Sabat-Pośpiech, D., Strączyńska, P., Ishikawa, T., Milewski, R., et al. (2019). Postovulatory ageing modifies sperm-induced Ca2+ oscillations in mouse oocytes through a conditions-dependent, multi-pathway mechanism. *Sci. Rep.* 9, 11859. doi:10.1038/s41598-019-48281-3

Takahashi, T., Igarashi, H., Amita, M., Hara, S., Matsuo, K., and Kurachi, H. (2013). Molecular mechanism of poor embryo development in postovulatory aged oocytes: mini review. *J. Obstet. Gynaecol. Res.* 39, 1431–1439. doi:10.1111/jog.12111

Tamai, Y., Ishikawa, T. O., Bösl, M. R., Mori, M., Nozaki, M., Baribault, H., et al. (2000). Cytokeratins 8 and 19 in the mouse placental development. *J. Cell Biol.* 151, 563–572. doi:10.1083/jcb.151.3.563

Tan, J.-H. J. H., Wang, H. L. H.-L., Sun, X. S. X.-S., Liu, Y., Sui, H. S. H.-S., and Zhang, J. (2009). Chromatin configurations in the germinal vesicle of mammalian oocytes. *Mol. Hum. Reprod.* 15, 1–9. doi:10.1093/molehr/gan069

Taneja, N., and Burnette, D. T. (2019). Myosin IIA drives membrane bleb retraction. *Mol. Biol. Cell* 30, 1051–1059. doi:10.1091/mbc.E18-11-0752

Tang, B. L. (2012). Membrane trafficking components in cytokinesis. *Cell. Physiol. biochem.* 30, 1097–1108. doi:10.1159/000343301

Tatone, C., Di Emidio, G., Vento, M., Ciriminna, R., and Artini, P. G. (2010). Cryopreservation and oxidative stress in reproductive cells. *Gynecol. Endocrinol.* 26, 563–567. doi:10.3109/09513591003686395

Thayil, A., Jesacher, A., Wilson, T., Booth, M., Watanabe, T., and Srinivas, S. (2011). Long-term imaging of mouse embryos using adaptive harmonic generation microscopy. *J. Biomed. Opt.* 16, 046018. doi:10.1117/1.3569614

Togashi, K., Kumagai, J., Sato, E., Shirasawa, H., Shimoda, Y., Makino, K., et al. (2015). Dysfunction in gap junction intercellular communication induces aberrant behavior of the inner cell mass and frequent collapses of expanded blastocysts in mouse embryos. *J. Assist. Reprod. Genet.* 32, 969–976. doi:10.1007/s10815-015-0479-1

Toralova, T., Kinterova, V., Chmelikova, E., and Kanka, J. (2020). The neglected part of early embryonic development: maternal protein degradation. *Cell. Mol. Life Sci.* 77, 3177–3194. doi:10.1007/s00018-020-03482-2

Tsai, T. Y. C., Collins, S. R., Chan, C. K., Hadjitheodorou, A., Lam, P. Y., Lou, S. S., et al. (2019). Efficient front-rear coupling in neutrophil chemotaxis by dynamic myosin II localization. *Dev. Cell* 49, 189–205. doi:10.1016/j.devcel.2019.03.025

Vander Borght, M., and Wyns, C. (2018). Fertility and infertility: definition and epidemiology. *Clin. Biochem.* 62, 2–10. doi:10.1016/j.clinbiochem.2018.03.012

Venturas, M., Shah, J. S., Yang, X., Sanchez, T. H., Conway, W., Sakkas, D., et al. (2022). Metabolic state of human blastocysts measured by fluorescence lifetime imaging microscopy. *Hum. Reprod.* 37, 411–427. doi:10.1093/humrep/deab283

Venturas, M., Yang, X., Sakkas, D., and Needleman, D. (2023). Noninvasive metabolic profiling of cumulus cells, oocytes, and embryos via fluorescence lifetime imaging microscopy: a mini-review. *Hum. Reprod.* 38, 799–810. doi:10.1093/humrep/dead063

Viana, J. H. (2019). 2018 Statistics of embryo production and transfer in domestic farm animals Embryo industry on a new level: over one million embryos produced *in vitro*. *Embryo Technol. Newsl.* 36, 8–25.

Viljoen, A., Mathelié-Guinlet, M., Ray, A., Strohmeyer, N., Oh, Y. J., Hinterdorfer, P., et al. (2021). Force spectroscopy of single cells using atomic force microscopy. *Nat. Rev. Methods Prim.* 11 (1), 63–24. doi:10.1038/s43586-021-00062-x

Walls, M. L., Hunter, T., Ryan, J. P., Keelan, J. A., Nathan, E., and Hart, R. J. (2015). *In vitro* maturation as an alternative to standard *in vitro* fertilization for patients diagnosed with polycystic ovaries: a comparative analysis of fresh, frozen and cumulative cycle outcomes. *Hum. Reprod.* 30, 88–96. doi:10.1093/humrep/deu248

Watanabe, Y., Miyasaka, K. Y., Kubo, A., Kida, Y. S., Nakagawa, O., Hirate, Y., et al. (2017). Notch and Hippo signaling converge on Strawberry Notch 1 (Sbno1) to synergistically activate Cdx2 during specification of the trophectoderm. *Sci. Rep.* 7, 46135–46217. doi:10.1038/srep46135

Westerweel, J. (1997). Fundamentals of digital particle image velocimetry. *Meas. Sci. Technol.* 8, 1379–1392. doi:10.1088/0957-0233/8/12/002

Winkel, G. K., Ferguson, J. E., Takeichi, M., and Nuccitelli, R. (1990). Activation of protein kinase C triggers premature compaction in the four-cell stage mouse embryo. *Dev. Biol.* 138, 1–15. doi:10.1016/0012-1606(90)90171-E

Xie, H.-L. L., Wang, Y.-B. B., Jiao, G.-Z. Z., Kong, D.-L. L., Li, Q., Li, H., et al. (2016). Effects of glucose metabolism during *in vitro* maturation on cytoplasmic maturation of mouse oocytes. *Sci. Rep.* 6, 20764. doi:10.1038/srep20764

Yamamoto, K., Miura, H., Ishida, M., Mii, Y., Kinoshita, N., Takada, S., et al. (2021). Optogenetic relaxation of actomyosin contractility uncovers mechanistic roles of cortical tension during cytokinesis. *Nat. Commun.* 12, 7145. doi:10.1038/s41467-021-27458-3

Yanez, L. Z., Han, J., Behr, B. B., Pera, R. A. R., and Camarillo, D. B. (2016). Human oocyte developmental potential is predicted by mechanical properties within hours after fertilization. *Nat. Commun.* 7, 10809–10812. doi:10.1038/ncomms10809

Yin, H., Jiang, H., He, R., Wang, C., Zhu, J., and Li, Y. (2016). The effects of blastocyst morphological score and blastocoele re-expansion speed after warming on pregnancy outcomes. *Clin. Exp. Reprod. Med.* 43, 31–37. doi:10.5653/cerm.2016.43.1.31

Yu, C. H., Langowitz, N., Wu, H. Y., Farhadifar, R., Brugues, J., Yoo, T. Y., et al. (2014). Measuring microtubule polarity in spindles with second-harmonic generation. *Biophys. J.* 106, 1578–1587. doi:10.1016/j.bpj.2014.03.009

Zaninovic, N., and Rosenwaks, Z. (2020). Artificial intelligence in human *in vitro* fertilization and embryology. *Fert. Steril.* 114, 914–920. doi:10.1016/j.fertnstert.2020.09.157

Zenker, J., White, M. D., Gasnier, M., Alvarez, Y. D., Lim, H. Y. G., Bissiere, S., et al. (2018). Expanding actin rings zipper the mouse embryo for blastocyst formation. *Cell* 173, 776–791. doi:10.1016/j.cell.2018.02.035

Zenker, J., White, M. D., Templin, R. M., Parton, R. G., Thorn-Seshold, O., Bissiere, S., et al. (2017). A microtubule-organizing center directing intracellular transport in the early mouse embryo. *Science* 357, 925–928. doi:10.1126/science.aam9335

Zhao, J., Yan, Y., Huang, X., Sun, L., and Li, Y. (2019). Blastocoele expansion: an important parameter for predicting clinical success pregnancy after frozen-warmed blastocysts transfer. *Reprod. Biol. Endocrinol.* 17, 15–18. doi:10.1186/s12958-019-0454-2

Zhao, Q., Yin, T., Peng, J., Zou, Y., Yang, J., Shen, A., et al. (2013). Noninvasive metabolomic profiling of human embryo culture media using a simple spectroscopy adjunct to morphology for embryo assessment in *in vitro* fertilization (IVF). *Int. J. Mol. Sci.* 14, 6556–6570. doi:10.3390/ijms14046556

Zhu, M., Leung, C. Y., Shahbazi, M. N., and Zernicka-Goetz, M. (2017). Actomyosin polarisation through PLC-PKC triggers symmetry breaking of the mouse embryo. *Nat. Commun.* 8, 921–1016. doi:10.1038/s41467-017-00977-8

Zumbusch, A., Langbein, W., and Borri, P. (2013). Nonlinear vibrational microscopy applied to lipid biology. *Prog. Lipid Res.* 52, 615–632. doi:10.1016/j.plipres.2013.07.003

frontiers | Frontiers in Cell and Developmental Biology

TYPE Mini Review
PUBLISHED 07 March 2024
DOI 10.3389/fcell.2024.1325565

Check for updates

OPEN ACCESS

EDITED BY
Jason Knott,
Michigan State University, United States

REVIEWED BY
Antonio R. L. Teixeira,
University of Brasilia, Brazil

*CORRESPONDENCE
Ivan Varga,
ivan.varga@fmed.uniba.sk

RECEIVED 21 October 2023
ACCEPTED 27 February 2024
PUBLISHED 07 March 2024

CITATION
Visnyaiová K, Varga I, Feitscherová C, Pavlíková L, Záhumenský J and Mikušová R (2024), Morphology of the immune cells in the wall of the human uterine tube and their possible impact on reproduction—uterine tube as a possible immune privileged organ. *Front. Cell Dev. Biol.* 12:1325565. doi: 10.3389/fcell.2024.1325565

COPYRIGHT
© 2024 Visnyaiová, Varga, Feitscherová, Pavlíková, Záhumenský and Mikušová. This is an open-access article distributed under the terms of the Creative Commons Attribution License (CC BY). The use, distribution or reproduction in other forums is permitted, provided the original author(s) and the copyright owner(s) are credited and that the original publication in this journal is cited, in accordance with accepted academic practice. No use, distribution or reproduction is permitted which does not comply with these terms.

Morphology of the immune cells in the wall of the human uterine tube and their possible impact on reproduction—uterine tube as a possible immune privileged organ

Kristína Visnyaiová[1], Ivan Varga[2]*, Claudia Feitscherová[2], Lada Pavlíková[3], Jozef Záhumenský[1] and Renáta Mikušová[2]

[1]Second Department of Gynecology and Obstetrics, Faculty of Medicine, Comenius University in Bratislava and University Hospital, Bratislava, Slovakia, [2]Institute of Histology and Embryology, Faculty of Medicine, Comenius University in Bratislava, Bratislava, Slovakia, [3]Department of Rehabilitation Studies, Faculty of Health Care Studies, University of Western Bohemia, Pilsen, Czechia

The uterine tube, as well as other parts of the upper female reproductive system, is immunologically unique in its requirements for tolerance to allogenic sperm and semi-allogenic embryos, yet responds to an array of sexually transmitted pathogens. To understand this dichotomy, there is a need to understand the functional morphology of immune cells in the wall of the uterine tube. Thus, we reviewed scientific literature regarding immune cells and the human uterine tube by using the scientific databases. The human uterine tube has a diverse population of immunocompetent cells representing both the innate and adaptive immune systems. We describe in detail the possible roles of cells of the mononuclear phagocyte system (macrophages and dendritic cells), T and B lymphocytes, natural killer cells, neutrophils and mast cells in association with the reproductive functions of uterine tubes. We are also discussing about the possible "immune privilege" of the uterine tube, as another mechanism to tolerate sperm and embryo without eliciting an inflammatory immune response. In uterine tube is not present an anatomical blood-tissue barrier between antigens and circulation. However, the immune cells of the uterine tube probably represent a type of "immunological barrier," which probably includes the uterine tube among the immunologically privileged organs. Understanding how immune cells in the female reproductive tract play roles in reproduction is essential to understand not only the mechanisms of gamete transport and fertilization as well as embryo transport through the uterine tube, but also in improving results from assisted reproduction.

KEYWORDS

uterine tube, macrophage, dendritic cell, T lymphocyte, B lymphocyte, natural killer cell, mast cell, fertility

1 Introduction

Uterine tubes (fallopian tubes, oviducts) are important organs of the female internal reproductive system, responsible for cardinal processes needed for successful reproduction. The uterine tube is the only tubular organ of the human body that, even under physiological conditions, performs a transport function in opposing directions. The picked-up oocyte

released during ovulation or formation of the early embryo is transported proximally, to the uterine cavity. Concomitantly, the uterine tube also facilitates transport of spermatozoa distally, to the ampullary portion, where fertilization usually occurs. However, the uterine tube has many other unique functions, such as sperm selection (an essential mechanism for preventing polyspermatic fertilization) or formation of a unique tubal fluid. Tubal fluid is important not only during fertilization but activates sperm before fertilization and nourishes the embryo during transport to the uterine cavity (Csöbönyeiová et al., 2022b; Varga et al., 2022; Hamranová et al., 2023).

The uterine tube, as well as other parts of the upper female reproductive system, is immunologically unique in its requirements for tolerance to allogenic sperm and semi-allogenic embryos, yet responds to an array of sexually transmitted pathogens. Although uterine tubes are considered sterile, microorganisms can ascend from the lower reproductive tract, causing pelvic inflammatory disease and/or reproductive alterations such as ectopic pregnancy (Caven and Carabeo, 2023; Jenabi et al., 2023; Pant et al., 2023) and tubal infertility (Hoenderboom et al., 2019; Liu et al., 2022). In general, uterine tube diseases account for 25%–35% of female factor infertility. Pelvic inflammatory disease is the most common cause of tubal disease, representing more than 50% of cases (Chua et al., 2017). However, the lumen of uterine tubes is not sterile. Uterine tubes harbor highly variable microbial communities among women, especially a variety of bacteria growing in mildly alkaline conditions. These diverse microbial communities of uterine tubes are affected by hormones and antibiotics, and exhibit biogeographical tropism (Liptáková et al., 2022). Epithelial cell secretions filled with several cytokines and chemokines from the human female upper reproductive tract inhibit sexually transmitted pathogens (including *Neisseria gonorrhoeae* and yeast *Candida albicans*), as well as reduce HIV-1 infection of target cells. In contrast, these secretions have no inhibitory effect on *Lactobacillus* (Wira et al., 2011). Probably because of this specific tubal microenvironment, the presence of lymphatic follicles in the wall of uterine tubes (indicating a massive presence of B lymphocytes and their activated antibody-producing plasma cells, usually present in the mucosae of other organs) is rare yet detectable during histological examination only in 2.1% of surgically removed healthy uterine tubes (Hunt and Lynn, 2002).

There is a diverse range of immunocompetent cells in uterine tubes. Ulrich et al. (2022) in their study applied single-cell RNA-sequencing to analyze more than 59.000 unselected cells from 10 specimen of human uterine tubes from 4 healthy subjects. They define 12 major cell types in healthy uterine tubes, from 4 are immune cells (B lymphocytes, T lymphocytes/NK cells, mast cells and macrophages). Ramraj et al. (2018), in a flow cytometric analysis of immunocompetent cells from dispersed tubal specimens, indicates that the predominant cell type is M1 macrophages (20% of total cells); followed by regulatory T lymphocytes (7%), CD8 cytotoxic T lymphocytes (3%), M2 macrophages (1%), perforin-positive natural killer (NK) cells (0.52%), and granzyme B-positive NK cells (0.13%). The aim of this narrative review is to present a comprehensive overview of the immune cell populations in the wall of human uterine tubes. We describe in detail the possible roles of cells of the mononuclear phagocyte system (macrophages and dendritic cells), T and B lymphocytes, NK cells, and mast cells in association with the reproductive functions of uterine tubes. All mentioned immunocompetent cells residing in the reproductive tract play paradoxical roles since they maintain immunity against pathogens yet also establish immune tolerance for sperm and embryos/fetuses (Lee et al., 2015). However, we are also discussing about the possible mechanism of "immune privilege" within the lumen of the uterine tube, as another mechanism to tolerate the foreign antigens as sperm and embryo without eliciting an inflammatory immune response. Understanding how immune cells in the female reproductive tract play roles in reproduction is essential to understand not only the mechanisms of gametes transport and fertilization as well as embryo transport through the uterine tube, but also in improving results from assisted reproduction and clinical embryology.

2 Methods

Recent and relevant scientific literature was reviewed herein on the topic of the functional morphology of immune cells in the wall of the human uterine tube. Scientific literature regarding morphologically different types of immune cells and the human uterine tube was reviewed by using scientific databases PubMed/Medline, SCOPUS, and Web of Knowledge.

A total of 109 references consisting of reviews, case reports, and original articles from the fields of histology, immunology, gynecology, and reproductive medicine published mostly in recent years were selected to document the present manuscript. The collected data were organized as a narrative literature review synthesis structured in paragraphs.

3 Cells of the mononuclear phagocyte system in the uterine tube

The mononuclear phagocyte system is defined as a cell lineage in which committed bone marrow progenitors give rise to monocytes of the peripheral blood and tissue macrophages. This nomenclature and definition were first time proposed by a Dutch scientist Ralph van Furth and his co-workers in 1972 (van Furth et al., 1972). In the following years, dendritic cells were also incorporated into this system. The mononuclear phagocyte system represents a critical regulator of innate and adaptive immune responses. Additionally, tissue macrophages also play a crucial role in tissue homeostasis, wound healing, and tissue regeneration in prenatal as well as postnatal development (Hume et al., 2019; Sreejit et al., 2020; Miah et al., 2021). Macrophages are a major cell population in most of the tissues in the body; and their numbers increase further in inflammation, wounding, and malignancy (Hume, 2006). There are two hypotheses about the exact origin of tissue macrophages. First, tissue-resident macrophages are a separate lineage seeded exclusively during embryonic development and maintained through adulthood by longevity and self-renewal. Second, other experiments suggesting that during postnatal life, circulating blood monocytes can replace tissue resident macrophages in all major organs and adopt their tissue-specific gene expression (Varol et al., 2015; Hume et al., 2019). In uterine tubes, macrophages and their pro-inflammatory and anti-inflammatory functions play a critical

role during *Chlamydia* infection and subsequent development of hydrosalpinx and/or pelvic inflammatory disease and ectopic pregnancy (Harvie et al., 2019; Wang et al., 2020; Zhang et al., 2022).

3.1 Macrophages in the uterine tube

In uterine tubes, macrophages are localized within the epithelium and in the connective tissue of the lamina propria. In an immunohistochemical study by Gaytán et al. (2007), performed on uterine tubes in different phases of the menstrual cycle, macrophages exhibited cyclic changes in both numbers and location in the uterine tube mucosa. Macrophages were relatively abundant in both the epithelium and the underlying connective tissue (lamina propria) during the early follicular phase, yet were scarce—particularly within the epithelium—during the late follicular phase. During the luteal phase, macrophages exhibited relevant changes in numbers, anatomical location, and morphology. Macrophages were abundant within the epithelium during the early and mid-luteal phases. These macrophages exhibited dendritic features with cytoplasmic projections among epithelial cells, even located at the apical zone of the epithelium. During the late luteal phase, macrophages were still abundant but were preferentially located at the basal zone of the epithelium. Changes in macrophages located in the lamina propria were not as relevant (Gaytán et al., 2007). The number of macrophages decreased with age, in postmenopausal women (Safwat et al., 2008; Rodriguez–Garcia et al., 2021).

Lu et al. (2023) was the first to describe an interesting immune phenomenon: macrophage extracellular trap formation during sperm phagocytosis due to interactions between sperm and macrophages *in vitro* (cell cultures co-incubation). This is a possible mechanism of sperm phagocytosis by macrophages; morphologically abnormal and hypomotile sperm of patients with asthenozoospermia (reduced sperm motility) are more effectively cleared by macrophage extracellular traps compared with sperm from healthy patients. It is possible that such a mechanism of sperm selection also takes place within the uterine tubes. However, this preliminary study by Lu et al. (2023) was realized in cell cultures, and further research will be needed to confirm whether the same mechanism applies *in vivo*, inside the uterine tube. Moreover, spermatozoa interaction with tubal epithelium *in vitro* modifies expression of cytokines, chemokines and growth factors from tubal epithelial cells (Mousavi et al., 2021).

The role of macrophages in the pathogenesis of tubal ectopic pregnancy is not clear, but macrophages might dysregulate both tubal motility and propensity of the uterine tube. In the early or mid-luteal phases, high progesterone levels could recruit macrophage infiltration in the uterine tubes and enhance production of prostaglandin E2 by macrophages. Macrophage type M1 is also capable of secreting large quantities of interleukin 6. Notably, progesterone, prostaglandin E2, and interleukin 6 restrain smooth muscle contraction and induce dysfunction of the ciliated epithelium; resulting in retention of the embryo within the uterine tubes. Macrophages are capable of producing inflammatory cytokines and growth factors (such as interleukin 1 alpha, tumor necrosis factor alpha, and transforming growth factor beta), which could induce a marked upregulation of molecules necessary for embryo implantation such as leukemia inhibitory factor, indicating a crucial role of macrophages in facilitating a tubal environment permissive for embryo implantation (Wang et al., 2019).

Macrophages are abundant in the wall of the uterine tube; however, histiocytic lesions of uterine tubes—the presence of sheets and clusters of histiocytes (an alternative term for tissue resident macrophages in histopathology)—are relatively rare (Tran and Holloway, 2021).

3.2 Dendritic cells in the uterine tube

Dendritic cells are specialized antigen-presenting cells; orchestrating innate and adaptive immunity during infections, autoimmune diseases, and malignancies (Kvedaraite and Ginhoux, 2022). After capturing antigens, dendritic cells move to nearby regional lymph nodes via efferent lymph vessels as they mature and then present those antigens to naive T lymphocytes for activation or tolerance induction. There are two main lineages of human dendritic cells: conventional (types 1 and 2) and plasmacytoid. Different subtypes of conventional dendritic cells have different functions: some have an anti-inflammatory function, whereas others produce pro-inflammatory cytokines tumor necrosis factor alpha and interleukin 6. Plasmacytoid dendritic cells were initially called interferon-producing cells because they rapidly produce large quantities of type I interferons after recognizing nucleic acids of viruses or bacteria (Ohteki et al., 2021). Plasmacytoid dendritic cells also induce tolerance through interferon alpha production, by suppressing T lymphocyte proliferation and inducing regulatory T lymphocytes. By using flow cytometry, Shaw et al. (2011) found a relatively large percentage of CD123+ plasmacytoid dendritic cells in human uterine tube and a significantly higher percentage of CD123+ plasmocytoid dendritic cells compared with CD11c+ conventional dendritic cells. Given that the uterine tube is exposed to allogeneic spermatozoa and the semi-allogeneic embryo, and must exhibit tolerance toward these cells for reproduction, plasmacytoid dendritic cells might play a role in facilitating a tolerant phenotype within the tubal microenvironment (Shaw et al., 2011).

3.3 Langerhans cells in the uterine tube

Langerhans cells are specific antigen-presenting dendritic cells localized typically in the epidermis; however, they are present in other surface and lining epithelial tissues of the human body, as in the vagina and uterine cervix. Hagiwara et al. (1998) investigated human uterine tubes by electron microscopy and immunohistochemistry by using anti-CD1a antibodies. They discovered Langerhans cells in the tubal epithelium. Moreover, Rabi et al. (2014) described various subtypes of Langerhans cells in the human uterine tube. In accordance with their immunohistochemical study, CD1a-positive Langerhans cells were significantly fewer and smaller in diameter than zinc iodide–osmium-positive Langerhans cells in the uterine tube and both types of cells were significantly more prevalent in *postpartum*

tubes. They described perivascular clusters of zinc iodide–osmium-positive Langerhans cells in tissues from the *postpartum* tube, as well as close association of CD1a-positive Langerhans cells with $CD4^+$ and $CD8^+$ T lymphocytes in the *postpartum* uterine tube. The role of Langerhans cells in the upper female reproductive tract is not fully understood. Tubal Langerhans cells have typical morphological features of Langerhans cells localized in other epithelia, as extended cytoplasmic projections along the basal part of the epithelium and presence of intracytoplasmatic rod-shaped Birbeck granules (visible only by electron microscopy) (Hagiwara et al., 1998).

4 T lymphocytes in the wall of the uterine tube

T lymphocytes represent the dominant immune cell population in the healthy uterine tube and account for approximately 40%–60% of all leucocytes. They are predominantly localized as single cells within the epithelium, along the basement membrane. Focused on the epithelium of the uterine tube, intraepithelial T lymphocytes represent the dominant lymphoid subset of human tubal epithelium. In the tubal epithelium, the average ratio of $CD3^+$ T lymphocytes to epithelial cells is 1:16. Intraepithelial B lymphocytes are 4× less frequent. The average ratio of immune cells to epithelial cells is 1: 400 for $CD4^+$ T lymphocytes and 1:15 for $CD8^+$ T lymphocytes (Ardighieri et al., 2014; Rigby et al., 2022). Most intraepithelial lymphocytes express estrogen receptor beta at both mRNA and protein levels (Ulziibat et al., 2006).

Surprisingly, for many decades tubal intraepithelial T lymphocytes were described as tubal "basal cells" in various morphological publications; including in official histological nomenclature, the *Terminologia Histologica* (FICAT, 2008). These tubal "basal cells" exhibit small, hyperchromatic nuclei and pale cytoplasm (clear cytoplasmic halo). They are located in the epithelium adjacent to the basement membrane, and are non-mitotically active. Varga et al. (2019) conducted an immunohistochemical study that confirmed that these tubal "basal cells" are intraepithelial T lymphocytes; mostly regulatory T lymphocytes ($CD3^+$, $CD8^+$, $CD45RO^+$, $CD4^-$, $CD20^-$, $CD56^-$, and granzyme B^-). Intraepithelial T lymphocytes can be involved in immune tolerance, which could lead to the tolerance of non-self cells (sperm) and partially non-self cells (a developing embryo) without activating local immune responses. Considering the important role of regulatory T lymphocytes in modulating immunological balance and supporting the embryo, further research is required on the distribution patterns and functions of regulatory T lymphocytes in the uterine tubes, especially regarding women with tubal ectopic pregnancy.

5 B lymphocytes and lymphoid follicles in the uterine tube

B lymphocytes account for approximately 5%–10% of all leucocytes in healthy uterine tubes. They are less frequently detected than T lymphocytes and predominantly localize within the connective tissue lamina propria (Rigby et al., 2022). Only a small number of B lymphocytes as well as B dependent lymphoid follicles are present in the mucosa of the uterine tube (Wang et al., 2019; Mills, 2020). In the histological study of Hunt and Lynn (2002), lymphoid follicles within the tubal mucosal folds were present only in 2.1% of bioptic samples. Even the mucosae of most of other tubular organs have a higher prevalence of lymphoid follicles; the cited authors consider their occurrence as evidence of tubal mucosa associated lymphoid tissue as a potential protective mechanism.

Wollen et al. (1994) histologically studied sections from the human uterine tubes of women who were using an intrauterine contraceptive device. The number of cells positive for immunoglobulins IgA, IgG, or IgM (activated forms of B lymphocytes) was significantly higher in the intrauterine contraceptive device user group than in the control group. Therefore, the intrauterine contraceptive device can incite inflammatory cells, resulting in inflammation of the uterine tube; and thus might interfere with the immunological function of the uterine tube and the uterine tube's role in reproduction.

6 NK cells in the wall of the uterine tube

NK cells are relatively common in the mucosa of the uterus (endometrium), especially during pregnancy. They represent 70% of endometrial/decidual leukocytes during pregnancy. These uterine NK cells differ from peripheral blood NK cells (less cytotoxic) and exhibit critical immunomodulatory functions with the potential to control embryo implantation and trophoblast invasion, regulate placental vascular remodeling, and facilitate embryonic/fetal growth (Lapides et al., 2023). In the human uterine tube, NK cells are less numerous and are present in the epithelium, lamina propria, and tubal wall. In the epithelium they are evenly distributed between the epithelial cells with an average ratio of NK cells to epithelial cells of 1:70 (Ardighieri et al., 2014). Shaw et al. (2011) demonstrated the presence of $CD56dimCD16^-$ NK cells in the non-pregnant uterine tube. NK cells at the ectopic tubal pregnancy implantation site express lower percentages of perforin and granulysin, but express a higher percentage of tumor necrosis factor related apoptosis inducing ligand) than do ectopic pregnancy uterine decidual and peripheral NK cells (Laskarin et al., 2010).

7 Neutrophils in the wall of the uterine tube

In the human body, neutrophils are the most dominant cellular component of innate immunity. As the human body's first line of defense against microorganisms, neutrophils execute a variety of potent effector mechanisms for mediating innate immunity. In the cervix and vagina, neutrophils contribute to removal of harmful microbes entering the vagina, or phagocytosis of damaged or dead sperm (Pandya and Cohen, 1985; Milligan et al., 2001). Regarding the uterine tube, the role of neutrophils is largely unknown. Uterine tube neutrophils exhibit a phenotype distinct from peripheral blood neutrophils (expressed significantly higher levels of CD64, human class II histocompatibility antigen DR,

gamma-interferon, and vascular endothelial growth factor), suggesting functional activation of innate immune defense in the female reproductive tract as well as a potential role in maintaining normal uterine tube physiology (Smith et al., 2006). In animals (e.g., buffalo), neutrophils are present within the epithelium and also inside the lumen of the uterine tube around the estrus period. Additionally, the preovulatory tubal fluid suppresses sperm phagocytosis by neutrophils via prostaglandin E2 action (Marey et al., 2016; Yousef et al., 2019).

8 Mast cells in the wall of the uterine tube

Mast cells (mastocytes) are common in connective tissue or in the mucosa of many organs; including the skin, airways, and digestive tract. They are also present in male and female reproductive organs. Mast cells are involved in inflammatory, hypersensitivity, and fibrotic disorders; their effects are hypothesized to be mediated by biogenic amines, proteoglycans, and prostaglandins but also by neutral proteases. They are widely known for their role in allergic reactions via their binding to immunoglobulin E receptor. In addition, there is growing evidence for a role of mast cells in host immune defense and autoimmunity (Weidinger et al., 2003). From a histological point of view, mast cell density is higher in the muscle layer of uterine tube than in tubal lamina propria. Most mast cells of the muscle layer are more closely related to smooth muscle cells than to blood vessels (Sandvei et al., 1986).

Numerous authors have demonstrated expression of estradiol and progesterone receptors in human, mouse, and rat mast cells. For this reason, many mast cell-related pathophysiological alterations have a different prevalence in females and males; e.g., there is much higher asthma prevalence in women at reproductive age compared with that in men, and serum levels of estradiol and progesterone have been directly correlated with the clinical and functional features of asthma (Zierau et al., 2012). Although COVID-19 hyper-inflammation and post-COVID-19 syndrome might be based on mast cell activation syndrome, the available clinical data do not provide grounds for treating this mechanism as significantly increasing the risk of abnormal female reproductive function (Szukiewicz et al., 2022).

The exact role of mast cells in the wall of the uterine tube is largely unknown. Weidinger et al. (2003) demonstrated that the mast cell product tryptase interacts with human spermatozoa during migration through the female genital tract and directly reduces sperm motility. In women who were using an intrauterine contraceptive device, the number of mast cells in the wall of the uterine tube was higher than in a control group of non-pregnant women. This increased number of mast cells in intrauterine contraceptive device users might be a factor in the pathogenesis of pelvic inflammatory disease and the ectopic pregnancies that occur in intrauterine contraceptive device users (Sandvei et al., 1986). From an immunological point of view, mast cells also play an important role in shaping immune responses in *Chlamydia* reproductive tract infection through both effector cell recruitment and modification of the chemokine microenvironment (Mayavannan et al., 2023).

9 Possible "immune privilege" of uterine tube

The immune privilege represents a specific tissue microenvironment where the systemic immune responses to allo- and autoantigens are reduced. Immune privilege is thought to reflect an adaptation to protect vital structures from damage by inflammatory responses directed against pathogens. It was originally believed that antigens in immune-privileged sites are separated from the immune system by anatomical barriers (to be sealed from the blood circulation) and therefore ignored. Nowadays we know that immune privilege is maintained thanks to immune cells by an active rather than passive process (Hong and Van Kaer, 1999). Immune privileged organs include the eye (Du and Yan, 2023; Wang et al., 2023) and the brain (Rustenhoven and Kipnis, 2022; González-Hernández and Mukouyama, 2023) as well as the pregnant uterus (Zhang et al., 2016) and testis (Kaur et al., 2021). However, so far no one has described a similar "immune privilege" inside the uterine tube.

Male germ cells are immunogenic. The immune privilege is well described in male genital system; mostly in testis, but less direct evidence support that the whole epididymis is immune-privileged (Mital et al., 2011). The immune microenvironment of the male genital organs, specifically the testis and epididymis, is characterized by the formation of a specific barrier between the immune system and haploid sperm. These barriers are the blood-testis barrier and blood-epididymis barrier. The ultrastructural composition of both mentioned anatomical barriers is well known and consists of Sertoli cell-Sertoli cell tight junctions or tight junctions between the epithelial cells in the epididymal duct (Gregory and Cyr, 2014; Luaces et al., 2023). However, both barriers contain also functional parts, the so-called physiological and immunological barriers (Mital et al., 2011), which are similarly important for the immune privilege. Inside ovary, the presence of blood-follicle barrier is discussed. From anatomical point of view, the layers of this barrier are: the vascular endothelium, endothelial basement membrane, the thecal interstitium, the follicular basement membrane, and the membrana granulosa (Siu and Cheng, 2012). But according to our knowledge, no similar anatomical barrier is inside the uterine tube.

The presence of anatomical blood-tissue barrier is not the only basis for the immune privilege. Similar important is the presence of immunological barrier. E.g., in testis, T lymphocytes play an imperative role in testicular immunity, thus maintaining a tolerance status in terms of the physiological condition and arousing an immune response under threat of infection and tumorigenesis (Gong et al., 2020). From embryological point of view, the male epididymis is analogous to female uterine tube. Inside epididymis, numerous immune cells preventing induction of an autoimmune reaction as, mononuclear phagocytic cells, $CD4^+$ T lymphocytes, and $CD8^+$ T lymphocytes, which are located throughout the epididymal epithelium and interstitial space (Da Silva and Smith, 2015; Zhao et al., 2022). Similar key cells of the immune system have also been described in the uterine tube. This is also why it is possible that the immune cells of the uterine tube represent a type of "immunological barrier," which in a certain way includes the uterine tube among the immunologically privileged organs. Additionally, anti-inflammatory cytokines, TGFB1 and

IL10, are strongly and constantly expressed in the uterine tube epithelial and endothelial cells of the surrounding vasculature (Yousef et al., 2016). This constant expression of both epithelial-derived T helper type 2-driving (Th2, anti-inflammatory) cytokines suppressed the immune system, thereby inducing a state of immune-tolerance toward sperm and early embryo in the uterine tube. These findings suggest that under physiological conditions, the uterine tube mucosal epithelium provides a strong and stable anti-inflammatory environment (Marey et al., 2020).

To our knowledge, only one study investigated *in vivo* the uterine tube (even only its intramural portion) as an immunoprivileged organ in baboons (the anatomical structure of baboon's female reproductive system resembles that of human). Hernandez et al. (2021) placed silver nitrate loaded fiber devices in uteruses and intramural portions of uterine tubes of baboons to probe the fibrotic response. Cited authors found no evidence of inflammation, collagen deposition or abnormal immune cell infiltration in either the endometrium or intramural portion of uterine tube. In other hand, the same electrospun fibers initiating fibrosis after subcutaneous application. This experimental study may be the first confirmation that at least the intramural portion of the uterine tube is an immune privileged organ.

10 The role of tubal fluid in immune privilege of uterine tube

The tubal fluid inside the uterine tube consists of components that are either passively or actively transported over the tubal epithelial barrier from the circulating blood or the interstitial tissue, and/or secreted by the tubal epithelial cells (Leese et al., 2001). Probably the uterine tube-specific lymphatic lacunae (width lymphatic capillaries), which run through the central part of each uterine mucosal fold and fimbria, may play an important role in the formation and/or absorption of tubal fluid (Varga et al., 2018; Csöbönyeiová et al., 2022a). The composition of tubal fluid differs significantly from the blood plasma (Ménézo et al., 2015). Tubal fluid protein concentrations are low compared to those of blood serum; although some proteins such as albumin are in abundance (Pérez-Cerezales et al., 2018). The unique tubal liquid microenvironment contains a variety of molecules, including tubal extracellular vesicles (both exosomes and microvesicles), specific glycoproteins as oviductin, nutrients such as glucose, lactate, pyruvate and amino acids, and bicarbonate ions. All these components provide an optimal environment for sperm survival and capacitation, fertilization and early embryo development in the uterine tube (Harris et al., 2020; Cajas et al., 2021; Zhao et al., 2022). The volume, chemical composition and even temperature of the tubal fluid is influenced by the cyclically changing level of female sex hormones (Saint-Dizier et al., 2019). Additionally, tubal fluid contains immune cells as neutrophils (Marey et al., 2013), and macrophages, which may arise from peritoneal macrophages that migrate into the uterine tubes (Haney et al., 1983). The significant presence of neutrophils in the tubal fluid was described in the bovine especially during preovulatory period (Marey et al., 2016). Little is known about the tubal fluid local immunological microenvironment and how tubal fluid immune cells interact with sperm and embryo. Insemination always stimulates neutrophil migration into the female reproductive tract, which eliminates excess spermatozoa and bacterial contaminants introduced by the coitus (Alghamdi and Foster, 2005). The composition of tubal fluid/secretion of tubal epithelial cells through mainly prostaglandin E2 suppresses the phagocytic activity of neutrophils for sperm, which is also hormonally regulated through luteinizing hormone (Marey et al., 2013). In the time window of ovulation, follicular and tubal fluids seem to have opposite effects on the uterine tube immunotolerance. The follicular fluid collected from buffalo pre-ovulatory follicles enhanced sperm phagocytosis by neutrophils through the formation of neutrophil extracellular traps and hydrogen peroxide formation, whereas tubal fluid inhibited this activity *in vitro* (Yousef et al., 2016).

The tubal fluid bidirectionally carries signaling molecules between sperm/pre-implantation embryo on the one hand and tubal epithelial cells and immune cells on the other hand. Arrival of spermatozoa and/or preimplantation embryo within the uterine tube is now known to regulate gene expression in tubal epithelial cells, inducing up- and downregulation of various proteins. The sperm-uterine tube interaction generates an anti-inflammatory immune response, which supports sperm survival until fertilization (Yousef et al., 2016). Moreover, tubal fluid appears to protect against activated leucocyte-induced sperm DNA fragmentation, thus preserving the integrity of the paternal genome (Navarrete Gómez et al., 2009). The positive influence of the tubal fluid on early embryonic growth and development is well established in non-human species (Rizos et al., 2016). During the embryo-uterine tube interaction, the embryo might play a role as a modulator of the immune system in the maternal tract, inducing the downregulation of immune related genes to allow the refractory uterine tube and uterus to tolerate the embryo and support its development (Almiñana et al., 2012). From the mentioned preliminary studies, it is probable that the tubal fluid plays not only an important role in the survival of the sperm and embryo, but also regulates the immune reactions inside the lumen of the uterine tube. This is also why further research will be needed to accurately describe the mechanism of the relationship between tubal fluid and immune reactions inside the uterine tube.

11 Female sex hormone and the tubal immune privilege

Progesterone and estrogen are steroid female sex hormones produced cyclically by the ovaries. Within the female reproductive tract, the mucosal immune system is precisely regulated by both sex hormones to protect against potential pathogens without compromising fetal survival. This regulation leads to changes in innate and adaptive immune responses throughout the cycle and to differential regulation of the immune cell populations present in the female reproductive system. Sex hormones can act directly on cells or indirectly via intermediate cells to modulate cytokine and chemokine secretion (Wira et al., 2015). For example, both hormones are known to regulate the quantity of macrophages present within the uterus, as well as the expression of these macrophages in the anti-inflammatory, M2 polarization state (Chambers et al., 2021). For successful fertilization and embryo survival, the immune system must be modulated during mid-cycle of the menstrual cycle. On other

hand, this period lasting 7–10 days, when components of innate, humoral, and cell-mediated immunity are suppressed by estrogen and/or progesterone, enhancing the potential for viral infection. The period of fertilization and early development of the embryo is also a period of vulnerability for HIV infection (Wira and Fahey, 2008).

Despite significant progress in reproductive immunology and endocrinology, much remains to be done to more fully understand the complexities of the immune system in the female reproductive system. According to Wira et al. (2015), the most important questions we need to get answers to include:

1) defining the balance between direct effects of sex hormones and their indirect effects that are mediated through cytokines, chemokines, and growth factors made by immune cells, stromal cells, and epithelial cells that modulate female reproductive tract mucosal immune function;
2) defining the role of the female reproductive tract tissue microenvironment in regulating immune phenotype and function given that blood immune cells are different from their counterparts in the female reproductive system;
3) determining the extent to which immune cells function vary with their site of residence in the female reproductive system (e.g., uterus vs. uterine tube).

Additionally, very little is known about the effect of endocrine disruptors on the function of immune cells within the female reproductive system. There have been numerous studies and reviews demonstrating effects of endocrine disruptors on embryonic development and germ cell development and these are discussed in detail elsewhere, even less is known about their effects on the immune system of the female reproductive system (Dunbar et al., 2012).

12 Conclusion and further perspectives

The human uterine tube has a diverse population of immunologically active cells representing both the innate and adaptive immune systems; including lymphocytes, macrophages, NK cells, dendritic cells, and mast cells. In comparison with the uterus and its endometrium, studies examining immune cell populations and their functions in the uterine tube are not as numerous. Recent years have revealed that the obsolete notion of uterine tubes as simply a passive tubular organ for gametes and embryos could not be further from the truth. Active cross-talk between spermatozoa, oocytes, preimplantation embryos, and the wall of the uterine tube (including immunocompetent cells) occurs before, at, as well as after fertilization; yet also during transport of the early embryo toward the uterine cavity. However, immune crosstalk between the pre-hatching embryo in uterine tube and the mother has received little attention (Talukder et al., 2020). Recent animal studies indicate that the pre-hatching bovine embryo secretes bioactive molecules that can be detected by epithelial and immune cells of the female reproductive system and induces anti-inflammatory effect (Talukder et al., 2017; Talukder et al., 2018). Therefore, understanding these processes and its translation into clinical practice could substantially impact further development of the field of reproductive medicine (improvement of fertility and pregnancy outcomes) and in the management of sexually transmitted infections. Additionally, understanding how immune protection changes in the female reproductive tract during the menstrual cycle or in menopause is essential to understanding the pathogenesis of gynecological cancers.

This review has some limitations due to a relative lack of data regarding immune cells in the wall of the human uterine tube. In various scientific reports there are inconsistent data in terms of the immune cell populations in the female reproductive tract; this discrepancy comes from differences in the sampling phase in the menstrual cycle, laboratory methods (histology *versus* flow cytometry), and antibodies used to identify immune cells. In conclusion, scientific research of the immune system in the female reproductive tract can help solve the puzzle of semi-allograft embryo/fetus acceptance during pregnancy and contribute to improved women's health.

Author contributions

KV: Conceptualization, Formal Analysis, Writing–original draft. IV: Funding acquisition, Project administration, Resources, Supervision, Writing–original draft. CF: Conceptualization, Investigation, Writing–review and editing. LP: Investigation, Writing–review and editing. JZ: Formal Analysis, Writing–review and editing. RM: Conceptualization, Formal Analysis, Investigation, Writing–original draft.

Funding

The author(s) declare that financial support was received for the research, authorship, and/or publication of this article. This study was supported by a grant from the Slovak Research and Development Agency number APVV-18-0499 entitled "Histomorphological basis of idiopathic tubal infertility" and by a grant of Ministry of Education, Research, Development and Youth of the Slovak Republic No. VEGA 1/0347/24 entitled "Morphological and molecular-biological study of hormone-dependent processes and immune functions of the uterine tube wall and interactions between the wall of the uterine tube and gametes."

Conflict of interest

The authors declare that the research was conducted in the absence of any commercial or financial relationships that could be construed as a potential conflict of interest.

Publisher's note

All claims expressed in this article are solely those of the authors and do not necessarily represent those of their affiliated organizations, or those of the publisher, the editors and the reviewers. Any product that may be evaluated in this article, or claim that may be made by its manufacturer, is not guaranteed or endorsed by the publisher.

References

Alghamdi, A. S., and Foster, D. N. (2005). Seminal DNase frees spermatozoa entangled in neutrophil extracellular traps. *Biol. Reprod.* 73 (6), 1174–1181. doi:10.1095/biolreprod.105.045666

Almiñana, C., Heath, P. R., Wilkinson, S., Sanchez-Osorio, J., Cuello, C., Parrilla, I., et al. (2012). Early developing pig embryos mediate their own environment in the maternal tract. *PloS one* 7 (3), e33625. doi:10.1371/journal.pone.0033625

Ardighieri, L., Lonardi, S., Moratto, D., Facchetti, F., Shih, I. M., Vermi, W., et al. (2014). Characterization of the immune cell repertoire in the normal fallopian tube. *Int. J. Gynecol. Pathol.* 33, 581–591. doi:10.1097/PGP.0000000000000095

Cajas, Y. N., Cañón-Beltrán, K., de la Blanca, M. G. M., Sánchez, J. M., Fernandez-Fuertes, B., González, E. M., et al. (2021). Role of reproductive fluids and extracellular vesicles in embryo–maternal interaction during early pregnancy in cattle. *Reprod. Fertil. Dev.* 34 (2), 117–138. doi:10.1071/RD21275

Caven, L. T., and Carabeo, R. A. (2023). The role of infected epithelial cells in *Chlamydia*-associated fibrosis. *Front. Cell. Infect. Microbiol.* 13, 1208302. doi:10.3389/fcimb.2023.1208302

Chambers, M., Rees, A., Cronin, J. G., Nair, M., Jones, N., and Thornton, C. A. (2021). Macrophage plasticity in reproduction and environmental influences on their function. *Front. Immunol.* 11, 607328. doi:10.3389/fimmu.2020.607328

Chua, S. J., Akande, V. A., and Mol, B. W. (2017). Surgery for tubal infertility. *Cochrane Database Syst. Rev.* 1 (1), CD006415. doi:10.1002/14651858.CD006415.pub3

Csöbönyeiová, M., Klein, M., Juríková, M., Feitscherová, C., Gálfiová, P., and Varga, I. (2022a). Immunohistochemical and scanning electron microscopic confirmation of the lymphatic lacunae in the uterine tube mucosal folds. What are the clinical implications? *Phys. Res.* 71 (1), S115–S123. doi:10.33549/physiolres.935029

Csöbönyeiová, M., Varga, I., Lapides, L., Pavlíková, L., Feitscherová, C., and Klein, M. (2022b). From a passive conduit to highly dynamic organ. What are the roles of uterine tube epithelium in reproduction? *Physiol. Res.* 71, S11–S20. doi:10.33549/physiolres.934954

Da Silva, N., and Smith, T. B. (2015). Exploring the role of mononuclear phagocytes in the epididymis. *Asian J. Androl.* 17 (4), 591–596. doi:10.4103/1008-682X.153540

Du, Y., and Yan, B. (2023). Ocular immune privilege and retinal pigment epithelial cells. *J. Leukoc. Biol.* 113 (3), 288–304. doi:10.1093/jleuko/qiac016

Dunbar, B., Patel, M., Fahey, J., and Wira, C. (2012). Endocrine control of mucosal immunity in the female reproductive tract: impact of environmental disruptors. *Mol. Cell. Endocrinol.* 354 (1-2), 85–93. doi:10.1016/j.mce.2012.01.002

FICAT (2008). *Terminologia Histologica: international terms for human cytology and histology*. First edition. Philadelphia: Wolters Kluwer.

Gaytán, M., Morales, C., Bellido, C., Sánchez-Criado, J. E., and Gaytán, F. (2007). Macrophages in human fallopian tube and ovarian epithelial inclusion cysts. *J. Reprod. Immunol.* 73, 66–73. doi:10.1016/j.jri.2006.06.002

Gong, J., Zeng, Q., Yu, D., and Duan, Y. G. (2020). T lymphocytes and testicular immunity: a new insight into immune regulation in testes. *Int. J. Mol. Sc.* 22 (1), 57. doi:10.3390/ijms22010057

González-Hernández, S., and Mukouyama, Y. S. (2023). Lymphatic vasculature in the central nervous system. *Front. Cell Dev. Biol.* 11, 1150775. doi:10.3389/fcell.2023.1150775

Gregory, M., and Cyr, D. G. (2014). The blood-epididymis barrier and inflammation. *Spermatogenesis* 4 (2), e979619. doi:10.4161/21565562.2014.979619

Hagiwara, H., Ohwada, N., Aoki, T., and Fujimoto, T. (1998). Langerhans cells in the human oviduct mucosa. *Ital. J. Anat. Embryol.* 103, 253–258.

Hamranová, N., Hocinec, N., Záhumenský, J., Csöbönyeiová, M., Klein, M., Feitscherová, C., et al. (2023). Traditional and contemporary views on the functional morphology of the fallopian tubes and their importance for gynecological practice. *Ceska Gynekol.* 88, 33–43. doi:10.48095/cccg202333

Haney, A. F., Misukonis, M. A., and Weinberg, J. B. (1983). Macrophages and infertility: oviductal macrophages as potential mediators of infertility. *Fertil. Steril.* 39 (3), 310–315. doi:10.1016/s0015-0282(16)46877-9

Harris, E. A., Stephens, K. K., and Winuthayanon, W. (2020). Extracellular vesicles and the oviduct function. *Int. J. Mol. Sci.* 21 (21), 8280. doi:10.3390/ijms21218280

Harvie, M. C., Carey, A. J., Armitage, C. W., O'Meara, C. P., Peet, J., Phillips, Z. N., et al. (2019). *Chlamydia*-infected macrophages are resistant to azithromycin treatment and are associated with chronic oviduct inflammation and hydrosalpinx development. *Immunol. Cell Biol.* 97, 865–876. doi:10.1111/imcb.12285

Hernandez, J. L., Park, J., Yao, S., Blakney, A. K., Nguyen, H. V., Katz, B. H., et al. (2021). Effect of tissue microenvironment on fibrous capsule formation to biomaterial-coated implants. *Biomaterials* 273, 120806. doi:10.1016/j.biomaterials.2021.120806

Hoenderboom, B. M., van Benthem, B. H. B., van Bergen, J. E. A. M., Dukers-Muijrers, N. H. T. M., Götz, H. M., Hoebe, C. J. P. A., et al. (2019). Relation between *Chlamydia trachomatis* infection and pelvic inflammatory disease, ectopic pregnancy and tubal factor infertility in a Dutch cohort of women previously tested for chlamydia in a chlamydia screening trial. *Sex. Transm. Infect.* 95, 300–306. doi:10.1136/sextrans-2018-053778

Hong, S., and Van Kaer, L. (1999). Immune privilege: keeping an eye on natural killer T cells. *J. Exp. Med.* 190 (9), 1197–1200. doi:10.1084/jem.190.9.1197

Hume, D. A. (2006). The mononuclear phagocyte system. *Curr. Opin. Immunol.* 18, 49–53. doi:10.1016/j.coi.2005.11.008

Hume, D. A., Irvine, K. M., and Pridans, C. (2019). The mononuclear phagocyte system: the relationship between monocytes and macrophages. *Trends Immunol.* 40, 98–112. doi:10.1016/j.it.2018.11.007

Hunt, J. L., and Lynn, A. A. (2002). Histologic features of surgically removed fallopian tubes. *Arch. Pathol. Lab. Med.* 126, 951–955. doi:10.1043/0003-9985(2002)126<0951:HFOSRT>2.0.CO;2

Jenabi, E., Ayubi, E., Khazaei, S., Soltanian, A. R., and Salehi, A. M. (2023). The environmental risk factors associated with ectopic pregnancy: an umbrella review. *J. Gynecol. Obstet. Hum. Reprod.* 52, 102532. doi:10.1016/j.jogoh.2022.102532

Kaur, G., Wright, K., Verma, S., Haynes, A., and Dufour, J. M. (2021). The good, the bad and the ugly of testicular immune regulation: a delicate balance between immune function and immune privilege. *Adv. Exp. Med. Biol.* 1288, 21–47. doi:10.1007/978-3-030-77779-1_2

Kvedaraite, E., and Ginhoux, F. (2022). Human dendritic cells in cancer. *Sci. Immunol.* 7, eabm9409. doi:10.1126/sciimmunol.abm9409

Lapides, L., Varga, I., Csöbönyeiová, M., Klein, M., Pavlíková, L., Visnyaiová, K., et al. (2023). The neglected uterine NK cells/hamperl cells/endometrial stromal granular cell, or K cells: a narrative review from history through histology and to medical education. *Int. J. Mol. Sci.* 24, 12693. doi:10.3390/ijms241612693

Laskarin, G., Redzovic, A., Vukelic, P., Veljkovic, D., Gulic, T., Haller, H., et al. (2010). Phenotype of NK cells and cytotoxic/apoptotic mediators expression in ectopic pregnancy. *Am. J. Reprod. Immunol.* 64, 347–358. doi:10.1111/j.1600-0897.2010.00844.x

Lee, S. K., Kim, C. J., Kim, D. J., and Kang, J. H. (2015). Immune cells in the female reproductive tract. *Immune Netw.* 15, 16–26. doi:10.4110/in.2015.15.1.16

Leese, H. J., Tay, J. I., Reischl, J., and Downing, S. J. (2001). Formation of Fallopian tubal fluid: role of a neglected epithelium. *Reprod. Camb. Engl.* 121 (3), 339–346. doi:10.1530/rep.0.1210339

Liptáková, A., Čurová, K., Záhumenský, J., Visnyaiová, K., and Varga, I. (2022). Microbiota of female genital tract – functional overview of microbial flora from vagina to uterine tubes and placenta. *Physiol. Res.* 71, S21–S33. doi:10.33549/physiolres.934960

Liu, L., Li, C., Sun, X., Liu, J., Zheng, H., Yang, B., et al. (2022). Chlamydia infection, PID, and infertility: further evidence from a case-control study in China. *BMC Womens Health* 22, 294. doi:10.1186/s12905-022-01874-z

Lu, C., Wu, Z., Gao, H., Li, H., Deng, R., Luo, N., et al. (2023). Sperm induce macrophage extracellular trap formation via phagocytosis-dependent mechanism. *Biol. Reprod.* 109, 319–329. doi:10.1093/biolre/ioad068

Luaces, J. P., Toro-Urrego, N., Otero-Losada, M., and Capani, F. (2023). What do we know about blood-testis barrier? current understanding of its structure and physiology. *Front. Cell Dev. Biol.* 11, 1114769. doi:10.3389/fcell.2023.1114769

Marey, M. A., Aboul Ezz, M., Akthar, I., Yousef, M. S., Imakawa, K., Shimada, M., et al. (2020). Sensing sperm via maternal immune system: a potential mechanism for controlling microenvironment for fertility in the cow. *J. animal Sci.* 98 (1), S88–S95. doi:10.1093/jas/skaa147

Marey, M. A., Liu, J., Kowsar, R., Haneda, S., Matsui, M., Sasaki, M., et al. (2013). Bovine oviduct epithelial cells downregulate phagocytosis of sperm by neutrophils: prostaglandin E2 as a major physiological regulator. *Reprod. Camb. Engl.* 147 (2), 211–219. doi:10.1530/REP-13-0375

Marey, M. A., Yousef, M. S., Kowsar, R., Hambruch, N., Shimizu, T., Pfarrer, C., et al. (2016). Local immune system in oviduct physiology and pathophysiology: attack or tolerance? *Domest. Anim. Endocrinol.* 56, S204–S211. doi:10.1016/j.domaniend.2016.02.005

Mayavannan, A., Shantz, E., Haidl, I. D., Wang, J., and Marshall, J. S. (2023). Mast cells selectively produce inflammatory mediators and impact the early response to *Chlamydia* reproductive tract infection. *Front. Immunol.* 14, 1166068. doi:10.3389/fimmu.2023.1166068

Ménézo, Y., Guérin, P., and Elder, K. (2015). The oviduct: a neglected organ due for re-assessment in IVF. *Reprod. Biomed. Online.* 30 (3), 233–240. doi:10.1016/j.rbmo.2014.11.011

Miah, M., Goh, I., and Haniffa, M. (2021). Prenatal development and function of human mononuclear phagocytes. *Front. Cell Dev. Biol.* 9, 649937. doi:10.3389/fcell.2021.649937

Milligan, G. N., Bourne, N., and Dudley, K. L. (2001). Role of polymorphonuclear leukocytes in resolution of HSV-2 infection of the mouse vagina. *J. Reprod. Immunol.* 49, 49–65. doi:10.1016/s0165-0378(00)00080-2

Mills, S. E. (2020). *Histology for pathologist*. Fifth edition. Philadelphia: Wolters Kluwer.

Mital, P., Hinton, B. T., and Dufour, J. M. (2011). The blood-testis and blood-epididymis barriers are more than just their tight junctions. *Biol. Reprod.* 84 (5), 851–858. doi:10.1095/biolreprod.110.087452

Mousavi, S. O., Mohammadi, R., Amjadi, F., Zandieh, Z., Aghajanpour, S., Aflatoonian, K., et al. (2021). Immunological response of fallopian tube epithelial cells to spermatozoa through modulating cytokines and chemokines. *J. Reprod. Immunol.* 146, 103327. doi:10.1016/j.jri.2021.103327

Navarrete Gómez, P., Espinoza Ruiz, J., Parodi Rivera, J., Alvarez, J. G., and Sánchez Gutiérrez, R. (2009). Protective effect of fallopian tubal fluid against activated leucocyte-induced sperm DNA fragmentation: preliminary results. *Andrologia* 41 (3), 196–198. doi:10.1111/j.1439-0272.2009.00922.x

Ohteki, T., Kawamura, S., and Onai, N. (2021). Commitment to dendritic cells and monocytes. *Int. Immunol.* 33, 815–819. doi:10.1093/intimm/dxab031

Pandya, I. J., and Cohen, J. (1985). The leukocytic reaction of the human uterine cervix to spermatozoa. *Fertil. Steril.* 43, 417–421. doi:10.1016/s0015-0282(16)48442-6

Pant, S., Bhati, T., Dimri, A., Arora, R., Siraj, F., Raisuddin, S., et al. (2023). *Chlamydia trachomatis* infection regulates the expression of tetraspanins, activin-A, and inhibin-A in tubal ectopic pregnancy. *Pathog. Dis.* 81, ftad018. doi:10.1093/femspd/ftad018

Pérez-Cerezales, S., Ramos-Ibeas, P., Acuña, O. S., Avilés, M., Coy, P., Rizos, D., et al. (2018). The oviduct: from sperm selection to the epigenetic landscape of the embryo. *Biol. Reprod.* 98 (3), 262–276. doi:10.1093/biolre/iox173

Rabi, S., Jacob, T. M., Lionel, J., and Indrasingh, I. (2014). Different subsets of Langerhans cells in human uterine tubes and uterus. *J. Obstet. Gynaecol. Res.* 40, 1833–1839. doi:10.1111/jog.12446

Ramraj, S. K., Smith, K. M., Janakiram, N. B., Toal, C., Raman, A., and Benbrook, D. M. (2018). Correlation of clinical data with fallopian tube specimen immune cells and tissue culture capacity. *Tissue Cell* 52, 57–64. doi:10.1016/j.tice.2018.04.001

Rigby, C. H., Aljassim, F., Powell, S. G., Wyatt, J. N. R., Hill, C. J., and Hapangama, D. K. (2022). The immune cell profile of human fallopian tubes in health and benign pathology: a systematic review. *J. Reprod. Immunol.* 152, 103646. doi:10.1016/j.jri.2022.103646

Rizos, D., Maillo, V., and Lonergan, P. (2016). Role of the oviduct and oviduct-derived products in ruminant embryo development. *Anim. Reprod.* 13 (3), 160–167. doi:10.21451/1984-3143-ar863

Rodriguez–Garcia, M., Patel, M. V., Shen, Z., and Wira, C. R. (2021). The impact of aging on innate and adaptive immunity in the human female genital tract. *Aging Cell* 20, e13361. doi:10.1111/acel.13361

Rustenhoven, J., and Kipnis, J. (2022). Brain borders at the central stage of neuroimmunology. *Nature* 612 (7940), 417–429. doi:10.1038/s41586-022-05474-7

Safwat, M. D., Habib, F. A., and Oweiss, N. Y. (2008). Distribution of macrophages in the human fallopian tubes: an immunohistochemical and electron microscopic study. *Folia Morphol. (Warsz.)* 67, 43–52.

Saint-Dizier, M., Schoen, J., Chen, S., Banliat, C., and Mermillod, P. (2019). Composing the early embryonic microenvironment: physiology and regulation of oviductal secretions. *Int. J. Mol. Sci.* 21 (1), 223. doi:10.3390/ijms21010223

Sandvei, R., Wollen, A. L., Flood, P. R., and Anker, C. (1986). Mast cells in the tubal wall in women using an intrauterine contraceptive device. *Br. J. Obstet. Gynaecol.* 93, 758–764. doi:10.1111/j.1471-0528.1986.tb08064.x

Shaw, J. L., Fitch, P., Cartwright, J., Entrican, G., Schwarze, J., Critchley, H. O. D., et al. (2011). Lymphoid and myeloid cell populations in the non-pregnant human fallopian tube and in ectopic pregnancy. *J. Reprod. Immunol.* 89, 84–91. doi:10.1016/j.jri.2011.01.014

Siu, M. K., and Cheng, C. Y. (2012). The blood-follicle barrier (BFB) in disease and in ovarian function. *Adv. Exp. Med. Biol.* 763, 186–192. doi:10.1007/978-1-4614-4711-5_9

Smith, J. M., Wira, C. R., Fanger, M. W., and Shen, L. (2006). Human fallopian tube neutrophils – a distinct phenotype from blood neutrophils. *Am. J. Reprod. Immunol.* 56, 218–229. doi:10.1111/j.1600-0897.2006.00410.x

Sreejit, G., Fleetwood, A. J., Murphy, A. J., and Nagareddy, P. R. (2020). Origins and diversity of macrophages in health and disease. *Clin. Transl. Immunol.* 9, e1222. doi:10.1002/cti2.1222

Szukiewicz, D., Wojdasiewicz, P., Watroba, M., and Szewczyk, G. (2022). Mast cell activation syndrome in COVID-19 and female reproductive function: theoretical background vs accumulating clinical evidence. *J. Immunol. Res.* 2022, 9534163. doi:10.1155/2022/9534163

Talukder, A. K., Marey, M. A., Shirasuna, K., Kusama, K., Shimada, M., Imakawa, K., et al. (2020). Roadmap to pregnancy in the first 7 days post-insemination in the cow: immune crosstalk in the corpus luteum, oviduct, and uterus. *Theriogenology* 150, 313–320. doi:10.1016/j.theriogenology.2020.01.071

Talukder, A. K., Rashid, M. B., Yousef, M. S., Kusama, K., Shimizu, T., Shimada, M., et al. (2018). Oviduct epithelium induces interferon-tau in bovine Day-4 embryos, which generates an anti-inflammatory response in immune cells. *Sci. Rep.* 8 (1), 7850. doi:10.1038/s41598-018-26224-8

Talukder, A. K., Yousef, M. S., Rashid, M. B., Awai, K., Acosta, T. J., Shimizu, T., et al. (2017). Bovine embryo induces an anti-inflammatory response in uterine epithelial cells and immune cells *in vitro*: possible involvement of interferon tau as an intermediator. *J. Reprod. Dev.* 63 (4), 425–434. doi:10.1262/jrd.2017-056

Tran, T. A. N., and Holloway, R. W. (2021). Intratubal pseudopapillary histiocytic hyperplasia: a new histologic variant in the spectrum of histiocytic lesions involving the fallopian tube. *Int. J. Gynecol. Pathol.* 40, 369–375. doi:10.1097/PGP.0000000000000740

Ulrich, N. D., Shen, Y. C., Ma, Q., Yang, K., Hannum, D. F., Jones, A., et al. (2022). Cellular heterogeneity of human fallopian tubes in normal and hydrosalpinx disease states identified using scRNA-seq. *Dev. Cell.* 57 (7), 914–929.e7. doi:10.1016/j.devcel.2022.02.017

Ulziibat, S., Ejima, K., Shibata, Y., Hishikawa, Y., Kitajima, M., Fujishita, A., et al. (2006). Identification of estrogen receptor beta-positive intraepithelial lymphocytes and their possible roles in normal and tubal pregnancy oviducts. *Hum. Reprod.* 21, 2281–2289. doi:10.1093/humrep/del176

van Furth, R., Cohn, Z. A., Hirsch, J. G., Humphrey, J. H., Spector, W. G., and Langevoort, H. L. (1972). The mononuclear phagocyte system: a new classification of macrophages, monocytes, and their precursor cells. *Bull. World Health Organ.* 46, 845–852.

Varga, I., Csöbönyeiová, M., Visnyaiová, K., Záhumenský, J., Pavlíková, L., Feitscherová, C., et al. (2022). Functional morphology of the human uterine tubes in the 21st century: anatomical novelties and their possible clinical applications. *Physiol. Res.* 71, S151–S159. doi:10.33549/physiolres.935036

Varga, I., Kachlík, D., Žišková, M., and Miko, M. (2018). Lymphatic lacunae of the mucosal folds of human uterine tubes - a rediscovery of forgotten structures and their possible role in reproduction. *Ann. Anat.* 219, 121–128. doi:10.1016/j.aanat.2018.06.005

Varga, I., Miko, M., Kachlík, D., Žišková, M., Danihel, Ľ., and Babál, P. (2019). How many cell types form the epithelial lining of the human uterine tubes? Revision of the histological nomenclature of the human tubal epithelium. *Ann. Anat.* 224, 73–80. doi:10.1016/j.aanat.2019.03.012

Varol, C., Mildner, A., and Jung, S. (2015). Macrophages: development and tissue specialization. *Annu. Rev. Immunol.* 33, 643–675. doi:10.1146/annurev-immunol-032414-112220

Wang, X., Lee, C. L., Li, R. H. W., Vijayan, M., Duan, Y. G., Yeung, W. S. B., et al. (2019). Alteration of the immune cell profiles in the pathophysiology of tubal ectopic pregnancy. *Am. J. Reprod. Immunol.* 81, e13093. doi:10.1111/aji.13093

Wang, X., Lee, C. L., Vijayan, M., Yeung, W. S. B., Ng, E. H. Y., Wang, X., et al. (2020). Adrenomedullin insufficiency alters macrophage activities in fallopian tube: a pathophysiologic explanation of tubal ectopic pregnancy. *Mucosal Immunol.* 13, 743–752. doi:10.1038/s41385-020-0278-6

Wang, X., Wang, T., Lam, E., Alvarez, D., and Sun, Y. (2023). Ocular vascular diseases: from retinal immune privilege to inflammation. *Int. J. Mol. Sci.* 24 (15), 12090. doi:10.3390/ijms241512090

Weidinger, S., Mayerhofer, A., Frungieri, M. B., Meineke, V., Ring, J., and Kohn, F. M. (2003). Mast cell-sperm interaction: evidence for tryptase and proteinase-activated receptors in the regulation of sperm motility. *Hum. Reprod.* 18, 2519–2524. doi:10.1093/humrep/deg476

Wira, C. R., and Fahey, J. V. (2008). A new strategy to understand how HIV infects women: identification of a window of vulnerability during the menstrual cycle. *AIDS Lond. Engl.* 22 (15), 1909–1917. doi:10.1097/QAD.0b013e3283060ea4

Wira, C. R., Ghosh, M., Smith, J. M., Shen, L., Connor, R. I., Sundstrom, P., et al. (2011). Epithelial cell secretions from the human female reproductive tract inhibit sexually transmitted pathogens and *Candida albicans* but not *Lactobacillus*. *Mucosal Immunol.* 4, 335–342. doi:10.1038/mi.2010.72

Wira, C. R., Rodriguez-Garcia, M., Patel, M. V., Biswas, N., and Fahey, J. V. (2015). "Chapter 110 - endocrine regulation of the mucosal immune system in the female reproductive tract," in *Mucosal immunology*. Fourth Edition (Berlin, Germany: Springer), Vol. 2, 2141–2156.

Wollen, A. L., Sandvei, R., Mørk, S., Marandon, J. L., and Matre, R. (1994). *In situ* characterization of leukocytes in the fallopian tube in women with or without an intrauterine contraceptive device. *Acta Obstet. Gynecol. Scand.* 73, 103–112. doi:10.3109/00016349409013411

Yousef, M. S., Abd–Elhafeez, H. H., Talukder, A. K., and Miyamoto, A. (2019). Ovulatory follicular fluid induces sperm phagocytosis by neutrophils, but oviductal fluid around oestrus suppresses its inflammatory effect in the buffalo oviduct *in vitro*. *Mol. Reprod. Dev.* 86, 835–846. doi:10.1002/mrd.23164

Yousef, M. S., Marey, M. A., Hambruch, N., Hayakawa, H., Shimizu, T., Hussien, H. A., et al. (2016). Sperm binding to oviduct epithelial cells enhances TGFB1 and IL10 expressions in epithelial cells as well as neutrophils *in vitro*: prostaglandin E2 as a main regulator of anti-inflammatory response in the bovine oviduct. *PloS one* 11 (9), e0162309. doi:10.1371/journal.pone.0162309

Zhang, J., Dunk, C., Croy, A. B., and Lye, S. J. (2016). To serve and to protect: the role of decidual innate immune cells on human pregnancy. *Cell Tissue Res.* 363 (1), 249–265. doi:10.1007/s00441-015-2315-4

Zhang, Z., Zhang, C., and Zhang, S. (2022). Irisin activates M1 macrophage and suppresses Th2-type immune response in rats with pelvic inflammatory disease. *Evid. Based Complement. Altern. Med.* 2022, 5215915. doi:10.1155/2022/5215915

Zhao, Y., Vanderkooi, S., and Kan, F. W. K. (2022). The role of oviduct-specific glycoprotein (OVGP1) in modulating biological functions of gametes and embryos. *Histochem. Cell Biol.* 157 (3), 371–388. doi:10.1007/s00418-021-02065-x

Zierau, O., Zenclussen, A. C., and Jensen, F. (2012). Role of female sex hormones, estradiol and progesterone, in mast cell behavior. *Front. Immunol.* 3, 169. doi:10.3389/fimmu.2012.00169

frontiers | Frontiers in Cell and Developmental Biology

TYPE Brief Research Report
PUBLISHED 08 March 2024
DOI 10.3389/fcell.2024.1337937

Check for updates

OPEN ACCESS

EDITED BY
Jason Knott,
Michigan State University, United States

REVIEWED BY
Zuzana Holubcová,
Masaryk University, Czechia
Nicole Camlin,
University of Southern Mississippi, United States

*CORRESPONDENCE
Greg FitzHarris,
greg.fitzharris@umontreal.ca

†These authors have contributed equally to this work

RECEIVED 13 November 2023
ACCEPTED 19 February 2024
PUBLISHED 08 March 2024

CITATION
Rémillard-Labrosse G, Cohen S, Boucher É, Gagnon K, Vasilev F, Mihajlović AI and FitzHarris G (2024), Oocyte and embryo culture under oil profoundly alters effective concentrations of small molecule inhibitors. *Front. Cell Dev. Biol.* 12:1337937. doi: 10.3389/fcell.2024.1337937

COPYRIGHT
© 2024 Rémillard-Labrosse, Cohen, Boucher, Gagnon, Vasilev, Mihajlović and FitzHarris. This is an open-access article distributed under the terms of the Creative Commons Attribution License (CC BY). The use, distribution or reproduction in other forums is permitted, provided the original author(s) and the copyright owner(s) are credited and that the original publication in this journal is cited, in accordance with accepted academic practice. No use, distribution or reproduction is permitted which does not comply with these terms.

Oocyte and embryo culture under oil profoundly alters effective concentrations of small molecule inhibitors

Gaudeline Rémillard-Labrosse[1†], Sydney Cohen[1†], Éliane Boucher[1†], Kéryanne Gagnon[1†], Filip Vasilev[1], Aleksandar I. Mihajlović[1] and Greg FitzHarris[1,2,3*]

[1]Centre de Recherche du Centre Hospitalier de l'Université de Montréal (CRCHUM), Montréal, QC, Canada, [2]Department of Obstetrics and Gynaecology, Université de Montréal, Montréal, QC, Canada, [3]Department of Pathology and Cell Biology, Université de Montréal, Montréal, QC, Canada

Culture of oocytes and embryos in media under oil is a cornerstone of fertility treatment, and extensively employed in experimental investigation of early mammalian development. It has been noted anecdotally by some that certain small molecule inhibitors might lose activity in oil-covered culture systems, presumably by drug partitioning into the oil. Here we took a pseudo-pharmacological approach to appraise this formally using mouse oocytes and embryos. Using different culture dish designs with defined media:oil volume ratios, we show that the EC_{50} of the widely employed microtubule poison nocodazole shifts as a function of the media:oil ratio, such that nocodazole concentrations that prevent cell division in oil-free culture fail to in oil-covered media drops. Relatively subtle changes in culture dish design lead to measurable changes in EC_{50}. This effect is not specific to one type of culture oil, and can be readily observed both in oocyte and embryo culture experiments. We subsequently applied a similar approach to a small panel of widely employed cell cycle-related inhibitors, finding that most lose activity in standard oil-covered oocyte/embryo culture systems. Our data suggest that loss of small molecule activity in oil-covered oocyte and embryo culture is a widespread phenomenon with potentially far-reaching implications for data reproducibility, and we recommend avoiding oil-covered culture for experiments employing inhibitors/drugs wherever possible.

KEYWORDS

oocyte, embryo, culture, artefact, inhibitor

Introduction

Oocyte and embryo culture in fertility clinics and research labs is routinely performed in plastic Petri dishes in drops of media under a covering layer of oil to prevent contamination and evaporation, often termed the 'closed system' (Gardner et al., 2014; Eskew and Jungheim, 2017; Gardner et al., 2019). Culture under oil allows dishes to be moved easily within the lab, permits longer-term manipulation out of the incubator such as for micromanipulation or imaging of live oocytes/embryos, and enables *ex-vivo* experimental access that has been fundamental in understanding early development. Typical dish setups in many labs involve multiple ~20–50 µL drops of culture media under commercially-

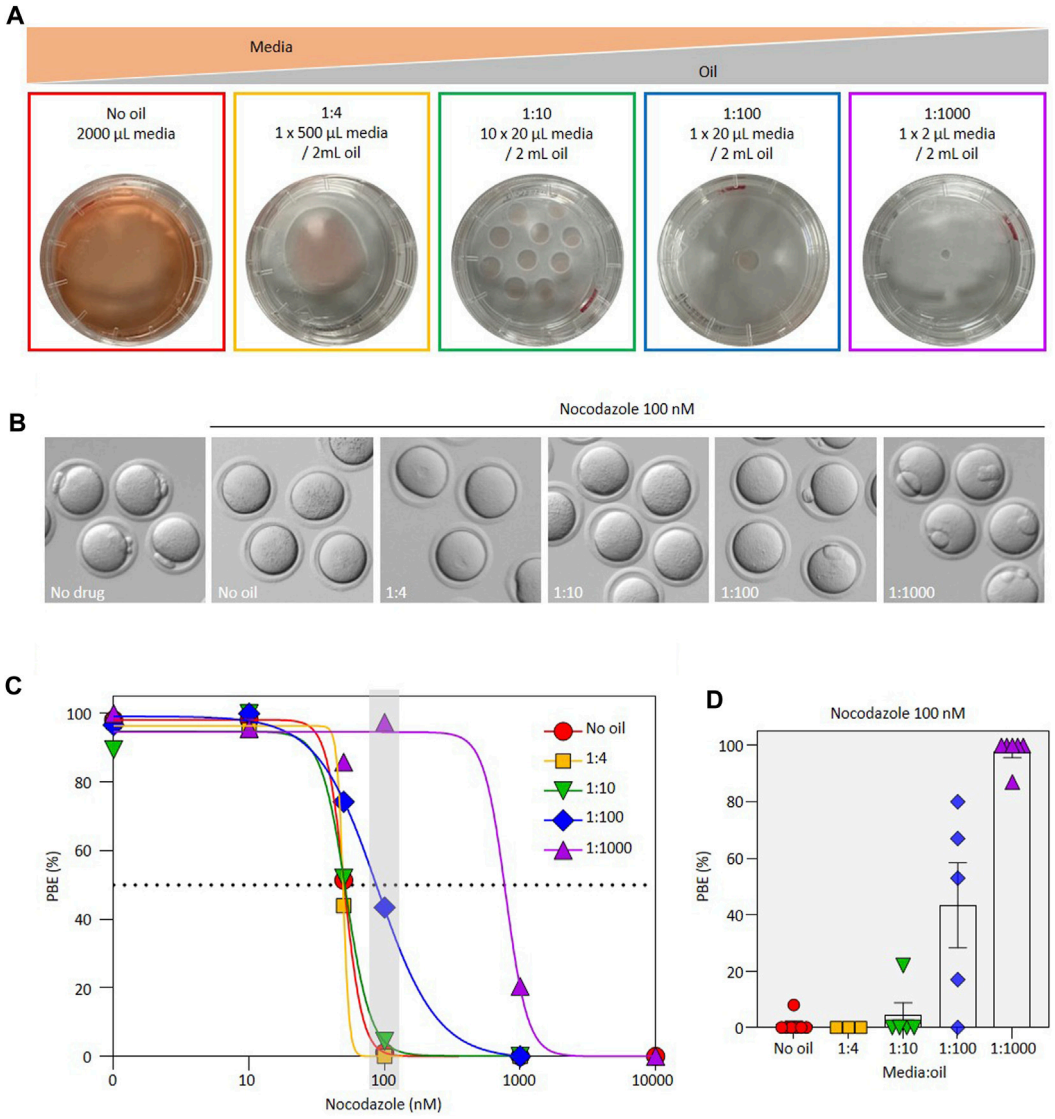

FIGURE 1
Effect of media:oil ratio on the EC_{50} of nocodazole during oocyte maturation. **(A)** Schematic representation of the experimental design to address impact of media:oil ratio on drug effects. Conditions were: no oil (2 mL media without oil); 1:4 (1 × 500 µL media covered with 2 mL oil); 1:10 (10 × 20 µL media covered with 2 mL oil); 1:100 (1 × 20 µL media covered with 2 mL oil) and 1:1000 (1 × 2 µL media covered with 2 mL oil). **(B)** Bright-field images illustrating different outcomes of PBE in oocytes incubated in 100 nM nocodazole for different media:oil ratios. **(C)** Dose-response curves for oocytes incubated in varying concentrations of nocodazole in different media:oil conditions. For this graph, each data point is an average of three to eight replicates, ~10 oocytes per replicate, *n* = 1367 oocytes in total. Specific replicate numbers for Figure 1C are as follows for no oil, 1:4, 1:10, 1:100 and 1:1000 conditions, respectively. For 1 nM nocodazole, N = 4, 4, 4, 3, 3; 10 nM, N = 8, 4, 4, 4, 5; for 50 nM N = 8, 5, 5, 5, 4; for 100 nM, N = 8, 3, 5, 6, 7; for 1000 nM, N = 3, 4, 3, 6, 5; for 10,000 nM, N = 3, 0, 0, 0, 3 respectively. **(D)** Bar chart representation highlighting impact of different media:oil ratios for oocytes incubated in 100 nM nocodazole. Data from same experiments as **(D)**; each data point is a replicate of ~10 oocytes, *n* = 332 oocytes in total. Bars represent mean ± SEM.

available mineral oils in plastic Petri dishes of diameter 3–5 cm, but many variations on this standard setup are used in different experimental contexts (discussed below). Extensive investigation and development takes place to ensure oils are embryo culture-safe, such as examination of the rate of media evaporation using different oils, and reducing the extent to which oils introduce pathogens or contaminants (Otsuki et al., 2009; Swain, 2018; Swain, 2019). Here we document a further hazard of culture oil with important consequences in oocyte and embryo studies.

The past few decades have seen major advances in our understanding of oogenesis and early embryogenesis owing to the ability to pair *ex-vivo* culture with specific experimental interventions such as conditional transgenics (Kudo et al., 2006; Sasaki et al., 2021), acute gene knockdown approaches (Stein et al., 2003; Homer et al., 2005), and use of small molecule inhibitors ("drugs") to interrogate molecular mechanisms (Pratt et al., 1981; Longo and Chen, 1985). In this context it has occasionally been noted by some investigators that they avoided oil-covered culture when using some drugs that appear to lose activity under oil, presumably a result of the ability of the drug to partition into the oil. However, a formal appraisal of the effect of oil on drug activities has not to our knowledge been presented, and whether the

phenomenon is limited to just a few niche drugs, or impacts diverse and commonly used inhibitors, is unclear.

Here we quantitatively assessed the impact of oil upon the effectiveness of several cell-cycle-related inhibitors that are widely used in oocyte and embryo research. Our results show that changing media:oil ratio profoundly impacts effective drug concentrations of many, and suggest that this is a widespread phenomenon. We argue that the impacts of this upon interpretation of some published data may be significant, and make proposals for experimental design and data reporting in such experiments.

Results

Media:oil ratios change the EC_{50} of nocodazole in oocyte maturation experiments

We reasoned that if oil reduces the effectiveness of inhibitors, then this should be quantitively demonstrable by altering the media: oil ratio in the culture dish. In this study we used a standardized series of dish setups, as illustrated in Figure 1, all employing the same 35 mm diameter plastic dish. At one extreme, we employed an oil-free culture dish wherein oocytes were cultured in 2 mL of media in a humidified incubator in the complete absence of oil. Our groups also included one 20 µL drop under 2 mL oil, and ten 20 µL drops under 2 mL oil (i.e., 1:100 and 1:10 media:oil ratio respectively), reminiscent of many standard culture systems. At the other extreme we included a setup in which 2 µL of media were placed under 2 mL of oil (1:1000 media:oil ratio). Low media:oil ratios such as this are often employed for live imaging experiments where it is important for oocytes/embryos to remain immobile, co-culture experiments, and also arise in micromanipulation studies where small media drops are used in oversized oil-filled dishes. A ratio of 1: 4 comprising 500 µl of media under 2 mL of oil was included, 500 µl of media being approximately the biggest drop that can be made under 2 mL of oil in this dish type whilst retaining a full oil covering to prevent evaporation. Throughout the study we focused on well characterized inhibitors that are documented to prevent first polar body (PB1) extrusion (PBE) at the end of oocyte maturation. We first centered on nocodazole, a mitotic/meiotic spindle poison that causes spindle disassembly by buffering free tubulin, and thus at high concentrations prevents PBE by activating the Spindle Checkpoint (Kubiak et al., 1993; Duncan et al., 2009). Nocodazole is widely employed to explore cell cycle regulation in oocytes and embryos, and used routinely in micromanipulation studies to soften the cytoplasm for enucleation (Darbandi et al., 2017; Nakagawa and FitzHarris, 2017). Importantly, to our knowledge, nocodazole has not previously been noted to lose activity under oil.

Nocodazole is well established to prevent PBE during oocyte maturation by depolymerizing the spindle and therefore activating the spindle assembly checkpoint (Homer et al., 2005; Duncan et al., 2009; Illingworth et al., 2010). To establish an accurate EC_{50} for this effect, we initially cultured oocytes in a range of nocodazole concentrations in the absence of oil. We found that the EC_{50} for prevention of PBE in the complete absence of oil was 50.7nM, 100 nM nocodazole enforcing a 100% block to PBE. However, EC_{50} was substantially shifted in oil-covered culture (Figure 1). Notably, in the 1:100 media:oil dish setup, which reflects standard culture, the EC_{50} was shifted to 88.4nM, with 50% of oocytes extruding PB1. Strikingly, in the 1:1000 dish setup analogous to that used in many labs for live imaging, all oocytes extruded PB1 even at 100 nM nocodazole (EC_{50} of 785 nM). Thus, the EC_{50} of nocodazole for preventing PBE shifted more than tenfold across a range of media:oil ratios reflective of commonly used experimental setups, such that concentrations of nocodazole that prevent PBE in the absence of oil fail to do so in certain oil-covered dish setups.

Many different embryo culture oils are commercially available and used by various investigators. Therefore, to determine whether this effect was specific to one type of embryo culture oil, we cultured oocytes in 100 nM nocodazole at different media:oil ratios using two different commercially available oils, one heavy oil and one light oil. Both oils are compatible with complete preimplantation embryo development in our lab (not shown). Notably, PBE occurred at lower media:oil ratios despite the presence of nocodazole, regardless of oil type (Figure 2). The extent to which nocodazole was inactivated was significantly less in Heavy oil compared to light ($p < 0.0001$, ANOVA with Sidak's multiple comparison test at 1:1000 ratio), but nonetheless the inactivation of nocodazole was pronounced and significant in both oil types. Thus, media:oil ratios used commonly in standard experimental setups substantially impact the EC_{50} of nocodazole for preventing first PBE, and this is not specific to one type of oil.

Media:oil ratio alters the EC_{50} of nocodazole during embryo development

To determine whether the same phenomenon could be observed in preimplantation embryos, we collected 2-cell embryos from mated females, and cultured them in the presence of nocodazole in similar dish setups as described above. Analogous to PBE, in the absence of oil, progression to the 4-cell stage was completely inhibited by 100 nM nocodazole, embryos instead arresting in M-phase of the 2-4 cell division, consistent with the activation of the spindle assembly checkpoint as expected (Figure 3). Notably however, some cells were able to divide in 100 nM nocodazole in a single 20 µL drop under oil (1:100), and only 6% of cells remained M-phase arrested in 2 µL drops under oil (1:1000). Most cells either divided to make normal 4 cell stage cells, or underwent chaotic cell divisions, suggesting low level spindle disruption that failed to activate SAC. Thus the loss of activity under oil of nocodazole that can prevent activation of the SAC in oocytes can also be observed in embryo culture experiments.

Impact of oil on diverse cell cycle inhibitors

Our pseudo-pharmacological analysis of the impact of media:oil ratios across a concentration range of nocodazole clearly demonstrates the impact of oil on the EC_{50} for preventing the completion of cell division, either in meiosis or mitosis. However, assembling the data presented in Figure 1D alone required 1367 mouse oocytes across dozens of experimental days. We therefore sought a simplified approach that could feasibly be

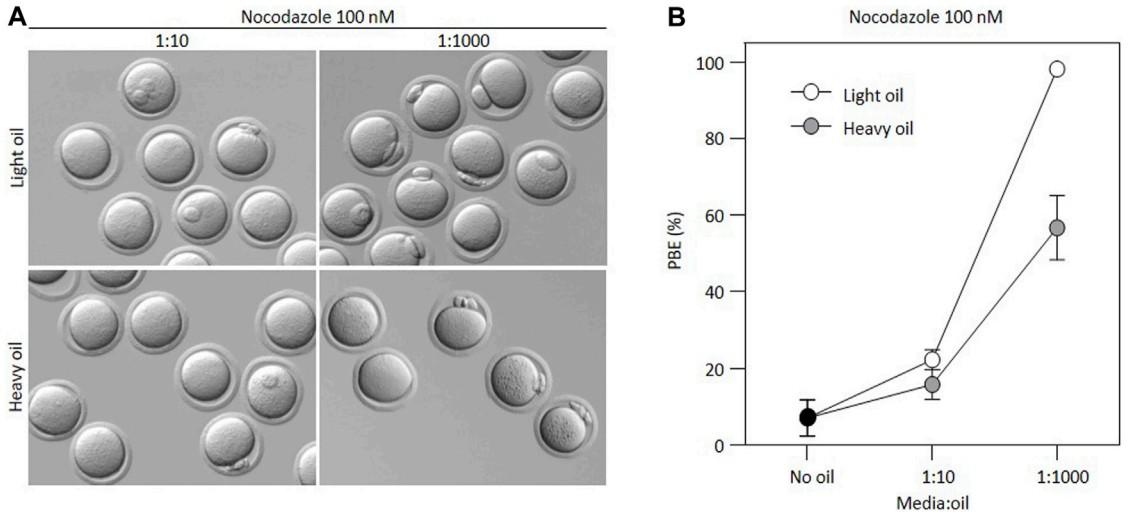

FIGURE 2
Loss of nocodazole activity is not specific to only one type of oil. **(A)** Bright-field images illustrating outcomes for oocytes incubated in 100 nM nocodazole for different media:oil ratios in light *versus* heavy mineral oil. **(B)** Graph representing changing PBE rate for oocytes incubated in 100 nM nocodazole in different media:oil conditions comparing two oil types (light vs. heavy mineral oil). For this graph, each data point is an average of four replicates, ~10 oocytes per replicate, n = 223 oocytes in total. Bars represent mean ± SEM.

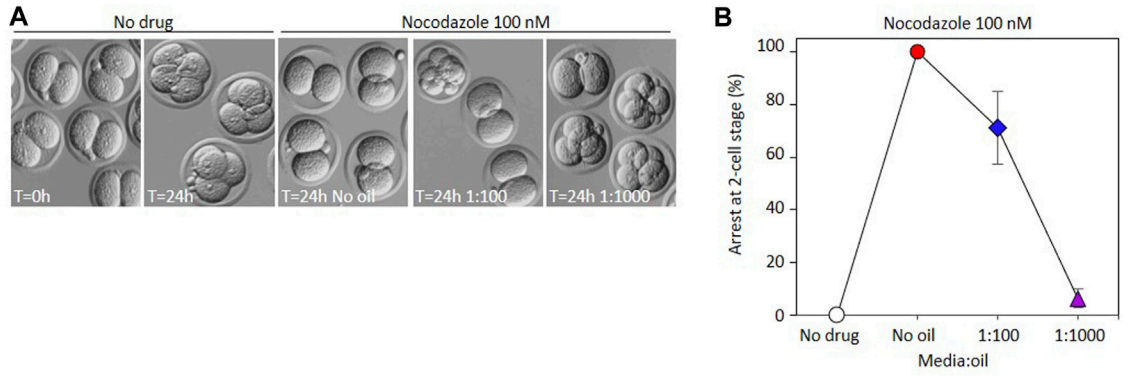

FIGURE 3
Impact of oil on the EC_{50} of nocodazole during embryo development. **(A)** Bright-field representative images illustrating appearance of embryos incubated in 100 nM nocodazole with different media:oil ratio conditions. Arrowheads indicate embryos characterized as chaotic. **(B)** Arrest at 2-cell stage was measured after embryos were incubated in 100 nM nocodazole in different media:oil ratios. Bars represent mean ± SEM. For B and C, each data point is an average mean of four replicates, 120 embryos in total.

used by labs to test the effect of oil on a given drug. We decided to first establish the concentration-dependency for PBE of a given drug in the complete absence of oil, and then use a minimum effective concentration to investigate the impact of different media:oil ratios. Although this approach does not allow formal appraisal of EC_{50} shift, it provides a quantifiable indication of the extent to which drug activity is lost under oil (Figure 4). We applied this approach to an additional five drugs that have been heavily employed in mouse oocyte studies: the proteasome inhibitor MG132 (Mailhes et al., 2002), the kinesin-5 inhibitors STLC and monastrol, the APC inhibitor APCin (Mihajlović et al., 2021), and the CDK1 inhibitor roscovitine. In all cases we added the drugs at the time of IBMX washout, as for nocodazole. APCin, MG132, STLC and monastrol are all compatible with GVBD but prevent PBE, similar to nocodazole. Roscovitine prevents GVBD, and thus our analyses were on the ability of oil to permit GVBD in the presence of roscovitine. Strikingly, as for nocodazole, the ability to prevent PBE was substantially reduced for MG132, STLC and monastrol. Oil potently prevented roscovitine from inhibiting GVBD, even the 1:4 media:oil dish setup permitting GVBD in ~50% of cases. Thus, oil coverings potently inactivate a range of cell cycle related drugs.

In contrast, it was noteworthy that 50 μM APCin retained the ability to prevent PBE even at low media:oil ratios. We wondered whether this indicated a slower loss of activity, and perhaps loss of activity might become evident over a longer time-course. We therefore examined APCin after a 24 h pre-incubation under oil, and found that the ability to prevent PBE was preserved (Figure 4, dashed curve). Thus,

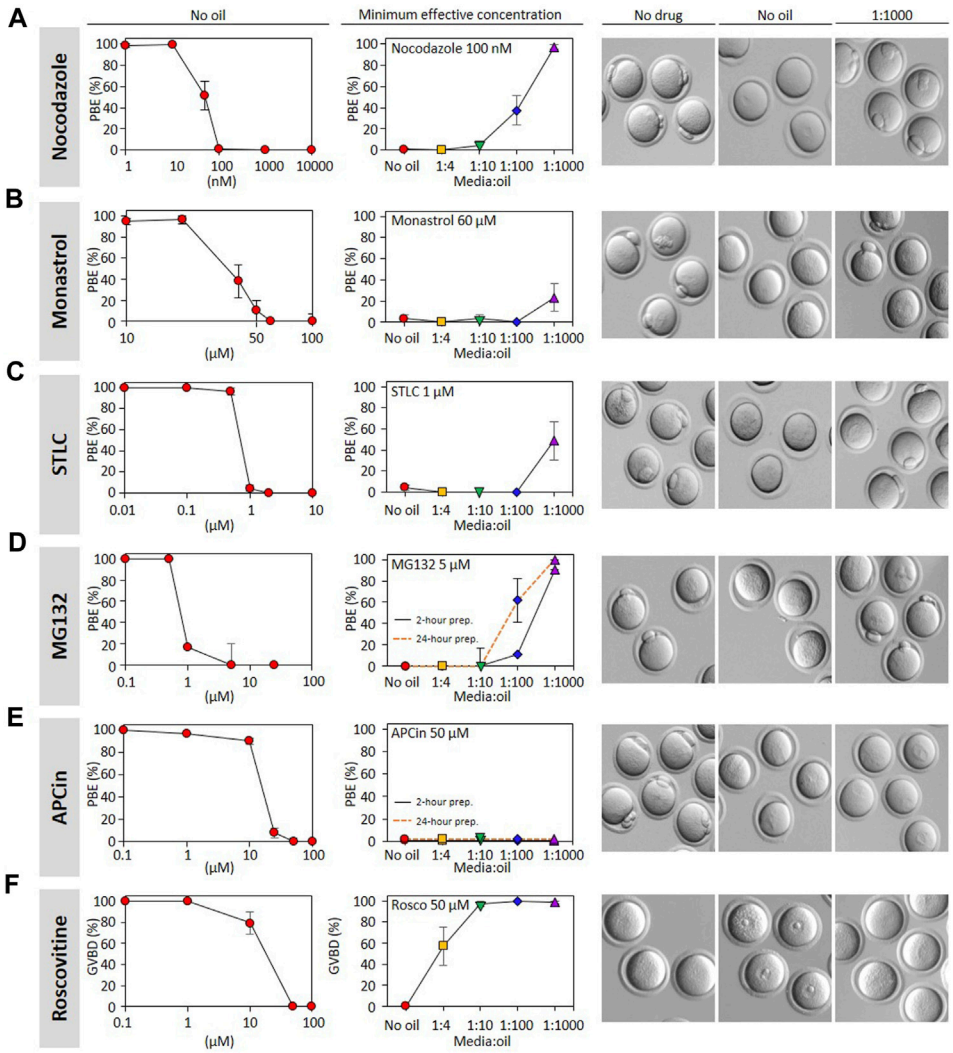

FIGURE 4
Oil covered culture affects the action of many inhibitors. Polar body extrusion (PBE) was assessed following incubation of GV oocytes with **(A)** nocodazole; **(B)** monastrol; **(C)** STLC; **(D)** MG132; **(E)** APCin. Germinal vesicle breakdown (GVBD) was evaluated with GV oocytes treated with **(F)** roscovitine. Oocytes were first incubated in varying concentrations of inhibitors without oil in order to determine the effective concentration of these drugs (i.e., concentration-response curves). In the central column, the lowest maximally effective concentration was used to analyze the impact of media:oil ratios. Dishes with media containing inhibitors ± oil were prepared and pre-equilibrated at 37°C with 5% CO_2 for 2 h prior to oocytes being transferred to them, as elsewhere in the study, and for MG132 **(D)** and APCin **(E)**, a parallel set of dishes were additionally pre-equilibrated for 24 h prior to oocytes incubation. On the right, bright-field images represent oocytes status when evaluating PBE and GVBD. Each data point is the mean of a minimum of three replicates, ~10 oocytes/replicate, a total of 2245 oocytes throughout the figure. Bars represent mean ± SEM. Specific replicate numbers for Figure 4 are as follows. Nocodazole without oil => 1 nM, N = 4; 10 nM N = 8; 50 nM, N = 8; 100 nM, N = 8; 1,000 nM, N = 3; 10,000 nM, N = 3. Nocodazole 100 nM N = 8, 3, 5, 6, 7 for no oil, 1:4, 1:10, 1:100 and 1:1000, respectively. Monastrol without oil => 10 µM: N = 3; 20µM, N = 3; 40 µM, N = 3; 50 µM, N = 4; 60 µM, N = 4; 100 µM, N = 3. Monastrol 60 µM => N = 3 for each media:oil conditions. STLC without oil => 0.01 µM N = 3; 0.1 µM N = 3; 0.5 µM N = 3; 1 µM N = 5; 2 µM N = 3; 10 µM N = 3. STLC 1 µM=> N = 5, 3, 3, 3, 3 for no oil, 1:4, 1:10, 1:100 and 1:1000 conditions respectively. For MG132, N = 3 for all conditions. For APCin without oil => 0.1 µM, N = 3; 1µM, N = 4; 10 µM, N = 4; 25 µM, N = 4; 50 µM, N = 4; 100 µM N = 3. APCin 50 µM 2-h or 24-h conditioned dishes N = 3 for all media:oil conditions. Roscovitine without oil N = 3 for all concentrations. Roscovitine 50 µM N = 3, 3, 3, 3, 5 for no oil, 1:4, 1:10, 1:100 and 1:1000, respectively.

although nocodazole, MG132, STLC, monastrol, and roscovitine clearly lose activity under oil, we were unable to find evidence that APCin activity is lost, even after long-term media-oil contact.

Finally, we wondered whether drugs that lose activity under oil may do so even more profoundly after a 24 h incubation. To test this we examined the impact of a 24 h preincubation under oil upon MG132, one of the drugs that most profoundly lost activity even in our standard experimental setup (2 h preincubation under oil). We found that MG132 was even further inactivated by a 24 h incubation under oil, such that ~60% of oocytes extruded PB1 in the 1:100 dish setup compared to only ~10% in the standard 2 h experiment (all at 5 µM MG132) (Figure Fig4, dashed curve). This indicates that even the timing of dish setup (e.g., whether dishes are prepared the night before) affects drug EC_{50}s.

To summarise, our analysis of a panel of 6 drugs suggests that although some specific drugs may retain their activity under oil, as exemplified by APCin, five of the six we tested are very clearly

inactivated by a covering layer of oil, and that the extent of this inactivation can be dependent upon time spent under oil.

Discussion

Here we have used a conceptually simple experimental approach to demonstrate that the effective concentration of an array of commonly used cell cycle drugs is dramatically changed by culturing under oil. Although we have not formally measured the presence of drugs within oil after culture, and other possible explanations such as altered drug dynamics or availability in different culture conditions and drop sizes can be conceived, the simplest interpretation is that each drug partitions into the oil, and the oil acts as a sink. Some level of hydrophobicity is necessary for most drugs to enter cells. Moreover, LogP values that are provided with most inhibitors provide a broad indication of oil solubility based on water/octanol partitioning, and these values tend to support the notion that these drugs should partition into oil. Whilst our data suggest that the extent of drug partitioning into the oil might differ between oil types (Figure 2), the effect was nonetheless very pronounced both in heavy and light oils, and so we recommend that it be presumed that drugs are likely to partition into the oil regardless of oil type/brand employed, unless clearly demonstrated not to.

In some cases partial drug loss under oil may have little impact on broad experimental conclusions, particularly where supra-maximal concentrations are used to elicit well characterised effects. However, there are several types of conclusions that are more precarious. For example, 'negative results' in which a drug appears to have no impact upon a cellular process, or circumstances in which unexpectedly high concentrations are needed to elicit expected effects, may warrant revisiting. Moreover, interpretations of which molecular species are being inhibited by selective inhibitors at specific concentrations should be interpreted with extreme caution if oil-covered culture was employed. Instances in which different inhibitor concentrations were required between studies to achieve a given phenotype could be explained by different dish setups and even the timing of their preparation.

Although here we have formally examined the loss of activity under oil of only 6 drugs, there are strong clues that many others behave similarly. Blegini and Schindler (Blengini et al., 2022) have noted that they avoid oil for Aurora-Kinase inhibitors. The Wassmann group noted that when using the MPS1/AurK inhibitor Reversine they supplemented the culture oil with drug (Gryaznova et al., 2021). Halet et al. used the PI3K inhibitor LY294002 in oil free conditions, noting a dramatic reduction in the required concentration to prevent preimplantation embryo development compared to other studies (Riley et al., 2005, Halet et al., 2008). Doubtless many other examples exist. Other drugs that we have anecdotally observed in our lab to lose activity under oil include the CENPE inhibitor GSK923295 (Vázquez-Diez et al., 2019), the APC^{cdh1} inhibitor Protame (Vázquez-Diez et al., 2019), and the myosin ATPase blocker Blebbistatin (Paim and FitzHarris, 2019). Nonetheless our data show that at least one small molecule inhibitor, APCin, did not partition into the oil, even after a 24 h incubation. Why this is the case is unclear, since LogP value for APCin and inferred polarity based on DMSO solubility would lead one to predict that APCin might do so. The case of APCin thus demonstrates that it is possible for a drug to remain in the media under oil, but this is the minority case and impossible to predict, and thus needs to be demonstrated empirically on a drug-by-drug basis if oil covering is to be used. Overall, while we believe the present study is the first to formally quantitate and highlight the effect, loss of drug activity under oil has certainly been noted by others, and is likely a widespread phenomenon.

To conclude, we advise caution when employing small molecule inhibitors, avoiding oil-covered culture wherever possible. Where the use of oil is unavoidable given the experimental context, in some live imaging studies, for example, thorough testing should be carried out to demonstrate that the media:oil ratio employed is far below the threshold where results are affected. Most importantly, detailed experimental information including exact media:oil ratios and timing of dish setup should be clearly reported when drugs are used under oil. As increasing importance is rightly placed upon data reproducibility, elimination of factors that inadvertently change experimental conditions in a manner that could critically alter results is paramount.

Materials and methods

Oocyte and embryo collection

Mouse oocytes were collected at the GV stage from the ovaries of CD1 females (Charles River Crl:CD1(ICR) 022) aged 6–12 weeks, after intraperitoneal injection of 5 IU pregnant mare serum gonadotropin (PMSG; Aviva system biotech OPPA01037). Oocytes were collected in M2 media containing 200 µM 3-isobutyl-I-methylxanthine (IBMX; Sigma I5879). Following collection oocytes were kept in M16 medium supplemented with IBMX to prevent GVBD (Wisent 311-630-QL) at 37C under 5% CO_2, prior to transfer to experimental dishes (see below). Mouse two-cell embryos were collected from the oviducts of CD1 females aged 6–12 weeks, following intraperitoneal injection of 5 IU pregnant mare serum gonadotropin (~90 h pre-collect) and 5 IU human chorionic gonadotropin (hCG; Sigma; ~40–48 h pre-collect) and mating with BDF1 male mice (Jackson 100006). Embryos were collected in M2 media and cultured in KSOM (Wisent 003–026-XL) under 5% CO_2 at 37 C. All animal experiments were performed in accordance with relevant CIPA (Comité institutionnel de protection des animaux - CHUM) guidelines and regulations under protocol IP22054GFs.

Small molecule treatments and analysis

Following collection oocytes were incubated in M16 + IBMX for 1–3 h to allow zona release (Tartia et al., 2009) and a final selection of healthy fully-grown oocytes was performed. To test the effect of oil on inhibitors, 35-mm plastic culture dishes (Sarstedt 83900) were prepared with different media:oil ratios as indicated in Figure 1 ("experimental dishes"). Importantly, experimental dishes were prepared exactly 2 h prior to the addition of oocytes/embryos for examination of the effect of drugs/oil in all cases, with the exception of Figures 4D, E which also included a group in which the dishes were assembled 24 h prior. Light oil (Sigma M8410) was used for all experiments, and heavy oil (Sigma 330760) was used in addition in

Figure 2. The media:oil ratios used in experimental dishes were: no oil (2 mL media without oil); 1:4 (1 × 500 uL media covered with 2 mL oil); 1:10 (10 × 20 uL media covered with 2 mL oil); 1:100 (1 × 20 uL media covered with 2 mL oil) and 1:1000 (1 × 2 uL media covered with 2 mL oil)). For embryo experiments, two-cell embryos were collected and then transferred in inhibitors 2 h after collection, which was again exactly 2 h after dish setup.

Oocyte maturation was triggered by washing oocytes into IBMX-free media. Immediately thereafter, oocytes were transferred into the experimental dishes. Oocytes or embryos was washed through four drops of media with inhibitor in a similar setup (concentration, and media:oil ratio) as the final experimental dish, and then transferred to the experimental dish. On any given experimental day each investigator cultured an additional control group of oocytes or embryos incubated entirely without inhibitors—data was included in the final dataset from any experimental day only if >90% development (GVBD, PBE, or 2–4 cell division) was observed in this sentinel group. Inhibitors used in this project were: nocodazole (Calbiochem/Millipore 487928); monastrol (Calbiochem/Millipore 475879); S-Trityl-L-cysteine (STLC; Tocris 2191); MG132 (Calbiochem/Millipore 474790); APCin (Tocris 5747) and roscovitine (Sigma R7772). Effects of the treatment was assessed 16–18 h post transfer into inhibitors. Bright-field images were captured using a Leica M165C dissection scope equipped with a camera (Camera Opti-Vision 4K LITE- 8 MP Opti-Tech Scientific). Calculation of EC_{50} was performed in graphpad prism. Data were entered as XY table, where X = concentration and Y=PBE. A nonlinear regression analysis was performed and a dose response curve was fitted. EC_{50} was calculated by the software from the fitted curve.

Data availability statement

The raw data supporting the conclusion of this article will be made available by the authors, without undue reservation.

Ethics statement

The animal study was approved by Comité institutionnel de protection des animaux—Centre Hospitalier de l'Université de Montréal (CIPA) (protocol IP22054GFs—GF) under the aegis of the Canadian Council on Animal Care (CCAC). The study was conducted in accordance with the local legislation and institutional requirements.

Author contributions

GR: Conceptualization, Data curation, Formal Analysis, Investigation, Methodology, Validation, Writing–review and editing. SC: Conceptualization, Data curation, Formal Analysis, Investigation, Methodology, Validation, Writing–review and editing. ÉB: Conceptualization, Data curation, Formal Analysis, Investigation, Methodology, Validation, Writing–review and editing. KG: Conceptualization, Data curation, Formal Analysis, Investigation, Methodology, Validation, Writing–review and editing. FV: Conceptualization, Data curation, Formal Analysis, Investigation, Methodology, Writing–review and editing. AM: Conceptualization, Data curation, Formal Analysis, Methodology, Writing–review and editing. GF: Conceptualization, Data curation, Formal Analysis, Methodology, Writing–review and editing, Funding acquisition, Investigation, Project administration, Resources, Supervision, Validation, Writing–original draft.

Funding

The author(s) declare financial support was received for the research, authorship, and/or publication of this article. This research was supported by the grants from Canadian Institute for Health Research (CIHR), Foundation Jean-Louis Levesque, and Natural Sciences and Engineering Research Council of Canada (NSERC) to GF. EB received a scholarship from McGill University's Centre for Research in Reproduction and Development (CRRD), and SC received a scholarship from Université de Montréal Centre de recherche en reproduction et fertilité (CRRF).

Acknowledgments

We thank François Proulx, Karen Schindler, and Guillaume Halet for valuable discussions and for critical reading of the manuscript. A version of this manuscript has been published as a preprint on the BioRxiv website (Rémillard Labrosse et al., 2023).

Conflict of interest

The authors declare that the research was conducted in the absence of any commercial or financial relationships that could be construed as a potential conflict of interest.

Publisher's note

All claims expressed in this article are solely those of the authors and do not necessarily represent those of their affiliated organizations, or those of the publisher, the editors and the reviewers. Any product that may be evaluated in this article, or claim that may be made by its manufacturer, is not guaranteed or endorsed by the publisher.

References

Blengini, C. S., Ik Jung, G., Aboelenain, M., and Schindler, K. (2022). A field guide to Aurora kinase inhibitors: an oocyte perspective. *Reproduction* 164, V5–V7. doi:10.1530/REP-22-0292

Darbandi, S., Darbandi, M., Khorram Khorshid, H. R., Shirazi, A., Sadeghi, M. R., Agarwal, A., et al. (2017). Reconstruction of mammalian oocytes by germinal vesicle transfer: a systematic review. *Int. J. Reprod. Biomed.* 15, 601–612. doi:10.29252/ijrm.15.10.2

Duncan, F. E., Chiang, T., Schultz, R. M., and Lampson, M. A. (2009). Evidence that a defective spindle assembly checkpoint is not the primary cause of maternal age-associated aneuploidy in mouse eggs. *Biol. Reprod.* 81, 768–776. doi:10.1095/biolreprod.109.077909

Eskew, A. M., and Jungheim, E. S. (2017). A history of developments to improve *in vitro* fertilization. *Mo Med.* 114, 156–159.

Gardner, D. K., and Lane, M. (2014). "Chapter 6 - culture of viable mammalian embryos *in vitro*," in *Principles of cloning*. Editors J. Cibelli, R. Lanza, K. H. S. Campbell, and M. D. West Second Edition (Academic Press), 63–84. doi:10.1016/B978-0-12-386541-0.00006-0

Gardner, D. K., and Truong, T. T. (2019). "Culture of the mouse preimplantation embryo," in *Comparative embryo culture: methods and protocols*. Editor J. R. Herrick (Springer), 13–32. doi:10.1007/978-1-4939-9566-0_2

Gryaznova, Y., Keating, L., Touati, S. A., Cladière, D., El Yakoubi, W., Buffin, E., et al. (2021). Kinetochore individualization in meiosis I is required for centromeric cohesin removal in meiosis II. *EMBO J.* 40, e106797. doi:10.15252/embj.2020106797

Halet, G., Viard, P., and Carroll, J. (2008). Constitutive PtdIns(3,4,5)P3 synthesis promotes the development and survival of early mammalian embryos. *Development* 135, 425–429. doi:10.1242/dev.014894

Homer, H. A., McDougall, A., Levasseur, M., Yallop, K., Murdoch, A. P., and Herbert, M. (2005). Mad2 prevents aneuploidy and premature proteolysis of cyclin B and securin during meiosis I in mouse oocytes. *Genes. Dev.* 19, 202–207. doi:10.1101/gad.328105

Illingworth, C., Pirmadjid, N., Serhal, P., Howe, K., and Fitzharris, G. (2010). MCAK regulates chromosome alignment but is not necessary for preventing aneuploidy in mouse oocyte meiosis I. *Development* 137, 2133–2138. doi:10.1242/dev.048306

Kubiak, J. Z., Weber, M., de Pennart, H., Winston, N. J., and Maro, B. (1993). The metaphase II arrest in mouse oocytes is controlled through microtubule-dependent destruction of cyclin B in the presence of CSF. *EMBO J.* 12, 3773–3778. doi:10.1002/j.1460-2075.1993.tb06055.x

Kudo, N. R., Wassmann, K., Anger, M., Schuh, M., Wirth, K. G., Xu, H., et al. (2006). Resolution of chiasmata in oocytes requires separase-mediated proteolysis. *Cell* 126, 135–146. doi:10.1016/j.cell.2006.05.033

Longo, F. J., and Chen, D.-Y. (1985). Development of cortical polarity in mouse eggs: involvement of the meiotic apparatus. *Dev. Biol.* 107, 382–394. doi:10.1016/0012-1606(85)90320-3

Mailhes, J. B., Hilliard, C., Lowery, M., and London, S. N. (2002). MG-132, an inhibitor of proteasomes and calpains, induced inhibition of oocyte maturation and aneuploidy in mouse oocytes. *Cell and Chromosome* 1, 2. doi:10.1186/1475-9268-1-2

Mihajlović, A. I., Haverfield, J., and FitzHarris, G. (2021). Distinct classes of lagging chromosome underpin age-related oocyte aneuploidy in mouse. *Dev. Cell* 56, 2273–2283.e3. doi:10.1016/j.devcel.2021.07.022

Nakagawa, S., and FitzHarris, G. (2017). Intrinsically defective microtubule dynamics contribute to age-related chromosome segregation errors in mouse oocyte meiosis-I. *Curr. Biol.* 27, 1040–1047. doi:10.1016/j.cub.2017.02.025

Otsuki, J., Nagai, Y., and Chiba, K. (2009). Damage of embryo development caused by peroxidized mineral oil and its association with albumin in culture. *Fertil. Steril.* 91, 1745–1749. doi:10.1016/j.fertnstert.2008.03.001

Paim, L. M. G., and FitzHarris, G. (2019). Tetraploidy causes chromosomal instability in acentriolar mouse embryos. *Nat. Commun.* 10, 4834. doi:10.1038/s41467-019-12772-8

Pratt, H. P., Chakraborty, J., and Surani, M. A. (1981). Molecular and morphological differentiation of the mouse blastocyst after manipulations of compaction with cytochalasin D. *Cell* 26, 279–292. doi:10.1016/0092-8674(81)90310-x

Rémillard Labrosse, G., Cohen, S., Boucher, É., Gagnon, K., Vasilev, F., Mihajlović, A., et al. (2023). *Oocyte and embryo culture under oil profoundly alters effective concentrations of small molecule inhibitors*. bioRxiv. doi:10.1101/2023.11.10.566607

Riley, J. K., Carayannopoulos, M. O., Wyman, A. H., Chi, M., Ratajczak, C. K., and Moley, K. H. (2005). The PI3K/Akt pathway is present and functional in the preimplantation mouse embryo. *Dev. Biol.* 284, 377–386. doi:10.1016/j.ydbio.2005.05.033

Sasaki, K., Takaoka, S., and Obata, Y. (2021). Oocyte-specific gene knockdown by intronic artificial microRNAs driven by Zp3 transcription in mice. *J. Reprod. Dev.* 67, 229–234. doi:10.1262/jrd.2020-146

Stein, P., Svoboda, P., and Schultz, R. M. (2003). Transgenic RNAi in mouse oocytes: a simple and fast approach to study gene function. *Dev. Biol.* 256, 187–193. doi:10.1016/s0012-1606(02)00122-7

Swain, J. E. (2018). Different mineral oils used for embryo culture microdrop overlay differentially impact media evaporation. *Fertil. Steril.* 109, e53. doi:10.1016/j.fertnstert.2018.02.101

Swain, J. E. (2019). Controversies in ART: considerations and risks for uninterrupted embryo culture. *Reprod. Biomed. Online* 39, 19–26. doi:10.1016/j.rbmo.2019.02.009

Tartia, A. P., Rudraraju, N., Richards, T., Hammer, M. A., Talbot, P., and Baltz, J. M. (2009). Cell volume regulation is initiated in mouse oocytes after ovulation. *Development* 136, 2247–2254. doi:10.1242/dev.036756

Vázquez-Diez, C., Paim, L. M. G., and FitzHarris, G. (2019). Cell-size-independent spindle checkpoint failure underlies chromosome segregation error in mouse embryos. *Curr. Biol.* 29, 865–873. doi:10.1016/j.cub.2018.12.042

frontiers | Frontiers in Cell and Developmental Biology

TYPE Original Research
PUBLISHED 13 March 2024
DOI 10.3389/fcell.2024.1355979

Check for updates

OPEN ACCESS

EDITED BY
Satoshi Kishigami,
University of Yamanashi, Japan

REVIEWED BY
Carlos Conde,
Universidade do Porto, Portugal
Chengjie Zhou,
Harvard Medical School, United States

*CORRESPONDENCE
Martin Anger,
martin.anger@vri.cz

RECEIVED 14 December 2023
ACCEPTED 20 February 2024
PUBLISHED 13 March 2024

CITATION
Horakova A, Konecna M, Radonova L and Anger M (2024), Early onset of APC/C activity renders SAC inefficient in mouse embryos. *Front. Cell Dev. Biol.* 12:1355979. doi: 10.3389/fcell.2024.1355979

COPYRIGHT
© 2024 Horakova, Konecna, Radonova and Anger. This is an open-access article distributed under the terms of the Creative Commons Attribution License (CC BY). The use, distribution or reproduction in other forums is permitted, provided the original author(s) and the copyright owner(s) are credited and that the original publication in this journal is cited, in accordance with accepted academic practice. No use, distribution or reproduction is permitted which does not comply with these terms.

Early onset of APC/C activity renders SAC inefficient in mouse embryos

Adela Horakova[1,2,3], Marketa Konecna[1,2,3], Lenka Radonova[1,2] and Martin Anger[1,2]*

[1]Department of Genetics and Reproductive Biotechnologies, Veterinary Research Institute, Brno, Czechia, [2]Institute of Animal Physiology and Genetics, Academy of Sciences of the Czech Republic (ASCR), Libechov, Czechia, [3]Faculty of Science, Masaryk University, Brno, Czechia

Control mechanisms of spindle assembly and chromosome segregation are vital for preventing aneuploidy during cell division. The mammalian germ cells and embryos are prone to chromosome segregation errors, and the resulting aneuploidy is a major cause of termination of development or severe developmental disorders. Here we focused on early mouse embryos, and using combination of methods involving microinjection, immunodetection and confocal live cell imaging, we concentrated on the Spindle Assembly Checkpoint (SAC) and Anaphase Promoting Complex/Cyclosome (APC/C). These are two important mechanisms cooperating during mitosis to ensure accurate chromosome segregation, and assessed their activity during the first two mitoses after fertilization. Our results showed, that in zygotes and 2-cell embryos, the SAC core protein Mad1 shows very low levels on kinetochores in comparison to oocytes and its interaction with chromosomes is restricted to a short time interval after nuclear membrane disassembly (NEBD). Exposure of 2-cell embryos to low levels of spindle poison does not prevent anaphase, despite the spindle damage induced by the drug. Lastly, the APC/C is activated coincidentally with NEBD before the spindle assembly completion. This early onset of APC/C activity, together with precocious relocalization of Mad1 from chromosomes, prevents proper surveillance of spindle assembly by SAC. The results contribute to the understanding of the origin of aneuploidy in early embryos.

KEYWORDS

spindle, spindle assembly checkpoint, chromosome segregation, anaphase, embryo, Mad1, anaphase-promoting complex

Introduction

Mammalian oocytes and embryonic blastomeres are known to be prone to errors during chromosome segregation. Such errors might lead to chromosome loss or gain, and the resulting aneuploidy compromises the future development of the embryo or causes severe developmental disorders (Nagaoka et al., 2012). In oocytes, the origin of chromosome segregation errors was extensively studied in multiple species, including mice and humans. The problem, at least in mouse, seems to be caused by an inability to respond adequately to the spindle assembly defects, as reported by several laboratories, including our laboratory (Nagaoka et al., 2011; Gui and Homer, 2012; Kolano et al., 2012; Lane et al., 2012; Sebestova et al., 2012; Allais and FitzHarris, 2022). In human oocytes, chromosome segregation is even more compromised (Mihajlovic and FitzHarris, 2018; Charalambous et al., 2022). In early

embryos, the mechanisms underlying chromosome segregation were not studied extensively, and thus, the reasons why embryonic blastomeres are frequently affected by aneuploidy are less clear (Vázquez-Diez and FitzHarris, 2018).

The embryos are usually mosaic, and the number of cells affected dictates the possibility of further development (Shahbazi et al., 2020). We have previously shown that in mouse 1–8-cell *in vivo* embryos, the frequency of aneuploidy per blastomere fluctuates between 4% and 7%, with a further increase of 11% during the 8–16-cell transition (Pauerova et al., 2020). Because of the increasing number of blastomeres within the embryo, such incidence of aneuploidy translates into more than half of the embryos carrying aneuploid blastomeres in the later stages of preimplantation development. Similar numbers were also reported in human (Carbone and Chavez, 2015), bovine (Destouni et al., 2016; Tšuiko et al., 2017), porcine (Hornak et al., 2012), and rhesus monkey embryos (Daughtry et al., 2019), indicating that aneuploidy represents a general problem for mammalian embryos.

Given the much higher frequency of aneuploidy in embryos compared to somatic cells, answering the question of whether chromosome segregation in early embryos fails more frequently or whether the control mechanisms are compromised is important. During mitosis, the spindle assembly and chromosome segregation are monitored through the spindle assembly checkpoint (SAC) pathway (Musacchio, 2015; Lara-Gonzalez et al., 2021; McAinsh et al., 2023). In response to the defects in the spindle apparatus and erroneous connections of kinetochores, SAC delays anaphase until all chromosomes are properly attached to the spindle. This ensures accurate segregation of chromosomes between daughter cells. SAC depends on the ability of unoccupied kinetochores to catalyze a conformational change in Mad2, which leads to the formation of the mitotic checkpoint complex (MCC). This complex, by sequestration of CDC20 from anaphase-promoting complex/cyclosome (APC/C), arrests cells in metaphase. Anaphase entry requires cessation of SAC activity, which is followed by swift APC/C activation. It is, however, not clear whether such a pathway also operates in early embryos and if so, whether it is fully functional.

In some metazoan species, such as ascidians, *Xenopus*, and zebrafish, SAC in embryos is active only after midblastula transition (MBT) (Clute and Masui, 1995; Zhang et al., 2015; Chenevert, 2020). In other species, such as *Caenorhabditis elegans*, SAC is already active before MBT (Encalada et al., 2005). In mammals, the situation is not very clear. Human embryos respond to nocodazole, and during later stages of development, the exposure leads to apoptosis (Jacobs et al., 2017). In mouse, the gene targeting studies showed that Mad2 and BubR1, which are both essential genes for the SAC pathway, did not prevent development to the blastocyst stage (Dobles et al., 2000). In addition, the deletion of various SAC proteins in zygotes affected chromosome segregation (Wei et al., 2011). Recently, SAC was also studied in mouse embryos, and the authors showed that 2-cell embryos exposed to nocodazole prolong mitosis and that during morula and blastocyst stages, the congression defects and lagging chromosomes are ignored (Vázquez-Diez et al., 2019).

Here, we assessed the SAC function during the first two mitotic divisions in mouse embryos. We focused on the ability of SAC to postpone APC/C activity. A combination of various techniques, such as immunodetection, live cell imaging, and pharmacological perturbations, revealed that SAC in early mouse embryos is unable to postpone anaphase in the case of defects in spindle assembly. This is consistent with the inability of embryos to effectively prevent chromosome segregation errors and aneuploidy.

Results

Detection of endogenous Mad1 on kinetochores in zygotes and 2-cell embryos

The function of SAC critically depends on the ability of Mad1/Mad2 to localize to unattached kinetochores, where it resides until connections to the spindle apparatus are established (Luo et al., 2018). Mad1 kinetochore localization, therefore, serves as a direct reporter of the local SAC activity. First, we focused on endogenous Mad1 to specifically determine whether the localization is consistent with its potential function in SAC. The Mad1 expression levels in zygotes and 2-cell embryos were compared to those in meiosis I oocytes with a known localization pattern (Zhang et al., 2005). For Mad1 detection, cells were collected in metaphase, meiosis I oocytes four hours after GVBD, and zygotes and 2-cell embryos 30–50 min after NEBD (Figure 1A). After processing for immunodetection of Mad1 and CREST, the signal of Mad1 was measured in the region of CREST localization (Supplementary Figure S1A), and the Mad1 cytoplasmic signal was subtracted. A comparison of the signal in zygotes and 2-cell embryos with oocytes showed significantly lower levels of endogenous Mad1 in embryos (Figures 1B, C).

Inhibition of Mps1 has different consequences in zygotes and 2-cell embryos

Our previous results showed that the crucial SAC component Mad1 was almost absent in the kinetochores of zygotes and 2-cell embryos. Inhibition of SAC in mitosis (Shindo et al., 2021) or meiosis (McGuinness, 2009) causes M phase acceleration and increases the frequency of chromosome segregation defects. To inhibit SAC, we used reversine, a potent Mps1 kinase inhibitor (Santaguida et al., 2010), which was previously used in mouse oocytes (Hached et al., 2011; El Yakoubi et al., 2017) and embryos (Bolton et al., 2016). Mps1 inhibition should prevent Mad1 localizing to the kinetochores (Santaguida et al., 2010). Zygotes and 2-cell embryos were microinjected with cRNAs encoding tubulin-EGFP and histone H2B-mCherry fusion proteins. For all experiments, the identical concentration of reversine was employed for both embryos since they were in the same dish. The division was monitored by confocal microscopy. The results showed that reversine significantly affected chromosome segregation in both embryos, although it affected zygotes more severely (Figure 2A). In the majority of cells, the congression was profoundly affected, and chromosomes were scattered along the spindle axis. Whereas the length of mitosis in zygotes was unaffected by reversine, the length of mitosis in 2-cell embryos was accelerated by approximately one-third (Figures 2B, C). Mps1 inhibition

10.3389/fcell.2024.1355979

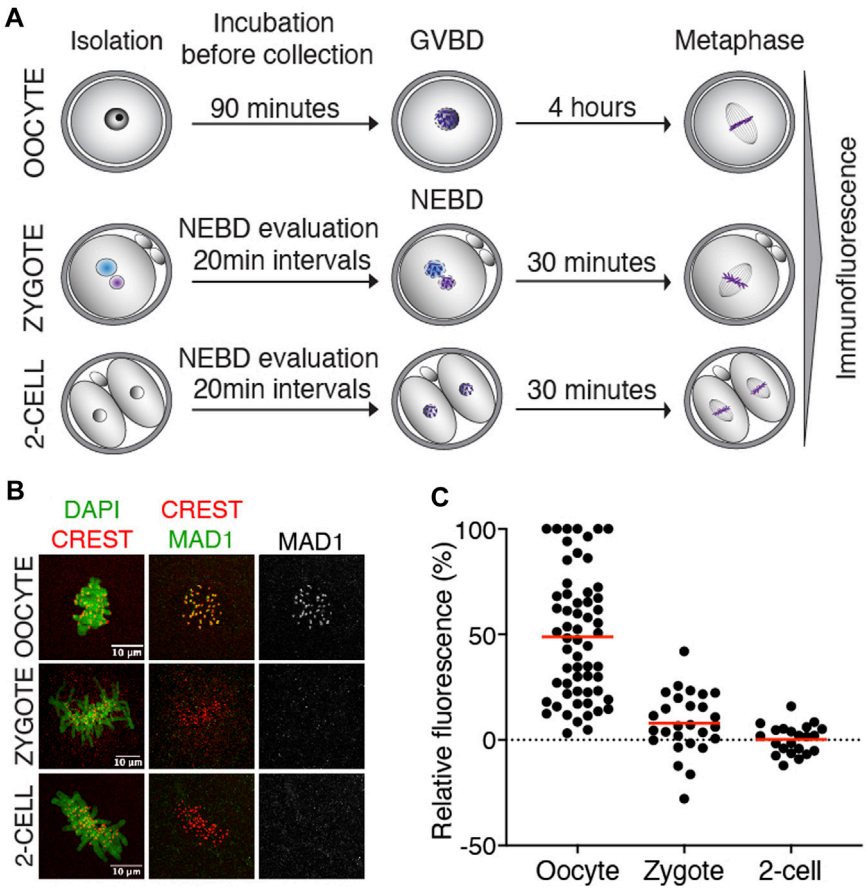

FIGURE 1
Endogenous Mad1 in oocytes and early embryos. **(A)** Scheme of synchronization protocol for obtaining oocytes and embryos in meiosis or mitosis. **(B)** Representative images of oocytes and early mouse embryos after immunostaining. DNA (green) was visualized by DAPI, centromeres were detected by the anti-CREST antibody (red), and Mad1 was detected by the anti-Mad1 antibody (green or gray). The scale bar represents 10 µm. **(C)** Scatterplot showing the signal of Mad1 detected by the antibody in control oocytes, zygotes, and 2-cell embryos. The average per group was 48.8 ± 29.5% in oocytes, 7.9 ± 14.5% in zygotes, and 0.3 ± 6.8% in 2-cell embryos. The difference between oocytes and zygotes or oocytes and 2-cell embryos was statistically significant ($\alpha < 0.05$, ****p = <0.0001). The data were obtained from two independent experiments (oocytes: n = 60; zygotes: n = 27; 2-cell embryos: n = 22).

accelerated meiosis I (Hached et al., 2011), reducing the timing to almost 50% of its normal duration. Such an acceleration is similar to the depletion of SAC components, for example, Bub1 (McGuinness, 2009) or BubR1 (Touati et al., 2015). Compared to oocytes, the effect of Mps1 inhibition on the duration of mitosis was apparent only in 2-cell embryos. Although the 2-cell embryos eventually divided, the division of zygotes was compromised and frequently resulted in cell fragmentation (Figures 2D, E). In conclusion, these experiments revealed different sensitivity of zygotes and 2-cell embryos to the pharmacological inhibition of SAC, with catastrophic consequences, but unchanged mitosis time length in zygotes and shortened mitosis in 2-cell embryos.

Challenging SAC does not prevent anaphase in 2-cell embryos

Quantification of endogenous chromosomal Mad1 demonstrated its dramatically low levels on chromosomes in 1–2-cell embryos (Figure 1C). However, we could not exclude that a strong trigger, for example, uncongressed chromosomes, might cause Mad1 relocalization to the kinetochores. To address this, we assessed the Mad1 signal in zygotes and 2-cell embryos during a relatively rare event when chromosomes were visibly separated from the metaphase plate (Figure 3). The data were obtained from live cell imaging and showed, that Mad1 signal was not always associated with kinetochores of chromosomes outside of the metaphase plate. In another case, we show that the Mad1 signal was retained even during anaphase entry. Nevertheless, the overall frequency of congression defects in embryos was low and did not allow for drawing any conclusion. Therefore, we decided to challenge SAC by nocodazole (Figure 4). Cells were microinjected with tubulin-CFP, Mad1-Venus, and histone H2B-mCherry cRNAs and exposed to 266 nM nocodazole. Same as in reversine experiments, all cells were cultured in the same dish and therefore were exposed to the same concentration of the inhibitor. Confocal live cell imaging monitoring showed that all cells remained arrested in mitosis and had no spindle (Figures 4A, B). The Mad1 signal, albeit reduced, was detectable on

10.3389/fcell.2024.1355979

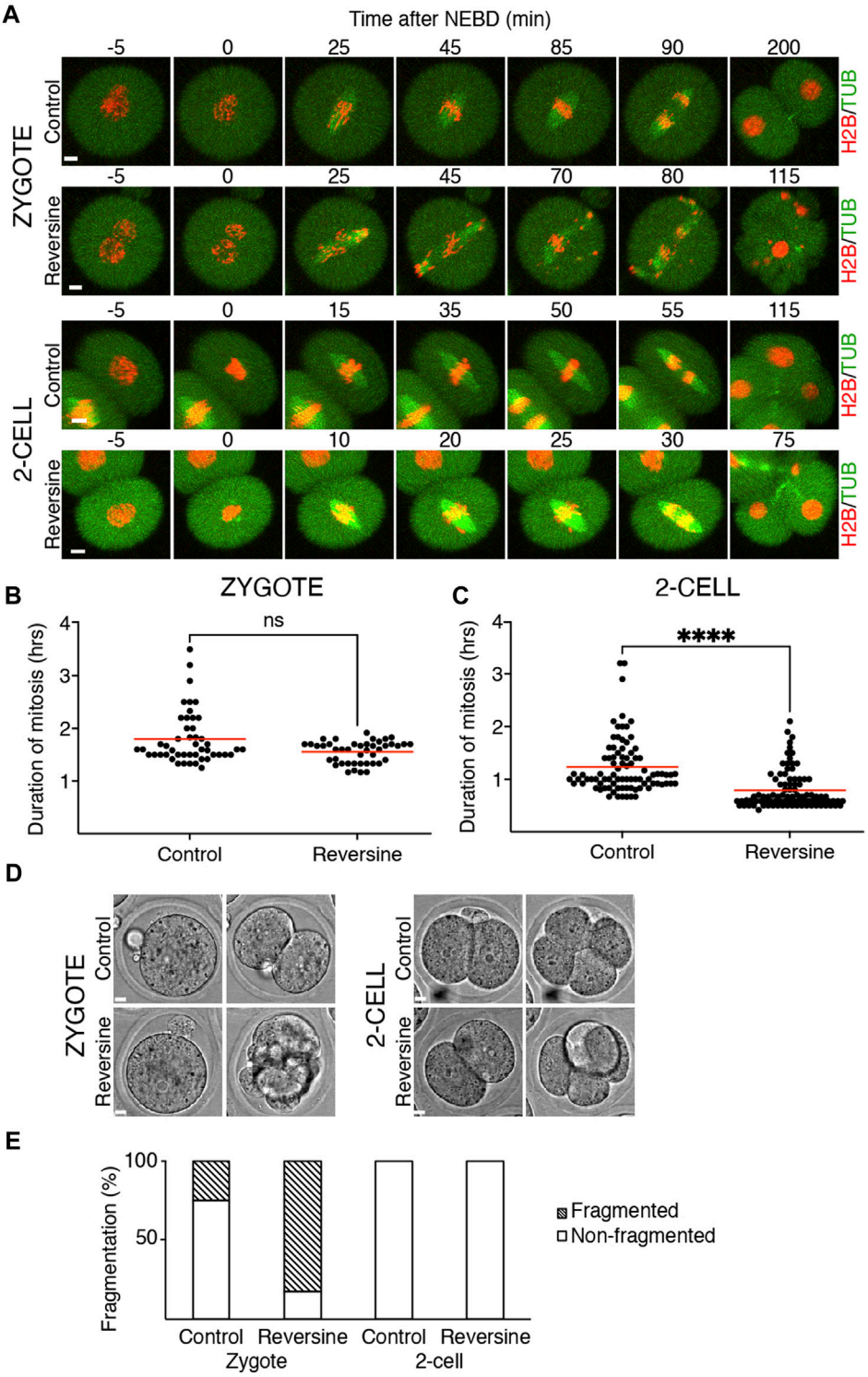

FIGURE 2
Reversine impacts chromosome segregation in oocytes and early mouse embryos. **(A)** Representative frames of mitosis from the time-lapse confocal microscopy of control and reversine-treated zygotes and 2-cell embryos. Cells were microinjected with histone H2B (red) and tubulin (green) fusion proteins. The scale bar represents 10 μm. **(B)** Scatterplot shows duration of mitosis from NEBD until anaphase in zygotes cultured without and with reversine (control: n = 48; reversine: n = 43). The average per group was 1.8 ± 0.5% in control zygotes and 1.55 ± 0.21% in reversine-treated zygotes. The difference between control and reversine-treated zygotes was not significant (p = <0.0991). The data were obtained from six experiments. **(C)** Scatterplot shows duration of mitosis from NEBD until anaphase in 2-cell embryos cultured without and with reversine (control: n = 86; reversine: n = 92). The average per group was 1.23 ± 0.52% in control 2-cell embryos and 0.79 ± 0.36% in reversine-treated 2-cell embryos. The difference between control and reversine-treated 2-cell embryos was significant ($\alpha < 0.05$, ****p = <0.0001). The data were obtained from six experiments. **(D)** Representative images of division of control and reversine-treated zygotes and 2-cell embryos illustrating the fragmentation in zygotes. The scale bar represents 10 μm. **(E)** Fragmentation of control and reversine-treated zygotes and 2-cell embryos. The chart shows the percentage of fragmentation in the control group

(*Continued*)

FIGURE 2 (Continued)
(zygotes: n = 24; 2-cell embryos: n = 46) and reversine group (zygotes: n = 23; 2-cell embryos: n = 47). In zygotes, the fragmentation was observed in 25% of the control group and 82.6% of the reversine group. The 2-cell embryos show no fragmentation. The chart shows data from three independent experiments.

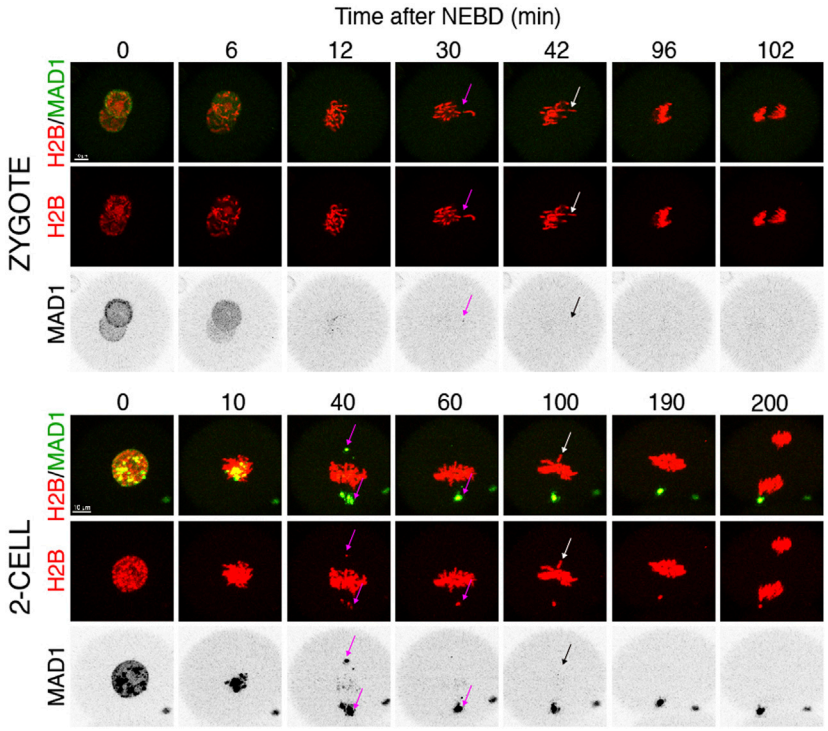

FIGURE 3
Mad1 signal on uncongressed chromosomes in zygotes and 2-cell embryos. Frames from the time-lapse experiments showing division of zygotes and 2-cell embryos from NEBD to anaphase. Early mouse embryos were microinjected with cRNAs encoding histone H2B (red) and Mad1 (green and black in the inverted part) fused to fluorescent proteins. The magenta arrow points to a chromosome with the Mad1 signal, whereas the white arrow (in inverted pictures black) points to a chromosome without the Mad1 signal. The scale bar represents 10 μm.

chromosomes for a prolonged time interval (Figures 4C, D), which was on average longer in zygotes than in 2-cell embryos.

We also tested a lower 100 nM concentration of nocodazole (Figure 5) in the same experimental setup. A lower concentration of the drug will allow for building the spindle, but it should challenge the SAC. The spindle morphology was, however, significantly affected by nocodazole, more so in zygotes than in 2-cell embryos (Figures 5A, B). The spindle assembly in zygotes therefore seems to be more sensitive to tubulin depolymerization than that in 2-cell embryos. The residence time of Mad1 on kinetochores was extended (Figures 5C, D) and was comparable to the higher doses of the drug (Figures 4C, D). The main difference therefore was in the presence of spindle apparatus in cells exposed to a lower dose. Although the 2-cell embryos eventually divided, they spent a much longer time in division compared to the control embryos (Figure 5E). Importantly, this experiment revealed that the 2-cell embryos were able to execute chromosome division even with visibly damaged spindles and that Mad1 was displaced from the chromosomes only just before anaphase entry.

Early onset of APC/C activity in 2-cell embryos after entry into mitosis

It was shown that in zygotes, the destruction of cyclin B is delayed, whereas in 2-cell embryos, the cyclin B destruction seems to be initiated earlier (Ajduk et al., 2017). Here, we used securin, which is also an APC/C substrate, to assess a link between spindle assembly and APC/C activity (Figure 6). For our experiments, we used tagged wild-type securin (WT securin), as well as tagged securin with mutations in KEN box and D box (DK securin), which should render securin resistant to APC/C (Thomas et al., 2021). Our results showed that the destruction of securin in 2-cell embryos starts immediately after NEBD, whereas in zygotes, it is delayed (Figures 6A–D). The DK securin showed that the onset of securin destruction in zygotes and 2-cell embryos is dependent on APC/C. Importantly, although in zygotes, the onset of securin destruction was delayed until the completion of the spindle assembly and establishment of the metaphase plate, the link between the initiation of securin destruction and completion of spindle assembly in 2-cell embryos is lost (Figures 7A, B).

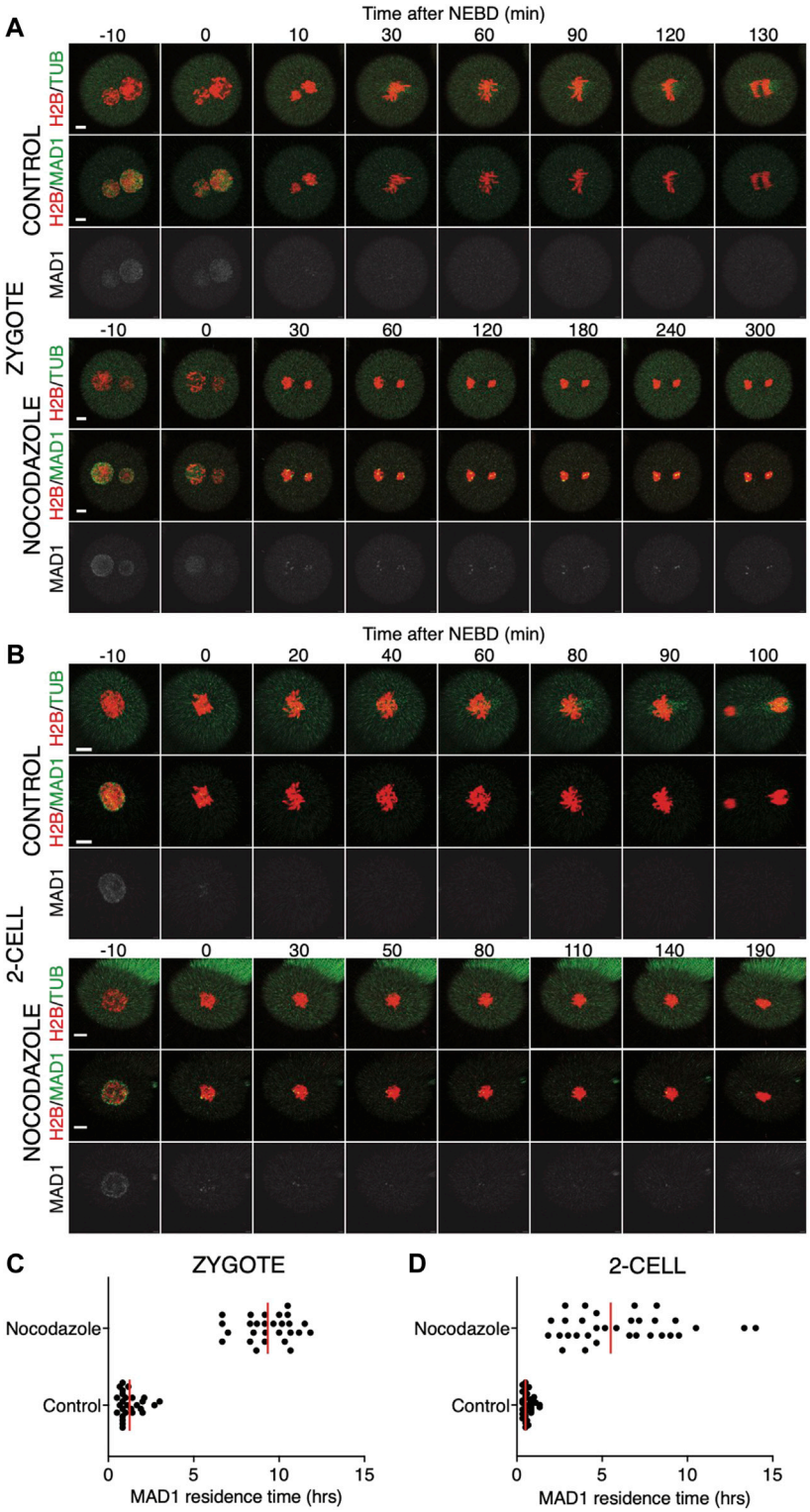

FIGURE 4
Impact of higher concentrations of nocodazole on division in zygotes and 2-cell embryos. **(A)** Representative mitosis of zygotes dividing with and without nocodazole. Embryos were microinjected with cRNAs encoding histone H2B (red), tubulin (green), and Mad1 (green and gray) fusion proteins. Cell division and chromosome segregation were assessed by time-lapse confocal microscopy. The scale bar represents 10 μm. **(B)** Representative mitosis of 2-cell embryos dividing with and without nocodazole. Embryos were microinjected with cRNAs encoding histone H2B (red), tubulin (green), and Mad1 (green and gray) fusion proteins. Cell division and chromosome segregation were assessed by time-lapse confocal microscopy. The scale bar represents 10 μm. **(C)** Scatterplot showing the residence time of the Mad1 signal on kinetochores throughout mitosis in zygotes. Time was scored in control zygotes (n = 27) and nocodazole-treated zygotes (n = 27). The presence of Mad1 was 1.25 ± 0.66% in control zygotes and 9.33 ± 1.47% in nocodazole-treated zygotes. The difference between groups was significant ($\alpha < 0.05$, ****$p = <0.0001$). The data were obtained from three independent experiments. **(D)** Scatterplot showing the residence time of the Mad1 signal on kinetochores throughout mitosis in 2-cell embryos. Time was scored in
(*Continued*)

FIGURE 4 (Continued)
control 2-cell embryos (n = 32) and nocodazole-treated 2-cell embryos (n = 24). The presence of Mad1 was 0.64 ± 0.3% in control embryos and 6.1 ± 3.1% in nocodazole embryos. The difference between groups was significant (α < 0.05, ****p = <0.0001). The data were obtained from three independent experiments.

We also compared the stability of cyclin B in zygotes and 2-cell embryos (Figure 8). For this, we used the first 90 amino acids of cyclin B1 (1–90 cyB1) that contain the D box but lack the ability to interact with CDK1 (Glotzer et al., 1991), which minimizes the risk of mitosis perturbation. Our results showed that similar to the full-length cyclin, the destruction of 1–90 cyB1 fragments was delayed in zygotes but commenced immediately after NEBD in 2-cell embryos (Figure 8A). We also tested the ability of nocodazole to prevent APC/C activation and destruction of 1–90 cyB1. Our results showed that in zygotes and 2-cell embryos exposed to 100 nM nocodazole (lower dose, allowing the 2-cell embryos to divide), the destruction of 1–90 cyB1 was slower in the majority of cells but not abolished (Figures 8B, C). A prolonged residence time of Mad1 was shown at this concentration of nocodazole (Figures 5C, D). Therefore, the APC/C seems to be active in these cells despite the association between Mad1 and chromosomes.

Discussion

In dividing cells, the control of spindle assembly, more specifically the control of microtubule–kinetochore connections, is of paramount importance for the fidelity of chromosome segregation (Curtis et al., 2020; Lara-Gonzalez et al., 2021; McAinsh et al., 2023). The importance of these surveillance mechanisms is undisputable as potential errors in chromosome segregation have severe consequences in daughter cells and in the case of multicellular organisms, for the entire body. However, mammalian germ cells and embryos suffer from exceptionally high incidences of chromosome segregation errors. In addition, the aneuploidy in these cells leads to the termination of development or causes severe developmental disorders (Hassold and Hunt, 2001; Nagaoka et al., 2012; Mihajlovic and FitzHarris, 2018; Charalambous et al., 2022).

The canonical function of SAC is to postpone APC/C activation until the completion of spindle assembly when all kinetochores are correctly attached to the spindle microtubules and the sister kinetochores are oriented to the opposite spindle poles (Musacchio, 2011). Once this is achieved, the SAC signaling turns off, which leads to the activation of APC/C and ubiquitination and proteolysis of cyclin B, securin, and other substrates. Therefore, during entry into mitosis, the CDC20-controlled substrates should be, at least initially, stabilized until the completion of spindle assembly and degraded afterward. This important ability of SAC to postpone APC/C activation is a cornerstone of chromosome segregation control, and its function was demonstrated in HeLa cells (Clute and Pines, 1999) and confirmed in many cell types thereafter.

Our data presented here show that during unperturbed division, mouse zygotes fully activate APC/C after the spindle assembly is completed, whereas the 2-cell embryos fully activate APC/C much earlier, simultaneously with NEBD. Our data in this regard are similar to a previous report (Ajduk et al., 2017). Here, we used 2 different substrates, securin and a fragment of cyclin B, to confirm this, with both showing similar results. As a consequence, the spindle is assembled when the APC/C is already fully active, and this might be the reason why the embryos lose the ability to respond to single uncongressed chromosomes (our results here and also Vázquez-Diez et al. (2019)). It does not, however, exclude a possibility of SAC reactivation by a strong impulse, such as spindle damage, induced after the initiation of spindle assembly. This might reactivate SAC even during ongoing APC/C activity. Nevertheless, it needs to be tested since in our experiments, we applied nocodazole before mitotic entry.

Using lower concentrations of nocodazole, we show that the SAC is unable to arrest cells in metaphase in response to substantial spindle damage. Although with significant delay, the cells were able to enter into anaphase. In this situation, it is difficult to assess whether the delay was caused by prolonged SAC activity. However, the gradual loss of the Mad1 signal from chromosomes during prolonged mitosis would perhaps favor the alternative explanation that the delay might rather be caused by the direct effect of nocodazole on spindle microtubules. During the time of nocodazole-induced mitotic arrest, in the majority of cells, the fragment of cyclin B is not completely stabilized but instead slowly degraded. This would also support our view that even strong activation of SAC, which is sufficient to keep the fraction of Mad1 on chromosomes, is not capable of preventing the destruction of the cyclin B fragment. On the other hand, the mutations in securin APC/C-dependent sequences prevented its degradation completely. The slow degradation of the cyclin B fragment is similar to its degradation during the process, which allows cells to escape from SAC arrest, which is called mitotic slippage (Lok et al., 2020). In that case, it would be another argument for weak SAC in embryos because the duration of arrest induced by lower nocodazole levels was up to 10 h, which is usually shorter compared to the 24-h arrest in somatic cells.

The conclusion drawn from APC/C activation is supported by Mad1 expression and localization in embryos. This protein was found to be essential for SAC functionality in all cells studied so far (Luo et al., 2018). Despite its indispensability for SAC, it shows low expression levels in both zygotes and 2-cell embryos. Its interaction with chromosomes takes place during unperturbed divisions restricted to a very narrow time interval, following NEBD. In addition, although we show that the exposure to nocodazole prolongs Mad1 interaction with chromosomes, when the levels of the nocodazole are low, allowing the assembly of residual spindles, the Mad1 loses its localization to chromosomes after prolonged mitosis anyway, and the cells initiate anaphase. We believe that this is another strong evidence that the SAC in embryos is unable to

10.3389/fcell.2024.1355979

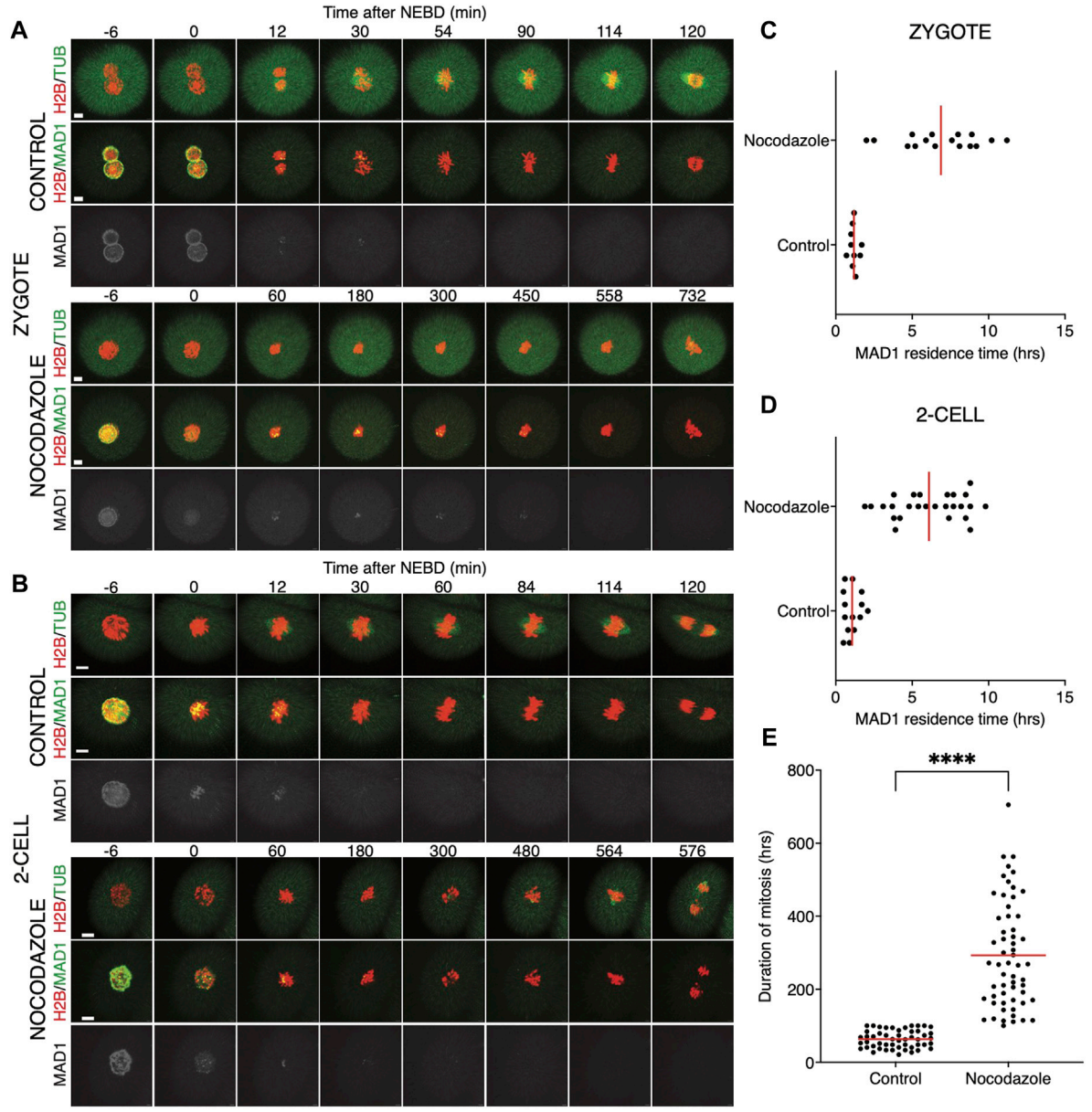

FIGURE 5
Low concentrations of nocodazole allows embryos to enter anaphase. **(A)** Representative mitosis of zygotes dividing with and without nocodazole. Embryos were microinjected with cRNAs encoding histone H2B (red), tubulin (green), and Mad1 (green and gray) fusion proteins. Cell division and chromosome segregation were assessed by time-lapse confocal microscopy. The scale bar represents 10 μm. **(B)** Representative mitosis of 2-cell embryos dividing with and without nocodazole. Embryos were microinjected with cRNAs encoding histone H2B (red), tubulin (green), and Mad1 (green and gray) fusion proteins. Cell division and chromosome segregation were assessed by time-lapse confocal microscopy. The scale bar represents 10 μm. **(C)** Scatterplot showing the residence time of the Mad1 signal on kinetochores throughout mitosis in zygotes. Time was scored in control zygotes (n = 10) and nocodazole-treated zygotes (n = 16). The presence of Mad1 was 1.19 ± 0.29% in control zygotes and 6.88 ± 2.60% in nocodazole-treated zygotes. The difference between groups was significant ($\alpha < 0.05$, ****$p = <0.0001$). The data were obtained from two experiments. **(D)** Scatterplot showing the residence time of the Mad1 signal on kinetochores throughout mitosis in 2-cell embryos. Time was scored in control 2-cell embryos (n = 14) and nocodazole-treated 2-cell embryos (n = 26). The presence of Mad1 was 1.07 ± 0.52% in control embryos and 6.1 ± 2.28% in nocodazole embryos. The difference between groups was significant ($\alpha < 0.05$, ****$p = <0.0001$). The data were obtained from two experiments. **(E)** Scatterplot of the duration of mitosis of 2-cell embryos with and without nocodazole (control 2-cell embryos: n = 51; nocodazole-treated 2-cell embryos: n = 58). The length of division in control 2-cell embryos was 63.2 ± 23.9%, and that in nocodazole-treated 2-cell embryos was 293.1 ± 145.5%. The difference between groups was significant ($\alpha < 0.05$, ****$p = <0.0001$). The data were obtained from four experiments.

prevent anaphase for a long time, even in the situation when the spindle is substantially damaged. We still could not exclude that low expression of Mad1 in 2-cell embryos and perhaps other molecules from the SAC pathway is simply insufficient to produce enough MCC to delay APC/C activation. However, our data with overexpressed Mad1 indicate that rather than the expression itself, the association with kinetochores could be the problem.

Pharmacological inhibition of Mps1 is an effective way to prevent SAC activity. In our experiments, we used reversine, a potent Mps1 kinase inhibitor (Santaguida et al., 2010). Previously

10.3389/fcell.2024.1355979

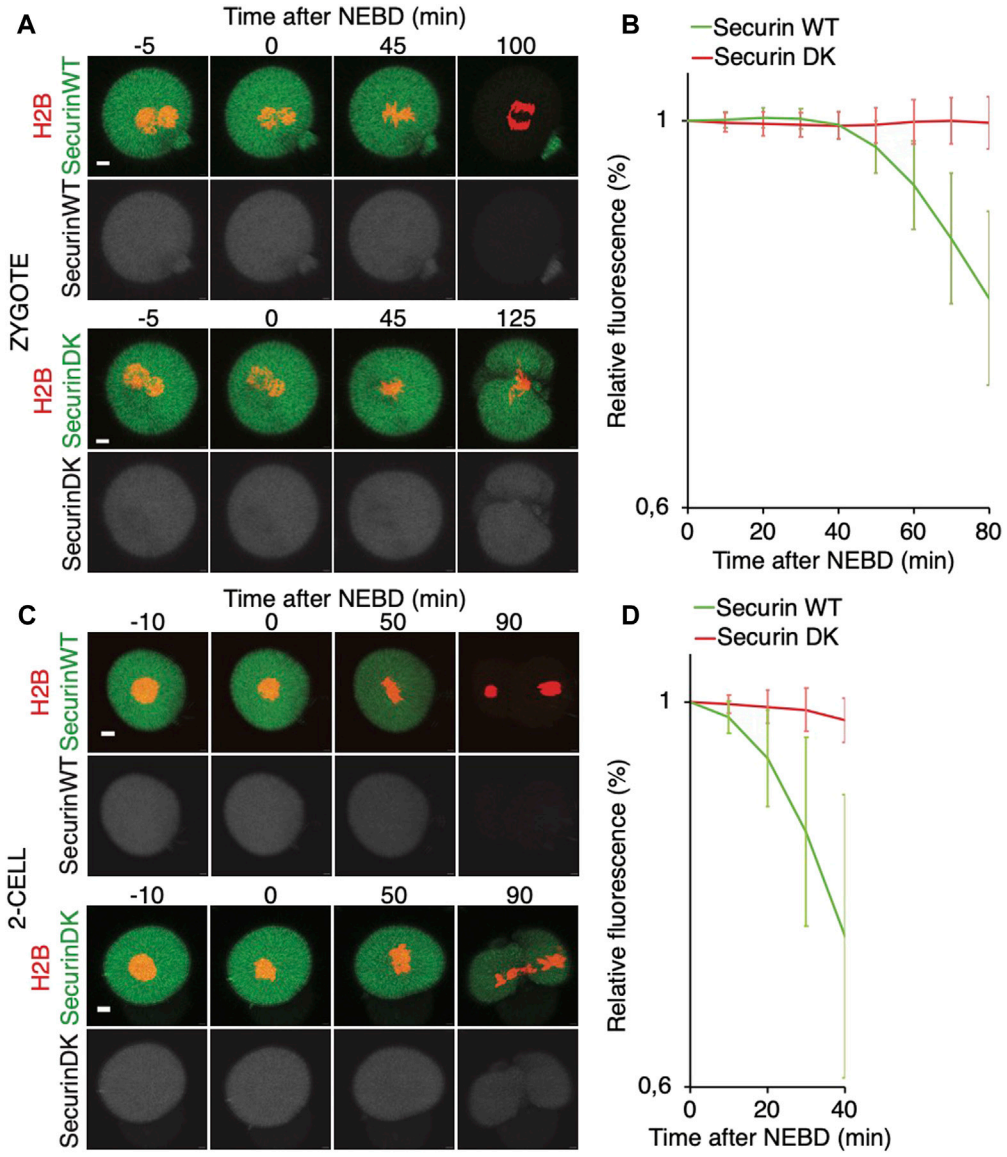

FIGURE 6
Onset of securin destruction in zygotes and 2-cell embryos. **(A)** Zygotes were microinjected with cRNAs encoding WT securin or securin with mutated K/D boxes (securin DK) and histone H2B (red) fused to fluorescent protein, and subsequently, the fluorescence signal was measured by time-lapse confocal microscopy. The scale bar represents 10 μm. **(B)** Fluorescence signal profiles of securin WT (green, n = 56) and securin DK (red, n = 52) during mitosis I. The graph shows the average relative values from NEBD to the shortest anaphase. The data were obtained from four independent experiments. **(C)** 2-cell embryos were microinjected with cRNAs encoding WT securin or securin with mutated K/D boxes (securin DK) and histone H2B (red) fused to fluorescent protein, and subsequently, the fluorescence signal was measured by time-lapse confocal microscopy. The scale bar represents 10 μm. **(D)** Fluorescence signal profiles of securin WT (green; n = 11) and securin DK (red; n = 11) in 2-cell embryos. The graph shows the average relative values from NEBD to the shortest anaphase. The data were obtained from two independent experiments.

published results using different inhibitors showed that in zygotes, Mps1 inhibition negatively impacts chromosome segregation and compromises further development (Ju et al., 2021). In our experiments, we observed a much stronger effect. Chromosome segregation in zygotes was severely affected, and cells fragmented at anaphase. In contrast to the zygotes, 2-cell embryos were able to execute anaphase in the same concentration of the inhibitor. On the other hand, the length of their mitoses was significantly shorter. We can speculate to what extent the effect we observed in zygotes might have been caused by the side effects of reversine. This small molecule was originally discovered as an inhibitor of aurora kinases, and it was later found to inhibit Mps1 more potently than auroras (Hiruma et al., 2016). The assembly of the spindle in zygotes is, however, a more complex process than in ordinary cells because it involves a stage during which paternal genomes build their spindles which later join into a single spindle (Reichmann et al., 2018). It is conceivable that partial inhibition of aurora kinases, which are crucial for spindle assembly and function, might prevent the formation of the definitive spindle prior to division and be responsible for the phenotype we observed in zygotes.

We believe that our results support the overall conclusion that mouse 2-cell embryos normally do not require SAC activity for

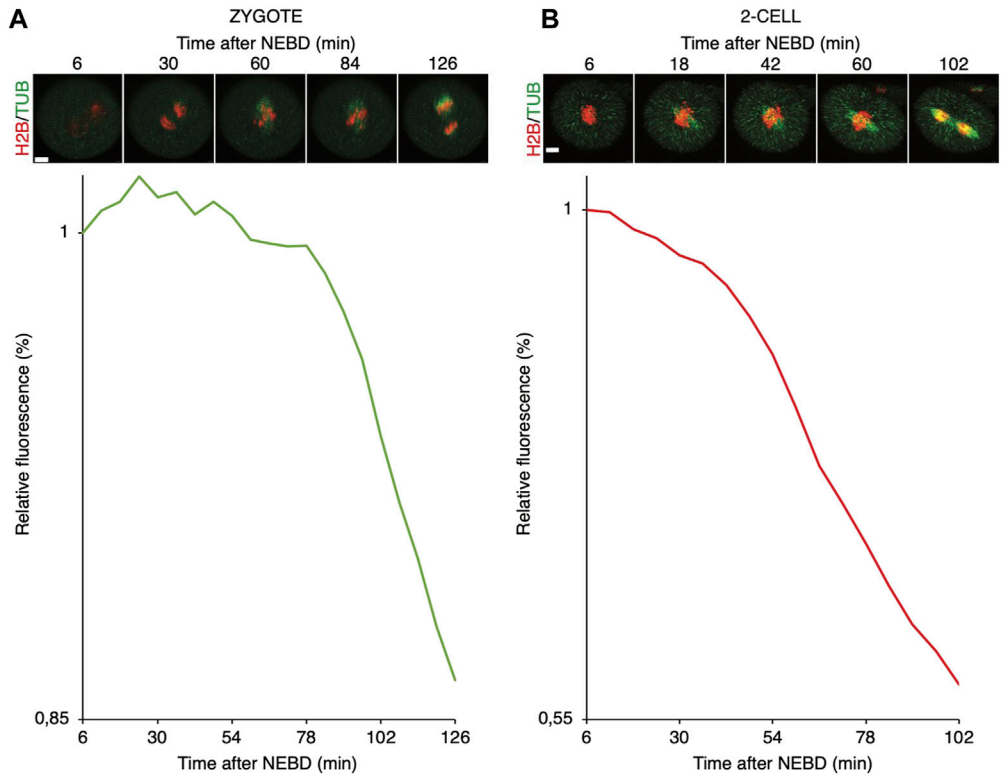

FIGURE 7
Relationship between the spindle assembly and APC/C activity in mouse zygotes and 2-cell embryos. **(A)** Upper panel represents selected frames from the time-lapse experiment showing the division of representative zygote. Cell was microinjected with cRNAs encoding histone H2B (red), tubulin (green), and 90 cyB1 (not shown) fused to fluorescent proteins. The scale bar represents 10 μm. The lower panel shows fluorescence levels of 90 cyB1 during mitosis of the same cell. **(B)** Upper panel represents selected frames from the time-lapse experiment showing division of representative 2-cell blastomere. The cell was microinjected with cRNAs encoding histone H2B (red), tubulin (green), and 90 cyB1 (not shown) fused to fluorescent proteins. The scale bar represents 10 μm. The lower panel shows fluorescence levels of 90 cyB1 during mitosis of the same cell.

progression during mitosis. This is similar to some other vertebrates, in which the SAC is activated only after MBT, such as *Xenopus* and zebrafish (Clute and Masui, 1995; Zhang et al., 2015). In contrast to those species, however, we show that in mice, exposure to nocodazole delays anaphase and slows down the degradation of cyclin B. It remains to be tested, however, whether the activation of SAC within mitosis would be sufficient to revert APC/C activity.

Materials and methods

Animals, isolation, and culture of oocytes and embryos and inhibitors

CD-1 mice were purchased from the Animal Breeding and Experimental Facility, Faculty of Medicine, Masaryk University, Brno, Czech Republic; BDF1 males were purchased from AnLab, Prague, Czech Republic. CD-1/BDF1 mice were obtained by crossing CD-1 female mice and BDF1 male mice. For all experiments, at least 3-month-old females were used. All animal work was conducted according to Act No 246/1992 Coll. on the protection of animals against cruelty and was approved by the Central Commission for Animal Welfare, under approval ID 37/2021. The methods for the collection of oocytes and embryos were described previously (Pauerova et al., 2021). In brief, to collect embryos, mice were stimulated with 5 IU of pregnant mare serum gonadotropin (PMSG; BioVendor, Brno, Czech Republic), followed by stimulation with 5 IU of human chorionic gonadotropin (hCG; Merck, Darmstadt, Germany) 44–48 h later, and mated with BDF1 males. Zygotes and 2-cell embryos were isolated 18–27 and 41–46 h after hCG stimulation by the manual rupture of the oviduct in M2 medium, respectively, and zygotes were incubated with 1 mg/mL hyaluronidase (Merck) in M2 medium for cumulus cell removal. We cultured embryos in KSOM (Merck) covered with mineral oil (Nidacon, Mölndal, Sweden) at 37 °C and 5% CO_2. GV-stage oocytes were isolated in M2 (Merck) and cultured in M16 media (Merck). In some experiments, oocytes and embryos were treated with 500 nM reversine (Merck) or with 100 nM and 266 nM of nocodazole (Merck) diluted in KSOM (Merck).

Microinjection of GV oocytes and embryos

The microinjection of mouse oocytes and embryos was performed in M2 media (Merck), as previously described

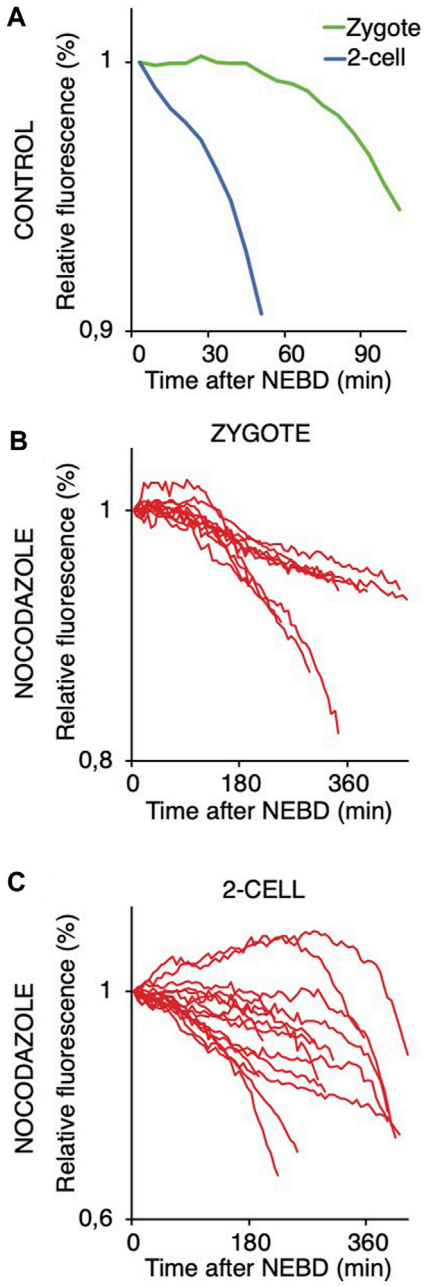

FIGURE 8
Targeting 1–90 cyB1 for destruction after NEBD in zygotes and 2-cell embryos with and without nocodazole. **(A)** Fluorescence signal profiles of 90 cyB1 in zygotes (green; n = 13) and 2-cell embryos (blue; n = 20) during mitosis. The graph shows the average relative values from NEBD to the shortest anaphase. The data were obtained from two independent experiments. **(B)** Fluorescence signal profiles of 90 cyB1 in zygotes (red; n = 10) during mitosis I. The graph shows the relative values from NEBD to the anaphase. The data were obtained from two independent experiments. **(C)** Fluorescence signal profiles of 90 cyB1 in 2-cell embryos (red; n = 15) during mitosis II. The graph shows the relative values from NEBD to the anaphase. The data were obtained from two independent experiments.

(Pauerova et al., 2021). The cRNAs used were as follows: securin-CFP, securin-EGFP, securin-DK EGFP, a fragment of the first 90 aa of cyclin B1 (1–90 cyB1) fused to Venus, tubulin-CFP, tubulin-EGFP, Mad1-Venus, histone H2B-mCherry, and histone H2B-mPlum. cRNAs for microinjection were diluted in RNase-free water to a concentration of 2–4 ng per µL.

Immunodetection

The immunofluorescence protocol was described by Pauerova et al. (2021). In brief, oocytes and embryos were harvested after the previous culture. The zona pellucida was removed with acid Tyrode solution (Merck). Cells were fixed in 2% paraformaldehyde (Merck) for 20 min, permeabilized with 0.1% Triton X-100 (Merck) for 15 min, and blocked for 15 min at RT. The antibodies rabbit anti-Mad1 (1:200 dilution, GeneTex, Irvine, CA, United States), human anti-CREST (1:500 dilution, ImmunoVision, Springdale, AR, United States), Alexa Fluor 488 goat anti-rabbit (1:500 dilution, Thermo Fisher Scientific, Waltham, MA, United States), and Alexa Fluor 647 goat anti-human (1:500 dilution, Thermo Fisher Scientific) were used. VECTASHIELD with DAPI (Vector Laboratories, Burlingame, CA, United States) was used for mounting on microscope slides.

Microscopy and live cell imaging

Fixed sample staining was scanned on the Olympus FV3000 confocal microscope equipped with an HCPL APO 60XS2/1.30 silicone immersion objective and HSDs. Absorbance at 405 nm, 488 nm, and 640 nm excitation wavelengths was measured using HSDs for the detection of DAPI, Alexa Fluor 488, and Alexa Fluor 647, respectively. Imaging of live cells was performed on a Leica SP5 confocal microscope and Olympus FLUOVIEW 3000 confocal microscope, both equipped with an EMBL incubator (37°C; 5% CO_2) (EMBL, Heidelberg, Germany). The following objectives were used: Leica HCX PL APO ×40/1.1 water immersion objective and Olympus UPLSAPO 30xs/1.05 silicone immersion objective. Absorbance at 458 nm or 445 nm, 488 nm, 514 nm, and 561 nm excitation wavelengths were measured using hybrid detectors (Leica) and HSDs (Olympus) for the detection of CFP, EGFP, Venus, and mCherry fluorescent proteins.

Image analysis and statistical analysis

Fiji (ImageJ, National Institutes of Health, Bethesda, MA, USA), LAS AF (http://www.leica-microsystems.com), and Imaris software (www.bitplane.com) was used for image analysis. For the quantification of the securin and 1–90 cyclin B1 signal the expression level was normalized to the level at GVBD or NEBD, as previously (Pauerova et al., 2021). To quantify the Mad1 signal on the kinetochores, the CREST signal was used to define the ROI. The background of the area with the same size was subtracted from the level of the Mad1 fluorescence signal on the kinetochore area. GraphPad Prism was used for the statistical testing of data. To

analyze the difference between groups, the Mann–Whitney test was used.

Data availability statement

The original contributions presented in the study are included in the article/Supplementary Material; further inquiries can be directed to the corresponding author.

Ethics statement

The animal study was approved by the Ethics Committee of the Ministry of Agriculture of the Czech Republic. The study was conducted in accordance with the local legislation and institutional requirements.

Author contributions

AH: data curation, formal analysis, investigation, methodology, and writing–review and editing. MK: data curation, formal analysis, investigation, methodology, and writing–review and editing. LR: data curation, formal analysis, investigation, methodology, and writing–review and editing. MA: conceptualization, formal analysis, funding acquisition, project administration, supervision, and writing–original draft.

Funding

The author(s) declare that financial support was received for the research, authorship, and/or publication of this article. This work was supported by the Czech Science Foundation Project 20-25850S and by Grant RO 0523 of the Ministry of Agriculture of the Czech Republic.

Acknowledgments

The authors are grateful to all members of the Mammalian Reproduction Group at the Veterinary Research Institute and all members of the Laboratory of Cell Division Control at the Institute of Animal Physiology and Genetics in Libechov.

Conflict of interest

The authors declare that the research was conducted in the absence of any commercial or financial relationships that could be construed as a potential conflict of interest.

Publisher's note

All claims expressed in this article are solely those of the authors and do not necessarily represent those of their affiliated organizations, or those of the publisher, the editors, and the reviewers. Any product that may be evaluated in this article, or claim that may be made by its manufacturer, is not guaranteed or endorsed by the publisher.

Supplementary material

The Supplementary Material for this article can be found online at: https://www.frontiersin.org/articles/10.3389/fcell.2024.1355979/full#supplementary-material

References

Ajduk, A., Strauss, B., Pines, J., and Zernicka-Goetz, M. (2017). Delayed APC/C activation extends the first mitosis of mouse embryos. *Sci. Rep.* 7, 9682. doi:10.1038/s41598-017-09526-1

Allais, A., and Fitzharris, G. (2022). Absence of a robust mitotic timer mechanism in early preimplantation mouse embryos leads to chromosome instability. *Development* 149, dev200391. doi:10.1242/dev.200391

Bolton, H., Graham, S. J. L., Van der Aa, N., Kumar, P., Theunis, K., Fernandez Gallardo, E., et al. (2016). Mouse model of chromosome mosaicism reveals lineage-specific depletion of aneuploid cells and normal developmental potential. *Nat. Commun.* 7, 11165. doi:10.1038/ncomms11165

Carbone, L., and Chavez, S. L. (2015). Mammalian pre-implantation chromosomal instability: species comparison, evolutionary considerations, and pathological correlations. *Syst. Biol. Reprod. Med.* 61, 321–335. doi:10.3109/19396368.2015.1073406

Charalambous, C., Webster, A., and Schuh, M. (2022). Aneuploidy in mammalian oocytes and the impact of maternal ageing. *Nat. Rev. Mol. Cell. Biol.* 24, 27–44. doi:10.1038/s41580-022-00517-3

Chenevert, J., Roca, M., Besnardeau, L., Ruggiero, A., Nabi, D., McDougall, A., et al. (2020). The spindle assembly checkpoint functions during early development in non-chordate embryos. *Cells* 9, 1087. doi:10.3390/cells9051087

Clute, P., and Masui, Y. (1995). Regulation of the appearance of division asynchrony and microtubule-dependent chromosome cycles in *Xenopus laevis* embryos. *Dev. Biol.* 171, 273–285. doi:10.1006/dbio.1995.1280

Clute, P., and Pines, J. (1999). Temporal and spatial control of cyclin B1 destruction in metaphase. *Nat. Cell. Biol.* 1, 82–87. doi:10.1038/10049

Curtis, N. L., Ruda, G. F., Brennan, P., and Bolanos-Garcia, V. M. (2020). Deregulation of chromosome segregation and cancer. *Annu. Rev. Cancer Biol.* 4, 257–278. doi:10.1146/annurev-cancerbio-030419-033541

Daughtry, B. L., Rosenkrantz, J. L., Lazar, N. H., Fei, S. S., Redmayne, N., Torkenczy, K. A., et al. (2019). Single-cell sequencing of primate preimplantation embryos reveals chromosome elimination via cellular fragmentation and blastomere exclusion. *Genome Res.* 29, 367–382. doi:10.1101/gr.239830.118

Destouni, A., Zamani Esteki, M., Catteeuw, M., Tšuiko, O., Dimitriadou, E., Smits, K., et al. (2016). Zygotes segregate entire parental genomes in distinct blastomere lineages causing cleavage-stage chimerism and mixoploidy. *Genome Res.* 26, 567–578. doi:10.1101/gr.200527.115

Dobles, M., Liberal, V., Scott, M. L., Benezra, R., and Sorger, P. K. (2000). Chromosome missegregation and apoptosis in mice lacking the mitotic checkpoint protein Mad2. *Cell.* 101, 635–645. doi:10.1016/s0092-8674(00)80875-2

El Yakoubi, W., Buffin, E., Cladière, D., Gryaznova, Y., Berenguer, I., Touati, S. A., et al. (2017). Mps1 kinase-dependent Sgo2 centromere localisation mediates cohesin protection in mouse oocyte meiosis I. *Nat. Commun.* 8, 694. doi:10.1038/s41467-017-00774-3

Encalada, S. E., Willis, J., Lyczak, R., and Bowerman, B. (2005). A spindle checkpoint functions during mitosis in the early *Caenorhabditis elegans* embryo. *Mol. Biol. Cell.* 16, 1056–1070. doi:10.1091/mbc.e04-08-0712

Glotzer, M., Murray, A. W., and Kirschner, M. W. (1991). Cyclin is degraded by the ubiquitin pathway. *Nature* 349, 132–138. doi:10.1038/349132a0

Gui, L., and Homer, H. (2012). Spindle assembly checkpoint signalling is uncoupled from chromosomal position in mouse oocytes. *Development* 139, 1941–1946. doi:10.1242/dev.078352

Hached, K., Xie, S. Z., Buffin, E., Cladière, D., Rachez, C., Sacras, M., et al. (2011). Mps1 at kinetochores is essential for female mouse meiosis I. *Development* 138, 2261–2271. doi:10.1242/dev.061317

Hassold, T., and Hunt, P. (2001). To err (meiotically) is human: the genesis of human aneuploidy. *Nat. Rev. Genet.* 2, 280–291. doi:10.1038/35066065

Hiruma, Y., Koch, A., Dharadhar, S., Joosten, R. P., and Perrakis, A. (2016). Structural basis of reversine selectivity in inhibiting Mps1 more potently than aurora B kinase. *Proteins* 84, 1761–1766. doi:10.1002/prot.25174

Hornak, M., Oracova, E., Hulinska, P., Urbankova, L., and Rubes, J. (2012). Aneuploidy detection in pigs using comparative genomic hybridization: from the oocytes to blastocysts. *PLoS One* 7, e30335. doi:10.1371/journal.pone.0030335

Jacobs, K., Van De Velde, H., De Paepe, C., Sermon, K., and Spits, C. (2017). Mitotic spindle disruption in human preimplantation embryos activates the spindle assembly checkpoint but not apoptosis until Day 5 of development. *Mol. Hum. Reprod.* 23, 321–329. doi:10.1093/molehr/gax007

Ju, J. Q., Li, X. H., Pan, M. H., Xu, Y., Xu, Y., Sun, M. H., et al. (2021). Mps1 controls spindle assembly, SAC, and DNA repair in the first cleavage of mouse early embryos. *J. Cell. Biochem.* 122, 290–300. doi:10.1002/jcb.29858

Kolano, A., Brunet, S., Silk, A. D., Cleveland, D. W., and Verlhac, M. H. (2012). Error-prone mammalian female meiosis from silencing the spindle assembly checkpoint without normal interkinetochore tension. *Proc. Natl. Acad. Sci. U. S. A.* 109, E1858–E1867. doi:10.1073/pnas.1204686109

Lane, S. I., Yun, Y., and Jones, K. T. (2012). Timing of anaphase-promoting complex activation in mouse oocytes is predicted by microtubule-kinetochore attachment but not by bivalent alignment or tension. *Development* 139, 1947–1955. doi:10.1242/dev.077040

Lara-Gonzalez, P., Pines, J., and Desai, A. (2021). Spindle assembly checkpoint activation and silencing at kinetochores. *Semin. Cell. Dev. Biol.* S1084-9521 (21), 00160. doi:10.1016/j.semcdb.2021.06.009

Lok, T. M., Wang, Y., Xu, W. K., Xie, S., Ma, H. T., and Poon, R. Y. C. (2020). Mitotic slippage is determined by p31^{comet} and the weakening of the spindle-assembly checkpoint. *Oncogene* 39, 2819–2834. doi:10.1038/s41388-020-1187-6

Luo, Y., Ahmad, E., and Liu, S. T. (2018). MAD1: kinetochore receptors and catalytic mechanisms. *Front. Cell. Dev. Biol.* 6, 51. doi:10.3389/fcell.2018.00051

Mcainsh, A. D., and Kops, G. J. P. L. (2023). Principles and dynamics of spindle assembly checkpoint signalling. *Nat. Rev. Mol. Cell. Biol.* 24, 543–559. doi:10.1038/s41580-023-00593-z

Mcguinness, B. E., Anger, M., Kouznetsova, A., Gil-Bernabé, A. M., Helmhart, W., Kudo, N. R., et al. (2009). Regulation of APC/C activity in oocytes by a Bub1-dependent spindle assembly checkpoint. *Curr. Biol.* 19, 369–380. doi:10.1016/j.cub.2009.01.064

Mihajlovic, A. I., and Fitzharris, G. (2018). Segregating chromosomes in the mammalian oocyte. *Curr. Biol.* 28, R895–R907. doi:10.1016/j.cub.2018.06.057

Musacchio, A. (2011). Spindle assembly checkpoint: the third decade. *Philos. Trans. R. Soc. Lond B Biol. Sci.* 366, 3595–3604. doi:10.1098/rstb.2011.0072

Musacchio, A. (2015). The molecular Biology of spindle assembly checkpoint signaling dynamics. *Curr. Biol.* 25, R1002–R1018. doi:10.1016/j.cub.2015.08.051

Nagaoka, S. I., Hassold, T. J., and Hunt, P. A. (2012). Human aneuploidy: mechanisms and new insights into an age-old problem. *Nat. Rev. Genet.* 13, 493–504. doi:10.1038/nrg3245

Nagaoka, S. I., Hodges, C. A., Albertini, D. F., and Hunt, P. A. (2011). Oocyte-specific differences in cell-cycle control create an innate susceptibility to meiotic errors. *Curr. Biol.* 21, 651–657. doi:10.1016/j.cub.2011.03.003

Pauerova, T., Radonova, L., Horakova, A., Knott, J. G., and Anger, M. (2021). Accumulation of securin on spindle during female meiosis I. *Front. Cell. Dev. Biol.* 9, 1752. doi:10.3389/fcell.2021.701179

Pauerova, T., Radonova, L., Kovacovicova, K., Novakova, L., Skultety, M., and Anger, M. (2020). Aneuploidy during the onset of mouse embryo development. *Reproduction* 160, 773–782. doi:10.1530/REP-20-0086

Reichmann, J., Nijmeijer, B., Hossain, M. J., Eguren, M., Schneider, I., Politi, A. Z., et al. (2018). Dual-spindle formation in zygotes keeps parental genomes apart in early mammalian embryos. *Science* 361, 189–193. doi:10.1126/science.aar7462

Santaguida, S., Tighe, A., D'alise, A. M., Taylor, S. S., and Musacchio, A. (2010). Dissecting the role of MPS1 in chromosome biorientation and the spindle checkpoint through the small molecule inhibitor reversine. *J. Cell. Biol.* 190, 73–87. doi:10.1083/jcb.201001036

Sebestova, J., Danylevska, A., Novakova, L., Kubelka, M., and Anger, M. (2012). Lack of response to unaligned chromosomes in mammalian female gametes. *Cell. Cycle* 11, 3011–3018. doi:10.4161/cc.21398

Shahbazi, M. N., Wang, T., Tao, X., Weatherbee, B. A. T., Sun, L., Zhan, Y., et al. (2020). Developmental potential of aneuploid human embryos cultured beyond implantation. *Nat. Commun.* 11, 3987. doi:10.1038/s41467-020-17764-7

Shindo, N., Otsuki, M., Uchida, K. S. K., and Hirota, T. (2021). Prolonged mitosis causes separase deregulation and chromosome nondisjunction. *Cell. Rep.* 34, 108652. doi:10.1016/j.celrep.2020.108652

Thomas, C., Wetherall, B., Levasseur, M. D., Harris, R. J., Kerridge, S. T., Higgins, J. M. G., et al. (2021). A prometaphase mechanism of securin destruction is essential for meiotic progression in mouse oocytes. *Nat. Commun.* 12, 4322. doi:10.1038/s41467-021-24554-2

Touati, S. A., Buffin, E., Cladière, D., Hached, K., Rachez, C., van Deursen, J. M., et al. (2015). Mouse oocytes depend on BubR1 for proper chromosome segregation but not for prophase I arrest. *Nat. Commun.* 6, 6946. doi:10.1038/ncomms7946

Tšuiko, O., Catteeuw, M., Zamani Esteki, M., Destouni, A., Bogado Pascottini, O., Besenfelder, U., et al. (2017). Genome stability of bovine *in vivo*-conceived cleavage-stage embryos is higher compared to *in vitro*-produced embryos. *Hum. Reprod.* 32, 2348–2357. doi:10.1093/humrep/dex286

Vázquez-Diez, C., and Fitzharris, G. (2018). Causes and consequences of chromosome segregation error in preimplantation embryos. *Reproduction* 155, R63–R76. doi:10.1530/REP-17-0569

Vázquez-Diez, C., Paim, L. M. G., and Fitzharris, G. (2019). Cell-size-independent spindle checkpoint failure underlies chromosome segregation error in mouse embryos. *Curr. Biol.* 29, 865–873. doi:10.1016/j.cub.2018.12.042

Wei, Y., Multi, S., Yang, C. R., Ma, J., Zhang, Q. H., Wang, Z. B., et al. (2011). Spindle assembly checkpoint regulates mitotic cell cycle progression during preimplantation embryo development. *PLoS One* 6, e21557. doi:10.1371/journal.pone.0021557

Zhang, D., Li, M., Ma, W., Hou, Y., Li, Y. H., Li, S. W., et al. (2005). Localization of mitotic arrest deficient 1 (MAD1) in mouse oocytes during the first meiosis and its functions as a spindle checkpoint protein. *Biol. Reprod.* 72, 58–68. doi:10.1095/biolreprod.104.032987

Zhang, M., Kothari, P., and Lampson, M. A. (2015). Spindle assembly checkpoint acquisition at the mid-blastula transition. *PLoS One* 10, e0119285. doi:10.1371/journal.pone.0119285

frontiers | Frontiers in Cell and Developmental Biology

TYPE Original Research
PUBLISHED 21 March 2024
DOI 10.3389/fcell.2024.1345669

Check for updates

OPEN ACCESS

EDITED BY
Jason Knott,
Michigan State University, United States

REVIEWED BY
Kenneth White,
Utah State University, United States
Jian Sun,
University of Delaware, United States

*CORRESPONDENCE
Yongxun Jin,
jyx0429@jlu.cn
Il-Keun Kong,
ikong7900@gmail.com

RECEIVED 28 November 2023
ACCEPTED 12 March 2024
PUBLISHED 21 March 2024

CITATION
Kang S-M, Idrees M, Perera CD, Lee S-H, Zhang M, Yu X, Jin Y and Kong I-K (2024), GDF-8 improves *in vitro* implantation and cryo-tolerance by stimulating the ALK5-SMAD2/3 signaling in bovine IVF embryo development. *Front. Cell Dev. Biol.* 12:1345669. doi: 10.3389/fcell.2024.1345669

COPYRIGHT
© 2024 Kang, Idrees, Perera, Lee, Zhang, Yu, Jin and Kong. This is an open-access article distributed under the terms of the Creative Commons Attribution License (CC BY). The use, distribution or reproduction in other forums is permitted, provided the original author(s) and the copyright owner(s) are credited and that the original publication in this journal is cited, in accordance with accepted academic practice. No use, distribution or reproduction is permitted which does not comply with these terms.

GDF-8 improves *in vitro* implantation and cryo-tolerance by stimulating the ALK5-SMAD2/3 signaling in bovine IVF embryo development

Seon-Min Kang[1], Muhammad Idrees[1,2], Chalani Dilshani Perera[1], Seo-Hyun Lee[1], Mingjun Zhang[3], Xianfeng Yu[3], Yongxun Jin[3]* and Il-Keun Kong[1,2]*

[1]Division of Applied Life Science (BK21 Four), Graduate School of Applied Life Science, Gyeongsang National University, Jinju, Republic of Korea, [2]Division of Animal Science, Institute of Agriculture and Life Science, Gyeongsang National University, Jinju, Republic of Korea, [3]Jilin Provincial Key Laboratory of Animal Model, College of Animal Science, Jilin University, Changchun, China

Transforming growth factor-beta (TGF-β) plays a critical role in regulating trophoblast invasion and proliferation. Growth differentiation factor-8 (GDF-8) is a member of the TGF-β superfamily and is categorized as a myostatin subtype. It is primarily a secreted protein synthesized in skeletal muscle cells. It is expressed in the placenta, reproductive tissues, and cells. In this study, we investigated the role of GDF-8 in the development and hatching rate of bovine embryos. We noted a notable elevation ($p < 0.05$) in the development and hatching rates compared to the control embryos. Furthermore, the GDF-8 group showed a significantly improved total cell number ($p < 0.05$) and an increase in trophectoderm ratio inner cell mass (trophectoderm: inner cell mass) cells ($p < 0.001$) compared to the control group. Additionally, blastocysts treated with GDF-8 exhibited significantly higher mRNA levels of caudal-type homeobox 2 (*CDX2*) ($p < 0.05$). The trophoblast invasion area was significantly larger in the GDF-8 group than in the control group ($p < 0.01$). Furthermore, qRT-PCR analysis revealed significantly higher mRNA levels ($p < 0.05$) of matrix metalloproteinases 9 (*MMP9*) and follistatin-like 3(*FSTL3*), both of which are associated with the ALK5-SMAD2/3 signaling pathway, in the GDF-8 group than those in the control group. The mRNA expression levels of genes related to tight junctions (TJ) and adherent junctions were higher in the GDF-8 group than those in the control group ($p < 0.05$). After 24 h of thawing, blastocysts were analyzed using 4-kDa FITC-dextran, which revealed a higher TJ integrity in the GDF-8 group ($p < 0.01$). Thus, GDF-8 plays a crucial role in bovine embryonic development, *in vitro* implantation, and cryotolerance.

KEYWORDS

GDF-8, ALK5-SMAD2/3 signaling, embryo development, *in vitro* implantation, cryotolerance, bovine

1 Introduction

Embryo transfer and *in vitro* embryo production (IVP) represent indispensable assisted reproductive technologies in the commercial cattle industry for high-capacity cattle and serve as vital tools for controlling gene expression in blastocysts. Assisted reproductive technology has undergone significant advancements, particularly cryopreservation, which is unhindered by spatial and temporal constraints (Thibier, 2005). Nevertheless, the disparities between *in vitro* and *in vivo* embryo culture conditions within the female reproductive tract subject embryos to diverse physical and chemical stimuli, ultimately resulting in limitations regarding their developmental rate and quality (King et al., 1988; Underhill et al., 1991).

Despite extensive efforts to mitigate these differences, disparities persist between developing embryos cultured *in vivo* and those cultured *in vitro*. These disparities include morphological and molecular factors compromising IVP effectiveness (D. Lechniak et al., 1997; Thompson, 1997; Peter Holm, 1998; Khurana and Niemann, 2000; Corcoran et al., 2006; Camargo et al., 2018). Due to its inability to faithfully replicate *in vivo* culture conditions, IVP technology exhibits inherent developmental rate and quality differences. Consequently, the development rate of *in vitro* cultured bovine embryos remains limited to a 20%–30% range (Thompson, 1997; Camargo et al., 2006). Moreover, *in vitro* cultured embryos display a slower cell cycle division rate than *in vivo* cultured embryos, resulting in negative effects (Thompson, 1997). Furthermore, when embryos undergo cryopreservation, they are subjected to significant damage in their morphology and function. The extent of damage varies depending on membrane permeability, shape, and cell size (Marsico et al., 2019). Subsequently, the viability and quality of cryopreserved embryos depend on their cellular competence, which affects their ability to survive cryopreservation, potential for successful *in vitro* implantation, and preservation of structural integrity during *in vitro* culture (Thibier, 2005; Moussa et al., 2014). During the thawing process following cryopreservation, the trophectoderm (TE) cells of bovine blastocysts are susceptible to damage due to cryo-shrinkage, resulting in detrimental effects on their re-expansion capability (Kaidi et al., 2001; Camargo et al., 2011). Recent studies have emphasized the significant contribution of TE cells to early embryonic development and uterine implantation (Gauster et al., 2022). These cells undergo differentiation as part of the embryonic developmental process, controlling the movement of small molecules and H_2O, which are crucial for forming of the blastocoel cavity. Consequently, if these cells experience damage to their intercellular junctions due to cryo-shrinkage, they cannot maintain pressure within the blastocoel cavity (Choi et al., 2012; Marikawa and Alarcon, 2012). Moreover, previous research has indicated that TE cells are more sensitive to cryopreservation and exhibit a more pronounced response to thawing than inner cell mass (ICM) cells (Kaidi et al., 2001). The preservation of the epithelial integrity of TE cells requires specific conditions.

Transforming growth factor-beta (TGF-β) is also critical in regulating trophoblast invasion and proliferation (Adu-Gyamfi et al., 2020). Additionally, *in vitro* porcine embryo systems enhance blastocyst formation rates during early embryonic development and influence *in vitro* implantation (Massuto et al., 2010). Multiple studies have indicated that the proliferative activity of TE cells substantially affects the developmental ability of embryos. These findings underscore the significance of TGF-β as a key regulatory factor in embryo development and *in vitro* implantation, particularly through its effect on TE cell proliferation. Understanding the specific mechanisms by which TGF-β affects embryo development and *in vitro* implantation can potentially lead to advancements in IVP technology and enhance developmental outcomes.

Growth differentiation factor-8 (GDF-8) is a member of the TGF-β superfamily and is a myostatin subtype, primarily a secreted protein synthesized in skeletal muscle cells (McPherron et al., 1997). It is also expressed in the placenta, reproductive tissues, and cells (McPherron et al., 1997; Wong et al., 2009; Peiris and Mitchell, 2012; Peiris et al., 2014; Xie et al., 2020). Myostatin is a widely recognized inhibitor of muscle development that impedes cell proliferation and differentiation. However, it has been observed that both cell proliferation and migration are increased. Additionally, the elevated presence of myostatin in placental tissues during early pregnancy implies its potential involvement in early pregnancy, possibly contributing to the formation and development of the human placenta (Peiris et al., 2014). GDF-8 is expressed in extra villous trophoblasts and promotes the migration of trophoblasts (Peiris et al., 2014). Trophoblasts essential in regulating embryo development, *in vitro* implantation, and sustaining healthy pregnancies. In hamsters, GDF-8 induces proliferation exclusively in TE cells, stimulating the proliferation of extraembryonic trophoblast cells in preimplantation embryos and facilitating hatching (Wong et al., 2009), which underscores the significance of GDF-8 in regulating various aspects of embryonic development and *in vitro* implantation.

The GDF-8-related pathway involves the ALK5-SMAD2/3 signaling pathway. GDF-8 binds to a specific receptor, ALK5, in the trophoblast membrane. Upon binding of GDF-8 to its receptor, the receptor is activated, resulting in phosphorylation of SMAD2/3. Following phosphorylation, SMAD2/3 forms complexes with SMAD4 and relocates to the nucleus, where it conjugates to target genes, ultimately stimulating the expression of invasion-related genes (Peiris and Mitchell, 2012). The SMAD complex induces the transcription and expression of genes, such as follistatin-like 3 (*FSTL3*), matrix metalloproteinases 9 (*MMP9*), caudal-type homeobox 2 (*CDX2*), and SRY-box transcription factor 2, which increases TE cell proliferation, thereby enhancing their invasive capabilities (Yoon et al., 2019; Xie et al., 2020) (Supplementary Figure S1).

Cell invasion involves two primary processes: control of cell adhesion and migration, degradation of the extracellular matrix (ECM), and remodeling (Fang et al., 2021). Matrix metalloproteinases (MMPs) are also associated with ECM degradation. Matrix metalloproteinases 2 (*MMP2*)-mediated ECM degradation in humans enhances trophoblast cell invasion (Nagase and Woessner, 1999; Cohen et al., 2006). Furthermore, the expression of *MMP2* and *MMP9* is intricately linked to *in vitro* implantation capability, as it affects the capacity of embryos to degrade uterine epithelial ECM (Zhang et al., 2020). *FSTL3* binds to GDF-8, and its deficiency inhibits trophoblast invasion (Schneyer et al., 2004). It is also highly expressed in the human placenta (Xie

et al., 2020). GDF-8 has been shown to modulate *FSTL3* expression in human trophoblasts by triggering *FSTL3* expression via the SMAD2/3 signaling pathway SMAD2/3 in human trophoblasts plays a role in upregulating GDF-8-induced *FSTL3* expression (Xie et al., 2020). Under hypoxic conditions, trophoblasts exhibit increased *FSTL3* expression, and the absence of *FSTL3* impedes trophoblast invasion (Xie et al., 2020). Upregulated *FSTL3* expression in trophoblasts under low-oxygen culture conditions is associated with regulating trophoblast functions, including apoptosis, invasion, lipid storage, and migration (Xie et al., 2020).

Tight junctions (TJ) and adherent junctions (AJ) determine the maintenance of TE cell integrity. Sustaining blastocoels is challenging when these structures undergo deformation or damage, and it becomes difficult to maintain the blastocoel (Sidrat et al., 2022). Additionally, the Na^+/K^+-ATPase pump involving the ATPase Na^+/K^+ Transporting Subunit Alpha 1 (*ATP1a1*) located at the basal membrane of the TE facilitates the movement of Na^+ into the blastocoel through the TE, creating an osmotic pressure gradient that leads to fluid accumulation and blastocoel formation (Kidder, 2002; Barcroft et al., 2003; Barcroft et al., 2004). Furthermore, aquaporins (AQPs), membrane transporters, play a significant role in water transport (Edashige et al., 2007; Ribeiro et al., 2022). Previous studies have demonstrated that inhibition of AQPs suppresses blastocoel expansion, indicating their role in transporting water across the TE (Barcroft et al., 2003). Moreover, TJ, which seals the TE cells, is crucial for blastocyst formation. Incomplete sealing can result in fluid leakage around cells, reducing blastocoel size (Moriwaki et al., 2007). TJ seal spaces between adjacent cells (Tsukita et al., 2001; Schneyer et al., 2004). TJ comprises proteins, such as occludin and claudin, pivotal for structural integrity and barrier functionality (Wilcox et al., 2001; Ikenouchi et al., 2005; Moriwaki et al., 2007) (Supplementary Figure S2).

GDF-8 supplementation stimulates ALK5-SMAD2/3 signaling pathway activation, resulting in the upregulation of genes linked to implantation and TE cells. Activating this pathway augments the number of TE cells, enhancing *in vitro* implantation competence and functionality. This study investigated the enhancement of TE cell number and functionality through the ALK5-SMAD2/3 signaling pathway and its activation by supplementation with GDF-8, which led to improve *in vitro* implantation and developmental rates. The primary objective of this study was to confirm that the improved function of TE cells achieved through supplementation with GDF-8 enhances the functionality of AJ and TJ, thereby ensuring the preservation of post-thawing embryo survival and hatching rates.

In conclusion, adding GDF-8 to the culture medium could influence the quality of *in vitro* embryos, ultimately contributing to an improved *in vitro* implantation rate and TE cell function.

1.1 Experimental design

1.1.1 Experiment 1

To confirm the effect of GDF-8 supplementation on IVP, one control group and four experimental groups (treated with 0.2, 2, 10, or 20 ng/mL GDF-8) were used to evaluate the optimal concentration in bovine embryos. After 8 d, the developmental and hatching rates in the control and experimental groups were evaluated.

1.1.2 Experiment 2

To investigate whether GDF-8 supplementation affected TE cell proliferation, differential staining was performed using day 8 blastocysts, and variations in the mRNA levels of TE-related genes were analyzed in the control and GDF-8 groups.

1.1.3 Experiment 3

Genes associated with cell invasion are crucial to regulating TE cell invasion. Hence, this study aimed to assess the impact of GDF-8 on invasion by stimulating the ALK5-SMAD2/3 signaling pathway, thereby upregulating the genes involved in cell invasion.

1.1.4 Experiment 4

Experiments were conducted to evaluate the relative expression of TJ mRNA, AJ-related genes, and TJ permeability following GDF-8 supplementation. TJ assembly (claudin family, occludin, and actinγ2) was analyzed using day 8 blastocyst, and TJ permeability was investigated using a 4-kDa FITC-dextran assay after thawing blastocysts.

1.1.5 Experiment 5

To determine the effect of GDF-8 supplementation during cryopreservation, blastocysts from the control and GDF-8 groups were recovered and cryopreserved on day 7. The survival rates were assessed at 24 and 48 h. The survival rate was evaluated based on the presence or absence of blastocoels in the cultured post-thaw blastocysts. The hatching rate was estimated at 24 h and 48 h. Furthermore, qRT-PCR was conducted to assess the relative expression of genes involved in the osmotic pressure gradient.

2 Materials and methods

All experiments were approved by the Animal Care Facility of the Gyeongsang National University Institute of Animal Care Committee (GNU-130902-A0059). No animals were used directly in this study, and all bovine ovaries for experiments were collected from local slaughterhouse. Recombinant human GDF-8, obtained from a mouse myeloma cell line (88-G8/CF), was purchased from R&D Systems (Minneapolis, MN, United States). Unless otherwise stated, all chemicals and reagents were purchased from Merck (Sigma–Aldrich, St. Louis, MO, United States).

2.1 Cumulus–oocyte complex (COC) recovery

Ovaries were collected from a slaughterhouse in Gimhae, immersed in a 0.9% NaCl solution at 37.5°C, and transferred to the laboratory within 1 h. After washing the ovaries with saline, COCs were retrieved from the follicles (2–8 mm in diameter) using an 18-gauge needle connected to a 10-mL disposable syringe. Aspirated follicle fluid was discharged into the 50-mL tube containing Tyrode lactate-HEPES [TL-HEPES, calcium chloride 2 mM (C-7902), HEPES 10 mM (H-6147), 100 IU/mL penicillin, phenol red 1 μL/mL (P-0290), potassium chloride 3.2 mM (P-5405), sodium bicarbonate 2 mM (S-5761), sodium biphosphate 0.34 mM (S-5011), sodium chloride 114 mM (S-5886), sodium lactate 10 mM

(L-4263), and 0.1 mg/mL streptomycin] solution at 38.5°C and oocytes were recovered using a stereomicroscope. After washing with TL-HEPES, COCs with three layers of densely compacted cumulus cells were selected.

2.2 *In vitro* maturation (IVM)

The COCs were washed six times with IVM medium [Tissue Culture Medium-199 (TCM199, 11,150-059) with cysteine 0.6 mM, epidermal growth factor 10 ng/mL (EGF, E-4127), 10% (v/v) fetal bovine serum (16,000-044), follicle-stimulating hormone 10 μg/mL (HOR-285), 1 μg/mL estradiol-17β, and sodium pyruvate 0.2 mM (P-5280)] and the COCs, typically ranging from 30 to 35 in each well, were contained in 500 μL of IVM medium and then incubated at 38.5°C under a controlled humidified atmosphere of 5% CO_2 for 22 h.

2.3 *In vitro* fertilization (IVF) and *in vitro* culture (IVC)

After IVM, the semen was thawed, washed with sperm Dulbecco's phosphate-buffered saline, and then centrifuged at 750 × g for 5 min at 25°C. The sperm pellet was diluted with 500 μL of heparin (20 μg/mL) and incubated for 15 min at 38.5°C in humid conditions of 5% CO_2. Subsequently, it was diluted with IVF medium (Tyrode lactate solution supplemented with 6 mg/mL BSA, 22 μg/mL sodium pyruvate, 100 IU/M penicillin, and 0.1 mg/mL streptomycin) to form 5 mL (final concentration of 1×10^6 sperm/mL) and then matured COCs were transferred to a four-well dish containing sperm for 20 h in IVF medium. After IVF, the presumed zygotes from which the cumulus cells were removed were cultured in four-well dishes filled with 500 μL of synthetic oviductal fluid (SOF) medium (5 ng/mL ITS (insulin, transferrin, sodium selenite, 11074547001), 100 ng/mL EGF, and 4 mg/mL BSA) for 8 d (day 0 = day of IVF).

2.4 Supplementation of GDF-8

The solubility of GDF-8 is 4 mM HCl, and a 100 μg/mL GDF-8 stock solution was prepared by diluting 10 μg of GDF-8 in 100 μL of 4 mM HCl. Subsequently, SOF medium containing 10 ng/mL of GDF-8 used in the experiment was prepared by adding 0.5 μL of GDF-8 stock solution to 5 mL of SOF medium. The degree of development at each embryonic culture stage was compared between the control and GDF-8 groups.

2.5 Differential staining of blastocysts

Day 8 blastocysts were differentially stained to count ICM and TE cells. Blastocysts were permeabilized by a 20-s incubation in 0.2% Triton X-100 in PBS containing 2 mg/mL BSA, followed by two immediate washes in PBS-BSA solution (n = 5 per group). The ICM cells were stained by incubation in the dark at 37.5°C for 5 min with a PBS-BSA solution containing propidium iodide 30 μg/mL (PI, P-4864) and then washed twice in PBS-BSA solution. TE cells were stained by incubation in the dark for 30 min at 25°C with 4% paraformaldehyde fixation solution containing 10 μg/mL Hoechst 33,342 and washed twice in PBS-BSA solution. The stained samples were imaged using an Olympus IX71 microscope and analyzed using the ImageJ software (National Institutes of Health, Bethesda, MD, United States; https://imagej.nih.gov/ij).

2.6 Invasion assay

Day 8 hatched blastocysts were cultured in an invasion chamber insert (6.4 mm; Corning Inc. Life Sciences) to analyze the invasion area. The insert was coated with Matrigel (356,234) and incubated at 37.5°C for 2 h. The blastocysts were transferred to the chamber (three blastocysts per insert) and incubated at 37.5°C for 72 h, and the SOF medium was changed after 48 h. After 10 d of culture, the insert was washed thrice in PBS, fixed with 4% paraformaldehyde fixation solution at 4°C for 30 min, stained with 4',6-diamidino-2-phenylindole (DAPI) for 5 min, and washed thrice with PBS. Images of the invasion area were captured using an Olympus IX71 microscope and analyzed using the ImageJ software.

2.7 Long term culture

To recovery the TE cells, Day 8 Hatched blastocysts were cultured in four-well dish. Four well dish was coated 2% gelatin and dried at least 2 h. The blastocysts were transferred to the well (Three blastocysts per well) and incubated at 37.5°C for 72 h in SOF medium and changed after 48 h. After blastocysts attached on plate beyond Day 8 and use the scrapper for gathering the attached cells.

2.8 Extraction of mRNA and complementary DNA (cDNA) synthesis

The manufacturer protocol was used to extract mRNA using the Arcturus PicoPure RNA Isolation Kit (Cat. No. 12204-01; Arcturus, Foster, United States). Day 8 blastocysts and TE cells were washed four times with nuclease-free water, placed in a 1.5 mL tube containing 30 μL nuclease-free water, frozen in liquid nitrogen, and stored at −80°C. The isolated mRNA samples were reverse-transcribed into single-stranded cDNA.

2.9 Quantitative reverse transcription polymerase chain reaction (qRT-PCR) analysis of target genes

The expression of the ALK5-SMAD2/3 signaling pathway, TJ, and AJ-related genes was investigated using qRT-PCR. The expression levels of these genes were normalized to that of glyceraldehyde-3-phosphate dehydrogenase (*GAPDH*). Primers designed based on the mRNA sequences of the genes were purchased from Macrogen (Seoul, Korea). qRT-PCR was performed using CFX98 devices (Bio-Rad Laboratories) with 1x iQ SYBR Green Supermix (iQ™SYBR®327Green 328 Supermix kit, Bio-Rad Laboratories) and 3 μL of diluted DNA. All cDNA samples were subjected to qRT-PCR to detect variations in the expression of other genes using GAPDH

primers. After confirming that GAPDH expression was not significantly different between samples, all transcripts were quantified using qRT-PCR. The cycling conditions were as follows. 95°C for 3 min, 95°C for 15 s, 62°C for 20 s, 72°C for 30 s, and final extension for 5 min. Quantitative analysis was performed using the $^{\Delta\Delta}$Ct method. The results are reported as values relative to the mean value of the endogenous control, *GAPDH*, compared with the calibrator after normalization. The intra- and inter-assay variance coefficients were calculated using qRT-PCR for all genes. The primers sequences are mentioned in Table 1.

2.10 Cryopreservation and thawing procedure

An ethylene glycol-based freezing protocol and a conventional gold-standard freezing procedure were used for cryopreservation. Day 7 expanded blastocysts were immediately washed with a 0.5% (w/v) BSA solution prepared in PBS. After washing, the blastocysts were incubated with 0.1 M sucrose and 0.5% BSA solutions in an ethylene glycol cryoprotectant medium for 10 min. The blastocysts were then loaded into a 0.25-mL plastic straw. Embryos were slowly frozen using a controlled freezing system (CL-8800i; Cryo-Logic, Blackburn, Victoria, Australia). The straw was carefully transferred, immersed in liquid N_2, and stored until further use. The thawing of frozen straw was exposed to air for 10 s and soaked in water at 37.5°C for 20 s. The thawed embryos were washed with SOF medium to remove the cryoprotectant medium and then cultured in a humidified atmosphere of 5% CO_2 at 38.5°C for 48 h.

2.11 Assessment of embryo survival

After thawing, the survival rate was assessed by examining the presence or absence of blastocoels in the surviving blastocysts at 24 and 48 h. Additionally, the hatching rate of each group was evaluated 24 and 48 h after thawing.

2.12 Tight junction permeability assay

Post-thaw blastocysts were cultured in SOF medium for 24 h. The re-expanded blastocysts were stained with 1 mg/mL 4-kDa FITC-dextran (CAT# 60842-46-8, Sigma-Aldrich) in SOF medium at 25°C under dark conditions for 10 min and then washed with SOF medium. The fluorescence intensity that detected TJ permeability was measured using an Olympus IX71 microscope. The fluorescence intensity was analyzed using ImageJ software.

2.13 Immunofluorescence stain

Day 8 blastocysts were fixed using 4% paraformaldehyde fixation solution at 25°C for 30 min. Blastocysts were washed 3 times with 2% PBS-PVA and proteinase K-treated fixed blastocysts for 5 min to increase permeability. The blastocysts were washed 3 times and incubated with the blocking solution (5% BSA in PBS-PVA) at 25°C for 90 min. Then, the blastocysts were stained overnight with primary antibodies at 4°C. The blastocysts were washed 3 times with PBS-PVA and then incubated with TRITC secondary antibodies (Santa Cruz Biotechnology, Dallas, Texas, United States) at 25°C for 90 min. The nucleus was stained with DAPI at 25°C for 10 min. After washing, all blastocysts were mounted on slide glass. A laser scanning confocal microscope (Fluoview FV 1000; Olympus, Tokyo, Japan) was used for confocal imaging. Fluorescence intensities were measured using ImageJ software (National Institutes of Health, Bethesda, MD, United States; https://imagej.nih.gov/ij).

2.14 Statistical analysis

Statistical analysis was performed using one-way analysis of variance (ANOVA) with GraphPad Prism software (GraphPad Software, Franklin Street, Boston, MA; www.graphpad.com) and analyzed by multiple pairwise companies (Tukey's test) for comparisons between groups. One-way ANOVA was used to compare embryonic development (blastocyst and hatching rates). Differential staining, invasion assays, and qRT-PCR were performed using randomly selected blastocysts from each group (five embryos per replicate). Triplicate sets of experiments were performed to analyze the data. Data concerning blastocyst quality (ICM, TE, TE:ICM ratio) and expression levels of various genes between the control and GDF-8 groups were compared using t-tests. The mean fluorescence intensities from all imaging data were quantified per blastocyst (n = 15–20) in each group. The ImageJ software (version: ij154) (National Institutes of Health, Bethesda, MD, United States) generated all histogram values. Data are expressed as the mean ± standard deviation (mean ± SE). $^{*}p < 0.05$; $^{**}p < 0.01$; $^{***}p < 0.001$ indicate a significant difference.

3 Results

3.1 Setting the concentration of GDF-8 and cleavage and developmental rates

We conducted experiments using a range of concentrations to determine the most optimal GDF-8 supplementation concentration. GDF-8 treatment groups were established using GDF-8 concentrations of 0.2, 2, 10, and 20 ng/mL. We observed a notable increase in both development and hatching rates ($p < 0.05$) when the GDF-8 group was set at 10 ng/mL (Control vs Treatment; 31.00 ± 1.82 vs 47.77 ± 3.52) (Control vs Treat; 7.04 ± 2.68 vs 28.04 ± 6.11; Table 2). GDF-8 supplementation to the SOF medium improved the development and hatching rates. Therefore, the GDF-8 treatment group was selected at a 10 ng/mL concentration, and the experimental process was performed accordingly.

3.2 Effect of GDF-8 supplementation on the competence-related gene of trophectoderm cells

The GDF-8 treatment group showed significantly improved total cell numbers ($p < 0.05$) compared to the control

10.3389/fcell.2024.1345669

TABLE 1 List of qRT-PCR primers.

Gene name	Primer sequences	Accession number
MMP2	F: CCATTGAGACCATGCGGAAG	NM_174745.2
	R: ACATCGCTCCAGACTTGGAA	
MMP9	F: CACGCACGACATCTTTCAGT	NM_174744.2
	R: TTCAGGAGGTCGAAGGTCAC	
FSTL3	F: GATGTACCGTGGTCGCTGC	NM_001075710.2
	R: GTAGGTGACGTTGTTGTTGCC	
CDX2	F: TGAGGAGCATGGACTCTGCTA	NM_001206299.1
	R: GGGCTAGGTCAGCTGGTAAAC	
CLDN2	F: AGCTACAGCCAGCAGACAAG	NM_205781.2
	R: TGCTGGCACCAACATAGGAG	
CLDN4	F: TGTCCTGGACGGCTAACAAC	NM_001014391.2
	R: TTAGCGGAGTAGGGCTTGTC	
OCLN	F: AATCACTACACACCAAGCAATGAC	NM_001082433.2
	R: AAGCATAGACAGGATCCGAATTAC	
ACTINγ2	F: CCACCATGTACCCTGGCATT	BT021005.1
	R: ACTCTGGCTTGCTGATCCAC	
CD44	F: CCGGAACATAGGGTTTGAGA	NM_174013.3
	R: GGTATAACGGGTGCCATCAC	
CDH1	F: CCGTGAGAGTTTTCCCACAT	NM_001002763.1
	R: CATTGGTGACTGGGTCTGTG	
AQP3	F: AGAAGGAGCTGGTGAACCG	NM_001079794.1
	R: ACAGAGCCACAGCCAAACAT	
AQP8	F: CACTGGATCTACTGGCTGGG	NM_001206607.3
	R: CAGGGGAAGCGTATCAGTCA	
AQP9	F: CTGTTGTCATTGGCTTCCTG	NM_001205833.3
	R: AACCAAAGGTCCCACTACAG	
ATP1a1	F: AATGCCGAAGTGCTGGAATC	NM_001076798.1
	R: GTCCTGGCGAACACAATCTC	
ALK5	F: GGCAGTAAGGCATGATTCGG	NM_174621.2
	R: ATCGTCGAGCTACTTCCCAG	
SMAD2	F: AGAGACCTTCCATGCCTCAC	NM_001046218.1
	R: CACTTAGGCACTCGGCAAAA	
SMAD3	F: AACCATGTCGTCCATCCTG	NM_001205805.1
	R: CAGTAGATGACGTGGGGGAG	
GAPDH	F: CCCAGAATATCATCCCTGCT	NM_001034034.2
	R: CTGCTTCACCACCTTCTTGA	

TABLE 2 Effect of GDF-8 supplementation during *in vitro* culture on embryonic development of *in vitro* fertilization.

Treatments	No. of oocytes[a]	No. of presumed zygotes	No. of embryos cleaved (% ± SE)[b]	No. of blastocysts (% ± SE)[b]	No. of hatched blastocysts (% ± SE)[b]
Control	240	229	201 (87.77 ± 2.34)	71 (31.00 ± 1.82)[c]	5 (7.04 ± 2.68)[c]
0.2 ng/mL GDF-8	240	217	187 (86.18 ± 2.43)	83 (38.25 ± 2.69)[c,d]	13 (15.66 ± 4.36)[c,d]
2 ng/mL GDF-8	240	210	180 (85.71 ± 3.34)	93 (44.29 ± 2.82)[d]	21 (22.58 ± 3.72)[c,d]
10 ng/mL GDF-8	240	224	190 (84.82 ± 2.60)	107 (47.77 ± 3.52)[d]	30 (28.04 ± 6.11)[d]
20 ng/mL GDF-8	240	232	193 (83.19 ± 1.53)	66 (28.45 ± 1.28)[c]	16 (24.24 ± 3.96)[d]

[a]Six replicates were performed.
[b]Rates are relative to the number of presumed zygotes.
[c]$p < 0.05$ with different superscripts indicates the significant difference.
[d]$p < 0.05$ with different superscripts indicates the significant difference.

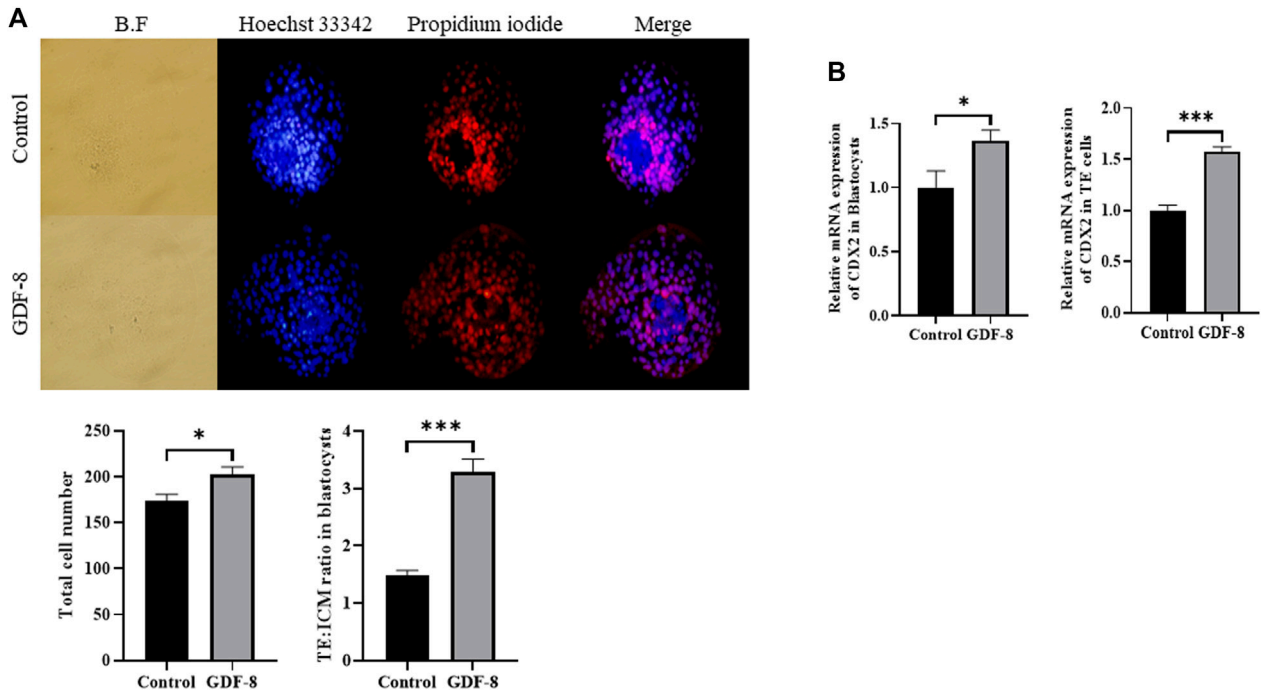

FIGURE 1
Number of ICM and TE cells in the control group and GDF-8 treatment group treated with Hoechst 33,342 and propidium iodide. **(A)** Differential stain of day 8 blastocysts showing propidium iodide localization in TE cells. Total cells were stained blue with Hoechst 33,342. TE cells were stained red with propidium iodide. Images were obtained using an epifluorescence microscope. Total cell number and TE: ICM cell ratio. Day 8 blastocysts were quantified after differential staining. Original magnification: ×200. Values represent the mean ± SE (n = 20, *$p < 0.05$, ***$p < 0.001$). **(B)** Relative mRNA expression levels of *CDX2* related to trophectoderm cell proliferation in the control and GDF-8 groups of blastocysts and TE cells. Three replicates were performed. Values represent the mean ± SE (*$p < 0.05$, ***$p < 0.001$). BF, bright field; GDF-8, 10 ng/mL GDF-8; ICM, inner cell mass; TE, trophectoderm.

group. Moreover, the control group exhibited more TE cells than did GDF-8 group, leading to a significant difference ($p < 0.01$) in the ratio of ICM cells to TE cell numbers between the control and GDF-8 groups (Figure 1A). Furthermore, blastocysts and TE cells treated with GDF-8 had significantly higher (Control, Treat; $p < 0.05$, $p < 0.001$) mRNA levels of *CDX2* (Figure 1B). These findings suggest that the addition of GDF-8 to the SOF medium stimulates TE cell proliferation by enhancing the expression of genes associated with TE cells.

3.3 GDF-8 supplementation improved *in vitro* implantation ability and related genes

The area of trophoblast invasion, assessed using ImageJ software, was significantly increased ($p < 0.01$) in the GDF-8 group compared to that in the control group (Figure 2A). Furthermore, we investigated the expression of genes associated with the ALK5-SMAD2/3 signaling pathway. The low *in vitro* implantation ability of IVC blastocysts has been attributed to a

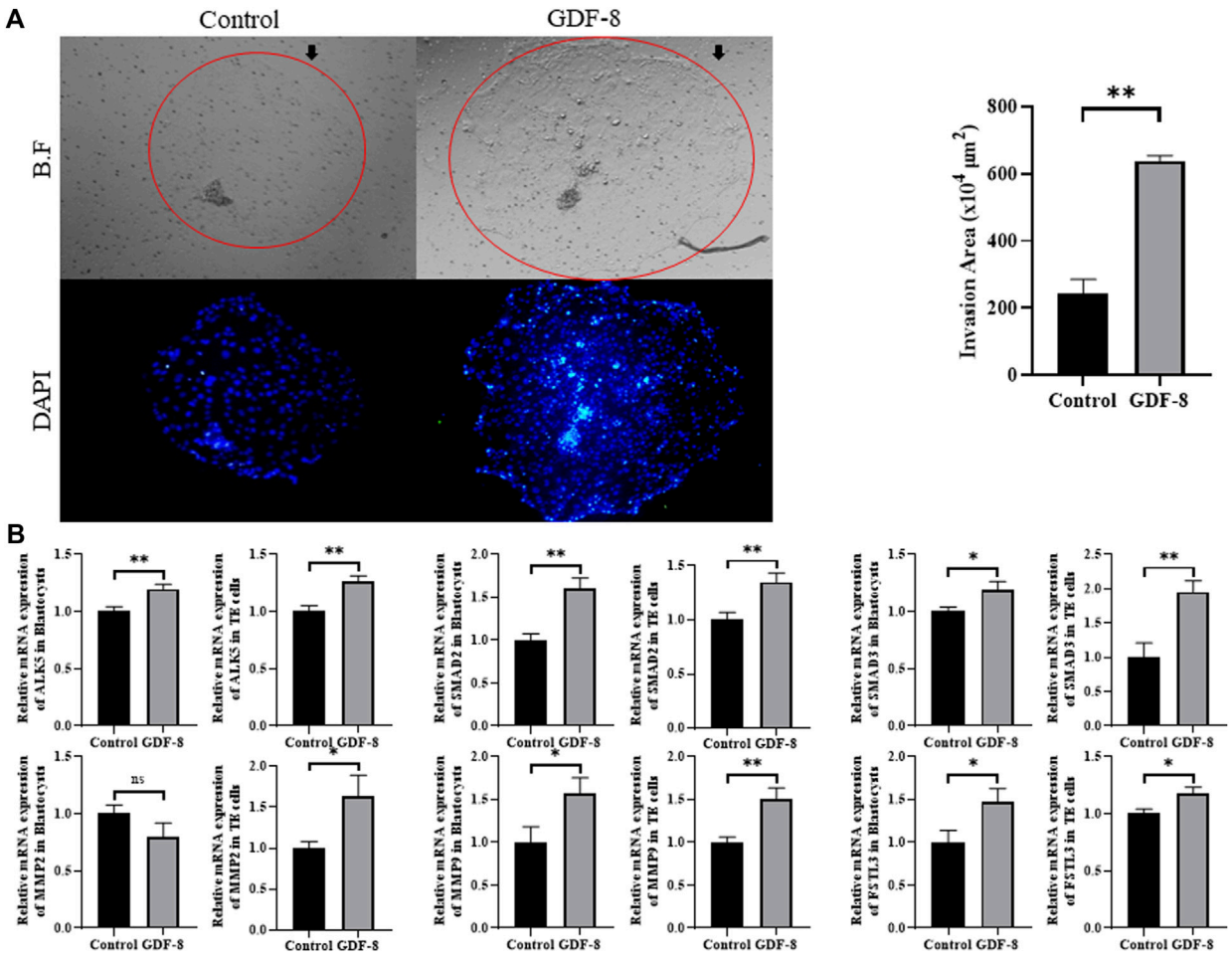

FIGURE 2
Invasion ability of trophoblast. **(A)** Bright-field and DAPI image showing the invasion area in the control and GDF-8 groups. Original magnification: ×40. Mean invasion area analyzed using ImageJ. n = 3 blastocysts per group were used in triplicates. **(B)** Relative mRNA expression level of ALK5, SMAD2 and SMAD3 related with ALK5-SMAD2/3 signaling pathway, *MMP2*, *MMP9* and *FSTL3* related to implantation in control and GDF-8 groups of blastocysts and TE cells. Three replicates were performed. Values represent the mean ± SE. (ns = not significant, *$p < 0.05$, **$p < 0.01$). BF, bright field; DAPI, 4′,6-diamidino-2-phenylindole; GDF-8, 10 ng/mL GDF-8.

decrease in the ability and/or function of the TE cells. qRT-PCR analysis demonstrated significant upregulation ($p < 0.05$, $p < 0.01$) in the mRNA expression of *ALK5*, *SMAD2*, and *SMAD3* in the GDF-8 group compared to that in the control group (Figure 2B). Moreover, the mRNA expression of *ALK5*, *SMAD2*, and *SMAD3* were significantly higher ($p < 0.01$) in the GDF-8 treated TE cells compared to that in the control group (Figure 2B). Therefore, GDF-8 supplementation stimulated activation of the ALK5-SMAD2/3 signaling pathway. Moreover, the mRNA expression of *MMP9* and *FSTL3*, both linked to the ALK5-SMAD2/3 signaling pathway, was significantly upregulated ($p < 0.05$) in the GDF-8 group compared with that in the control group. These genes' increased relative mRNA levels suggest that supplementation with GDF-8 stimulates the ALK5-SMAD2/3 signaling pathway, thereby improving *in vitro* implantation ability. However, *MMP2* levels were not significantly different (Figure 2B). The mRNA expression of *MMP2*, *MMP9*, and *FSTL3* related to invasion ability, were significantly increased ($p < 0.05$, $p < 0.01$) in the GDF-8 treated TE cells compared to that in the control group (Figure 2B). These findings indicate that supplementation of GDF-8 to SOF medium stimulates the ALK5-SMAD2/3 signaling pathway and enhances *in vitro* implantation gene expression.

3.4 GDF-8 supplementation improved TJ complexes and AJ in blastocysts

Maintenance of AJ and TJ integrity within the inner layer of TE epithelium is paramount in developing expanded blastocysts. Following a 24 h culture post-thawing, blastocysts were assessed via 4-kDa FITC-dextran analysis, and a significant reduction in fluorescence was observed within the GDF-8 group relative to the control group. ($p < 0.01$). This decrease indicates a significant reduction in the permeability of TJ in the blastocysts after GDF-8 treatment ($p < 0.01$) (Figure 3A). Moreover, qRT-PCR analysis offered further confirmation, showing that the mRNA expression of genes regulated by TJ (*actiny2*, *CLDN2*, *CLDN4*, and *OCLN*) was significantly elevated in the GDF-8 group relative to that in the

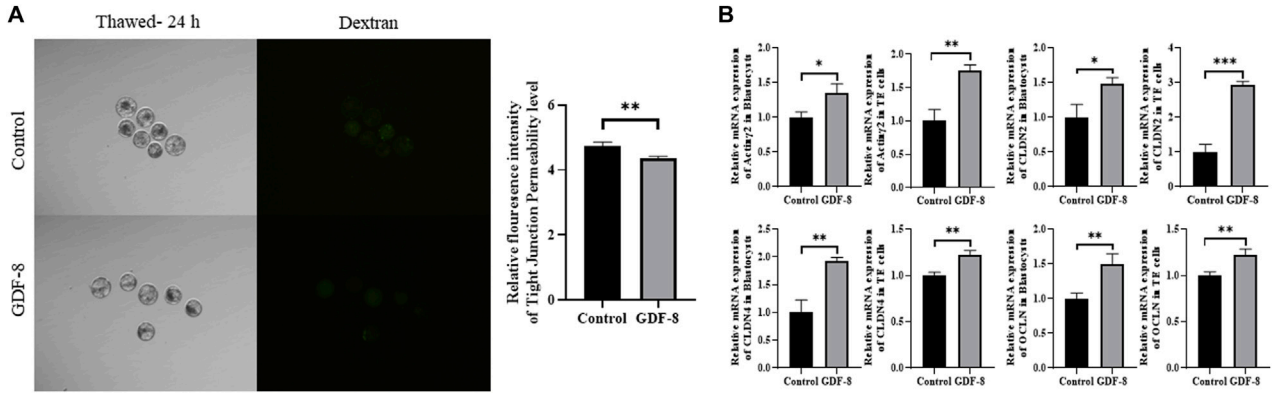

FIGURE 3
Tight junction sealing assay in post-thawing blastocyst cultures in control and GDF-8 groups. **(A)** Representative images of post-thawed blastocysts cultured for 24 h in the control and GDF-8 groups and then subjected to a dextran assay to assess tight junction sealing. Original magnification: ×100. Fluorescent signal in blastocysts cultured in the control and GDF-8 groups and then treated with dextran for 24 h n = 3 blastocysts per group were used in triplicates. **(B)** Relative mRNA levels of *Actinγ2*, *CLDN2*, *CLDN4*, and *OCLN* in the control and GDF-8 groups of blastocysts and TE cells. Three replicates were performed. Values represent the mean ± SE (*$p < 0.05$; **$p < 0.01$). Dexran, 4 kDa FITC-labelled dextran; GDF-8, 10 ng/mL GDF-8.

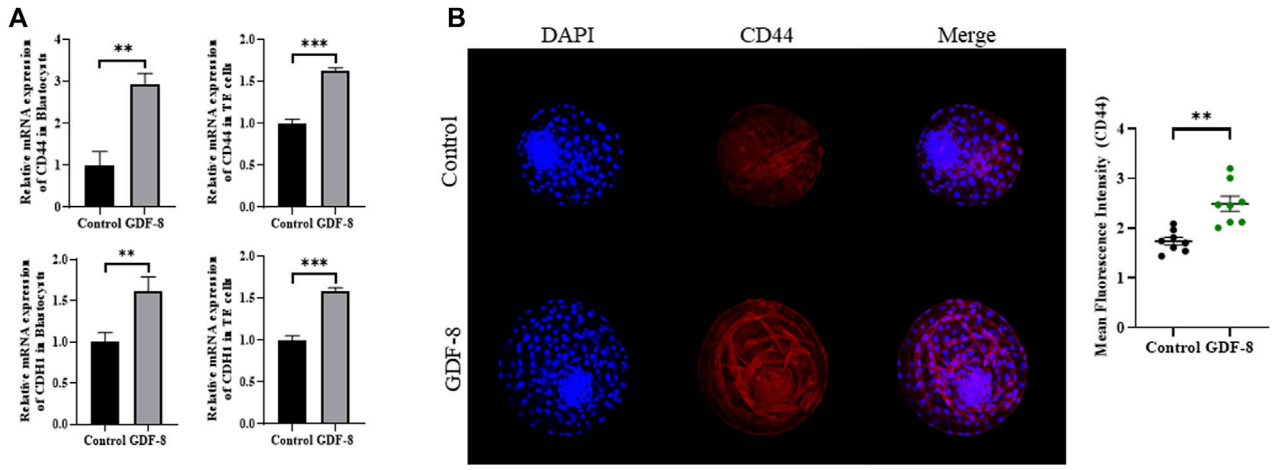

FIGURE 4
Expression of Adherent junction protein in control and GDF-8 groups. **(A)** Relative mRNA level of *CD44*, and *CDH1* in control and GDF-8 groups of blastocysts and TE cells. Three replicates were performed. Values represent the mean ± SE (*$p < 0.05$; **$p < 0.01$). **(B)** Confocal images of immunofluorescence CD44 in control and GDF-8 groups. Original magnification: ×200. The quantification of signal intensities of CD44 expression. n = 3 blastocysts per group were used in triplicates. DAPI, 4′,6-diamidino-2-phenylindole; GDF-8, 10 ng/mL GDF-8.

control group ($p < 0.05$) (Figure 3B). Moreover, the mRNA expression of the gene related to TJ (*actinγ2*, *CLDN2*, *CLDN4*, and *OCLN*) was significantly improved ($p < 0.01$, $p < 0.001$) in the GDF-8 treated TE cells compared to that in the control group (Figure 3B). Furthermore, the mRNA expression levels of genes related to AJ (*CD44* and *CDH1*) were significantly higher in the GDF-8 group than those in the control group ($p < 0.05$) (Figure 3B; Figure 4A). In addition, the mRNA expression level of gene related to AJ (*CD44* and *CDH1*) was higher ($p < 0.001$) in the GDF-8 treated TE cells compared to that in the control group (Figure 4B). The CD44 protein level was higher in the GDF-8 group than those in the control group ($p < 0.01$) (Figure 4B). These results imply that including GDF-8 in the SOF medium positively influences gene expression associated with AJ and TJ, contributing to the observed alterations in trophoblast cell morphology and function.

3.5 Effect of GDF-8 supplementation on post-thaw blastocysts

When assessing the blastocoel re-expansion rate at 12 h post-thawing, it was observed that the GDF-8-treated group exhibited blastocysts with over 70% re-expanded blastocoel cavities compared to the control group (Figures 5A,B). Blastocysts treated with GDF-8 exhibited significantly higher blastocoel expansion 24 and 48 h post-thawing, indicating improved

10.3389/fcell.2024.1345669

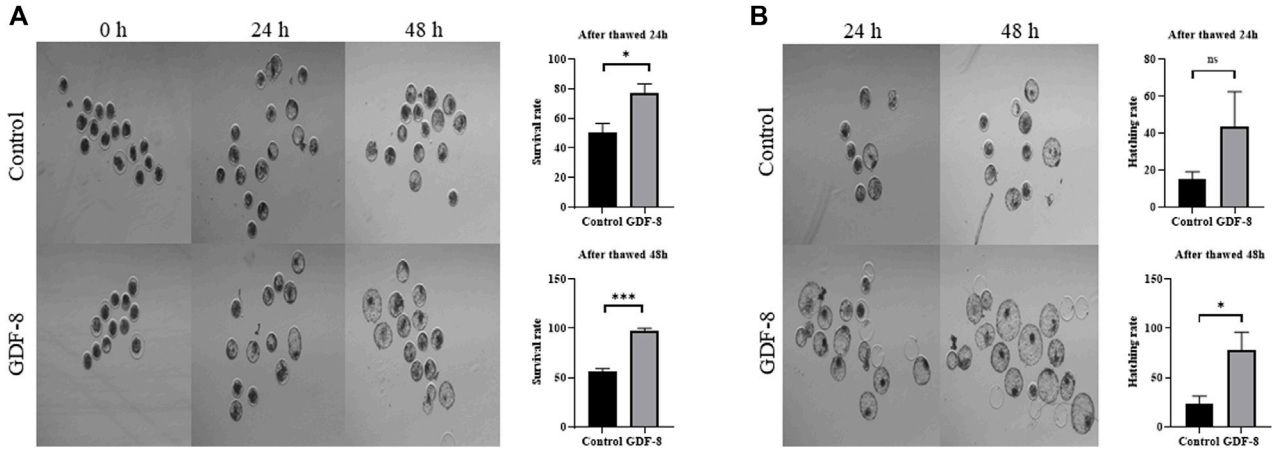

FIGURE 5
Survival and hatching in post-thawed bovine blastocysts cultured in the control and GDF-8 groups. **(A)** Representative images of surviving blastocysts cultured in the control and GDF-8 groups after 24 and 48 h of thawing. Original magnification: ×64. After thawing, investigate the survival rate. Three replicates were performed. Values represent the mean ± SE (ns = not significant, *$p < 0.05$; ***$p < 0.001$). **(B)** Representative images of hatching blastocysts cultured in the control and GDF-8 groups after 24 and 48 h of thawing. After thawing, investigate the hatching rate. Three replicates were performed. Values represent the mean ± SE (ns = not significant, *$p < 0.05$; ***$p < 0.001$). Original magnification: ×64. GDF-8, 10 ng/mL GDF-8.

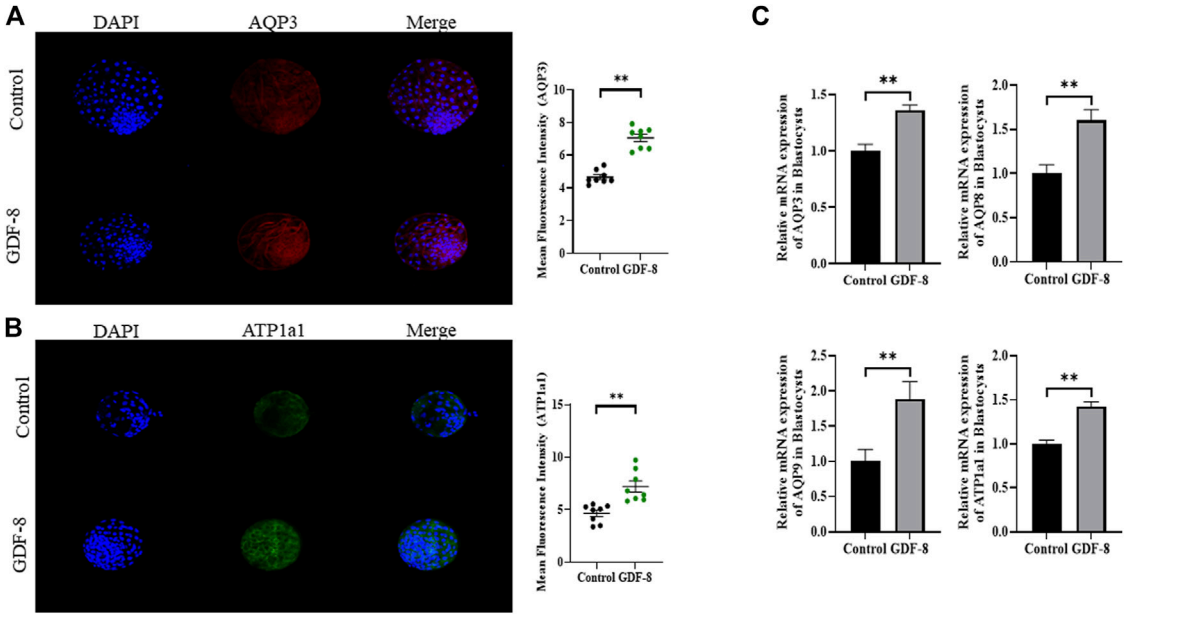

FIGURE 6
Expression of blastocoel expansion protein in control and GDF-8 groups. **(A)** Confocal images of immunofluorescence AQP3 in control and GDF-8 groups. Original magnification ×200. The quantification of signal intensities of AQP3 and expression. (n = 8). **(B)** Confocal images of immunofluorescence ATP1a1 in control and GDF-8 groups. Original magnification ×200. The quantification of signal intensities of ATP1a1 expression. (n = 8). **(C)** Relative mRNA expression levels of AQP3, AQP8, AQP9, and ATP1a1 related to re-expansion in the control and GDF-8 groups. Three replicates were performed. Values represent the mean ± SE (**$p < 0.01$). DAPI, 4′,6-diamidino-2-phenylindole; GDF-8, 10 ng/mL GDF-8.

survival rates (Figure 5A). Furthermore, the hatching rate was significantly higher ($p < 0.05$) 48 h post-thawing in the GDF-8 group than that in the control group (Figure 5B). While upregulating AQP3, ATP1a1 protein level in GDF-8 group those in the control group ($p < 0.01$) (Figures 6A,B). Additionally, in blastocysts that survived post-thawing, mRNA expression of genes related to *AQP3*, *AQP8*, *AQP9*, and *ATP1a1* was significantly upregulated in blastocysts treated with GDF-8 (Figure 6C). This suggests that GDF-8 supplementation promotes the upregulation of genes associated with *AQPs*, leading to increased fluid accumulation, thus implicating GDF-8 in influencing the post-thaw re-expansion and hatching rates.

4 Discussion

IVP is a critically assisted reproductive technology that is commercially employed to induce genetic improvement (Thibier, 2005). Over the years, concerted research efforts have been dedicated to overcoming several inherent constraints of IVP. Nevertheless, these limitations persist and substantially influence embryonic development and implantation rates (Thibier, 2005; Moussa et al., 2014). Consequently, this study was designed to investigate the impact of GDF-8 supplementation on the activation of the ALK5-SMAD2/3 signaling pathway in bovine *in vitro* embryo production and embryonic quality. This study examined the proliferation and functionality of TE cells, particularly their effects on implantation and cryopreservation *in vitro*.

GDF-8, classified as a member of the TGF-β superfamily, has been acknowledged as an activator of the ALK5-SMAD2/3 signaling pathway (Fang et al., 2021). Additionally, it has been demonstrated that activating this signaling pathway stimulates the expression of *MMP2*, thereby mediating the upregulation of invasive capabilities in human extra villous trophoblast cells (Fang et al., 2021). Moreover, it facilitates trophoblast mobility, regulates invasion, and promotes the expression of FSTL3, thereby influencing invasive capabilities (Xie et al., 2020; Fang et al., 2021; Chen et al., 2023). According to previous studies, GDF-8 binds to the receptor ALK5, activating the SMAD2/3 complex. Subsequently, the SMAD complex is transferred to the nucleus to activate implantation-related genes (Zheng et al., 2022). Our research involved the administration of GDF-8, resulting in the activation of the ALK5-SMAD2/3 signaling pathway, and an assessment of the mRNA expression of genes related to cellular invasion, specifically *ALK5*, *SMAD2*, *SMDA3*, *MMP2*, *MMP9*, and *FSTL3*. Notably, we demonstrated that GDF-8 supplementation stimulated the ALK5-SMAD2/3 signaling pathway. Moreover, we detected a significant increase in the mRNA expression levels of *MMP9* and *FSTL3* in the GDF-8-treated group. Furthermore, invasion assays confirmed that the *in vitro* implantation ability of GDF-8-treated embryos was significantly enhanced.

Previous studies have reported that GDF-8 treatment of hamster blastocysts promotes TE cell proliferation (Wong et al., 2009). Additionally, previous studies have established that the ratio of ICM to total cell number is reduced *in vitro* blastocysts cultured *in vitro* compared to those cultured *in vivo* (Koo et al., 2002). In our study, we conducted a differential staining analysis of control and GDF-8-treated blastocysts. In GDF-8 treated blastocysts, we observed enhanced proliferation of TE cells, and the ICM:total cell number ratio was approximately 20%, similar to that observed in blastocysts cultured *in vivo*. One previous study stated that Wnt signaling activator can increase the TE:ICM ratio (Denicol et al., 2014). Few other studies also claimed variation in TE:ICM ratio, using various conditions (Sakatani et al., 2008; Wooldridge and Ealy, 2019), but mostly the number is between 2.9 and 3.5. *In vivo* produced bovine embryos is the standard example and several researches claimed that difference is present between *in vivo* and *in vitro* produced bovine embryos in TE:ICM ratio (Iwasaki et al., 1990). *CDX2* initiates the differentiation of early TE cells and plays a crucial role in TE function and maintenance (Wu et al., 2010). Furthermore, previous studies have indicated that *CDX2* is essential for the integrity of the AJ and TJ in the TE epithelium surrounding the blastocoel of expanded mouse blastocysts (Strumpf et al., 2005; Qu et al., 2017). We observed a significant increase in the mRNA expression level of *CDX2* in GDF-8-treated blastocysts. Therefore, the upregulation of *CDX2* expression was facilitated by GDF-8 supplementation, which enhanced the proliferation and functionality of TE cells.

Previous studies have discovered that TJ and AJ play a crucial role in maintaining the integrity of TJ during cryo-shrinkage (Sidrat et al., 2022). TJ functions as a gate for the transport of ions and small molecules, whereas AJ provides structural support (Eckert and Fleming, 2008; Marikawa and Alarcon, 2012). When these components are compromised during cryo-shrinkage, TJ integrity is not maintained, resulting in ineffective sealing of TJ post-thawing (Sidrat et al., 2022). This difficulty in sealing prevents fluid accumulation within the blastocoel, making re-expansion difficult. Therefore, the development of the TE epithelium plays a pivotal role in blastocoel formation, and effective sealing of TJ regulates the balance between osmotic pressure gradients and fluid accumulation within the blastocoel (Chan et al., 2019). In the event of damage during cryo-shrinkage, TJ integrity is disrupted, leading to inadequate sealing (Miller et al., 2003). Therefore, fluid accumulation within the blastocoel after thawing becomes problematic and hinders re-expansion.

Therefore, we assess their permeability by conducting a 4-kDa FITC-dextran assay on control and GDF-8-treated blastocysts. We observed significant maintenance of TJ integrity in GDF-8-treated blastocysts at 24 h post-thawing. Additionally, AJ in TE cells is associated with TE integrity and is substantially affected by cryo-shrinkage. Genes related to AJ, such as *CDH1* and *CD44*, were upregulated in GDF-8-treated blastocysts. *CD44* is also expressed in the embryo (Wheatley et al., 1993; Haegel et al., 1994; Campbell et al., 1995) and associated with embryonic attachment during the early stages of implantation (Berneau et al., 2019). To confirm that the expression of *CD44* is related to AJ, immunofluorescence staining was performed, and the *CD44* protein level in GDF-8-treated blastocyst was upregulated. Therefore, GDF-8 supplementation has the potential to sustain accumulated fluid pressure during blastocoel re-expansion after thawing (Kirschner et al., 2011; Reardon et al., 2012). Furthermore, mRNA expression levels in GDF-8-treated blastocysts of genes associated with TJ and blastocoel re-expansion, including *CLDN2*, *CLDN4*, *OCLN*, and *actinγ2*, were upregulated (Eckert and Fleming, 2008). Thus, supplementation of GDF-8 induces increased AJ- and TJ-related gene expression within blastocysts, reducing cellular sealing defects.

One of the factors promoting blastocoel formation is the osmotic pressure gradient facilitated by *AQPs* and *ATP1a1*, which regulate the osmotic pressure and water transport pathways (Robinson and Benos, 1991; Frank et al., 2019; Kosyl and Ajduk, 2023). Therefore, we examined the expression of *AQP3*, *AQP8*, *AQP9*, and *ATP1a1* to assess the blastocyst blastocoel formation ability. A substantial increase in gene expression was observed in the GDF-8-treated blastocysts. *AQP3* is an H_2O transport channel located on the

basolateral membrane of the TE (Johnston et al., 2000; Bell and Watson, 2013). This channel facilitates water transfer into the blastocyst cavity, establishing an osmotic gradient accumulating fluid (Barcroft et al., 2003). Additionally, *ATP1a1* elevates the intracellular osmotic pressure, contributing to fluid accumulation in the blastocoel (Barcroft et al., 2003; Bell and Watson, 2013). We conducted immunofluorescence experiments to determine the expression of the genes related to blastocyst formation, *AQP3*, and *ATP1a1*. *AQP3* and *ATP1a1* protein levels in GDF-8-treated blastocyst were upregulated. In addition, post-thaw GDF-8-treated blastocysts exhibited significantly higher survival and hatching rates. The post-thaw survival and hatching rates of blastocysts also increased with increasing expression levels of *AQPs* and *ATP1a1*. The supplementation of GDF-8 to the IVC culture medium positively impacted the development and hatching rates of bovine IVP embryos, which significantly enhanced cryo-tolerance and *in vitro* implantation by stimulating TE cell function and proliferation.

Data availability statement

The original contributions presented in the study are included in the article/Supplementary Material, further inquiries can be directed to the corresponding authors.

Ethics statement

The animal study was approved by Animal Care Facility of the Gyeongsang National University Institute of Animal Care Committee (GNU-130902-A0059). The study was conducted in accordance with the local legislation and institutional requirements.

Author contributions

S-MK: Writing–original draft, Methodology, Investigation, Data curation, Conceptualization. MI: Writing–review and editing, Visualization, Data curation, Conceptualization. CP: Software, Methodology, Writing–review and editing. S-HL: Writing–review and editing, Software, Methodology. MZ: Visualization, Validation, Project administration, Writing–review and editing. XY: Supervision, Formal Analysis, Writing–review and editing. YJ: Writing–review and editing, Supervision. I-KK: Resources, Project administration, Funding acquisition, Writing–review and editing, Supervision.

Funding

The author(s) declare that financial support was received for the research, authorship, and/or publication of this article. This work was partially supported by a National Research Foundation of Korea (NRF) grant funded by the Korean Government (MSIT; no. RS-2023-00208894), Cooperative Research Program for Agriculture Science and Technology Development (Project title: Carbon Reduction Korean Beef Selection and Carbon Emission Evaluation Base Construction Research, Project No. RS-2023-00237137)", Rural Development Administration, Republic of Korea, and a scholarship from BK21. Institutional Review Board Statement: The experiments were carried out under the guidelines of GNU and the Institutional Animal Care and Use Committee (Approval ID: GNU-230425-A0088).

Acknowledgments

The authors are thankful to all the members of Kong's lab.

Conflict of interest

The authors declare that the research was conducted in the absence of any commercial or financial relationships that could be construed as a potential conflict of interest.

The author(s) declared that they were an editorial board member of Frontiers, at the time of submission. This had no impact on the peer review process and the final decision.

Publisher's note

All claims expressed in this article are solely those of the authors and do not necessarily represent those of their affiliated organizations, or those of the publisher, the editors and the reviewers. Any product that may be evaluated in this article, or claim that may be made by its manufacturer, is not guaranteed or endorsed by the publisher.

Supplementary material

The Supplementary Material for this article can be found online at: https://www.frontiersin.org/articles/10.3389/fcell.2024.1345669/full#supplementary-material

References

Adu-Gyamfi, E. A., Ding, Y.-B., and Wang, Y.-X. (2020). Regulation of placentation by the transforming growth factor beta superfamily. *Biol. Reproduction* 102, 18–26. doi:10.1093/biolre/ioz186

Barcroft, L. C., Offenberg, H., Thomsen, P., and Watson, A. J. (2003). Aquaporin proteins in murine trophectoderm mediate transepithelial water movements during cavitation. *Dev. Biol.* 256, 342–354. doi:10.1016/s0012-1606(02)00127-6

Barcroft, L., Moseley, A., Lingrel, J., and Watson, A. (2004). Deletion of the Na/K-ATPase alpha1-subunit gene (Atp1a1) does not prevent cavitation of the preimplantation mouse embryo. *Mech. Dev.* 121, 417–426. doi:10.1016/j.mod.2004.04.005

Bell, C. E., and Watson, A. J. (2013). p38 MAPK regulates cavitation and tight junction function in the mouse blastocyst. *PloS one* 8, e59528. doi:10.1371/journal.pone.0059528

Berneau, S., Ruane, P., Brison, D. R., Kimber, S., Westwood, M., and Aplin, J. (2019). Investigating the role of CD44 and hyaluronate in embryo-epithelial interaction using an *in vitro* model. *MHR Basic Sci. reproductive Med.* 25, 265–273. doi:10.1093/molehr/gaz011

Camargo, L. D. A., Viana, J., Sã, W., Ferreira, A., Ramos, A., and Vale Filho, V. (2018). Factors influencing *in vitro* embryo production. *Anim. Reprod. Ar.* 3, 19–28.

Camargo, L. S. A., Boite, M. C., Wohlres-Viana, S., Mota, G. B., Serapiao, R. V., Sa, W. F., et al. (2011). Osmotic challenge and expression of aquaporin 3 and Na/K ATPase genes in bovine embryos produced *in vitro*. *Cryobiology* 63, 256–262. doi:10.1016/j.cryobiol.2011.09.135

Camargo, L. S. A., Ferreira, A. M., Ramos, A. A., and Vale Filho, V. R. (2006). Factors influencing *in vitro* embryo production. *Anim. Reprod.* 3, 19.

Campbell, S., Swann, H., Aplin, J., Seif, M., Kimber, S., and Elstein, M. (1995). Fertilization and early embryology: CD44 is expressed throughout pre-implantation human embryo development. *Hum. Reprod.* 10, 425–430. doi:10.1093/oxfordjournals.humrep.a135955

Chan, C. J., Costanzo, M., Ruiz-Herrero, T., MøNKE, G., Petrie, R. J., Bergert, M., et al. (2019). Hydraulic control of mammalian embryo size and cell fate. *Nature* 571, 112–116. doi:10.1038/s41586-019-1309-x

Chen, J., Song, T., Yang, S., Meng, Q., Han, X., Wu, Z., et al. (2023). Snail mediates GDF-8-stimulated human extravillous trophoblast cell invasion by upregulating MMP2 expression. *Cell Commun. Signal.* 21, 93–13. doi:10.1186/s12964-023-01107-2

Choi, I., Carey, T. S., Wilson, C. A., and Knott, J. G. (2012). Transcription factor AP-2γ is a core regulator of tight junction biogenesis and cavity formation during mouse early embryogenesis. *Development* 139, 4623–4632. doi:10.1242/dev.086645

Cohen, M., Meisser, A., and Bischof, P. (2006). Metalloproteinases and human placental invasiveness. *Placenta* 27, 783–793. doi:10.1016/j.placenta.2005.08.006

Corcoran, D., Fair, T., Park, S., Rizos, D., Patel, O., Smith, G., et al. (2006). Suppressed expression of genes involved in transcription and translation in *in vitro* compared with *in vivo* cultured bovine embryos. *Reproduction* 131, 651–660. doi:10.1530/rep.1.01015

Denicol, A. C., Block, J., Kelley, D. E., Pohler, K. G., Dobbs, K. B., Mortensen, C. J., et al. (2014). The WNT signaling antagonist Dickkopf-1 directs lineage commitment and promotes survival of the preimplantation embryo. *FASEB J.* 28, 3975–3986. doi:10.1096/fj.14-253112

Eckert, J. J., and Fleming, T. P. (2008). Tight junction biogenesis during early development. *Biochimica Biophysica Acta (BBA)-Biomembranes* 1778, 717–728. doi:10.1016/j.bbamem.2007.09.031

Edashige, K., Ohta, S., Tanaka, M., Kuwano, T., Valdez, D. M., JR, Hara, T., et al. (2007). The role of aquaporin 3 in the movement of water and cryoprotectants in mouse morulae. *Biol. reproduction* 77, 365–375. doi:10.1095/biolreprod.106.059261

Fang, L., Wang, Z., Wu, Z., Yan, Y., Gao, Y., Li, Y., et al. (2021). GDF-8 stimulates trophoblast cell invasion by inducing ALK5-SMAD2/3-mediated MMP2 expression. *Reproduction* 162, 331–338. doi:10.1530/REP-21-0197

Frank, L., Rose, R., Anastasi, M., Tan, T., Barry, M., Thompson, J., et al. (2019). Artificial blastocyst collapse prior to vitrification significantly improves Na+/K+-ATPase-dependent post-warming blastocoel re-expansion kinetics without inducing endoplasmic reticulum stress gene expression in the mouse. *Reproduction, Fertil. Dev.* 31, 294–305. doi:10.1071/RD17500

Gauster, M., Moser, G., Wernitznig, S., Kupper, N., and Huppertz, B. (2022). Early human trophoblast development: from morphology to function. *Cell. Mol. Life Sci.* 79, 345. doi:10.1007/s00018-022-04377-0

Haegel, H., Dierich, A., and Ceredig, R. (1994). CD44 in differentiated embryonic stem cells: surface expression and transcripts encoding multiple variants. *J. Immunol. Res.* 3, 239–246. doi:10.1155/1994/25484

Ikenouchi, J., Furuse, M., Furuse, K., Sasaki, H., Tsukita, S., and Tsukita, S. (2005). Tricellulin constitutes a novel barrier at tricellular contacts of epithelial cells. *J. Cell Biol.* 171, 939–945. doi:10.1083/jcb.200510043

Iwasaki, S., Yoshiba, N., Ushijima, H., Watanabe, S., and Nakahara, T. (1990). Morphology and proportion of inner cell mass of bovine blastocysts fertilized *in vitro* and *in vivo*. *Reproduction* 90, 279–284. doi:10.1530/jrf.0.0900279

Johnston, H., Koukoulas, I., Jeyaseelan, K., Armugam, A., Earnest, L., Baird, R., et al. (2000). Ontogeny of aquaporins 1 and 3 in ovine placenta and fetal membranes. *Placenta* 21, 88–99. doi:10.1053/plac.1999.0445

Kaidi, S., Bernard, S., Lambert, P., Massip, A., Dessy, F., and Donnay, I. (2001). Effect of conventional controlled-rate freezing and vitrification on morphology and metabolism of bovine blastocysts produced *in vitro*. *Biol. Reproduction* 65, 1127–1134. doi:10.1095/biolreprod65.4.1127

Khurana, N. K., and Niemann, H. (2000). Energy metabolism in preimplantation bovine embryos derived *in vitro* or *in vivo*. *Biol. reproduction* 62, 847–856. doi:10.1095/biolreprod62.4.847

Kidder, G. M. (2002). Trophectoderm development and function: the roles of Na+/K+-ATPase subunit isoforms. *Can. J. physiology Pharmacol.* 80, 110–115. doi:10.1139/y02-017

King, W., Xu, K., Sirard, M. A., Greve, T., Leclerc, P., Lambert, R., et al. (1988). Cytogenetic study of parthenogenetically activated bovine oocytes matured *in vivo* and *in vitro*. *Gamete Res.* 20, 265–274. doi:10.1002/mrd.1120200303

Kirschner, N., Haftek, M., Niessen, C. M., Behne, M. J., Furuse, M., Moll, I., et al. (2011). CD44 regulates tight-junction assembly and barrier function. *J. Investigative Dermatology* 131, 932–943. doi:10.1038/jid.2010.390

Koo, D. B., Kang, Y. K., Choi, Y. H., Park, J. S., Kim, H. N., Oh, K. B., et al. (2002). Aberrant allocations of inner cell mass and trophectoderm cells in bovine nuclear transfer blastocysts. *Biol. Reprod.* 67, 487–492. doi:10.1095/biolreprod67.2.487

Kosyl, E., and Ajduk, A. (2023). O-163 the influence of aquaporin 3 on dynamics of cavitation, implantation and re-expansion after vitrification/warming. *Hum. Reprod.* 38, dead093–196. doi:10.1093/humrep/dead093.196

Lechniak, D., Cieslak, D., and Sosnowski, J. (1997). Cytogenetic analysis of bovine parthenotes after spontaneous activation *in vitro*. *Theriogenology* 49, 779–785. doi:10.1016/S0093-691X(98)00027-2

Marikawa, Y., and Alarcon, V. B. (2012). Creation of trophectoderm, the first epithelium, in mouse preimplantation development. *Mouse Dev. Oocyte Stem Cells* 55, 165–184. doi:10.1007/978-3-642-30406-4_9

Marsico, T. V., Camargo, J. D., Valente, R. S., and Sudano, M. J. (2019). Embryo competence and cryosurvival: molecular and cellular features. *Anim. Reprod.* 16, 423–439. doi:10.21451/1984-3143-AR2019-0072

Massuto, D. A., Kneese, E. C., Johnson, G. A., Burghardt, R. C., Hooper, R. N., Ing, N. H., et al. (2010). Transforming growth factor beta (TGFB) signaling is activated during porcine implantation: proposed role for latency-associated peptide interactions with integrins at the conceptus-maternal interface. *Reproduction* 139, 465–478. doi:10.1530/REP-09-0447

Mcpherron, A. C., Lawler, A. M., and Lee, S.-J. (1997). Regulation of skeletal muscle mass in mice by a new TGF-beta superfamily member. *Nature* 387, 83–90. doi:10.1038/387083a0

Miller, D. J., Eckert, J. J., Lazzari, G., Duranthon-Richoux, V., Sreenan, J., Morris, D., et al. (2003). Tight junction messenger RNA expression levels in bovine embryos are dependent upon the ability to compact and *in vitro* culture methods. *Biol. reproduction* 68, 1394–1402. doi:10.1095/biolreprod.102.009951

Moriwaki, K., Tsukita, S., and Furuse, M. (2007). Tight junctions containing claudin 4 and 6 are essential for blastocyst formation in preimplantation mouse embryos. *Dev. Biol.* 312, 509–522. doi:10.1016/j.ydbio.2007.09.049

Moussa, M., Shu, J., Zhang, X., and Zeng, F. (2014). Cryopreservation of mammalian oocytes and embryos: current problems and future perspectives. *Sci. China Life Sci.* 57, 903–914. doi:10.1007/s11427-014-4689-z

Nagase, H., and Woessner, J. F. (1999). Matrix metalloproteinases. *J. Biol. Chem.* 274, 21491–21494. doi:10.1074/jbc.274.31.21491

Peiris, H. N., and Mitchell, M. D. (2012). The expression and potential functions of placental myostatin. *Placenta* 33, 902–907. doi:10.1016/j.placenta.2012.06.021

Peiris, H. N., Salomon, C., Payton, D., Ashman, K., Vaswani, K., Chan, A., et al. (2014). Myostatin is localized in extravillous trophoblast and up-regulates migration. *J. Clin. Endocrinol. Metabolism* 99, E2288–E2297. doi:10.1210/jc.2014-2615

Peter Holm, H. C., and Callesen, H. (1998). *In vivo* versus *in vitro* produced bovine ova similarities and differences relevant for practical application. *Reprod. Nutr. Dev.* 38, 579–594. doi:10.1051/rnd:19980601

Qu, P., Qing, S., Liu, R., Qin, H., Wang, W., Qiao, F., et al. (2017). Effects of embryo-derived exosomes on the development of bovine cloned embryos. *PloS one* 12, e0174535. doi:10.1371/journal.pone.0174535

Reardon, S. N., King, M. L., Maclean, J. A., Mann, J. L., Demayo, F. J., Lydon, J. P., et al. (2012). CDH1 is essential for endometrial differentiation, gland development, and adult function in the mouse uterus. *Biol. reproduction* 86 (141), 1–10. doi:10.1095/biolreprod.112.098871

Ribeiro, J. C., Carrageta, D. F., Bernardino, R. L., Alves, M. G., and Oliveira, P. F. (2022). Aquaporins and animal gamete cryopreservation: advances and future challenges. *Animals* 12, 359. doi:10.3390/ani12030359

Robinson, D. H., and Benos, D. J. (1991). Chapter 4 ion and solute transport in preimplantation mammalian embryos. *Curr. Top. Membr.* 39, 121–150. doi:10.1016/S0070-2161(08)60802-3

Sakatani, M., Yamanaka, K., Kobayashi, S., and Takahashi, M. (2008). Heat shock-derived reactive oxygen species induce embryonic mortality in *in vitro* early stage bovine embryos. *J. Reproduction Dev.* 54, 496–501. doi:10.1262/jrd.20017

Schneyer, A., Sidis, Y., Xia, Y., Saito, S., Del Re, E., Lin, H. Y., et al. (2004). Differential actions of follistatin and follistatin-like 3. *Mol. Cell. Endocrinol.* 225, 25–28. doi:10.1016/j.mce.2004.02.009

Sidrat, T., Khan, A. A., Joo, M. D., Xu, L., El-Sheikh, M., Ko, J. H., et al. (2022). Extracellular vesicles improve embryo cryotolerance by maintaining the tight junction integrity during blastocoel re-expansion. *Reproduction* 163, 219–232. doi:10.1530/REP-21-0320

Strumpf, D., Mao, C.-A., Yamanaka, Y., Ralston, A., Chawengsaksophak, K., Beck, F., et al. (2005). Cdx2 is required for correct cell fate specification and differentiation of trophectoderm in the mouse blastocyst. *Development* 132, 2093–2102. doi:10.1242/dev.01801

Thibier, M. (2005). The zootechnical applications of biotechnology in animal reproduction: current methods and perspectives. *Reprod. Nutr. Dev.* 45, 235–242. doi:10.1051/rnd:2005016

Thompson, J. G. (1997). Comparison between *in vivo*-derived and *in vitro*-produced pre-elongation embryos from domestic ruminants. *Reproduction, Fertil. Dev.* 9, 341–354. doi:10.1071/r96079

Tsukita, S., Furuse, M., and Itoh, M. (2001). Multifunctional strands in tight junctions. *Nat. Rev. Mol. Cell Biol.* 2, 285–293. doi:10.1038/35067088

Underhill, K., Downey, B., Mcfarlane, C., and King, W. (1991). Cytogenetic analysis of Day-4 embryos from PMSG/hCG-treated prepuberal gilts. *Theriogenology* 35, 779–784. doi:10.1016/0093-691x(91)90419-e

Wheatley, S. C., Isacke, C. M., and Crossley, P. H. (1993). Restricted expression of the hyaluronan receptor, CD44, during postimplantation mouse embryogenesis suggests key roles in tissue formation and patterning. *Development* 119, 295–306. doi:10.1242/dev.119.2.295

Wilcox, E. R., Burton, Q. L., Naz, S., Riazuddin, S., Smith, T. N., Ploplis, B., et al. (2001). Mutations in the gene encoding tight junction claudin-14 cause autosomal recessive deafness DFNB29. *Cell* 104, 165–172. doi:10.1016/s0092-8674(01)00200-8

Wong, C. L., Huang, Y. Y., Ho, W. K., Poon, H. K., Cheung, P. L., O, W. S., et al. (2009). Growth-differentiation factor-8 (GDF-8) in the uterus: its identification and functional significance in the golden hamster. *Reprod. Biol. Endocrinol.* 7, 134. doi:10.1186/1477-7827-7-134

Wooldridge, L. K., and Ealy, A. D. (2019). Interleukin-6 increases inner cell mass numbers in bovine embryos. *BMC Dev. Biol.* 19, 2–11. doi:10.1186/s12861-019-0182-z

Wu, G., Gentile, L., Fuchikami, T., Sutter, J., Psathaki, K., Esteves, T. C., et al. (2010). Initiation of trophectoderm lineage specification in mouse embryos is independent of Cdx2. *Development* 137, 4159–4169. doi:10.1242/dev.056630

Xie, J., Zhu, H., Chang, H. M., Klausen, C., Dong, M., and Leung, P. C. K. (2020). GDF8 promotes the cell invasiveness in human trophoblasts by upregulating the expression of follistatin-like 3 through the ALK5-SMAD2/3 signaling pathway. *Front. Cell Dev. Biol.* 8, 573781. doi:10.3389/fcell.2020.573781

Yoon, J. D., Hwang, S. U., Kim, M., Lee, G., Jeon, Y., and Hyun, S. H. (2019). GDF8 enhances SOX2 expression and blastocyst total cell number in porcine IVF embryo development. *Theriogenology* 129, 70–76. doi:10.1016/j.theriogenology.2019.02.007

Zhang, S., Mesalam, A., Joo, M. D., Lee, K. L., Hwang, J. Y., Xu, L., et al. (2020). Matrix metalloproteinases improves trophoblast invasion and pregnancy potential in mice. *Theriogenology* 151, 144–150. doi:10.1016/j.theriogenology.2020.02.002

Zheng, X., Zheng, Y., Qin, D., Yao, Y., Zhang, X., Zhao, Y., et al. (2022). Regulatory role and potential importance of GDF-8 in ovarian reproductive activity. *Front. Endocrinol. (Lausanne)* 13, 878069. doi:10.3389/fendo.2022.878069

frontiers | Frontiers in Cell and Developmental Biology

TYPE Original Research
PUBLISHED 28 March 2024
DOI 10.3389/fcell.2024.1280797

Check for updates

OPEN ACCESS

EDITED BY
Katerina Komrskova,
Institute of Biotechnology (ASCR), Czechia

REVIEWED BY
Renee J. Chosed,
University of South Carolina, United States
William Kinsey,
University of Kansas Medical Center,
United States

*CORRESPONDENCE
Guohong Zhang,
g_ghzhang@stu.edu.cn

RECEIVED 21 August 2023
ACCEPTED 19 February 2024
PUBLISHED 28 March 2024

CITATION
Ma T, Zhou S, Xie X, Chen J, Wang J and Zhang G (2024), A case report of a family with developmental arrest of human prokaryotic stage zygote.
Front. Cell Dev. Biol. 12:1280797.
doi: 10.3389/fcell.2024.1280797

COPYRIGHT
© 2024 Ma, Zhou, Xie, Chen, Wang and Zhang. This is an open-access article distributed under the terms of the Creative Commons Attribution License (CC BY). The use, distribution or reproduction in other forums is permitted, provided the original author(s) and the copyright owner(s) are credited and that the original publication in this journal is cited, in accordance with accepted academic practice. No use, distribution or reproduction is permitted which does not comply with these terms.

A case report of a family with developmental arrest of human prokaryotic stage zygote

Tianzhong Ma[1], Songxia Zhou[2], Xuezhen Xie[2], Jingyao Chen[2], Jing Wang[2] and Guohong Zhang[2]*

[1]Reproductive Medicine Center, Affiliated Hospital of Guangdong Medical University, Zhanjiang, Guangdong, China, [2]Department of Pathology, Shantou University Medical College, Shantou, Guangdong, China

To study the genetic variation leading to the arrest phenotype of pronuclear (PN) zygotes. We recruited a family characterized by recurrent PN arrest during *in vitro* fertilization (IVF) and intracytoplasmic sperm injection cycles (ICSI) and performed whole-exome sequencing for 2 individuals. The transcriptome profiles of PN-arrest zygotes were assessed by single-cell RNA sequencing analysis. The variants were then validated by PCR amplification and Sanger sequencing in the affected individuals and other family members. A family characterized by recurrent PN arrest during IVF and ICSI cycles were enrolled after giving written informed consent. Peripheral blood samples were taken for DNA extraction. Three PN-arrest zygotes from patient III-3 were used for single-cell RNA-seq as described. This phenotype was reproduced after multiple cycles of egg retrieval and after trying different fertilization methods and multiple ovulation regimens. The mutant genes of whole exon sequencing were screened and verified. The missense variant c. C1630T (p.R544W) in *RGS12* was responsible for a phenotype characterized by paternal transmission. *RGS12* controls Ca^{2+} oscillation, which is required for oocyte activation after fertilization. Single-cell transcriptome profiling of PN-arrest zygotes revealed defective established translation, RNA processing and cell cycle, which explained the failure of complete oocyte activation. Furthermore, we identified proximal genes involved in Ca^{2+} oscillation–cytostatic factor–anaphase-promoting complex (Ca^{2+} oscillation–CSF–APC) signaling, including upregulated *CaMKII*, *ORAI1, CDC20,* and *CDH1* and downregulated *EMI1* and *BUB3*. The findings indicate abnormal spontaneous Ca^{2+} oscillations leading to oocytes with prolonged low CSF level and high APC level, which resulted in defective nuclear envelope breakdown and DNA replication. We have identified an RGS12 variant as the potential cause of female infertility characterized by arrest at the PN stage during multiple IVF and ICSI.

KEYWORDS

pronuclear arrest, zygote, *RGS12*, Ca^{2+} oscillation, case report

Abbreviations: APC, anaphase-promoting complex; BUB3, mitotic checkpoint protein; CaMKII, Calcium/calmodulin-dependent protein kinase II; CCNA2, cyclin A2; CDC, cell division cycle; CDH1, cadherin 1; CENPE, centromere protein E; CSF, cytostatic factor; EMI1, F-box protein 5; GMNN, geminin DNA replication inhibitor; ICSI, intracytoplasmic sperm injection; IVF, *in vitro* fertilization; ORAI1, calcium release-activated calcium modulator 1; PN, pronuclear; RGS12, regulator of G protein signaling 12.

Background

In vitro fertilization (IVF) is now routine for treating infertile women and has brought at least 8 million babies into the world. Indeed, the earliest embryonic development after fertilization is a complex process, including the formation of spermatozoa and oocyte pronuclei (two-pronuclear [2PN] zygote), cytoskeletal rearrangement, singamy, and initiation of cleavage of the zygote. After IVF trials, about 5% of fertilized human oocytes present early developmental arrest at the PN stage (Schmiady et al., 1987). Homozygous mutations in *TLE6* (MIM: 612399) and *PADI6* (MIM: 10363) have been reported to cause embryonic arrest at the 2- to 4-cell stage with normal cleavage in consanguineous families (Alazami et al., 2015; Xu et al., 2016). A patient presenting complete cleavage failure in 2PN oocytes after IVF carried the homozygous mutation c.322G > A (p.Glu108Lys) in *TUBB8* (Yuan et al., 2018). However, the crucial gene responsible for PN-arrest zygotes from familial individuals remains largely unknown.

Oocyte activation is Ca^{2+}-dependent, characterized by an increase in and spreading of intracellular Ca^{2+} waves. After formation of the male and female pronuclei, calcium signaling continues to play a crucial role in 2PN fusion, DNA synthesis, and initiation of the first cleavage. Therefore, optimal Ca^{2+} oscillation is required for both oocyte activation and 2PN fusion. Chemical artificial oocyte activation with the A23187 Ca^{2+} ionophore improved embryo development to the cleavage stage for zygotes with arrest at the PN stage. However, artificial oocyte activation with a Ca^{2+} ionophore resulted in partial success (Darwish and Magdi, 2015; Xi et al., 2020), so defects in an unknown mechanism can also contribute to Ca^{2+} oscillations causing 2PN fusion failure.

Here, we performed whole exome sequencing (WES) and single-cell RNA sequencing (RNA-seq) in a family characterized by recurrent PN arrest during IVF and intracytoplasmic sperm injection cycles. Our analysis implicated the causative variant in *RGS12*, a gene that controls Ca^{2+} oscillation, which is required for oocyte activation after fertilization.

Material and methods

Ethics approval and consent to participate

This study was approved by the Ethics Committee of Guangdong Medical University Affiliated Hospital (YS2018010), and written informed consent was obtained from participants. Patients gave written informed consent for the use of abandoned zygotes and peripheral blood for research on the arrest mechanism of PN stage, with no monetary payment. All procedures used were performed in accordance with the relevant guidelines and regulations.

Family recruitment

Families were recruited in the Reproductive Medicine Center at the Affiliated Hospital of Guangdong Medical University based on the observation of PN arrest during regular IVF treatment of 2 siblings. Eligible families and controls were enrolled after giving written informed consent. Peripheral blood samples were taken for DNA extraction.

Patients, ovarian stimulation, oocyte retrieval, and IVF/intracytoplasmic sperm injection (ICSI) procedures

Females III-2 and III-3 were 29 and 25 years old, with BMI of 18.82 and 18.92 kg/m^2. They both had primary infertility due to unexplained infertility. In the family, the women's ovarian function and sex hormones were normal, and the men's semen was normal. The peripheral blood chromosomes of both woman and man were normal as well (Supplementary Table S1).

IVF and ICSI were performed according to the laboratory routine insemination procedures on the day of oocyte retrieval (Day 0). The presence of 2 pronuclei (2PN) was observed 16–18 h after insemination or injection, then zygotes were cultured in 25 μL pre-equilibrated cleavage medium at 37°C under 6% CO_2. Embryo morphology was evaluated at 42–46 h (Day 2) and 68–72 h (Day 3) after insemination. Male and female pronuclei that continued to separate on Day 2 and 3 without fusion were defined as PN-arrest zygotes. More details of IVF/ICSI procedures are given in the following.

Ovarian stimulation

The ovulation promotion scheme and embryo development of patients with different egg retrieval cycles are described in detail in Supplementary Table S2.

Long agonist protocol: Briefly, 5–7 days after ovulation or after 15 days of being on pre-IVF Marvelon (N.V. Organon, Netherlands), gonadotropin-releasing hormone analogue (GnRH-a; single dose of 0.8–1.875 mg; Decapepty, Ferring, Germany) was administered. The GnRH-a administration phase ended on the human chorionic gonadotropin (hCG) administration day. The Gn phase of therapy, which started 14 days after starting GnRH-a delivery and finished on the hCG injection day, included a natural or synthetic follicle stimulating hormone (FSH) preparation (dose Gonal-F, Merck Serono, Germany), a luteinizing hormone (LH) preparation (dose Luveris, Merck Serono, Germany), and, finally, hCG (10,000 IU, Livzon Pharmaceutical Group, China). Eggs were harvested 34–36 h after hCG injection (generally, a single follicle with diameter of up to 19 mm, 2 follicles with diameter up to 18 mm, or 3 follicles with diameter up to 17 mm), when E2 levels were monitored (generally reaching a mean of 250–300 ng/L per dominant follicle [≥16 mm], and a proportion of dominant follicles as high as 60%).

Mild stimulation protocol: Without GnRH-a downregulation, a small number of ovulation-stimulating drugs is usually applied from the first 3–5 days of menstruation. Simple Gn was used to promote ovulation, or Gn was combined with oral ovulation-stimulating drugs to promote follicle growth After follicles grew and matured, after giving the hCG trigger, the egg was retrieved the next day.

Sperm preparation

Ejaculated samples were obtained after 3–5 days of abstinence. Semen was screened by the direct upstream method of fertilization culture fluid (G-IVF, Vitrolife Sweden AB). The pellet was resuspended in 0.3 mL fertilization culture fluid.

Oocyte retrieval

Transvaginal follicular aspiration was performed 36 h after recombinant hCG administration. After cumulus oocyte complexes were retrieved in 1 mL modified human tubal fluid medium (G-MOPS, Vitrolife Sweden AB) at 37°C, they were cultured in cleavage medium (G-1, Vitrolife Sweden AB) covered with light mineral oil (Vitrolife Sweden AB) at 37°C in 6% CO_2 for 2–4 h before conventional IVF, ICSI or IVF + ICSI (half the eggs were fertilized as routine and half by microinjection).

Oocyte preparation and insemination

All cumulus oocyte complexes were enzymatically treated with 80 μL hyaluronidase (Vitrolife Sweden AB) for 30–60 s with the aid of mechanical denudation to remove cumulus cells. The denuded oocytes were examined for maturity and integrity. Only metaphase II (MII) oocytes that had extruded the first polar body were injected by spermatozoa.

Zygote and embryo assessment

Fertilization was assessed 16–18 h after IVF or ICSI. On day 3 (68–72 h), cleaved embryos were morphologically graded by evaluating cell number, size, fragmentation and nucleation.

Whole-exome sequencing (WES) and data

WES was performed for 2 affected individuals and 3 unaffected individuals, including an unaffected sibling and parents. Germline genomic DNA was subjected to exome capture (60 Mb) with the Agilent SureSelect Human All ExonV6 kit according to the manufacturer's instructions (Agilent, Santa Clara, CA). Paired-end sequencing, resulting in 150 bases from each end of the fragments, involved using a HiSeq PE150 Genome Analyzer (Illumina) at Novogene Bioinformatics Technology (Beijing). Sequencing reads were mapped to the reference genome (GRCh37, UCSC hg19) by using the Burrow-Wheller Aligner and were analyzed by using the Genome Analysis Toolkit (GATK, v3.1) for calling single nucleotide variants, insertions and deletions. The 1,000 Genomes, Exome Sequencing Project (ESP6500), Exome Aggregation Consortium (ExAC) and an in-house database were used to annotate the minor allele frequency for each variant. *In silico* analysis, Sort Intolerant from Tolerant (SIFT), Polymorphism Phenotyping v2 (PolyPhen-2), MutationAssessor, and Genomic Evolutionary Rate Profiling (GERP++) were used to predict the impact of each non-synonymous variant.

Variant filtering

The pipeline was designed to filter heterozygous variants 1) shared by both affected individuals; 2) absent in other unaffected family members; 3) not previously reported or reported to have a frequency <0.1% in the public databases 1,000 Genomes, ESP6500, and ExAC and the in-house database; and 4) frameshift, nonsense, splice-site and missense variants predicted to be damaging in at least 3 of the 4 algorithms SIFT, PolyPhen-2, MutationAssessor, and GERP++.

Sanger sequencing validation and segregation analysis for candidate variants

The variants were then validated by PCR amplification and Sanger sequencing in the affected individuals and other family members. The *RGS12* gene-specific primers to generate the variation were 5′-CAGGTTCTGGGACCTAAACAAG-3′ (forward) and 5′-GAC TGTGCAAGCTGGTGACT-3′ (reverse). Variants were evaluated for co-segregation based on an autosomal-dominant mode of inheritance.

RNA library preparation and RNA sequencing (RNA-seq)

Three PN-arrest zygotes from patient III-3 were used for single-cell RNA-seq as described (Zhang et al., 2018). Briefly, zygotes were transferred into lysate buffer by using a mouth pipette, and whole-cell lysates underwent reverse transcription reaction according to the manufacturer's instructions. Terminal deoxynucleotidyl transferase was used to add a poly(A) tail to the 3′ end of the first-strand cDNA, then 20 + 10 cycles of PCR were used to amplify the single-cell cDNA. The libraries were sequenced on the HiSeq PE150 Genome Analyzer platform at Annoroad Gene Technology (Beijing; http://www.annoroad.com).

Transcript alignment and assembly

Overall read quality was checked by using FASTQC v.0.11.5. The raw sequence data, in the form of FASTQ files, were aligned to the human genome (GRCh38, Ensembl Homo_sapiens) by using HISAT2 (v. 2.1.0) and SAMTOOLS (v1.3.1). Read count and Fragments Per Kilobase Million (FPKM) mapped reads for each sample were generated by using HTSeq v0.6.0.

Differential expression analysis

HTSeq read counts were uploaded into RNA-seq 2G (http://52.90.192.24:3838/rnaseq2g/) for DESeq2 analysis. Normalization involved default settings ("normalize count by DESeq/normalize logged by Loess"). P-values were adjusted with the Benjamini and Hochberg method for controlling the false discovery rate (FDR). Genes with FDR $p < 0.05$ and fold change >2 or <0.5 were considered differentially expressed.

Functional enrichment analysis

RNA-seq normalized data (FPKM) were subjected to principal component analysis (PCA) by using an unsupervised approach to observe the whole clustering profile. Gene Ontology (GO, biological processes) and pathway enrichment involved using DAVID (http://david.abcc.ncifcrf.gov/) with the Benjamini and Hochberg FDR to adjust the *p*-value. Significantly enriched GO categories were visualized by using REVIGO (Supek et al., 2011) (http://revigo.irb.hr/). The network of enriched terms was evaluated by using Metascape (Zhou et al., 2019) (http://metascape.org/). To infer the transcription factor regulatory network of this study, we used all

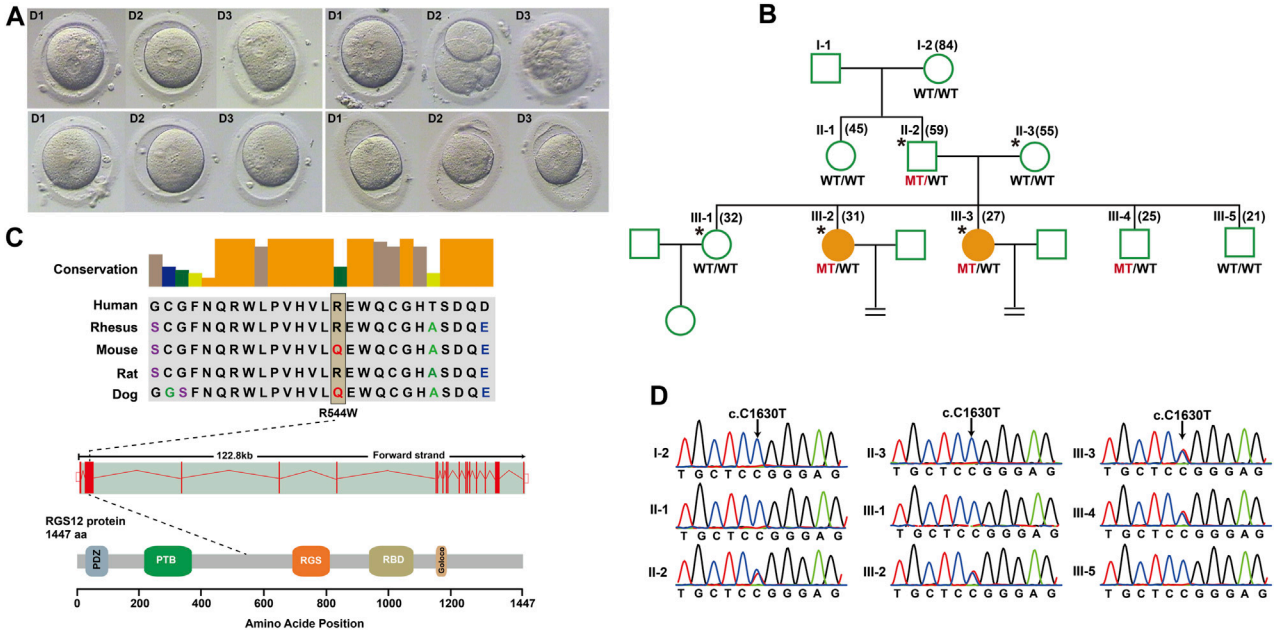

FIGURE 1
Structure of *RGS12* and sites of pathogenic mutations associated with pronuclear (PN)-arrest zygotes. **(A)** Morphology of zygotes on days 1–3 after IVF. Most zygotes from affected individuals remained at the one-cell stage, and maternal and paternal pronuclei were separated. **(B)** Pedigrees of the family affected by infertility due to arrest at PN zygote stage. Squares denote male family members, circles denote female members, and solid symbols represent affected members. Equal signs indicate infertility. MT, mutant type; WT, wild type. **(C)** Conservation of amino acid residues affected by mutations in different species, structure of *RGS12*, and known domains of the gene product. Exons are red vertical bars, introns are dashed lines, and open rectangles at each end are noncoding exons. **(D)** Sanger sequencing confirmation of *RGS12* variant (c.C1630T) in the family members.

1,665 human transcription factors in the human TFDB 3.0 database (http://bioinfo.life.hust.edu.cn/AnimalTFDB#!/).

Data availability

All RNA-seq datasets generated in this study have been deposited in Gene Expression Omnibus. Human oocyte, pre-implantation embryo RNA-seq data were obtained from GSE44183 (Xue et al., 2013). The RNA-seq data for normal PN zygotes (n = 22) were downloaded from GSE6548 (Yanez et al., 2016). The list of differentially expressed genes from RNA-seq data for validation were from a previous publication (Suo et al., 2018).

Statistical analysis

Statistical analysis was performed on original data by using GraphPad Prism 8.0 and Student's t-test with a significance threshold of $p < 0.05$.

Results

Identification of variant in *RGS12* responsible for phenotype of PN arrest of human zygotes

To identify novel PN zygote arrest-specific genes, we recruited a family with multiple infertile individuals who presented recurrent visible PN zygotes with second polar-body emission that failed to complete PN fusion after 24–68 h during IVF (Figure 1A; Supplementary Table S2). The affected individuals had primary infertility with an unknown cause. Initially, the affected individuals presented complete cleavage failure in all 2PN fertilized oocytes after 2 cycles of IVF. Subsequently, the affected individuals underwent 2 cycles of ICSI, with similar outcomes. We performed WES for 2 affected individuals (III-2 and III-3), an unaffected individual (III-1), and their parents (II-2 and II-3) (Figure 1B). Given the pedigree structure, we used an autosomal-dominant inheritance pattern and identified heterozygous, rare, potential pathogenic variants co-segregated with PN zygote arrest. Initially, 13 candidate genes were filtered by WES (Supplementary Table S3), and only the missense variant c. C1630T (minor allele frequency = 0.00018 in ExAC database) resulting in a p. R544W of regulator of G protein signaling-12 (*RGS12*) was confirmed by Sanger sequencing results available for relatives and was characterized by paternal transmission (Figure 1D).

RGS12 is the largest protein in the regulators of the G-protein signaling (RGS) family and is a negative regulator of specific G-protein–coupled receptor (GPCR) signals. *RGS12* p. R544W is located between the RGS and PTB domains and presents a non-conserved pattern between human and mouse (Figure 1C), so it might have a species-specific functional effect. The predicted protein structure of R544W mutant RGS12 was further rendered with ChimeraX (28710774). We observed that the predicted structures of mutational intolerance corresponding to amino acids with inward-facing side chains (Figure 2). Consequently, mutant protein has decreased efficiency of PTB structural domain (PTB),

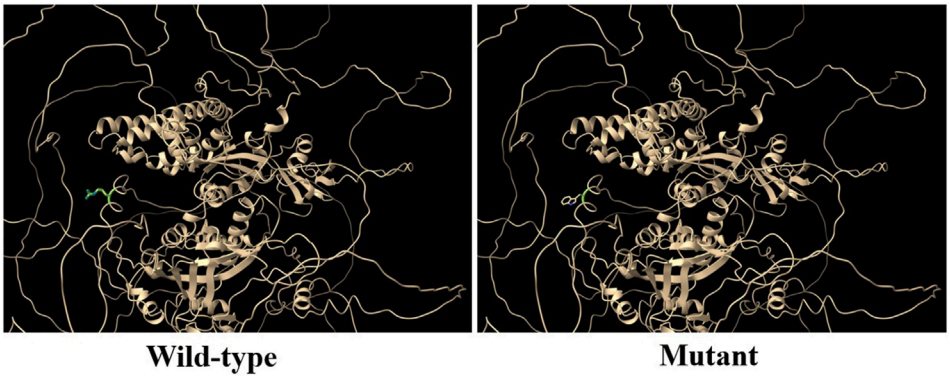

FIGURE 2
Three-dimensional structural analysis of wild-type and mutant RGS12 protein. Modeled structure of the RGS12 protein was painted by Chimera X software. Green indicated RGS protein structure in wild type, and the blue represent mutated RGS12 protein structure.

which can bind to N-type calcium channels. RGS12 inhibits Ca^{2+} oscillations through PTB inhibition of G protein activity.

Identification of the molecular landscape underlying PN-arrest zygotes caused by *RGS12* mutation

To describe the molecular landscape underlying the PN-arrest zygote (Figure 3A), we performed single-cell RNA-seq of PN-arrest zygotes (n = 3) from patient III-3 to explore the transcriptional profiles of PN-arrest zygotes by comparison with normal PN zygotes (n = 22, GSE65481) (Yanez et al., 2016). We found significant upregulation of 1,415 genes (fold change >2, $p < 0.001$) and downregulation of 1,545 genes (Figure 3B; Supplementary Table S4). Differentially expressed genes were enriched in the Gene Ontology (GO) terms (biological processes) RNA processing (FDR = 1.13×10^{-21}), translational elongation (FDR = 1.25×10^{-16}), intracellular transport (FDR = 1.63×10^{-15}), and cell cycle (FDR = 4.11×10^{-13}), so the oocyte-specific transcription and translation machinery is not completely established (Figures 3C, D). Pathway enrichment analysis revealed that differentially expressed genes in PN-arrest zygotes were also mainly involved in RNA processing and translation, such as ribosome (FDR = 6.40×10^{-22}) and spliceosome (FDR = 1.52×10^{-5}) (Figure 3F). The transition from oocyte to embryo is driven by a maternal stockpile of mRNA and translational machinery that is "packed" into the oocyte. Furthermore, oocyte activation after fertilization includes changes to oocyte coverings to prevent polyspermy, release of oocyte meiotic arrest, generation of haploid female and male pronuclei, changes in maternal mRNA and protein populations, and cytoskeletal rearrangements. Our transcriptional prolife results implied that the PN-arrest zygotes had properties of failure of complete oocyte activation after fertilization.

Mutant *RGS12* affects Ca^{2+} oscillations during oocyte activation after fertilization

Oocyte activation events present different Ca^{2+} requirements: 1) for cortical granules and blocking polyspermy; 2) inducing the resumption of meiosis including second meiotic polar body extrusion and initiating recruitment of maternal mRNAs; and 3) promoting pronuclear formation and initiation of embryonic mitosis. On oocyte activation, after PN formation, Ca^{2+} signaling continues to play a role in PN fusion and DNA synthesis for initiating embryonic mitosis during the oocyte-to-embryo transition.

Mature oocytes await fertilization while arrested at MII, which is maintained by the maturation promoting factor (MPF) consisting of cyclin B1/CDK1 subunits. Cytostatic factor (CSF) mediates MPF stabilization by inhibiting the anaphase-promoting complex (APC), which would otherwise destroy cyclin B. Fertilization breaks the MII arrest via cytoplasmic Ca^{2+} oscillation and triggers the APC, which mediates the degradation of cyclin B and thus inactivation of MPF. To confirm the spontaneous and abnormal Ca^{2+} oscillations, we traced the transcriptional change in genes that participate in vital processes from Ca^{2+} oscillation, CSF and APC (Figure 3E).

PN-arrest zygotes showed 9.54-fold increased *ZP3* expression, which indicates sustained *ZP3*-evoked Ca^{2+} entry by Ca^{2+} influx and activation of G protein (Patel, 2004). ZP3-mediated calcium in-flow is important for fertilization, but abnormal calcium in-flow may be an important manifestation of PN arrest zygotes. Furthermore, plasma membrane Ca^{2+} channel *ORAI1* mediates Ca^{2+} influx of oocytes after fertilization. In PN-arrest zygotes, *ORAI1* showed 7.2-fold upregulation, which further confirmed the Ca^{2+} influx. These results indicate a spontaneous and abnormal Ca^{2+} oscillation in PN-arrest zygotes.

Next, we explored further evidence to support spontaneous and abnormal Ca^{2+} oscillation and its effects. *CAMKII* (*CAMK2A*) links Ca^{2+} oscillations and inactivates the MPF as well as translation and degradation of maternal mRNAs. PN-arrest zygotes showed upregulated *CAMK2A*, which implies the existence of prolonged Ca^{2+} oscillations. *CaMKII* activation by Ca^{2+} oscillations leads to activation of the APC by inhibiting CSF activity, which suppresses APC via *EMI1* working with proto-oncogene, serine/threonine kinase (MOS). Because of abnormal Ca^{2+} oscillations, *EMI1* (*FBXO5*) was significantly downregulated (12.25-fold) in PN-arrest zygotes, which indicates the lower CSF level and possible high APC level.

Activation of APC is regulated by 2 activators, *CDC20* and *CDH1*. *CDC20* and *CDH1* expression was 2.7- and 10.3-fold increased, respectively, in PN-arrest zygotes. *CDC20* and *CDH1* bind to APC7, whose level was also increased in PN-arrest zygotes.

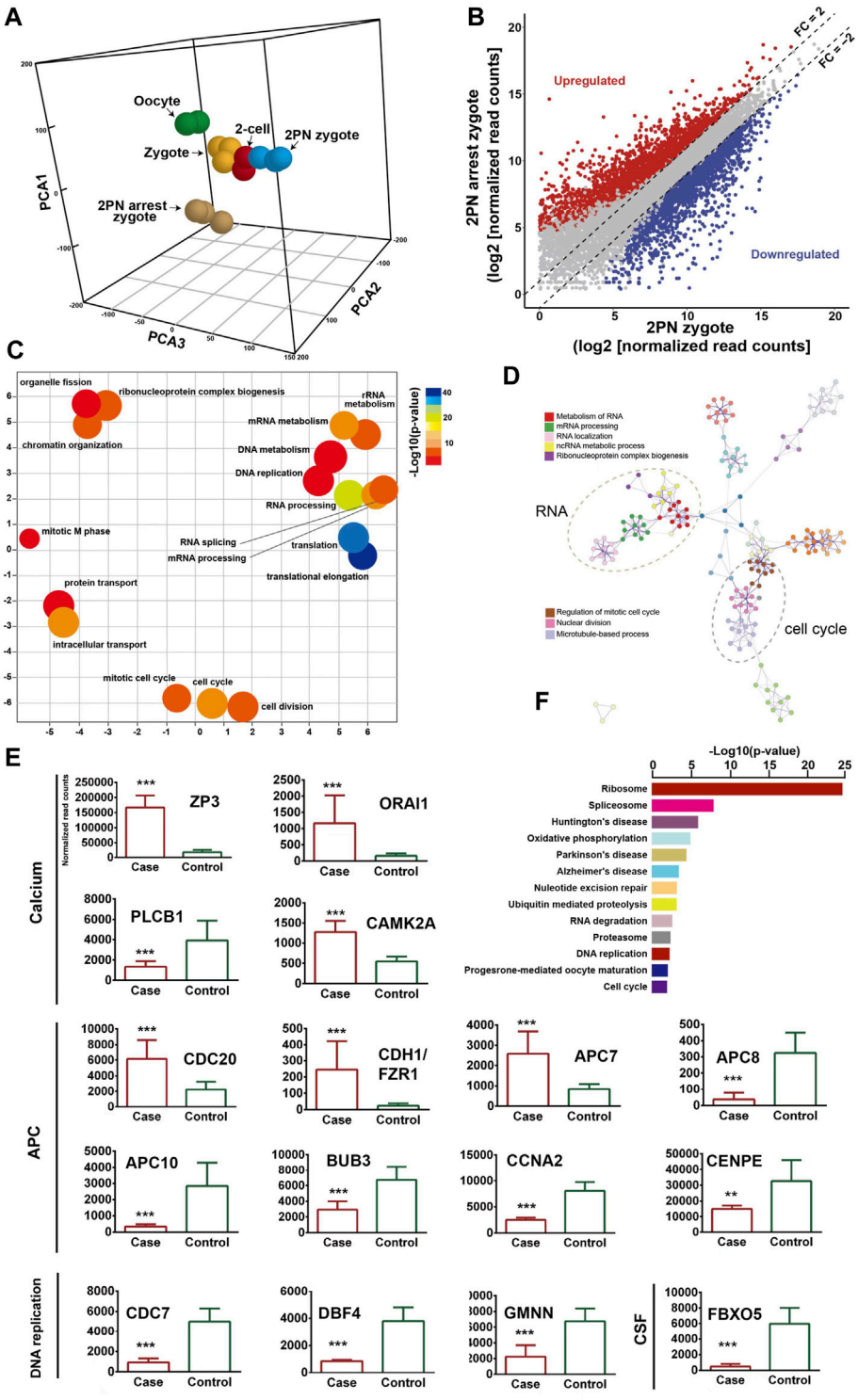

FIGURE 3
Transcriptome profile of PN arrest zygote by single-cell RNA-sequencing. **(A)** 3-D principal-component analysis (PCA) of the transcriptome of human oocytes, preimplantation embryos and PN-arrest zygotes. Cells of different preimplantation stages form distinct clusters, and PN-arrest zygotes had a specific transcriptome character. **(B)** Scatter plots comparing expression of genes with fold change >2, false discovery rate (FDR) < 0.05. **(C)** REVIGO scatter plot showing the cluster representatives in a 2-D space derived by applying multidimensional scaling to a matrix of semantic similarities for the Gene Ontology (GO) terms (biological processes). **(D)** Metascape enrichment network showing intra- and inter-cluster similarities of enriched GO terms. Cluster annotations are shown in color code. **(E)** Comparative analysis of genes in the Ca^{2+} oscillation–CSF–APC signaling pathway by average RNA-sequencing of normalized read counts for human PN and PN-arrest zygotes. FDR value, Data are mean ± SD. **, $p < 0.001$; ***, $p < 0.0001$. **(F)** Significantly enriched KEGG pathways in PN-arrest zygotes; length of column indicates the−log10 p-value.

The mitotic checkpoint complex (MCC), composed of *CDC20, MAD2, BUBR1, CENPE* and *BUB3*, acts as an APC inhibitor (Chao et al., 2012), but we found downregulated *BUB3* and *CENPE* in PN-arrest zygotes. Downregulation of *EMI1* and *BUB3* and upregulation of *CDC20, CDH1,* and *APC7* implied continually increased APC level in PN-arrest zygotes.

APC10 and cyclin A2 (*CCNA2*) were downregulated in PN-arrest zygotes, with no change in *CCNB1* expression. We also found downregulation of *GMNN* (geminin), an APC substrate and essential for regulation of DNA replication for zygotes. In PN-arrest zygotes, *CDC7/DBF4* expression was decreased ~ five-fold. Therefore, continuous APC disrupted nuclear envelope breakdown (NEBD) and DNA replication in PN-arrest zygotes.

Increased expression of ZP3 and Orai1 in PN arrest zygotes may lead to disturbances in calcium inward flow and promote APC activity. Here we speculate that spontaneous and abnormal Ca^{2+} oscillation increased APC level by the mutant *RGS12*, thus leading to defective NEBD and DNA replication after 24–68 h in IVF trials. The trigger for the oocyte-to-embryo transition is oocyte activation. Therefore, our evidence supports that the PN arrest is due to spontaneous and abnormal Ca^{2+} oscillation causing prolonged APC activation. Hence, a precise pattern of Ca^{2+} oscillations after fertilization should be evaluated for further treating optimal oocyte activation.

Validation of Ca^{2+} oscillation–CSF–APC signaling in PN arrest zygotes

We identified 589 common genes enriched in the GO terms translational elongation (FDR = 5.88×10^{-34}) and translation (FDR = 2.45×10^{-17}) and confirmed the incomplete oocyte activation. The key components of Ca^{2+} oscillation, CSF and APC signaling, *EMI1, CCNA2, CDC7/DBF4,* and *GMNN* were also identified (Figures 4A–D). To investigate the master regulators and construct the transcriptional regulatory network in the PN-arrest zygotes, we used the ARACNe method to analyze transcription factors. Only the transcription factor *MAX* was upregulated (Figure 4E), so *MYC-MAX* may play a critical role in the cell cycle entry of PN-arrest zygotes.

We found upregulation of 2- to 4-cell arrest-specific genes *TLE6* and *PATL2*; hence, the *RGS12* mutation caused earlier embryonic development arrest (Figure 4E). Furthermore, *SYCP3* and *TUBB8* were downregulated, which indicates defective cytoskeletal rearrangements. We did not find a disruption of zygotic arrest 1 (*ZAR1*), a oocyte-specific maternal-effect gene for mouse oocyte-to-embryo transition (Wu et al., 2003).

Discussion

In this study, we used WES to explore mutations affecting familial individuals with recurrent PN arrest during IVF and ICSI cycles. We identified a heterozygous pathogenic variant in RGS12 that was responsible for the phenotype. Moreover, single-cell RNA-seq identified proximal genes involved in Ca^{2+} oscillation–CSF–APC signaling. The findings indicate that abnormal spontaneous Ca^{2+} oscillations led to oocytes with prolonged low CSF level and high APC level, which resulted in defective NEBD and DNA replication.

Maternal genes have a critical effect in the earliest stages of embryonic development. *ZAR1* was first identified as an oocyte-specific maternal-effect gene that functions at the oocyte-to-embryo transition in mice (Wu et al., 2003), Novel synonymous variation (c.516C>T) and intron variation (c.964-55A>T) of *ZAR1* were identified in individuals with recurrent uncleaved zygotes in IVF (Tian et al., 2020). Homozygous mutations in *BTG4* caused zygotic cleavage failure in 4 independent affected females with infertility of unknown cause (Zheng et al., 2020). *BTG4/CCR4-NOT*–induced mRNA deadenylation is involved in regulating maternal mRNA stability (Sha et al., 2020). However, nothing is known about the genetic cause of the phenotype of human PN-arrest zygotes from familial individuals.

Here we describe a rare family with multiple infertile female members with phenotypes of human PN-arrest zygotes. Use of WES revealed that the affected members carried a paternally originated autosomal-dominant mutation (p.R544W) in *RGS12*, a member of the family of regulators of G-protein signaling. *RGS12* variants have been considered the most promising candidates in multiple families affected by bipolar disorder identified by WES (Forstner et al., 2020). To the best of our knowledge, this is the first report to describe a variant in the *RGS12* responsible for female infertility characterized by arrest at the PN stage during multiple IVF. The genetic basis for infertility characterized by abnormalities in human oocyte development and early embryogenesis (2- to 4-cell) has been described (Alazami et al., 2015; Feng et al., 2016; Xu et al., 2016). A variant in *RGS12* extends the genetic causes of infertility. Therefore, our findings will facilitate genetic diagnoses for *RGS12* mutation in identifying patients with infertility who are undergoing IVF and ICSI.

ZAR1 regulates mRNA translation during the oocyte-to-embryo transition (Tian et al., 2020). *BTG4* variants impair the decay of maternal mRNA in zygotes of the affected individual with zygotic cleavage failure (Zheng et al., 2020). Unlike *ZAR1* and *BTG4*, which affect maternal mRNA translation, *RGS12* plays an important role in Ca^{2+} oscillations in osteoblasts, neurons and other cell types (Schiff et al., 2000; Richman et al., 2005; Li et al., 2019). Therefore *RGS12* controls Ca^{2+} oscillations, which provides an important spatially restricted Ca^{2+} signal required for complete oocyte activation after fertilization and triggers CSF–APC signaling to switch from meiosis to mitotis. Our single-cell transcriptome sequencing data revealed unique features in translation, RNA processing and cell-cycle impairments of failure of complete oocyte activation and uncovered the Ca^{2+} oscillation–CSF–APC signaling pathway by which mutant *RGS12* exerts its maternal effect on PN arrest. The genes involved in PN arrest of the Ca^{2+} oscillation–CSF–APC signaling pathway were validated in other studies (Suo et al., 2018). The partially activated oocytes not progressing further and becoming arrested again in the PN stage were described as a new MII arrest (Kubiak, 1989). The key genes underlying the PN-arrest zygote (Figure 5) improve our understanding of why and how *RGS12* mutation causes the phenotype.

Our validated single-cell transcriptional data support that a loss-of-function effect of *RGS12* p. R544W causes spontaneous and abnormal Ca^{2+} oscillations in zygotes with 2PN arrest after fertilization. Our findings could explain why artificial oocyte activation using the A23187 Ca^{2+} ionophore improved embryo development only to the cleavage stage at a limited rate (one of 4 couples) (Darwish and Magdi, 2015). Spontaneous and abnormal Ca^{2+} oscillations in zygotes with 2PN arrest also raise the possibility of developing antagonists to block the excessive free Ca^{2+}, such as Ca^{2+} chelators BAPTA and EGTA.

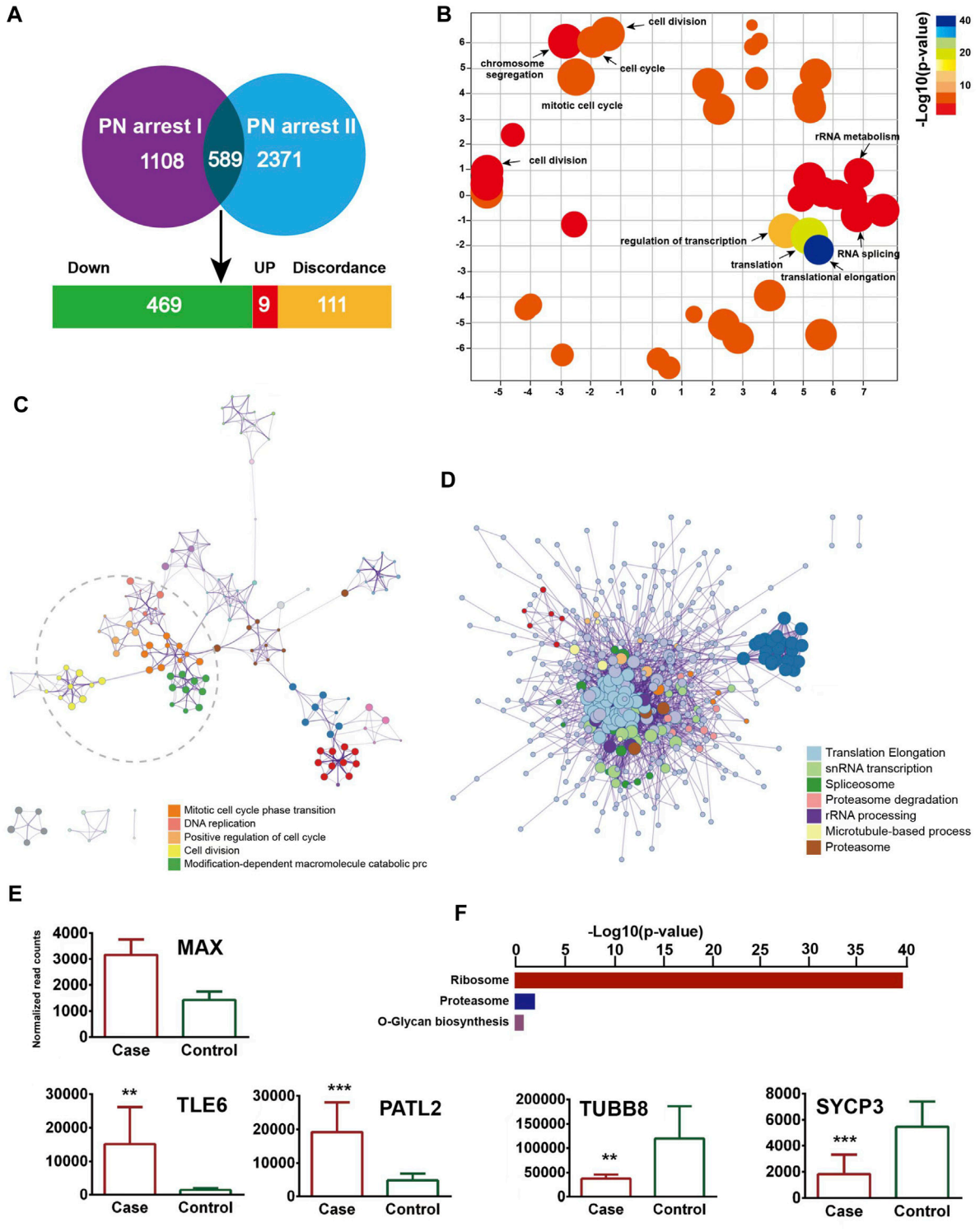

FIGURE 4
Validation of transcriptome profile in other PN-arrest zygotes. **(A)** Venn diagram shows overlapped differentially expressed genes between previous study by Suo et al. (2018) (PN arrest I) and our study (PN arrest II) for PN arrest groups each compared with their control group. **(B)** REVIGO scatterplot summarizes the overrepresented GO terms (biological processes) for representative subsets of terms. **(C)** Metascape enrichment network of the intra-cluster and inter-cluster similarities of enriched GO terms. **(D)** Metascape interactome network formed by all GO terms, confirming the defective RNA processing and translation in both PN-arrest zygote groups. **(E)** Relative expression of particularly interesting DEGs. FDR value, Data are mean ± SD. **, $p < 0.001$; ***, $p < 0.0001$. **(F)** Significantly enriched KEGG pathways shared in PN-arrest zygotes.

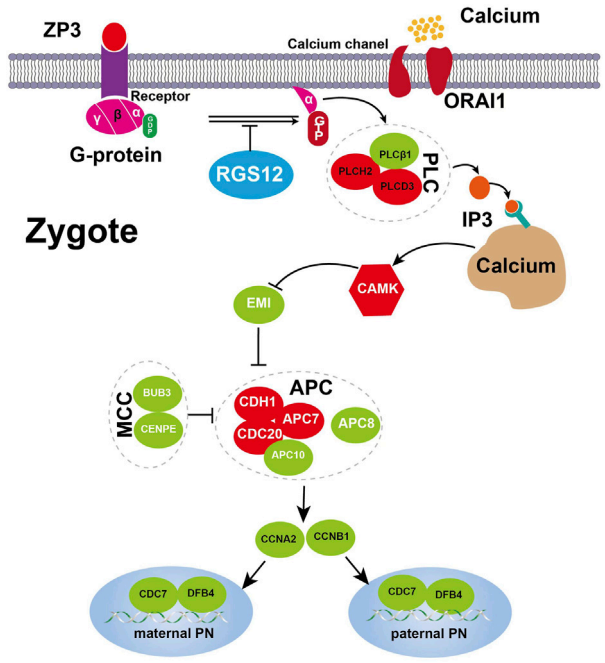

FIGURE 5
Expression changes of key genes involved Ca^{2+} oscillation–CSF–APC signaling. A proposed model for the *RGS12*-mutant oocyte with spontaneous and abnormal Ca^{2+} oscillations leading to prolonged low CSF and high APC level resulting in defective nuclear envelope breakdown and DNA replication. The key component genes are represented by green (downregulation) and red (upregulation), respectively. Detailed explanations are provided in the text.

Conclusion

We have identified an *RGS12* variant as the potential cause of female infertility characterized by arrest at the PN stage during multiple IVF and ICSI. This gene should be further screened in individuals with infertility caused by arrest at the PN stage during IVF and ICSI. These findings expand our knowledge of the genetic basis of human early embryonic arrest and provide the basis for genetic diagnoses of clinically infertile individuals with this phenotype.

Data availability statement

Sequencing data have been deposited in public, open access repository of the Genome Sequence Archive for Human (http://bigd.big.ac.cn/gsa-human/) with the accession no. HRA006945.

Ethics statement

The studies involving humans were approved by the Ethics Committee of Guangdong Medical University Affiliated Hospital. The studies were conducted in accordance with the local legislation and institutional requirements. The participants provided their written informed consent to participate in this study. The manuscript presents research on animals that do not require ethical approval for their study. Written informed consent was obtained from the individual(s) for the publication of any potentially identifiable images or data included in this article.

Author contributions

TM: Data curation, Funding acquisition, Resources, Writing–original draft, Writing–review and editing. SZ: Methodology, Data curation, Formal Analysis, Writing–review and editing. XX: Methodology, Data curation, Investigation, Formal Analysis, Writing–review and editing. JC: Methodology, Conceptualization, Data curation, Formal Analysis, Writing–review and editing. JW: Methodology, Data curation, Investigation, Formal Analysis, Writing–review and editing. GZ: Formal Analysis, Project administration, Writing–original draft, Writing–review and editing.

Funding

The author(s) declare financial support was received for the research, authorship, and/or publication of this article. This study was supported by grants from the Nature Science Foundation of Guangdong Province (2022A1515010849) and the National Nature Science Foundation of China (81300484).

Acknowledgments

We acknowledge J. L. for excellent technical assistance.

Conflict of interest

The authors declare that the research was conducted in the absence of any commercial or financial relationships that could be construed as a potential conflict of interest.

Publisher's note

All claims expressed in this article are solely those of the authors and do not necessarily represent those of their affiliated organizations, or those of the publisher, the editors and the reviewers. Any product that may be evaluated in this article, or claim that may be made by its manufacturer, is not guaranteed or endorsed by the publisher.

Supplementary material

The Supplementary Material for this article can be found online at: https://www.frontiersin.org/articles/10.3389/fcell.2024.1280797/full#supplementary-material

References

Alazami, A. M., Awad, S. M., Coskun, S., Al-Hassan, S., Hijazi, H., Abdulwahab, F. M., et al. (2015). TLE6 mutation causes the earliest known human embryonic lethality. *Genome Biol.* 16, 240. doi:10.1186/s13059-015-0792-0

Chao, W. C., Kulkarni, K., Zhang, Z., Kong, E. H., and Barford, D. (2012). Structure of the mitotic checkpoint complex. *Nature* 484 (7393), 208–213. doi:10.1038/nature10896

Darwish, E., and Magdi, Y. (2015). A preliminary report of successful cleavage after calcium ionophore activation at ICSI in cases with previous arrest at the pronuclear stage. *Reprod. Biomed. Online* 31 (6), 799–804. doi:10.1016/j.rbmo.2015.08.012

Feng, R., Sang, Q., Kuang, Y., Sun, X., Yan, Z., Zhang, S., et al. (2016). Mutations in TUBB8 and human oocyte meiotic arrest. *N. Engl. J. Med.* 374 (3), 223–232. doi:10.1056/NEJMoa1510791

Forstner, A. J., Fischer, S. B., Schenk, L. M., Strohmaier, J., Maaser-Hecker, A., Reinbold, C. S., et al. (2020). Whole-exome sequencing of 81 individuals from 27 multiply affected bipolar disorder families. *Transl. Psychiatry* 10 (1), 57. doi:10.1038/s41398-020-0732-y

Kubiak, J. Z. (1989). Mouse oocytes gradually develop the capacity for activation during the metaphase II arrest. *Dev. Biol.* 136 (2), 537–545. doi:10.1016/0012-1606(89)90279-0

Li, Z., Liu, T., Gilmore, A., Gómez, N. M., Fu, C., Lim, J., et al. (2019). Regulator of G Protein signaling protein 12 (Rgs12) controls mouse osteoblast differentiation via calcium channel/oscillation and gαi-ERK signaling. *J. Bone Min. Res.* 34 (4), 752–764. doi:10.1002/jbmr.3645

Patel, T. B. (2004). Single transmembrane spanning heterotrimeric g protein-coupled receptors and their signaling cascades. *Pharmacol. Rev.* 56 (3), 371–385. doi:10.1124/pr.56.3.4

Richman, R. W., Strock, J., Hains, M. D., Cabanilla, N. J., Lau, K. K., Siderovski, D. P., et al. (2005). RGS12 interacts with the SNARE-binding region of the Cav2.2 calcium channel. *J. Biol. Chem.* 280 (2), 1521–1528. doi:10.1074/jbc.M406607200

Schiff, M. L., Siderovski, D. P., Jordan, J. D., Brothers, G., Snow, B., De Vries, L., et al. (2000). Tyrosine-kinase-dependent recruitment of RGS12 to the N-type calcium channel. *Nature* 408 (6813), 723–727. doi:10.1038/35047093

Schmiady, H., Kentenich, H., and Stauber, M. (1987). Developmental arrest of fertilized human oocytes in the pronuclear stage after *in vitro* fertilization (IVF). *Geburtshilfe Frauenheilkd* 47 (6), 406–409. doi:10.1055/s-2008-1036145

Sha, Q. Q., Zheng, W., Wu, Y. W., Li, S., Guo, L., Zhang, S., et al. (2020). Dynamics and clinical relevance of maternal mRNA clearance during the oocyte-to-embryo transition in humans. *Nat. Commun.* 11 (1), 4917. doi:10.1038/s41467-020-18680-6

Suo, L., Zhou, Y. X., Jia, L. L., Wu, H. B., Zheng, J., Lyu, Q. F., et al. (2018). Transcriptome profiling of human oocytes experiencing recurrent total fertilization failure. *Sci. Rep.* 8 (1), 17890. doi:10.1038/s41598-018-36275-6

Supek, F., Bosnjak, M., Skunca, N., and Smuc, T. (2011). REVIGO summarizes and visualizes long lists of gene ontology terms. *PLoS One* 6 (7), e21800. doi:10.1371/journal.pone.0021800

Tian, Y., Yang, J., Peng, Y., Chen, T., Huang, T., Zhang, C., et al. (2020). Variation screening of zygote arrest 1(ZAR1) in women with recurrent zygote arrest during IVF/ICSI programs. *Reprod. Sci.* 27 (12), 2265–2270. doi:10.1007/s43032-020-00246-y

Wu, X., Viveiros, M. M., Eppig, J. J., Bai, Y., Fitzpatrick, S. L., and Matzuk, M. M. (2003). Zygote arrest 1 (Zar1) is a novel maternal-effect gene critical for the oocyte-to-embryo transition. *Nat. Genet.* 33 (2), 187–191. doi:10.1038/ng1079

Xi, H., Fu, Y., Liu, C., Lu, X., Sui, L., Chen, Y., et al. (2020). Assisted oocyte activation with calcium ionophore 44 hours after intracytoplasmic sperm injection resulting in successful pregnancy. *Gynecol. Endocrinol.* 36 (11), 1035–1037. doi:10.1080/09513590.2020.1737667

Xu, Y., Shi, Y., Fu, J., Yu, M., Feng, R., Sang, Q., et al. (2016). Mutations in PADI6 cause female infertility characterized by early embryonic arrest. *Am. J. Hum. Genet.* 99 (3), 744–752. doi:10.1016/j.ajhg.2016.06.024

Xue, Z., Huang, K., Cai, C., Cai, L., Jiang, C. Y., Feng, Y., et al. (2013). Genetic programs in human and mouse early embryos revealed by single-cell RNA sequencing. *Nature* 500 (7464), 593–597. doi:10.1038/nature12364

Yanez, L. Z., Han, J., Behr, B. B., Pera, R. A. R., and Camarillo, D. B. (2016). Human oocyte developmental potential is predicted by mechanical properties within hours after fertilization. *Nat. Commun.* 7, 10809. doi:10.1038/ncomms10809

Yuan, P., Zheng, L., Liang, H., Li, Y., Zhao, H., Li, R., et al. (2018). A novel mutation in the TUBB8 gene is associated with complete cleavage failure in fertilized eggs. *J. Assist. Reprod. Genet.* 35 (7), 1349–1356. doi:10.1007/s10815-018-1188-3

Zhang, Y., Yan, Z., Qin, Q., Nisenblat, V., Chang, H. M., Yu, Y., et al. (2018). Transcriptome landscape of human folliculogenesis reveals oocyte and granulosa cell interactions. *Mol. Cell* 72 (6), 1021–1034. doi:10.1016/j.molcel.2018.10.029

Zheng, W., Zhou, Z., Sha, Q., Niu, X., Sun, X., Shi, J., et al. (2020). Homozygous mutations in BTG4 cause zygotic cleavage failure and female infertility. *Am. J. Hum. Genet.* 107 (1), 24–33. doi:10.1016/j.ajhg.2020.05.010

Zhou, Y., Zhou, B., Pache, L., Chang, M., Khodabakhshi, A. H., Tanaseichuk, O., et al. (2019). Metascape provides a biologist-oriented resource for the analysis of systems-level datasets. *Nat. Commun.* 10 (1), 1523. doi:10.1038/s41467-019-09234-6

frontiers | Frontiers in Cell and Developmental Biology

TYPE Original Research
PUBLISHED 03 June 2024
DOI 10.3389/fcell.2024.1398684

Check for updates

OPEN ACCESS

EDITED BY
Martin Anger,
Academy of Sciences of the Czech Republic (ASCR), Czechia

REVIEWED BY
Shawn L. Chavez,
Oregon Health & Science University, United States
Pavel Travnik,
Repromeda s.r.o., Czechia

*CORRESPONDENCE
Mattan Levi,
mattanlevi@gmail.com

RECEIVED 10 March 2024
ACCEPTED 13 May 2024
PUBLISHED 03 June 2024

CITATION
Nemerovsky L, Ghetler Y, Wiser A and Levi M (2024), Two types of cleavage, from zygote to three cells, result in different clinical outcomes and should be treated differently.
Front. Cell Dev. Biol. 12:1398684.
doi: 10.3389/fcell.2024.1398684

COPYRIGHT
© 2024 Nemerovsky, Ghetler, Wiser and Levi. This is an open-access article distributed under the terms of the Creative Commons Attribution License (CC BY). The use, distribution or reproduction in other forums is permitted, provided the original author(s) and the copyright owner(s) are credited and that the original publication in this journal is cited, in accordance with accepted academic practice. No use, distribution or reproduction is permitted which does not comply with these terms.

Two types of cleavage, from zygote to three cells, result in different clinical outcomes and should be treated differently

Luba Nemerovsky[1,2], Yehudith Ghetler[1], Amir Wiser[1,2] and Mattan Levi[1,2]*

[1]IVF Unit, Department of Obstetrics and Gynecology, Meir Medical Center, Kefar Sava, Israel, [2]Faculty of Medicine, Tel Aviv University, Tel Aviv, Israel

Research Question: What is the utilization rate of embryos that exert inadequate zygote cleavage into three daughter cells?

Design: This study used a retrospective dataset from a single IVF Unit. A total of 3,060 embryos from 1,811 fresh IVF cycles were analyzed. The cleavage pattern, morphokinetics, and outcome were recorded. Only 2pn embryos, fertilized by ejaculated sperm, and cultured in a time-lapse system for at least 5 days were included. We generated three study groups according to the embryo's cleavage pattern: (I) Control, normal cleavage (n = 551); (II) fast cleavage, zygote to three cells within 5 h (n = 1,587); and (III) instant direct tripolar cleavage (IDC) from zygote to three cells (n = 922).

Results: The rate of usable fast cleavage blastocysts was 108/1,587 (6.81%) and usable control blastocysts was 180/551 (32.67%). The time of PN fading and from fading to first cleavage differed significantly between the three groups. Although the pregnancy rate of control and fast cleavage blastocysts were comparable (40.35% and 42.55%, respectively), the amount of instant direct cleavage embryos that reached blastocyst stage was neglectable (only four embryos out of 922 analyzed IDC embryos) and unsuitable for statistical comparison of pregnancy rates.

Conclusion: Our results indicate the need to culture instant direct cleavage embryos for 5 days, up to the blastocyst stage, and avoid transfer of embryos that are fated to arrest even when their morphological grade on day 3 is acceptable, whereas fast cleavage embryos could be transferred on day 3 when there is no alternative.

KEYWORDS

zygote, direct cleavage, Z-score, embryo, blastocyst

Introduction

Identifying embryos with the highest implantation potential and early identification of those that are abnormal is very challenging in ART (Anagnostopoulou et al., 2022; Coticchio et al., 2022). Time-lapse imaging in incubating systems enable continuous observation of embryos' morphological and kinetic parameters. Zygote morphology is one of the earliest embryonic stages investigated. Several zygote grading systems have been proposed (Nicoli et al., 2013) based on the size and distribution of pronuclei (PN) and nucleolus precursor bodies (NPB). Evaluating

the size of the PN just before their membranes breakdown is an effective indicator of the embryo's potential to result in a live birth (Otsuki et al., 2017). NPB are aggregations of dense fibrillar material that are visible in the PN of fertilized oocytes. Spatial distribution and size of these particles is associated with chromatin rearrangement during fertilization, in preparation for the first cleavage (Cavazza et al., 2021), as they serve as the major heterochromatin-organizing sites. The arrangement of NPB in human zygotes at the pronuclear interface is an indicator of efficient chromosome clustering (required for correct unification of the parental genomes after fertilization) and suggests accurate chromosome segregation and adequate embryo development (Scott, 2003; Cavazza et al., 2021). Chromosome segregation errors, such as misaligned, unattached, or lagging chromosomes, occur mainly in the first cleavage cycle (Currie et al., 2022).

Time-lapse cinematography reveals the occurrence of abnormal cleavage patterns, such as abnormal zygote mitosis resulting in three or more daughter cells, that are otherwise morphologically indistinguishable (Milewski and Ajduk, 2017). Mitotic abnormalities that arise in early cleavage stages affect a large portion of the lineage of the embryonic cells and have a critical effect on the developing embryo (Currie et al., 2022). By using time-lapse monitoring, we can observe cleavage of one cell into three daughter cells through either single tripolar mitosis or two consecutive mitoses separated by a very short interval (cleavage in less than 5 h), defined as direct cleavage (DC; Rubio et al., 2012). This phenomenon might occur at the first, second, or even later cleavage cycles. The mechanisms causing multipolar spindles are not clear, involving abnormal centriole distribution, abnormal centriole replication, or additional formation of a microtubule organizing center, leading to an additional spindle (Kalatova et al., 2015; Ottolini et al., 2017). DC in early stages strongly correlates with impaired blastocyst formation, implantation, and clinical outcome, whereas DC at later stages has a milder impact (Zhan et al., 2016). In two-pronuclear (2PN) human embryos, the frequency of DC at the first cleavage varied widely, ranging from 8.3% to 26% (Athayde Wirka et al., 2014; Yang et al., 2015; Zhan et al., 2016). Moreover, the exact timing of DC could assist in predicting the future of the developing embryo (Bamford et al., 2022). The aim of this study was to differentiate between zygote instant direct cleavage (IDC), defined as cleavage directly into three daughter cells, and fast cleavage (FC), defined as cleavage within less than 5 h from zygote to three daughter cells, comparing and investigating their occurrence and clinical outcomes. We also analyzed zygote morphological parameters of IDC embryos and compared them with those of normally cleaving siblings, in search of signs to predict and identify abnormal cleavage patterns at the zygote stage.

Materials and methods

Research approval

This retrospective cohort study was approved by the institutional Helsinki committee, No. 0043-22-MMC from 09/02/2022.

Study design and participants

The study was conducted from 2014 to 2022. A total of 6024 ART cycles were performed during this period. Only 2PN embryos, fertilized by ejaculated sperm and cultured in time-lapse incubators (EmbryoScope1, Vitrolife, Sweden) for more than 113 h, were retrospectively analyzed. This timeframe was selected as minimal period from insemination (both ICSI and IVF) to the occurrence of the fifth day of incubation in our laboratory protocol (the latest insemination was at 14:00 of day 0 and the earliest annotation was at 7:00 of day 5). In our unit, the EmbryoScope image acquisition system is set to capture images from seven focal planes for each embryo every 15 min during the entire culture period. The time-lapse video created from these images allowed monitoring of specific cell cycle events, as well as embryo morphology. A total of 3,060 embryos from 1,811 cycles were included. The time-lapse annotations were performed independently by three senior embryologists following the same annotation protocol. A rigorous IQC program is used in our laboratory, with an average of CV = 6.2 in the past 3 years.

Embryo culture and study groups

All embryos in our laboratory are cultured in single-step Global culture media, (LifeGlobal, Brussels, Belgium) with incubation conditions of 37°C, 5% (±0.3) O_2, and 5.5% (±0.5) CO_2. Day 5 embryo grading was performed according to Gardner's classification (Gardner and Schoolcraft, 1999). According to unit policy, blastocysts BB or above were used, whereas embryos classified as C were not transferred or cryopreserved. In this study, first cleavage patterns were classified as follows (Figure 1): instant direct cleavage (IDC) from zygote to three or four daughter cells, fast cleavage (FC) from zygote to three or four daughter cells in less than 5 h, and normally cleaving embryos were defined as three to four cells in more than 5 h (Wong et al., 2010). Follow-up of these embryos and their outcomes were monitored: arrested (developmental stage recorded), blastocyst used (transferred or cryopreserved), and blastocyst discarded (classified as C grade of ICM or TE). Interval from fertilization to PN fading and from PN fading to first cleavage was also recorded.

Zygote morphological assessment

Meticulous assessment in search of predictive signs for upcoming IDC was performed in a series of consecutive treatment cycles. The measures of Z-score and classifications were performed by a single senior embryologist. A total of 138 cycles out of 692 IDC cycles analyzed met the following inclusion criteria: IDC–from zygote to three or four daughter cells (FC within less than 5 h was excluded), two visible pronuclei without major overlapping in the zygote, at least one sibling neighbor 2PN embryo with normal cleavage to two cells and analyzable pronuclei, and time-lapse culture up to day 5/6.

Measures

For every cycle meeting the inclusion criteria, the IDC embryo, as well as the sibling neighbor 2PN embryo with normal cleavage to two cells, which served as own control to avoid bias, were analyzed as follows: last image was taken just before nuclear envelope breakdown (Zygote grading based on Scott, 2003, pronuclei

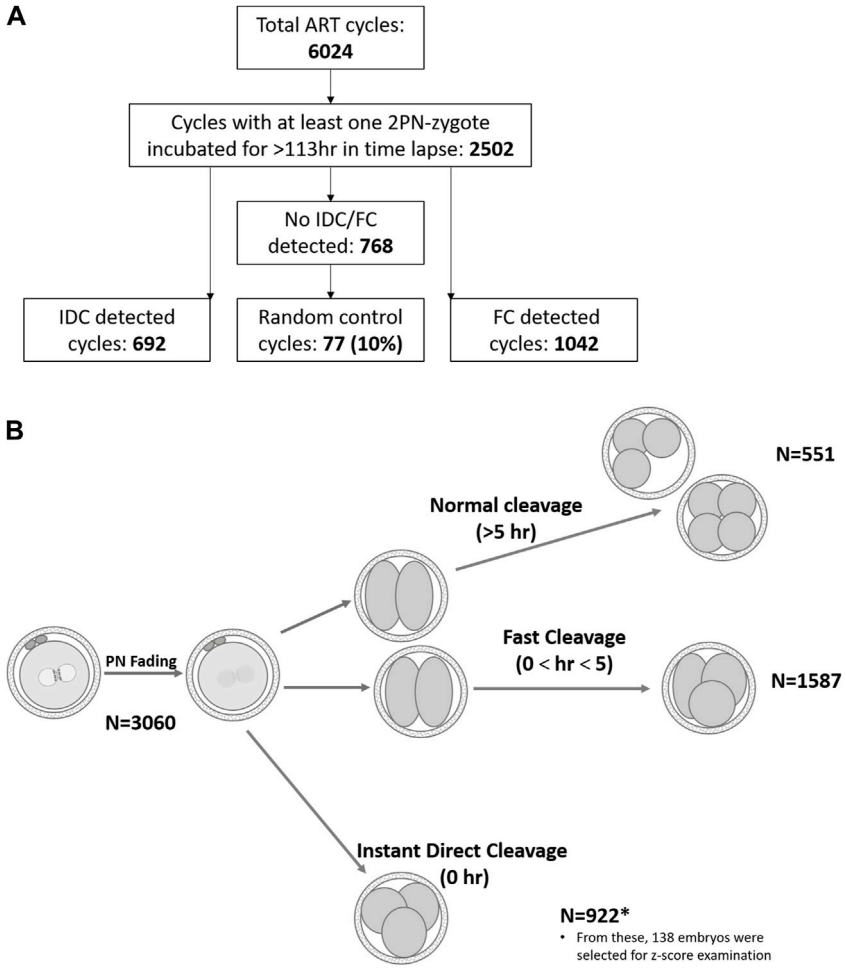

FIGURE 1
Schematic demonstration of retrospective data analyzed. **(A)**. Treatment cycles subgrouping. **(B)**. Graphical illustration of cleavage patterns and their prevalence. Normal cleavage was defined as cc2 > 5 h (Wong et al., 2010) and fast cleavage as cc2 < 5 h (Rubio et al., 2012). The length of the second cell cycle, cc2 = t3−t2.

diameter measured, number, size, and distribution of the NPB were classified); interval from PN fading to first cleavage was measured; embryonic stage was monitored up to day 5/6; the fate of each embryo was documented; the number of "usable" blastocysts (for ET or cryopreservation) and arrested or rejected blastocysts as well as the last developmental stage were also documented. An arrested embryo was defined as an embryo that did not reach the blastocyst stage, remaining in earlier cleavage stages up to day 5 of culture. A rejected embryo was defined as an embryo that continued to cleave to the blastocyst stage, but the resulting blastocyst was of poor quality (less than 3BB according to Gardner's classification) and therefore unsuitable for use (transfer or cryopreservation).

Statistical analysis

All analyses were performed using SPSS 23.0 (IBM Corp., Armonk, NY, United States). Chi-square test was used to compare rates and proportions. Normality of the data was assessed using Kolmogorov-Smirnov test. ANOVA was used to analyze continuous variables. If normal distribution was not detected, and/or homogeneity of distribution was not met, the Kruskal-Wallis test was performed and was followed by the original FDR method of Benjamini and Hochberg *post hoc* analysis. Student's t-test was applied for Z-score analysis of two experimental groups. All *p*-values were tested as two-tailed and considered significant if <0.05.

Results

Our results show that, out of 14,462 embryos that were 2PN and incubated for >113 h, 82.7% (11,953/14,462) resulted in normal cleavage and 17.3% were direct cleavage (922/14,462 IDC and 1,587/14,462 FC). A total of 922 IDC, 1,587 FC, and 551 control embryos, resulting from 692, 1,042, and 77 treatment cycles, respectively, were included in this study. Patient's age, number of aspirated oocytes, and insemination method were not significantly different among groups. Significant differences were recorded only for morphokinetic events of PN fading time and time from fading to the first cleavage (Table 1). Among the 922 IDC embryos analyzed, 881 (95.54%) arrested and did not reach the blastocyst stage, as

TABLE 1 Patient data and morphokinetics (average ± SD), Embryo development and outcomes, Outcomes of usable blastocysts.

	Control	FC	IDC	PV
Number of embryos	551	1,587	922	–
Number of cycles	77	1,042	692	–
Female age (years)	34.69 ± 5.01	33.69 ± 5.92	33.90 ± 6.14	NS
Aspirated oocytes/cycle	11.24 ± 8.24	12.51 ± 7.25	12.36 ± 7.27	NS
% ICSI cycles	68.83	59.88	63.73	NS
PN fading time (hr.)	24.68 ± 4.29	27.19 ± 5.86	29.45 ± 8.62	<0.0001
Time from fading to cleavage (hr.)	2.38 ± 2.12	3.03 ± 2.45	4.20 ± 4.01	<0.0001
Usable blastocysts (%)	180/551 (32.67)	108/1,587 (6.81)	4/922 (0.43)	<0.0001
Rejected blastocysts (%)	107/551 (19.42)	359/1,587 (22.62)	37/922 (4.01)	<0.0001
Arrested embryos (%)	264/551 (47.91)	1,120/1,587 (70.57)	881/922 (95.55)	<0.0001
Pregnancy per transfer (%)	23/57 (40.35)	20/47 (42.55)	0 (0)	NE

PN, Pronuclei; FC, fast cleavage; IDC, Instant direct cleavage; NS, not significant; NE, not eligible for statistical analysis. Usable blastocysts–transferred or frozen embryos.

TABLE 2 Z-Score, Pronuclei (PN), and nucleoli measurements of IDC embryos (average ± SD).

	Control	IDC	PV
Z-Score 1 (%)	29.71	38.41	NS
Z-Score 2 (%)	25.36	20.28	NS
Z-Score 3 (%)	41.3	34.06	NS
Z-Score 4 (%)	3.62	7.25	NS
Diameter of PN (μm)	27.25 ± 2.42	27.30 ± 2.22	NS
Delta between PN sizes (μm)	2.47 ± 2.53	2.44 ± 2.1	NS
Nucleoli number	4.60 ± 1.48	4.51 ± 1.49	NS
Nucleoli Asymmetry (%)	29.71	28.99	NS
Day of embryo arrest	4.33 ± 0.93*	3.16 ± 0.66	<0.0001

FC, fast cleavage; IDC, Instant direct cleavage; NS, not significant.

compared to 1,120/1,587 FC embryos (70.57%) and 264/551 (47.91%) controls (Table 1). In the control group, 180 embryos were usable (57 transferred and 123 frozen), whereas only 108 were usable in the FC group (47 transferred and 61 frozen) and only four were usable in the IDC group (two transferred and two frozen). Although 41 IDC embryos formed blastocysts, only four (0.43%) were of usable grade. The proportion of arrested, rejected, and usable blastocysts differed significantly among the groups (Table 1). The outcomes of usable transferred blastocysts originating from FC were comparable to the controls and resulted in similar pregnancy rates (40.35% and 42.55%, respectively). Although a smaller proportion of FC embryos reached blastocyst stage compared to embryos that underwent normal first cycle cleaving (29.43% vs 52.09%, respectively), the pregnancy rate of the transferred blastocysts was comparable to the general pregnancy rate (42.55%). The IDC embryos did not result in any pregnancies (Table 1). The morphological assessment of IDC zygotes *versus* sibling, normally cleaving controls was performed in 138 treatment cycles. Patient age, number of retrieved oocytes, and ICSI proportion did not differ from the data reported in Table 1 (data not shown). Zygote scores (adapted from Scott, 2003) are summarized in Table 2. The IDC embryos arrested significantly earlier than their sibling control embryos in the Z-Score analyzed cycles (3.16 ± 0.66 vs 4.33 ± 0.93 days, respectively; p <0.0001). None of the other parameters analyzed, such as PN size and nucleoli number and size, were associated with IDC (Table 2).

Discussion

The use of time-lapse incubation revealed several abnormal cleavage patterns (Boucret et al., 2021). Cleavage of one cell into three daughter cells was defined as direct cleavage (DC). This phenomenon might happen during various cleavage cycles. DC was earlier identified as cleavage from one to three cells within 5 h (Rubio et al., 2012). However, the phase of embryonic life at which this phenomenon occurs has a major impact on the outcome. The current study "fine-tuned" the first developmental stages, discriminating between tripolar cleavage from zygote into three daughter cells as IDC and from zygote to three daughter cells within 5 h as FC, as suggested by Ciray et al. (2014) and described as trichotomous *versus* rapid. Our results demonstrate that this differentiation is crucial because the outcomes of these embryos differ. Most IDC embryos arrested at day 3 and no pregnancies were achieved in this group. Due to these small numbers, no statistical analysis was suitable. When the zygote divides directly into three daughter cells, the chromosomal distribution among these cells is chaotic and most cells in the resulting embryo are highly aneuploid (Chatzimeletiou et al., 2005). When the embryo cleaves first into two cells and then one of the blastomeres divides again within 5 h, at least one of the blastomeres in the resulting three-cell embryo is normal. Although presumably mosaic, some of these FC-developing embryos can reach the blastocyst stage and result in pregnancy. Capalbo et al. (2021) reported that low- and medium-grade mosaic embryos have similar reproductive potentials to uniformly euploid

embryos. Human embryos exhibit self-correction mechanisms through their ability to eliminate abnormal blastomeres as cell fragments or through apoptosis (Orvieto et al., 2020; Coticchio et al., 2021).

By analyzing the timetable of the first cell cycle, we found significant differences between IDC, FC, and control embryos. PN fading time, as well as time from fading to first cleavage, were significantly longer in both abnormal cleavage patterns as compared to control blastocysts. Significantly longer times to PN fading were reported in poor quality embryos that failed to blastulate (Vera-Rodriguez et al., 2015), as well as in embryos carrying nonviable translocations compared with those carrying potentially viable translocations (Braude et al., 1988). The time between PN fading and first cleavage is of special interest because it can be measured in both conventional IVF and in ICSI. Vera-Rodriguez et al. (2015) reported that the interval between PN fading and first cleavage measured in a time-lapse incubation system was significantly longer in aneuploid-embryos compared to euploid embryos, as confirmed by single-cell RT-qPCR. These kinetic differences might reflect the maternal genome because embryonic genome activation and expression occur around the four-to eight-cell stage (Braude et al., 1988). Abnormal cleavage patterns are characterized by delayed first cleavage and a high proportion of developmental arrest. The proportion of arrested embryos in the current study differed significantly between IDC, FC, and controls. The IDC embryos arrested significantly earlier than their sibling control embryos in the Z-Score analyzed cycles. It is possible that the arrested IDC embryos failed to activate the embryonic genome due to chaotic chromosomal distribution.

In search of early signs of IDC, we analyzed several morphological zygote parameters in detail, as zygote morphology was reported as predictive of treatment outcomes (Nicoli et al., 2013). Moreover, suboptimal PN clustering at the interphase of the zygote might lead to segregation errors (Cavazza et al., 2021). In the current study, we did not find any significant differences concerning Z-scores, PN diameters, nucleoli appearance, or number among IDC embryos and their sibling controls. Therefore, we suggest that the Z-score cannot predict future cleavage patterns. Analyzing the cohort of treatment cycles in which IDC embryos originated revealed that at least one usable blastocyst was available in 93.30%, indicating that the treatment cycle was adequate. In search of tools for effective embryo assessments that can predict reproductive outcomes, several morphokinetic algorithms have been proposed that also consider the early cleavage timetable (Milewski and Ajduk, 2017). Wong et al. (2010) identified a correlation between the ability to achieve the blastocyst stage with an interval from the end of the first division and the onset of the second (the length of the second cell cycle) in human embryos. Divisions that are too fast may result in incorrect segregation of the genetic material and lead to aneuploidy, whereas divisions that are too slow might be a sign of dysfunction in cell cycle checkpoints.

Conclusion

Based on our results, we propose that the decision regarding the fate of IDC and FC embryos should rely on the pattern of cleavage during the first developmental cycles, since the potential outcomes differ significantly. Most IDC embryos stopped at day 3 developmental stage. The proportion of FC embryos that arrested after day 3 was also significantly greater than that of the controls. Therefore, we recommend not to transfer IDC at day 3, even when their morphological grade is good, but to culture them for 5 days, to the blastocyst stage, instead. On the other hand, FC embryos could be transferred on day 3 when there is no alternative. Further investigation should be conducted regarding the aneuploidy of FC embryos compared to controls.

Data availability statement

The raw data supporting the conclusions of this article will be made available by the authors, without undue reservation.

Ethics statement

The studies involving humans were approved by Meir Medical Center Helsinki committee, No. 0043-22-MMC from 09/02/2022. The studies were conducted in accordance with the local legislation and institutional requirements. The ethics committee/institutional review board waived the requirement of written informed consent for participation from the participants or the participants' legal guardians/next of kin because Retrospective Study with no impact on the medical treatment.

Author contributions

LN: Conceptualization, Data curation, Formal Analysis, Investigation, Methodology, Project administration, Software, Validation, Visualization, Writing–original draft, Writing–review and editing. YG: Conceptualization, Data curation, Formal Analysis, Investigation, Methodology, Software, Validation, Visualization, Writing–original draft, Writing–review and editing. AW: Funding acquisition, Project administration, Resources, Supervision, Writing–review and editing. ML: Conceptualization, Data curation, Formal Analysis, Investigation, Methodology, Project administration, Software, Validation, Visualization, Writing–original draft, Writing–review and editing, Funding acquisition, Resources, Supervision.

Funding

The author(s) declare that no financial support was received for the research, authorship, and/or publication of this article.

Conflict of interest

The authors declare that the research was conducted in the absence of any commercial or financial relationships that could be construed as a potential conflict of interest.

Publisher's note

All claims expressed in this article are solely those of the authors and do not necessarily represent those of their affiliated organizations, or those of the publisher, the editors and the reviewers. Any product that may be evaluated in this article, or claim that may be made by its manufacturer, is not guaranteed or endorsed by the publisher.

References

Anagnostopoulou, C., Maldonado, R. I., Singh, N., Gugnani, N., Chockalingham, A., Singh, K., et al. (2022). Oocyte quality and embryo selection strategies: a review for the embryologists, by the embryologists. *Panminerva Med.* 64, 171–184. doi:10.23736/S0031-0808.22.04680-8

Athayde Wirka, K., Chen, A. A., Conaghan, J., Ivani, K., Gvakharia, M., Behr, B., et al. (2014). Atypical embryo phenotypes identified by time-lapse microscopy: high prevalence and association with embryo development. *Steril* 101, 1637–1648. e1–5. doi:10.1016/j.fertnstert.2014.02.050

Bamford, T., Barrie, A., Montgomery, S., Dhillon-Smith, R., Campbell, A., Easter, C., et al. (2022). Morphological and morphokinetic associations with aneuploidy: a systematic review and meta-analysis. *Hum. Reprod. Update* 28, 656–686. doi:10.1093/humupd/dmac022

Boucret, L., Tramon, L., Saulnier, P., Ferré-L'Hôtellier, V., Bouet, P.-E., and May-Panloup, P. (2021). Change in the strategy of embryo selection with time-lapse system implementation—impact on clinical pregnancy rates. *J. Clin. Med.* 10, 4111. doi:10.3390/jcm10184111

Braude, P., Bolton, V., and Moore, S. (1988). Human gene expression first occurs between the four- and eight-cell stages of preimplantation development. *Nature* 332, 459–461. doi:10.1038/332459a0

Capalbo, A., Poli, M., Rienzi, L., Girardi, L., Patassini, C., Fabiani, M., et al. (2021). Mosaic human preimplantation embryos and their developmental potential in a prospective, non-selection clinical trial. *Am. J. Hum. Genet.* 108, 2238–2247. doi:10.1016/j.ajhg.2021.11.002

Cavazza, T., Takeda, Y., Politi, A. Z., Aushev, M., Aldag, P., Baker, C., et al. (2021). Parental genome unification is highly error-prone in mammalian embryos. *Cell* 184, 2860–2877.e22. doi:10.1016/j.cell.2021.04.013

Chatzimeletiou, K., Morrison, E. E., Prapas, N., Prapas, Y., and Handyside, A. H. (2005). Spindle abnormalities in normally developing and arrested human preimplantation embryos *in vitro* identified by confocal laser scanning microscopy. *Hum. Reprod.* 20, 672–682. doi:10.1093/humrep/deh652

Ciray, H. N., Campbell, A., Agerholm, I. E., Aguilar, J., Chamayou, S., Esbert, M., et al. (2014). Proposed guidelines on the nomenclature and annotation of dynamic human embryo monitoring by a time-lapse user group. *Hum. Reprod.* 29, 2650–2660. doi:10.1093/humrep/deu278

Coticchio, G., Barrie, A., Lagalla, C., Borini, A., Fishel, S., Griffin, D., et al. (2021). Plasticity of the human preimplantation embryo: developmental dogmas, variations on themes and self-correction. *Hum. Reprod. Update* 27, 848–865. doi:10.1093/humupd/dmab016

Coticchio, G., Borini, A., Zacà, C., Makrakis, E., and Sfontouris, I. (2022). Fertilization signatures as biomarkers of embryo quality. *Hum. Reprod.* 37, 1704–1711. doi:10.1093/humrep/deac123

Currie, C. E., Ford, E., Benham Whyte, L., Taylor, D. M., Mihalas, B. P., Erent, M., et al. (2022). The first mitotic division of human embryos is highly error prone. *Nat. Commun.* 13, 6755. doi:10.1038/s41467-022-34294-6

Gardner, D. K., and Schoolcraft, W. B. (1999). Culture and transfer of human blastocysts. *Curr. Opin. Obstet. Gynaecol.* 11, 307–311. doi:10.1097/00001703-199906000-00013

Kalatova, B., Jesenska, R., Hlinka, D., and Dudas, M. (2015). Tripolar mitosis in human cells and embryos: occurrence, pathophysiology and medical implications. *Acta Histochem.* 117, 111–125. doi:10.1016/j.acthis.2014.11.009

Milewski, R., and Ajduk, A. (2017). Time-lapse imaging of cleavage divisions in embryo quality assessment. *Reproduction* 154, R37–R53. doi:10.1530/REP-17-0004

Nicoli, A., Palomba, S., Capodanno, F., Fini, M., Falbo, A., and La Sala, G. B. (2013). Pronuclear morphology evaluation for fresh *in vitro* fertilization (IVF) and intracytoplasmic sperm injection (ICSI) cycles: a systematic review. *J. Ovarian Res.* 6, 64. doi:10.1186/1757-2215-6-64

Orvieto, R., Shimon, C., Rienstein, S., Jonish-Grossman, A., Shani, H., and Aizer, A. (2020). Do human embryos have the ability of self-correction? *Reprod. Biol. Endocrinol.* 18, 98. doi:10.1186/s12958-020-00650-8

Otsuki, J., Iwasaki, T., Tsuji, Y., Katada, Y., Sato, H., Tsutsumi, Y., et al. (2017). Potential of zygotes to produce live births can be identified by the size of the male and female pronuclei just before their membranes break down. *Reprod. Med. Biol.* 16, 200–205. doi:10.1002/rmb2.12032

Ottolini, C. S., Kitchen, J., Xanthopoulou, L., Gordon, T., Summers, M. C., and Handyside, A. H. (2017). Tripolar mitosis and partitioning of the genome arrests human preimplantation development *in vitro*. *Sci. Rep.* 7, 9744. doi:10.1038/s41598-017-09693-1

Rubio, I., Kuhlmann, R., Agerholm, I., Kirk, J., Herrero, J., Escribá, M.-J., et al. (2012). Limited implantation success of direct-cleaved human zygotes: a time-lapse study. *Fertil. Steril.* 98, 1458–1463. doi:10.1016/j.fertnstert.2012.07.1135

Scott, L. (2003). Pronuclear scoring as a predictor of embryo development. *Reprod. Biomed. Online* 6, 201–214. doi:10.1016/S1472-6483(10)61711-7

Vera-Rodriguez, M., Chavez, S. L., Rubio, C., Pera, R. A. R., and Simon, C. (2015). Prediction model for aneuploidy in early human embryo development revealed by single-cell analysis. *Nat. Commun.* 6, 7601. doi:10.1038/ncomms8601

Wong, C. C., Loewke, K. E., Bossert, N. L., Behr, B., De Jonge, C. J., Baer, T. M., et al. (2010). Non-invasive imaging of human embryos before embryonic genome activation predicts development to the blastocyst stage. *Nat. Biotechnol.* 28, 1115–1121. doi:10.1038/nbt.1686

Yang, S. T., Shi, J. X., Gong, F., Zhang, S. P., Lu, C. F., Tan, K., et al. (2015). Cleavage pattern predicts developmental potential of day 3 human embryos produced by IVF. *Reprod. Biomed. Online* 30, 625–634. doi:10.1016/j.rbmo.2015.02.008

Zhan, Q., Ye, Z., Clarke, R., Rosenwaks, Z., and Zaninovic, N. (2016). Direct unequal cleavages: embryo developmental competence, genetic constitution and clinical outcome. *PLoS One* 11, e0166398. doi:10.1371/journal.pone.0166398

frontiers | Frontiers in Cell and Developmental Biology

TYPE Original Research
PUBLISHED 30 July 2024
DOI 10.3389/fcell.2024.1429292

Check for updates

OPEN ACCESS

EDITED BY
Katerina Komrskova,
Institute of Biotechnology (ASCR), Czechia

REVIEWED BY
Pavla Postlerova,
Czech University of Life Sciences Prague, Czechia
A. Marie Lefrançois-Martinez,
Université Clermont Auvergne, France

*CORRESPONDENCE
Ana Katusic Bojanac,
ana.katusic@mef.hr

†These authors have contributed equally to this work

RECEIVED 07 May 2024
ACCEPTED 09 July 2024
PUBLISHED 30 July 2024

CITATION
Planinic A, Maric T, Himelreich Peric M, Jezek D and Katusic Bojanac A (2024), Dynamics of HSD17B3 expression in human fetal testis: implications for the role of Sertoli cells in fetal testosterone biosynthesis.
Front. Cell Dev. Biol. 12:1429292.
doi: 10.3389/fcell.2024.1429292

COPYRIGHT
© 2024 Planinic, Maric, Himelreich Peric, Jezek and Katusic Bojanac. This is an open-access article distributed under the terms of the Creative Commons Attribution License (CC BY). The use, distribution or reproduction in other forums is permitted, provided the original author(s) and the copyright owner(s) are credited and that the original publication in this journal is cited, in accordance with accepted academic practice. No use, distribution or reproduction is permitted which does not comply with these terms.

Dynamics of HSD17B3 expression in human fetal testis: implications for the role of Sertoli cells in fetal testosterone biosynthesis

Ana Planinic[1,2†], Tihana Maric[2†], Marta Himelreich Peric[2], Davor Jezek[1,2] and Ana Katusic Bojanac[2,3*]

[1]Department of Histology and Embryology, University of Zagreb School of Medicine, Zagreb, Croatia, [2]Scientific Centre of Excellence for Reproductive and Regenerative Medicine, University of Zagreb School of Medicine, Zagreb, Croatia, [3]Department of Medical Biology, University of Zagreb School of Medicine, Zagreb, Croatia

Introduction: Androgens play a pivotal role in shaping male sexual characteristics, with testosterone being an essential hormone in orchestrating various developmental processes. Testosterone biosynthesis involves a series of enzymatic reactions, among which the 17β-hydroxysteroid dehydrogenase type 3 (HSD17B3) holds significance. While its role in adult Leydig cells is well established, its localization and importance during the fetal period remain less known, especially in humans. This study aims to delineate the dynamics of HSD17B3 expression in human fetal testes to clarify the contribution of specific cell types to testosterone biosynthesis.

Methods: Using immunofluorescence staining, we investigated the expression pattern of HSD17B3 in human fetal and adult testicular tissues.

Results and discussion: The findings of this study revealed a distinct temporal and cellular expression pattern of HSD17B3 protein in the fetal period. We detected its expression exclusively in Sertoli cells, the highest during the second trimester. This unique localization suggests the inclusion of fetal Sertoli cells in testosterone production during the critical masculinization-programming window. Furthermore, we demonstrated a shift in HSD17B3 expression from Sertoli cells to Leydig cells in adulthood, corroborating findings from rodent studies. This study sheds light on the intricate, still underexplored regulation of steroidogenesis during fetal development, whose disturbance might lead to testicular dysgenesis. Further research is warranted to elucidate the regulatory pathways governing the expression of HSD17B3 and its transition between Sertoli and Leydig cells, potentially paving the way for novel therapeutic interventions in disorders of sexual development.

KEYWORDS

testosterone, Sertoli, testis, human, fetal, Leydig

1 Introduction

Androgens are steroid hormones that regulate the development and maintenance of the male sexual phenotype. The primary androgen in males is testosterone, but the more potent dihydrotestosterone (DHT) and less potent androstenedione and dehydroepiandrosterone (DHEA) also have important roles (Roy et al., 1999). Testosterone has anabolic effects on

male musculoskeletal development as well as androgenic effects such as spermatogenesis and fertility, voice deepening, sebum production, sex drive, and erection (Chang, 2002). The majority of testosterone in adults is produced by Leydig cells through steroidogenesis. The classical testosterone production pathway uses cholesterol as a precursor molecule, mobilized by the steroidogenic acute regulatory (STAR) protein from lipid droplets or the cell membrane into mitochondria. The enzyme cytochrome P450 family 11 subfamily A member 1 (CYP11A1) then converts cholesterol into pregnenolone, which is further converted into DHEA by the cytochrome P450 family 17 subfamily A member 1 (CYP17A1) enzyme in the smooth endoplasmic reticulum. DHEA is then converted to androstenediol by HSD17B3, which is then converted into testosterone by HSD3B2 and secreted into the blood (Payne and Hardy, 2007). Circulating testosterone is further converted in peripheral tissues such as the prostate, skin, liver, and hair follicles by 5α-reductase (SRD5A) into dihydrotestosterone (DHT), which exhibits a more potent agonistic effect on the androgen receptor (Chang, 2002). Although circulating testosterone is the primary source for the majority of intracellular DHT production (Okon et al., 1980), the latter can also be produced from androsterone via a so-called backdoor biochemical pathway, which includes other enzymes, such as aldo-keto reductase family 1 member C2 and C4 (AKR1C2, AKR1C4), and 17β-hydroxysteroid dehydrogenase 6 (HSD17B6) (Swerdloff et al., 2017).

HSD17B3 is a member of the 17β-hydroxysteroid dehydrogenase (HSD17B) family, a group of enzymes that catalyze the last step in the synthesis of androgens, a conversion of androstenedione to testosterone (Labrie et al., 1997). This superfamily of enzymes consists of 15 isoforms, which are expressed in various tissues and have multiple functions (Wang et al., 2016; Hilborn et al., 2017). For example, the HSD17B3 isoform is expressed in the Leydig cells of the adult testis, while HSD17B5 (AKR1C3) is expressed in other tissues such as the adrenal gland and the ovarian thecal cells, thus referred to as the peripheral HSD17B (Melmed, 2016; Penning, 2019). HSD17B3 deficiency causes male pseudohermaphroditism, leading to ambiguous or female external genitalia, cryptorchidism, and infertility (Longo et al., 1975). Affected individuals are usually raised as females, and the diagnosis is made at puberty when they start to show virilization and have a high androstenedione/testosterone ratio (Furtado et al., 2012). Virilization is caused either by an abnormal enzyme that produces enough testosterone or by peripheral conversion of androstenedione to testosterone via HSD17B5 (Faienza et al., 2020). Patients with HSD17B3 deficiency exhibit the highest rates of gender dysphoria, with incidence up to 63%, similar to those with SRD5A deficiency (Furtado et al., 2012). Moreover, mutations of AKR1C genes involved in the backdoor pathway also appear to cause a similar pathology, pointing to the crucial role of testosterone and DHT in human gonadal development (Fluck et al., 2011; Furtado et al., 2012).

In rodents, fetal LCs were shown to have low CYP11A1, HSD3B1, and CYP17A1 levels in the cytoplasm, allowing them to produce androgens such as androstenedione and androsterone. However, it has been discovered that, in rat and mouse fetuses, HSD17B3 is not expressed in Leydig cells but, surprisingly, in Sertoli cells, implicating them as testosterone producers during gestation in rodents (Shima et al., 2013). Even 10 days after birth, HSD17B3 expression is still limited to Sertoli cells, but later, at day 30, which corresponds to the puberty period in humans, it is switched to Leydig cells (O'Shaughnessy et al., 2000). Importantly, HSD17B3 KO male mice exhibit normal masculinization and fertility, indicating that HSD17B3 is probably important for maximal but not basal testosterone production in the mouse testis (Rebourcet et al., 2020).

Recent studies on transcriptomes of human fetuses showed that HSD17B3 mRNA was not found in human fetal Leydig cells but in the Sertoli cell lineage (Guo et al., 2021), thus supporting the results from rodent studies. However, due to a lack of human fetal samples, no studies have confirmed this exclusivity in testicular tissues at the protein level. Hence, this study aimed to prove the abovementioned observation and showed for the first time the dynamics of HSD17B3 protein expression during various stages of human development, implying that Sertoli cells are local testosterone producers in fetuses.

2 Materials and methods

2.1 Sample collection and ethical approval

Human fetal (gestational age 14–33) paraffin-embedded testicular tissue (n = 16) from stillbirths was acquired from the archive of the Department of Histology and Embryology, School of Medicine, University of Zagreb, Croatia. The provision was approved by the Ethics Committee of the University of Zagreb Medical School (no.: 04-1130-2006). According to Articles 232 (Okon et al., 1980), 235 (Chang, 2002), and 236 (Chang, 2002) of the Law on Healthcare (Republic of Croatia), written consent from patients was not necessary.

Adult human paraffin-embedded testicular tissue (n = 3) was provided by the Department of Urology, University Hospital Zagreb, Croatia. Samples were obtained via testicular biopsy from men diagnosed with obstructive azoospermia (OA) with preserved tubular spermatogenesis and interstitial tissue. Each patient provided written consent for the procedure and the histological analysis/current study. Approval was granted by the Ethics Committee of the School of Medicine at the University of Zagreb (380-59-10106-20-111/171).

2.2 Immunofluorescence and imaging

Immunofluorescent (IF) staining was performed on human adult and fetal FFPE (formalin-fixed paraffin-embedded) testis sections (4 μm thickness). Slides were incubated at 55°C, deparaffinized in xylol, rehydrated in 100%, 96%, and 70% EtOH, and then washed in distilled H_2O. Heat-induced antigen retrieval was performed using a pressure cooker and the Tris-EDTA buffer (10 mM Tris Base, 1 mM EDTA Solution, 0.05% Tween 20, pH 9.0) for 60 min, followed by 30 min of cooling at room temperature (RT). The slides were then washed in PBS (phosphate-buffered saline) 1x buffer. Non-specific binding was blocked by incubating the slides in 2.5% normal horse serum for 20 min. Primary antibodies were prepared in PBS

10.3389/fcell.2024.1429292

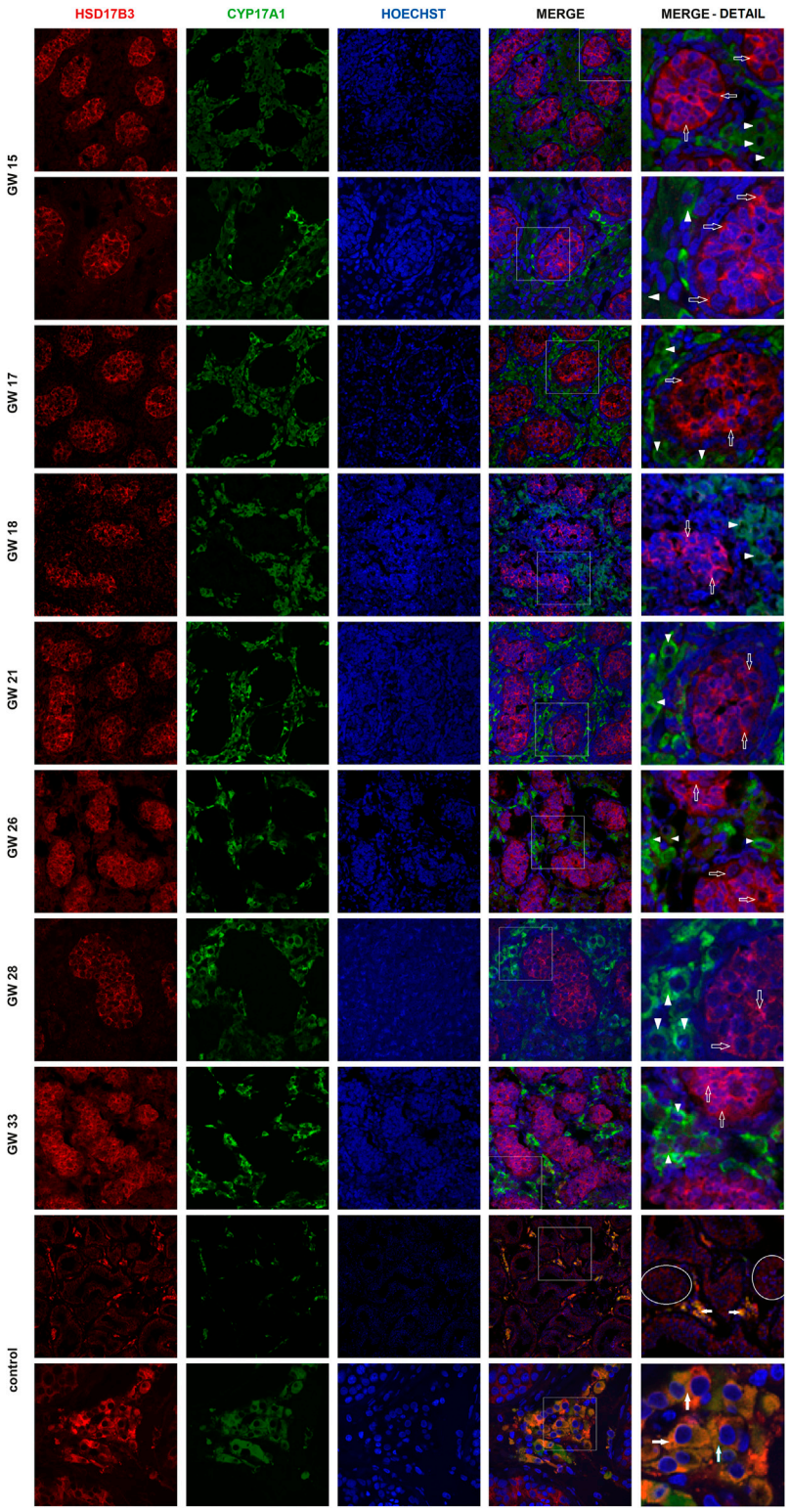

FIGURE 1
Colocalization of HSD17B3 and CYP17A1 in the human fetal testis. Representative images of immunofluorescent staining showing HSD17B3 and CYP17A1 expression in human fetal testes from gestational week (GW) 15 to GW 33 and in controls, the adult testis. The images show the expression of HSD17B3 in Sertoli cells cytoplasm in the tubules of fetal testes (empty arrows) and their noncolocalization with CYP17A1, expressed in Leydig cells (arrowheads). In adult testis (control), HSD17B3 and CYP17A1 show almost complete colocalization (filled arrows) in adult Leydig cell cytoplasm. Some seminiferous tubules are encircled. The most right column represents enlarged area of a merged image (marked by square). Images are recorded under ×400, except the second row of GW 15, GW 28 samples, and the second row of controls (×600).

10.3389/fcell.2024.1429292

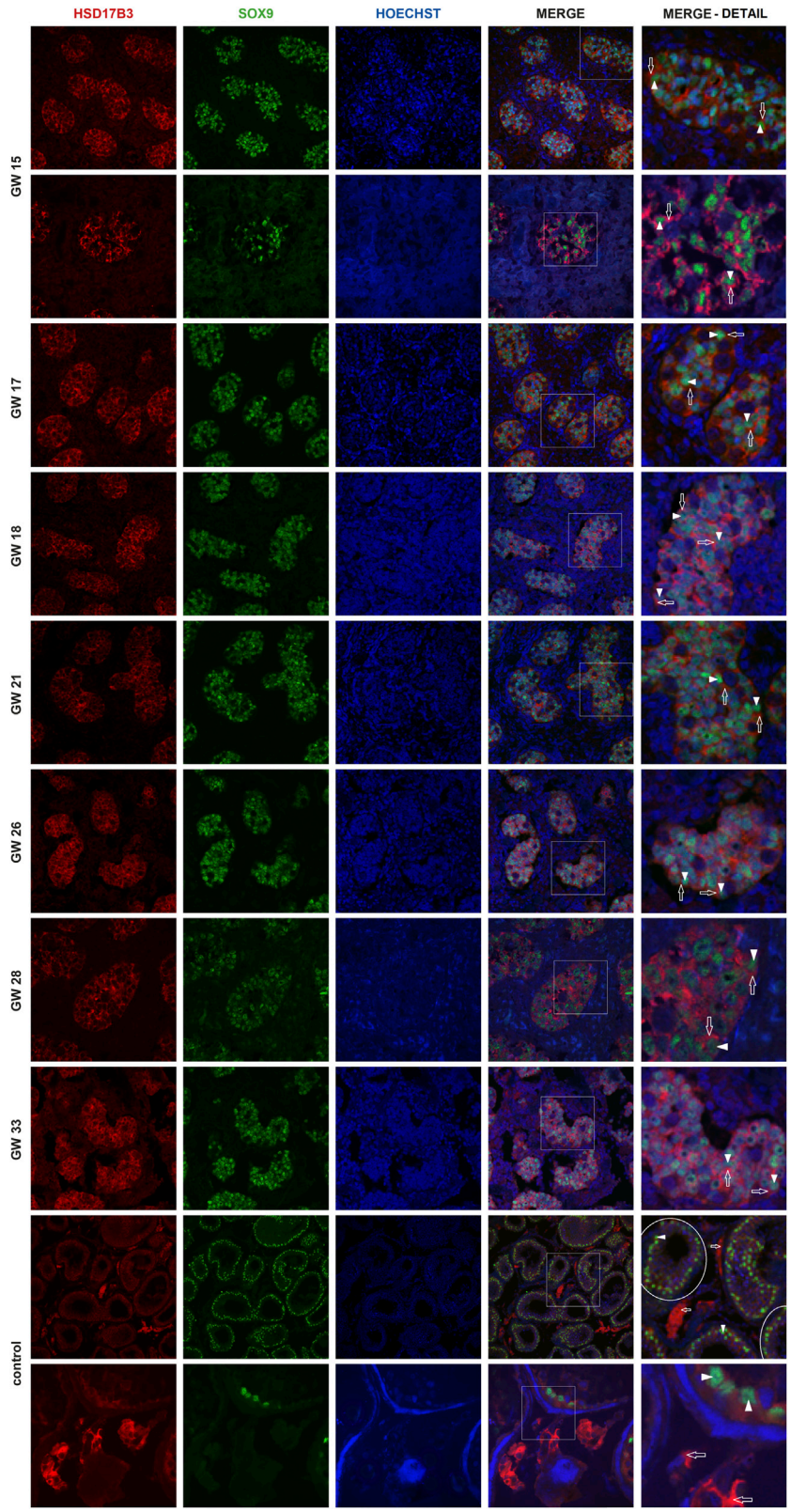

FIGURE 2
Colocalization of HSD17B3 and SOX9 in the human fetal testis. Representative images of immunofluorescent staining showing HSD17B3 and SOX9 expression in human fetal testes from GW 15 to GW 33 and in controls, the adult testis. The images show the expression of HSD17B3 in Sertoli cell cytoplasm in the tubules of fetal testes (empty arrows), specifically around the nuclei of Sertoli cells, where SOX9 is expressed (arrowheads). In controls, HSD17B3 is expressed in the interstitial Leydig cells, while SOX9 is again observed in Sertoli cell nuclei. Some seminiferous tubules are encircled. The most right column represents enlarged area of a merged image (marked by square). Images are recorded under ×400, except the second row of GW 15, GW 28, and the second row of controls (×600).

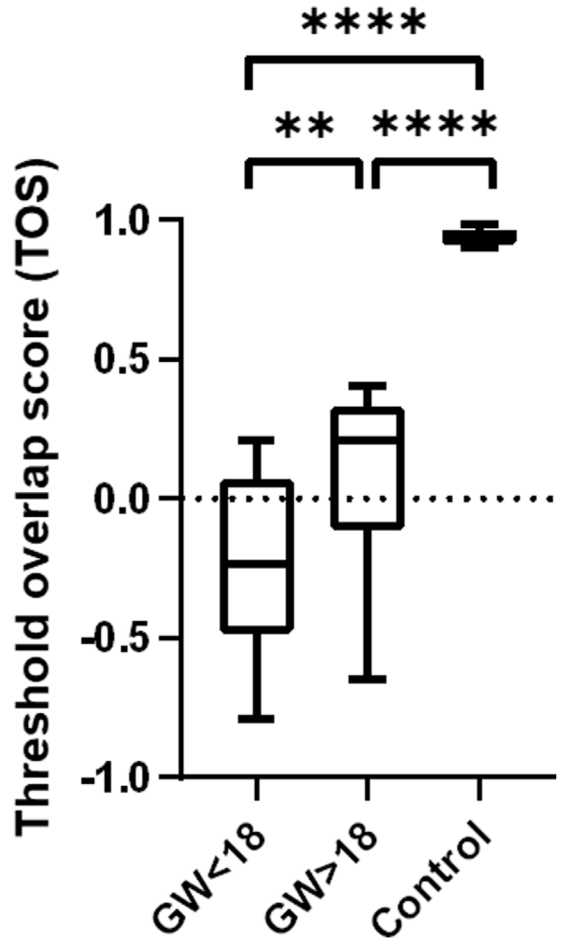

FIGURE 3
Colocalization analysis of HSD17B3 and CYP17A1 in the human fetal and adult testis (control). Box plot that shows quantification of colocalization through the threshold overlap score (TOS). The TOS points to almost complete colocalization of HSD17B3 and CYP17A1 in the adult human testis, while there is noncolocalization and even weak anticolocalization in the fetal testes. Differences in the TOS are statistically significant between all groups *$p < 0.05$, **$p < 0.01$, ***$p < 0.001$, ****$p < 0.0001$.

1x (13.7 mM NaCl, 0.27 mM KCl, 0.65 mM Na_2HPO_4, 0.14 mM KH_2PO_4, Kemika, HR) containing 0.1% Triton X and 1% normal horse serum in the following dilutions: rabbit polyclonal anti-HSD17B3 antibody 1:500 (13415-1-AP, Proteintech, United States), mouse monoclonal anti-CYP17A1 antibody 1:1000 (sc-374244, Santa Cruz Biotechnology, United States), mouse monoclonal anti-SOX9 antibody 1:100 (AMAb90795, Atlas Antibodies, Sweden). The anti-HSD17B3 antibody was verified in a previous study (Flippo et al., 2022). All samples were double-labeled with anti-HSD17B3 and anti-SOX9 or with anti-HSD17B3: anti-CYP17A and incubated in a humid chamber at 4°C overnight (ON). Testicular tissue with complete spermatogenesis from men with OA was used as positive controls, and samples on which primary antibodies weren't used were included as negative controls. The next day, slides were washed twice in PBS 1x for 10 min. Slides were also incubated with an amplifier anti-rabbit antibody for 15 min. Slides were then incubated with secondary antibodies, donkey anti-mouse (Alexa Fluor 488; ab150109, Abcam, United Kingdom) diluted 1:200 and horse anti-rabbit antibody (VectaFluor™ Excel Amplified Anti-Rabbit IgG, DyLight™ 594 Antibody Kit, Vector Laboratories, United States) diluted in PBS 1x for 2 h at RT in a dark humid chamber. Next, samples were washed 3 × 10 min in PBS 1x and incubated with TrueBlack® lipofuscin autofluorescence quencher solution (Biotium, United States) for 30 s, freshly diluted 20x with 70% EtOH, to reduce the immunofluorescence background. Samples were counterstained with the Hoechst solution (1 ng/mL) for 10 min, air dried for 3 min, covered with mounting medium (Vectashield, Vector Laboratories, United States), and stored at 4°C overnight. Confocal microscopy images were acquired using an Olympus FV1000 microscope with the FV10-ASW software with filters (Olympus, Japan). Images were processed using ImageJ.

2.3 Colocalization analysis

Signal colocalization was conducted in the ImageJ software using the EZcolocalization plugin (Stauffer et al., 2018). Colocalization was quantified by calculating the threshold overlap score (TOS), which measures the overlap in signals above threshold intensity values (Sheng et al., 2016). Thresholds were determined automatically using the Otsu algorithm. The TOS was calculated for HSD17B3 and CYP17A1 since both proteins are cytoplasmic.

2.4 Signal intensity quantification

HSD17B3 signal intensity was quantified with the ImageJ software by calculating the integrated density and mean gray value of ROIs (Regions of Interest) determined by the automated thresholding algorithm Moments. Integrated density is the sum of pixel values in the selection. The mean gray value is the sum of the values of all the pixels in the selection divided by the number of pixels.

2.5 Statistical analysis

Results were statistically analyzed using GraphPad Prism v7.00 Software (California, United States). Differences in quantitative variables were determined by the Student's t-test and one-way ANOVA. Results were considered statistically significant if $p < 0.05$.

3 Results

3.1 HSD17B3 is expressed in Sertoli cells of the human fetal testis

Immunofluorescent imaging showed the differential expression of HSD17B3 in human fetal and adult testicular tissue. In the adult testis, HSD17B3 colocalizes with CYP17A1 in the cytoplasm of adult

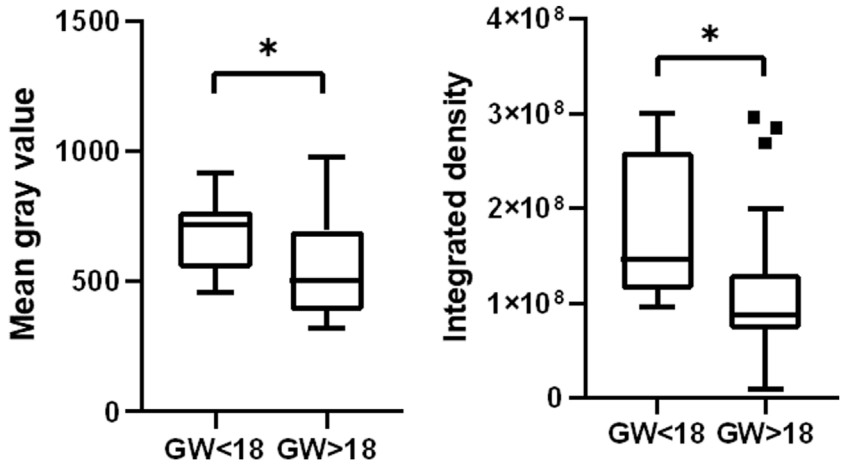

FIGURE 4
HSD17B3 signal intensity declines during the fetal period. Box plots show higher mean gray value and integrated density in the group before GW 18 than in the group after GW 18 *$p < 0.05$, **$p < 0.01$, ***$p < 0.001$, ****$p < 0.0001$.

Leydig cells in the interstitial compartment (Figure 1), while the colocalization is not observed with SOX9, a Sertoli cell marker (Figure 2). On the other hand, HSD17B3 clearly shows anti-colocalization with CYP17A1 in the fetal testis (Figure 1). The cytoplasmic HSD17B3 signal is detected around the nuclear SOX9 signal, indicating its presence in the fetal Sertoli cells (Figure 2).

Colocalization was quantified by determining the threshold overlap score (TOS), which measures the overlap in signals above threshold intensity values. The TOS showed almost complete colocalization of CYP17A1 and HSD17B3 in the adult testis. In contrast, the fetal testis showed noncolocalization and weak anticolocalization in the fetal samples before gestational week (GW) 18. Differences in colocalization of CYP17A1 and HSD17B3 were statistically significant between fetal testes before and after GW 18 ($p < 0.01$). Compared with the TOS of the adult testis, which served as a control tissue with known localization of HSD17B3 in Leydig cells, fetal testes before GW 18 and after GW 18 also showed a statistically significant difference. ($p < 0.0001$) (Figure 3). The sample group before GW 18 includes samples from GW 14 to GW 18, while the group after GW 18 includes samples from GW 18 to GW 33.

3.2 HSD17B3 expression in the human fetal testis declines during the fetal period

To further investigate the dynamics of HSD17B3 expression in the human fetal testis, we performed a quantitative analysis of HSD17B3 signal intensity across different gestational weeks. Utilizing ImageJ software, we calculated the integrated density and mean gray value of regions of interest (ROIs) identified by the automated thresholding algorithm Moments. The quantitative analysis revealed a statistically significant decrease in HSD17B3 expression as fetal development progresses. Specifically, we observed that the HSD17B3 signal intensity was higher in testicular tissues obtained from fetuses before gestational week 18 (GW 18) than after GW 18. The integrated density values, representing the sum of pixel values within the selected ROIs, indicated a robust presence of HSD17B3 protein in early fetal development, with a marked reduction in later stages. The mean gray value, the average pixel intensity within the selected ROIs, also supported this trend, showing higher values in samples from fetuses before GW 18 (Figure 4). To ensure the reliability of the findings in this study, we performed statistical analyses, and the results demonstrated a statistically significant difference ($p < 0.05$) in HSD17B3 expression, confirming the observed decline in protein levels during the later stages of fetal development.

4 Discussion

Using immunofluorescence staining, we demonstrated for the first time that the HSD17B3 protein is highly expressed in the human fetal testis during the second trimester, while expression decreases slightly after GW 18. Hence, this study confirms that the previously observed HSD17B3 mRNA (Guo et al., 2021) is successfully translated in the fetal testis. However, the primary finding of this study is that the HSD17B3 protein is present exclusively in fetal Sertoli cells, while its expression is further switched to Leydig cells in adulthood. Hence, these findings are in accordance with data from the human fetal testis transcriptome (Guo et al., 2021). Finally, they confirm the long-standing hypothesis that human Sertoli cells will likely be the testosterone synthesis's primary site in the testis.

Moreover, the HSD17B3 antibody could be used as a fetal Sertoli cell marker. While HSD17B3 doesn't seem to be crucial for basal testosterone production in mice (Rebourcet et al., 2020), HSD17B3 deficiency in humans causes abnormal masculinization, infertility, and very high rates of gender dysphoria, which confirms its role in the development of major sexual characteristics (Longo et al., 1975). Moreover, testosterone levels peak from GW 12 to 18, which overlaps with the masculinization programming window

(Tapanainen et al., 1981; O'Shaughnessy and Fowler, 2014) and is reflected in the results of this study, indicating higher HSD17B3 signal intensity in the abovementioned period. Hence, we propose that these disorders in male sexual development could be related to fetal Sertoli cells impairment and not to Leydig cells. This finding also implies a tight, still unresolved, crosstalk between fetal Sertoli and Leydig cells in testosterone production and complex regulation of HSD17B3 expression. In mice, activin A seems to activate the relevant genes in Sertoli cells, but its role in humans still needs to be elucidated (Whiley et al., 2020). HSD17B3 was also found to be highly expressed in adult Sertoli cells in a patient with complete androgen insensitivity syndrome (CAIS), which could be due to a lack of HSD17B3 shift from Sertoli to Leydig cells and could point to a role of androgen signaling in that process (O'Shaughnessy et al., 2012). The elucidation of the hormone regulation switch between Sertoli and Leydig cells could transform the research of novel hormonal treatments.

In this study, we analyzed 14 samples of fetal testicular tissue from GW 14 to GW 33, and thus, we established HSD17B3 protein expression throughout human fetal development for the first time. These samples are rare and difficult to obtain and present a strength of this study. The main limitation of this study is that we analyzed protein expression using immunofluorescence and not Western blot, which is the gold standard, but it was unfortunately not possible to perform since we only had access to paraffin-embedded samples.

This study demonstrated HSD17B3 protein expression in Sertoli cells throughout fetal development and pointed to Sertoli cells as the primary site of fetal testosterone production. Further research is needed to elucidate the background of the HSD17B3 expressional switch and to discover other regulatory players in fetal steroidogenesis.

Data availability statement

The original contributions presented in the study are included in the article/Supplementary Material, further inquiries can be directed to the corresponding author.

Ethics statement

The studies involving humans were approved by the Ethics Committee of the University of Zagreb Medical School. The studies were conducted in accordance with the local legislation and institutional requirements. The human samples used in this study were acquired from the archive of the Department of Histology and Embryology, School of Medicine, University of Zagreb, Croatia. The provision was approved by the Ethics Committee of the University of Zagreb Medical School (No. 04-1130-2006). Written informed consent for participation was not required from the participants or the participants' legal guardians/next of kin in accordance with the national legislation and institutional requirements.

Author contributions

AP: Data curation, Formal Analysis, Investigation, Methodology, Software, Writing–original draft, Writing–review and editing. TM: Data curation, Formal Analysis, Investigation, Methodology, Software, Writing–original draft, Writing–review and editing. MH: Investigation, Methodology, Visualization, Writing–original draft. DJ: Funding acquisition, Resources, Supervision, Writing–review and editing. AK: Conceptualization, Funding acquisition, Project administration, Supervision, Writing–original draft, Writing–review and editing.

Funding

The author(s) declare that financial support was received for the research, authorship, and/or publication of this article. This study was supported by Scientific Center of Excellence for Reproductive and Regenerative Medicine, Republic of Croatia, and by the European Union through the European Regional Development Fund, under projects: "Reproductive and Regenerative Medicine—Exploring New Platforms and Potentials" (grant agreement No. KK.01.1.1.01.0008), "Development and strengthening of research and innovation capacities, and application advanced technologies" and by University of Zagreb Supportive Fund No. 10106-23-2493.

Conflict of interest

The authors declare that the research was conducted in the absence of any commercial or financial relationships that could be construed as a potential conflict of interest.

Publisher's note

All claims expressed in this article are solely those of the authors and do not necessarily represent those of their affiliated organizations, or those of the publisher, the editors and the reviewers. Any product that may be evaluated in this article, or claim that may be made by its manufacturer, is not guaranteed or endorsed by the publisher.

References

Chang, C. (2002). *Androgens and androgen receptor: mechanisms, functions, and clinical applications*. Springer Science & Business Media., 451.

Faienza, M. F., Baldinotti, F., Marrocco, G., TyuTyusheva, N., Peroni, D., Baroncelli, G. I., et al. (2020). 17β-hydroxysteroid dehydrogenase type 3 deficiency: female sex assignment and follow-up. *J. Endocrinol. Investig.* 43 (12), 1711–1716. doi:10.1007/s40618-020-01248-y

Flippo, C., Kolli, V., Andrew, M., Berger, S., Bhatti, T., Boyce, A. M., et al. (2022). Precocious puberty in a boy with bilateral leydig cell tumors due to a somatic gain-

of-function LHCGR variant. *J. Endocr. Soc.* 6 (10), bvac127. doi:10.1210/jendso/bvac127

Fluck, C. E., Meyer-Boni, M., Pandey, A. V., Kempna, P., Miller, W. L., Schoenle, E. J., et al. (2011). Why boys will be boys: two pathways of fetal testicular androgen biosynthesis are needed for male sexual differentiation. *Am. J. Hum. Genet.* 89, 201–218. doi:10.1016/j.ajhg.2011.06.009

Furtado, P. S., Moraes, F., Lago, R., Barros, L. O., Toralles, M. B., and Barroso, U., Jr (2012). Gender dysphoria associated with disorders of sex development. *Nat. Rev. Urol.* 9 (11), 620–627. doi:10.1038/nrurol.2012.182

Guo, J., Sosa, E., Chitiashvili, T., Nie, X., Rojas, E. J., Oliver, E., et al. (2021). Single-cell analysis of the developing human testis reveals somatic niche cell specification and fetal germline stem cell establishment. *Cell.Cell Stem Cell.* 28 (4), 764–778.e4. doi:10.1016/j.stem.2020.12.004

Hilborn, E., Stål, O., and Jansson, A. (2017). Estrogen and androgen-converting enzymes 17β-hydroxysteroid dehydrogenase and their involvement in cancer: with a special focus on 17β-hydroxysteroid dehydrogenase type 1, 2, and breast cancer. *Oncotarget* 8 (18), 30552–30562. doi:10.18632/oncotarget.15547

Labrie, F., Luu-The, V., Lin, S. X., Labrie, C., Simard, J., Breton, R., et al. (1997). The key role of 17 beta-hydroxysteroid dehydrogenases in sex steroid biology. *Steroids* 62 (1), 148–158. doi:10.1016/s0039-128x(96)00174-2

Longo, F. J., Coleman, S. A., and Givens, J. R. (1975). Ultrastructural analysis of the testes in male pseudohermaphrodism reductase. *Am. J. Clin. Pathol.* 64, 145–154. doi:10.1093/ajcp/64.2.145

Melmed, S. (2016). *Williams textbook of endocrinology*. Elsevier Health Sciences, 904.

Okon, E., Livni, N., Rösler, A., Yorkoni, S., Segal, S., Kohn, G., et al. (1980). Male pseudohermaphroditism due to 5 alpha-reductase deficiency. Ultrastructure of the gonads. *Arch. Pathol. Lab. Med.* 104, 363–367.

O'Shaughnessy, P. J., Baker, P. J., Heikkilä, M., Vainio, S., and McMahon, A. P. (2000). Localization of 17beta-hydroxysteroid dehydrogenase/17-ketosteroid reductase isoform expression in the developing mouse testis--androstenedione is the major androgen secreted by fetal/neonatal leydig cells. *Endocrinology* 141, 2631–2637. doi:10.1210/endo.141.7.7545

O'Shaughnessy, P. J., and Fowler, P. A. (2014). Development of the human fetal testis. *Ann. Endocrinol. Paris.* 75 (2), 48–53. doi:10.1016/j.ando.2014.03.009

O'Shaughnessy, P. J., Monteiro, A., Bhattacharya, S., Fraser, M. J., and Fowler, P. A. (2012). Steroidogenic enzyme expression in the human fetal liver and potential role in the endocrinology of pregnancy. *Mol. Hum. Reprod.* 9 (3), 177–187. doi:10.1093/molehr/gas059

Payne, A., and Hardy, M. (2007). *The Leydig cell in Health and disease*.

Penning, T. M. (2019). AKR1C3 (type 5 17β-hydroxysteroid dehydrogenase/prostaglandin F synthase): roles in malignancy and endocrine disorders. *Mol. Cell. Endocrinol.* 489, 82–91. doi:10.1016/j.mce.2018.07.002

Rebourcet, D., Mackay, R., Darbey, A., Curley, M. K., Jørgensen, A., Frederiksen, H., et al. (2020). Ablation of the canonical testosterone production pathway via knockout of the steroidogenic enzyme HSD17B3, reveals a novel mechanism of testicular testosterone production. *FASEB J.* 34 (8), 10373–10386. doi:10.1096/fj.202000361R

Roy, A. K., Lavrovsky, Y., Song, C. S., Chen, S., Jung, M. H., Velu, N. K., et al. (1999). Regulation of androgen action. *Vitam. Horm.* 55, 309–352. doi:10.1016/s0083-6729(08)60938-3

Sheng, H., Stauffer, W., and Lim, H. N. (2016). Systematic and general method for quantifying localization in microscopy images. *Biol. Open* 5 (12), 1882–1893. doi:10.1242/bio.019893

Shima, Y., Miyabayashi, K., Haraguchi, S., Arakawa, T., Otake, H., Baba, T., et al. (2013). Contribution of Leydig and Sertoli cells to testosterone production in mouse fetal testes. *Mol. Endocrinol.* 27 (1), 63–73. doi:10.1210/me.2012-1256

Stauffer, W., Sheng, H., and Lim, H. N. (2018). *EzColocalization: an ImageJ plugin for visualizing and measuring colocalization in cells and organisms*.

Swerdloff, R. S., Dudley, R. E., Page, S. T., Wang, C., and Salameh, W. A. (2017). Dihydrotestosterone: biochemistry, physiology, and clinical implications of elevated blood levels. *Endocr. Rev.* 38 (3), 220–254. doi:10.1210/er.2016-1067

Tapanainen, J., Koivisto, M., Vihko, R., and Huhtaniemi, I. (1981). Enhanced activity of the pituitary-gonadal axis in premature human infants. *J. Clin. Endocrinol. Metab.* 52 (2), 235–238. doi:10.1210/jcem-52-2-235

Wang, C. T., Li, C. F., Wu, W. J., Huang, C. N., Li, C. C., Li, W. M., et al. (2016). High expression of 17β-hydroxysteroid dehydrogenase type 2 is associated with a better prognosis in urothelial carcinoma of the urinary tract. *J. Cancer* 7 (15), 2221–2230. doi:10.7150/jca.16777

Whiley, P. A. F., O'Donnell, L., Moody, S. C., Handelsman, D. J., Young, J. C., Richards, E. A., et al. (2020). Activin A determines steroid levels and composition in the fetal testis. *Endocrinology* 161 (7), bqaa058. doi:10.1210/endocr/bqaa058

frontiers | Frontiers in Cell and Developmental Biology

TYPE Review
PUBLISHED 01 August 2024
DOI 10.3389/fcell.2024.1358649

Check for updates

OPEN ACCESS

EDITED BY
Paolo Rinaudo,
University of California, San Francisco, United States

REVIEWED BY
Sadie L. Marjani,
Central Connecticut State University, United States
Inchul Choi,
Chungnam National University, Republic of Korea

*CORRESPONDENCE
Kiho Lee,
kiholee@missouri.edu

RECEIVED 20 December 2023
ACCEPTED 23 July 2024
PUBLISHED 01 August 2024

CITATION
Montgomery T, Uh K and Lee K (2024), TET enzyme driven epigenetic reprogramming in early embryos and its implication on long-term health.
Front. Cell Dev. Biol. 12:1358649.
doi: 10.3389/fcell.2024.1358649

COPYRIGHT
© 2024 Montgomery, Uh and Lee. This is an open-access article distributed under the terms of the Creative Commons Attribution License (CC BY). The use, distribution or reproduction in other forums is permitted, provided the original author(s) and the copyright owner(s) are credited and that the original publication in this journal is cited, in accordance with accepted academic practice. No use, distribution or reproduction is permitted which does not comply with these terms.

TET enzyme driven epigenetic reprogramming in early embryos and its implication on long-term health

Ty Montgomery[1], Kyungjun Uh[2] and Kiho Lee[1]*

[1]Division of Animal Sciences, University of Missouri, Columbia, MO, United States, [2]Futuristic Animal Resource and Research Center, Korea Research Institute of Bioscience and Biotechnology, Cheongju-si, Republic of Korea

Mammalian embryo development is initiated by the union of paternal and maternal gametes. Upon fertilization, their epigenome landscape is transformed through a series of finely orchestrated mechanisms that are crucial for survival and successful embryogenesis. Specifically, maternal or oocyte-specific reprogramming factors modulate germ cell specific epigenetic marks into their embryonic states. Rapid and dynamic changes in epigenetic marks such as DNA methylation and histone modifications are observed during early embryo development. These changes govern the structure of embryonic genome prior to zygotic genome activation. Differential changes in epigenetic marks are observed between paternal and maternal genomes because the structure of the parental genomes allows interaction with specific oocyte reprogramming factors. For instance, the paternal genome is targeted by the TET family of enzymes which oxidize the 5-methylcytosine (5mC) epigenetic mark into 5-hydroxymethylcytosine (5hmC) to lower the level of DNA methylation. The maternal genome is mainly protected from TET3-mediated oxidation by the maternal factor, STELLA. The TET3-mediated DNA demethylation occurs at the global level and is clearly observed in many mammalian species. Other epigenetic modulating enzymes, such as DNA methyltransferases, provide fine tuning of the DNA methylation level by initiating *de novo* methylation. The mechanisms which initiate the epigenetic reprogramming of gametes are critical for proper activation of embryonic genome and subsequent establishment of pluripotency and normal development. Clinical cases or diseases linked to mutations in reprogramming modulators exist, emphasizing the need to understand mechanistic actions of these modulators. In addition, embryos generated via *in vitro* embryo production system often present epigenetic abnormalities. Understanding mechanistic actions of the epigenetic modulators will potentially improve the well-being of individuals suffering from these epigenetic disorders and correct epigenetic abnormalities in embryos produced *in vitro*. This review will summarize the current understanding of epigenetic reprogramming by TET enzymes during early embryogenesis and highlight its clinical relevance and potential implication for assisted reproductive technologies.

KEYWORDS

TET family enzymes, epigenetics (DNA methylation), DNA methylation (5mC), fertilization, DNA demethylation during development

1 Introduction

Mammalian embryo development is initiated by the fertilization event. The haploid genome of oocyte and sperm are combined after fertilization and the genomes undergo origin-specific remodeling of their epigenome. After the remodeling, embryonic cells, i.e., blastomeres, start to possess unique epigenomic make-ups at the time of lineage specification. Proper remodeling of the epigenome is necessary for normal development and the dynamic changes are governed by a series of finely orchestrated events. The epigenetic reprogramming that embryos undergo includes changes to chromatin structure due to the remodeling of histone modifications and DNA methylation. This first wave of reprogramming initiates the change from germ cell specific epigenetic marks to embryo specific marks. Also, lineage-specific epigenetic markers are established as embryonic cells differentiate into fetal and placental lineages.

Global reprogramming of DNA methylation marks in early embryos has been intensively studied because disruption to the remodeling can have severe impact on development. Upon fertilization, a rapid decrease in DNA methylome is observed in multiple species, including humans (Dean et al., 2001; Santos et al., 2002; Guo H. et al., 2014). This demethylation event organizes the epigenetic structure of the embryonic genome prior to zygotic genome activation. Recent studies point out that the DNA demethylation is orchestrated by the ten-eleven translocation (TET1/2/3) enzyme family by oxidizing 5-methylcytosine (5mC) into 5-hydroxymethylcytosine (5hmC) (Tahiliani et al., 2009). Then, the 5hmC are ultimately converted into non-methylated cytosine (He et al., 2011; Shen et al., 2013). Demethylation of the genome is important for embryo survival and normal development, but the specific mechanisms underlying the remodeling are still under investigation (Wossidlo et al., 2011).

Disruption of the *TET* family during early development increases frequency of infertility, neurological defects, and cancer development in animal models (Dawlaty et al., 2011; Dawlaty et al., 2013; Zhang et al., 2013; Fahrner, 2023). The ablation of Tet1 causes neurological defects in spatial learning and short-term memory in mouse models (Rudenko et al., 2013; Zhang et al., 2013). Mouse models lacking functional Tet2 have an increased propensity of hematopoietic cell lineage malignancies (Li et al., 2011). Dysregulation of TET1 or TET2 is also associated with diseases in the clinic (Good et al., 2017; Cao et al., 2019; Jiang, 2020). The mutation or silencing of TET3 causes the onset of Beck-Farhner syndrome, an autosomal dominant epigenetic disorder, in humans (Fahrner, 2023). Clinical data and animal studies highlight conserved roles of the TET family in mammals and their importance for normal development.

In this review, we summarize and discuss recent findings underlying mechanisms regulating epigenetic reprogramming upon fertilization, particularly related with DNA methylation dynamics during preimplantation development in mammals. The mechanism of the reprogramming events will be outlined while emphasizing species specific characteristics. Epigenetic disorders found in patients that are rooted to dysregulated genes involved in the reprogramming process will also be discussed.

2 Epigenetic marks derive successful development

Biochemists and cytologists from the late 19th century were the first to observe that a DNA and protein complex existed in the cell's nucleus, and the complex was named 'chromatin' by Walther Flemming in the 1880's (Olins and Olins, 2003; Deichmann, 2015). Although the role of chromatin was not clear, it was suggested to influence gene expression without changing gene structure. Research on the modification of chromatin structure demonstrated that their conformation is linked to the expression of a gene without changing the DNA sequence, paving the concept of epigenetics.

The family of proteins called histones are the primary protein component of chromatin (Li, 2002). An octamer of these small and highly conserved proteins is associated with approximately 200 base pairs of DNA to form a nucleosome (Li, 2002). The lysine, arginine, and serine residues on the amino-terminal tail of histones can be modified to influence the accessibility of chromatin, thus highlighting the impact of histone tails on gene expression (Li, 2002). For example, transcriptional activation is associated with methylation of lysine on histone H3 at the fourth residue (H3K4me3), H3K36me, and H3K79me (Miao and Natarajan, 2005; Morgan et al., 2005). Alternatively, transcription suppression is accompanied by H3K9me3, H3K27me3, and H4K20me3 marks (Miao and Natarajan, 2005; Morgan et al., 2005). Other post-translational modifications such as phosphorylation, acetylation, and ubiquitylation of histones can also regulate gene activity (Li, 2002). Chromatin structure is also influenced by direct methylation of the nucleic acids within the DNA strand. The 5-methylcytosine (5mC) was first observed by Johnson and Coghill in 1925 (Johnson and Coghill, 1925); however, it wasn't until 1975 when DNA methylation was labeled as an epigenetic mark (Holliday and Pugh, 1975; Riggs, 1975). After identifying presence of 5mC in mammalian, insect, and plant DNA in 1950, their distribution patterns on the genome were confirmed 4 years later (Wyatt, 1950; Sinsheimer et al., 1954). The 5mC marks were specifically detected before guanine (CpG dinucleotides), rather than being randomly distributed throughout the genome (Sinsheimer et al., 1954). In mammalian cells, DNA methylation is predominantly found at CpG dinucleotides, and methylation of CpG dinucleotides in the promoters of genes is typically associated with epigenetic silencing of gene transcription (Weber et al., 2007; Meissner et al., 2008; Jones, 2012). Histone modification and DNA methylation mechanisms are linked together (Li, 2002; Morgan et al., 2005) as DNA methylation marks are added to the genome by DNA methyltransferases (DNMT) and their activity are highly correlated to the local chromatin states that are controlled by histone modifications (Burgers et al., 2002).

Epigenetic marks are in general maintained consistently during cell division, i.e., mitosis. Interestingly, during preimplantation development, highly methylated genomes, inherited from germ cells, are dramatically demethylated until blastocyst stage except for imprinting control regions (ICRs) and certain retrotransposons (Borgel et al., 2010; Smallwood et al., 2011; Kobayashi et al., 2012; Smith et al., 2012; Smith et al., 2014). The maternal and paternal genomes exhibit different rates of DNA demethylation during preimplantation development and distinct demethylation

pathways are involved; the maternal genome is passively demethylated, whereas the paternal genome is actively demethylated (Borgel et al., 2010; Smallwood et al., 2011; Kobayashi et al., 2012; Smith et al., 2012; Smith et al., 2014). Specifically, the paternal pronuclei are demethylated by the TET3 enzymes while the maternal pronuclei are protected by the protein STELLA (Wossidlo et al., 2011; Nakamura et al., 2012). Later in development, DNA methylation marks of the genes that are critical for pluripotency of embryos are re-established by *de novo* methylation (Li et al., 2007; Meissner, 2010). Although the key sequential reprogramming events are conserved across most mammals, species specific differences such as degree of demethylation and timing of onset in *de novo* methylation have been reported (Young and Beaujean, 2004; Hou et al., 2007). Mechanistic actions driving the reprogramming of gamete genome after fertilization have not been fully elucidated.

3 DNA methylation as the main epigenetic marker and its regulation

In mammalian cells, the presence of methylated CpG dinucleotides, specifically 5-methylcytosine (5mC), in the promoter regions is in general interpreted as silencing of genes (Weber et al., 2007; Meissner et al., 2008; Jones, 2012). Non-CpG methylation has recently been identified in other cell types such as oocytes, embryonic stem cells (ESCs), and neurons (Lister et al., 2009; Xie et al., 2012; Lister et al., 2013; Shirane et al., 2013). Methylation of cytosine preceding cytosine (CpC), thymine (CpT), and adenine (CpA) accounts for approximately 15% of cytosine DNA methylation (Ziller et al., 2011) but the epigenetic role of such methylation marks remains to be identified. The role of non-CpG methylation during early embryo development is largely unknown. Interestingly, an average of non-CpG methylation level, mostly CpA bases, is greater in oocytes (~3%) than any other stage of development, including post-implantation (~1%) (Li C. et al., 2018). There is little evidence it has a widespread impact on gene expression during embryogenesis. DNA methylation marks are established by two major *de novo* methyltransferases, DNA methyltransferase 3A (DNMT3A) and DNA methyltransferase 3B (DNMT3B) (Okano et al., 1998; Okano et al., 1999). A catalytically in-active DNMT, DNMT3L, is also involved in *de novo* methylation specifically in germline by stimulating activities of DNMT3A and DNMT3B through direct interaction (Suetake et al., 2004; Ooi et al., 2007). Maintenance of DNA methylation marks is led by DNA methyltransferase 1 (DNMT1). Since DNA replication occurs in semiconservative manner, newly synthesized complimentary sequence on daughter DNA strands lacks DNA methylation. Because DNMT1 preferably bind to hemi-methylated CpG dinucleotides, it functions as a key regulator, which maintain symmetrical DNA methylation levels throughout cell divisions (Bestor et al., 1988; Bestor, 1992). A depletion of DNMT1 results in the passive demethylation of the genome as DNA methylation is diluted after DNA replication (Holliday and Pugh, 1975; Hermann et al., 2004; Nishiyama et al., 2013).

The role and maintenance of 5mC have been intensively studied. Other modifications to the cytosine have been reported; however, their functions are largely unknown. For instance, the hydroxylated form of 5mC, 5-hydroxymethylcytosine (5hmC) was first reported in 1972; and it was originally reported that 5hmC accounted for ~15% of total cytosines in DNA isolated from brain tissues of rat, mouse, and frog (Penn et al., 1972). The presence of 5hmC in mammalian DNA could not be confirmed by other studies until it was robustly detected in the mouse cerebellum and ESCs by two research groups in 2009 (Kriaucionis and Heintz, 2009; Tahiliani et al., 2009). The 5hmC residue accounted for 0.6% of the total nucleotides in mouse Purkinje neurons and 0.03% of the total nucleotides in mouse ESCs (Kriaucionis and Heintz, 2009; Tahiliani et al., 2009). Another study identified 5hmC in various mouse and human tissues with high levels in the central nervous system (Song et al., 2011). Other cytosine bases such as 5-formylcytosine (5fC) and 5-carboxycytosine (5caC) have also been reported. However, the role of the bases is not clearly understood.

Discovery of the diverse cytosine bases prompt investigations on how the bases are converted. Identifying enzymes responsible for converting 5mC into 5hmC was inspired by the production of base J (β-D-glucosyl hydroxymethyluracil) in trypanosomes (Borst and Sabatini, 2008). Base J is a modified thymine associated with gene silencing, similar in function to 5mC in mammals and is synthesized by the hydroxylation of a methyl group of thymine (Borst and Sabatini, 2008). It was suggested enzymes JBP1 and JBP2 catalyzed the hydroxylation of the methyl group of thymine as a part of the 2-oxoglutarate (2OG)- and Fe(II)-dependent oxygenase superfamily (Yu et al., 2007; Cliffe et al., 2009). Following the studies, Tahiliani et al. (2009) identified the ten-eleven translocation (TET) proteins as mammalian homologs of the trypanosome proteins JBP1 and JBP2 and demonstrated that the TET enzymes are 2OG- and Fe(II)-dependent enzymes that catalyze the conversion of 5mC to 5hmC (Tahiliani et al., 2009). Subsequent studies revealed that 5hmC can be further oxidized to 5-formylcytosine (5fC) and 5-carboxycytosine (5caC) by the TET enzymes (He et al., 2011; Ito et al., 2011). The discovery and conversion of the three 5mC derivatives suggested a new demethylation mechanism orchestrated by the TET enzymes. Recent studies found that thymine DNA glycosylase (TDG), an enzyme mediating base excision repair of DNA, has direct activity with 5fC and 5caC, implying that these two cytosine bases are intermediates of the active demethylation process (He et al., 2011; Shen et al., 2013). In addition, conversion of 5mC to 5hmC by the TET enzymes may aid in the acceleration of passive demethylation because affinity of DNMT1 towards 5hmC is much lower than for 5mC in hemi-methylated DNA strands, thus preventing the addition of 5mC to a newly synthesized strand (Hashimoto et al., 2012; Ji et al., 2014). The discovery of the DNA demethylation pathways greatly expanded our understanding of how DNA methylation marks are regulated. Conventionally, it was hypothesized that the lack of DNMT would derive DNA demethylation in cells; however, the theory could not explain some of rapid changes in DNA methylation marks seen in cells especially during embryogenesis. The TET enzyme-mediated DNA demethylation pathway offers more detailed explanation to the dynamic changes in epigenetic marks and provide clues for successful cellular reprogramming and mechanistic understanding to certain diseases associated with aberrant DNA methylation.

TABLE 1 Comparison of the human TET family proteins to domestic species orthologs. Length (number of amino acids) of human TET family member denoted on the left. The percentage of identity shared between each species ortholog and the human protein.

	Length of human protein (AA)	Mouse	Pig	Cattle	Sheep
		Identity (%)	Identity (%)	Identity (%)	Identity (%)
TET1	2165	55.0	77.5	77.5	77.9
TET2	2002	60.1	84.7	82.4	82.8
TET3	1795	89.3	91.6	91.4	91.3

4 DNA methylation during pre-implantation development

The establishment of DNA methylation marks has been extensively studied and its impact on gene regulation is generally understood. Yet, mechanistic pathways of active DNA demethylation and its influence on gene regulation are still under investigation. Active DNA demethylation in mammalian tissues is mediated by the TET enzymes which oxidize the 5mC mark into 5hmC (Kriaucionis and Heintz, 2009; Tahiliani et al., 2009). This discovery quickly advanced our understanding of epigenetic regulation during early embryo development in mammals. Following fertilization, genome wide demethylation process rapidly erases DNA methylation marks, which were inherited from germ cells, and starts to establish embryonic DNA methylation patterns.

Amino acid sequences of TET family are highly conserved among species and share key domains in all species (Table 1). The conserved sequences highlight the importance of TET enzymes in leading epigenetic reprogramming for successful embryo development in mammals. Three TET enzymes, TET1/2/3, are differentially expressed throughout the stages of preimplantation development and responsible for the formation of 5hmC in different stages (Tahiliani et al., 2009; Ito et al., 2010). The TET3 protein is detected in oocytes and zygotes and highly expressed in neurons (Iqbal et al., 2011; Wossidlo et al., 2011; Perera et al., 2015; Yu et al., 2015). The Tet1 and Tet2 proteins are highly expressed in the inner cell mass (ICM) of blastocysts, ESCs, and PGCs (Ito et al., 2010; Vincent et al., 2013). The *TET2* is also highly expressed in hematopoietic stem cells (HSCs) and essential in hematopoiesis, including HSCs self-renewal and lineage commitment (Solary et al., 2014). A *Tet1* knockout (KO) resulted in reduced birth weight and subfertility in both male and female mice, but the modification did not lead to embryo lethality (Dawlaty et al., 2011; Yamaguchi et al., 2012). The mild impact of *Tet1* KO on development has been thought to be due to functional redundancy between Tet1 and Tet2, as they possess overlapping expression patterns in ESCs and HSCs (Costa et al., 2013; Zhao et al., 2015). A double KO of *Tet1* and *Tet2* did not cause any visible abnormalities in mice while its influence on epigenome remains unclear (Wang et al., 2013) Homozygous *Tet3* KO resulted in neonatal lethality (Wang et al., 2013; Tsukada et al., 2015), and the loss of maternal Tet3 caused embryonic sub-lethality (Gu et al., 2011).

The conversion of 5mC to 5hmC is directly mediated by the catalytic domain of TET enzymes. The catalytic domain is located at the carboxyl terminal region of TET enzymes and consists of a cysteine-rich domain (CRD) and two double-stranded beta-helixes (DSBH) (Iyer et al., 2009; Tahiliani et al., 2009) (Figure 1). Two zinc fingers bind the CRD and the DSBH domain to each other to form a compact catalytic domain (Hu et al., 2013). While the catalytic domain is present in all members of the TET family (TET1/2/3), the CXXC domain, which is located at the amino terminal region, is not present in TET2. The CXXC domain mediates specific binding of TET enzymes to DNA containing CpG dinucleotides (Xu et al., 2011; Xu et al., 2012). TET1 and TET3 have a tendency to bind preferentially to CpG-rich promoter regions, and the DNA binding property of the CXXC domain is thought to confer this property (Williams et al., 2011; Wu et al., 2011; Xu et al., 2012). The CXXC domain of an ancestral TET2 was lost through chromosomal inversion during evolution and then became a separate gene, IDAX (also called CXXC4) (Ko et al., 2013). In contrast to TET1 and TET3, 5hmC regulated by TET2 is abundant in gene body and exon regions rather than in promoter regions (Huang et al., 2014). The structural similarities, especially between TET1 and TET3, indicate their overlapping function (Figure 1). However, it is unclear why the TET family genes are differentially expressed during early embryo development.

4.1 Active demethylation of paternal genome

Upon fertilization, the paternal genome exhibits higher methylation level than maternal genome (Bestor, 2000). In mice, the level of CpG methylation of the mature sperm is between 80% and 90%, while mature oocytes show relatively lower-level levels (~40%) (Popp et al., 2010). The highly methylated paternal genome is almost completely demethylated shortly after fertilization while demethylation of maternal genome occurs gradually as embryos divide (Oswald et al., 2000). The removal of methylation marks of paternal genome is almost completed before the onset of DNA replication at pronuclear stage 3 (PN3), suggesting existence of an enzyme-mediated active DNA demethylation although no "demethylase" was identified (Mayer et al., 2000; Oswald et al., 2000). Bisulfite sequencing was difficult to interpret especially in the paternal pronuclei, even though immunofluorescence assays clearly demonstrated a loss of 5mC at the same stage (Hajkova et al., 2008; Wossidlo et al., 2010). The discrepancy between bisulfite sequencing and immunofluorescence assay detection of methylation status was due to the formation of 5hmC. Specifically, both 5mC and 5hmC are read as cytosine in the conventional bisulfite sequencing, thus 5hmC cannot be discriminated from 5mC (Huang et al., 2010).

The discovery of TET enzymes and 5hmC in mature oocytes and zygotes provided clues to understand the active demethylation of

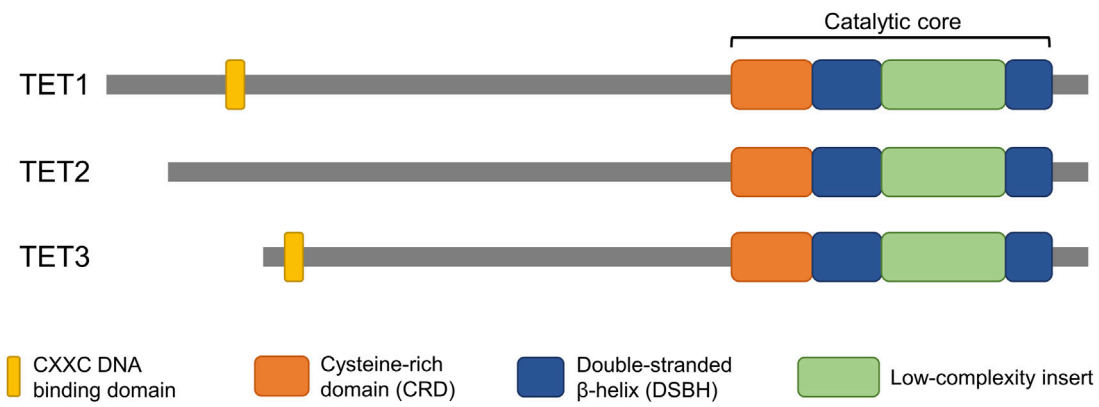

FIGURE 1
Domain structure of TET proteins. The catalytic domain, which is conserved in all members of the TET family, is located at the C-terminus. The CXXC domain, which confers DNA binding properties, is located at the N-terminus of TET1 and TET3 but is not present in TET2. The structural similarities highlight potential overlapping function of the genes.

paternal genome in zygotes (Gu et al., 2011). The TET3 enzyme mediates active demethylation by catalyzing the conversion of 5mC to 5hmC in paternal pronuclei (Gu et al., 2011; Iqbal et al., 2011; Wossidlo et al., 2011). The 5hmC signal is enriched in paternal pronuclei of zygotes (Tahiliani et al., 2009; Ito et al., 2010). Subsequently, the 5hmC is further oxidized to 5fC and 5caC by TET3 in zygotes (Inoue et al., 2011). Immunofluorescent staining of 5hmC has been the main technique to capture the level of 5hmC. Development of diverse molecular tools now allow for more detailed identification of 5hmC signals. Specifically, advanced sequencing methods such as TET-assisted bisulfite sequencing (TAB-Seq), oxidative bisulfite sequencing (oxBS), and TET-assisted pyridine borane sequencing (TAPS) have been developed for detection of 5hmC at base-resolution (Booth et al., 2012; Yu et al., 2012; Liu Y. et al., 2019).

The Tet3 enzyme is enriched in the paternal pronucleus where it catalyzes the oxidation of 5mC to 5hmC (Gu et al., 2011; Wossidlo et al., 2011). In the absence of Tet3, the level of 5mC remained constant in the paternal genome in zygotes (Gu et al., 2011). The Tet3 deficiency also impeded the demethylation of paternal alleles essential for embryo development and pluripotency, such as Oct4 and Nanog and delayed activation of paternal genes in preimplantation embryos (Gu et al., 2011). These findings demonstrate that demethylation of the paternal genome in zygotes is initiated by Tet3-mediated conversion of 5mC to 5hmC and is critical for proper activation of genes essential for embryo development and pluripotency. However, it was argued that a passive demethylation pathway, reliant on DNA replication, was also involved in removal of methylation marks in the paternal pronuclei (Guo F. et al., 2014; Shen et al., 2014). Blocking DNA replication, using a DNA replication inhibitor, maintained DNA methylation level of paternal pronuclei at the same level of sperm DNA, even under Tet3-mediated 5hmC mark formation (Guo F. et al., 2014; Shen et al., 2014). Although the involvement of TET3 on initiating DNA demethylation is widely accepted, a study demonstrated that newly formed 5mC marks via *de novo* methylation are also targeted TET3 and converted into 5hmC (Amouroux et al., 2016). These findings illustrate methylation reprogramming of the paternal genome is a complex process which involves active and passive demethylation and *de novo* methylation processes.

Although deficiency of maternal Tet3 results in sublethality in mice, it is due to haploinsufficiency rather than impaired 5mC oxidation (Inoue et al., 2015). Mouse embryos that bypassed Tet3-mediated 5mC oxidation develop to term normally, and demethylation of paternal genome proceeds as they reached to blastocyst stage, suggesting an existence of compensatory mechanism for defective 5mC oxidation during preimplantation development (Inoue et al., 2015). In particular, Tet1 and Tet3 are on the same branch of the evolutionary tree (Liu D. et al., 2019) and have a similar gene structure (Figure 1). Tet1 expression is relatively lower than Tet3 in developing embryos before the blastocyst stage, but Tet1 protein is apparently detected in early stages such as 2-cell embryos (Kang et al., 2015). In Tet1/3 double knockout embryos strong 5hmC loss and increase of 5mC is observed at 8-cell embryos (Kang et al., 2015). Furthermore, the loss of 5hmC is increased in Tet1/2/3 deficient embryos compared to Tet3 deficient embryos in paternal pronuclei at the zygote stage, suggesting that Tet1 and Tet2 are involved in active demethylation of the paternal genome (Arand et al., 2022). Indeed, Tet1/2 deficiency reduces the levels of 5hmC and 5caC in paternal pronuclei compared to wild-type embryos, implying a distinct role for Tet1 and Tet2 in the sequential oxidation of 5mC to 5caC (Arand et al., 2022). Connection between the loss of 5mC in paternal pronuclei and TET3-driven active demethylation is highly established; however, mechanistic actions underlying the changes remains elusive. In addition to 5hmC, 5fC, and 5caC appear in zygotes concurrently with the loss of 5mC, suggesting that 5hmC is further oxidized potentially by TET3 before cleavage (Inoue et al., 2011). The three 5mC derivatives (5hmC, 5fC, and 5caC) can be direct targets for base-excision repair (BER) pathways mediated by thymine DNA glycosylase (TDG) (He et al., 2011; Maiti and Drohat, 2011). However, depletion of maternal TDG had no effect on zygotic 5fC and 5caC levels (Guo F. et al., 2014), suggesting that TDG is dispensable for paternal pronuclear demethylation. Further studies are necessary to clarify the subsequent demethylation process that

reverts oxidized 5mC to unmethylated cytosine because TDG is not consistently detectable in zygotes (Hajkova et al., 2010).

4.2 Active and passive demethylation of maternal genome

In contrast to the paternal genome, 5mC in the maternal pronucleus is not targeted by TET3 and rather protected from active demethylation in zygotes (Wossidlo et al., 2011). A maternal factor, STELLA is known to play a key protective role against TET3-mediated 5mC oxidation in maternal pronucleus (Wossidlo et al., 2011; Nakamura et al., 2012). The STELLA, also known as PGC7 and DPPA3, is essential for embryo viability and is a nuclear polypeptide that is highly expressed in PGCs, oocytes, and pluripotent cells (Sato et al., 2002; Bowles et al., 2003). The mating of heterozygous *STELLA*-mutant mice resulted in the birth of STELLA-null offspring without developmental defects (Payer et al., 2003; Bortvin et al., 2004). However, embryos derived from oocytes of STELLA-deficient females were arrested during early cleavage, mostly around the 4-cell stage (Payer et al., 2003; Bortvin et al., 2004). The developmental abnormality was due to the lack of maternally inherited STELLA in the oocytes (Payer et al., 2003; Bortvin et al., 2004). It was suggested that STELLA likely protected the maternal genome from demethylation by localizing to the maternal pronucleus in zygotes, although mechanistic actions of the *STELLA* was unknown (Nakamura et al., 2007).

The discovery of 5hmC and TET proteins in mammals has provided clues to the actions of STELLA. Indeed, STELLA deficiency resulted in TET3-mediated 5hmC accumulation in the maternal pronucleus, demonstrating that STELLA was an important maternal factor for protecting the genome of maternal pronucleus against TET3-mediated demethylation (Wossidlo et al., 2011; Nakamura et al., 2012). It has been demonstrated that the protective role of STELLA is determined by its interaction with demethylated histone H3 Lys9 (H3K9me2), a histone methylation mark enriched only in the maternal pronucleus (Nakamura et al., 2012). STELLA preferentially binds to the maternal genome harboring H3K9me2 marks in zygotes and alters chromatin configuration, thus preventing TET3 binding and inhibiting TET3-mediated 5mC oxidation (Nakamura et al., 2012; Bian and Yu, 2014). A recent study demonstrated that the presence of maternal STELLA sequestered UHRF1, a cofactor of DNMT1, from nuclei of oocytes to protect against hypermethylation (Li Y. et al., 2018). A deficiency in STELLA leads to increased methylation levels in metaphase II oocytes and accumulation of 5hmC, presumably due to a higher availability of 5mC that converts into 5hmC (Li Y. et al., 2018; Han et al., 2019). These findings support the interaction and competition between STELLA and TET3 to steer proper demethylation of the maternal genome upon fertilization.

Despite the protective role of STELLA, demethylation of maternal DNA is not solely mediated by replication-dependent dilution. Maternal genome also partially undergoes Tet3-mediated active demethylation in mouse embryos. Tet3 protein and 5mC oxidation derivatives including 5hmC and 5fC are also detected in maternal pronuclei (Guo F. et al., 2014; Shen et al., 2014; Wang et al., 2014). In Tet3 knockout zygotes, demethylation of maternal DNA is partially blocked (Guo F. et al., 2014; Shen et al., 2014). The 5mC bases, or its oxidized derivatives, are converted to unmodified cytosines at the majority of demethylated CpG dinucleotides in maternal DNA, independent of DNA replication dilution during development from oocytes to four-cell stage (Guo F. et al., 2014; Wang et al., 2014). The existence of both active and passive demethylation in the maternal genome is apparent; however, no clear demethylation pathway has been identified. A recent study has demonstrated that differential distribution of hemi-5mC is found in active genes of the maternal genome, and it indicates demethylation strategies to regulate gene expression in the maternal genome (Cao et al., 2023).

5 The DNA demethylation mechanism is conserved in other species

Dynamic changes in DNA methylation levels during preimplantation embryo development exhibit similar patterns in mammalian species (Figure 2). For example, a rapid demethylation of the paternal pronucleus occurs in mice, rats, pigs, and cattle (Dean et al., 2001). However, quantitative differences in the level of DNA methylation exist among the species (Kobayashi et al., 2012; Guo H. et al., 2014; Okae et al., 2014; Smith et al., 2014; Ivanova et al., 2020). For instance, differences in DNA methylation levels between species are apparent in cleavage stage embryos. Pig embryos have higher CpG methylation levels (55%) (Ivanova et al., 2020) than mouse embryos (23%–28%) (Altschuler et al., 1985; Smith et al., 2012) at 8–16 cells stage. The higher DNA methylation level in pig embryos decreases dramatically at the blastocyst stage, reaching the lowest level (13%) (Ivanova et al., 2020) compared to other species (19%–29%) (Altschuler et al., 1985; Smith et al., 2012; Smith et al., 2014; Zhu et al., 2018). In contrast to other species, dramatic DNA demethylation is not observed during preimplantation development in sheep (Beaujean et al., 2004; Zhang et al., 2021). During development from gametes to the 16-cells stage, very limited demethylation occurs, then the level of methylation increases until the blastocyst stage (Beaujean et al., 2004; Zhang et al., 2021).

Consistent with the DNA demethylation process, similar expression patterns of TET enzymes are observed in preimplantation embryos of different species (Figure 2). Transcripts of *TET3* are abundant in oocytes and zygotes, while *TET1* is highly expressed in the relatively late-stage embryos in mice, pigs, cows, and sheep (Ito et al., 2010; Gu et al., 2011; Iqbal et al., 2011; Wossidlo et al., 2011; Lee et al., 2014; Jafarpour et al., 2017; Duan et al., 2019; Uh et al., 2020; Uh and Lee, 2022). In mouse zygotes, the role of Tet3 in the demethylation and formation of 5hmC in paternal pronuclei has been identified (Gu et al., 2011; Iqbal et al., 2011; Wossidlo et al., 2011). Similarly, disruption of TET3 impaired 5hmC formation in porcine zygotes and bovine 2-cell embryos (Lee et al., 2014; Zhang et al., 2017; Cheng et al., 2019), suggesting a conserved role of TET3 in the demethylation of fertilized mammalian embryos. Furthermore, the fine-tuning of post-fertilization demethylation by TET3 is required for the regulation of pluripotency gene expression in mammalian embryos. Impaired DNA methylation and expression levels of pluripotency genes due to *TET3* disruption have been detected in developing embryos of mice, pigs, and cows (Gu et al., 2011; Lee et al., 2014; Zhang et al., 2017; Cheng et al., 2019; Uh and Lee, 2022).

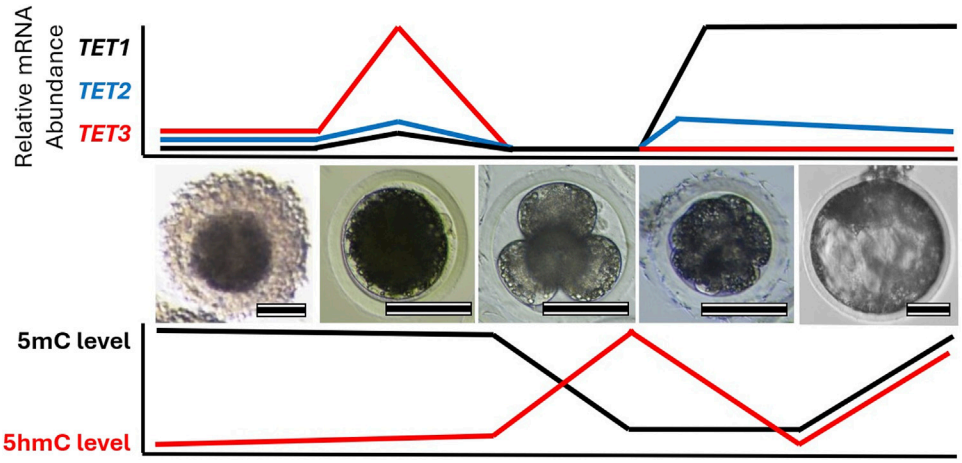

FIGURE 2
Change in TET family transcript abundance with global 5-methylcytosine (5mC) and 5-hydroxymethylcytosine (5hmC) profiles during early embryo development. Images highlight different stages of porcine oocyte and embryo development: (left-to-right) cumulus-oocyte complex, MII oocyte, 4-cell embryo, compacted morula, and blastocyst. Relative mRNA abundance of each TET family member and DNA methylation levels corresponds to each stage are illustrated. Scale bare represents 100 μm.

Genetic ablation of Tet3 leads to perinatal death without pregnancy failure in mice (Gu et al., 2011), but the impact of TET3 deficiency beyond the preimplantation stage has not been reported in other species. TET1, which is enriched in pluripotent stem cells and in the inner cell mass of blastocysts, plays an important role in the regulation of pluripotency. Although Tet1 is dispensable for maintaining pluripotency of mouse embryonic stem cells (Dawlaty et al., 2011), the disruption of *TET1* leads to impaired lineage specification, particularly of the inner cell mass in both mouse and pig blastocysts (Ito et al., 2010; Uh et al., 2020). Conservation of embryonic reprogramming among our domesticated species allows greater understanding of the impact that TET family disruption has on embryo development and their epigenetic landscape (Table 2).

6 Long-term health effects due to TET enzyme disruption

Disruption of epigenetic machinery is known to be linked to several neurodevelopmental and growth abnormalities in the clinic. For example, immunodeficiency-centromeric instability-facial anomalies (ICF) syndrome and Tatton-Brown-Rahman syndrome are caused by mutations in *DNMT3B* and *DNMT3A*, respectively (Vukic and Daxinger, 2019; Kumps et al., 2023). Patients with either syndrome show signs of epigenetic abnormalities. There is global hypomethylation of the genome in patients with Tatton-Brown-Rahman syndrome (Kumps et al., 2023) while regions surrounding the centromeres are hypomethylated in patients with ICF syndrome (Vukic and Daxinger, 2019). Beck-Fahrner syndrome is an autosomal dominant disorder with mutations in the catalytic domain to reduce TET3 enzymatic activity (Beck et al., 2020; Fahrner, 2023). Individuals suffering from Beck-Fahrner syndrome commonly have intellectual disability, autistic traits, movement disorders, hypotonia, and facial dysmorphism (Beck et al., 2020; Fahrner, 2023). There are no consensus diagnostic criteria for Beck-Fahrner syndrome except modifications to the *TET3* gene (Fahrner, 2023).

No other genetic diseases are known to have a direct link to mutations in the TET family. However, there are clinical cases that are rooted to abnormal TET activity or somatic mutation of TET family. These clinical cases are difficult to pinpoint clear association of abnormal TET family to their pathogenesis; however, animal studies indicate potential outcomes if the level of TET family is misregulated (Table 2). Mice with *Tet1* KO had a reduction in birthweight and increased infertility (Dawlaty et al., 2011). Reduced follicle size and follicle number contributed to the subfertile phenotype, but progeny was still viable (Dawlaty et al., 2011). It was observed that the ablation of TET1 caused several neurological defects such as reduced spatial learning and impaired short-term memory although their brain weight, neuron number, synaptic activity, or eyesight memory seemed to be normal (Rudenko et al., 2013; Zhang et al., 2013). The disruption of *TET1* caused promoter hypermethylation and subsequent downregulation of genes associated with neural progenitor proliferation, neuroprotection, and mitochondrial function (Rudenko et al., 2013; Zhang et al., 2013). A different phenotype emerges when *TET2* was disrupted. The *Tet2* KO mice had expanded hematopoietic stem cell and progenitor cell populations (Li et al., 2011; Moran-Crusio et al., 2011; Ito et al., 2019), which induced disorders in myeloid and lymphoid cell lineages mimicking chronic myelomonocytic leukemia (CMML) (Moran-Crusio et al., 2011; Ito et al., 2019). Similar phenotypes are seen in the human clinic as several myeloid malignancies have loss-of-function mutations in TET2 (Li et al., 2011). There are fewer functional studies of *TET3* as the knockout mice model appears to be neonatal lethal (Wang et al., 2013; Tsukada et al., 2015). It was demonstrated that a conditional *Tet3* knockout in brain neurons increased anxiety-like behavior and cortisol production that's similar to Cushing's disease (Antunes et al., 2021).

Various somatic-cell diseases are associated with disruption of the TET family. For example, it has been shown that TET1 is downregulated in many tumor cell lines (Li et al., 2016). In breast cancer, uterine cancer, or glioblastoma, there is an enrichment of a

TABLE 2 Summary of outcomes of disrupting normal TET family function during early embryo development. The targeted TET family member is denoted on the left along with model species and the type of model generated. The impact of TET family disruption on embryo development, epigenetic landscape, and other relevant outcomes are recorded.

Gene	Species	Model	Outcome	Reference
Tet1	Mouse	Global knockout	Reduced birthweight and increased infertility. Severe neurological defects. Promoter hypermethylation and down-regulation of neural-associated genes	Dawlaty et al. (2011); Yamaguchi et al. (2012); Rudenko et al. (2013); Zhang et al. (2013)
TET1	Swine	siRNA knockdown in zygotes	Reduced blastocyst development. Abnormal methylation patterns and abnormal pluripotency gene expression	Uh et al. (2020)
Tet2	Mouse	Global knockout	Expanded hematopoietic progenitor cell populations inducing myeloid and lymphoid lineage disorders	Li et al. (2011); Moran-Crusio et al. (2011); Ito et al. (2019)
Tet1, 2	Mouse	Global double knockout	Successful generation of double-gene mutant mice by zygote injection. Normal birth-rate and no visible developmental abnormalities. Epigenetic profiles were not examined	Wang et al. (2013)
Tet3	Mouse	Global knockout	Neonatal lethal	Wang et al. (2013); Tsukada et al. (2015)
		Germline-specific knockout	Failure to demethylate paternal pronucleus. Disruption of pluripotency genes. Females have reduced fecundity	Gu et al. (2011)
		Neuronal-specific knockout	Increased anxiety-like behavior and cortisol production; like Cushing's disease	Antunes et al. (2021)
TET3	Swine	siRNA knockdown in zygotes	Embryo development was not affected, but expression of pluripotency related genes was suppressed	Lee et al. (2014); Uh and Lee (2022)
		Zygotes overexpressed TET3-mutant only containing CXXC domain	Rapid genome-wide demethylation by 2-cell embryo. Upregulation of pluripotency genes in blastocyst	Uh and Lee (2022)
TET3	Cattle	siRNA knockdown in GV oocytes	Disrupted embryo development. Increased 5mC levels and decreased 5hmC levels. Decreased pluripotency-related gene expression	Cheng et al. (2019)
		TET3 overexpressed in SCNT embryo	Improved embryo development. Decreased methylation and subsequent increased transcriptional activity of pluripotency-related genes	Zhang et al. (2020)
TET3	Goat	siRNA knockdown in MII oocytes	Disruption of DNA demethylation at 2-cell and 4-cell stage. Decreased pluripotency gene expression	Han et al. (2018)
		TET3 overexpressed in SCNT embryo	Improved embryo development, pregnancy rates, and birth rates. Prevented hypermethylation of pluripotency gene promoters	Han et al. (2018)

truncated TET1 isoform that lacks the CXXC domain (Good et al., 2017), thus presumably inhibit normal action of TET1. The promoter methylation of tumor suppressing genes in these cells remained to be high and silenced these genes (Li et al., 2016; Good et al., 2017). Proper regulation of the TET family is necessary to avoid disease onset. It is well established that deregulation of WNT signaling pathway induces early-stage cancer formation (Klaus and Birchmeier, 2008). Normal TET1 expression supports WNT pathway inhibitors that inhibit cell migration, cell division, and epithelial-mesenchymal transition (Duan et al., 2017; Fan et al., 2018; Wu et al., 2019). This disruption of TET2 is common in hematopoietic cancers as its enzymatic activity mediates the formation of immune cells, especially T cells, B cells, and macrophages. Specifically, the loss of TET2 causes hypermethylation in enhancer regions within immune progenitor cells which induces their tumorigenesis (Jiang, 2020). Somatic-cell cancers such as ovarian, head/neck squamous cell carcinoma, gastric, and colorectal cancers have been implicated with TET3 disruption but the mechanistic influence of TET3 remains unclear (Misawa et al., 2018; Cao et al., 2019; Mo et al., 2020).

Abnormal TET family disruption is linked to several neurological diseases found in the clinic. The level of 5hmC is enriched in mammalian brain compared to other tissues (Tahiliani et al., 2009; Globisch et al., 2010; Song et al., 2011). As one of the main regulators of 5hmC, it is not a surprise TET3 is highly present in many brain regions, including the cerebral cortex, hippocampus and cerebellum, and its expression level is stable across different brain regions (Szwagierczak et al., 2010). As aforementioned, mutation in *TET3* causes Beck-Fahrner syndrome where patients present intellectual disability and developmental delay ranging from mild to severe affecting both motor and speech abilities (Beck et al., 2020; Fahrner, 2023). To date, studies using animal models carrying neurons with a disrupted *TET3* gene have reported increased anxiety-like behavior, impaired spatial orientation and short-term memory (Antunes et al., 2021; Antunes et al., 2022; Fan et al., 2022), suggesting potential risks of *TET3*-related neurological disorders in humans. Rare variations of TET2 were often found in patients with early onset Alzheimer's diseases (AD) and frontotemporal dementia (FTD) (Cochran et al., 2020). Similarly, a mouse model carrying repressed level of *Tet2* accelerated at presenting age-related neurogenic decline and the overexpression of *Tet2* could rescue the abnormalities by protecting the animals from age-related neurodegenerative decline and enhanced their cognitive function

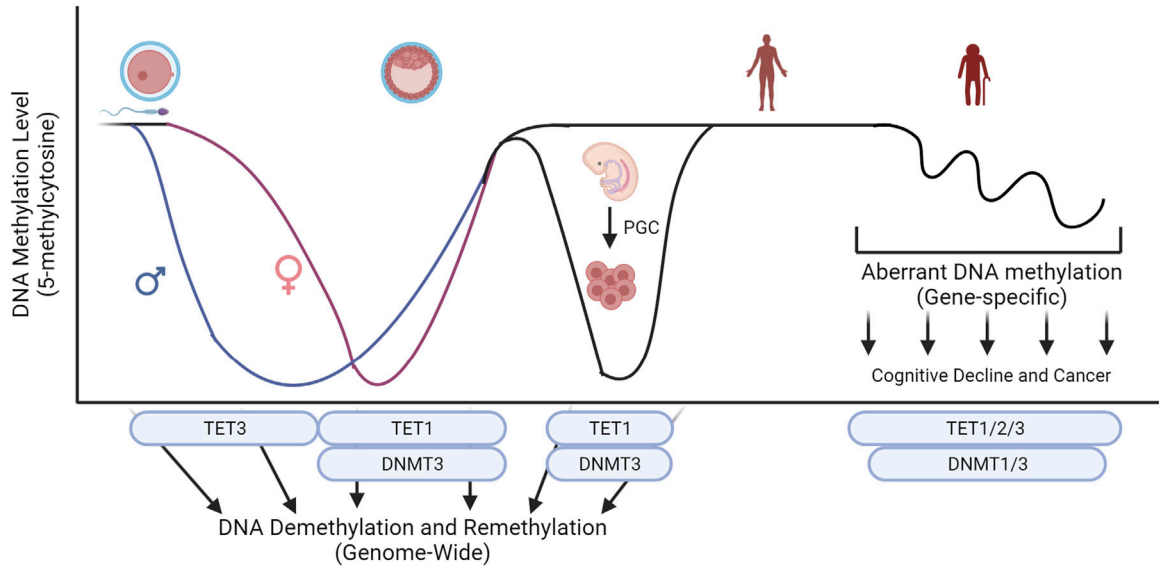

FIGURE 3
Key epigenetic machinery during embryo development and their influence on global levels of 5-methylcytosine. Conversion of 5-methylcytosine by the TET family and *de novo* methylation by DNMT3 sculpture the level of DNA methylation during development. Abnormal global epigenetic reprogramming during development or somatic mutations on key epigenetic regulators can cause diseases including neurological disorders and cancers. Created with BioRender.com.

(Gontier et al., 2018). Patients with psychosis, such as schizophrenia or bipolar disorders, do have increased expression of TET1 and altered levels of 5hmC in their brain (Dong et al., 2012; Kwon et al., 2018). The level of 5hmC is enriched in various neuronal cells (Kriaucionis and Heintz, 2009; Globisch et al., 2010; Ruzov et al., 2011; Mellén et al., 2012) and maintains for months without further modifications in the brain (Bachman et al., 2014). Unlike 5mC levels, which are relatively consistent across different tissue types (Li and Liu, 2011), the level of 5hmC is highly tissue specific, ranging from 0.03% of all cytosines in the spleen to 0.7% in the brain (Globisch et al., 2010; Li and Liu, 2011). The enrichment of 5hmC indicates the base is more than an intermediate during DNA demethylation process, but rather a stable epigenetic mark that regulates activity of nervous system (Gontier et al., 2018).

Improper maintenance of DNA methylation is linked to clinical diseases, and abnormal levels of *TET* family are often associated with the diseases. Abnormal global epigenetic reprogramming during development or somatic mutations on key epigenetic regulators can cause diseases including neurological disorders and cancers (Figure 3). Understanding mechanistic actions of *TET* family using cell and animal models will lead to the development of clinical interventions that can be used to design customized treatment options against these epigenetic disorders.

7 Influence of assisted reproductive technology on embryonic reprogramming

Assisted reproductive technologies (ART) are widely used in the clinic and as a technology to sustain food production around the world. In the clinic, it is estimated that over eight million children have been born via ART in western countries to date, and that approximately 6% of births in Europe in 2014 were conceived through ART (Wennerholm and Bergh, 2020). Although commonly applied, the long-term impact of ART has not been clear. It is estimated that children born using ART have a 1.4 to 1.9-fold higher risk of birth defects than children born naturally (Olson et al., 2005; El-Chaar et al., 2009; Giorgione et al., 2018). A retrospective study also states ART-pregnancies has a risk factor for epigenetic diseases three times higher than normal pregnancy (Uk et al., 2018). Beckwith-Wiedemann and Silver-Russel syndrome, both of which occur due to disruption of epigenetic imprints, have a 10-fold greater frequency in ART-conceived children compared to natural conception (Hiura et al., 2012). In addition, the methylation of CpG sites in placental and umbilical appears to be dysregulated (Katari et al., 2009).

Due to the lack of *in vitro* models for human implantation and placentation, studies in animal models reflect how ART may impact embryo quality and subsequent development. When compared to embryo development *in vivo*, ART-derived blastocysts contain a lower total number of cells and a reduced ratio of inner cell mass to trophectoderm cell numbers (Macháty et al., 1998; Yoshioka et al., 2002; Canovas et al., 2017). Similar to humans, the DNA methylomes are disrupted in domesticated species by the *in vitro* culture system (Barrera et al., 2017; Mani and Mainigi, 2018; Salilew-Wondim et al., 2018). In addition, ART-derived embryos would have a relatively hypermethylated global genome (Deshmukh et al., 2011; Cao et al., 2014; Zhang et al., 2016; Han et al., 2018). ART-induced epigenetic abnormalities are also well-documented in rodent models (Doherty et al., 2000; Market-Velker et al., 2010; Market Velker et al., 2012; Vrooman et al., 2022). Aberrant methylation, in ART-derived embryos, often occurs at promoter and intergenic regions (Canovas et al., 2017; Cao et al., 2020), but

some imprinted regions can be disrupted as well (Canovas et al., 2017). Interestingly, a large proportion of embryos generated from somatic cell nuclear transfer (SCNT) present epigenetic abnormalities because of incomplete epigenetic reprogramming of donor cell DNA (Rideout et al., 2001; Mann and Bartolomei, 2002; Bonk et al., 2007). Embryos derived from SCNT have greater global DNA methylation than other ART-derived embryos (Kwon et al., 2008; Huan et al., 2014). In addition, SCNT-derived embryos that are arrested during early cleavage stages have greater genomic methylation than those that developed into blastocyst (Gao et al., 2018). The hypermethylation of SCNT-embryonic genome appears to disrupt transcription of genes essential for zygotic-genome activation, such as Dppa2 and Dppa4 (Cao et al., 2020). Aberrant *de novo* methylation has been linked to the transcriptional dysregulation of SCNT-embryos (Song et al., 2017; Gao et al., 2018). However, embryonic reprogramming of SCNT-embryos appears to be locus-specific (Zhang et al., 2016), implicating multiple epigenetic modulators being dysregulated.

It is not clear if abnormal activity of epigenetic modulators, such as TET family, in ART-embryos is directly responsible for the epigenetic abnormalities. However, since expression of these pluripotency factors are decreased in cattle and pig *in vitro* embryos (Cheng et al., 2019; Uh et al., 2020), and *TET* family is directly related to pluripotency (Costa et al., 2013), presumably, activity of *TET* family is associated with the epigenetic abnormalities in ART-embryos. Stress from *in vitro* culture systems often disrupt reprogramming ability of the TET family and other epigenetic modulators. Mouse and bovine embryos derived from *in vitro* fertilization have abnormal level of the TET family as it develops into a blastocyst (Chu et al., 2021). Additionally, epigenetic changes occur when embryos are removed from a low oxygen environment (~5%) (Gaspar et al., 2015; Skiles et al., 2018). Bovine embryos exposed to atmospheric levels oxygen (~20%) carry disrupted transcript level of epigenetic modulators such as polycomb repressor complex, histone methyltransferases, histone demethylases, and TET family enzymes (Skiles et al., 2018). Cryopreservation of mouse and bovine oocytes results in a global abnormality in 5mC and 5hmC (Chen et al., 2016; Fu et al., 2019). These abnormalities may be corrected by functioning TET family enzymes. The presence of functional *TET3* greatly influences the transcript abundance of pluripotent factors, such as *NANOG* or *OCT4*, in domesticated species (Gu et al., 2011; Skiles et al., 2018; Cheng et al., 2019; Uh et al., 2020). For instance, cattle and goat embryos that overexpress *TET3* have been shown to perform much better during *in vitro* culture (Han et al., 2018; Zhang et al., 2020). The inclusion of embryokines (such as FGF2 and LIF) does not rescue TET enzyme suppression by *in vitro* culture (Chu et al., 2021), but the activity of available TET enzymes has been stimulated by Vitamin C supplementation which improved 5mC and 5hmC levels (Zhang et al., 2016; Fu et al., 2019; Zhang et al., 2019; Chu et al., 2021). It may be fruitful to investigate how *in vitro* culture systems influence the function of the TET enzymes or their cofactors as the TET family appear to be major contributors to ART-derived embryo success.

Use of embryos produced via ART is an important part of sustaining livestock productivity. Elite genetics can be rapidly introduced into the production system and ART-embryos between elite animals can enhance genetic improvement (Vishwanath, 2003; Sirard, 2018). Although successful animal production from ART-embryos, even at industry scale, is possible, the ART-embryos and subsequent animals may have epigenetic abnormalities. For example, *in vitro* conceived cattle often suffer from large offspring syndrome (LOS), which is caused by aberrant expression of insulin-like growth factor 2 receptor (*IGF2R*) due to abnormal imprinting errors (Urrego et al., 2014). In addition, loss-of-imprinting was detected in ART-induced LOS fetus tissues (Chen et al., 2015). Oocytes derived via *in vitro* maturation is known to have differentially methylated regions, compared to their *in vivo* counterparts (Jiang et al., 2018). Several other developmentally important genes have been shown to be disrupted in *in vitro* bovine embryos, such as X (inactive)-specific transcript (*XIST*) and insulin-like growth factor 2 (*IGF2*) (Urrego et al., 2014). As mentioned earlier, the TET-mediated epigenetic reprogramming is conserved in many species, including livestock. Utilizing mechanistic actions of epigenetic modulators such as the TET family will assist us to correct epigenetic abnormalities associated with ART-embryos.

8 Conclusion

Proper epigenetic reprogramming upon fertilization is coordinated by the *TET* family and is essential for successful development. These enzymes are indispensable as several neurological disorders and cancers are associated with the malfunction of TET enzymes. While species differences do exist, the role of *TET* family is highly conserved among different mammals. Understanding mechanistic actions of the TET family can provide clues to improve the well-being of individuals suffering from epigenetic disorders and maintain epigenetic integrity of embryos produced via assisted reproductive technologies.

Author contributions

TM: Writing–original draft, Writing–review and editing. KU: Writing–original draft, Writing–review and editing. KL: Writing–original draft, Writing–review and editing.

Funding

The author(s) declare that financial support was received for the research, authorship, and/or publication of this article. The authors' work reported herein was supported by 2015-67015-23288 and 2022-67015-36299 from the USDA National Institute of Food and Agriculture.

Conflict of interest

The authors declare that the research was conducted in the absence of any commercial or financial relationships that could be construed as a potential conflict of interest.

Publisher's note

All claims expressed in this article are solely those of the authors and do not necessarily represent those of their affiliated organizations, or those of the publisher, the editors and the reviewers. Any product that may be evaluated in this article, or claim that may be made by its manufacturer, is not guaranteed or endorsed by the publisher.

References

Altschuler, R. A., Hoffman, D. W., Reeks, K. A., and Fex, J. (1985). Localization of dynorphin B-like and alpha-neoendorphin-like immunoreactivities in the Guinea pig organ of Corti. *Hear Res.* 17, 249–258. doi:10.1016/0378-5955(85)90069-3

Amouroux, R., Nashun, B., Shirane, K., Nakagawa, S., Hill, P. W. S., D'Souza, Z., et al. (2016). *De novo* DNA methylation drives 5hmC accumulation in mouse zygotes. *Nat. Cell Biol.* 18, 225–233. doi:10.1038/ncb3296

Antunes, C., Da Silva, J. D., Guerra-Gomes, S., Alves, N. D., Ferreira, F., Loureiro-Campos, E., et al. (2021). Tet3 ablation in adult brain neurons increases anxiety-like behavior and regulates cognitive function in mice. *Mol. Psychiatry* 26, 1445–1457. doi:10.1038/s41380-020-0695-7

Antunes, C., Da Silva, J. D., Guerra-Gomes, S., Alves, N. D., Loureiro-Campos, E., Pinto, L., et al. (2022). Tet3 deletion in adult brain neurons of female mice results in anxiety-like behavior and cognitive impairments. *Mol. Neurobiol.* 59, 4892–4901. doi:10.1007/s12035-022-02883-7

Arand, J., Chiang, H. R., Martin, D., Snyder, M. P., Sage, J., Reijo Pera, R. A., et al. (2022). Tet enzymes are essential for early embryogenesis and completion of embryonic genome activation. *EMBO Rep.* 23, e53968. doi:10.15252/embr.202153968

Bachman, M., Uribe-Lewis, S., Yang, X., Williams, M., Murrell, A., and Balasubramanian, S. (2014). 5-Hydroxymethylcytosine is a predominantly stable DNA modification. *Nat. Chem.* 6, 1049–1055. doi:10.1038/nchem.2064

Barrera, A. D., García, E. V., Hamdi, M., Sánchez-Calabuig, M. J., López-Cardona, Á. P., Balvís, N. F., et al. (2017). Embryo culture in presence of oviductal fluid induces DNA methylation changes in bovine blastocysts. *Reproduction* 154, 1–12. doi:10.1530/REP-16-0651

Beaujean, N., Hartshorne, G., Cavilla, J., Taylor, J., Gardner, J., Wilmut, I., et al. (2004). Non-conservation of mammalian preimplantation methylation dynamics. *Curr. Biol.* 14, R266–R267. doi:10.1016/j.cub.2004.03.019

Beck, D. B., Petracovici, A., He, C., Moore, H. W., Louie, R. J., Ansar, M., et al. (2020). Delineation of a human mendelian disorder of the DNA demethylation machinery: TET3 deficiency. *Am. J. Hum. Genet.* 106, 234–245. doi:10.1016/j.ajhg.2019.12.007

Bestor, T., Laudano, A., Mattaliano, R., and Ingram, V. (1988). Cloning and sequencing of a cDNA encoding DNA methyltransferase of mouse cells. The carboxyl-terminal domain of the mammalian enzymes is related to bacterial restriction methyltransferases. *J. Mol. Biol.* 203, 971–983. doi:10.1016/0022-2836(88)90122-2

Bestor, T. H. (1992). Activation of mammalian DNA methyltransferase by cleavage of a Zn binding regulatory domain. *EMBO J.* 11, 2611–2617. doi:10.1002/j.1460-2075.1992.tb05326.x

Bestor, T. H. (2000). The DNA methyltransferases of mammals. *Hum. Mol. Genet.* 9, 2395–2402. doi:10.1093/hmg/9.16.2395

Bian, C., and Yu, X. (2014). PGC7 suppresses TET3 for protecting DNA methylation. *Nucleic Acids Res.* 42, 2893–2905. doi:10.1093/nar/gkt1261

Bonk, A. J., Cheong, H. T., Li, R., Lai, L., Hao, Y., Liu, Z., et al. (2007). Correlation of developmental differences of nuclear transfer embryos cells to the methylation profiles of nuclear transfer donor cells in swine. *Epigenetics* 2, 179–186. doi:10.4161/epi.2.3.4844

Booth, M. J., Branco, M. R., Ficz, G., Oxley, D., Krueger, F., Reik, W., et al. (2012). Quantitative sequencing of 5-methylcytosine and 5-hydroxymethylcytosine at single-base resolution. *Science* 336, 934–937. doi:10.1126/science.1220671

Borgel, J., Guibert, S., Li, Y., Chiba, H., Schübeler, D., Sasaki, H., et al. (2010). Targets and dynamics of promoter DNA methylation during early mouse development. *Nat. Genet.* 42, 1093–1100. doi:10.1038/ng.708

Borst, P., and Sabatini, R. (2008). Base J: discovery, biosynthesis, and possible functions. *Annu. Rev. Microbiol.* 62, 235–251. doi:10.1146/annurev.micro.62.081307.162750

Bortvin, A., Goodheart, M., Liao, M., and Page, D. C. (2004). Dppa3/Pgc7/stella is a maternal factor and is not required for germ cell specification in mice. *BMC Dev. Biol.* 4, 2. doi:10.1186/1471-213X-4-2

Bowles, J., Teasdale, R. P., James, K., and Koopman, P. (2003). Dppa3 is a marker of pluripotency and has a human homologue that is expressed in germ cell tumours. *Cytogenet. Genome Res.* 101, 261–265. doi:10.1159/000074346

Burgers, W. A., Fuks, F., and Kouzarides, T. (2002). DNA methyltransferases get connected to chromatin. *Trends Genet.* 18, 275–277. doi:10.1016/S0168-9525(02)02667-7

Canovas, S., Ivanova, E., Romar, R., García-Martínez, S., Soriano-Úbeda, C., García-Vázquez, F. A., et al. (2017). DNA methylation and gene expression changes derived from assisted reproductive technologies can be decreased by reproductive fluids. *Elife* 6, e23670. doi:10.7554/eLife.23670

Cao, P., Li, H., Zuo, Y., and Nashun, B. (2020). Characterization of DNA methylation patterns and mining of epigenetic markers during genomic reprogramming in SCNT embryos. *Front. Cell Dev. Biol.* 8, 570107. doi:10.3389/fcell.2020.570107

Cao, T., Pan, W., Sun, X., and Shen, H. (2019). Increased expression of TET3 predicts unfavorable prognosis in patients with ovarian cancer-a bioinformatics integrative analysis. *J. Ovarian Res.* 12, 101. doi:10.1186/s13048-019-0575-4

Cao, Y., Bai, Y., Yuan, T., Song, L., Fan, Y., Ren, L., et al. (2023). Single-cell bisulfite-free 5mC and 5hmC sequencing with high sensitivity and scalability. *Proc. Natl. Acad. Sci. U. S. A.* 120, e2310367120. doi:10.1073/pnas.2310367120

Cao, Z., Zhou, N., Zhang, Y., Zhang, Y., Wu, R., Li, Y., et al. (2014). Dynamic reprogramming of 5-hydroxymethylcytosine during early porcine embryogenesis. *Theriogenology* 81, 496–508. doi:10.1016/j.theriogenology.2013.10.025

Chen, H., Zhang, L., Deng, T., Zou, P., Wang, Y., Quan, F., et al. (2016). Effects of oocyte vitrification on epigenetic status in early bovine embryos. *Theriogenology* 86, 868–878. doi:10.1016/j.theriogenology.2016.03.008

Chen, Z., Hagen, D. E., Elsik, C. G., Ji, T., Morris, C. J., Moon, L. E., et al. (2015). Characterization of global loss of imprinting in fetal overgrowth syndrome induced by assisted reproduction. *Proc. Natl. Acad. Sci. U. S. A.* 112, 4618–4623. doi:10.1073/pnas.1422088112

Cheng, H., Zhang, J., Zhang, S., Zhai, Y., Jiang, Y., An, X., et al. (2019). Tet3 is required for normal *in vitro* fertilization preimplantation embryos development of bovine. *Mol. Reprod. Dev.* 86, 298–307. doi:10.1002/mrd.23105

Chu, M., Yao, F., Xi, G., Yang, J., Zhang, Z., Yang, Q., et al. (2021). Vitamin C rescues *in vitro* embryonic development by correcting impaired active DNA demethylation. *Front. Cell Dev. Biol.* 9, 784244. doi:10.3389/fcell.2021.784244

Cliffe, L. J., Kieft, R., Southern, T., Birkeland, S. R., Marshall, M., Sweeney, K., et al. (2009). JBP1 and JBP2 are two distinct thymidine hydroxylases involved in J biosynthesis in genomic DNA of African trypanosomes. *Nucleic Acids Res.* 37, 1452–1462. doi:10.1093/nar/gkn1067

Cochran, J. N., Geier, E. G., Bonham, L. W., Newberry, J. S., Amaral, M. D., Thompson, M. L., et al. (2020). Non-coding and loss-of-function coding variants in TET2 are associated with multiple neurodegenerative diseases. *Am. J. Hum. Genet.* 106, 632–645. doi:10.1016/j.ajhg.2020.03.010

Costa, Y., Ding, J., Theunissen, T. W., Faiola, F., Hore, T. A., Shliaha, P. V., et al. (2013). NANOG-dependent function of TET1 and TET2 in establishment of pluripotency. *Nature* 495, 370–374. doi:10.1038/nature11925

Dawlaty, M. M., Breiling, A., Le, T., Raddatz, G., Barrasa, M. I., Cheng, A. W., et al. (2013). Combined deficiency of Tet1 and Tet2 causes epigenetic abnormalities but is compatible with postnatal development. *Dev. Cell* 24, 310–323. doi:10.1016/j.devcel.2012.12.015

Dawlaty, M. M., Ganz, K., Powell, B. E., Hu, Y. C., Markoulaki, S., Cheng, A. W., et al. (2011). Tet1 is dispensable for maintaining pluripotency and its loss is compatible with embryonic and postnatal development. *Cell Stem Cell* 9, 166–175. doi:10.1016/j.stem.2011.07.010

Dean, W., tima Santos, F., Stojkovic, M., Zakhartchenko, V., rn Walter, J., Wolf, E., et al. (2001). Conservation of methylation reprogramming in mammalian development: aberrant reprogramming in cloned embryos. *Proc. Natl. Acad. Sci. U. S. A.* 98, 13734–13738. doi:10.1073/pnas.241522698

Deichmann, U. (2015). Chromatin: its history, current research, and the seminal researchers and their philosophy. *Perspect. Biol. Med.* 58, 143–164. doi:10.1353/pbm.2015.0024

Deshmukh, R. S., Østrup, O., Østrup, E., Vejlsted, M., Niemann, H., Lucas-Hahn, A., et al. (2011). DNA methylation in porcine preimplantation embryos developed *in vivo* and produced by *in vitro* fertilization, parthenogenetic activation and somatic cell nuclear transfer. *Epigenetic* 6, 177–187. doi:10.4161/epi.6.2.13519

Doherty, A. S., Mann, M. R., Tremblay, K. D., Bartolomei, M. S., and Schultz, R. M. (2000). Differential effects of culture on imprinted H19 expression in the preimplantation mouse embryo. *Biol. Reprod.* 62, 1526–1535. doi:10.1095/biolreprod62.6.1526

Dong, E., Gavin, D. P., Chen, Y., and Davis, J. (2012). Upregulation of TET1 and downregulation of APOBEC3A and APOBEC3C in the parietal cortex of psychotic patients. *Transl. Psychiatry* 2, e159. doi:10.1038/tp.2012.86

Duan, H., Yan, Z., Chen, W., Wu, Y., Han, J., Guo, H., et al. (2017). TET1 inhibits EMT of ovarian cancer cells through activating Wnt/β-catenin signaling inhibitors DKK1 and SFRP2. *Gynecol. Oncol.* 147, 408–417. doi:10.1016/j.ygyno.2017.08.010

Duan, J., Zhu, L., Dong, H., Zheng, X., Jiang, Z., Chen, J., et al. (2019). Analysis of mRNA abundance for histone variants, histone- and DNA-modifiers in bovine *in vivo* and *in vitro* oocytes and embryos. *Sci. Rep.* 9, 1217. doi:10.1038/s41598-018-38083-4

El-Chaar, D., Yang, Q., Gao, J., Bottomley, J., Leader, A., Wen, S. W., et al. (2009). Risk of birth defects increased in pregnancies conceived by assisted human reproduction. *Fertil. Steril.* 92, 1557–1561. doi:10.1016/j.fertnstert.2008.08.080

Fahrner, J. (2023). "TET3-Related beck-fahrner syndrome," in *GeneReviews*. Editors M. Adam, J. Feldman, G. Mirzaa, R. A. Pagon, S. E. Wallace, L. J. H. Bean, et al. (Seattle: University of Washington).

Fan, B.-F., Hao, B., Dai, Y.-D., Xue, L., Shi, Y.-W., Liu, L., et al. (2022). Deficiency of Tet3 in nucleus accumbens enhances fear generalization and anxiety-like behaviors in mice. *Brain Pathol.* 32, e13080. doi:10.1111/bpa.13080

Fan, J., Zhang, Y., Mu, J., He, X., Shao, B., Zhou, D., et al. (2018). TET1 exerts its anti-tumor functions via demethylating DACT2 and SFRP2 to antagonize Wnt/β-catenin signaling pathway in nasopharyngeal carcinoma cells. *Clin. Epigenetics* 10, 103. doi:10.1186/s13148-018-0535-7

Fu, L., Chang, H., Wang, Z., Xie, X., Chen, H., Lei, Z., et al. (2019). The effects of TETs on DNA methylation and hydroxymethylation of mouse oocytes after vitrification and warming. *Cryobiology* 90, 41–46. doi:10.1016/j.cryobiol.2019.09.001

Gao, R., Wang, C., Gao, Y., Xiu, W., Chen, J., Kou, X., et al. (2018). Inhibition of aberrant DNA Re-methylation improves post-implantation development of somatic cell nuclear transfer embryos. *Cell Stem Cell* 23, 426–435. doi:10.1016/j.stem.2018.07.017

Gaspar, R. C., Arnold, D. R., Corrêa, C. A. P., da Rocha, C. V., Penteado, J. C. T., del Collado, M., et al. (2015). Oxygen tension affects histone remodeling of *in vitro*-produced embryos in a bovine model. *Theriogenology* 83, 1408–1415. doi:10.1016/j.theriogenology.2015.01.002

Giorgione, V., Parazzini, F., Fesslova, V., Cipriani, S., Candiani, M., Inversetti, A., et al. (2018). Congenital heart defects in IVF/ICSI pregnancy: systematic review and meta-analysis. *Ultrasound Obstetrics Gynecol.* 51, 33–42. doi:10.1002/uog.18932

Globisch, D., Münzel, M., Müller, M., Michalakis, S., Wagner, M., Koch, S., et al. (2010). Tissue distribution of 5-hydroxymethylcytosine and search for active demethylation intermediates. *PLoS One* 5, e15367. doi:10.1371/journal.pone.0015367

Gontier, G., Iyer, M., Shea, J. M., Bieri, G., Wheatley, E. G., Ramalho-Santos, M., et al. (2018). Tet2 rescues age-related regenerative decline and enhances cognitive function in the adult mouse brain. *Cell Rep.* 22, 1974–1981. doi:10.1016/j.celrep.2018.02.001

Good, C. R., Madzo, J., Patel, B., Maegawa, S., Engel, N., Jelinek, J., et al. (2017). A novel isoform of TET1 that lacks a CXXC domain is overexpressed in cancer. *Nucleic Acids Res.* 45, 8269–8281. doi:10.1093/nar/gkx435

Gu, T. P., Guo, F., Yang, H., Wu, H. P., Xu, G. F., Liu, W., et al. (2011). The role of Tet3 DNA dioxygenase in epigenetic reprogramming by oocytes. *Nature* 477, 606–610. doi:10.1038/nature10443

Guo, F., Li, X., Liang, D., Li, T., Zhu, P., Guo, H., et al. (2014a). Active and passive demethylation of male and female pronuclear DNA in the mammalian zygote. *Cell Stem Cell* 15, 447–459. doi:10.1016/j.stem.2014.08.003

Guo, H., Zhu, P., Yan, L., Li, R., Hu, B., Lian, Y., et al. (2014b). The DNA methylation landscape of human early embryos. *Nature* 511, 606–610. doi:10.1038/nature13544

Hajkova, P., Ancelin, K., Waldmann, T., Lacoste, N., Lange, U. C., Cesari, F., et al. (2008). Chromatin dynamics during epigenetic reprogramming in the mouse germ line. *Nature* 452, 877–881. doi:10.1038/nature06714

Hajkova, P., Jeffries, S. J., Lee, C., Miller, N., Jackson, S. P., and Surani, M. A. (2010). Genome-wide reprogramming in the mouse germ line entails the base excision repair pathway. *Science* 329, 78–82. doi:10.1126/science.1187945

Han, C., Deng, R., Mao, T., Luo, Y., Wei, B., Meng, P., et al. (2018). Overexpression of Tet3 in donor cells enhances goat somatic cell nuclear transfer efficiency. *FEBS J.* 285, 2708–2723. doi:10.1111/febs.14515

Han, L., Ren, C., Zhang, J., Shu, W., and Wang, Q. (2019). Differential roles of Stella in the modulation of DNA methylation during oocyte and zygotic development. *Cell Discov.* 5, 9. doi:10.1038/s41421-019-0081-2

Hashimoto, H., Liu, Y., Upadhyay, A. K., Chang, Y., Howerton, S. B., Vertino, P. M., et al. (2012). Recognition and potential mechanisms for replication and erasure of cytosine hydroxymethylation. *Nucleic Acids Res.* 40, 4841–4849. doi:10.1093/nar/gks155

He, Y.-F., Li, B.-Z., Li, Z., Liu, P., Wang, Y., Tang, Q., et al. (2011). Tet-mediated formation of 5-carboxylcytosine and its excision by TDG in mammalian DNA. *Science* 333, 1303–1307. doi:10.1126/science.1210944

Hermann, A., Gowher, H., and Jeltsch, A. (2004). Biochemistry and biology of mammalian DNA methyltransferases. *Cell. Mol. Life Sci.* 61, 2571–2587. doi:10.1007/s00018-004-4201-1

Hiura, H., Okae, H., Miyauchi, N., Sato, F., Sato, A., Van De Pette, M., et al. (2012). Characterization of DNA methylation errors in patients with imprinting disorders conceived by assisted reproduction technologies. *Hum. Reprod.* 27, 2541–2548. doi:10.1093/humrep/des197

Holliday, R., and Pugh, J. E. (1975). DNA modification mechanisms and gene activity during development. *Science* 187, 226–232. doi:10.1126/science.187.4173.226

Hou, J., Liu, L., Lei, T. H., Cui, X. H., An, X. R., and Chen, Y. F. (2007). Genomic DNA methylation patterns in bovine preimplantation embryos derived from *in vitro* fertilization. *Sci. China C Life Sci.* 50, 56–61. doi:10.1007/s11427-007-0003-7

Hu, L., Li, Z., Cheng, J., Rao, Q., Gong, W., Liu, M., et al. (2013). Crystal structure of TET2-DNA complex: insight into TET-mediated 5mC oxidation. *Cell* 155, 1545–1555. doi:10.1016/j.cell.2013.11.020

Huan, Y. J., Zhu, J., Wang, H. M., Wu, Z. F., Zhang, J. G., Xie, B. T., et al. (2014). Epigenetic modification agents improve genomic methylation reprogramming in porcine cloned embryos. *J. Reprod. Dev.* 60, 377–382. doi:10.1262/jrd.2014-062

Huang, Y., Chavez, L., Chang, X., Wang, X., Pastor, W. A., Kang, J., et al. (2014). Distinct roles of the methylcytosine oxidases Tet1 and Tet2 in mouse embryonic stem cells. *Proc. Natl. Acad. Sci. U. S. A.* 111, 1361–1366. doi:10.1073/pnas.1322921111

Huang, Y., Pastor, W. A., Shen, Y., Tahiliani, M., Liu, D. R., and Rao, A. (2010). The behaviour of 5-hydroxymethylcytosine in bisulfite sequencing. *PLoS One* 5, e8888. doi:10.1371/journal.pone.0008888

Inoue, A., Shen, L., Dai, Q., He, C., and Zhang, Y. (2011). Generation and replication-dependent dilution of 5fC and 5caC during mouse preimplantation development. *Cell Res.* 21, 1670–1676. doi:10.1038/cr.2011.189

Inoue, A., Shen, L., Matoba, S., and Zhang, Y. (2015). Haploinsufficiency, but not defective paternal 5mC oxidation, accounts for the developmental defects of maternal Tet3 knockouts. *Cell Rep.* 10, 463–470. doi:10.1016/j.celrep.2014.12.049

Iqbal, K., Jin, S. G., Pfeifer, G. P., and Szabó, P. E. (2011). Reprogramming of the paternal genome upon fertilization involves genome-wide oxidation of 5-methylcytosine. *Proc. Natl. Acad. Sci. U. S. A.* 108, 3642–3647. doi:10.1073/pnas.1014033108

Ito, K., Lee, J., Chrysanthou, S., Zhao, Y., Josephs, K., Sato, H., et al. (2019). Non-catalytic roles of Tet2 are essential to regulate hematopoietic stem and progenitor cell homeostasis. *Cell Rep.* 28, 2480–2490. doi:10.1016/j.celrep.2019.07.094

Ito, S., Dalessio, A. C., Taranova, O. V., Hong, K., Sowers, L. C., and Zhang, Y. (2010). Role of tet proteins in 5mC to 5hmC conversion, ES-cell self-renewal and inner cell mass specification. *Nature* 466, 1129–1133. doi:10.1038/nature09303

Ito, S., Shen, L., Dai, Q., Wu, S. C., Collins, L. B., Swenberg, J. A., et al. (2011). Tet proteins can convert 5-methylcytosine to 5-formylcytosine and 5-carboxylcytosine. *Science* 333, 1300–1303. doi:10.1126/science.1210597

Ivanova, E., Canovas, S., Garcia-Martínez, S., Romar, R., Lopes, J. S., Rizos, D., et al. (2020). DNA methylation changes during preimplantation development reveal inter-species differences and reprogramming events at imprinted genes. *Clin. Epigenetics* 12, 64. doi:10.1186/s13148-020-00857-x

Iyer, L. M., Tahiliani, M., Rao, A., and Aravind, L. (2009). Prediction of novel families of enzymes involved in oxidative and other complex modifications of bases in nucleic acids. *Cell Cycle* 8, 1698–1710. doi:10.4161/cc.8.11.8580

Jafarpour, F., Hosseini, S. M., Ostadhosseini, S., Abbasi, H., Dalman, A., and Nasr-Esfahani, M. H. (2017). Comparative dynamics of 5-methylcytosine reprogramming and TET family expression during preimplantation mammalian development in mouse and sheep. *Theriogenology* 89, 86–96. doi:10.1016/j.theriogenology.2016.10.010

Ji, D., You, C., Wang, P., and Wang, Y. (2014). Effects of tet-induced oxidation products of 5-methylcytosine on DNA replication in mammalian cells. *Chem. Res. Toxicol.* 27, 1304–1309. doi:10.1021/tx500169u

Jiang, S. (2020). Tet2 at the interface between cancer and immunity. *Commun. Biol.* 3, 667. doi:10.1038/s42003-020-01391-5

Jiang, Z., Lin, J., Dong, H., Zheng, X., Marjani, S. L., Duan, J., et al. (2018). DNA methylomes of bovine gametes and *in vivo* produced preimplantation embryos. *Biol. Reprod.* 99, 949–959. doi:10.1093/biolre/ioy138

Johnson, T. B., and Coghill, R. D. (1925). Researches on pyrimidines. C111. The discovery of 5-methyl-cytosine in tuberculinic acid, the nucleic acid of the tubercle Bacillus[1]. *J. Am. Chem. Soc.* 47, 2838–2844. doi:10.1021/ja01688a030

Jones, P. A. (2012). Functions of DNA methylation: islands, start sites, gene bodies and beyond. *Nat. Rev. Genet.* 13, 484–492. doi:10.1038/nrg3230

Kang, J., Lienhard, M., Pastor, W. A., Chawla, A., Novotny, M., Tsagaratou, A., et al. (2015). Simultaneous deletion of the methylcytosine oxidases Tet1 and Tet3 increases transcriptome variability in early embryogenesis. *Proc. Natl. Acad. Sci. U. S. A.* 112, E4236–E4245. doi:10.1073/pnas.1510510112

Katari, S., Turan, N., Bibikova, M., Erinle, O., Chalian, R., Foster, M., et al. (2009). DNA methylation and gene expression differences in children conceived *in vitro* or *in vivo*. *Hum. Mol. Genet.* 18, 3769–3778. doi:10.1093/hmg/ddp319

Klaus, A., and Birchmeier, W. (2008). Wnt signalling and its impact on development and cancer. *Nat. Rev. Cancer* 8, 387–398. doi:10.1038/nrc2389

Ko, M., An, J., Bandukwala, H. S., Chavez, L., Aijö, T., Pastor, W. A., et al. (2013). Modulation of TET2 expression and 5-methylcytosine oxidation by the CXXC domain protein IDAX. *Nature* 497, 122–126. doi:10.1038/nature12052

Kobayashi, H., Sakurai, T., Imai, M., Takahashi, N., Fukuda, A., Yayoi, O., et al. (2012). Contribution of intragenic DNA methylation in mouse gametic DNA methylomes to establish Oocyte-specific heritable marks. *PLoS Genet.* 8, e1002440. doi:10.1371/journal.pgen.1002440

Kriaucionis, S., and Heintz, N. (2009). The nuclear DNA base 5-hydroxymethylcytosine is present in purkinje neurons and the brain. *Science* 324, 929–930. doi:10.1126/science.1169786

Kumps, C., D'haenens, E., Kerkhof, J., McConkey, H., Alders, M., Sadikovic, B., et al. (2023). Methylation signatures in clinically variable syndromic disorders: a familial DNMT3A variant in two adults with Tatton-Brown–Rahman syndrome. *Eur. J. Hum. Genet.* 31, 1350–1354. doi:10.1038/s41431-023-01459-w

Kwon, D. J., Park, C. K., Yang, B. K., and Cheong, H. T. (2008). Control of nuclear remodelling and subsequent *in vitro* development and methylation status of porcine nuclear transfer embryos. *Reproduction* 135, 649–656. doi:10.1530/REP-06-0387

Kwon, W., Kim, H., Jeong, J., Sung, Y., Choi, M., Park, S., et al. (2018). Tet1 overexpression leads to anxiety-like behavior and enhanced fear memories *via* the activation of calcium-dependent cascade through Egr1 expression in mice. *FASEB J.* 32, 390–403. doi:10.1096/fj.201601340RR

Lee, K., Hamm, J., Whitworth, K., Spate, L., Park, K. W., Murphy, C. N., et al. (2014). Dynamics of TET family expression in porcine preimplantation embryos is related to zygotic genome activation and required for the maintenance of NANOG. *Dev. Biol.* 386, 86–95. doi:10.1016/j.ydbio.2013.11.024

Li, C., Fan, Y., Li, G., Xu, X., Duan, J., Li, R., et al. (2018a). DNA methylation reprogramming of functional elements during mammalian embryonic development. *Cell Discov.* 4, 41. doi:10.1038/s41421-018-0039-9

Li, E. (2002). Chromatin modification and epigenetic reprogramming in mammalian development. *Nat. Rev. Genet.* 3, 662–673. doi:10.1038/nrg887

Li, J.-Y., Pu, M.-T., Hirasawa, R., Li, B.-Z., Huang, Y.-N., Zeng, R., et al. (2007). Synergistic function of DNA methyltransferases Dnmt3a and Dnmt3b in the methylation of Oct4 and Nanog. *Mol. Cell Biol.* 27, 8748–8759. doi:10.1128/mcb.01380-07

Li, L., Li, C., Mao, H., Du, Z., Chan, W., Murray, P., et al. (2016). Epigenetic inactivation of the CpG demethylase TET1 as a DNA methylation feedback loop in human cancers. *Sci. Rep.* 6, 26591. doi:10.1038/srep26591

Li, W., and Liu, M. (2011). Distribution of 5-hydroxymethylcytosine in different human tissues. *J. Nucleic Acids* 2011, 870726. doi:10.4061/2011/870726

Li, Y., Zhang, Z., Chen, J., Liu, W., Lai, W., Liu, B., et al. (2018b). Stella safeguards the oocyte methylome by preventing *de novo* methylation mediated by DNMT1. *Nature* 564, 136–140. doi:10.1038/s41586-018-0751-5

Li, Z., Cai, X., Cai, C. L., Wang, J., Zhang, W., Petersen, B. E., et al. (2011). Deletion of Tet2 in mice leads to dysregulated hematopoietic stem cells and subsequent development of myeloid malignancies. *Blood* 118, 4509–4518. doi:10.1182/blood-2010-12-325241

Lister, R., Mukamel, E. A., Nery, J. R., Urich, M., Puddifoot, C. A., Johnson, N. D., et al. (2013). Global epigenomic reconfiguration during mammalian brain development. *Science* 341, 1237905. doi:10.1126/science.1237905

Lister, R., Pelizzola, M., Dowen, R. H., Hawkins, R. D., Hon, G., Tonti-Filippini, J., et al. (2009). Human DNA methylomes at base resolution show widespread epigenomic differences. *Nature* 462, 315–322. doi:10.1038/nature08514

Liu, D., Li, G., and Zuo, Y. (2019a). Function determinants of TET proteins: the arrangements of sequence motifs with specific codes. *Brief. Bioinform* 20, 1826–1835. doi:10.1093/bib/bby053

Liu, Y., Siejka-Zielińska, P., Velikova, G., Bi, Y., Yuan, F., Tomkova, M., et al. (2019b). Bisulfite-free direct detection of 5-methylcytosine and 5-hydroxymethylcytosine at base resolution. *Nat. Biotechnol.* 37, 424–429. doi:10.1038/s41587-019-0041-2

Macháty, Z., Day, B. N., and Prather, R. S. (1998). Development of early porcine embryos *in vitro* and *in vivo*. *Biol. Reprod.* 59, 451–455. doi:10.1095/biolreprod59.2.451

Maiti, A., and Drohat, A. C. (2011). Thymine DNA glycosylase can rapidly excise 5-formylcytosine and 5-carboxylcytosine: potential implications for active demethylation of CpG sites. *J. Biol. Chem.* 286, 35334–35338. doi:10.1074/jbc.C111.284620

Mani, S., and Mainigi, M. (2018). Embryo culture conditions and the epigenome. *Semin. Reprod. Med.* 36, 211–220. doi:10.1055/s-0038-1675777

Mann, M. R. W., and Bartolomei, M. S. (2002). Epigenetic reprogramming in the mammalian embryo: struggle of the clones. *Genome Biol.* 3, REVIEWS1003. doi:10.1186/gb-2002-3-2-reviews1003

Market Velker, B. A., Denomme, M. M., and Mann, M. R. W. (2012). Loss of genomic imprinting in mouse embryos with fast rates of preimplantation development in culture. *Biol. Reprod.* 86 (143), 1–16. doi:10.1095/biolreprod.111.096602

Market-Velker, B. A., Fernandes, A. D., and Mann, M. R. W. (2010). Side-by-side comparison of five commercial media systems in a mouse model: suboptimal *in vitro* culture interferes with imprint maintenance. *Biol. Reprod.* 83, 938–950. doi:10.1095/biolreprod.110.085480

Mayer, W., Niveleau, A., Walter, J., Fundele, R., and Haaf, T. (2000). Demethylation of the zygotic paternal genome. *Nature* 403, 501–502. doi:10.1038/35000656

Meissner, A. (2010). Epigenetic modifications in pluripotent and differentiated cells. *Nat. Biotechnol.* 28, 1079–1088. doi:10.1038/nbt.1684

Meissner, A., Mikkelsen, T. S., Gu, H., Wernig, M., Hanna, J., Sivachenko, A., et al. (2008). Genome-scale DNA methylation maps of pluripotent and differentiated cells. *Nature* 454, 766–770. doi:10.1038/nature07107

Mellén, M., Ayata, P., Dewell, S., Kriaucionis, S., and Heintz, N. (2012). MeCP2 binds to 5hmC enriched within active genes and accessible chromatin in the nervous system. *Cell* 151, 1417–1430. doi:10.1016/j.cell.2012.11.022

Miao, F., and Natarajan, R. (2005). Mapping global histone methylation patterns in the coding regions of human genes. *Mol. Cell Biol.* 25, 4650–4661. doi:10.1128/MCB.25.11.4650-4661.2005

Misawa, K., Imai, A., Mochizuki, D., Mima, M., Endo, S., Misawa, Y., et al. (2018). Association of TET3 epigenetic inactivation with head and neck cancer. *Oncotarget* 9, 24480–24493. doi:10.18632/oncotarget.25333

Mo, H. Y., An, C. H., Choi, E. J., Yoo, N. J., and Lee, S. H. (2020). Somatic mutation and loss of expression of a candidate tumor suppressor gene TET3 in gastric and colorectal cancers. *Pathol. Res. Pract.* 216, 152759. doi:10.1016/j.prp.2019.152759

Moran-Crusio, K., Reavie, L., Shih, A., Abdel-Wahab, O., Ndiaye-Lobry, D., Lobry, C., et al. (2011). Tet2 loss leads to increased hematopoietic stem cell self-renewal and myeloid transformation. *Cancer Cell* 20, 11–24. doi:10.1016/j.ccr.2011.06.001

Morgan, H. D., Santos, F., Green, K., Dean, W., and Reik, W. (2005). Epigenetic reprogramming in mammals. *Hum. Mol. Genet.* 14, R47–R58. doi:10.1093/hmg/ddi114

Nakamura, T., Arai, Y., Umehara, H., Masuhara, M., Kimura, T., Taniguchi, H., et al. (2007). PGC7/Stella protects against DNA demethylation in early embryogenesis. *Nat. Cell Biol.* 9, 64–71. doi:10.1038/ncb1519

Nakamura, T., Liu, Y. J., Nakashima, H., Umehara, H., Inoue, K., Matoba, S., et al. (2012). PGC7 binds histone H3K9me2 to protect against conversion of 5mC to 5hmC in early embryos. *Nature* 486, 415–419. doi:10.1038/nature11093

Nishiyama, A., Yamaguchi, L., Sharif, J., Johmura, Y., Kawamura, T., Nakanishi, K., et al. (2013). Uhrf1-dependent H3K23 ubiquitylation couples maintenance DNA methylation and replication. *Nature* 502, 249–253. doi:10.1038/nature12488

Okae, H., Chiba, H., Hiura, H., Hamada, H., Sato, A., Utsunomiya, T., et al. (2014). Genome-wide analysis of DNA methylation dynamics during early human development. *PLoS Genet.* 10, e1004868. doi:10.1371/journal.pgen.1004868

Okano, M., Bell, D. W., Haber, D. A., and Li, E. (1999). DNA methyltransferases Dnmt3a and Dnmt3b are essential for *de novo* methylation and mammalian development. *Cell* 99, 247–257. doi:10.1016/S0092-8674(00)81656-6

Okano, M., Xie, S., and Li, E. (1998). Cloning and characterization of a family of novel mammalian DNA (cytosine-5) methyltransferases. *Nat. Genet.* 19, 219–220. doi:10.1038/890

Olins, D. E., and Olins, A. L. (2003). Chromatin history: our view from the bridge. *Nat. Rev. Mol. Cell Biol.* 4, 809–814. doi:10.1038/nrm1225

Olson, C. K., Keppler-Noreuil, K. M., Romitti, P. A., Budelier, W. T., Ryan, G., Sparks, A. E. T., et al. (2005). *In vitro* fertilization is associated with an increase in major birth defects. *Fertil. Steril.* 84, 1308–1315. doi:10.1016/j.fertnstert.2005.03.086

Ooi, S. K. T., Qiu, C., Bernstein, E., Li, K., Jia, D., Yang, Z., et al. (2007). DNMT3L connects unmethylated lysine 4 of histone H3 to *de novo* methylation of DNA. *Nature* 448, 714–717. doi:10.1038/nature05987

Oswald, J., Engemann, S., Lane, N., Mayer, W., Olek, A., Fundele, R., et al. (2000). Active demethylation of the paternal genome in the mouse zygote. *Curr. Biol.* 10, 475–478. doi:10.1016/S0960-9822(00)00448-6

Payer, B., Saitou, M., Barton, S. C., Thresher, R., Dixon, J. P. C., Zahn, D., et al. (2003). Stella is a maternal effect gene required for normal early development in mice. *Curr. Biol.* 13, 2110–2117. doi:10.1016/j.cub.2003.11.026

Penn, N. W., Suwalski, R., O'Riley, C., Bojanowski, K., and Yura, R. (1972). The presence of 5-hydroxymethylcytosine in animal deoxyribonucleic acid. *Biochem. J.* 126, 781–790. doi:10.1042/bj1260781

Perera, A., Eisen, D., Wagner, M., Laube, S. K., Künzel, A. F., Koch, S., et al. (2015). TET3 is recruited by REST for context-specific hydroxymethylation and induction of gene expression. *Cell Rep.* 11, 283–294. doi:10.1016/j.celrep.2015.03.020

Popp, C., Dean, W., Feng, S., Cokus, S. J., Andrews, S., Pellegrini, M., et al. (2010). Genome-wide erasure of DNA methylation in mouse primordial germ cells is affected by AID deficiency. *Nature* 463, 1101–1105. doi:10.1038/nature08829

Rideout, W., Eggan, K., and Jaenisch, R. (2001). Nuclear cloning and epigenetic reprogramming of the genome. *Science* 293, 1093–1098. doi:10.1126/science.1063206

Riggs, A. D. (1975). X inactivation, differentiation, and DNA methylation. *Cytogenet Genome Res.* 14, 9–25. doi:10.1159/000130315

Rudenko, A., Dawlaty, M. M., Seo, J., Cheng, A. W., Meng, J., Le, T., et al. (2013). Tet1 is critical for neuronal activity-regulated gene expression and memory extinction. *Neuron* 79, 1109–1122. doi:10.1016/j.neuron.2013.08.003

Ruzov, A., Tsenkina, Y., Serio, A., Dudnakova, T., Fletcher, J., Bai, Y., et al. (2011). Lineage-specific distribution of high levels of genomic 5-hydroxymethylcytosine in mammalian development. *Cell Res.* 21, 1332–1342. doi:10.1038/cr.2011.113

Salilew-Wondim, D., Saeed-Zidane, M., Hoelker, M., Gebremedhn, S., Poirier, M., Pandey, H. O., et al. (2018). Genome-wide DNA methylation patterns of bovine blastocysts derived from *in vivo* embryos subjected to *in vitro* culture before, during or after embryonic genome activation. *BMC Genomics* 19, 424. doi:10.1186/s12864-018-4826-3

Santos, F., Hendrich, B., Reik, W., and Dean, W. (2002). Dynamic reprogramming of DNA methylation in the early mouse embryo. *Dev. Biol.* 241, 172–182. doi:10.1006/dbio.2001.0501

Sato, M., Kimura, T., Kurokawa, K., Fujita, Y., Abe, K., Masuhara, M., et al. (2002). Identification of PGC7, a new gene expressed specifically in preimplantation embryos and germ cells. *Mech. Dev.* 113, 91–94. doi:10.1016/S0925-4773(02)00002-3

Shen, L., Inoue, A., He, J., Liu, Y., Lu, F., and Zhang, Y. (2014). Tet3 and DNA replication mediate demethylation of both the maternal and paternal genomes in mouse zygotes. *Cell Stem Cell* 15, 459–471. doi:10.1016/j.stem.2014.09.002

Shen, L., Wu, H., Diep, D., Yamaguchi, S., D'Alessio, A. C., Fung, H. L., et al. (2013). Genome-wide analysis reveals TET- and TDG-dependent 5-methylcytosine oxidation dynamics. *Cell* 153, 692–706. doi:10.1016/j.cell.2013.04.002

Shirane, K., Toh, H., Kobayashi, H., Miura, F., Chiba, H., Ito, T., et al. (2013). Mouse oocyte methylomes at base resolution reveal genome-wide accumulation of non-CpG methylation and role of DNA methyltransferases. *PLoS Genet.* 9, e1003439. doi:10.1371/journal.pgen.1003439

Sinsheimer, R. L., Koerner, J. F., Vadla, J., and Lunan, K. (1954). The action of pancreatic desoxyribonuclease. I. Isolation of mono- and dinucleotides. *J. Biol. Chem.* 208, 445–459. doi:10.1016/s0021-9258(18)65663-7

Sirard, M.-A. (2018). 40 years of bovine IVF in the new genomic selection context. *Reproduction* 156, R1–R7. doi:10.1530/REP-18-0008

Skiles, W. M., Kester, A., Pryor, J. H., Westhusin, M. E., Golding, M. C., and Long, C. R. (2018). Oxygen-induced alterations in the expression of chromatin modifying enzymes and the transcriptional regulation of imprinted genes. *Gene Expr. Patterns* 28, 1–11. doi:10.1016/j.gep.2018.01.001

Smallwood, S. A., Tomizawa, S. I., Krueger, F., Ruf, N., Carli, N., Segonds-Pichon, A., et al. (2011). Dynamic CpG island methylation landscape in oocytes and preimplantation embryos. *Nat. Genet.* 43, 811–814. doi:10.1038/ng.864

Smith, Z. D., Chan, M. M., Humm, K. C., Karnik, R., Mekhoubad, S., Regev, A., et al. (2014). DNA methylation dynamics of the human preimplantation embryo. *Nature* 511, 611–615. doi:10.1038/nature13581

Smith, Z. D., Chan, M. M., Mikkelsen, T. S., Gu, H., Gnirke, A., Regev, A., et al. (2012). A unique regulatory phase of DNA methylation in the early mammalian embryo. *Nature* 484, 339–344. doi:10.1038/nature10960

Solary, E., Bernard, O. A., Tefferi, A., Fuks, F., and Vainchenker, W. (2014). The Ten-Eleven Translocation-2 (TET2) gene in hematopoiesis and hematopoietic diseases. *Leukemia* 28, 485–496. doi:10.1038/leu.2013.337

Song, C. X., Szulwach, K. E., Fu, Y., Dai, Q., Yi, C., Li, X., et al. (2011). Selective chemical labeling reveals the genome-wide distribution of 5-hydroxymethylcytosine. *Nat. Biotechnol.* 29, 68–72. doi:10.1038/nbt.1732

Song, X., Liu, Z., He, H., Wang, J., Li, H., Li, J., et al. (2017). Dnmt1s in donor cells is a barrier to SCNT-mediated DNA methylation reprogramming in pigs. *Oncotarget* 8, 34980–34991. doi:10.18632/oncotarget.16507

Suetake, I., Shinozaki, F., Miyagawa, J., Takeshima, H., and Tajima, S. (2004). DNMT3L stimulates the DNA methylation activity of Dnmt3a and Dnmt3b through a direct interaction. *J. Biol. Chem.* 279, 27816–27823. doi:10.1074/jbc.M400181200

Szwagierczak, A., Bultmann, S., Schmidt, C. S., Spada, F., and Leonhardt, H. (2010). Sensitive enzymatic quantification of 5-hydroxymethylcytosine in genomic DNA. *Nucleic Acids Res.* 38, e181. doi:10.1093/nar/gkq684

Tahiliani, M., Koh, K. P., Shen, Y., Pastor, W. A., Bandukwala, H., Brudno, Y., et al. (2009). Conversion of 5-methylcytosine to 5-hydroxymethylcytosine in mammalian DNA by MLL partner TET1. *Science* 324, 930–935. doi:10.1126/science.1170116

Tsukada, Y. I., Akiyama, T., and Nakayama, K. I. (2015). Maternal TET3 is dispensable for embryonic development but is required for neonatal growth. *Sci. Rep.* 5, 15876. doi:10.1038/srep15876

Uh, K., and Lee, K. (2022). Ten-Eleven Translocation-3 CXXC domain is critical for postfertilization demethylation and expression of pluripotency genes in pig embryos†. *Biol. Reprod.* 107, 1205–1216. doi:10.1093/biolre/ioac129

Uh, K., Ryu, J., Farrell, K., Wax, N., and Lee, K. (2020). TET family regulates the embryonic pluripotency of porcine preimplantation embryos by maintaining the DNA methylation level of NANOG. *Epigenetics* 15, 1228–1242. doi:10.1080/15592294.2020.1762392

Uk, A., Collardeau-Frachon, S., Scanvion, Q., Michon, L., and Amar, E. (2018). Assisted Reproductive Technologies and imprinting disorders: results of a study from a French congenital malformations registry. *Eur. J. Med. Genet.* 61, 518–523. doi:10.1016/j.ejmg.2018.05.017

Urrego, R., Rodriguez-Osorio, N., and Niemann, H. (2014). Epigenetic disorders and altered gene expression after use of Assisted Reproductive Technologies in domestic cattle. *Epigenetics* 9, 803–815. doi:10.4161/epi.28711

Vincent, J. J., Huang, Y., Chen, P. Y., Feng, S., Calvopiña, J. H., Nee, K., et al. (2013). Stage-specific roles for Tet1 and Tet2 in DNA demethylation in primordial germ cells. *Cell Stem Cell* 12, 470–478. doi:10.1016/j.stem.2013.01.016

Vishwanath, R. (2003). Artificial insemination: the state of the art. *Theriogenology* 59, 571–584. doi:10.1016/S0093-691X(02)01241-4

Vrooman, L. A., Rhon-Calderon, E. A., Suri, K. V., Dahiya, A. K., Lan, Y., Schultz, R. M., et al. (2022). Placental abnormalities are associated with specific windows of embryo culture in a mouse model. *Front. Cell Dev. Biol.* 10, 884088. doi:10.3389/fcell.2022.884088

Vukic, M., and Daxinger, L. (2019). DNA methylation in disease: immunodeficiency, Centromeric instability, Facial anomalies syndrome. *Essays Biochem.* 63, 773–783. doi:10.1042/EBC20190035

Wang, H., Yang, H., Shivalila, C. S., Dawlaty, M. M., Cheng, A. W., Zhang, F., et al. (2013). One-step generation of mice carrying mutations in multiple genes by CRISPR/cas-mediated genome engineering. *Cell* 153, 910–918. doi:10.1016/j.cell.2013.04.025

Wang, L., Zhang, J., Duan, J., Gao, X., Zhu, W., Lu, X., et al. (2014). Programming and inheritance of parental DNA methylomes in mammals. *Cell* 157, 979–991. doi:10.1016/j.cell.2014.04.017

Weber, M., Hellmann, I., Stadler, M. B., Ramos, L., Pääbo, S., Rebhan, M., et al. (2007). Distribution, silencing potential and evolutionary impact of promoter DNA methylation in the human genome. *Nat. Genet.* 39, 457–466. doi:10.1038/ng1990

Wennerholm, U.-B., and Bergh, C. (2020). Perinatal outcome in children born after assisted reproductive technologies. *Ups. J. Med. Sci.* 125, 158–166. doi:10.1080/03009734.2020.1726534

Williams, K., Christensen, J., Pedersen, M. T., Johansen, J. V., Cloos, P. A. C., Rappsilber, J., et al. (2011). TET1 and hydroxymethylcytosine in transcription and DNA methylation fidelity. *Nature* 473, 343–348. doi:10.1038/nature10066

Wossidlo, M., Arand, J., Sebastiano, V., Lepikhov, K., Boiani, M., Reinhardt, R., et al. (2010). Dynamic link of DNA demethylation, DNA strand breaks and repair in mouse zygotes. *EMBO J.* 29, 1877–1888. doi:10.1038/emboj.2010.80

Wossidlo, M., Nakamura, T., Lepikhov, K., Marques, C. J., Zakhartchenko, V., Boiani, M., et al. (2011). 5-Hydroxymethylcytosine in the mammalian zygote is linked with epigenetic reprogramming. *Nat. Commun.* 2, 241. doi:10.1038/ncomms1240

Wu, H., D'Alessio, A. C., Ito, S., Xia, K., Wang, Z., Cui, K., et al. (2011). Dual functions of Tet1 in transcriptional regulation in mouse embryonic stem cells. *Nature* 473, 389–393. doi:10.1038/nature09934

Wu, J., Li, H., Shi, M., Zhu, Y., Ma, Y., Zhong, Y., et al. (2019). TET1-mediated DNA hydroxymethylation activates inhibitors of the Wnt/β-catenin signaling pathway to suppress EMT in pancreatic tumor cells. *J. Exp. Clin. Cancer Res.* 38, 348. doi:10.1186/s13046-019-1334-5

Wyatt, G. R. (1950). Occurrence of 5-methylcytosine in nucleic acids. *Nature* 166, 237–238. doi:10.1038/166237b0

Xie, W., Barr, C. L., Kim, A., Yue, F., Lee, A. Y., Eubanks, J., et al. (2012). Base-resolution analyses of sequence and parent-of-origin dependent DNA methylation in the mouse genome. *Cell* 148, 816–831. doi:10.1016/j.cell.2011.12.035

Xu, Y., Wu, F., Tan, L., Kong, L., Xiong, L., Deng, J., et al. (2011). Genome-wide regulation of 5hmC, 5mC, and gene expression by Tet1 hydroxylase in mouse embryonic stem cells. *Mol. Cell* 42, 451–464. doi:10.1016/j.molcel.2011.04.005

Xu, Y., Xu, C., Kato, A., Tempel, W., Abreu, J. G., Bian, C., et al. (2012). Tet3 CXXC domain and dioxygenase activity cooperatively regulate key genes for Xenopus eye and neural development. *Cell* 151, 1200–1213. doi:10.1016/j.cell.2012.11.014

Yamaguchi, S., Hong, K., Liu, R., Shen, L., Inoue, A., Diep, D., et al. (2012). Tet1 controls meiosis by regulating meiotic gene expression. *Nature* 492, 443–447. doi:10.1038/nature11709

Yoshioka, K., Suzuki, C., Tanaka, A., Anas, I. M.-K., and Iwamura, S. (2002). Birth of piglets derived from porcine zygotes cultured in a chemically defined medium. *Biol. Reprod.* 66, 112–119. doi:10.1095/biolreprod66.1.112

Young, L. E., and Beaujean, N. (2004). DNA methylation in the preimplantation embryo: the differing stories of the mouse and sheep. *Anim. Reprod. Sci.* 82–83, 61–78. doi:10.1016/j.anireprosci.2004.05.020

Yu, H., Su, Y., Shin, J., Zhong, C., Guo, J. U., Weng, Y. L., et al. (2015). Tet3 regulates synaptic transmission and homeostatic plasticity via DNA oxidation and repair. *Nat. Neurosci.* 18, 836–843. doi:10.1038/nn.4008

Yu, M., Hon, G. C., Szulwach, K. E., Song, C. X., Zhang, L., Kim, A., et al. (2012). Base-resolution analysis of 5-hydroxymethylcytosine in the mammalian genome. *Cell* 149, 1368–1380. doi:10.1016/j.cell.2012.04.027

Yu, Z., Genest, P. A., ter Riet, B., Sweeney, K., DiPaolo, C., Kieft, R., et al. (2007). The protein that binds to DNA base J in trypanosomatids has features of a thymidine hydroxylase. *Nucleic Acids Res.* 35, 2107–2115. doi:10.1093/nar/gkm049

Zhang, J., Hao, L., Wei, Q., Zhang, S., Cheng, H., Zhai, Y., et al. (2020). TET3 overexpression facilitates DNA reprogramming and early development of bovine SCNT embryos. *Reproduction* 160, 379–391. doi:10.1530/REP-20-0021

Zhang, J., Zhang, S., Wang, Y., Cheng, H., Hao, L., Zhai, Y., et al. (2017). Effect of TET inhibitor on bovine parthenogenetic embryo development. *PLoS One* 12, e0189542. doi:10.1371/journal.pone.0189542

Zhang, R. R., Cui, Q. Y., Murai, K., Lim, Y. C., Smith, Z. D., Jin, S., et al. (2013). Tet1 regulates adult hippocampal neurogenesis and cognition. *Cell Stem Cell* 13, 237–245. doi:10.1016/j.stem.2013.05.006

Zhang, S., Chen, X., Wang, F., An, X., Tang, B., Zhang, X., et al. (2016). Aberrant DNA methylation reprogramming in bovine SCNT preimplantation embryos. *Sci. Rep.* 6, 30345. doi:10.1038/srep30345

Zhang, Z., He, C., Zhang, L., Zhu, T., Lv, D., Li, G., et al. (2019). Alpha-ketoglutarate affects murine embryo development through metabolic and epigenetic modulations. *Reproduction* 158 (2), 123–133. doi:10.1530/REP-19-0018

Zhang, Z., Xu, J., Lyu, S., Xin, X., Shi, Q., Huang, Y., et al. (2021). Whole-genome DNA methylation dynamics of sheep preimplantation embryo investigated by single-cell DNA methylome sequencing. *Front. Genet.* 12, 753144. doi:10.3389/fgene.2021.753144

Zhao, Z., Chen, L., Dawlaty, M. M., Pan, F., Weeks, O., Zhou, Y., et al. (2015). Combined loss of Tet1 and Tet2 promotes B cell, but not myeloid malignancies, in mice. *Cell Rep.* 13, 1692–1704. doi:10.1016/j.celrep.2015.10.037

Zhu, P., Guo, H., Ren, Y., Hou, Y., Dong, J., Li, R., et al. (2018). Single-cell DNA methylome sequencing of human preimplantation embryos. *Nat. Genet.* 50, 12–19. doi:10.1038/s41588-017-0007-6

Ziller, M. J., Müller, F., Liao, J., Zhang, Y., Gu, H., Bock, C., et al. (2011). Genomic distribution and inter-sample variation of non-CpG methylation across human cell types. *PLoS Genet.* 7, e1002389. doi:10.1371/journal.pgen.1002389

frontiers | Frontiers in Cell and Developmental Biology

TYPE Original Research
PUBLISHED 25 October 2024
DOI 10.3389/fcell.2024.1447630

Check for updates

OPEN ACCESS

EDITED BY
Maria Eugenia Teves,
Virginia Commonwealth University,
United States

REVIEWED BY
Eduardo R. S. Roldan,
Spanish National Research Council (CSIC),
Spain
Rafael Oliva,
University of Barcelona, Spain

*CORRESPONDENCE
Katerina Komrskova,
katerina.komrskova@ibt.cas.cz

†These authors have contributed equally to this work

RECEIVED 13 June 2024
ACCEPTED 27 September 2024
PUBLISHED 25 October 2024

CITATION
Sanovec O, Frolikova M, Kraus V, Vondrakova J, Qasemi M, Spevakova D, Simonik O, Moritz L, Caswell DL, Liska F, Ded L, Cerny J, Avidor-Reiss T, Hammoud SS, Schorle H, Postlerova P, Steger K and Komrskova K (2024) Protamine 2 deficiency results in Septin 12 abnormalities.
Front. Cell Dev. Biol. 12:1447630.
doi: 10.3389/fcell.2024.1447630

COPYRIGHT
© 2024 Sanovec, Frolikova, Kraus, Vondrakova, Qasemi, Spevakova, Simonik, Moritz, Caswell, Liska, Ded, Cerny, Avidor-Reiss, Hammoud, Schorle, Postlerova, Steger and Komrskova. This is an open-access article distributed under the terms of the Creative Commons Attribution License (CC BY). The use, distribution or reproduction in other forums is permitted, provided the original author(s) and the copyright owner(s) are credited and that the original publication in this journal is cited, in accordance with accepted academic practice. No use, distribution or reproduction is permitted which does not comply with these terms.

Protamine 2 deficiency results in Septin 12 abnormalities

Ondrej Sanovec[1,2†], Michaela Frolikova[1†], Veronika Kraus[1], Jana Vondrakova[1], Maryam Qasemi[1], Daniela Spevakova[1], Ondrej Simonik[1], Lindsay Moritz[3], Drew Lewis Caswell[4], Frantisek Liska[5], Lukas Ded[1], Jiri Cerny[6], Tomer Avidor-Reiss[4,7], Saher Sue Hammoud[3], Hubert Schorle[8], Pavla Postlerova[1], Klaus Steger[9] and Katerina Komrskova[1,10]*

[1]Laboratory of Reproductive Biology, Institute of Biotechnology, Czech Academy of Sciences, BIOCEV, Vestec, Czechia, [2]Department of Physiology, Faculty of Science, Charles University, Prague, Czechia, [3]Department of Human Genetics, University of Michigan, Ann Arbor, MI, United States, [4]Department of Biological Sciences, College of Natural Sciences and Mathematics, University of Toledo, Toledo, OH, United States, [5]Institute of Biology and Medical Genetics, First Faculty of Medicine, Charles University and General University Hospital in Prague, Prague, Czechia, [6]Laboratory of Structural Bioinformatics of Proteins, Institute of Biotechnology Czech Academy of Sciences, BIOCEV, Vestec, Czechia, [7]Department of Urology, College of Medicine and Life Sciences, University of Toledo, Toledo, OH, United States, [8]Department of Developmental Pathology, Institute of Pathology, University Hospital Bonn, Bonn, Germany, [9]Clinic of Urology, Paediatric Urology and Andrology, Molecular Andrology, Justus Liebig University of Giessen, Giessen, Germany, [10]Department of Zoology, Faculty of Science, Charles University, Prague, Czechia

There is a well-established link between abnormal sperm chromatin states and poor motility, however, how these two processes are interdependent is unknown. Here, we identified a possible mechanistic insight by showing that Protamine 2, a nuclear DNA packaging protein in sperm, directly interacts with cytoskeletal protein Septin 12, which is associated with sperm motility. Septin 12 has several isoforms, and we show, that in the *Prm2*$^{-/-}$ sperm, the short one (Mw 36 kDa) is mis-localized, while two long isoforms (Mw 40 and 41 kDa) are unexpectedly lost in *Prm2*$^{-/-}$ sperm chromatin-bound protein fractions. Septin 12 co-immunoprecipitated with Protamine 2 in the testicular cell lysate of WT mice and with Lamin B1/2/3 in co-transfected HEK cells despite we did not observe changes in Lamin B2/B3 proteins or SUN4 expression in *Prm2*$^{-/-}$ testes. Furthermore, the *Prm2*$^{-/-}$ sperm have on average a smaller sperm nucleus and aberrant acrosome biogenesis. In humans, patients with low sperm motility (asthenozoospermia) have imbalanced histone–protamine 1/2 ratio, modified levels of cytoskeletal proteins and we detected retained Septin 12 isoforms (Mw 40 and 41 kDa) in the sperm membrane, chromatin-bound and tubulin/mitochondria protein fractions. In conclusion, our findings present potential interaction between Septin 12 and Protamine 2 or Lamin B2/3 and describe a new connection between their expression and localization, contributing likely to low sperm motility and morphological abnormalities.

KEYWORDS

Protamine 2 deficiency, Septin 12, sperm, asthenozoospermia, sperm immotility, annulus

Introduction

Spermiogenesis is a complex process essential for transforming round spermatids into mature sperm. A crucial step in this process is the histone–protamine exchange, which plays an important role in DNA hyper-condensation. This exchange is initiated in elongating spermatids and is completed during epididymal maturation. During spermiogenesis, spermatids reduce their size by releasing most organelles and residual cytoplasm in the form of the cytoplasmic droplet (Cooper, 2005), and consequently, by histone–protamine exchange in the nucleus, the highly condensed DNA structure is formed. This DNA hyper-condensation is secured by protamines, small arginine-rich proteins, which bind to the minor as well as major grooves of the DNA, resulting in about a 6-fold increase in DNA compaction compared to histones-loaded DNA (Coelingh et al., 1969; Balhorn, 1982; Ward and Coffey, 1991; Mukherjee et al., 2021). This extensive compaction is not only essential for the efficient packaging of DNA and gene silencing but also to protect sperm DNA during the passage through the female reproductive tract (Schneider et al., 2020a). Notably, the replacement of histones by protamines is incomplete, and histone retention in mature sperm varies significantly among species, from 15% in humans to 1% in mice (Gatewood et al., 1987; Brunner et al., 2014; Hammoud et al., 2009; Erkek et al., 2013; Hisano et al., 2013).

There are two known types of protamines, Protamine 1 (P1) and Protamine 2 (P2), in mammals. While Protamine 1 is present in all mammals, Protamine 2 protein is lost in some species (Ammer et al., 1986). Humans have a 1:1 ratio of P1:P2, whereas in mice, Protamine 2 is more abundant, comprising about 65% of the total Protamine level (Corzett et al., 2002). On the other hand, in mammals such as bulls or boars, Protamine 2 is absent due to the mutation in the promoter region (Maier et al., 1990), and in these species, DNA packaging is organized solely by Protamine 1. It was shown in humans and could be true for other species, that the protamine ratio is important for sperm fertilizing ability (Schagdarsurengin et al., 2012) and that the relative proportion of sperm Protamine 1 to Protamine 2 mRNA can serve as a valuable clinical parameter to estimate men's fertility and fertilizing capacity in an assisted reproductive techniques such as IVF (*in vitro* fertilization) or ICSI (intracytoplasmic sperm injection) (Rogenhofer et al., 2013). Moreover, a protamine mRNA ratio likely affects the fertilization ability of sperm and plays a significant role in the initiation of gene expression in the early embryo (Rogenhofer et al., 2017). The negative impact of an aberrant protamine mRNA ratio in embryonic development may be due to changes in chromatin composition and abnormal histone retention (Rogenhofer et al., 2017; Schagdarsurengin and Steger, 2016). P1:P2 protein level ratio reflects the sperm quality and fertilization potential (De Yebra et al., 1993; Oliva, 2006; Nanassy et al., 2011), ranging in fertile men from 0.54 to 1.43 (Nanassy et al., 2011) being on average 0.99 while higher (20%) or lower (3.5%) P1 abundance is reported in sub-fertile patients.

Based on the evidence that the histone–protamine ratio impacts sperm fertilization ability in humans, a Protamine 2 knock-out mouse strain (*Prm2*$^{-/-}$) was established (Schneider et al., 2016) to investigate the consequence of loss of Protamine 2. Interestingly, *Prm2*$^{+/-}$ males are fertile, and sperm retain physiologically normal head morphology and motility, while *Prm2*$^{-/-}$ males are sterile, and their sperm display severe phenotypical abnormalities, including fragmented DNA, detached acrosomes at the acrosome-nuclear interface, a higher abundance of reactive oxygen species (ROS), damaged plasma membrane, atypically bent flagellum and loss of motility (Schneider et al., 2016; Schneider et al., 2020b). Further, the deletion of *Prm2* in mice affected sperm DNA hyper-condensation and integrity and resulted in abnormal acrosome anchorage and flagellum bending, both of which are likely linked to the cytoskeleton function (Schneider et al., 2016).

In spermiogenesis, the cytoskeleton plays a crucial role during acrosome formation, when an actin-keratin structure called acroplaxome emerges. In sperm, the acroplaxome is located in the subacrosomal region and is composed of F-actin and Keratin-5 (Kierszenbaum et al., 2003). This structure is essential for anchoring the acrosome to the nucleus as well as to facilitate myosin-Va mediated vesicular transport by contributing to sperm maturation (Kierszenbaum et al., 2004; Dunleavy et al., 2019). The position of the acroplaxome is likely directed by some proteins of the LINC (LInker of Nucleoskeleton and Cytoskeleton) complex and the ability of keratin-5 to bind to the nuclear lamina (Dunleavy et al., 2019). The LINC complex, which facilitates the connection between the cytoskeleton and nucleoskeleton, is composed of SUN (Sad1/UNc84 homology domain-containing) proteins situated in the inner nuclear membrane and KASH (Klarsicht/Anc1/Syne1 homology domain-containing) proteins located in the outer nuclear membrane (reviewed in Kmonickova et al., 2020).

Regarding our study, during spermiogenesis, the localization of SUN protein was shown to be affected by testis-specific Septin 12 (Yeh et al., 2019), which is essential for the correct positioning of the testis-specific SUN4-Lamin B1 complex and sperm head shaping. Lamin Bs are type V intermediate filaments and play various roles in spermiogenesis. Lamin B1 is present in all stages of spermatogenesis, and its function is to decrease the mechanical strength of the nuclear envelope during meiotic chromosome movements (Pereira et al., 2019). On the other hand, Lamin B3 is a spermiogenesis-specific protein. Lamin B3 replaces its longer splicing variant, Lamin B2, during spermiogenesis, and it is suggested that Lamin B3 is essential for nuclear reshaping during spermiogenesis by making the nuclear envelope less stable and more flexible (Furukawa and Hotta, 1993; Schütz et al., 2005a; Schütz et al., 2005b). In relevance to above mentioned connection between SUN and Septin 12 (Yeh et al., 2019), the *Prm2*$^{-/-}$ phenotype resembles *SUN4*$^{-/-}$and *Sept12*$^{+/-}$ mouse models, particularly the loss of tail elongation and abnormal sperm head shaping, and for *Septin12*$^{+/-}$ sperm additionally aberrantly formed tails and decreased motility (Lin et al., 2009; Calvi et al., 2015). Septin 12, as a member of the Septin cytoskeleton protein family, has a conserved GTP binding domain and forms filamentous structures (Mostowy and Cossart, 2012). Septin 12 also contributes to the organization of cytoskeletal proteins and can interact with actin and tubulin and mediates their crosstalk (Nakos et al., 2022). Testis-specific Septin 12 is primarily expressed in male postmeiotic germ cells (Lin et al., 2009; Lin et al., 2011b) with six isoforms described in mice (isoform 1 with calculated molecular mass of 36.0 kDa, isoform 2 of 31.8 kDa, isoform 3 of 40.9 kDa, isoform X1 of 41.3 kDa, isoform X2 of 34.6 kDa, and isoform X3 of 33.3 kDa) and five in humans (isoform 1 with calculated molecular mass of 35.2 kDa, isoform 2 and X2 of 40.7 kDa, isoform X1 of 41.6 kDa, isoform X3 of

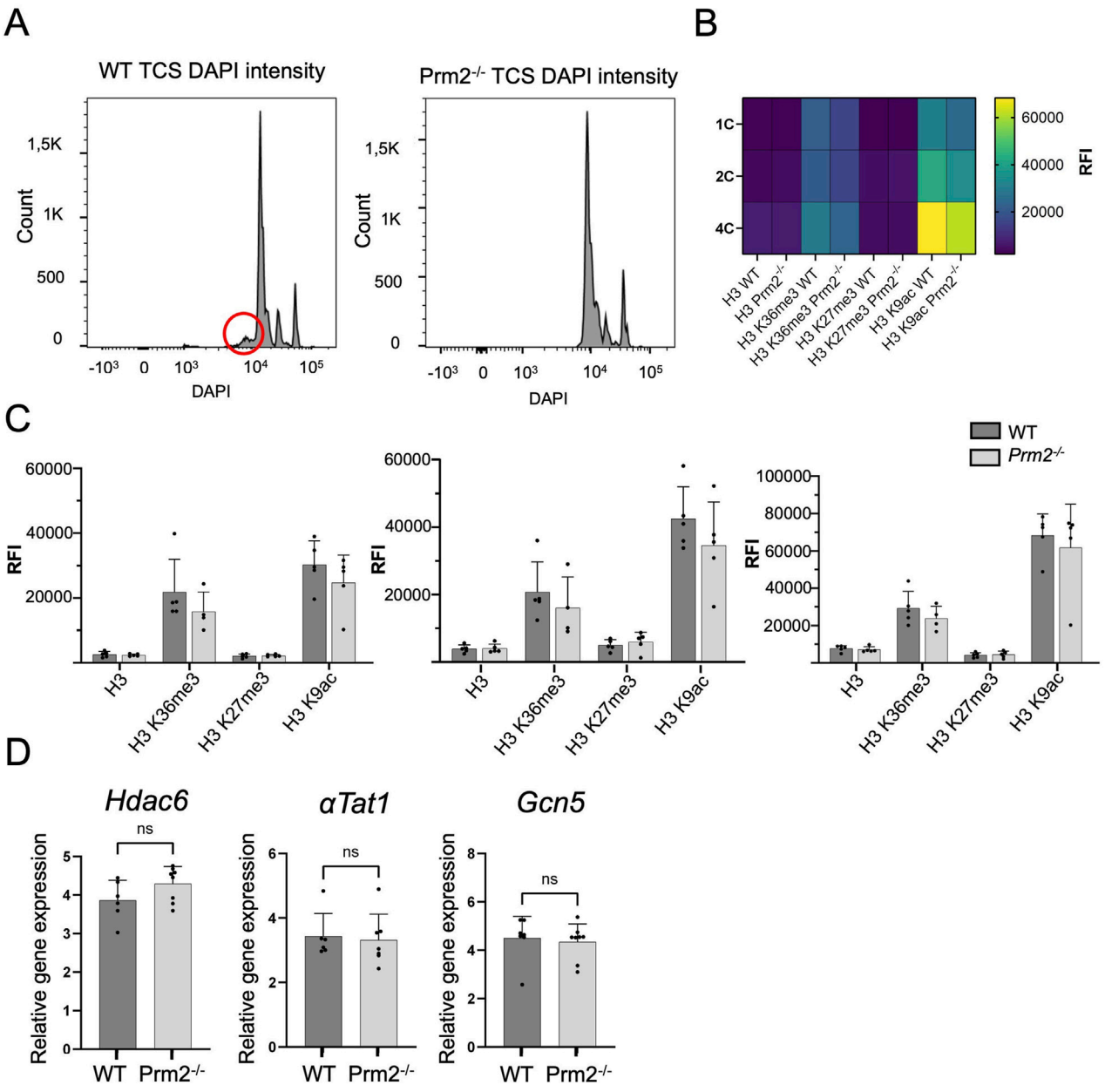

FIGURE 1
Protamine 2 deletion resulted in histone abundance in testicular cells. **(A)** Distribution of testicular cells based on DAPI intensity (ploidy). The red circle indicates sub-haploid cells present only in WT mouse testis. **(B)** Heat map summarising relative fluorescent intensity (RFI) of all histones stained in all cell populations in both WT and *Prm2*$^{-/-}$ testicular cells. 1C - haploid cells; 2C - diploid cells; 4C - tetraploid cells. n = 5, *t*-Test, at least 50,000 events were recorded for each measurement. **(C)** Comparison of RFI of individual histones in WT and *Prm2*$^{-/-}$ in testicular cells. **(D)** qPCR showing no difference in relative gene expression of Hdac6 (Histone deacetylase 6), αTat1 (Alpha-tubulin N-acetyltransferase), and Gcn5 (General control non-depressible 5 also called lysine acetyltransferase 2A) in testicular cells. n = 8, Mann-Whitney test.

34.0 kDa) (https://www.ncbi.nlm.nih.gov/protein/). In mice, Septin 12 is localized to the manchette in elongating spermatids, the neck in elongated spermatids, and the annulus, head, and acrosome in maturated sperm (Yeh et al., 2019). In humans, Septin 12 is present in sperm mainly within the annulus and, to a lesser extent, in the midpiece and head (Lin et al., 2009), particularly to the nucleus edge (Lin et al., 2011a), where it is likely associated with the nuclear membrane, connecting piece, mitochondrial sheet, and annulus (Lin et al., 2011b). Previous studies reported a decreased level of Septin 12 in men suffering from asthenozoospermia and correlated Septin 12 malfunction with sperm morphology abnormalities (Kuo et al., 2012; Ihara et al., 2005; Sugino et al., 2008; Lhuillier et al., 2009). Notably, patients with asthenozoospermia exhibited differences in the Protamine 1 to Protamine 2 ratio compared to the control group (Mengual et al., 2003). Point mutations of Septin 12 affecting the GTP-binding region of human Septin 12 were also linked to pathozoospermia, and these mutations are known to disrupt the Septin 12 filamentous structure (Kuo et al., 2012; Lin et al., 2011a). Besides, Septin 12 interaction with α- and β-tubulin are thought to influence

head and tail development, supported by sperm of *Septin12*$^{+/-}$ males, which displayed unphysiologically formed heads and scattered α- and β-tubulin patterns, resulting in bent and disorganized tails results (Kuo et al., 2012).

To extend the knowledge, we aimed to address the molecular mechanism and protein interactions underlying the above-described phenotypes. We studied the interplay between histone–protamine exchange in connection to sperm motility using the *Prm2*$^{-/-}$ mouse model and compared the results with those of asthenozoospermic men with aberrant Protamine 1/2 ratio. Using biochemical and advanced microscopical techniques, we addressed the localization of Septin 12 during spermiogenesis and in mature mouse and human sperm and defined new potential interaction partners such as Protamine 2, Lamin B2, and Lamin B3.

Results

Protamine 2 deletion disrupted DNA packaging, histone abundance, and selected epigenetic modifications

DNA Flow cytometric (FCM) analysis of testicular cell populations represents a rapid, sensitive, and quantitative method for evaluating germ cell maturation during spermatogenesis. Staining DNA in testicular cell suspension followed by FCM allows discrimination of cell populations with different ploidy based on their fluorescence intensity (Rodríguez-Casuriaga and Geisinger, 2021). In our study, using this method, we revealed differences in DNA hyper-condensation during spermiogenesis between WT and *Prm2*$^{-/-}$ (Figure 1A), specifically a peak, that represents elongated spermatids and sperm containing sub-haploid DNA content in *Prm2*$^{-/-}$ testicular cell samples, was absent. The sub-haploid peak in adult mouse testis cell suspensions reflects the transition from histone–complexed to protamine-complexed DNA, as tight chromatin packaging reduces DNA sites available for fluorochrome binding resulting in an apparent sub-haploid DNA content (Zante et al., 1977; Spanò and Evenson, 1993). The absence of this peak representing sub-haploid cells indicate disruption of DNA hyper-condensation in *Prm2*$^{-/-}$ germ cells and signifies that the DNA condensation in *Prm2*$^{-/-}$ sperm is likely resembling elongating spermatids in WT. The other main peaks, which represent haploid cells (1C), diploid cells (2C), and tetraploid cells (4C) were detected in both WT and *Prm2*$^{-/-}$ mice (n = 5).

During the histone–protamine exchange, specific histone modifications (H1, H2A, H2B, H3) play a crucial role (Wang et al., 2019). However, the histone epigenetic modifications in the *Prm2*$^{-/-}$ mouse model have remained unexplored. We employed immunofluorescent staining followed by FCM (gating strategy Supplementary Figure S1) to investigate potential alterations in epigenetic histone modifications within the *Prm2*$^{-/-}$ testicular cells. In the first step, we evaluated the abundance of core histone H3, as well as selected histone modifications, such as H3K27Me3, H3K36Me3, and H3K9Ac in testicular cells (Figures 1B, C). The FCM analysis revealed no significant differences in the levels of studied histones and their modifications among the haploid (1C), diploid (2C), and tetraploid (4C) cell populations of both WT and *Prm2*$^{-/-}$ mice (n = 5) (Figure 1C). Additionally, qRT-PCR analysis of *Hdac6* (Histone deacetylase 6), *αTat1* (Alpha-tubulin N-acetyltransferase), and *Gcn5* (General control non-depressible five also called lysine acetyltransferase 2A) in testes did not reveal any difference in the gene expression of these enzymes (Figure 1D). The results of gene and protein expression indicate that the depletion of *Prm2* does not significantly change H3K27Me3, H3K36Me3, H3K9Ac histone modifications when normalised to core histone H3.

Sperm morphology is impaired in *Prm2*$^{-/-}$ mice

Previous studies characterizing the *Prm2*$^{-/-}$ mouse model focused on possible disruption of spermiogenesis and reported mainly sperm damage during the epididymal maturation (Schneider et al., 2016; Schneider et al., 2020b). In our study, we focused on the morphology of sperm isolated from the testes, caput, corpus, and cauda of epididymis using Coomassie Brilliant Blue staining (Figure 2A). Four morphological types of sperm were identified; type 1 – morphologically normal looking; type 2 – tail bent around the head; type 3 – tail partially wrapped around the head; and type 4 – tail completely wrapped around the head (Figure 2A). Statistical analysis revealed no significant difference in the number of morphologically normal testicular sperm between WT and *Prm2*$^{-/-}$ (Figure 2B, straight dashed line). However, in all epididymal regions, the number of morphologically normal sperm was significantly lower in the *Prm2*$^{-/-}$ compared to WT (caput $p = 0.0005$; corpus and cauda $p < 0.0001$; Figure 2B, bend full line). The number of abnormal sperm was also significantly increased in epididymal regions of *Prm2*$^{-/-}$ mice compared to WT (caput $p = 0.0004$; corpus and cauda $p < 0.0001$). Based on the obtained data and the observation of Schneider and colleagues (2016 and 2020) we concluded that the *Prm2*$^{-/-}$ sperm morphology is mainly disturbed during individual stages of epididymal maturation, and the sperm of testicular origin did not display altered morphology compared to WT (Schneider et al., 2016; Schneider et al., 2020b).

A more in-depth analysis of the caudal sperm revealed a decreased area of the nuclei in *Prm2*$^{-/-}$ sperm (Figure 2C), which is overall in accordance with previously reported findings (Schneider et al., 2020b). The detailed measurements delivered more robust data and revealed that the average area of the WT nucleus is 18.47 μm^2 ± 1.13 (n = 106), and that of the *Prm2*$^{-/-}$ is 9.57 ± 1.99 (n = 176), which is about 50% smaller ($p < 0.0001$). The small nuclei size in *Prm2*$^{-/-}$ is independent of the sperm type. Interestingly, there is a significant difference between the *Prm2*$^{-/-}$ sperm Type 2 and Type 3 ($p = 0.006$) and between Type 2 and Type 4 ($p = 0.042$), indicating that Type 2 *Prm2*$^{-/-}$ sperm nuclei are larger than the others. In addition, we measured the length of the nuclear indentation of caudal sperm (Figure 2D) and found out that the average length of the indentation is 1.87 μm ± 0.19 (n = 101) in WT, compared to 1.39 μm ± 0.24 (n = 128) in *Prm2*$^{-/-}$, which is about 25% smaller ($p < 0.0001$). The nucleus indentation size is independent of the sperm type for both WT and *Prm2*$^{-/-}$ sperm. There is also a significant difference in the number of sperm 90-degree post-neck tail kink between WT and *Prm2*$^{-/-}$ (Figure 1E). We never observed a 90-degree post-neck tail kink in WT sperm and 32% of *Prm2*$^{-/-}$ sperm (n = 176). The kink was present in 60% of Type 2 *Prm2*$^{-/-}$ sperm (n = 75), 13% of Type 3 (n = 61), and 7.9% of Type 4 sperm. The 90-degree post-neck tail kink in *Prm2*$^{-/-}$ is observed predominantly in Types 2 and 3 of *Prm2*$^{-/-}$ sperm.

10.3389/fcell.2024.1447630

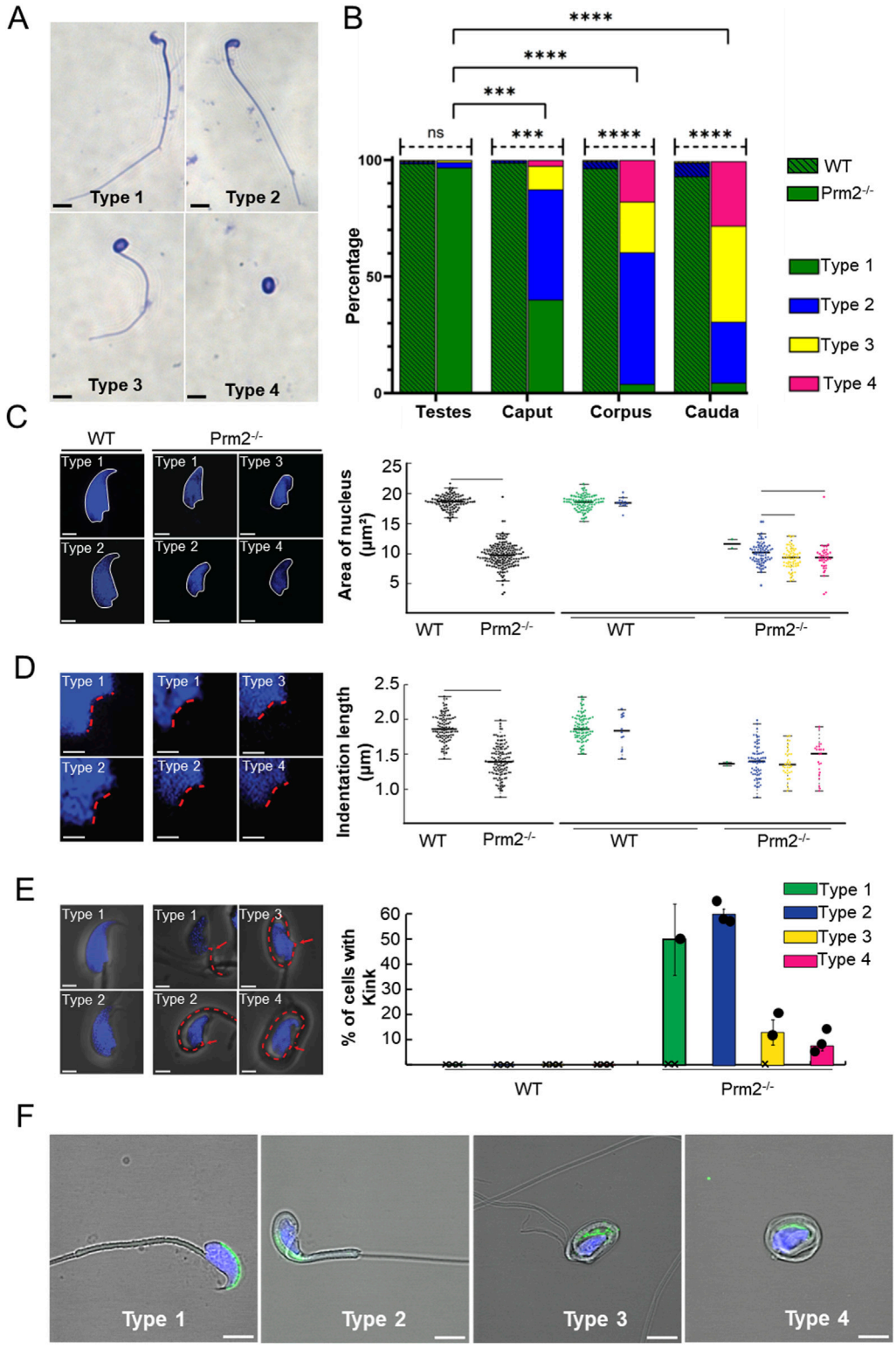

FIGURE 2
Prm2$^{-/-}$ sperm have pathological morphology during epididymal maturation. **(A)** Representative examples of sperm morphological types present in *Prm2*$^{-/-}$ cauda epididymis, scale bar = 10 µm. **(B)** Graph shows a significant gradual increase of morphologically abnormal sperm during epididymal maturation. Straight dashed lines indicate the difference in Type 1 sperm between *Prm2*$^{-/-}$ and WT. The full bent bar represents a decrease of morphologically normal sperm (Type 1) in *Prm2*$^{-/-}$ in epididymal regions compared to testes. *t*-test, ***$p < 0.0005$; ****$p < 0.0001$; n = 3, at least 200 cells were counted for each individual. **(C)** Area of the nucleus of the cauda epididymis sperm. Left, visualization of sperm head shapes in WT and *Prm2*$^{-/-}$ stained by DAPI (blue) in the four types we observed, scale bar = 2 µm. The right panel shows nuclei size distribution. The average area of the WT nucleus is 18.47 µm^2 ± 1.13 (n = 106), and that of the *Prm2*$^{-/-}$ is 9.57 ± 1.99 (n = 176), ($p < 0.0001$). The small nuclei size in *Prm2*$^{-/-}$ is independent of the
(*Continued*)

FIGURE 2 (Continued)
sperm type. A significant difference between the *Prm2*$^{-/-}$ Type 2 and *Prm2*$^{-/-}$ Type 3 (p = 0.006) and between Type 2 and Type 4 (p = 0.042). **(D)** Nucleus indentations differ in WT and *Prm2*$^{-/-}$ sperm. Visualization of sperm head shapes in WT and *Prm2*$^{-/-}$ stained by DAPI (blue) in the four types of sperm. The red line marks the nucleus indentation. The average length of control nucleus indentation is 1.87 µm ± 0.19 (n = 101), and that of the *Prm2*$^{-/-}$ is 1.39 µm ± 0.24 (n = 128), (p < 0.0001). The nucleus indentation size in *Prm2*$^{-/-}$ is independent of the sperm type for both control and *Prm2*$^{-/-}$ sperm. **(E)** Visualization of WT and *Prm2*$^{-/-}$ sperm that present a 90-degree post-neck tail kink (red dashed line). The 90-degree post-neck tail kink frequency was 0% in WT sperm and 31.8% in *Prm2*$^{-/-}$sperm (n = 176). The kink was present in 60% of Type 2 *Prm2*$^{-/-}$ sperm (n = 75), 13% of Type 3 mutant sperm (n = 61), and 7.9% of Type 4 mutant sperm. The 90-degree post-neck tail kink in Prm2 is observed mainly in Types 2 and 3 of mutant sperm. **(F)** Visualization of the acrosomal membrane in *Prm2*$^{-/-}$ cauda sperm via CD46 (green) immunohistochemistry. Nuclei are visualized in blue (DAPI). Scale bar = 5 µm.

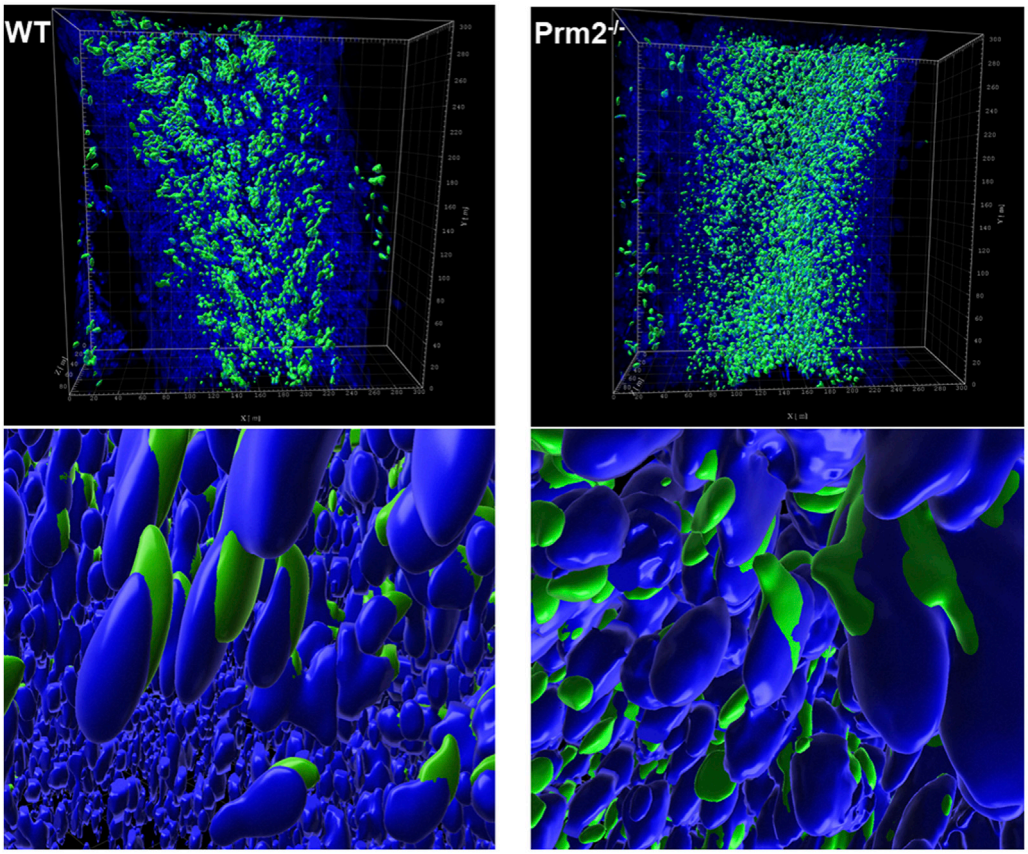

FIGURE 3
Acrosome formation is aberrant in *Prm2*$^{-/-}$ seminiferous tubules. 3D visualization of surface-rendered sperm acrosomes (green, PNA-AF488 stained) and nuclei (blue, DAPI stained) in the seminiferous tubule. Surface rendering was postprocessed by Imaris software. The upper panel shows the overall look of half of the seminiferous tubule with surface-rendered acrosomes only. The lower panel shows details of spermatids nuclei and acrosomes in the seminiferous tubule with surface-rendered acrosomes and nuclei.

Further, the acrosome integrity of *Prm2*$^{-/-}$ caudal sperm was evaluated. Utilizing immunofluorescent labeling against the CD46 protein as a marker of the acrosomal membranes (Frolikova et al., 2016), we detected the acrosome disintegration in sperm obtained from cauda epididymis (Figure 2F). Consequently, we examined the acrosomal status of testicular sperm and 3D reconstruction of PNA-stained acrosomes in the individual seminiferous tubule was employed. Using 3D confocal imaging and Imaris software surface rendering, we visualized the abnormal development of acrosomes. Within the sperm head of elongating spermatids, acrosomes of WT could be described as smooth and adjacent to the apical part of the nucleus, whereas in *Prm2*$^{-/-}$ the acrosomes were distorted to the side with notable protrusions (Figure 3). These findings indicate that the abnormal phenotype of *Prm2*$^{-/-}$ sperm might be established at the beginning or during early stages of spermiogenesis, however, it is fully expanded during epididymal maturation.

Protamine 2 deficiency leads to Septin 12 abnormalities

In spermiogenesis, the cytoskeleton plays a pivotal role in shaping the spermatid head and forming the acrosome, and it is

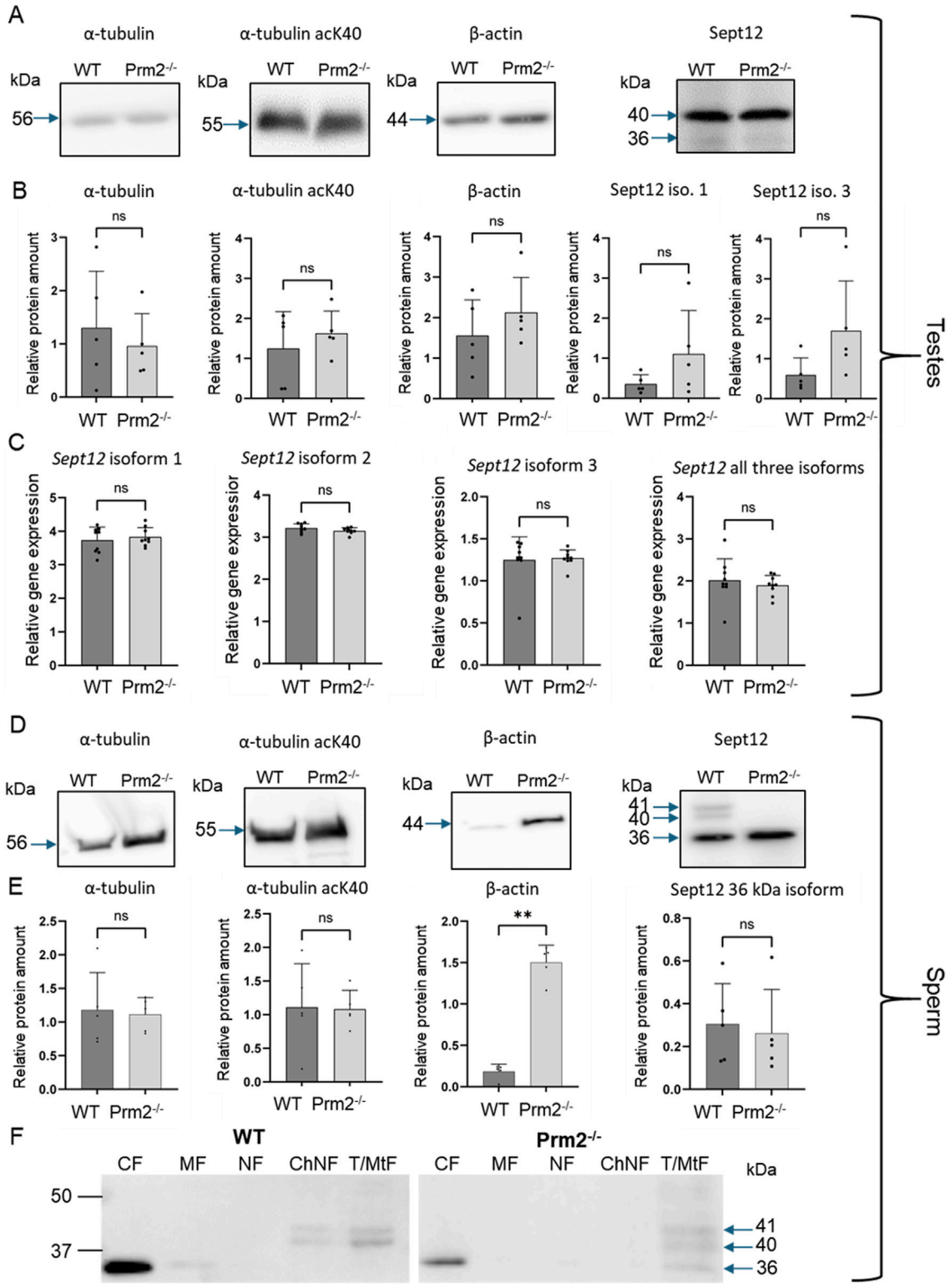

FIGURE 4
Cytoskeletal protein abundance and gene expression in *Prm2*$^{-/-}$ sperm and testes is modified for β-Actin, and Septin12 subcellular localization is altered. **(A, D)** Western blots of specified cytoskeletal proteins in testes **(A)** or sperm **(D)** of WT and *Prm2*$^{-/-}$ mice. Blue arrows indicate the molecular size of the antibody-detected bands. **(B, E)** A relative protein amount quantification. Band intensities were normalized to the CBB-stained membrane. n = 5, Mann-Whitney test, $^{**}p = 0.0079$. **(C)** qPCR of total testes lysate showing no difference in relative gene expression of all individual Septin 12 isoforms and total Septin 12. n = 8, Mann-Whitney test. **(F)** Detection of Septin 12 in subcellular fractions of WT and *Prm2*$^{-/-}$ sperm. CF - Cytoplasmic fraction; MF - Membrane fraction; NF - Nuclear fraction; ChNF - Chromatin-bound nuclear fraction; T/MtF -Tubulin/mitochondria protein fraction. Blue arrows indicate the molecular size of the antibody-detected bands.

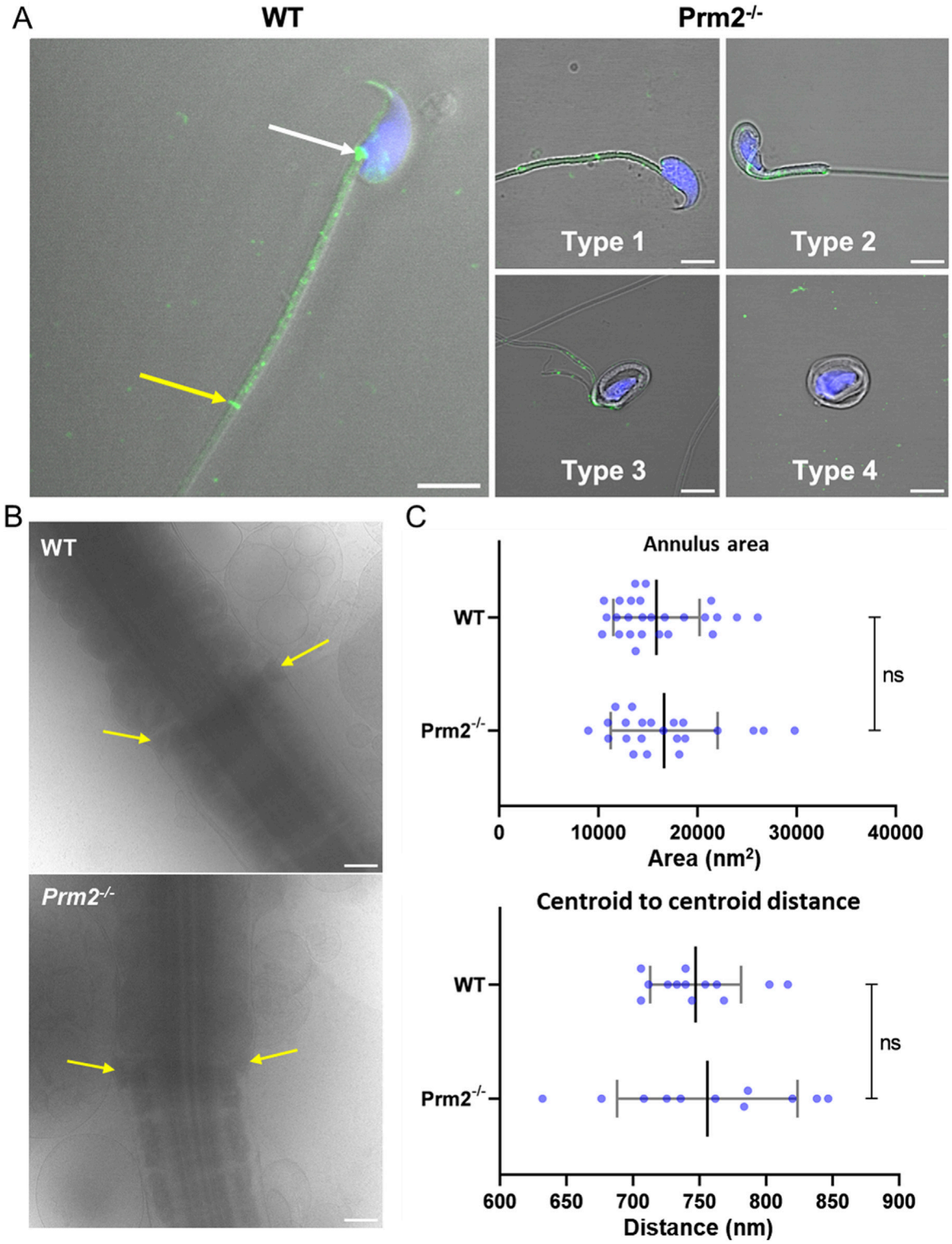

FIGURE 5
Protamine 2 deletion resulted in aberrant Septin12 localization in epididymal sperm. **(A)** Left panel: A localization of Septin 12 in WT sperm connecting piece (white arrow), annulus (yellow arrow), and midpiece (the area between arrows). Right panel: A mislocalization of Septin 12 in the tail of four morphologically aberrant types of *Prm2*$^{-/-}$ sperm. Septin 12 (green) and DAPI (Blue), scale bar = 5 µm. **(B)** Annulus (yellow arrows) detail visualized by cryoelectron microscopy. Scale bar = 500 nm. **(C)** Scatterplot visualizing statistical evaluation of mean annulus area and mean of annulus distance from centroid to centroid within one sperm. Mann-Whitney test, n = 13 (WT) and 11 (*Prm2*$^{-/-}$).

tightly involved in sperm motility. Based on the identification of the abnormal acrosomal shaping in testicular sperm of *Prm2*$^{-/-}$ mice coupled with the observation of epididymal sperm motility loss in *Prm2*$^{-/-}$, we evaluated selected cytoskeletal proteins, which could be impaired in *Prm2*$^{-/-}$ sperm. The protein abundance of α-tubulin, acetylated α-tubulin at lysine 40 (acK40), β-actin, and Septin 12 in mouse testes and sperm was investigated.

In testicular tissue lysates, Western blot analysis, followed by densitometry, was performed (Figures 4A, B), and the quantification of the obtained data showed no significant difference in the abundance of tubulin and actin proteins between WT and *Prm2*$^{-/-}$ mice. The presence of two different Septin 12 isoforms in molecular weights of 36 and 40 kDa was detected in both *Prm2*$^{-/-}$ and WT testicular tissue. As the antibody used failed to visualize other isoforms, we additionally performed qRT-PCR analysis of *Sept12* in WT and *Prm2*$^{-/-}$ testes. Using primers specific for mouse Septin 12 isoforms (1, 2, 3) and a common part of the *Sept12* gene, relative gene expression was calculated with no significant difference between the WT and *Prm2*$^{-/-}$ (Figure 4C).

In sperm, similarly to the testicular tissue and using the same methodology, the levels of α-tubulin and α-tubulin acK40 remained unchanged (Figures 4D, E), but we detected a significant increase ($p = 0.0079$) of β-actin abundance in *Prm2*$^{-/-}$ sperm. Importantly, in the sperm lysate from *Prm2*$^{-/-}$ males, only the Septin 12 isoform of 36 kDa was detected while the other two isoforms of 40 and 41 kDa were absent in contrast to WT, where all these isoforms were detected (Figure 4D). The abundance of 36 kDa isoform in WT and *Prm2*$^{-/-}$ showed no significant difference (Figure 4E).

Using immunofluorescence staining of mature mouse sperm, Septin 12 was shown to be localized in the head, neck, and midpiece of the tail (Lin et al., 2009). To assess potential differences in the localization of individual Septin 12 isoforms across different sperm compartments, we employed Western blot analysis of proteins in enriched subcellular fractions from caudal sperm of WT and *Prm2*$^{-/-}$ mice (Figure 4F). Our results revealed that isoform of 36 kDa was present in the cytoplasmic proteins containing fraction (CF) of both WT and *Prm2*$^{-/-}$ mouse sperm, as well as in the fraction containing tubulin and mitochondria (T/MtF) of *Prm2*$^{-/-}$ sperm. A small amount was also detected in the membrane fraction (MF) of WT, where membrane proteins are enriched. In contrast, both higher-molecular-weight isoforms (40 and 41 kDa) were detected in T/MtF of both WT and *Prm2*$^{-/-}$mouse sperm; however, in WT sperm, both these isoforms were additionally present in chromatin-bound nuclear protein fraction (ChNF) whereas, in *Prm2*$^{-/-}$ sperm, was notably absent. The specificity of the Septin 12 antibody was verified on transfected HEK293T/17 cells with mouse Septin 12 plasmid (Supplementary Figure S2).

The follow-up detailed analysis of Septin 12 in individual sperm compartments further revealed its presence in the perforatorium and post-acrosomal region of the sperm head, in the connecting piece and midpiece of the tail with notably intense signal observed at the site of the annulus (Figure 5A) in WT sperm. Although in sperm of *Prm2*$^{-/-}$ mice, Septin 12 was also identified in both head and tail, it appears that it does not localize into the same compartmental structures as observed in WT sperm. Specifically, the distinct signal detected in the annulus and connecting piece of WT sperm was not observed in *Prm2*$^{-/-}$, nor in the detection of Septin 12 in the perforatorium, which remains unclear. The detailed confocal data provided additional evidence of altered localization of Septin 12 in sperm absence of Protamine 2. To assess whether Septin 12 absence affects its formation in sperm annulus, we employed cryoelectron microscopy (Figure 5B). There was no visible difference in the annulus shape or localization in *Prm2*$^{-/-}$ caput sperm to WT; therefore, we analyzed data in FIJI software using Labkit, MorpholibJ and 3DSuite plugins. The applied statistical analysis (Figure 5C) did not reveal a difference in the annulus area or distance between the centers of the two annular anchoring points (centroid to centroid distance).

There was previously reported interaction between Septin 12 and Pericentriolar material 1 (PCM1) (Yeh et al., 2019), as a component of centriolar satellites, which likely plays a role in the precise localization of various centrosomal proteins and anchoring microtubules to the centrosomes (Dammermann and Merdes, 2002; Schatten et al., 2011), as demonstrated by yeast two-hybrid assay. Due to the presence of Septin 12 in the sperm connecting piece, where the centrioles are situated, along with a potential link between Septin 12 and centriole function (note that mice have structurally remnant centrioles that maintain centriole proteins (Khanal et al., 2024), we evaluated sperm centriole status in *Prm2*$^{-/-}$ mice and implied immunofluorescent staining of Centrosomal Protein 135 (CEP135) (Figure 6A; Supplementary Figure S3). Using the Leica LAS-X software algorithm we analyzed confocal images concluding, that *Prm2*$^{-/-}$ sperm centriole remnant is abnormal. Both the mean (Figure 6B) and maximum (Figure 6C) intensities of the CEP135 signal are reduced by about 35% ($p = 4.4 \times 10^{-6}$ and $p = 5.8 \times 10^{-7}$, respectively). Moreover, the *Prm2*$^{-/-}$ Cep135-labeled centriole is 10% longer (Figure 6D) than the WT ($p = 0.04$). The average length of the control group Cep135-labeled centriole was 0.74 ± 0.20 μm while the length of *Prm2*$^{-/-}$ centriole was 0.81 ± 0.15 μm. Interestingly, the average width (Figure 6E) of control and *Prm2*$^{-/-}$ Cep135-labeled centrioles was 0.47 ± 0.09 μm and 0.48 ± 0.10 μm, respectively, showing no significant difference. Measurement strategy of centriolar width and length is shown in the Figure 6F.

Interaction of Septin 12 with Protamine 2 and Lamin B2/3 intermediate filaments

Based on findings that the lack of Protamine 2 might be responsible for the absence of Septin 12 isoform 3 in *Prm2*$^{-/-}$ mouse sperm, we employed a co-immunoprecipitation assay to explore their potential interaction. The Septin 12 – Protamine 2 complex was precipitated from mouse testes lysate using an anti-Protamine 2 antibody. Subsequently, the samples were immunodetected with an anti-Septin 12 antibody (Figure 7A). Two bands corresponding to the molecular weights of 36 and 41 kDa were observed in the precipitated sample, while it was absent in the IgG control, indicating a possible interaction between Septin 12 and Protamine 2.

Within the sperm nucleus, Septin 12 was shown to interact with the SUN4/Lamin B1 complex (Yeh et al., 2015). In the current study, HEK293T/17 cells were co-transfected with the Septin 12-GFP and LaminBx-Myc plasmids, followed by co-immunoprecipitation assay to investigate the possible interaction of Septin 12 with other Lamin family members–specifically Lamin B2 and Lamin B3. Co-

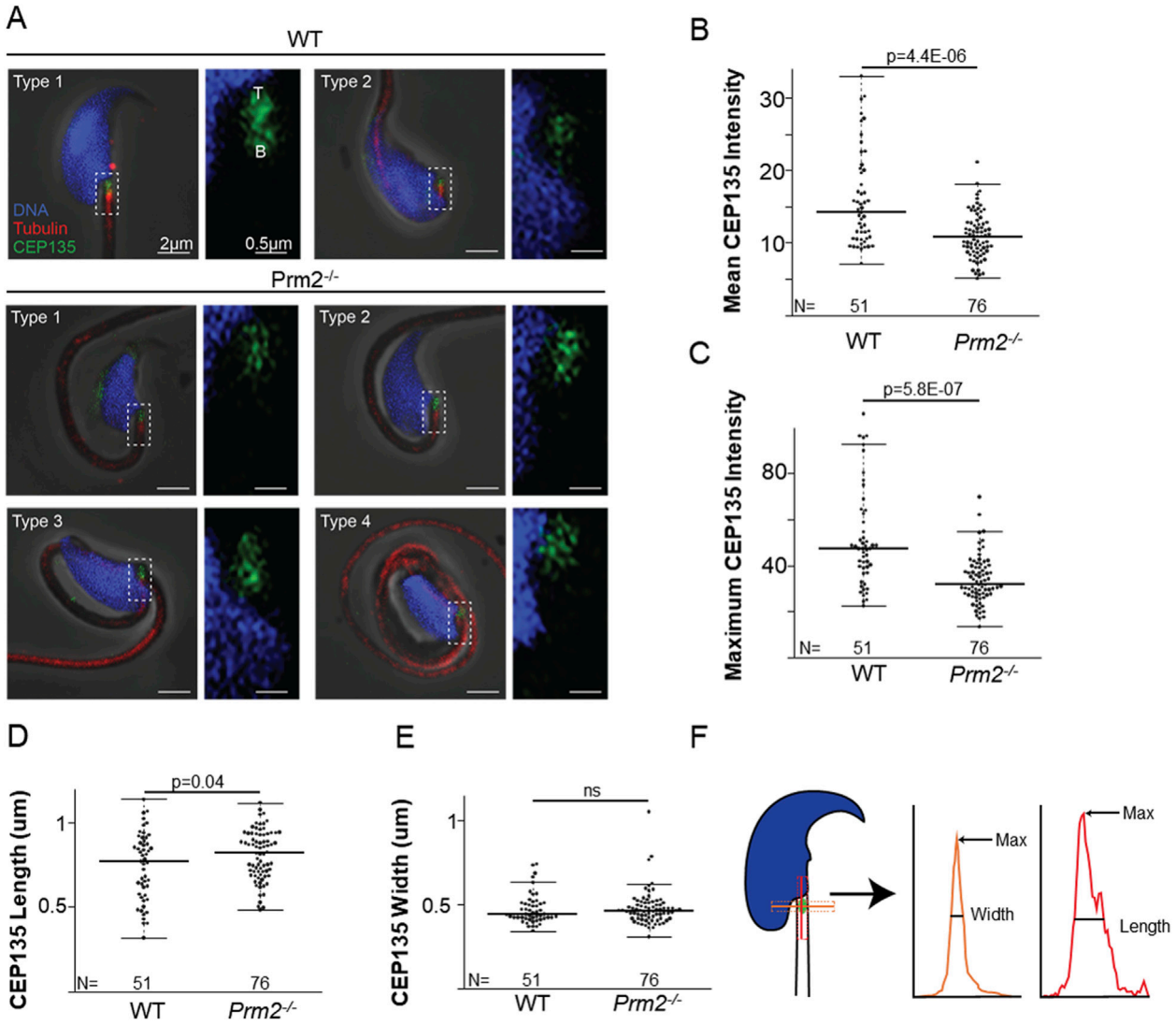

FIGURE 6
Prm2$^{-/-}$ spermatozoa remnant centrioles are abnormal. **(A)** Examples of WT types 1 and 2 spermatozoa and the four types of *Prm2*$^{-/-}$ spermatozoa. The left panel shows a low-magnification view of the sperm head, and the right panel illustrates a high-magnification view focusing on the centriolar staining. CEP135 (in green) the tail axoneme (in red), and the nucleus (in blue). All sperm were oriented with the tip of the centriole (T) at the top of the image and the base of the centriole **(B)** at the bottom. Scale bar = 2 and 0.5 μm, respectively. **(B)** Graph illustrating CEP135 mean intensity. The wild-type spermatozoa average intensity was 15.92 ± 6.46 (n = 51), and the average for the *Prm2*$^{-/-}$ was 11.00 ± 3.13 (n = 76), p = 4.4E-06. **(C)** Graph representing CEP135 maximum intensity. The average maximum intensity for the wild-type sperm was 51.36 ± 21.07 (n = 51), and for the *Prm2*$^{-/-}$ sperm was 33.62 ± 10.22 (n = 76), (p = 5.8E-07). **(D)** The average CEP135 length of the WT sperm was 0.74 ± 0.20 μm (n = 51), and the *Prm2*$^{-/-}$ was 0.81 ± 0.15 μm (n = 76), p = 0.04. **(E)** The average CEP135 width of WT sperm was 0.47 ± 0.09 μm (n = 51), and of the *Prm2*$^{-/-}$ was 0.48 ± 0.10 μm (n = 76), p = 0.705. **(F)** Schematic illustration showing CEP135 length and width measurement strategy. Width is shown in orange, and length in red.

transfection of Septin 12 with Lamin B1 served as a positive control. The Septin 12-Lamin Bx complex was precipitated via GFP-tag on Septin 12 using an anti-GFP antibody, followed by immunodetection using an anti-Myc antibody. Myc-tag labeling revealed the double band corresponding to two isoforms of Lamin B1 (118 kDa, 92 kDa), as well as two bands for Lamin B2 (111 kDa, 89 kDa). Only a single band with a molecular weight of 111 kDa corresponding to Lamin B3 was detected. No immunodetection was observed in the non-transfected cell lysate or the IgG control (Figure 7B). Co-transfected HEK293T/17 cells are shown in representative Figure 7C. These data suggested that Septin 12 interacts with the investigated Lamin B proteins either directly or indirectly within a protein complex.

To inspect the potential influence of lack of *Prm2* on the abundance of Lamin B proteins, we performed a Western blot analysis using mouse testes lysates (Figure 7D). The bands corresponding to molecular weights of Lamin B2 (68 kDa) and Lamin B3 (53 kDa) were detected. However, densitometric analysis revealed no significant change in the levels of Lamin B2 or B3 in the *Prm2*$^{-/-}$ testes compared to WT. Furthermore, using qRT-PCR analysis of cDNA from mouse testes, we also did not detect a significant difference between WT and *Prm2*$^{-/-}$ and the relative gene expression levels of *LaminB2* and *LaminB3*, as well as *SUN4*

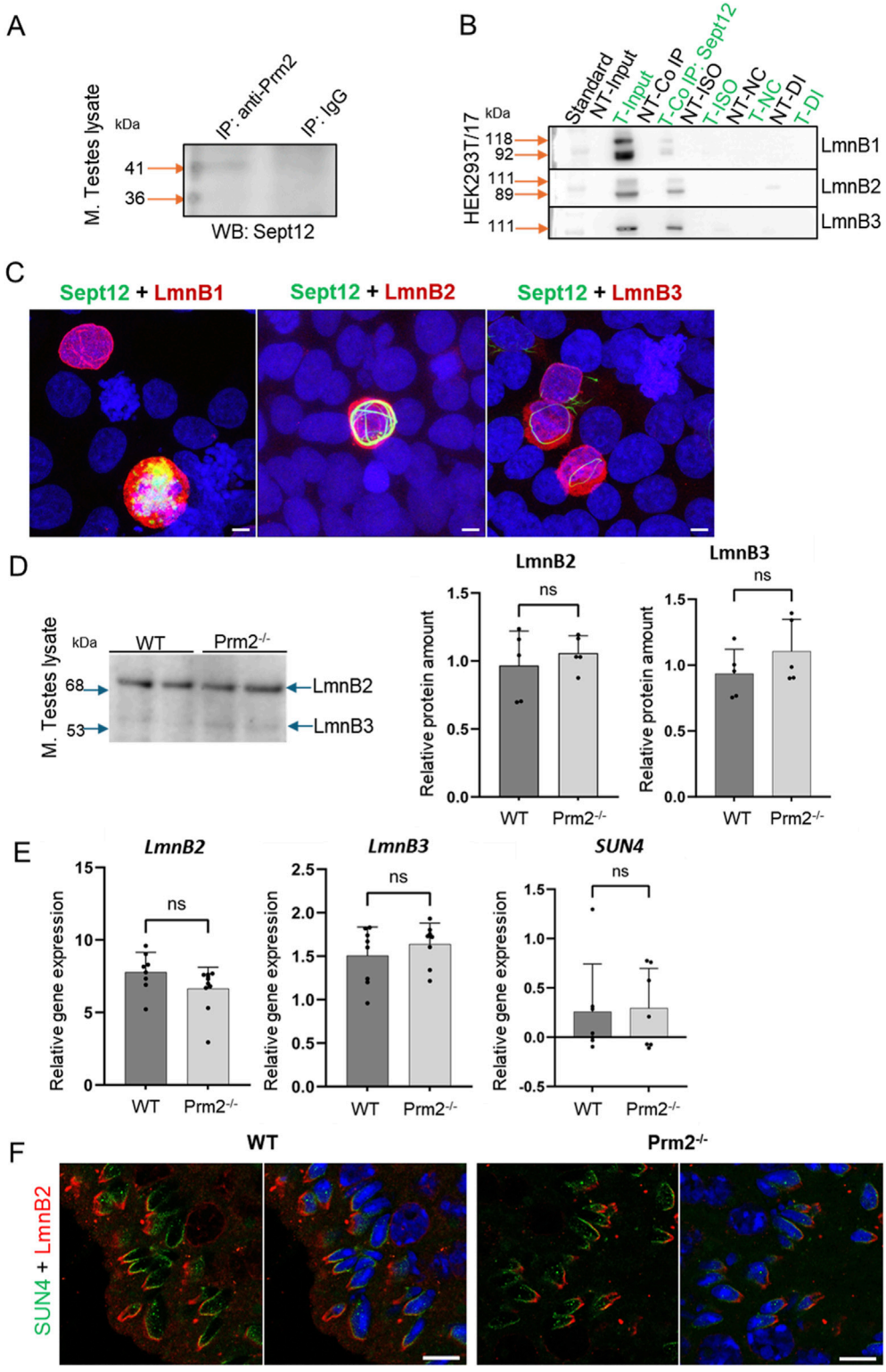

FIGURE 7
Analysis of Septin 12 interacting proteins reveals positive interaction with Protamine 2 and Lamin B2/3. **(A)** Co-immunoprecipitation of Protamine 2 with Septin 12 in mouse testes lysate. Blue arrows indicate a molecular weight standard; orange arrows indicate a precipitate in predicted molecular weights. Isotype IgG control shows no precipitate. **(B)** Co-immunoprecipitation of transfected HEK cells with mouse Septin 12 and Lamin B1, Lamin B2, or Lamin B3. NT - non-transfected cells; T - Transfected cells; Input-only cell lysate (without Co-IP); Iso - Isotype control; NC - Negative control for

(*Continued*)

FIGURE 7 (Continued)
Co-IP (without ab); DI - Depleted input (the last wash of Co-IP). **(C)** 3D illustrative images showing positive transfection of HEK cells with Septin 12-GFP (green) and Lamin Bs-Myc (red). Nuclei are stained by DAPI (blue). Scale bar = 5 μm. **(D)** Western blot shows no significant difference in the relative abundance of Lamin B2 and Lamin B3 in mouse testes. Blue arrows indicate the molecular size of the antibody-detected bands. **(E)** qPCR of mouse testes shows no significant difference in relative gene expression of Lamin B2, Lamin B3, and SUN4 in testicular cells of WT and *Prm2*$^{-/-}$ mice. n = 8, Mann-Whitney test. **(F)** Immunohistochemistry of mouse SUN4 (green) and Lamin B2 (red). Scale bar = 10 μm.

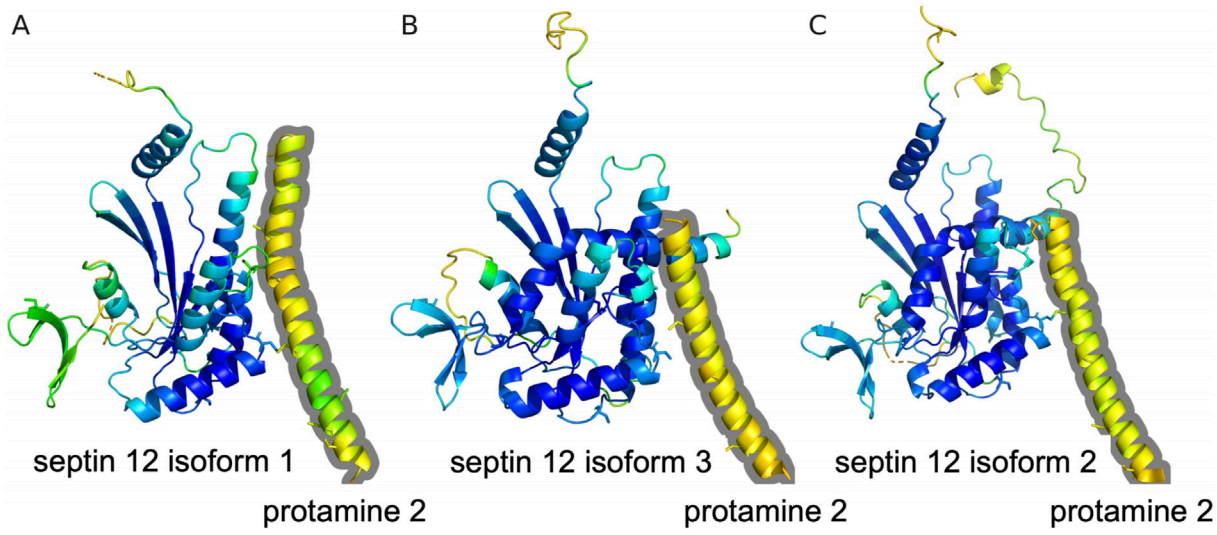

FIGURE 8
Prediction of Protamine 2/Septin 12 complexes with AlphaFold multimer. The proteins are shown in cartoon representation with Cysteine residues in sticks representation. Residues are color coded according to the transformed pLDDT confidence score using 100-pLDDT with the standard B-factor color scale with cold colors corresponding to high confidence regions. Only residues with pLDDT score higher than 40 are shown. The Protamine 2 moieties are outlined with a grey contour. **(A)** Predicted complex of mouse Protamine 2 and Septin 12 isoform 1. **(B)** Predicted complex of mouse Protamine 2 and Septin 12 isoform 3. **(C)** Predicted complex of human Protamine 2 and Septin 12 isoform 2.

(Figure 7E), suggesting no difference in the regulation of these proteins on expression level. To compare the localization of Lamin B2 and SUN4 in testicular cells, we employed indirect immunohistochemistry of FFPE mouse testes. We were able to detect SUN4 as well as Lamin B2 in postmeiotic cells, in particular in elongating/elongated spermatids (Figure 7F) in the lateral posterior part of the spermatid head, where the manchette is localized, with absence in the head-to-tail coupling apparatus. These results suggest that the absence of Protamine 2 does not significantly affect Lamin B2/3 and SUN4 expression, protein abundance, and localization within nuclear lamina composition in *Prm2*$^{-/-}$ mice testicular cells.

A potential interaction is also predicted by the AlphaFold multimer for Protamine 2 with Septin 12 model complexes. The modeling predicts association of a helical C-terminal Protamine 2 region (residues from about 60 to 100) with the Septin 12 protein. Although the structure of the C-terminal Protamine region is modeled with relatively low confidence (pLDDT between 50 and 60), the potential interaction could be further stabilized by predicted disulfide bridges between Protamine 2 and Septin 12. The potential disulfide bridges involve mouse Protamine 2 Cys88 and Septin 12 isoform 1 Cys217, mouse Protamine 2 Cys70 and Septin 12 isoform 3 Cys217, and human Protamine 2 Cys74 and Septin 12 isoform 2 Cys219 (homologous to the murine Cys217), respectively. The Cysteine residues in predicted complexes are shown in sticks representation in Figure 8.

Septin 12 is retained in asthenozoospermic human sperm

We used immunofluorescent labeling to visualize Septin 12 localization in human sperm (Figure 9) and detected it predominantly in connecting piece and annulus in normozoospermic donors and asthenozoospermic patients' samples. A weak signal was also detected across the whole midpiece of the tail, where mitochondria are located (Figure 9A). To compare the Septin 12 accumulation within sperm tail of asthenozoospermic and normozoospermic men, relative fluorescent intensity (RFI) were calculated using Zen Blue software, which did not detect change in the localization of Septin 12 in the annulus, or midpiece analyzing a signal between the neck and annulus (Figure 9B). Subsequent analysis of fluorescent data and normalization to relative length (percentage of the distance) did not again provide a significant change among the patients and healthy donors.

Based on our *Prm2*$^{-/-}$ results reporting differences in the Septin 12 isoforms (40 and 41 kDa) compared to WT males, we determined

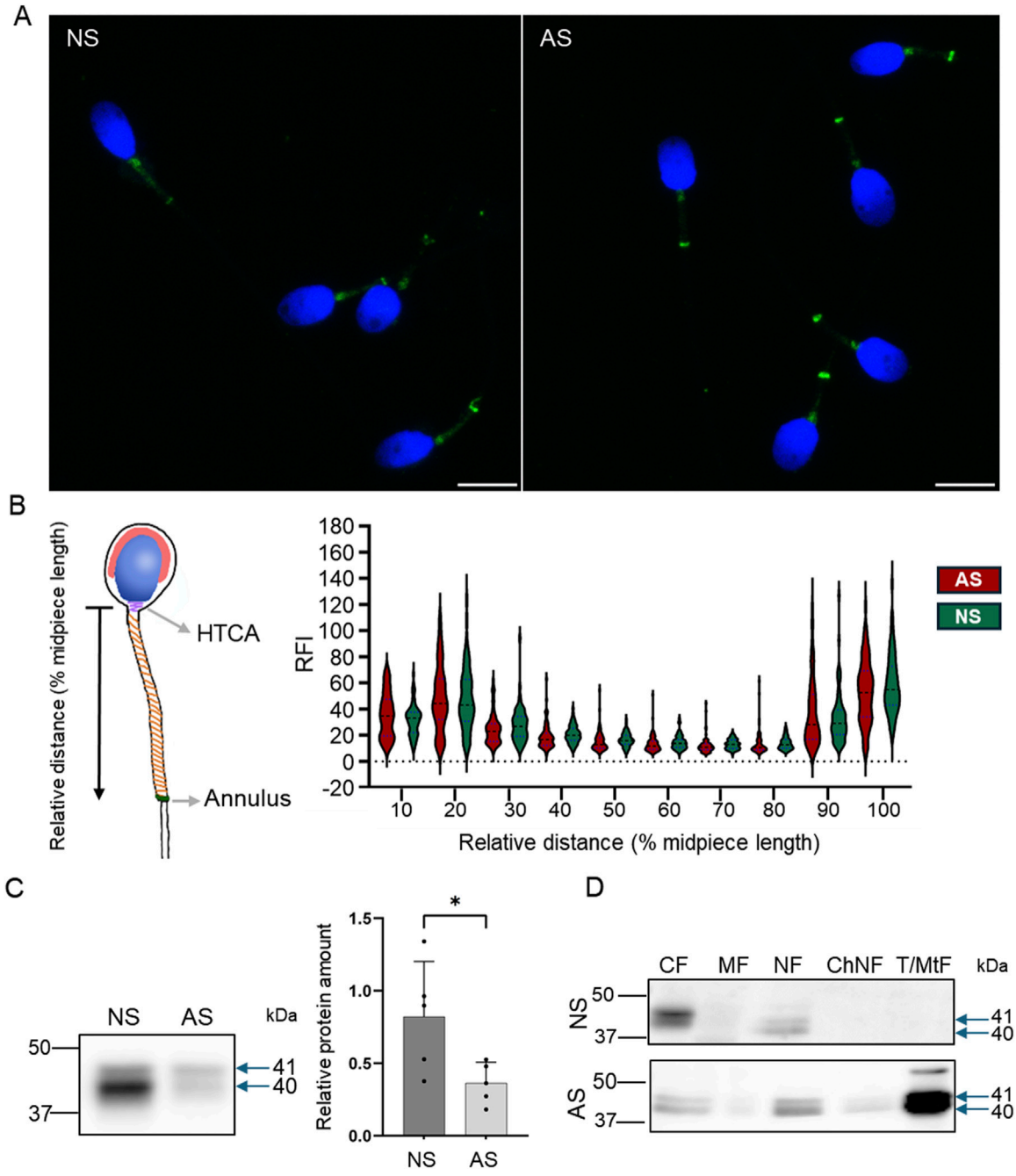

FIGURE 9
Septin 12 distribution is modified in human asthenozoospermic sperm. **(A)** Comparison of localization of Septin 12 between NS (normozoospermic) and AS (asthenozoospermic) men. Scale bar = 10 μm. **(B)** Graphical visualization of the relative length measurement. The graph shows changes in the relative fluorescence intensity of the Septin 12 signal in the sperm midpiece. Measured relative fluorescent intensity (RF) was compared based on the relative distance (percentage) from the neck. n = 3, at least 20 sperm from each patient were measured. *t*-test, no significant results. **(C)** Western blot shows a decreased abundance of Septin 12 in AS sperm. Blue arrows indicate the molecular size of antibody-detected bands. The graph represents Relative protein amount quantification. n = 5, Mann-Whitney test, $p = 0.0317$. **(D)** Subcellular fractionations of human sperm and Western blot detection of Septin 12. CF - Cytoplasmic fraction; MF - Membrane fraction; NF - Nuclear fraction; ChNF - Chromatin-bound nuclear fraction. T/MtF -Tubulin/mitochondria protein fraction.

the total Septin 12 protein level using Western blot densitometry, normalized to tubulin, in human samples. The analyzed data revealed a significantly ($p = 0.0317$) decreased level of detected Septin 12 isoforms in asthenozoospermic patients (Figure 9C). Using in-depth analysis of subcellular localization of Septin 12 we isolated subcellular protein fractions and detected a strong signal for Septin 12 (isoforms of 40 and 41 kDa) only in cytoplasmic and nuclear fractions in normozoospermic donor samples (Figure 9D). In comparison with asthenozoospermic patients' sperm, Septin 12 was additionally detected in the membrane and

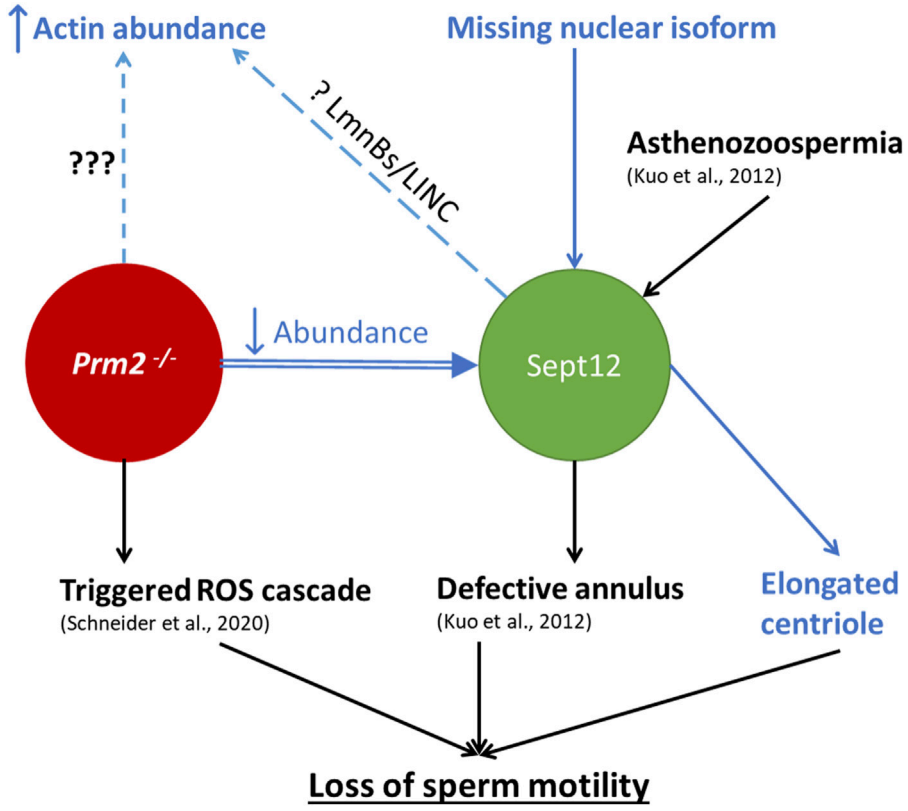

FIGURE 10
Schematic illustration summarizing the current knowledge regarding the connection between *Prm2*$^{-/-}$ phenotype and Septin 12 role in mouse sperm. The text in blue represents the results delivered by this study. Arrows up/down represent increased/decreased effect on the described mechanism, dashed lines represent a phenotype without a described cause. ??? represents an unknown cause of the abnormality; The question mark (?) represents a possible mechanism behind the abnormality.

nuclear-bound protein fractions apart from the other fraction of normozoospermic donors (Figure 9D) with very strong signal in fraction defined as tubulin/mitochondria proteins. The retention of Septin 12 in the nuclear-bound fraction of asthenozoospermic men may have a significant value and possibly point to impaired docking of Septin 12 during spermiogenesis, contributing to poor sperm motility.

Results summary

The schematic illustration (Figure 10) summarizes the results of this study in connection with current available knowledge relevant to the scope of this work. It describes the connection between *Prm2*$^{-/-}$ phenotype and Septin 12 and highlights the new possible pathways and missing links. Our results demonstrate distinct localization patterns of Septin 12 individual isoforms in sperm, suggesting that these isoforms could play different roles in sperm organelle biogenesis and function, and the absence of Septin 12 isoforms in the chromatin-bound nuclear protein fraction of *Prm2*$^{-/-}$ sperm could be due to absence of Protamine 2. Based on co-immunoprecipitation detecting potential interactions between Septin 12 and Lamin B2/3, we hypothesize that in the absence of Protamine 2, the interplay between Lamin B2/3 and other nuclear lamina-associated proteins might be modified. The differences in the protein abundance pattern of Septin 12 isoforms in caudal sperm may further suggest a role of Septin 12 during the late stages of sperm development and/or during epididymal maturation. Based on these findings, we propose that Septin 12 and Protamine 2 could potentially directly or indirectly interact within the sperm nucleus.

Discussion

Protamines are known to play a pivotal role in sperm function, its fertilizing ability, and proper early embryogenesis (Arévalo et al., 2022a; Arévalo et al., 2022b), and Protamine 2 is one of the most abundant sperm proteins in humans and mice (Retief and Dixon, 1993). The establishment of *Prm2*$^{-/-}$ mouse strain has unveiled a notable link between Protamine 2 deficiency and male infertility characterized by morphologically impaired and immotile sperm (Schneider et al., 2016), and a follow-up study (Schneider et al., 2020a) suggested a possible molecular mechanism behind described sperm dysfunction. Our current study provides new evidence suggesting that Protamine 2 deficiency might significantly impact the cytoskeleton function, especially the testis-specific Septin 12 protein, whose impairment could likely contribute to the development of morphological abnormalities and lack of motility of *Prm2*$^{-/-}$ sperm.

In this study, we employed the DNA FCM analysis and showed differences in DNA hyper-condensation during spermiogenesis between WT and *Prm2*$^{-/-}$ males and discovered an absence of sub-haploid cells in *Prm2*$^{-/-}$ mouse testis compared to WT. Additionally, we investigated the potential impact of a lack of Protamine 2 on histone replacement and retention, including the abundance of a core histone and related epigenetic modifications. While the proteomic approach indicates that histone retention (Arévalo et al., 2022a) and DNA methylation may be affected in sperm with aberrant protamine replacement (Carrell et al., 2008), our new approach using FCM analysis did not reveal significant differences in histone H3 retention, or H3K27Me3, H3K36Me3, and H3K9Ac histone pattern between WT and *Prm2*$^{-/-}$sperm. This finding may suggest a dominant role of Protamine 1 in sperm DNA packaging in mice but also a need for further in-depth studies of sperm epigenome and DNA structure to visualize Protamine 1 coils assembly and histone localization in the absence of Protamine 2.

Morphological characterization of *Prm2*$^{-/-}$ germ cells did not indicate significant differences in nuclear shape or acrosome biogenesis between *Prm2*$^{-/-}$ and WT testicular sperm (Schneider et al., 2020b; Schneider et al., 2016). The first detectable morphological changes of *Prm2*$^{-/-}$ sperm were described during sperm passage through the *epididymis* (Schneider et al., 2016), which led to the conclusion that morphological aberrations of *Prm2*$^{-/-}$ sperm are predominantly acquired during epididymal maturation (Schneider et al., 2020b). In accordance with this knowledge, our study confirmed a significant increase in the number of abnormal sperm during sperm epididymal transit in *Prm2*$^{-/-}$ mice, and we further described several serious morphological aberrations in caudal *Prm2*$^{-/-}$ sperm compared to WT. Interestingly, our examination of testicular sperm acrosomes revealed their abnormal morphological shapes and modified structural appearance, i.e., before the epididymal maturation. These findings suggest a new role of Protamine 2 in spermatid development, which impacts acrosome biogenesis as a critical part of spermiogenesis. At this stage of sperm development, a formation of the acrosome and spermatid head shaping is orchestrated by the cytoskeleton network and represents a crucial process that also involves sperm motility. Identifying abnormal acrosomal shaping in testicular sperm of *Prm2*$^{-/-}$ mice, coupled with the observation of complete immotility in *Prm2*$^{-/-}$ sperm, points towards a potential impairment of cytoskeletal protein function.

Among other cytoskeletal proteins and their multiple roles, the organization of actin and tubulin network in sperm is facilitated by testis-specific Septin 12 (Nakos et al., 2022) a member of the Septin cytoskeleton family (Mostowy and Cossart, 2012). In both WT and *Prm2*$^{-/-}$ sperm immunofluorescent staining for Septin 12 was located to the neck, annulus with moderate signal over the tail midpiece, and Western blot data analysis showed significant differences in Septin 12 isoforms of 40 and 41 kDa corresponding to calculated molecular weights of Septin12 isoforms 3 and X1, which was absent in *Prm2*$^{-/-}$ sperm lysate, compared to WT. Subsequent assessment of Septin 12 subcellular localization revealed the presence of these two isoforms in the cytoplasmic fraction of both WT and *Prm2*$^{-/-}$ sperm but notably absent from the chromatin-bound nuclear protein fraction of *Prm2*$^{-/-}$ sperm. These findings suggest potential crosstalk between Septin 12 and Protamine 2 within the sperm nucleus, which aligns well with the reported interaction between Septin 12 and Protamine 2 using a yeast 2-hybrid system (Yeh et al., 2015) and our co-immunoprecipitation results in mouse testes lysate. Consistent with these observations are also our modeling results suggesting interactions between Septin 12 isoforms and Protamine 2. The predicted complexes could be stabilized by potential disulfide bridges involving different Protamine 2 Cysteine residues for each Septin 12 isoform. However, these potential interactions are still waiting for a more detailed experimental validation. Based on current knowledge, it might be plausible to believe that Septin 12 isoforms are likely to play different roles in sperm function, suggesting regulation of protein localization during later stages of sperm maturation. Septin 12 was previously shown to be essential for correct annulus formation (Lin et al., 2009). Its dysregulation by constitutive phosphorylation leads to immotile sperm with absent annulus (Shen et al., 2017). We employed cryo-transmission electron microscopy to study the annulus localization, size, and its distance. Contrary to Shen's observation (Shen et al., 2017), we can see the annulus of *Prm2*$^{-/-}$ to be present in the same position as in the WT. Moreover, its area and distance from each other are the same as in WT, even though the immunofluorescent microscopy showed the absence of Septin 12 form *Prm2*$^{-/-}$ annulus. These observations might suggest the Septin12 mislocalization during later stages of sperm maturation, potentially as a result of high oxidative stress of *Prm2*$^{-/-}$ sperm.

In relevance to the modified status of the cytoskeleton in response to Protamine 2 depletion, a significant increase in the abundance of β-actin was detected in *Prm2*$^{-/-}$ sperm lysate. The β-actin and its capping proteins are known to be abnormally regulated in patients with oligozoospermia and asthenozoospermia (Inagaki et al., 2021) and an abnormal regulation of testis-specific actin capping protein CPβ3 was described in sub-fertile patients (Soda et al., 2017). Moreover, the expression of F-actin-capping protein subunit beta (CAPZB) and Tektin 2 were significantly decreased in patients with low sperm motility, being supported by knowledge that CAPZB causes actin depolymerization meanwhile, tektins provide stability to axonemal microtubules, making these two proteins key factors in sperm motility (Xiong et al., 2018). To add more, the pivotal role of the septin filaments in the anchoring of actin filaments has been reported recently (Martins et al., 2023). Considering the above-reported abnormal acrosomal formation, which is dependent on the cytoskeletal network and the significantly elevated level of β-actin may be a result of miscommunication between cytoskeletal proteins and their associated proteins or from improper sequestration of septin membrane-anchored actin fraction during the spermiogenesis.

Notably, centrioles, which play a pivotal role in regulating sperm tail movement (Avidor-Reiss et al., 2020), exhibit changed morphology under Protamine 2 depletion. This aberration could represent a potential mechanistic link to the observed motility defects and in connection with the previously documented plasma membrane defects resulting in an exceptionally low cytoplasmic Ca^{2+} concentration, may contribute to the observed immotile phenotype (Schneider et al., 2016). This finding is in accordance with results from the yeast 2-hybrid system, which predicted interaction between Septin 12 and PCM1 (Yeh et al.,

2015), a component of centriolar satellites (Dammermann and Merdes, 2002). It has been shown that PCM1 and centriolar satellites play a role in regulating the composition of centrioles (Hall et al., 2023) and conversely, PCM1 requires centrosomal localization of CEP135 for efficient localization around centrosomes (Chu and Gruss, 2022). It suggests that the interaction between Septin 12 and PCM1 may regulate the structure and function of sperm centrioles and that the undetected expression of Septin 12 in the connecting piece of *Prm2*$^{-/-}$ sperm could indirectly result in their immotility.

In general, Septins tend to have various interaction partners (Desterke and Gassama-Diagne, 2019). Our results from HEK cells co-immunoprecipitation show the interaction of Septin 12 with Lamin B1, B2, and B3, suggesting its possibly crucial role in spermiogenesis. As described previously, Septin 12 can form a complex with Lamin B1 and SUN4 (a sperm-specific component of LINC complex) and is important for its correct positioning (Lin et al., 2009; Yeh et al., 2015; Yeh et al., 2019). Moreover (Thoma et al., 2023), it has recently been shown that Lamin B3 interacts with SUN4 *in vivo,* but its localization is independent of SUN4, as shown on the *SUN4*$^{-/-}$ mouse model. Based on our analysis, the amount of Lamin B2 and Lamin B3 in testicular cells of *Prm2*$^{-/-}$ remains unchanged compared to WT. Similarly, the localization of Lamin B2 and SUN4 in spermatids seems not to be affected by Protamine 2 depletion. Possibly, Septin 12 could be involved in the signal transduction between the nucleus to cytoplasm via the LINC complex, which can be disrupted despite the functional assembly of the LINC components and due to complex multiprotein machinery [revised in (Kmonickova et al., 2020)] further research addressing this topic is needed.

In an attempt to test our findings in relevance to the described clinical observation and human sperm pathologies, we aimed to test Septin 12 protein expression in sperm of asthenozoospermic patients and compare them with normozoospermic donors. Previous studies showed a connection between point mutations of the GTP binding domain of Septin12 with teratozoospermia (Lin et al., 2012), asthenoteratozoospermia, and oligoasthenozoospermia (Kuo et al., 2012). Moreover, the sperm of these patients possessed defective annulus. We discovered that the amount of two isoforms (40 and 41 kDa corresponding to calculated molecular weights of human Septin12 isoform of 2 and X1) of Septin 12 was reduced in asthenozoospermic patients, which is in accordance with previously reported data (Kuo et al., 2012). In contrast to Septin 12 overall reduction, we detected retention of Septin 12 isoforms in subcellular fraction containing specifically tubulin/mitochondrial proteins, and fractions with membrane and chromatin-bound proteins, whereas in normozoospermic donors' sperm there is none. Humans express less amount of Septin 12 isoforms compared to the expressed in the mouse, so it is likely that their role varies, and a comparison cannot be drawn between human and mouse Septin 12/Protamine 2 related phenotypes. However, the discovery of different localization of Septin 12 isoforms in sperm of asthenozoospermic and normozoospermic men expands our knowledge and contributes to a better understanding of the mechanism behind multiple causes, including idiopathic infertility, behind poor sperm motility in humans.

Conclusion

In conclusion, our present study provides new insights into sperm physiological abnormalities and immotility caused by Protamine 2 deficiency in mice. Detection of potential Septin 12 and Protamine 2 interaction in mouse testes, the absence of nuclear Septin 12 isoforms of 40 and 41 kDa in *Prm2*$^{-/-}$ sperm as well as the detected possible interaction of Septin 12 and Lamin B1/B2/B3 *in vitro* delivers new insight into the role of Protamine 2 in sperm biogenesis. The abundance and localization of Lamin B2 nor Lamin B2/3, as well as localization of SUN4, which were not detected to be influenced by Protamine 2 deletion, suggest a possible new role of Septin 12, which could be involved in the signal transduction between the nucleus to cytoplasm via the LINC complex. This signaling pathway may be disrupted due to Septin 12 modifications despite the functional assembly of the LINC components. This new consequence of Protamine 2 deficiency is also strengthened by the discovery of aberrant acrosome formation during spermiogenesis and results in several cytoskeletal abnormalities that might be caused by aberrant Septin 12 docking.

Material and methods

Animals

Protamine 2 knock-out mouse line (*Prm2*$^{-/-}$) was prepared by Schneider and his colleagues in 2016 (Schneider et al., 2016). Using CRISPR/Cas9 system, 97 bp deletion was introduced into *Prm2* exon 1 between 120 and 217 bp resulting in premature termination codon occurrence (Supplementary Figure S4). This mouse line was registered as C57BL/6J Prm2Δ^{97}. Wild-type C57BL/6J males served as a control. Mice were housed in a breeding colony of the Laboratory of Reproduction, IMG animal facilities, Institute of Molecular Genetics of the Czech Academy of Sciences; food and water were supplied *ad libitum*. The male mice used for all experiments were healthy, 10–14 weeks old, with no sign of stress or discomfort. All animal procedures and experimental protocols were approved by the Animal Welfare Committee of the Czech Academy of Sciences, Animal Ethical protocol code 66866/2015-MZE-17214, 18 December 2015.

Mouse sperm preparation

Sperm were retrieved from *caput, corpus or cauda epididymis*. The exact sperm source is listed in the corresponding results section. Appropriate parts of the epididymis were dissected, and sperm were released into two 200 µL droplets of M2-fertilizing medium (M7167) under paraffin oil (P14501, P-LAB, Prague, Czech Republic) in a Petri dish and pre-tempered at 37°C in the 5% CO_2 atmosphere. After 15 min, medium with released sperm was collected into the Eppendorf tube and centrifuged for 5 min at 300 x g. The supernatant was removed, and the pellet was gently resuspended in 500 µL PBS tempered to 37°C and centrifuged again.

Human sperm samples

Human ejaculates were obtained from men after 3–4 days of sexual abstinence, at the Centers for Assisted Reproduction (Prague, Czech Republic) with the informed consent of the donors and in accordance with the approval of the Ethical Committee, protocol code BIOCEV 012019, 20 January 2019. Biological materials and experimental protocols were approved by the Ethical Committee of the General University Hospital (Prague, Czech Republic), protocol code 617/17 S-IV.

Immunofluorescence of mouse and human sperm

For immunofluorescence analysis, the sperm smears were fixed for 10 min with 3.2% paraformaldehyde and permeabilized with the Intracellular Staining Perm Wash Buffer for 3 × 5 min (421,002, BioLegend, United States of America). Following permeabilization, the samples were blocked for 30 min with SuperBlock blocking buffer (Invitrogen) at room temperature (RT). After the anti-Septin12 primary antibody (H00124404-B01P, Bio-Techne, United States of America) diluted 1:50 in the Antibody diluent (Zytomed Systems GmbH) was applied and sperm smears were incubated at 4°C overnight. The next day, the slides with sperm smears were washed three times with PBS and then incubated with AlexaFluor 488 goat anti-mouse secondary antibody diluted 1:300 (A11029, Invitrogen, United States of America) for 60 min and with PNA 568 (Peanut Agglutinin, 6.66 µg/mL, Invitrogen, United States of America) for 20 min at RT. After, the samples were washed with PBS and incubated with DAPI (62,248, Thermo Fischer Scientific, United States of America) diluted in PBS to the concentration of 2 µg/mL for 5 min at RT. Slices were mounted with AD-Mount-F Mounting Medium (ADVI, Czech Republic) and sealed in coverslips. Images were taken by a laser scanning confocal microscope Carl Zeiss LSM 880 NLO, Zeiss, Germany, Objective Plan-Apochromat 420,782-9900, magnification ×63, N.A. 1,4.

Immunohistochemistry of the formalin-fixed paraffin-embedded testes sections

Mouse testes were harvested and fixed in 10% buffered formalin (Sigma-Aldrich, United States of America) overnight at 4°C. Fixed testes were transferred to 70% ethanol and embedded in paraffin (FFPE blocks). The 5 µm sections were prepared using the Leica microtome system. Testicular FFPE sections were deparaffinized using DIASOLV (DiaPath, Italy) two times for 5 min. After paraffine removal, samples were hydrated in decreasing ethanol series (100%, 90%, and 70%) for 5 min in each solution followed by rinsing in distilled water and PBS. Antigen retrieval was performed in a pressure cooker for 15 min in 0.1 M citrate buffer pH 6. After, samples were cooled down to RT for 30 min. After, samples were permeabilized with the Intracellular Staining Perm Wash Buffer for 3 × 5 min (421,002, BioLegend), followed by blocking in Superblock solution (Invitrogen, United States of America) and incubated with antibodies for 1 h at RT in the humid chamber. Primary antibodies against Lamin B2 (AB_2533107, Thermo Fisher Scientific) and SUN4 (sc-393115, Santa Cruz, United States of America) were diluted 1:100 and 1:50, respectively, in the Antibody diluent (Zytomed Systems GmbH, Germany) and incubated overnight at 4°C. The next day, samples were washed in PBS 3 × 5 min at RT with orbital shaking at 100 RPM. Secondary antibodies (Alexa Fluor, Invitrogen) were diluted 1:300 in Antibody diluent and incubated for 1 h in a humid chamber at RT. Samples were washed twice again. Next, DAPI at a concentration of 2 µg/mL was applied for 5 min to stain the nuclei followed by washing for 5 min in PBS again. Finally, slides were rinsed in distilled water, air-dried, and mounted using the AD-Mount-F Mounting Medium (ADVI, Czech Republic) and sealed with nail polish. Microscopic data were acquired using Carl Zeiss LSM 880 NLO, Zeiss, Germany, Objective Plan-Apochromat 420,782-9900, magnification ×63, N.A. 1,4 and processed in ImageJ/FIJI and Imaris software.

3D visualization of individual seminiferous tubules

Individual seminiferous tubules (iSTs) were processed using the CLARITY procedure (Chung et al., 2013). Briefly, iSTs were fixed in CLARITY gel monomer containing 4% formaldehyde for 2 h. After gel polymerization occurred, the iSTs were cleared overnight in a clearing buffer (20 mM lithium hydroxide monohydrate and 200 mM SDS, pH 8.5) at 37°C with gentle shaking. The next day, iSTs were stained by DAPI (2 µg/mL) and PNA 488 (Thermo Fisher Scientific) (2 µg/mL). Stained iSTs were mounted in PROTOS refractive index matching solution. Z-stacks were acquired using Carl Zeiss LSM 880 NLO confocal microscope, C-Apochromat 421,867-9970, magnification ×40, N.A. 1,1. For 3D visualization and surface rendering the Imaris software, Version 9.8.2 Package for Cell Biologists was utilized.

Cryo-transmission electron microscopy

4 µL of caput sperm suspension were applied to a glow-discharged Quantifoil cryoEM grid (R 2/1, 300 mesh) and incubated for 10 s in the Leica GP2 Plunge Freezer at room temperature and 80% relative humidity. The grid was then automatically blotted using filter paper for 4 s and frozen by immersion into the liquid ethane cooled down to −180°C.

CryoEM data were acquired in a semi-automated mode using SerialEM software (Mastronarde, 2005) on a Jeol JEM 2100Plus transmission electron microscope (TEM) equipped with a LaB6 electron gun and TVIPS XF416 CMOS camera, operated at 200 kV. Overview images were taken at magnification ×8000 (pixel size 14.04 Å) and details were acquired at x20,000 (pixel size 5.89 Å, electron dose ~40e/Å2).

Testicular cell suspensions preparation and flow cytometry analysis of testicular cells

Testes were harvested and *tunica albuginea* was removed. The rest of the tissue was incubated in RPMI medium with collagenase (35 µg/mL) and DNase (5 µg/mL) at 37°C, 100 RPM for 20 min.

Next, seminiferous tubules were resuspended by gentle pipetting using a wide-end tip. The suspension was filtered through the cell strainer (40 μm, Falcon) a flow-through fraction containing interstitial cells was discarded. Seminiferous tubules were harvested from the strainer and moved into fresh RPMI medium with collagenase (60 μg/mL) and DNase (5 μg/mL) and incubated for 30 min at 37°C with shaking 150 RPM. After, cells were resuspended by pipetting (20 times) a testicular cell suspension was filtered through the cell strainer (70 μm, Falcon). Flow through fraction containing testicular cells was centrifuged for 10 min, 400 × g at 4°C. The pellet was resuspended in 1 mL of cold PBS and transferred to a 1.5 mL Eppendorf tube and centrifuged again. The supernatant was removed, and the pellets were gently resuspended in 500 μL of 3.2% PFA in PBS. After 10 min fixation, cells were centrifuged and washed twice in PBS. All centrifugations were performed for 5 min at 400 × g at 4°C. After the second wash, cell pellets were resuspended in Superblock solution. After 1 h, cells were counted, and at least 1×10^6 cells were used for subsequent staining. Cells were incubated with primary antibodies (anti-H3 K27me3, ab6002; anti-H3K9ac, ab10812; anti-H3, ab1791; anti-H3K36me3, ab9050) diluted in the Intracellular Staining Perm Wash Buffer 1:100 (BioLegend) overnight at 4°C. The next day, cells were washed twice with PBS, and goat anti-mouse or anti-rabbit secondary antibody (dilution 1:300) was applied for 1 h at RT. Finally, cells were stained with DAPI (2 μg/mL) for 5 min and washed twice in PBS. Flow cytometry analyses of the testicular cells were performed using a BD LSRFortessa TM SORP instrument (Becton Dickinson, San Jose, CA, United States of America). The following lasers and filter parameters were selected, according to which a fluorescent probe was used: FITC blue laser = 488 nm (100 mW) excitation and 530/30 emission filter; PNA 568 = 561 nm (50 mW) laser line excitation and 586/15 nm emission filter; and DAPI = 405 nm (50 mW) laser line excitation and 450/50 nm emission filter. The voltages were set for the optimum resolution, and minimally, 50,000 gated events (based on FSC and SSC) were recorded for each sample. As a standard procedure before each specific parameter evaluation, positive and negative control samples were prepared to ensure the correct setting of the flow cytometer. DNA staining with dyes such as DAPI or Hoechst, combined with FACS analysis, is a well-established method for separating germ cells based on DNA content and light scattering properties. This approach can accurately distinguish mitotic, meiotic, and post-meiotic germ cells from each other, as well as from the somatic cells of the testis (Gaysinskaya et al., 2014; Bastos et al., 2005; Petrusová et al., 2022).

Protein isolation from sperm

To detect Septin 12, the pellet of mouse and human sperm was dissolved in Pellet Extraction Buffer (PEB) with protease inhibitors from the Subcellular Protein Fractionation Kit for Cultured cells (78,840, Thermo Fisher Scientific) for 20 min at RT. To detect other proteins, sperm pellets were dissolved in SDS sample buffer (2% SDS, 50 mM Tris-HCl (pH 8), 10 mM EDTA, 10% Glycerol) with Proteinase Inhibitors and incubated on ice for 30 min. Subsequently, the samples were centrifuged at 16,000 x g for 5 min. The supernatant was transferred to a new tube and a 1:1 SDS sample buffer was added to it. The samples were reduced by 5% β-mercaptoethanol and boiled for 5 min at 95°C. The protein lysate from sperm was used on SDS-Page.

Protein isolation from mouse testis

Freshly harvested mouse testes were placed in the Precellys tubes with beads (Bertin Technologies, France) and homogenized in corresponding lysis buffer with protease inhibitors by a Precellys tissue homogenizer (5,000 rpm, 10 s, 3 times, 4°C; Bertin Technologies). Used lysis buffers were: For Septin 12 PEB (from the Subcellular Protein Fractionation Kit for Cultured cells (78,840, Thermo Fisher Scientific), form Lamin B2/3 RHB lysis buffer (7M Urea, 2M Thio-urea, 4% CHAPS, 1% Triton X-100, 20 mM TRIS) and for other proteins SDS lysis buffer was used. Consequently, the samples were centrifuged at 16,000 × g, for 5 min, at RT, and the supernatant was transferred into a new tube. SDS sample buffer was added to it in a ratio of 1:1. The samples were reduced by 5% β-mercaptoethanol and boiled for 5 min at 95°C. The protein lysate from testis was used on SDS-Page.

Subcellular fractionation

The Subcellular Protein Fractionation Kit for Cultured cells (78,840, Thermo Fisher Scientific) was used for the separation and preparation of cytoplasmic, membrane, nuclear soluble, chromatin-bound, and cytoskeletal protein extracts from mouse and human sperm. The volume of buffers depended on the cell pellet volume, while the volume ratio of used buffers CEB: MEB:NEB:PEB was 200:200:100:100. As a first reagent was added cytoplasmic extraction buffer (CEB), incubated with the sperm for 10 min at 4°C with gentle mixing, followed by centrifugation 500 *g* for 5 min at 4°C. The supernatant with cytoplasmic proteins was transferred to a new tube and the membrane extraction buffer (MEB) was added to the pellet. After the 10 min incubation on ice, the samples were centrifuged 3,000 × g for 5 min at 4°C and the supernatant with membrane proteins was transferred to a new tube. Nuclear extraction buffer (NEB) was added to the pellet, vortexed on higher settings, and incubated with the sample for 30 min on ice. The sample was centrifuged at 5,000 × g for 5 min at 4°C and the supernatant with nuclear soluble proteins was transferred to a new tube. The NEB with 100 mM $CaCl_2$ and 300 units of Micrococcal Nuclease was added to the samples. The samples were incubated for 15 min at RT, followed by centrifugation at 16,000 × g for 5 min at RT. The supernatant with chromatin-bound proteins was transferred to a new tube and PEB was added to the rest of the pellet (Tubulin/mitochondria protein fraction). The sample was incubated for 10 min at RT and centrifuged at 16,000 × g for 5 min. The supernatant was transferred to a new tube and the pellet was discarded. SDS samples buffer was added to the all tubes with supernatant with different subcellular fractions in a ratio of 1:1. The samples were reduced by 5% β-mercaptoethanol and boiled for 5 min at 95°C and the protein fractions were used on SDS-Page.

SDS electrophoresis (SDS-Page) and western blot analysis

The protein extracts were separated by 10% SDS-PAGE and the proteins were transferred on the low fluorescence PVDF membrane (Bio-rad). The molecular weight of the proteins was assigned by Precision Plus Protein Dual Color Standards (Bio-Rad). The membranes were blocked in 5% Blotto, non-fat dry milk (Santa Cruz Biotechnology) diluted in PBS and incubated with rabbit polyclonal Septin-12 Antibody (NBP1-91640, Novus Biologicals) diluted 1:250 in PBS, at 4°C overnight. Other antibodies used in this article were α-tubulin (A11126, Thermo Fisher Scientific 1:600), α-tubulin acK40 (T7451 Sigma-Aldrich, 1:600), β-actin (ab 6276, Abcam, UK, 1:600), β-tubulin (T8355, Sigma-Aldrich, 1:600) and LmnB2/3 (ab151735, Abcam, 1:300). After incubation, the membranes were washed in PBS and incubated with a secondary antibody, goat anti-rabbit IgG or goat anti-mouse IgG conjugated to horseradish peroxidase (Bio-Rad), diluted 1:3,000 in PBS for 1 h at RT, and consequently washed in PBS. The membranes were developed with SuperSignal™ Chemiluminescent Substrate (Thermo Scientific) and images were captured using the Azure c600 imaging system (Azure Biosystems, Inc., CA, United States of America). As a negative control, a membrane without a primary antibody was used. The membranes were stained with Coomassie brilliant blue (7% acetic acid, 50% ethanol, dH_2O, 0.1% Coomassie brilliant blue) for 5 min at RT and washed in a destaining solution (35% ethanol, 10% acetic acid, dH_2O) to determine the total protein profile.

Transfection and immunofluorescent staining of HEK293T/17 cells

HEK293T/17 cells were co-transfected transiently with mouse Septin 12 and Lamin B1 or Lamin B2 or Lamin B3. Briefly, 1.1 × 10^6 cells were seeded in 60 mm cultivation dish containing a coverslip and incubated overnight. The following day, cells with 70%–80% confluency were transfected with Lipofectamine 3000 Transfection Reagent (L3000001, Invitrogen) kit using 3 μg of mouse Septin 12-GFP plasmid (pEGFP-C1, Addgene, United States of America) and 3 μg of mouse Lamin B1 or Lamin B2 or Lamin B3 plasmids conjugated with myc-tag (pCS2-MT, Addgene). Cells were incubated for 48 h in a DMEM cultivation medium (Gibco, United States of America) supplemented with 10% FBS (Gibco, United States of America) followed by immunofluorescent staining. Briefly, cells on the coverslips were fixed with Paraformaldehyde 3.2% (Scientific) in PBS for 10 min, washed twice with PBS followed by permeabilizing with 0.1% Triton X-100 (Serva, Germany) for 5 min. Super Block (Thermo Fisher Scientific) was used for 1 h blocking and cells were incubated with anti-myc tag primary antibody (MA1-21316, Invitrogen) diluted 1: 500 for 2 h in RT. After 3 times washing, the slides were incubated with donkey anti-mouse IgG secondary antibody conjugated with Alexa Fluor 568 (A10037, Invitrogen) diluted 1:300 for 1 h at RT. Subsequently, they were washed with PBS, incubated with DAPI (2 μg/mL) for 5 min, washed in PBS again, dried, and mounted in AD-Mount-F Mounting Medium. Septin 12 was conjugated with a GFP-tag and was not stained. Apochromat 420,782-9900, magnification ×63, N.A. 1,4 and processed in ImageJ/FIJI and Imaris software.

Co-immunoprecipitation (Co-IP)

Co-transfected cells with Septin 12 and Lamin B1 or Lamin B2 or Lamin B3 were incubated for 48 h followed by cell lysis with 1% CHAPS (Sigma-Aldrich) in 30 mM Tris-HCl (pH 7.5). Subsequently, Co-IP was performed on cell lysate supernatants by Dynabeads Protein G Immunoprecipitation kit (10007D, Invitrogen). Briefly, magnetic beads were conjugated with anti-GFP antibody (Ab290, Abcam) (against Septin 12) and incubated with cell lysate supernatants overnight at 4°C on a rotator. The samples were washed 3 times and precipitated proteins were eluted in the kit's elution buffer and incubated at 70°C for 5 min. Rabbit IgG Isotype control antibody (31,235, Invitrogen) was used for the isotype control group, and all the procedures were also performed on non-transfected cell lysate supernatant as the control. Then Western blot was performed to detect Lamin B1/B2/B3 in the eluted protein complexes as described above. Lamin B1/B2/B3 was detected with anti-myc tag primary antibody (MA1-21316, Invitrogen) diluted 1:500. Freshly harvested mouse testes were placed in the Precellys tubes with beads (Bertin Technologies, France) and homogenized in the 50 mM HEPES buffer with 3 mM $MgCl_2$, 500 mM KCl, 20% Glycerol, 1% NP40 (Roche, Switzerland) with protease inhibitors by a Precellys tissue homogenizer (5,000 rpm, 10 s, 3 times, 4°C; Bertin Technologies, France). The obtained protein lysate was subsequently used for Co-IP of the Prm2-Septin12 protein complex by Dynabeads Protein G Immunoprecipitation kit (10007D, Invitrogen, United States of America). Magnetic beads were conjugated with anti-protamine 2 antibody (Mab-Hup2B, Labome, United States of America) for 30 min at RT. As a control, magnetic beads conjugated with a mouse IgG isotype control (31,903, Invitrogen) were used. Subsequently, the beads were washed, and lysate obtained from the isolation of mouse testes was added to them. Samples were incubated overnight at 4°C with constant agitation. The next day, the supernatant was removed, the beads with protein complex were 3 times washed and the precipitated proteins were eluted from beads by elution buffer with SDS sample buffer and 5% β-mercaptoethanol was added to the beads and incubated at 70°C for 5 min. Subsequently, SDS-Page with Western blot Analysis was performed, followed by the detection of Septin 12 Antibody (NBP1-91640, Novus Biologicals, United States of America).

Centriole analysis

To analyze signal intensity, length, and width of the centrioles, we used CEP135 immunofluorescent staining using a rabbit polyclonal antibody raised against the first 233 amino acids of CEP135 (24428-1-AP, Thermo Fisher Scientific). Sperm samples were visualized using a Leica SP8 confocal microscope in BrightR mode using an HC PL APO CS2 63x/1.40 OIL lens, 100% gain, 1,024 × 1,024 pixels (62 μm × 62 μm) format, 3x zoom factor, line averaging of 3, and frame accumulation of 2. Three sequences were used to collect the fluorescence signals. DNA signal was detected using a 410 nm laser set to detect photons between 425 and 478 nm and was color-coded to blue. For phase-like images, the fluoro-turret was set to Scan-PH, and PMT Trans was set to ON with a gain of 300 in greyscale. CEP135 signal was detected using an anti-rabbit

Gene	Primer sequence (5′→3′)
Rps2	CTGACTCCCGACCTCTGGAAA
	GAGCCTGGGTCCTCTGAACA
Hdac6	CAGAGAAGCAGAGGAAGCCC
	ACCAGGATAGTGGGGTCACA
α-Tat1	CAGCGCTTTGAGGATGCAAA
	CTCCCGGTCATCCAGTACAA
Gcn5	ATGAGCAGGTCAAGGGCTATG
	AATGGCGTACTCGTCAGCAT
Sept12 isoform1	ACAGTAAGATTCGGGAGCAGAT
	ATGCCTGCAATGTTCCCAAAC
Sept12 isoform 2	GGGAGCAGATCCCTTTTGCT
	CCTGGAGATGGGAGCTTCG
Sept12 isoform 3	GGGGCATCATCGAAGTGGAA
	AGTCTGAGTACCCGGTAGTTCT
Sept12 all isoforms	GACTCATCCACCAGGAGCAG
	AATGCCCACAGGACCAAACA
LmnB2	CTGGCACACTACATCGACCGT
	TCCCGCTTCTTGGCACTCTTC
LmnB3	AGGACTTGGAACAACCACCTC
	GCCTTGTCATTCTGGTCCGA
SUN4	GAACCGTCTGGATCTTCTGTAGT
	AGTGAACAGGAAGCGGATGG

secondary conjugated with ALEXA 488 and activated with a 488 nm laser. The absorption spectrum was set to 505–550 nm and was color-coded to green. The Tubulin signal was detected using an anti-sheep secondary conjugated with ALEXA 555 and activated with a 561 nm laser. We set the absorption spectrum to 560–625 nm, and it was color-coded to red. We collected 10-15 Z-sections of 0.3 µm thickness from the bottom to the top of the sperm. The CEP135 intensity was quantified using a Leica LAS-X algorithm. Centriole length and width were determined using the line-profile tool in Leica LAS-X. A line 3 µm long and 0.5 µm wide was drawn through the CEP135 labeling, and a corresponding graph was calculated for each pixel value along the line. The distance from two points at half the distance of the graph's peak was measured to determine the length and width of CEP135.

RNA isolation, reverse transcription, qPCR

Total RNA was isolated from testicular tissue samples using TRI Reagent®. RNA extracts (2 µg) were treated with DNase I (1 U/µL, Fermentas, United States of America) in the presence of DNase I buffer 10× (Thermo Fisher Scientific) with MgCl2 for 30 min at 37°C, and EDTA (Fermentas) was added for 10 min at 65°C. The reverse transcription reaction contained 5× reaction Buffer (Fermentas), RNaseOUT Recombinant Ribonuclease Inhibitor (40 U/1 µL, Thermo Fisher Scientific), Universal RNA Spike II (0.005 ng/µL, TATAA biocenter, Göteborg, Sweden), 10 mM dNTP Mix (Thermo Fisher Scientific), oligo(dt)18 (Thermo Fisher Scientific) mixed 1:1 with Random primers (Thermo Scientific) and M-MuLV RevertAid transcriptase (200 U/µL, Fermentas), and run to generate cDNA. The RT^- negative control was prepared in the same conditions but with RNase/DNase-free water. For qRT-PCR, 10 ng/µL cDNA was used. Two times Maxima SYBR Green qPCR Master Mix (Thermo Fisher Scientific), reverse and forward primer and nuclease-free water were used, and all reactions were performed in duplets in a PCR cycler (CFX 96-qPCR cycler/CFX 384-qPCR, Bio-Rad). The RT^- negative control for cDNA synthesis, no template control, and spike control were also analyzed. Ribosomal protein S2 (*Rps2*) was used as a reference gene.

Statistical and data analysis

The intensity of Septin 12 signal among the tail was analyzed in ZEN Blue software. The line in the width of 5 pixels was drawn for each sperm from the head (0% of the distance) to the end of the annulus (100% of the distance). Intensities were normalized on the relative distance from the head (0%). Measured values were subsequently analyzed using Microsoft Excel. Nuclear area and indentation length were measured manually using Leica LAS-X software. Data from flow cytometry were gated and analyzed using Flow Jo software. The gating strategy is shown in Supplementary Figure S1. 3D microscopic data were processed using Imaris (version 9.8.2 Package for Cell Biologists) software. Cryo-TEM data were analysed in FIJI software using Labkit, MorpholibJ and 3DSuite plugins. Annulus was manually detected, and its area was marked using "masks" function. The distance of annulus centroids (geometric center of a structure) and the area of these structures were. Graphs and statistical analysis were done using GraphPad software (version 10.2.0) using Mann-Whitney or *t*-test. The number of animals and the amount of biological material used for each experiment are listed in Supplementary Figure S5.

Molecular modelling

The prediction of potential complexes of Protamine 2 with Septin 12 was performed using a local installation of the AlphaFold version 2.3.2 (Jumper et al., 2021). Three complexes were prepared using AlphaFold multimer with protein sequences of mouse Protamine 2 (NP_032959.1) with Septin 12 isoform 1 (NP_081945.1), mouse Protamine 2 (NP_032959.1) with Septin 12 isoform 3 (NP_001360874.1), and human Protamine 2 (NP_002753.2) with Septin 12 isoform 2 (NP_653206.2), respectively. The modelling results were visualized with the open-source PyMOL version 2.6.0 (The PyMOL Molecular Graphics System, Schrödinger, LLC). The pLDDT scores were transformed in PyMOL to 100-pLDDT for the visualization using the standard

B-factor color scale with cold colors corresponding to high confidence regions (see Figure 8).

Data availability statement

Source data files corresponding to individual panels in Figures are deposited in Zenodo as Source Data Archives: https://zenodo.org/records/11217661. A preprint version of this manuscript is available on bioRxiv with the No. BIORXIV/2024/596175 (https://doi.org/10.1101/2024.05.28.596175).

Ethics statement

The studies involving humans were approved by the Ethical Committee, protocol code BIOCEV 012019, 20 January 2019. Biological materials and experimental protocols were approved by the Ethical Committee of the General University Hospital (Prague, Czech Republic), protocol code 617/17 S-IV. The studies were conducted in accordance with the local legislation and institutional requirements. The participants provided their written informed consent to participate in this study. The animal study was approved by the Animal Welfare Committee of the Czech Academy of Sciences, Animal Ethical protocol code 66866/2015-MZE-17214, 18 December 2015. The study was conducted in accordance with the local legislation and institutional requirements.

Author contributions

OSa: Conceptualization, Data curation, Formal Analysis, Investigation, Methodology, Visualization, Writing–original draft. MF: Conceptualization, Data curation, Investigation, Methodology, Supervision, Visualization, Writing–original draft. VK: Formal Analysis, Investigation, Methodology, Validation, Writing–review and editing. JV: Methodology, Validation, Writing–review and editing. MQ: Investigation, Methodology, Writing–review and editing. DS: Investigation, Writing–review and editing. OSi: Formal Analysis, Methodology, Writing–review and editing. LM: Investigation, Validation, Writing–review and editing. DC: Formal Analysis, Investigation, Writing–review and editing. FL: Formal Analysis, Methodology, Writing–review and editing. LD: Conceptualization, Supervision, Writing–review and editing. JC: Investigation, Visualization, Writing–review and editing. TA-R: Supervision, Writing–review and editing, Funding acquisition. SH: Supervision, Writing–review and editing. HS: Writing–review and editing. PP: Conceptualization, Supervision, Writing–review and editing. KS: Conceptualization, Funding acquisition, Resources, Supervision, Writing–review and editing. KK: Conceptualization, Funding acquisition, Project administration, Resources, Supervision, Writing–original draft, Writing–review and editing.

Funding

The author(s) declare that financial support was received for the research, authorship, and/or publication of this article. This work was supported by the Czech Grant Agency (GC20-20217J and GA23-06591S), and German Research Foundation (DFG, STE 892/20-1); by institutional support from the Institute of Biotechnology of the Czech Academy of Sciences RVO (86652036); by BIOCEV project (CZ.1.05/1.1.00/02.0109) from the ERDF; European Regional Development Fund, project "Modernization and support of research activities of the national infrastructure for biological and medical imaging Czech-BioImaging" (No. CZ.02.1.01/0.0/0.0/16_013/0001775) Imaging Methods Core Facility at BIOCEV, institution supported by the MEYS CR (Large RI Project LM2018129 Czech-BioImaging) and MEYS CR (LM2023050 Czech-BioImaging); COST Action CA20119 (ANDRONET) supported by European Cooperation in Science and Technology (www.cost.eu). Eunice Kennedy Shriver National Institute of Child Health and Human Development (United States) 1R15HD110863 supported Tomer Avidor-Reiss research.

Acknowledgments

We acknowledge Michala Krejci for excellent technical assistance, David Liebl and Jiri Miksatko for cryo-TEM data acquisition, Zuzana Cockova for cry-TEM data analysis consultation, and Robert Selvek for statistical data analysis consultation.

Conflict of interest

The authors declare that the research was conducted in the absence of any commercial or financial relationships that could be construed as a potential conflict of interest.

Publisher's note

All claims expressed in this article are solely those of the authors and do not necessarily represent those of their affiliated organizations, or those of the publisher, the editors and the reviewers. Any product that may be evaluated in this article, or claim that may be made by its manufacturer, is not guaranteed or endorsed by the publisher.

Supplementary material

The Supplementary Material for this article can be found online at: https://www.frontiersin.org/articles/10.3389/fcell.2024.1447630/full#supplementary-material

References

Ammer, H., Henschen, A., and Lee, C. H. (1986). Isolation and amino-acid sequence analysis of human sperm protamines P1 and P2. Occurrence of two forms of protamine P2. *Biol. Chem. Hoppe Seyler* 367, 515–522. doi:10.1515/bchm3.1986.367.1.515

Arévalo, L., Merges, G. E., Schneider, S., Oben, F. E., Neumann, I. S., and Schorle, H. (2022a). Loss of the cleaved-protamine 2 domain leads to incomplete histone-to-protamine exchange and infertility in mice. *PLoS Genet.* 18, e1010272. doi:10.1371/journal.pgen.1010272

Arévalo, L., Merges, G. E., Schneider, S., and Schorle, H. (2022b). Protamines: lessons learned from mouse models. *Reproduction* 164, R57–R74. doi:10.1530/REP-22-0107

Avidor-Reiss, T., Carr, A., and Fishman, E. L. (2020). The sperm centrioles. *Mol. Cell Endocrinol.* 518, 110987. doi:10.1016/j.mce.2020.110987

Balhorn, R. (1982). A model for the structure of chromatin in mammalian sperm. *J. Cell Biol.* 93, 298–305. doi:10.1083/jcb.93.2.298

Bastos, H., Lassalle, B., Chicheportiche, A., Riou, L., Testart, J., Allemand, I., et al. (2005). Flow cytometric characterization of viable meiotic and postmeiotic cells by Hoechst 33342 in mouse spermatogenesis. *Cytom. Part A* 65A, 40–49. doi:10.1002/cyto.a.20129

Brunner, A. M., Nanni, P., and Mansuy, I. M. (2014). Epigenetic marking of sperm by post-translational modification of histones and protamines. *Epigenetics & Chromatin* 7, 2. doi:10.1186/1756-8935-7-2

Calvi, A., Wong, A. S., Wright, G., Wong, E. S., Loo, T. H., Stewart, C. L., et al. (2015). SUN4 is essential for nuclear remodeling during mammalian spermiogenesis. *Dev. Biol.* 407, 321–330. doi:10.1016/j.ydbio.2015.09.010

Carrell, D. T., Emery, B. R., and Hammoud, S. (2008). The aetiology of sperm protamine abnormalities and their potential impact on the sperm epigenome. *Int. J. Androl.* 31, 537–545. doi:10.1111/j.1365-2605.2008.00872.x

Chung, K., Wallace, J., Kim, S. Y., Kalyanasundaram, S., Andalman, A. S., Davidson, T. J., et al. (2013). Structural and molecular interrogation of intact biological systems. *Nature* 497, 332–337. doi:10.1038/nature12107

Chu, Z., and Gruss, O. J. (2022). Mitotic maturation compensates for premature centrosome splitting and PCM loss in human cep135 knockout cells. *Cells* 11, 1189. doi:10.3390/cells11071189

Coelingh, J. P., Rozijn, T. H., and Monfoort, C. H. (1969). Isolation and partial characterization of a basic protein from bovine sperm heads. *Biochim. Biophys. Acta* 188, 353–356. doi:10.1016/0005-2795(69)90091-9

Cooper, T. G. (2005). Cytoplasmic droplets: the good, the bad or just confusing? *Hum. Reprod.* 20, 9–11. doi:10.1093/humrep/deh555

Corzett, M., Mazrimas, J., and Balhorn, R. (2002). Protamine 1: protamine 2 stoichiometry in the sperm of eutherian mammals. *Mol. Reprod. Dev.* 61, 519–527. doi:10.1002/mrd.10105

Dammermann, A., and Merdes, A. (2002). Assembly of centrosomal proteins and microtubule organization depends on PCM-1. *J. Cell Biol.* 159, 255–266. doi:10.1083/jcb.200204023

Desterke, C., and Gassama-Diagne, A. (2019). Protein-protein interaction analysis highlights the role of septins in membrane enclosed lumen and mRNA processing. *Adv. Biol. Regul.* 73, 100635. doi:10.1016/j.jbior.2019.100635

De Yebra, L., Ballescà, J. L., Vanrell, J. A., Bassas, L., and Oliva, R. (1993). Complete selective absence of protamine P2 in humans. *J. Biol. Chem.* 268, 10553–10557. doi:10.1016/s0021-9258(18)82234-7

Dunleavy, J. E. M., O'Bryan, M. K., Stanton, P. G., and O'Donnell, L. (2019). The cytoskeleton in spermatogenesis. *Reproduction* 157, R53–R72. doi:10.1530/REP-18-0457

Erkek, S., Hisano, M., Liang, C.-Y., Gill, M., Murr, R., Dieker, J., et al. (2013). Molecular determinants of nucleosome retention at CpG-rich sequences in mouse spermatozoa. *Nat. Struct. & Mol. Biol.* 20, 868–875. doi:10.1038/nsmb.2599

Frolikova, M., Sebkova, N., Ded, L., and Dvorakova-Hortova, K. (2016). Characterization of CD46 and β1 integrin dynamics during sperm acrosome reaction. *Sci. Rep.* 6, 33714. doi:10.1038/srep33714

Furukawa, K., and Hotta, Y. (1993). cDNA cloning of a germ cell specific lamin B3 from mouse spermatocytes and analysis of its function by ectopic expression in somatic cells. *Embo J.* 12, 97–106. doi:10.1002/j.1460-2075.1993.tb05635.x

Gatewood, J. M., Cook, G. R., Balhorn, R., Bradbury, E. M., and Schmid, C. W. (1987). Sequence-specific packaging of DNA in human sperm chromatin. *Science* 236, 962–964. doi:10.1126/science.3576213

Gaysinskaya, V., Soh, I. Y., Van Der Heijden, G. W., and Bortvin, A. (2014). Optimized flow cytometry isolation of murine spermatocytes. *Cytom. Part A* 85, 556–565. doi:10.1002/cyto.a.22463

Hall, E. A., Kumar, D., Prosser, S. L., Yeyati, P. L., Herranz-Pérez, V., García-Verdugo, J. M., et al. (2023). Centriolar satellites expedite mother centriole remodeling to promote ciliogenesis. *eLife* 12, e79299. doi:10.7554/eLife.79299

Hammoud, S. S., Nix, D. A., Zhang, H., Purwar, J., Carrell, D. T., and Cairns, B. R. (2009). Distinctive chromatin in human sperm packages genes for embryo development. *Nature* 460, 473–478. doi:10.1038/nature08162

Hisano, M., Erkek, S., Dessus-Babus, S., Ramos, L., Stadler, M. B., and Peters, A. H. (2013). Genome-wide chromatin analysis in mature mouse and human spermatozoa. *Nat. Protoc.* 8, 2449–2470. doi:10.1038/nprot.2013.145

Ihara, M., Kinoshita, A., Yamada, S., Tanaka, H., Tanigaki, A., Kitano, A., et al. (2005). Cortical organization by the septin cytoskeleton is essential for structural and mechanical integrity of mammalian spermatozoa. *Dev. Cell* 8, 343–352. doi:10.1016/j.devcel.2004.12.005

Inagaki, Y., Fukuhara, S., Kuribayashi, S., Okada, K., Sekii, Y., Takezawa, K., et al. (2021). The expression of human testis-specific actin capping protein predicts *in vitro* fertilization outcomes: a novel biomarker of sperm function for assisted reproductive technology. *Reprod. Med. Biol.* 20, 537–542. doi:10.1002/rmb2.12407

Jumper, J., Evans, R., Pritzel, A., Green, T., Figurnov, M., Ronneberger, O., et al. (2021). Highly accurate protein structure prediction with AlphaFold. *Nature* 596, 583–589. doi:10.1038/s41586-021-03819-2

Khanal, S., Jaiswal, A., Chowdanayaka, R., Puente, N., Turner, K., Assefa, K. Y., et al. (2024). The evolution of centriole degradation in mouse sperm. *Nat. Commun.* 15, 117. doi:10.1038/s41467-023-44411-8

Kierszenbaum, A. L., Rivkin, E., and Tres, L. L. (2003). Acroplaxome, an F-Actin–Keratin-containing plate, anchors the acrosome to the nucleus during shaping of the spermatid head. *Mol. Biol. Cell* 14, 4628–4640. doi:10.1091/mbc.e03-04-0226

Kierszenbaum, A. L., Tres, L. L., Rivkin, E., Kang-Decker, N., and Van Deursen, J. M. A. (2004). The acroplaxome is the docking site of Golgi-derived myosin Va/Rab27a/b-containing proacrosomal vesicles in wild-type and Hrb mutant mouse spermatids. *Biol. Reproduction* 70, 1400–1410. doi:10.1095/biolreprod.103.025346

Kmonickova, V., Frolikova, M., Steger, K., and Komrskova, K. (2020). The role of the LINC complex in sperm development and function. *Int. J. Mol. Sci.* 21, 9058. doi:10.3390/ijms21239058

Kuo, Y.-C., Lin, Y.-H., Chen, H.-I., Wang, Y.-Y., Chiou, Y.-W., Lin, H.-H., et al. (2012). SEPT12 mutations cause male infertility with defective sperm annulus. *Hum. Mutat.* 33, 710–719. doi:10.1002/humu.22028

Lhuillier, P., Rode, B., Escalier, D., Lorès, P., Dirami, T., Bienvenu, T., et al. (2009). Absence of annulus in human asthenozoospermia: case report. *Hum. Reprod.* 24, 1296–1303. doi:10.1093/humrep/dep020

Lin, Y. H., Chou, C. K., Hung, Y. C., Yu, I. S., Pan, H. A., Lin, S. W., et al. (2011a). SEPT12 deficiency causes sperm nucleus damage and developmental arrest of preimplantation embryos. *Fertil. Steril.* 95, 363–365. doi:10.1016/j.fertnstert.2010.07.1064

Lin, Y. H., Kuo, Y. C., Chiang, H. S., and Kuo, P. L. (2011b). The role of the septin family in spermiogenesis. *Spermatogenesis* 1, 298–302. doi:10.4161/spmg.1.4.18326

Lin, Y. H., Lin, Y. M., Wang, Y. Y., Yu, I. S., Lin, Y. W., Wang, Y. H., et al. (2009). The expression level of septin12 is critical for spermiogenesis. *Am. J. Pathol.* 174, 1857–1868. doi:10.2353/ajpath.2009.080955

Lin, Y. H., Wang, Y. Y., Chen, H. I., Kuo, Y. C., Chiou, Y. W., Lin, H. H., et al. (2012). SEPTIN12 genetic variants confer susceptibility to teratozoospermia. *PLoS One* 7, e34011. doi:10.1371/journal.pone.0034011

Maier, W. M., Nussbaum, G., Domenjoud, L., Klemm, U., and Engel, W. (1990). The lack of protamine 2 (P2) in boar and bull spermatozoa is due to mutations within the P2 gene. *Nucleic Acids Res.* 18, 1249–1254. doi:10.1093/nar/18.5.1249

Martins, C. S., Taveneau, C., Castro-Linares, G., Baibakov, M., Buzhinsky, N., Eroles, M., et al. (2023). Human septins organize as octamer-based filaments and mediate actin-membrane anchoring in cells. *J. Cell Biol.* 222, e202203016. doi:10.1083/jcb.202203016

Mastronarde, D. N. (2005). Automated electron microscope tomography using robust prediction of specimen movements. *J. Struct. Biol.* 152, 36–51. doi:10.1016/j.jsb.2005.07.007

Mengual, L., Ballescá, J. L., Ascaso, C., and Oliva, R. (2003). Marked differences in protamine content and P1/P2 ratios in sperm cells from percoll fractions between patients and controls. *J. Androl.* 24, 438–447. doi:10.1002/j.1939-4640.2003.tb02692.x

Mostowy, S., and Cossart, P. (2012). Septins: the fourth component of the cytoskeleton. *Nat. Rev. Mol. Cell Biol.* 13, 183–194. doi:10.1038/nrm3284

Mukherjee, A., Saurabh, S., Olive, E., Jang, Y. H., and Lansac, Y. (2021). Protamine binding site on DNA: molecular dynamics simulations and free energy calculations with full atomistic details. *J. Phys. Chem. B* 125, 3032–3044. doi:10.1021/acs.jpcb.0c09166

Nakos, K., Alam, M. N. A., Radler, M. R., Kesisova, I. A., Yang, C., Okletey, J., et al. (2022). Septins mediate a microtubule–actin crosstalk that enables actin growth on microtubules. *Proc. Natl. Acad. Sci.* 119, e2202803119. doi:10.1073/pnas.2202803119

Nanassy, L., Liu, L., Griffin, J., and Douglas, T. C. (2011). The clinical utility of the protamine 1/protamine 2 ratio in sperm, *Protein Pept. Lett.* 18, 772–777. doi:10.2174/092986611795713934

Oliva, R. (2006). Protamines and male infertility. *Hum. Reprod. Update* 12, 417–435. doi:10.1093/humupd/dml009

Pereira, C. D., Serrano, J. B., Martins, F., Da Cruz, E. S. O. A. B., and Rebelo, S. (2019). Nuclear envelope dynamics during mammalian spermatogenesis: new insights on male fertility. *Biol. Rev. Camb Philos. Soc.* 94, 1195–1219. doi:10.1111/brv.12498

Petrusová, J., Manning, J., Kubovčiak, J., Kolář, M., and Filipp, D. (2022). Two complementary approaches for efficient isolation of Sertoli cells for transcriptomic analysis. *Front. Cell Dev. Biol.* 10, 972017. doi:10.3389/fcell.2022.972017

Retief, J. D., and Dixon, G. H. (1993). Evolution of pro-protamine P2 genes in primates. *Eur. J. Biochem.* 214, 609–615. doi:10.1111/j.1432-1033.1993.tb17960.x

Rodríguez-Casuriaga, R., and Geisinger, A. (2021). Contributions of flow cytometry to the molecular study of spermatogenesis in mammals. *Int. J. Mol. Sci.* 22, 1151. doi:10.3390/ijms22031151

Rogenhofer, N., Dansranjavin, T., Schorsch, M., Spiess, A., Wang, H., Von Schönfeldt, V., et al. (2013). The sperm protamine mRNA ratio as a clinical parameter to estimate the fertilizing potential of men taking part in an ART programme. *Hum. Reprod.* 28, 969–978. doi:10.1093/humrep/des471

Rogenhofer, N., Ott, J., Pilatz, A., Wolf, J., Thaler, C. J., Windischbauer, L., et al. (2017). Unexplained recurrent miscarriages are associated with an aberrant sperm protamine mRNA content. *Hum. Reprod.* 32, 1574–1582. doi:10.1093/humrep/dex224

Schagdarsurengin, U., Paradowska, A., and Steger, K. (2012). Analysing the sperm epigenome: roles in early embryogenesis and assisted reproduction. *Nat. Rev. Urol.* 9, 609–619. doi:10.1038/nrurol.2012.183

Schagdarsurengin, U., and Steger, K. (2016). Epigenetics in male reproduction: effect of paternal diet on sperm quality and offspring health. *Nat. Rev. Urol.* 13, 584–595. doi:10.1038/nrurol.2016.157

Schatten, H., Vanesa, Y. R., and Sun, Q.-Y. (2011). The sperm centrosome: its role and significance in nature and human assisted reproduction. *J. Reprod. Stem Cell Biotechno* 2, 121–127. doi:10.1177/205891581100200206

Schneider, S., Balbach, M., Jan, F. J., Fietz, D., Nettersheim, D., Jostes, S., et al. (2016). Re-visiting the Protamine-2 locus: deletion, but not haploinsufficiency, renders male mice infertile. *Sci. Rep.* 6, 36764. doi:10.1038/srep36764

Schneider, S., Shakeri, F., Trötschel, C., Arévalo, L., Kruse, A., Buness, A., et al. (2020a). Protamine-2 deficiency initiates a reactive oxygen species (ROS)-mediated destruction cascade during epididymal sperm maturation in mice. *Cells* 9, 1789. doi:10.3390/cells9081789

Schneider, S., Shakeri, F., Trötschel, C., Arévalo, L., Kruse, A., Buness, A., et al. (2020b). Protamine-2 deficiency initiates a reactive oxygen species (ROS)-Mediated destruction cascade during epididymal sperm maturation in mice. *Cells* 9, 1789. doi:10.3390/cells9081789

Schütz, W., Alsheimer, M., Ollinger, R., and Benavente, R. (2005a). Nuclear envelope remodeling during mouse spermiogenesis: postmeiotic expression and redistribution of germline lamin B3. *Exp. Cell Res.* 307, 285–291. doi:10.1016/j.yexcr.2005.03.023

Schütz, W., Benavente, R., and Alsheimer, M. (2005b). Dynamic properties of germ line-specific lamin B3: the role of the shortened rod domain. *Eur. J. Cell Biol.* 84, 649–662. doi:10.1016/j.ejcb.2005.03.001

Shen, Y.-R., Wang, H.-Y., Kuo, Y.-C., Shih, S.-C., Hsu, C.-H., Chen, Y.-R., et al. (2017). SEPT12 phosphorylation results in loss of the septin ring/sperm annulus, defective sperm motility and poor male fertility. *PLoS Genet.* 13, e1006631. doi:10.1371/journal.pgen.1006631

Soda, T., Miyagawa, Y., Ueda, N., Takezawa, K., Okuda, H., Fukuhara, S., et al. (2017). Systematic characterization of human testis-specific actin capping protein β3 as a possible biomarker for male infertility. *Hum. Reprod.* 32, 514–522. doi:10.1093/humrep/dew353

Spanò, M., and Evenson, D. P. (1993). Flow cytometric analysis for reproductive biology. *Biol. Cell.* 78 (1–2), 53–62. doi:10.1016/0248-4900(93)90114-t

Sugino, Y., Ichioka, K., Soda, T., Ihara, M., Kinoshita, M., Ogawa, O., et al. (2008). Septins as diagnostic markers for a subset of human asthenozoospermia. *J. Urol.* 180, 2706–2709. doi:10.1016/j.juro.2008.08.005

Thoma, H., Grünewald, L., Braune, S., Pasch, E., and Alsheimer, M. (2023). SUN4 is a spermatid type II inner nuclear membrane protein that forms heteromeric assemblies with SUN3 and interacts with lamin B3. *J. Cell Sci.* 136, jcs260155. doi:10.1242/jcs.260155

Wang, T., Gao, H., Li, W., and Liu, C. (2019). Essential role of histone replacement and modifications in male fertility. *Front. Genet.* 10, 962. doi:10.3389/fgene.2019.00962

Ward, W. S., and Coffey, D. S. (1991). DNA packaging and organization in mammalian spermatozoa: comparison with somatic cells. *Biol. Reprod.* 44, 569–574. doi:10.1095/biolreprod44.4.569

Xiong, Z., Zhang, H., Huang, B., Liu, Q., Wang, Y., Shi, D., et al. (2018). Expression pattern of prohibitin, capping actin protein of muscle Z-line beta subunit and tektin-2 gene in Murrah buffalo sperm and its relationship with sperm motility. *Asian-Australas J. Anim. Sci.* 31, 1729–1737. doi:10.5713/ajas.18.0025

Yeh, C. H., Kuo, P. L., Wang, Y. Y., Wu, Y. Y., Chen, M. F., Lin, D. Y., et al. (2015). SEPT12/SPAG4/LAMINB1 complexes are required for maintaining the integrity of the nuclear envelope in postmeiotic male germ cells. *PLoS One* 10, e0120722. doi:10.1371/journal.pone.0120722

Yeh, C. H., Wang, Y. Y., Wee, S. K., Chen, M. F., Chiang, H. S., Kuo, P. L., et al. (2019). Testis-specific SEPT12 expression affects SUN protein localization and is involved in mammalian spermiogenesis. *Int. J. Mol. Sci.* 20, 1163. doi:10.3390/ijms20051163

Zante, J., Schumann, J., Göhde, W., and Hacker, U. (1977). DNA-fluorometry of mammalian sperm. *Histochemistry* 54, 1–7. doi:10.1007/BF00493324

Frontiers in
Cell and Developmental Biology

Explores the fundamental biological processes of life, covering intracellular and extracellular dynamics.

The world's most cited developmental biology journal, advancing our understanding of the fundamental processes of life. It explores a wide spectrum of cell and developmental biology, covering intracellular and extracellular dynamics.

Discover the latest Research Topics

See more →

Frontiers

Avenue du Tribunal-Fédéral 34
1005 Lausanne, Switzerland
frontiersin.org

Contact us

+41 (0)21 510 17 00
frontiersin.org/about/contact